Vol. 193, February 14, 1987
Complete in one issue

ISSN 0003-2670

ANALYTICA CHIMICA ACTA

International journal devoted to all branches of analytical chemistry

ELSEVIER

ANALYTICA CHIMICA ACTA

International journal devoted to all branches of analytical chemistry
Revue internationale consacrée à tous les domaines de la chimie analytique
Internationale Zeitschrift für alle Gebiete der analytischen Chemie

PUBLICATION SCHEDULE FOR 1987

	J	F	M	A	M	J	J	A	S	O	N	D
Analytica Chimica Acta	192	193	194	195	196	197	198	199	200	201	202	20

Scope. *Analytica Chimica Acta* publishes original papers, short communications, and reviews dealing with a aspect of modern chemical analysis both fundamental and applied.

Submission of Papers. Manuscripts (three copies) should be submitted as designated below for rapid efficient handling:

Papers from the Americas to: Professor Harry L. Pardue, Department of Chemistry, Purdue University, Lafayette, IN 47907, U.S.A.

Papers from all other countries to: Dr. A. M. G. Macdonald, Department of Chemistry, The University, P.O. Box Birmingham B15 2TT, England. Papers dealing particularly with computer techniques to: Professor J. T. C Universität Bern, Pharmazeutisches Institut, Baltzerstrasse 5, CH-3012 Bern, Switzerland.

Submission of an article is understood to imply that the article is original and unpublished and is not b considered for publication elsewhere. Upon acceptance of an article by the journal, authors will be asked to tra the copyright of the article to the publisher. This transfer will ensure the widest possible disseminatio information.

Papers in English, French and German are published. There are no page charges. Manuscripts should confor layout and style to the papers published in this Volume. See inside back cover for "Information for Authors'

Reprints. Fifty reprints will be supplied free of charge. Additional reprints (minimum 100) can be ordered order form containing price quotations will be sent to the authors together with the proofs of their article.

Publication. *Analytica Chimica Acta* appears in 12 volumes in 1987. The subscription for 1987 (Vols. 192–20 Dfl. 2700.00 plus Dfl. 300.00 (p.p.h.) (total approx. US $1333.30). All earlier volumes (Vols. 1–191) except 23 and 28 are available at Dfl. 231.00 (US $102.70), plus Dfl. 17.00 (US $7.60) p.p.h., per volume.

Our p.p.h. (postage, packing and handling) charge includes surface delivery of all issues, except to subscribe the U.S.A., Canada, Japan, Australia, New Zealand, P.R. China, India, Israel, South Africa, Malaysia, Thai Singapore, South Korea, Taiwan, Pakistan, Hong Kong, Brazil, Argentina and Mexico, who receive all issues b delivery (S.A.L. — Surface Air Lifted) at no extra cost. For the rest of the world, airmail and S.A.L. charge available upon request.

Subscription. Subscription should be sent to: Elsevier Science Publishers B.V., Journals Department, P.O. 211, 1000 AE Amsterdam, The Netherlands. Tel: 5803 911, Telex: 18582, to which requests for sample copie also be sent.

Claims for issues not received should be made within three months of publication of the issues. If not they ca be honoured free of charge.

Readers in the U.S.A. and Canada can contact the following address: Elsevier Science Publishing Co. Inc., Jo Information Center, 52 Vanderbilt Avenue, New York, NY 10017, U.S.A., Tel: (212) 916-1250, for fu information, or a free sample copy of this or any other Elsevier Science Publishers journal.

Advertisements. Advertisement rates are available from the publisher.

0003-2670/87/

Printed in The Netherlands

CONTENTS

ANALYTICA CHIMICA ACTA
VOL. 193 (1987)

ANALYTICA CHIMICA ACTA

International journal devoted to all branches of analytical chemistry

ELSEVIER Amsterdam–Oxford–New York–Tokyo

0003-2670/86/$03.50

Printed in The Netherlands

Analytica Chimica Acta, 193 (1987) 1—18
Elsevier Science Publishers B.V., Amsterdam — Printed in The Netherlands

A MODIFIED COMBUSTION METHOD FOR THE DETERMINATION OF THE SURFACE AND BULK CARBON CONTENTS OF HIGH-PURITY METALS

K. GRETZINGER, E. GRALLATH* and G. TÖLG

Max-Planck-Institut für Metallforschung, Institut für Werkstoffwissenschaften, Laboratorium für Reinststoffanalytik, Dortmund (F.R.G.)

(Received 14th July 1986)

SUMMARY

A newly developed apparatus for the determination of carbon in high-purity metals is described. By controlled heating of samples in an oxygen or oxygen/helium flow, it is possible to distinguish between the carbon contents of a thin surface layer and of the bulk metal. The oxidation is done within a device of fused silica by means of micropyrometer-controlled h.f. induction heating. The carbon dioxide formed is quantified after absorption in 10^{-2} M sodium hydroxide by measurement of electrolytic conductivity. Calibration is done by injection of various volumes of a certified calibration gas from a gas syringe. Investigations on Si, Fe, Ni, Cu, Zr, Nb, Mo and W samples of high purity as well as of technical grade showed that the surface carbon can be determined by oxidation at 630—650° C. Its quantity depends on the kind of sample preparation chosen. Increasing the temperature to a maximum of 1500° C yields the carbon concentration of the bulk by complete combustion of the sample. Combustion additives are useful for a variety of matrices. At sample weights of $\leqslant 0.5$ g, bulk carbon concentrations of $\geqslant 0.1$ $\mu g\ g^{-1}$ can be determined.

Metals with extremely low carbon contents are not only of great importance in materials research, but also increasingly so in numerous technological materials, especially for electric and electronic applications [1, 2]. The accurate determination of carbon contents in the lower $\mu g\ g^{-1}$ and $ng\ g^{-1}$ ranges is therefore of increasing significance. For this range, activation analysis by charged particles [3—8] or photons [9—11] has been found very useful. The combustion method as commonly used in carbon determinations is not suitable for concentrations $\leqslant 1$ $\mu g\ g^{-1}$ [7, 12], although the detector systems available for the measurement of thermal conductivity [13—15], electrolytic conductivity [16, 17] and infrared absorption [18, 19] do permit the determination of nanogram amounts of separated carbon dioxide. Systematic errors possibly occurring during sample combustion and separation of carbon dioxide restrict the applicability of the method and permit determinations in the $ng\ g^{-1}$ range only with highly sophisticated modifications [15, 20].

The most prominent cause of systematic errors, which had not been taken sufficiently into account in earlier work [16], is the ubiquitous carbonaceous

0003-2670/87/$03.50

contamination layer [12, 20—25], which remains even after the most careful sample preparation. Surface carbon is determined together with bulk carbon when the commonly used combustion technique is applied, thus yielding erroneous results. Consequently, when samples with large surface-to-volume ratios (thin sheets, wires, powders) are analyzed, carbon concentration values may deviate by orders of magnitude from the true bulk concentration [12, 26]. Only activation methods have so far made it possible to distinguish between the surface and bulk carbon, when the procedure includes surface etching after irradiation of the sample.

If the expensive activation methods are to be replaced by a more economic method which can be applied in any analytical laboratory, the sample preparation step has to be an integral part of the procedure within the analytical system itself. Thereby, it must be ascertained that the sample surface is not re-contaminated between the cleaning procedure and the analytical process. Apart from sputter etching [27, 28], this is possible by oxidation of the sample by annealing in oxygen at temperatures between 500 and 900° C [12, 20]. The combination of this pretreatment with a vacuum heat extraction apparatus including mass spectrometric detection has been described for Si, Ni, Nb and Mo by Petrov et al. [20].

Treatment of metal sheets, which have undergone certain manufacturing processes, with oxygen at temperatures of $\leqslant 900°$ C for the determination of carbon and its compounds on the surface via the carbon dioxide formed, has been described before (e.g., for Ni [29], Cu [30] and steel [31—33]), and is commonly used today with commercially available instruments. Limits of detection of ca. 0.1 $\mu g\ cm^{-2}$ are usually obtained by the analysis of appropriately large areas (up to 100 cm^2). As preliminary experiments showed [12], this approach can also be applied in the analysis of high-purity metals.

It is the aim of this investigation, therefore, to combine the following analytical steps: cleaning surfaces by annealing in an oxygen flow, and determining the carbon content of the surface layer, and the carbon content in the bulk by subsequent complete combustion of the sample. The five prerequisites for application to the analysis of high-purity metals in limited amounts were: (1) independently controllable annealing and combustion temperatures; (2) low and easily controllable blank values; (3) a procedure for the separation of carbon dioxide from the sample, free from systematic error; (4) facilities for accurate calibration; and (5) a highly sensitive detection system for carbon dioxide.

High-frequency induction heating has already proved suitable for the combustion of small metal samples with low carbon contents [16]. With the aid of a pyrometer, one can control the power regulator of a frequency-adjustable h.f. generator and keep the sample temperature constant. As for the detection system, the measurement of electrolytic conductivity that had proved suitable for carbon dioxide measurement in the nanogram range [16] was utilized.

EXPERIMENTAL

Sample materials

Where available, one material with a carbon content below the detection limit and one with a favourably measurable concentration (lower $\mu g\ g^{-1}$ range), for which analytical values had already been established by other methods, were used for each metal. The following materials were used.

Silicon. (a) p-Si, 4×10^{17} atoms cm^{-3} carbon (infrared absorption), i.e., 3.5 $\mu g\ g^{-1}$ (AEG-Telefunken, Heilbronn); (b) p-Si, Czochralski-grown (Siemens, Erlangen).

Iron. (a) Very pure iron rod of 3.5-mm diameter (Johnson-Matthey); (b) a section of (a) decarbonized by annealing at 750°C (150 h) and at 840°C (16 h) in hydrogen.

Nickel. (a) Very pure nickel rod, 9-mm diameter (MRC; Material Research, München) cold-rolled to give a sheet 1.5 mm thick; (b) a section of (a) decarbonized by annealing at 1100°C and 80-Pa air pressure (7 h).

Copper. Technical grade (Hüttenwerke Kayser, Lünen).

Zirconium. Zr-800 No. 368, material from a preliminary round-robin of the BCR (Brussels) for the certification of carbon in zirconium. Carbon concentrations between 57 and 68 $\mu g\ g^{-1}$ were found in that exercise.

Niobium. (a) Nb-WCT-75 rod, 9-mm diameter (Teledyne Wah Chang, Albany, NY), cold-rolled into a sheet 1.3 mm thick, decarbonized at 2000°C and 10^{-5}—10^{-6} Pa oxygen (2 h) and subsequently annealed at 2000°C at a residual gas pressure of 10^{-8} Pa (24 h); (b) Nb-CBMM disk, cut from an electron-beam molten ingot of 140-mm diameter (Niobium Products Comp., Düsseldorf); (c) ES-Nb sheet, 1-mm thick (W. C. Heraeus, Hanau); (d) niobium wire, 1.5-mm diameter (Metallwerk Plansee, Reutte).

Molybdenum. (a) Sheet, 1.2-mm thick (Metallwerk Plansee); (b) BCR-RM No. 23, certified carbon content $\leqslant 0.2\ \mu g\ g^{-1}$ (BCR, Brussels).

Tantalum. Pieces, technical grade (Metallwerk Plansee).

Tungsten. Sheet, 1 mm thick, technical grade, analyzed in the course of an interlaboratory comparison in 1977 (Metallwerk Plansee).

Sample preparation

The metal samples were cut into a cuboid shape measuring $5 \times 5 \times (1—5)$ mm by a laboratory cut-off machine (Accutom, Struers GmbH, Erkrath). For most of the metals, silicon carbide cut-off wheels were used ($125 \times 0.5 \times 12.7$, Tyrolit 89-A-150-0.B-92; Schleifmittelges, München) at spindle speeds of 900—1000 rpm. For tungsten and silicon, diamond cut-off wheels at 600 rpm were used ($127 \times 0.3 \times 12.7$, Type 330-CA; Struers). An aqueous lubricator emulsion (cutting fluid; Struers) served as a cooling fluid during the cutting procedure. After the burr had been removed with a fine file, the samples were rinsed with water and ethanol to remove any remaining lubricant. They were then stored in glass containers until analysis.

Whenever possible, the sample preparation was started immediately before, and not exceeding 2 h before, the combustion was begun. The sample pieces

were measured with a micrometer and their surface areas calculated. For degreasing, the samples were rinsed with boiling toluene in a beaker, subsequently rinsed twice with acetone and then air-dried under dust-free conditions. For etching, acid mixtures which had been found suitable for oxygen determination [21] were mainly used. Etching conditions and etched layer thicknesses estimated from the loss in mass are listed in Table 1. After acid treatment, samples were rinsed three times with doubly-distilled water and acetone, and dried in a warm air stream under clean-bench conditions. The complete procedure was done under ultrasonic agitation.

For etching mixtures (Table 1), the following reagents were used (analytical grade; Merck, Darmstadt): 48% hydrofluoric acid, 65% nitric acid, 37% hydrochloric acid, 95—97% sulfuric acid, 96% acetic acid and 30% hydrogen peroxide. Ethanol, doubly-distilled acetone and toluene (Merck) and water doubly-distilled in a silica still were also used for sample preparation.

Combustion additives

Granulated copper and iron (Leco Instruments, Kirchheim near München) as well as molybdenum (Metallwerk Plansee) in the form of small strips, 1 mm thick, were used as additives. In some of the experiments, granular tungsten (Tungrit, Metallwerk Plansee) was used. Investigations showed that the carbon content of copper, molybdenum and tungsten was almost entirely on the sample surface (Cu, 6 $\mu g\ g^{-1}$; W, 0.9 $\mu g\ g^{-1}$) whereas the bulk carbon contents were found to be $\leqslant 0.1\ \mu g\ g^{-1}$ for these materials. Additives were cleaned by etching, in the same manner as described for the samples. The granular iron was decarbonized in a hydrogen stream at 1100° C for 2 h.

TABLE 1

Etching conditions used [21] and surface layer thicknesses removed

Metal	Etching bath		Temp. (° C)	Duration (s)	Removed layer thickness (μm)
	Composition	Ratio by volume			
Si	$HF/HNO_3/HAc$[a]	3:5:3	20	60	24—27
Fe	(1) H_2O_2/HF	14:1	20	30	
	(2) HCl	—	20	20	103—115
Ni	HAc[a]$/HNO_3/HF$	150:50:3	80	60	31—38
Cu	(1) HCl	—	20	120	
	(2) HNO_3/HAc[a]	1:1	20	30	22—29
Zr	$HNO_3/HF/H_2O$	10:1:10	20	50	11—14
Nb	$HNO_3/HF/H_2O$	2:2:1	20	60	18—25
Mo	(1) HF/HNO_3	4:1	20	10	
	(2) HCl	—	20	10	24—26
Ta	$HF/H_2SO_4/HNO_3$	2:5:2	20	20	11
W	HF/HNO_3	1:4	20	140	1.2—1.6

[a] Acetic acid.

After cleaning, the additives were stored dust-protected in ground-joint vessels of fused silica.

Apparatus

The construction of the system is shown schematically in Fig. 1 [34]. From the gas supply (1), oxygen (99.995%) or helium (99.996%; Messer Griesheim, Düsseldorf) as well as a mixture of both gases can be taken. Gas at 3 bar is purified in an assembly consisting of a stainless-steel tube (6) filled with a BTS catalyst [35] and molecular sieve 5 Å, followed by a glass tube filled with sodium hydroxide pellets (8). The stainless-steel tube can be heated with a tubular oven (7) in order to regenerate catalyst and molecular sieve. The BTS catalyst serves to catalyze the oxidation of the hydrocarbon impurities in the oxygen and helium; the molecular sieve and alkali absorb the water and carbon dioxide, respectively. Subsequently, the gas flow is divided by two bellows pressure regulators with metering valves (9); part goes directly

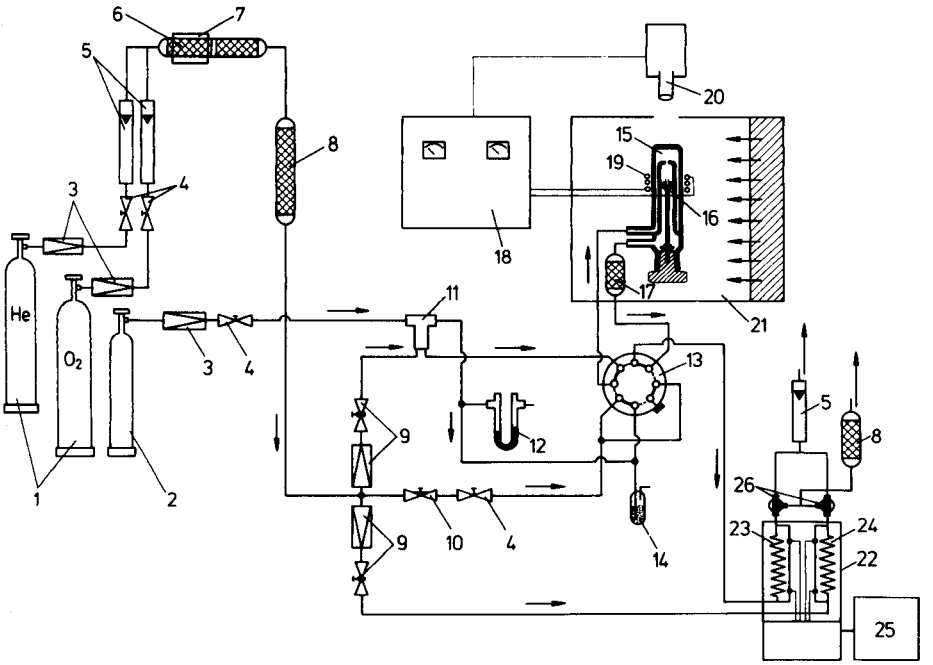

Fig. 1. The arrangement for the temperature-controlled combustion and measurement of carbon dioxide: (1) gas supply; (2) calibration gas; (3) cylinder regulator; (4) needle valve; (5) flowmeter; (6) stainless-steel tube with BTS catalyst/molecular sieve; (7) tubular oven; (8) CO_2 absorber (NaOH or soda lime); (9) low pressure-reducer with needle valve; (10) cut-off valve; (11) injection port for calibration gas; (12) pressure gauge; (13) eight-port valve; (14) bubble counter; (15) combustion chamber; (16) crucible; (17) SO_2 absorber; (18) h.f. generator, micropyrometer-controlled; (19) induction coil; (20) micropyrometer; (21) clean hood; (22) conductivity cell; (23) measuring branch; (24) reference branch; (25) recorder; (26) three-port valve.

to the reference branch (24) and part to the measuring branch (23) of the conductivity cell (22) via an 8-port valve (13) and the combustion chamber (15). In order to avoid recontamination of the cleaned gas, only transport pipes made of stainless steel or tubes made of fused silica are used. For the coupling of metal-to-metal or fused silica-to-metal tubing, Swagelok, Serto and specially designed fittings are used.

With the aid of a gas-tight injection syringe (Pressure-Lok, series A-2, Latek, Eppelheim), accurately measured volumes of calibration gas (certified content: 1005 vpm ± 2% carbon dioxide in nitrogen (Messer Griesheim) can be introduced into a specially designed injection port (11) situated in the measuring gas flow between the pressure regulator and the 8-port valve, and conducted directly to the conductivity cell or by-passing the combustion chamber (22). The upper space of the injection port (cf. Fig. 2) made of

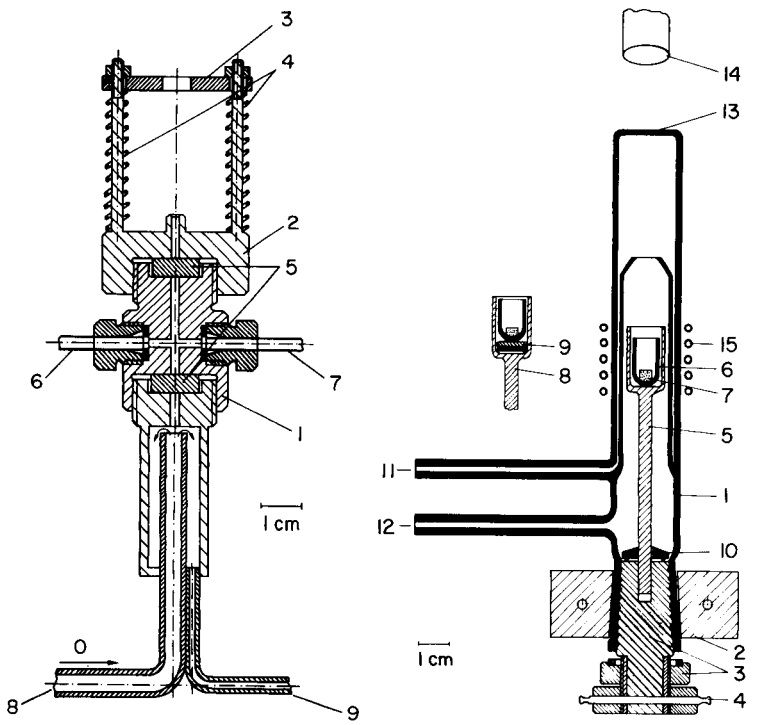

Fig. 2. Gas injection port for calibration gas dosage: (1) brass housing, nickel-plated; (2) needle guide; (3) guide plate; (4) helical springs; (5) silicone rubber septa; (6) calibration gas inlet; (7) calibration gas outlet; (8) O_2 inlet; (9) O_2 outlet.

Fig. 3. The combustion chamber: (1) encasement; (2) PVC holder; (3) PTFE stopper with detaching screw; (4) steel pin for fixing the stopper; (5) crucible holder; (6) crucible; (7) sample; (8) crucible holder with (9) Pt for better coupling to h.f. field; (10) fused silica plate; (11) gas inlet; (12) combustion gas outlet; (13) planar plate; (14) micropyrometer; (15) induction coil.

nickel-plated brass is separated by silicone rubber septa from the laboratory air and flowing oxygen. It is continuously flooded with calibration gas (excess pressure ca. 100 Pa). If the upper septum is pierced with the injection needle until the syringe body stops in position at the guide plate, the desired volume of the calibration gas can be taken up into the syringe. By pushing the needle further forward against the force of the helical springs, the lower septum is pierced and the calibration gas volume is injected into the oxygen flow passing the lower space of the injection port.

The surface oxidation and the subsequent entire combustion of the sample are effected in the combustion chamber made of fused silica (Fig. 3), positioned by an adjustable holding device in the induction coil of the h.f. furnace (4 windings made of silver-plated copper tubing, 2.4 mm external diameter). The sample is kept in a small fused silica crucible (diameter 10 mm, height 15 mm) which is held at the level of the coil by a crucible holder, so that coupling is optimum. For the combustion of very small samples or samples difficult to couple with the h.f. field, a thin platinum disk (6 mm diameter, height 1.5 mm) is placed into the crucible holder for improved coupling (8; Fig. 3). The crucible holder is fixed to a stopper made of graphite/PTFE, which is protected by a fused silica plate (10) against slag particles possibly splashing during combustion. Two metal springs fixed to the PVC holder (2) are hooked over the steel pin (4); the stopper is thus pressed into the glass joint. To loosen the usually tightly-fitted stopper, a detaching screw is provided. The gas flow passes from the top of the combustion chamber. In this way, coating of volatile metal oxides on the upper part of the chamber can be avoided. A fused silica tube filled with perhydrit (Merck, Darmstadt), which is connected at the outlet of the combustion chamber (cf. Fig. 1) absorbs sulfur dioxide from the combustion gas [36].

In order to avoid as far as possible any access of air into the system during sample exchange, the opened combustion chamber is flushed with cleaned gas from the gas inlet as are the gas combustion outlet paths. For this, a cut-off valve (10) and the 8-port valve (13; Fig. 1) are operated. Access of dust is avoided by a small "clean-bench" (SLEE, Mainz) protecting the vicinity of the combustion chamber and the work place by a laminar air flow.

The specially designed 1.5-kW h.f. generator (Type FS-1,5/16-27; Linn-Elektronik, Hirschbach) used for heating the sample is adjustable between 16—27 MHz. Its power, when adjusted to a frequency of 18—19 MHz, is controlled with a micropyrometer (Type TMRS 85-1; Dr. G. Maurer, Neuffen); the micropyrometer can be moved in vertical and horizontal directions by a brass support that is fixed to the encasement of the h.f. generator. The plane parallel disk of the combustion chamber (Fig. 3) enables the pyrometer to be aligned in the direction of the sample with a light beam justifier. At a distance of ca. 100 mm between lens and sample, the measuring spot has a diameter of 1.5 mm. The pyrometer covers a range of 630—1600°C and a useful spectral range of 0.8—1.1 μm. As most of the metals covered with an oxide layer have an emission factor of 0.7—0.9 [37], so a factor of 0.8 was generally used for temperature correction.

The measuring assembly for carbon dioxide is a highly sensitive, symmetric electrolytic conductivity cell including a specially matched 1-kHz measuring bridge developed particularly for this purpose [34]. In a commercially available measuring cell (Type G; H. Wösthoff OHG, Bochum), the original reference branch was replaced by a branch which is identical with its measuring branch and through which flows the reference gas [34]. The spiral absorption tubes and the attached measuring tubes equipped with platinized platinum electrodes were arranged in such a way that the amplifier could be integrated into the acrylic glass cylinder for thermostating. A steel wire net surrounding the acrylic housing protects the measuring assembly against interferences caused by the h.f. field of the generator. A 10-ml portion of absorption solution (0.01 M sodium hydroxide) is added by means of two proportioning pumps (Type P-40, Wösthoff) for each branch from a 5-l storage container made of polyethylene. The storage container is protected against laboratory air by a glass pipe filled with soda lime. Both branches are independently supplied with gas (80—90 ml min^{-1}). The gas flows are controlled by a flowmeter, which is connected to the gas outlets of the cell via two three-way stopcocks (cf. Fig. 1). The signal from the conductivity cell is amplified and recorded on a chart recorder (Type BD-8, Kipp & Zonen).

Procedure

For cleaning, the crucibles are treated with (1 + 1) hydrochloric acid for at least 24 h; they are then rinsed thoroughly with doubly-distilled water and dried under dust-free conditions. Prior to the combustion, the crucible is annealed at 1200—1500°C in the combustion chamber with the aid of a piece of platinum (ca. 2 g). After cooling, the platinum is removed and the appropriately prepared combustion additive (Table 2) is pre-annealed in the crucible at 650—700°C for 1—2 min. For introduction of the prepared sample, after a short cooling period the sample holder is removed, the

TABLE 2

Optimum conditions for combustion in fused silica crucibles

Metal	Additive	Sample/additive ratio (w/w)	Combustion temperature (°C)
Si	none	—	1420—1450
Fe	none	—	1350—1400
Ni	none	—	1480
Cu	Mo	Cu:Mo = 1:1	1300
Zr	Mo + Cu	Zr:Mo:Cu = 1:2:3	1450
Nb	Mo + Cu	Nb:Mo:Cu = 3:1:3	1400—1450
Mo	Cu	Mo:Cu = 1:1	1300
Ta	Mo + Cu	Ta:Mo:Cu = 5:1:3	1400
W	Cu	W:Cu = 2:1	1300

sample is placed into the crucible and the chamber is immediately closed. Sample materials which do not require additives (Table 2) are placed directly into the annealed vessel. During all manipulations, including sample preparation, storage, weighing and introduction to the crucible, strict care must be taken that the cleaned crucible as well as additives and sample are handled exclusively with clean, stainless-steel forceps, and that the crucible and the prepared sample come into contact only with cleaned fused silica containers.

The sample is heated to 630—640°C for a maximum of 2 min and the measuring signal pertaining to the carbon content of the surface is recorded. After this time, the measured value reaches a constant level. By gradual increase up to the appropriate combustion temperature required for the particular sample material (Table 2), within 0.5 min complete oxidation of the sample or of sample and additive, respectively, is achieved. The carbon dioxide corresponding to the bulk carbon is measured in this step (Fig. 4). When a constant value of the conductivity signal is achieved, commonly after a maximum of 4 min, the combustion procedure is ended by temperature reduction to 700°C and by switching off the h.f. power. The signal heights for the surface and the bulk carbon, respectively, are taken from the recorder chart and converted to the appropriate quantity of carbon via the calibration graph. The surface carbon content can then be calculated in $\mu g\ cm^{-2}$ and the bulk content in $\mu g\ g^{-1}$.

Calibration

Previous investigations have shown that instrumentation for carbon determination can be calibrated by burning of salts of organic acids (e.g., potassium hydrogenphthalate or sodium oxalate) or by injection of carbon dioxide, if experimental conditions are suitable [12, 16, 38]. With the gas-injection device used here, gas volumes in the 100 μl and ml range can be

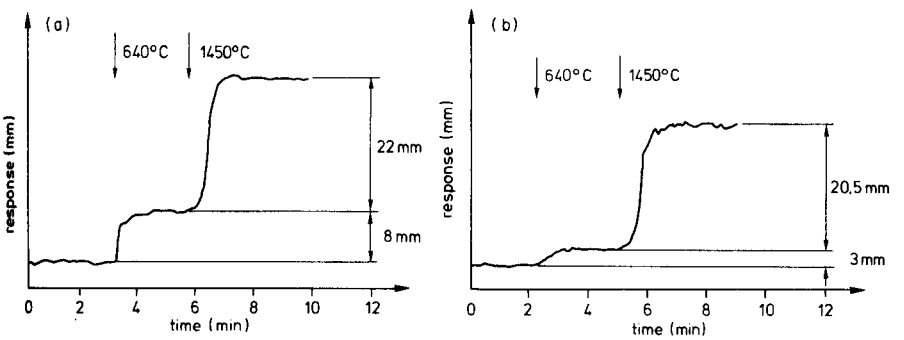

Fig. 4. Surface and bulk carbon of a degreased (a) and an etched (b) nickel sample. (Degreasing with toluene, etching conditions as in Table 1.) (a) Sample weight 327.7 mg, surface area 79.5 mm^2, surface carbon 1.09 $\mu g\ cm^{-2}$, bulk carbon 7.52 $\mu g\ g^{-1}$; (b) sample weight 306.5 mg, etched layer 33.5 μm, surface area 79.6 mm^2, surface carbon 0.35 $\mu g\ cm^{-2}$, bulk carbon 7.54 $\mu g\ g^{-1}$.

introduced reproducibly with the aid of gas-tight syringes. In the calibration gas used in this procedure, 1 ml at 1×10^5 Pa (750 torr) and 293 K corresponds to 0.495 μg of carbon. An inaccuracy in the pressure of 6.7×10^2 Pa (5 torr) would cause an error of 3.8 ng C ml^{-1} (0.78%) for the calibration gas; a temperature uncertainty of 5 K would give an error of 8 ng C ml^{-1} (1.65%). Generally, all values required for calibration can be measured with considerably better accuracy.

For any freshly prepared absorption solution, a calibration graph is established, by addition of calibration gas volumes between 0.1 and 5 ml. The graph is linear in the range 0.05—30 μg of carbon; 5 l of absorption solution is sufficient for several weeks of operation. The sensitivity of ca. 40-mm step height per μg of carbon at 50-mV full scale recording is checked daily by injections of calibration gas.

RESULTS AND DISCUSSION

Surface oxidation

Oxide layers of different thicknesses, characteristic of the metal, are formed on the sample surfaces by the annealing process at 630—640°C for the determination of surface carbon content (Table 3). These thicknesses generally amount to a few μm and are typically less than that of the layer removed by etching (Table 1). They are measured either by microscopic inspection of the metallographic specimen (Fe, Cu, Zr, Nb, Ta, W), by Auger-electron spectrometry (Si and Ni) [34] or calculated from the mass differences before and after the removal of the oxide layer, with hot ammonia for molybdenum or concentrated hydrochloric acid for copper. Figure 5 shows the oxide-layer thickness as a function of the oxidation time at 630—640°C for Ni, Cu, Nb and Mo. Only slight oxidation occurs even at relatively long annealing times for nickel and silicon, whereas for copper and niobium, the oxidation layer becomes considerably thicker. This increase is decreased, however, with increasing annealing time, because of the formation of dense

TABLE 3

Oxide-layer thicknesses after reaction for 1 min with O_2/He at 630—640°C

Metal	Oxide layer thickness (μm)	Method	Metal	Oxide layer thickness (μm)	Method
Si[a]	0.003	A.e.s.[b]	Nb	5	Metallography
Fe	8	Metallography	Mo	1—1.5	Differential weighing
Ni[a]	0.4	A.e.s.[b]	Ta	4	Metallography
Cu	4—5	Metallography	W	3—4	Metallography
Zr	1	Metallography			

[a]Oxidation in pure oxygen. [b]Auger-electron spectrometry.

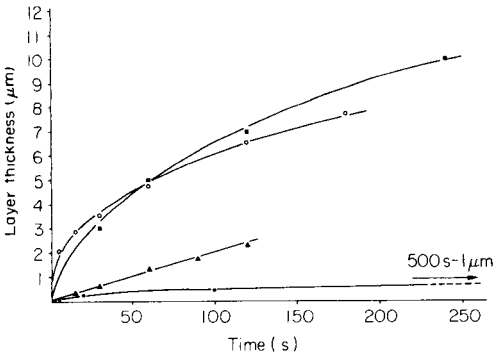

Fig. 5. Dependence of the oxide layer thickness on the oxidation time at 630—640° C: ■) niobium; (○) copper; (▲) molybdenum; (●) nickel.

ayers. On molybdenum, the oxygen always gains free access to the metal urface because of the loosely growing layer of MoO_3 crystals, so that with ufficiently long oxidation times, there is complete reaction of the sample.

Table 4 shows the progress of reaction for molybdenum and copper amples, ca. 5 × 5 × 1 mm, and 5 × 5 × 1.5 mm, respectively, during oxidaion. Thus the part of the samples oxidized during 1 min, when the surface arbon is removed, contributes only a negligible error to the final result for ts bulk content. As the storage time until the start of combustion is short, nly a very thin carbonaceous contamination layer is formed on the surface f an etched sample. A 1-min oxidation will therefore be more than sufficient o remove the surface carbon.

A further prerequisite for the separate determinations of surface and bulk arbon is that in the course of the annealing at 630—640° C, no carbon difuses from the non-oxidized bulk sample to the surface. As the diffusion oefficients at 640° C in the investigated metals (with the exception of iron) re in the range 10^{-10}—10^{-12} $cm^2\ s^{-1}$ [39], there is little danger of a decrease n the bulk concentration during surface oxidation. On the assumption that uboid samples are annealed for 1 min, the carbon transported to the sample urface by diffusion amounts to only 10^{-2}—10^{-6}% of the bulk content [34]. Even for iron at 640° C, in which carbon shows a diffusion coefficient of 3.5×10^{-7} $cm^2\ s^{-1}$, the possible loss of bulk carbon content of 0.5% can be eglected.

Combustion

The process of combustion of metal samples in a high-frequency induction urnace depends not only on the material of the sample, but also very strongly n its geometry. Powders, granules and thin sheets can be converted to the ppropriate oxide without difficulty, while compact samples oxidize on the urface only or to differing surface depths. This may lead to the screening f the sample against further attack by oxygen. The use of additives as

TABLE 4

Effect of time on the degree of oxidation at 640° C of molybdenum and copper

Oxidation time (s)	Molybdenum			Copper		
	Sample weight (mg)	Mo converted		Sample weight (mg)	Cu converted	
		(mg)	(%)		(mg)	(%)
5	—	—	—	339.2	1.4	0.4
15	252.5	0.2	0.1	311.2	1.9	0.6
30	257.2	0.4	0.2	295.3	2.3	0.8
60	258.9	0.9	0.3	307.6	3.1	1.0
90	257.5	1.2	0.5	—	—	—
120	257.2	1.5	0.6	296.8	3.6	1.2

combustion accelerators (W, Fe, Cu or CuO are used in different sample/additive ratios) guarantees complete sample combustion and quantitative release of carbon dioxide [12, 38]. Also, by using suitable additives, excessively violent combustion processes can be moderated and undesired evaporation of volatile metal oxides like MoO_3 or WO_3 can be decreased significantly [2, 34].

The oxide melts formed during combustions can in some cases produce intense reactions with the crucible material [2, 25, 34]. Crucibles made of Al_2O_3 (Degussit Al-23), $Al_2O_3 \cdot MgO$ (Degussit SP-23) and ZrO_2 (Degussit ZR-23, all from Degussa, Frankfurt) were tested for their suitability as vessel materials for combustion of Nb-Cu or Nb-Cu-Mo. It was found that the molten oxide permeated deeply into the crucible walls, often even fully penetrating them. By reaction with the partly acidic melts, carbon compounds in the vessel material can thus be converted to carbon dioxide, which cannot be removed merely by annealing. This results in increased blank values. Crucibles made of fused silica, however, showed much more suitable behaviour. Although in the combustion of Fe, Cu, Nb, W etc., reaction of the oxide melt with the silica cannot be fully avoided, such a reaction would be very slight, in the case of acidic oxides, or it can be fully suppressed by addition of suitable additives (cf. Table 2). Any blank value arising from the combustion crucible is then no longer detectable.

In Table 2, the established optimal combustion conditions for the investigated metals are listed. Nickel and silicon can be analyzed in a pure oxygen flow without additives. Full conversion to the respective oxides does not occur. For nickel, complete melting of the sample and a very rapid release of carbon dioxide takes place, but silicon merely melts slightly according to its purity, and the release of carbon dioxide proceeds slowly. Here, further investigations are necessary in order to achieve more rapid formation of carbon dioxide.

In the combustion of other metals, 10—30 vol.-% helium is mixed with the oxygen to avoid an excessively violent reaction and the resulting decrease in

pressure of the combustion system; falling pressure can cause an interruption of the gas flow through the conductivity cell.

The combination of copper and molybdenum, both of which are available with very low carbon content, proved most suitable for combustion in a fused silica crucible, because silica is not attacked by this oxide melt. Often, molybdenum can be replaced by tungsten, which is commercially available as very carbon-poor granules (Tungrit, Metallwerk Plansee) [40].

Surface carbon

The residual surface carbon on high-purity samples is listed in Table 5. It can be seen that the values for all metals are significantly decreased by etching, compared to merely degreasing with hot toluene. Often, the duration of the etching process is also of great influence as, in some cases, the carbon contamination expands to some extent into the sample bulk. Here, the production process used for the metal, such as rolling, hammering and wire-drawing, plays an important part (see also Table 7). For samples which have undergone a cleaning process in a vacuum melting apparatus or have been cleaned by etching, a short acid treatment prior to combustion is sufficient to remove the contamination layer. For optimum preparation of samples of unknown processing history, however, the etched layer thickness should not be less than 10 μm. In Table 6, the residual surface carbon layers found under the above conditions are compared to the values obtained by Quaglia et al. [21—24] by activation analysis. Good agreement was found between the results for metal samples of different origin, obtained by completely different analytical principles. This proves the general validity of the results, which can be referred to for correction of analytical values given by common instruments for carbon determination.

Determination of the bulk content

Figure 4 shows the recorder plot for the determination of the surface and bulk carbon contents of a non-etched and an etched nickel sample. The samples were degreased with toluene, and treated with an acetic/nitric/hydrofluoric acid mixture, respectively, then heated to 640° C for 2 min and to 1450° C for 3—4 min. Table 7 shows results of carbon determinations on metal samples of different grades of purity, each pretreated merely by degreasing or by additional chemical etching. In the fourth column the surface contents are shown. The sample "Nb-wire" is worthy of note, because it shows deep carbon contamination as a result of the drawing processing with drawing lubricants. Here, the surface oxidation time of 1 min seemed insufficient to fully remove the contamination layer, as was discovered by the resulting increased value compared to the etched sample. Table 7 (column 6) shows the total carbon content of the samples without differentiating between surface and bulk carbon. This apparent content is compared to the "true" bulk content. Particularly with samples of carbon content $\leqslant 1\ \mu g\ g^{-1}$, the co-determined surface carbon causes excessive errors when it is included

TABLE 5

Surface carbon content of high-purity metal samples after different treatments

Metal	Bulk content ($\mu g\ g^{-1}$)	Treatment[a]	Etching time (s)	Removed layer thickness (μm)	Surface C[b] ($\mu g\ cm^{-2}$)
Si	≤ 0.3	Degreasing	—	—	0.66 ± 0.02
		Etching	5	4	0.19 ± 0.02
		Etching	60	26	0.12 ± 0.01
Fe	≤ 0.15	Etching 1	30	118	1.10 ± 0.17
		Etching 1 + 2	30 + 10	88	0.17 ± 0.03
Ni	11	Degreasing	—	—	1.34 ± 0.34
		Etching	60	32	0.33 ± 0.07
	1.5[c]	Etching	60	30	0.33 ± 0.08
Cu	≤ 0.1	Degreasing	—	—	2.12 ± 0.10
		Etching 1 + 2	120 + 5	4	0.50 ± 0.12
		Etching 1 + 2	120 + 30	27	0.15 ± 0.02
Zr	61	Degreasing	—	—	0.95 ± 0.14
		Etching	50	12	≤ 0.25
Nb-CBMM	0.2	Degreasing	—	—	0.90 ± 0.20
		Etching	5	2	0.15 ± 0.04
		Etching	60	23	0.03 ± 0.02
Nb-TWCA	0.8	Degreasing	—	—	0.94 ± 0.12
		Etching	5	2	0.20 ± 0.01
		Etching	60	18	0.07 ± 0.01
Mo	≤ 0.15	Degreasing	—	—	1.28 ± 0.12
		Etching 1[d] + 2	45 + 20	≤ 0.1	0.61 ± 0.09
		Etching 1[e] + 2	15 + 20	0.6	0.24 ± 0.03
		Etching 1[e] + 2	10 + 20	25	0.21 ± 0.04
Ta	≤ 0.1	Degreasing	—	—	2.51 ± 0.25
		Etching	5	0.7	0.25 ± 0.05
		Etching	20	11	0.15 ± 0.02
W	≤ 0.1	Degreasing	—	—	2.52 ± 0.93
		Etching	15	0.2	0.73 ± 0.50
		Etching	140	1.3	0.12 ± 0.05

[a]Degreasing with hot toluene; for composition and temperature of etching, see Table 1. [b]Mean ± s.d. (n = 5). [c]Ni sample after annealing at 1100°C and 80 Pa for 7 h. [d]Diluted (2 + 3) with water. [e]Etching bath diluted (3 + 1) with water.

in the bulk content, as is done in common combustion procedures. In such cases, the relative excess values stated in Table 7, column 7, are several-fold high, even after optimum sample treatment. But also in the concentration range 1—10 $\mu g\ g^{-1}$, excessively high values can be found, as shown by the results on the sample "VP-Ni decarbonized".

For a check of the analytical procedure with an independent method, the samples Niobium WCT-75 (decarbonized) and CBMM as well as the molybdenum sheet were examined by instrumental activation with deuterons [8, 34] at the Instituut voor Nucleaire Wetenschappen, Rijksuniversiteit Gent.

TABLE 6

Residual surface carbon on high-purity metals after optimum sample preparation

Metal	Surface carbon ($\mu g\ cm^{-2}$)		Metal	Surface carbon ($\mu g\ cm^{-2}$)	
	Quaglia et al.	This paper		Quaglia et al.	This paper
Si	0.015—0.15	0.12—0.17	Nb	0.07	0.02—0.07
Fe	0.4—0.7[a]	0.17	Mo	0.1	0.21—0.22
Ni	0.15—0.2	0.25—0.34	Ta	0.03—0.18	0.15
Cu	0.04—0.1	0.15	W	—	0.12
Zr	0.1—0.2	$\leqslant$0.25			

[a]Treatment with concentrated hydrochloric acid.

This gave the following results for the bulk contents: Nb-WCT-75, 1.3 ± 0.3; Nb-CBMM, $\leqslant$0.12; molybdenum sheet, 0.11 $\mu g\ g^{-1}$ carbon. Taking into consideration the very low carbon contents, there is relatively good agreement with the values presented in Table 7. Thus, the procedure described, with the relatively low instrumental expense involved, can replace the activation method for numerous routine analyses of high-purity materials. Recent measurements made with a highly sensitive infrared gas analyzer (Type Binos, Leybold-Heraeus, Hanau) showed that replacing the conductivity detector by this specific carbon dioxide detector provides easier operation of the apparatus.

We thank Linn Elektronik, Hirschbach, for the construction of the specially adapted h.f. generator, and W. Werner for the development of the electronic measurement equipment. We also thank G. Kiessler for the metallographic investigations, Dr. S. Hofmann and B. Siegle for Auger-electron spectrometric measurements as well as Prof. Dr. H. M. Ortner, Metallwerk Plansee, Reutte, and Dr. K. Schulze for the supply of samples. We especially acknowledge the help of Prof. Dr. J. Hoste, Instituut voor Nucleaire Wetenschappen, Rijksuniversiteit Gent, who kindly facilitated the activation analysis, and of Dr. C. Vandecasteele and Dr. K. Strijckmans for their experimental support. Financial support by the Carl-Schneider Foundation assisting in the provision of the instrumentation is gratefully acknowledged. We also thank A. Masurowski for translating the manuscript.

TABLE 7

Results obtained with and without taking into account surface contamination

Sample	Range of sample weight (mg)	Sample treatment[a]	Surface carbon ($\mu g\ cm^{-2}$)	Bulk carbon[b] ($\mu g\ g^{-1}$)	Total content ($\mu g\ g^{-1}$)	Erroneous excess values (%)	Comparative values ($\mu g\ g^{-1}$)
Silicon							
p-Si (AEG-Telefunken)	180—260	Degreasing	0.63	2.7 (0.2; 4)	7.3	170	3.5[c]
		Etching	0.17	3.5 (1.3; 6)	3.7	—	
p-Si (Siemens)	170	Degreasing	0.66	⩽0.2 (—; 4)	2.9	⩾1350	
		Etching	0.12	⩽0.2 (—; 8)	1.1	⩾450	
Iron							
Delivery state	50—80	Etching[d]	0.92	12.1 (1.3; 4)	17.0	40	
Decarbonized	380—400	Etching[d]	1.06	⩽0.15 (—; 4)	2.4	⩾1500	
Decarbonized	390—520	Etching	0.17	⩽0.15 (—; 4)	0.4	⩾170	
Nickel							
Delivery state	200—220	Degreasing	1.34	11.0 (1.4; 4)	13.9	26	
		Etching	0.33	10.0 (1.0; 4)	10.9	9	
Decarbonized	500—530	Degreasing	0.63	1.6 (0.1; 3)	2.8	75	
		Etching	0.31	1.5 (0.14; 8)	2.3	53	
Copper	460—530	Degreasing	2.12	⩽0.1 (—; 4)	4.4	⩾4300	
		Etching	0.15	⩽0.1 (—; 4)	0.3	⩾200	
Zirconium							
Zr-800	36—38	Degreasing	0.95	60.5 (1, 3; 7)	65.6	8	53—86 [41], 65 [8]
		Etching	⩽0.25	61.4 (1, 4; 4)	62.8	—	
Niobium							
Nb wire	130—150	Degreasing	17.1	25.0 (3, 1; 7)	89.8	260	
		Etching	0.20	13.0 (0, 4; 4)	13.7	5	
Nb-ES	155—185	Degreasing	1.07	9.3 (0, 8; 4)	13.1	41	
		Etching	0.06	8.6 (0, 6; 4)	8.8	—	
Nb-WCT-75	280—310	Degreasing	0.94	0.8 (0, 44; 4)	3.6	350	
Decarbonized		Etching	⩽0.03	0.8 (0, 16; 4)	0.8	—	

Nb-CBMM	**300—330**	**Degreasing**	**0.90**	**0.4 (0, 18; 5)**	**3.6**	**800**	**2—4[e]**
		Etching	⩽0.03	0.3 (0, 16; 5)	0.3	—	
Molybdenum							
Mo sheet	360—400	Degreasing	1.28	⩽0.15 (—; 4)	3.3	⩾2100	Cf. [7]
		Etching	0.21	⩽0.15 (—; 4)	0.6	⩾300	
BCR-RM 23	240—330	Degreasing	1.24	⩽0.2 (—; 4)	4.5	⩾2200	⩽0.2[f]
		Etching	0.22	⩽0.2 (—; 4)	0.7	⩾250	
Tantalum	320—400	Degreasing	2.5	⩽0.15 (—; 4)	5.0	⩾3200	
		Etching	0.15	⩽0.15 (—; 4)	0.3	⩾100	
Tungsten	430—500	Degreasing	2.52	⩽0.1 (—; 4)	5.7	⩾5600	⩽0.015 (cf. [8, 41])
		Etching	0.12	⩽0.1 (—; 4)	0.2	⩾100	

[a]As in Table 1. [b]Mean with standard deviation and number of determinations in parentheses. [c]By i.r. absorption. [d]Etching bath only [1]. [e]Usual combustion method. [f]Certified value.

REFERENCES

1 K. Schulze, J. Metals, 33 (1981) 33.
2 H. M. Ortner, Talanta, 26 (1979) 629.
3 V. Krivan, Fresenius Z. Anal. Chem., 290 (1978) 193.
4 J. Petit, J. Gosset and Ch. Engelmann, Mem. Sci. Rev. Metall., 75 (1978) 395.
5 Ch. Engelmann, J. Radioanal. Chem., 58 (1980) 29.
6 M. L. Böttger, D. Birnstein and W. Helbig, J. Radioanal. Chem., 58 (1980) 183.
7 C. Vandecasteele, K. Strijckmans, Ch. Engelmann and H. M. Ortner, Talanta, 28 (1981) 1.
8 C. Vandecasteele, K. Strijckmans and J. Hoste, Anal. Chim. Acta, 108 (1979) 127.
9 M. Fédoroff, C. Loos-Neskovic and G. Revel, J. Radioanal. Chem., 38 (1977) 107.
10 C. Loos-Neskovic, M. Fédoroff, V. N. Samosyuk and B. A. Chapyzhnikov, Radiochem. Radioanal. Lett., 45 (1980) 185.
11 B. F. Schmitt and H.-U. Fusban, Metall, 33 (1979) 1265.
12 E. Grallath, F. Bühler, A. Meyer and G. Tölg, Erzmetall, 34 (1981) 591.
13 P. Cukor, C. Persiani and A. Russel, Talanta, 22 (1975) 571.
14 J. Ševčik, Detectors in the Gas Chromatography, Elsevier, Amsterdam, 1976.
15 V. A. Krylov, Yu. V. Revin and D. I. Pogudalov, Zh. Anal. Khim., 40 (1985) 679 (J. Anal. Chem. USSR, 40 (1985) 552).
16 P. Schoch, E. Grallath, P. Tschöpel and G. Tölg, Z. Anal. Chem., 271 (1974) 12.
17 P. Lanza and P. L. Buldini, Anal. Chim. Acta, 5 (1976) 61.
18 T. Carter and H. I. Shalgosky, Talanta, 15 (1968) 1199.
19 N. Kukla, Laborpraxis, 9 (1980) 35.
20 P. N. Petrov, Yu. A. Karpov, K. Yu. Natanson and O. V. Zav'yalov, Zavodsk. Lab., 46 (1980) 484 (Industr. Lab., 46 (1980) 517).
21 L. Quaglia, G. Weber, D. David, J. Triffaux, J. Geerts, J. van Audenhove and J. Pauwels, Surface Treatment of Non-ferrous Metals for the Purpose of Gas Analysis, BCR Information EUR 6602, Comm. Europ. Communities, Brussels 1979.
22 L. Quaglia, G. Weber, D. David, J. van Audenhove and J. Pauwels, ITE-Report No. 90 of Bureau Eurisotop, Comm. Europ. Communities, Brussels 1976.
23 L. Quaglia and G. Weber, J. Radioanal. Chem., 17 (1973) 91.
24 J. N. Barrandon, L. Quaglia, J. L. Debrun, M. Cuypers and G. Robayer, J. Radioanal. Chem., 4 (1970) 115.
25 K. Gretzinger, E. Grallath and G. Tölg, in D. Hirschfeld (Ed.), Gase in Metallen, Proceedings of the conference in Darmstadt 1984, Deutsche Gesellschaft für Metallkunde, Oberursel 1984, p. 101.
26 E. Grallath, in D. Hirschfeld (Ed.), Gase in Metallen, Proceedings of the conference in Darmstadt 1984, Deutsche Gesellschaft für Metallkunde, Oberursel 1984, p. 1.
27 R. Voigtmann, Mikrochim. Acta, 1980, I, 393.
28 J. H. Hill, C. J. Morris and J. W. Frazer, Analyst, 95 (1970) 215.
29 I. S. Solet, Anal. Chem., 38 (1966) 504.
30 J. Eisen, Erzmetall, 27 (1974) 596.
31 W. R. Lee and L. L. Lewis, Anal. Chem., 42 (1970) 103.
32 M. Kretschmer, K.-H. Koch and D. Grunenberg, Stahl und Eisen, 104 (1984) 193.
33 H. Lemm, F. Leiber, E. Voß, K.-H. Waldöfner and H. Böllert, Stahl und Eisen, 104 (1984) 141.
34 K. Gretzinger, Thesis, Stuttgart 1984.
35 M. Schütze, Angew. Chem., 70 (1958) 697.
36 W. Thomich, Gießerei-Forsch., 21 (1969) 195.
37 C. J. Smithells (Ed.), Metals Reference Book, Butterworth, London, 5th edn., 1976.
38 E. Lassner, Mikrochim. Acta, 1970, 820.
39 E. Fromm and E. Gebhardt (Eds.), Gase und Kohlenstoff in Metallen, Springer-Verlag, Berlin, 1976.
40 H. M. Ortner, H. Schedle and K. Katzengruber, Mikrochim. Acta, 1984, II, 263.
41 J. Pauwels, in Gase in Metallen, Proceedings of the conference in Darmstadt 1979, Deutsche Gesellschaft für Metallkunde, Oberursel 1979, p. 137.

Analytica Chimica Acta, 193 (1987) 19—27
Elsevier Science Publishers B.V., Amsterdam — Printed in The Netherlands

FLOW-INJECTION DETERMINATION OF AMMONIA IN KJELDAHL DIGESTS BY GAS DIFFUSION AND CONDUCTOMETRY

CELIO PASQUINI* and LOURIVAL CARDOSO DE FARIA

Instituto de Química, Universidade Estadual de Campinas, C.P. 6154, Campinas SP (Brazil)

(Received 15th July 1986)

SUMMARY

A flow injection/conductometric method is proposed for determing ammonia in solutions obtained from Kjeldahl digestion. The method is based on diffusion of ammonia through a PTFE membrane from an alkaline (NaOH/EDTA) medium to a deionized water stream. The change in conductance of the deionized water stream is proportional to the ammonia concentration present in the digest. The effects of flow parameters, temperature and potential interferences are reported. Approximately 100 samples can be injected per hour; the precision is about 1%. Results for total nitrogen in vegetable tissues, animal feeds and fertilizers are in good agreement with those obtained by the usual distillation/titration method.

The Kjeldahl digestion procedure for total nitrogen determination is widely used for food, animal feed, and fertilizer quality control as well as for other agricultural analysis. The procedure is to digest with concentrated sulfuric acid; mercury, selenium or copper is added as catalyst and potassium sulfate is added to increase the boiling point of the mixture. Under these conditions, almost all organic nitrogen compounds of biological or agricultural interest are converted to ammonia [1]. The ammonia is often quantified by distillation followed by titration or colorimetry. Direct spectrophotometric determination of ammonia in the digest is possible and is implemented in automatic analyzers like the Technicon Auto Analyzer. However, this direct determination can suffer from changes in acid concentration, presence of metal ions and sample turbidity [2]. Carlson [3] used diffusion through silicone-rubber hollow fibres to separate the ammonia from the alkaline sample digest. The ammonia diffused into a deionized water stream and the conductance of the resulting solution was measured. This method is attractive because it does not involve complex chemical reactions, and potential sources of interference in the spectrophotometric method do not affect the conductometric measurements. This method was based on a steady-state principle.

Flow injection analysis (f.i.a.) has been used with gas-diffusion membrane units [4—6] or with isothermal distillation [7] in spectrophotometric determinations of ammonia. The use of conductometric detection of ammonia,

0003-2670/87/$03.50

based on the Carlson [3] method, and its application to Kjeldahl digests, is described below.

EXPERIMENTAL

Apparatus

Conductance was measured with a Micronal B-330 conductivity meter. The output voltage was sent to a potentiometric chart recorder (ECB-RE 101). A Micronal model B-332 peristaltic pump was used with Tygon pumping tubes. Polyethylene tubes (0.8 mm i.d.) were used to construct the flow manifold. Samples were introduced by a proportional valve similar to one previously described [8]. The gas diffusion unit was similar to earlier models [5]. Each block, made of acrylic resin, had a shallow groove, 0.1 mm deep, 3 mm wide and 5 cm long. Commercial PTFE (teflon) tape was placed between the two pieces and the unit was secured with six screws.

The flow cell for conductance measurement is outlined in Fig. 1. The stainless-steel body acts as one of the electrodes; the other electrode is a stainless-steel needle (1.5 mm o.d.) that is inserted into a hole (2.2 mm diameter) bored through the body. The estimated volume of the cell is 60 μl. The cell is covered with epoxy resin to isolate it from the water bath in which it is immersed.

The final design of the flow-injection manifold for the ammonia determination in real samples is shown in Fig. 2. The donor stream is defined by the confluence of the sodium hydroxide/EDTA solution with the deionized water carrier into which the sample is introduced. The acceptor stream is deionized water that flows through a small column (a 10-ml disposable syringe) of mixed-bed ion exchanger for final purification before it enters the conductivity cell. For thermal equilibration, both streams flow through coils immersed in an insulated 8-l water bath, without temperature control, which also contains the diffusion cell and the conductance cell. The path from the outlet of the diffusion cell to the conductance cell is a 5-cm length of polyethylene tube (0.8 mm i.d.). Sample volume was fixed at 100 μl for Kjeldahl digests of leaves, fertilizers and animal feed. Sensitivity was adjusted by changing the conductivity meter control or the range of the recorder.

Reagents and standards

Sodium hydroxide solutions free of carbonate were prepared daily by dilution of ca. 12 M sodium hydroxide with boiled deionized water. The concentrations of these solutions were chosen in order to ensure excess over the acid content of samples. All the sodium hydroxide solutions used also contained 1% EDTA, to avoid precipitation of metals such as Fe, Ca, Mg and Zn usually present in the samples. For samples of plant tissues, fertilizers and animal feed, the sodium hydroxide concentrations were, respectively, 3.0, 2.0 and 3.0 M.

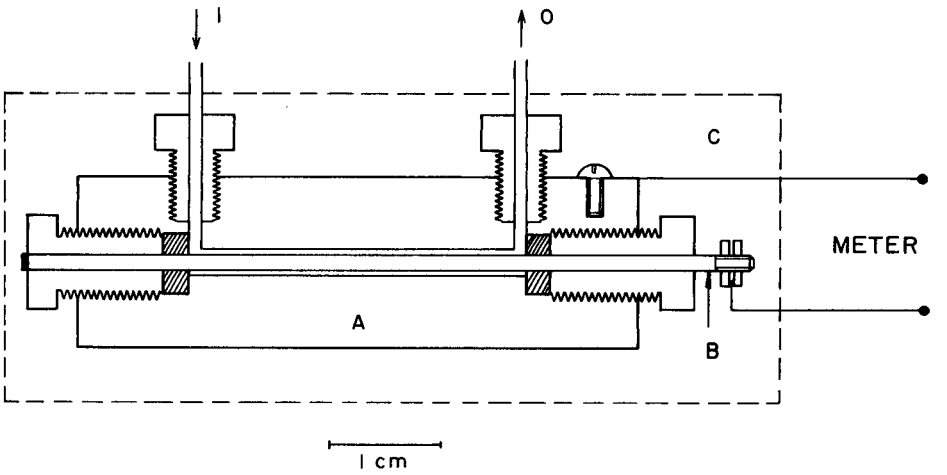

Fig. 1. Conductance flow cell: A, stainless-steel body electrode; B, stainless-steel tube electrode; C, epoxy isolation; I, inlet for fluid from diffusion cell; O, outlet for solution to waste. Nylon screws were used throughout.

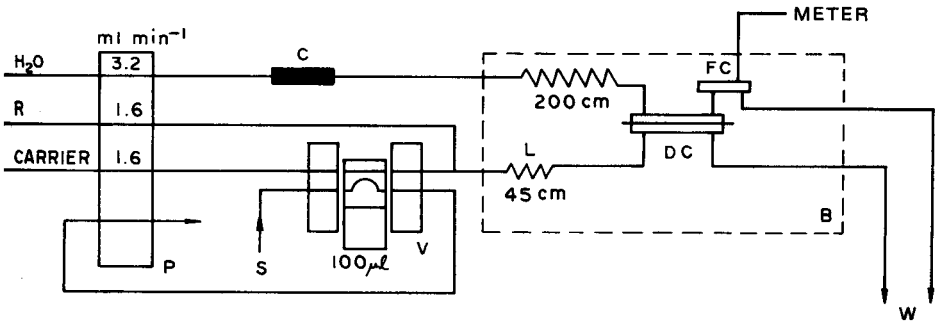

Fig. 2. Flow-injection manifold: C, mixed-bed ion-exchange resin column; P, peristaltic pump; S, sample inlet; V, sample introduction valve; L, mixing, thermal equilibration and reaction coil; B, insulated water bath; DC, ammonia diffusion cell; FC, conductance flow cell; W, waste; R, reagent stream of NaOH (3 M or 2 M)/1% EDTA solution. Carrier stream is deionized water.

Standard ammonium solutions ranging from 5 to 25 mM (for fertilizers) and 1 to 8 mM (for plant tissues and animal feed) were obtained by suitable dilution of a 100 mM stock solution prepared with analytical-grade ammonium sulfate. Standards and blanks, for plant tissue and animal feed, were prepared by matching the acid, salt and catalyst concentrations with the average composition of the sample after it had been digested. Standards for fertilizer samples were prepared by weighing an appropriate mass of ammonium sulfate and applying the same digestion procedure as for the samples.

Kjeldahl digestion procedure

For plant tissues and animal feed, 0.100 g of sample was treated with 3 m of concentrated sulfuric acid and 0.1 g of a 10:1 salt (K_2SO_4)/catalyst (HgO mixture. Digestion was done in a conventional digester block for 20—30 mi after a clear solution had been obtained. The resulting solution was dilute to 50 ml.

For fertilizers, 0.5—1.0 g of sample was treated with 10 ml of a solutio containing 50 g of salicylic acid per 1 l of concentrated sulfuric acid, followe by 0.17 g of HgO and 3.7 g of potassium sulfate. Digestion was done as des cribed above. The resulting digest was diluted to 250 ml.

RESULTS AND DISCUSSION

Various experiments were necessary to find the best flow-injection mani fold. The factors considered were the sensitivity, sample throughput, an reproducibility of the analytical signal. For these studies, the standard solu tions simulated real samples only in acid content (1.0 M sulfuric acid) an salt content (1.6 g of potassium sulfate per 100 ml); 3.0 M sodium hydroxid was used as the reagent stream. Figure 3 shows the calibration curves obtaine when the length of tube L (Fig. 2) from the confluence point to the diffusio cell was varied and when the injected sample volume was changed. Repro ducibility was the same in all cases but the sensitivity and the time necessar for the signal to return to baseline changed. More time is required to clear a large sample volume from the system, even though high sensitivity is achieved. When volumes larger than 250 μl were introduced and coil L was 45 cm long, a double peak signal was observed, i.e., the sample and reagent streams were not properly mixed. Further tests of differently arranged manifolds [4] led to the choice of a 45-cm coil length and a 100-μl sample volume. These conditions provided the required sensitivity without causing double peaks, and allowed 100 injections per hour.

The coil L also serves to provide thermal equilibration between the water bath and the sample stream. The water bath was at ambient temperature, so that equilibration started during the sample introduction. Under the conditions used, a temperature difference of 10°C between the sample prior to injection and the water bath caused no significant difference in the peak height of the signals.

When the distance from the outlet of the diffusion cell to the conductance cell was changed from 2 to 30 cm, the peak height decreased. This indicates that ionization equilibrium is reached rapidly and the contribution from physical dispersion predominates.

Flow rates were chosen in order to maintain a 1:1 relation between the donor and acceptor streams. This allows an equal pressure to be maintained on both sides of the membrane, so avoiding distortion of the membrane that can affect signal reproducibility. Lowering the flow rates of the acceptor and donor streams (while maintaining a 1:1 proportion) increased the sensitivity, but the sample injection rate was reduced. For example, when the

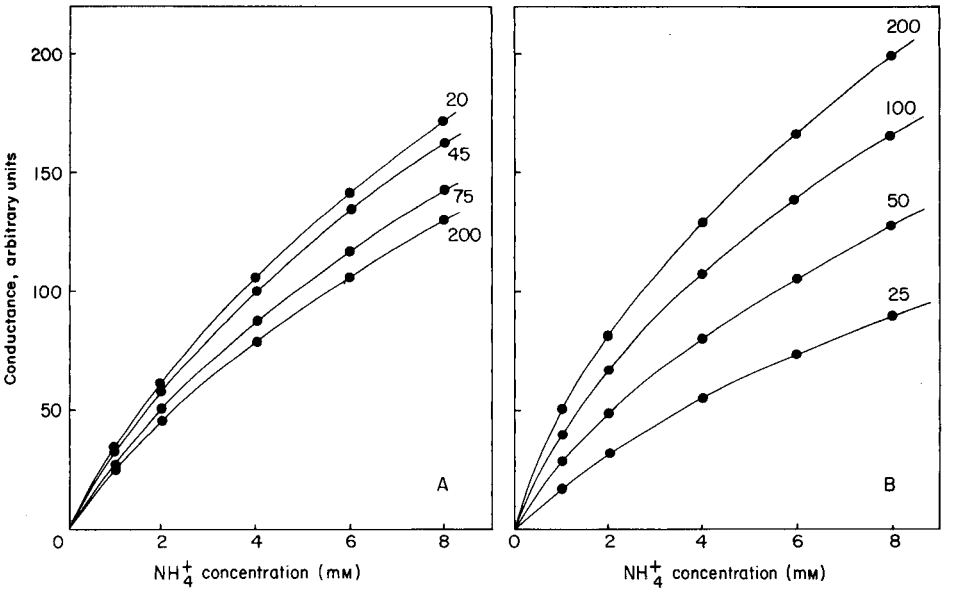

Fig. 3. Calibration curves for ammonia determination: (A) observed for varying lengths of coil L from 20 to 200 cm (sample volume 100 μl, 25° C); (B) observed for varying sample volumes from 25 to 200 μl (L = 45 cm, 27°C).

flow rates were decreased from 3.2 ml min^{-1} to 0.9 ml min^{-1}, a rise of about 80% in the signal height for a 1 mM ammonium sulfate solution was observed, but the time necessary for return of the signal to baseline increased about 300%. When the acceptor flow rate was decreased in relation to that of the donor one, sensitivity was increased. The sample injection rate was still reduced, however, although less than observed with the 1:1 flow ratios, if conditions of similar sensitivity are considered.

Figure 4 shows the effect of the water bath temperature on the signals for different concentrations of ammonium sulfate. As can be seen, there is an average increase of about 4%/°C in peak height around 25°C. Temperature control within ±0.1°C would be necessary to ensure a reproducibility better than 1%. However, the measurements are obtained very quickly, and the reproducibility can be maintained within 1% by using only an insulated water bath that changes its internal temperature very slowly. With the water bath used, signal reproducibility was within 1% over a 1-h work period. After this time, a new calibration run is recommended to account for possible temperature fluctuations.

Membrane

The membrane used in the diffusion cell was the commercial PTFE (teflon) tape which is widely available for household and plumbing purposes. Thus it does not have highly standardized chemical and physical characteristics.

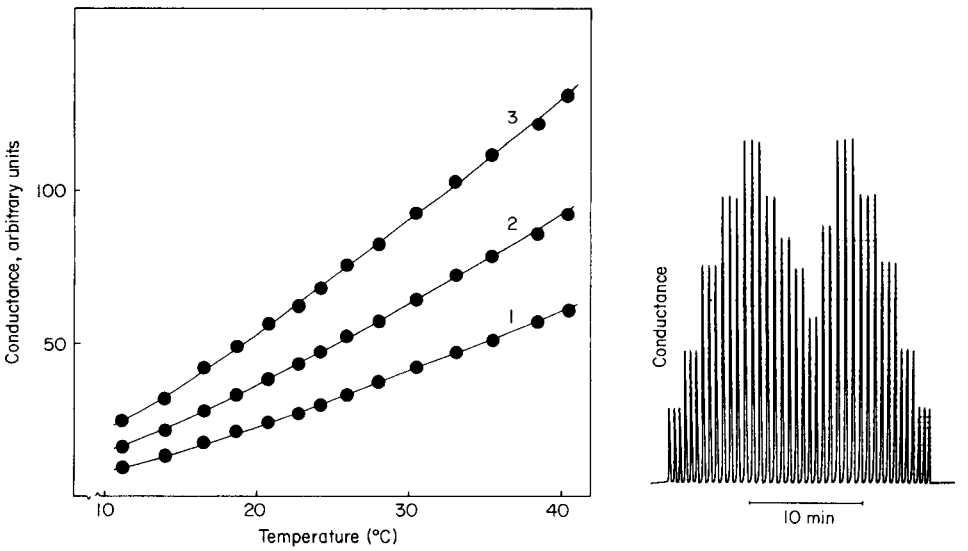

Fig. 4. Effect of water-bath temperature on signals. Data obtained with the manifold described in Fig. 2. Concentration of ammonium sulfate: (1) 2 mM; (2) 3.5 mM; (3) 6 mM.

Fig. 5. Calibration and sample runs for Kjeldahl digests. From left to right: triplicate signals for ammonium standards (1, 2, 4, 6 and 8 mM) 5 duplicate signals for vegetable tissues, and the standards in reverse order.

Variations in loading materials, polymer crystallinity and tape thickness can occur because of different production processes. Therefore, various PTFE tapes from several manufacturers were tested in the diffusion cell. All of them provided reproducible signals but sensitivity changes of ±20% were observed from manufacturer to manufacturer. Even among tapes from the same manufacturer, a ±10% change in sensitivity was observed. However, once selected, a single membrane can be used for at least a month, without drastic changes in sensitivity and reproducibility, and a roll of tape provides many membranes.

Interferences

Potential sources of error are interferences from metal-containing ions in the digests and differences in the composition of the final digests. The main source of problems was expected to be alteration of the acid content, because acid can be consumed in the digestion by different pathways depending on the sample, and production of sulfur trioxide is strongly dependent on temperature. The use of standards for each type of sample is unattractive. Tests were made in which the sulfuric acid concentration was varied from 0 to 1.75 M in standards containing 3 and 6 mM ammonium ion. The changes in response were not significant up to 1.25 M sulfuric acid and the effect can

be neglected if the standard resembles the average acid content. The effect of changing the potassium sulfate content was investigated over the range 7—30 g l^{-1} at constant acid concentration; there was no significant difference between the signals. The average acid concentration can be determined for each digestion procedure by simply titrating some samples after completing the digestion and selecting the concentration of sodium hydroxide accordingly. The addition of salt, acid and catalyst to the blank and standards avoids the effect of possible contamination deriving from the reagents. Fertilizer standards are best prepared by subjecting a pure salt such as ammonium sulfate to the digestion procedure, because a blank contribution can also come from nitrate contamination. In the presence of salicylic acid, some nitrate is converted to ammonia during digestion.

Table 1 shows the influence of some metals that can be found in Kjeldahl digests. Interferences were tested at ratios of 1:1 and 1:3 NH_4^+/interferent. With these proportions, only mercury(II) presents serious interference. For the digestion procedures described above, the final mercury concentrations of the digests are 3 mM for fertilizers and 0.9 mM for vegetable tissues and animal feeds. Detailed investigation of mercury interference showed that its effect is negligible at a level of 3 mM in a 2 or 6 mM ammonium solution. The effect of 6 mM mercury on the peak heights could be eliminated by using an alkaline 3% EDTA reagent, but the wash time increased significantly.

Calibration curves, precision and accuracy

The calibration graphs for the proposed method are not linear (Fig. 3). All calibration graphs obtained showed the same behaviour, even with

TABLE 1

Recovery of the signal in the presence of potential interferences

Species added	Recovery of signal[a] (%)			
	Without EDTA		With 1% EDTA	
	A	B	A	B
Ca(II)	100.0	100.0	100.0	100.0
Fe(III)	100.0	100.9	99.2	100.9
Al(III)	100.0	100.3	100.0	100.2
Mg(II)	102.8	100.1	100.9	100.0
Zn(II)	100.0	99.6	100.8	100.2
Cu(II)	100.2	100.2	100.1	100.0
Se(IV)	100.9	101.0	99.9	100.9
Hg(II)	70.0	73.9	99.5	98.6

[a](A) Solution 2 mM in NH_4^+ with 6 mM of the added species. (B) solution 6 mM in NH_4^+ with 6 mM of the added species. Recoveries are related to peak height in the absence of added substances.

TABLE 2

Comparative results for nitrogen by the proposed method and by the conventional method in various samples[a]

Sample	Nitrogen (%)		Sample	Nitrogen (%)	
	Usual method	Proposed method		Usual method	Proposed method
V_1	3.52 ± 0.17	3.46 ± 0.05	AF_1	2.60	2.61
V_2	1.83 ± 0.14	1.86 ± 0.01	AF_2	3.78	3.69
V_3	2.76 ± 0.17	2.65 ± 0.01	AF_3	3.45	3.59
V_4	3.18 ± 0.17	3.25 ± 0.03	AF_4	5.45	5.44
V_5	4.07 ± 0.14	4.10 ± 0.03	F_1	4.55	4.60
			F_2	3.00	3.08
			F_3	2.10	2.18
			F_4	3.64	3.63
			F_5	3.31	3.28

[a] V, Vegetable tissue (samples 1—5 are cotton, rice, orange, coffee and soy, respectively); AF, animal feed; F, fertilizer. The results for the vegetable tissues are the average of 13 interlaboratory determinations with the standard deviation found for the conventional method, and the average result with the standard deviation from 5 determinations of the same digest by the proposed method.

different manifold parameters and membranes. The ammonia concentrations in unknown samples can be evaluated by graphical interpolation with acceptable precision. Examination of the calibration data showed that the experimental points fit a curve with the equation $y = a + b\,x^c$ where y is the peak height, x the ammonia concentration, and a, b and c adjustable parameters. For twelve calibration curves in the range 1—8 mM ammonia, the mean value of the c parameter was 0.5842. This value agrees with the hypothesis that the curved nature of the calibration plots is due to ionization of the ammonia.

A typical output for standards and samples is shown in Fig. 5. Table 2 shows that the results obtained for real samples by the proposed flow injection/conductometric method are in good agreement with those obtained by the conventional distillation/titration method. There is no statistical difference between the results at the 99% confidence level. The precision of the method can be seen from the results for vegetable tissues, which are the average of five runs on the same digest and were obtained by using five calibration curves obtained on different days. The average precision was 1% in the range 1—4% nitrogen.

Overall evaluation of the proposed method

The proposed flow injection/conductometric method shows some advantages over the automatic methods already applied. The only reagent solution needed is stable, containing only sodium hydroxide and EDTA. The

equipment needed is simpler and less expensive than that required by the spectrophotometric and potentiometric methods. Interferences from solution turbidity and/or metallic species are negligible. Only one precaution was found to be necessary during six months of operation; that was periodic cleaning of the conductance cell to free it from a coating of organic material which probably originated from the ion-exchange resin column. This coating had no effect on reproducibility but could halve the sample throughput. The principal disadvantage of the method is the temperature dependence of the analytical signal but this could easily be avoided by proper thermostating.

This method is now being adapted and tested for use in determinations of low levels of ammonia in natural waters.

The authors are grateful to Micronal S.A. for providing the conductivity meter and peristaltic pump, and to O. C. Bataglia, M. M. Imai and C. H. Collins.

REFERENCES

1 F. A. Lowenheim, in F. D. Snell and L. S. Ettre (Eds.), Encyclopedia of Industrial Chemical Analysis, Wiley, New York, 1972, p. 458.
2 P. L. Searle, Analyst, 109 (1984) 549.
3 R. M. Carlson, Anal. Chem., 50 (1978) 1528.
4 J. Růžička and E. H. Hansen, Flow Injection Analysis, Wiley, New York, 1981.
5 W. E. Van der Linden, Anal. Chim. Acta, 151 (1983) 359.
6 M. Van Son, R. C. Schothorst and G. den Boef, Anal. Chim. Acta, 153 (1983) 271.
7 E. A. G. Zagatto, B. F. Reis, H. Bergamin F° and F. J. Krug, Anal. Chim Acta, 109 (1979) 45.
8 H. Bergamin F°, B. F. Reis, A. O. Jacintho and E. A. G. Zagatto, Anal. Chim. Acta, 117 (1980) 81.

Analytica Chimica Acta, 193 (1987) 29—39
Elsevier Science Publishers B.V., Amsterdam — Printed in The Netherlands

PHYSICAL, CHEMICAL AND IMMUNOLOGICAL CHARACTERISTICS OF CONTINUOUS-DENSITY LIPOPROTEINS ISOLATED BY SINGLE-SPIN GRADIENT ULTRACENTRIFUGATION

F. TALLET, R. COUDERC, G. LEFEVRE, M. P. BRUNET-COULHON, J. YONGER and D. RAICHVARG*

Laboratoire de Biochimie A, Hôpital Cochin, 27 rue du Faubourg Saint-Jacques, 75014 Paris (France)

S. LAOUSSADI

INSERM U.5, ERA CNRS no. 337, Institut de Rhumatologie, Hôpital Cochin, 27 rue du Faubourg Saint-Jacques, 75014 Paris (France)

(Received 22nd July 1986)

SUMMARY

The isolation of various lipoproteins of very low, intermediate, low and high density from 5 ml of serum was obtained by single-step ultracentrifugation in a potassium bromide density gradient obtained by smoothing a discontinuous gradient during the run (120 000g, 48 h, 4°C; Beckman SW27 rotor). The density profiles were reproducible. The lipoproteins were characterized by electron microscopy, fluorescence polarization, polyacrylamide gel electrophoresis and complete chemical assays. The composition of the entire lipoprotein spectrum was in accordance with previous results. The lipoprotein molecular mass, particle size distribution, Apo AI/AII ratio and microviscosity varied according to the density range.

Ultracentrifugation is the most widely used technique for the separation of plasma lipoproteins [1]. Techniques for separating lipoproteins which use a density gradient are the most consistent with good preservation of the lipoprotein integrity. Among these methods, the procedure described by Chapman et al. [2] seems to be very suitable. However, the sample size is limited (3 ml) and two gradients are normally required for each serum sample to provide sufficient material for subsequent examination. Moreover, one tube is lost in determining the density gradient profile and the published results do not appear to show good separation between very-low-density lipoproteins (VLDL, $0.96 < d < 1.006$ g ml^{-1}) and intermediate-density lipoproteins (IDL, $1.006 < d < 1.021$ g ml^{-1}).

In this paper, a method is described for the separation of VLDL, IDL, low-density lipoproteins (LDL, $1.021 < d < 1.063$ g ml^{-1}) and high-density lipoproteins (HDL_2, $1.063 < d < 1.125$ g ml^{-1}, HDL_3, $1.125 < d < 1.210$ g ml^{-1}) by single-step ultracentrifugation from 5 ml of serum in a SW27 swinging-bucket rotor. The force generated by this rotor plus the injection of plasma/potassium bromide mixture at the bottom of the tube were

sufficient to minimize contamination of HDL by other proteins, thus allowing a better study of the apolipoproteins. The method is shown to be suitable for elucidating the physical, chemical and immunological characteristics of lipoproteins in normal and various pathological states.

EXPERIMENTAL

Blood samples

Blood was collected in standard test tubes after 12-h fasting from 30 normolipidemic male and female subjects (20—40 years) and from patients with hyperlipoproteinemia or cholestasis. The cholesterol and triglyceride concentrations of normolipidemic subjects were 5.10 ± 0.80 and 0.95 ± 0.13 mmol l^{-1}, respectively. Ethylenediaminetetraacetic acid (EDTA) (2.7 mmol l^{-1}) and sodium azide (1.5 mmol l^{-1}) were added to the serum prior to ultracentrifugation.

Density-gradient ultracentrifugation

A Beckman model L5-65 ultracentrifuge was used throughout. Each potassium bromide solution (d = 1.126, 1.220 and 1.350 g ml^{-1}) contained 2.7 mmol l^{-1} EDTA. A discontinuous density gradient was constructed at 4°C in a 25 ×89 mm polyallomer tube (Beckman SW27 rotor, ref. 338820). With the use of a Technicon peristaltic pump, 18 ml of 2.7 mmol l^{-1} EDTA (d = 1.000 g ml^{-1}) was pumped into the bottom of the tube at 2 ml min^{-1}. The following solutions were then layered under the EDTA in the following order: 10 and 5 ml of potassium bromide solutions with densities of 1.126 and 1.220 g ml^{-1}, respectively, and 5 ml of serum adjusted to a density of 1.255 g ml^{-1}. Finally, the gradient was centrifuged at 120 000 g for 48 h at 4°C; no brake was used. The rotor content was displaced by injecting potassium bromide solution (d = 1.350 g ml^{-1}) into the bottom of the tube with a universal extracting gradient system (OSI, 75739, Paris); 35 fractions of 1.1 ml were collected with a density gradient fractionator (Gilson TGC-80). The density of each fraction was calculated from the formula: d (g ml^{-1}) = 0.0828[K^+](mol l^{-1}) + 1.00077, where the potassium concentration was determined by flame photometry with an Instrumentation Laboratories IL-343 spectrometer.

Procedures

Electron microscopy. Fractions were dialyzed exhaustively at 4°C against a 0.1 mol l^{-1} ammonium carbonate buffer adjusted to pH 7.4 with 1 mol l^{-1} acetic acid. Samples were prepared for microscopy by mixing equal volumes of solutions of lipoproteins and 2% sodium tungstophosphate (pH 7.2) in a small test tube. The final concentration of the lipoproteins in the mixture was ca. 2 g l^{-1}. One drop of this mixture was placed on a Formvar carbon-coated grid and left to stand for 45 s; excess of fluid was removed by touching the edge of the grid with filter paper [3]. Each fraction was examined

at 80 kV with a Siemens electron microscope (Elmiskop 1A) and then photographed with instrumental magnification of 40 000—120 000.

Fluorescence polarization. The fluorescence probe was 1,6-diphenyl-1,3,5-hexatriene (DPH, Sigma Chemical Co.). All solvents were glass-distilled, and all glassware was washed with chromic acid. An aqueous dispersion of the fluorophore was obtained by mixing 25 μl of DPH solution (2.6 mmol l^{-1} in tetrahydrofuran) with 5 ml of Tris-HCl buffer (0.03 mol l^{-1}, pH 8.9) [4]. Fluorescent derivatives of all lipoproteins were prepared by addition of 0.5 ml of the DPH dispersion to 1.5 ml of lipoprotein solution containing 50—150 nmol of phospholipids. Equilibrium was reached in about 40 min at 37°C. Fluorescent intensities were measured with a Jobin-Yvon JY 3D recording spectrofluorimeter with 360-nm excitation and 429-nm emission; the cell compartment was thermostatted at 25°C. The total polarized fluorescence intensity (F) was calculated from $F = I_1 + 2I_2$, and the microviscosity determination was based on the expression $\eta = [(I_1/I_2) - 1]/[0.73 - 0.27\ (I_1/I_2)]$ where I_1 and I_2 are the fluorescence intensities parallel and perpendicular to the exciting plane-polarized light, respectively [5].

Chemical assays. Total and free cholesterol, phospholipids and triglycerides were assayed by enzymatic methods with commercial kits (Boehringer, Mannheim or Wako, Osaka) [6—8]. Protein was determined by the method of Lowry with bovine serum albumin as standard [9]. The presence of up to 0.33 mol l^{-1} potassium bromide as contaminant in the lipoprotein fractions did not affect these assays. Under the conditions used, the potassium bromide concentration never exceeded 0.07 mol l^{-1}.

Immunological methods. The levels of albumin, apolipoprotein A (Apo AI + AII) and apolipoprotein B (Apo B) were measured by the electroimmunoassay technique of Laurell as described by Fujii et al. [10]. After an overnight dialysis against Tris-HCl buffer (0.03 mol l^{-1}, pH 8.9) at 4°C, immunoelectrophoresis was done in 1% (w/v) agarose in 0.065 mol l^{-1} barbital buffer (Corning, Palo Alto, CA). Total anti-human, anti-Apo A (AI + AII) or anti-Apo B sera (Behring, D-3550 Marburg) were used. Lines were stained for protein and lipids with Coomassie brilliant blue R250 and Fat red 7B (Sigma), respectively.

Lipoprotein electrophoresis. This was done by established methods with a linear polyacrylamide gradient gel (T = 2—30% and C = 2.5%, where T(%) is the weight of acrylamide + bisacrylamide (g) per 100 ml of gel and C (%) is the bisacrylamide/T ratio) [11]. The lipoprotein fractions (20 μg of protein) or 20 μl of standard protein mixture [high molecular weights (HMW) and low molecular weights (LMW) calibration kits; Pharmacia] were subjected to electrophoresis in Tris (0.09 mol l^{-1}/boric acid (0.08 mol l^{-1}) (pH 8.4) for 48 h at a constant 250 V at 4°C. Gels were stained with Coomassie brilliant blue R250 and the migration distance of each stained protein band was measured.

Apolipoprotein electrophoresis. Tetramethylurea-soluble apolipoproteins were examined by electrophoresis in 7.5% polyacrylamide gels containing

8 mol l^{-1} urea at pH 8.9, as described by Davis [12]. Gels were fixed, stained with Coomassie brilliant blue R250 and after destaining (>72 h in 10% acetic acid), scanned at 550 nm with a Cellosystem (Sebia, 92120, Issy-les-Moulineaux). The Apo AI/Apo AII ratio was calculated from measurements of the absorbance of bands after staining.

RESULTS

Preliminary experiments were done to achieve optimal separation of the lipoproteins. The calculation of density from the potassium bromide concentration was relatively simple. This method required only 10 μl of sample for each fraction and the results correlated significantly with the values measured by a digital density meter (PAAR DMA-46) (n = 140; r = 0.998). The density profiles obtained after different running times (12, 24, 36, 42 and 72 h) were examined. During the centrifugal procedure, a smoothing of the gradient was reached after 12 h and equilibrium for LDL was reached after 24 h. The variation of the density was linear from the ninth fraction to the bottom of the tube, i.e., 75% of the gradient. The density of the first fraction containing VLDL increased from 1.001 to 1.006 g ml^{-1} after centrifugation for 42—48 h. An increase in the running time (to 72 h) resulted in contamination of the first fraction by IDL (Table 1). Finally, VLDL (d = 1.006), LDL (d = 1.044), HDL_2 (d = 1.097) and HDL_3 (d = 1.127 g ml^{-1}) were simultaneously separated from each other and from the remaining plasma proteins after centrifugation for 48 h at 120 000 g. A high degree of reproducibility was found in density profiles for 30 serum samples. The relative standard deviations (r.s.d.) varied from 0.1% (first fraction) to 0.5% (30th fraction). Moreover, the profiles obtained simultaneously from a pooled serum sample were very similar (Fig. 1). These data affirm both the intra- and inter-run reproducibility of the fractionation.

Physicochemical investigations were then conducted on the lipoproteins isolated. Table 2 shows the chemical composition and mean diameters of the lipoprotein density classes. The apparent molecular mass of each HDL fraction decreased while the density showed a corresponding increase (Fig. 2). The validity of the HDL subfractionation was also confirmed by the distribution of Apo AI/AII mole ratios. In the density range between 1.075 and 1.105 g ml^{-1}, the ratio increased from 2.1 to 4.0 while the density decreased. Between 1.105 and 1.154 g ml^{-1}, this ratio was nearly constant at 1.83 ± 0.22. In the density range between 1.155 and 1.210 g ml^{-1}, this ratio increased from 1.9 to 8.9 as well as the density.

The purity of each fraction was estimated by electro-immunodiffusion and immuno-electrophoresis. The contamination of lipoproteins by albumin was negligible except for the HDL_3 fractions (d = 1.116 g ml^{-1}) in which, however, it did not exceed 1% (Table 1, Fig. 3). Electrophoresis on agarose indicated that VLDL, LDL and HDL travelled as single bands corresponding to pre-β-, β- and α-lipoproteins. Immuno-electrophoresis of each band showed

TABLE 1

Influence of ultracentrifugation time on density and albumin contamination of lipoproteins

Time (h)	Isolation density				Contamination[b] (%)
	VLDL[a]	LDL	HDL_2	HDL_3	
12	1.001	1.052	one peak	1.186	3.5
24	1.002	1.045	1.117	1.151	1.8
36	1.004	1.047	1.104	1.144	1.1
42	1.005	1.045	1.103	1.128	1.0
48	1.007	1.044	1.097	1.127	1.0
72	1.013	1.044	1.093	1.119	<1

[a]First collected fraction. [b]Albumin contamination of HDL_3 expressed as total proteins.

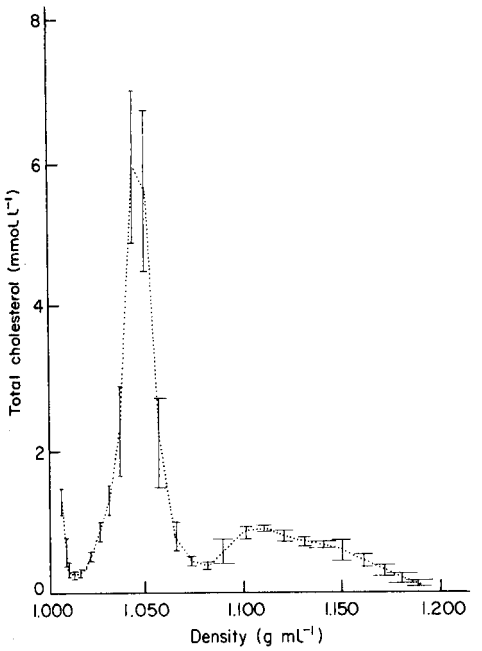

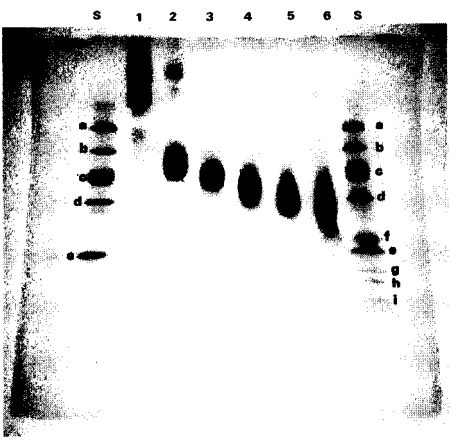

Fig. 1. Ultracentrifugation of normal pooled serum: intra-run reproducibility (n = 6). (···) Mean densities and cholesterol concentrations for each fraction. Vertical (——) and horizontal (——) bars show ±2 s.d. for the mean cholesterol and density values, respectively.

Fig. 2. HDL fractions in gradient gel electrophoresis. Lipoprotein densities (g ml^{-1}): (1) 1.071; (2) 1.089; (3) 1.108; (4) 1.127; (5) 1.148; (6) 1.170. Standards of known molecular mass: (a) thyroglobulin, 669 000; (b) ferritin, 440 000; (c) catalase, 232 000; (d) lactate dehydrogenase, 140 000; (e) albumin, 67 000; (f) phosphorylase b, 94 000; (g) ovalbumin, 43 000; (h) carbonic anhydrase, 30 000; (i) trypsin inhibitor, 20 100.

TABLE 2

Physical and chemical characteristics of isolated lipoproteins

Lipo-protein	Density (g ml^{-1})	Molecular mass[a] (D)	Molecular diameter (Å)[b]	Cholesterol		PL[c] (%)	TG[d] (%)	Protein (%)
				Free (%)	Esterified (%)			
VLDL	1.006	ND	340 ± 65	5.6	10.2	16.9	56.5	10.7
IDL	1.021	ND	250 ± 50	6.6	21.7	19.2	35.3	17.1
LDL	1.041	ND	185 ± 35	7.4	38.1	20.4	11.0	23.1
HDL_2	1.089	335 000	90 ± 15	9.4	18.3	29.2	2.8	40.3
	1.108	255 000	70 ± 15	6.8	17.1	29.1	2.5	44.5
HDL_3	1.127	185 000	60 ± 10	4.8	17.1	27.4	2.3	48.4
	1.148	135 000	45 ± 10	3.8	15.9	23.8	1.9	54.5
	1.170	128 000	40 ± 10	4.7	8.9	17.5	1.4	67.4

[a]ND, not determined. [b]Mean and standard deviation (n = 3). [c]Phospholipids. [d]Triglycerides.

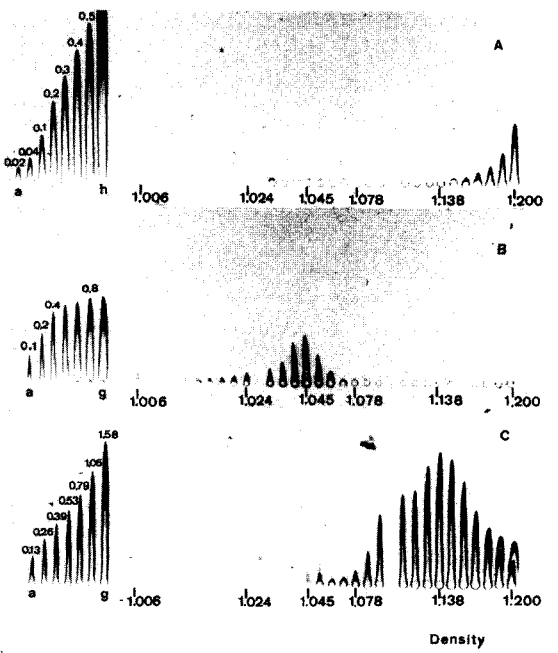

Fig. 3. Check on lipoprotein separation by electro-immunodiffusion. (A) Anti-albumin immunoserum (1.4%): (a—h) albumin standards, 0.02—0.70 g l^{-1}. (B) Anti-Apo B immunoserum (0.4%): (a—g) Apo B standards, 0.10—0.94 g l^{-1}. (C) Anti-Apo A (AI + AII) immunoserum (4%): (a—g) Apo A standards, 0.13—1.58 g l^{-1}.

neither cross-contamination nor plasma protein contamination. Only one lipid and protein-staining precipitin line was observed with an anti-human serum (Fig. 4). The Apo A and Apo B rockets confirmed good separation between LDL and HDL_2. Negligible overlap of Apo A and Apo B rockets was found between 1.045 and 1.061 g ml^{-1} (Fig. 3). The recovery of lipoprotein lipid from the gradient, estimated from the serum lipid content, was 96.9 ± 2.7% (n = 4) for the main lipids, i.e., cholesterol, triglycerides and phospholipids.

Fluorescence polarization techniques allowed certain parameters linked to the dynamic properties of lipids to be evaluated and the lipoprotein structure to be examined. The total polarization intensities measured for a constant quantity of phospholipids (50 nmol) decreased continuously from VLDL to HDL_3 (Fig. 5). These values correlated significantly with the ratio of esterified cholesterol (EC) plus triglycerides (TG) to phospholipids (PL) (n = 32; r = 0.986; $p < 0.001$). Figure 6 shows the lipoprotein microviscosity plotted as a function of density. There was a significant correlation between the microviscosity (η in poise) and the lipid-core composition of Apo B lipoproteins isolated from fractions of density 1.006–1.064 g ml^{-1}: η = 1.884 (±0.019) + 0.638 (±0.015) log EC/TG (n = 16; r = 0.996).

Finally, in order to establish if the method is suitable in all cases, 5-ml

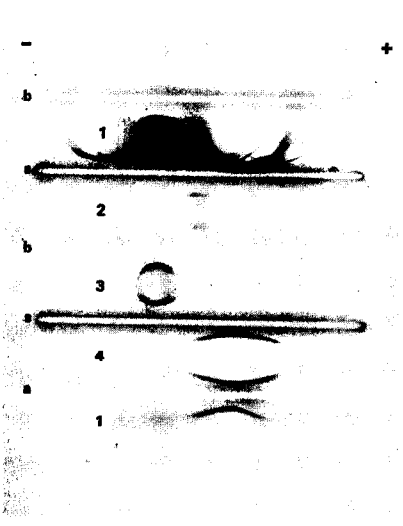

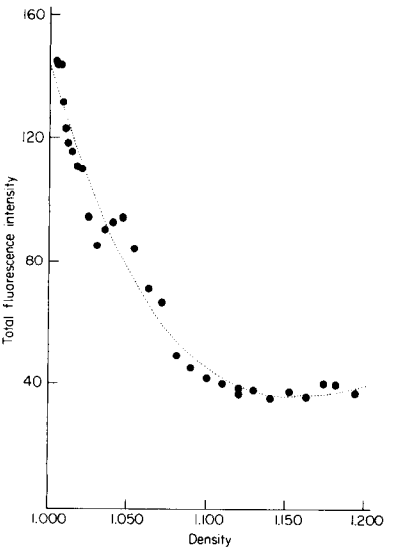

Fig. 4. Purity check of lipoproteins by immuno-electrophoresis of immunosera: (a) anti-Apo-A (AI + AII); (b) anti-Apo B; (s) anti-human serum. Samples: (1) human serum; (2) VLDL d = 1.006; (3) LDL d = 1.044; (4) HDL d = 1.116 g ml^{-1}.

Fig. 5. Variations in the total fluorescence intensity as a function of the density (g ml^{-1}) of the lipoproteins. The phospholipids and molecular probe (DPH) concentrations were constant at 33.3 and 4.3 μmol l^{-1}, respectively.

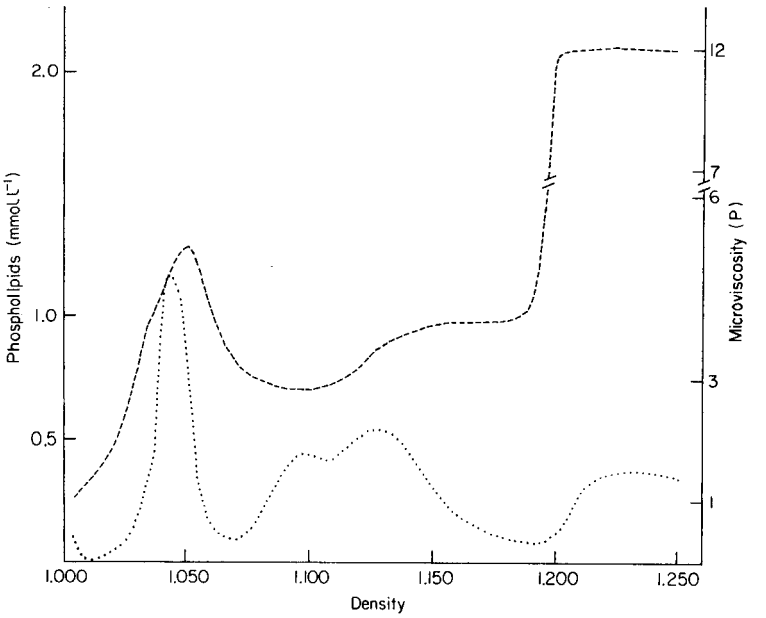

Fig. 6. Ultracentrifugation of a normal human serum. Variation of (···) phospholipids; (---) microviscosity.

samples of serum from different hyperlipemic patients were centrifuged (Fig. 7). No modification of running conditions was necessary to obtain a clear separation of the various lipoprotein density classes with total cholesterol and total triglyceride levels as high as 20 mmol l^{-1} or 15 mmol l^{-1}, respectively. The IDL was isolated with a dysbetalipoproteinemic serum (Fig. 7C).

DISCUSSION

Gradient ultracentrifugation is at present the most successful, easiest and most reliable method for obtaining highly pure, concentrated lipoprotein fractions [2, 13]. The fractionation and quantitative recovery of the major lipoprotein classes of both normo- and hyper-lipemic sera essentially free of other contaminating proteins was described above. This discontinuous density-gradient ultracentrifugation, which uses the SW27 Beckman rotor, widens the choice of rotors available for lipoprotein studies. The experimental procedure described above leads to high reproducibility in density profiles with good separation of the main lipoproteins (VLDL, LDL, HDL_2 and HDL_3).

Earlier results [14] showed that attention must be paid to the gradient constituents in order to reach a steady state. Other studies showed that sodium chloride has a stabilizing effect on proteins but causes preferential

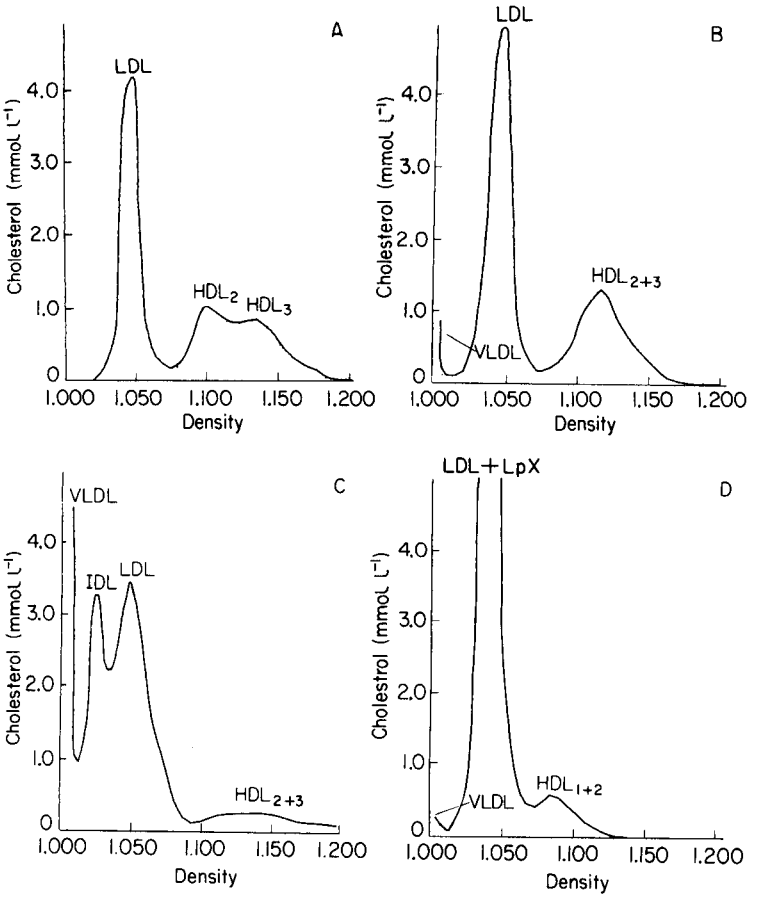

Fig. 7. Separation of lipoproteins. (A) Hyperalphalipoproteinemic serum (28-year old female, serum cholesterol 5.50 mmol l^{-1}, serum triglycerides 0.65 mmol l^{-1}); (B) hyperprebetalipoproteinemic serum, type IV (45-year old male, serum cholesterol 6.00 mmol l^{-1}, serum triglycerides 2.80 mmol l^{-1}); (C) dysbetalipoproteinemic serum, type III (35-year old male, serum cholesterol 12.30 mmol l^{-1}, serum triglycerides 11.30 mmol l^{-1}); (D) cholestatic serum (62-year old male, serum cholesterol 6.10 mmol l^{-1}, serum triglycerides 5.00 mmol l^{-1}, serum phospholipids 5.40 mmol l^{-1}, serum bilirubin 300 μmol l^{-1}).

hydration of the latter, and that sucrose is not an inert medium component [15—17]. The construction of the gradient with potassium bromide alone is rapid and simple and did not seem to alter the lipoprotein structure as judged by fluorescence polarization measurements. The microviscosity values obtained are in agreement with previous results obtained by techniques involving cumulative centrifugation [18]. Indeed, the physiological pathway between VLDL and LDL, which includes the loss of triglycerides and a relative increase in esterified cholesterol, was indicated by the linear relationship between microviscosity and the log EC/TG ratio. Thus, the microviscosity measurement can be used to detect metabolic disturbances related to structural abnormalities of lipoproteins of equal density.

The DPH probe is situated in the rigid lipid matrix, between the fatty acids of the phospholipid monolayer [5]. Given that fluorescence intensity has been found to be proportional to the phospholipid concentration [4], the present data show that both the hydrophobic core and the surface components of all the lipoprotein fractions regulate the total polarization intensity. Consequently, the total fluorescence intensity measured with constant DPH and phospholipid concentrations reflects the structure of the core indirectly.

The chemical composition of the gradient used permitted the calculation of the density by a direct potassium determination on 10-μl portions of each collected fraction. However, some procedures require a sample-free reference tube containing only the gradient solutions to establish the density profile [2, 13]. In particular, the procedure of Chapman et al. requires one tube for determination of the density-gradient profile and two sample gradients to provide sufficient quantities of lipoproteins from 6 ml of serum. Moreover, the methodologies described by Chapman et al. [2] and Foreman et al. [13] do not appear to allow adequate separation between VLDL and IDL. In contrast, the present technique is appropriate to the study of type III hyperlipidemic serum with use of a single gradient and 5 ml of serum.

With regard to HDL, electron microscopy and gradient gel electrophoresis showed a good separation of HDL_2 and HDL_3 (Table 2, Fig. 2). Furthermore, the Apo AI/Apo AII ratios found with the present single-step procedure were similar to those obtained with the two-step ultracentrifuge method of Cheung and Albers [19]. Finally, fractions with densities greater than 1.180 g ml^{-1} contained two HDL types, one of which could be considered as lipoprotein AI_2, previously described by Ayrault-Jarrier et al. (Fig. 3B) [20]. As judged by electro-immunodiffusion, there is a small quantity of Apo A in the LDL fractions (Fig. 3), this is in accordance with previous studies [21]. The presence of less than 5% of the total Apo A in the most dense fractions (>1.200 g ml^{-1}) could be explained by loss of Apo A from HDL and/or the presence of VHDL. The latter hypothesis is supported by the association of an increase in phospholipid concentration (Fig. 6) and the presence of non-polar lipids (triglycerides and esterified cholesterol) which was found in these fractions.

This relatively simple procedure, therefore, allows the study of the chemical composition and physical behaviour of the lipoprotein "spectrum" not only in normal subjects but also in patients with hyperlipoproteinemia or a cholestatic syndrome.

REFERENCES

1 F. T. Hatch and R. S. Lee, Adv. Lipid Res., 6 (1968) 1.
2 M. J. Chapman, S. Goldstein, D. Lagrange and P. M. Laplaud, J. Lipid Res., 22 (1981) 339.
3 G. M. Forte, A. V. Nichols and R. M. Glaeser, Chem. Phys. Lipids, 2 (1968) 396.
4 P. Jouanel, C. Motta, J. Delattre and B. Dastugue, Clin. Chim. Acta, 105 (1980) 173.

5 M. Shinitzky and Y. Barenholz, Biochim. Biophys. Acta, 515 (1978) 367.
6 C. C. Allain, L. S. Poon, C. S. G. Chan, W. Richmond and P. C. Fu, Clin. Chem., 20 (1974) 470.
7 M. Takayama, S. Itoh, T. Nagasaki and I. Tanimizu, Clin. Chim. Acta, 79 (1977) 93.
8 M. W. McGowan, J. D. Artiss, D. R. Strandbergh and B. Zak, Clin. Chem., 29 (1983) 538.
9 O. Lowry, N. Rosebrough, A. Farr and R. Randall, J. Biol. Chem., 193 (1951) 265.
10 S. Fujii, S. Koga, T. Shono, K. Yamamoto and H. Ibayashi, Clin. Chim. Acta, 115 (1981) 321.
11 A. V. Emes, A. L. Latner, M. Rahbani-Nobar and B. H. A. Tan, Clin. Chim. Acta, 71 (1976) 293.
12 B. J. Davis, Ann. NY Acad. Sci., 121 (1964) 404.
13 J. R. Foreman, J. B. Karlin, C. Edelstein, D. J. Juhn, A. H. Rubenstein and A. M. Scanu, J. Lipid Res., 18 (1977) 759.
14 J. R. Patsch, S. Sailer, G. Kostner, F. Sandhofer, A. Holasek and H. Braunsteiner, J. Lipid Res., 15 (1974) 356.
15 D. J. Cox and V. N. Schumaker, J. Am. Chem. Soc., 83 (1961) 2433.
16 V. N. Schumaker and D. J. Cox, J. Am. Chem. Soc., 83 (1961) 2439.
17 C. Edelstein, D. Pfaffinger and A. M. Scanu, J. Lipid Res., 25 (1984) 630.
18 A. Jonas, Biochim. Biophys. Acta, 486 (1977) 10.
19 M. C. Cheung and J. J. Albers, J. Lipid Res., 20 (1979) 200.
20 M. Ayrault-Jarrier, J. F. Alix and J. Polonovski, Biochimie, 62 (1980) 51.
21 S. Salmon, A. Van Wambeke, L. Theron, M. Ayrault-Jarrier and J. Polonovski, Biochim. Biophys. Acta, 710 (1982) 297.

Analytica Chimica Acta, 193 (1987) 41—50
Elsevier Science Publishers B.V., Amsterdam — Printed in The Netherlands

PREPARATION, ULTRAVIOLET SPECTROPHOTOMETRIC DETERMINATION, AND AQUEOUS DECOMPOSITION OF ALKYL XANTHIC ANHYDRIDES

MICHAEL H. JONES* and JAMES T. WOODCOCK

CSIRO Division of Mineral Chemistry, P.O. Box 124, Port Melbourne, Victoria 3207 (Australia)

(Received 29th July 1986)

SUMMARY

The preparation of alkyl xanthic anhydrides ($(ROCS)_2S$; dialkyl esters of thiodicarbonic acid) which are useful in flotation and in insecticide and rubber manufacture, is described. The ethyl and isopropyl homologues are crystalline solids and are readily purified. The isobutyl, sec-butyl, and n-amyl homologues, which are liquid, were found by reversed-phase liquid chromatography and u.v. spectrometry to be grossly contaminated with the corresponding dixanthogen. Ethyl xanthic anhydride can be quantitatively extracted by iso-octane or chloroform from aqueous solution. Molar absorptivities and analytical wavelengths for ethyl and isopropyl xanthic anhydrides in iso-octane and chloroform are reported. In alkaline solution, ethyl xanthic anhydride rapidly decomposes to xanthate ($ROCSS^-$) and monothiocarbonate ($ROCSO^-$); decomposition is faster at higher pH levels. In acidic solution, this compound is much more stable.

Alkyl xanthic anhydrides, $(ROCS)_2S$, were first prepared in 1877 by Welde [1] who reacted potassium ethyl xanthate with ethyl chloroformate. Subsequently, other methods of preparation were proposed which included reacting an alkyl dixanthogen with potassium cyanide [2] and reacting phosgene with potassium ethyl xanthate in toluene [3]. The compounds, currently named dialkyl esters of thiodicarbonic acid, have also been called anhydrosulphides of dialkyl dithiocarbonic acid, alkyl carbonodithioate anhydrosulphides, xanthogen monosulphides, xanthogen thioformates, xanthogen thioanhydrides, and monoxanthogen anhydrosulphides [4].

Xanthic anhydrides have been used as collectors in sulphide mineral flotation [5], as insecticides and as accelerators in rubber manufacture [6], and in stabilizing urethane rubber [7]. During the spectrophotometric analysis of liquors from industrial sulphide mineral flotation plants, broad absorption bands were observed at about 300 nm which could not be attributed to perxanthate [8], xanthyl thiosulphate [9], or dixanthogen [10] but could have been caused by a xanthic anhydride.

There was a need therefore to develop an analytical method for alkyl xanthic anhydrides in aqueous solutions to which they have been added as sulphide mineral collectors. In addition, it would be useful to establish

0003-2670/87/$03.50

whether some has been formed either as a result of the reaction between cyanide (a common sulphide mineral depressant) and dixanthogen [2] or from the decomposition of heavy metal xanthates [11]. There was also a need to understand the decomposition reactions of xanthic anhydrides in aqueous solution and the products formed.

This paper describes the preparation and purification of some alkyl xanthic anhydrides. Liquid-liquid extraction of ethyl xanthic anhydride from aqueous solution with iso-octane and chloroform is also described, and the molar absorptivities in iso-octane and chloroform are given. The decomposition rate in aqueous solution is also studied and the reaction products are identified.

EXPERIMENTAL

Preparation of alkyl xanthic anhydrides

Potassium methyl, ethyl, isopropyl, isobutyl, sec-butyl, and n-amyl xanthates were prepared by reacting the appropriate alcohol with a slurry of crushed potassium hydroxide in petroleum ether, and then slowly adding carbon disulphide ($ROH:KOH:CS_2$ = 1.1:1.1:1.0). The crude xanthates were purified by repeated dissolution in hot acetone, filtration, and precipitation from diethyl ether.

The corresponding alkyl dixanthogens were prepared by oxidation of a cooled aqueous solution of xanthate with an equimolar amount of sodium hypochlorite solution. The resultant yellow oil or solid was extracted with ether, the extract was dried over anhydrous magnesium sulphate and the ether was then evaporated under vacuum.

The alkyl xanthic anhydrides were prepared by reacting equimolar amounts of the dixanthogen in ethanol with aqueous potassium cyanide (pH 9) [2]. The resultant oil or solid was treated as described above for dixanthogen. The ethyl and isopropyl compounds, which are solid, were recrystallized from ethanol. The other compounds, which were liquids, were examined without purification.

Instrumentation and analytical procedures

Ultraviolet absorption spectra were recorded with a Hitachi Perkin-Elmer Model 330 spectrophotometer and stoppered 1-cm quartz cells, with linear wavelength and absorbance presentation.

Solutions of the alkyl xanthic anhydrides (approximately 50 mg l^{-1} in methanol/water 85:15, v/v) were examined by reversed-phase liquid chromatography. Injections were made onto a C_{18} (5-μm particle size) column (250 mm × 4.6 mm i.d.). The mobile phase was methanol/water (85:15 v/v) at a flow rate of 1 ml min^{-1} at 20°C. A Pye-Unicam SP6 single-beam detector with a 1-cm microcell was used and the chromatograms were recorded on a Rikadenki B6 recorder. Fractions absorbing at 302 or 303 nm were collected and their absorption spectra between 210 and 400 nm were recorded with a Perkin-Elmer Model 404 spectrophotometer.

Saturated aqueous solutions of ethyl xanthic anhydride at pH 1.5 or 7.3 were shaken for 2 min with equal volumes of iso-octane or chloroform and, after disengagement of the phases and filtration of the extract through a Whatman 1PS paper, the u.v. absorption spectrum was recorded. The extract from a similarly treated blank was used as reference.

The rate of dissolution of ethyl and isopropyl xanthic anhydrides in aqueous solution at pH 1.5, 7.3, 9.4, and 12.1 was measured by magnetically stirring 0.01 g of the finely crushed crystals in 50 ml of solution. The absorption spectrum of the supernatant liquor between 210 and 400 nm was recorded at intervals to measure the rate of dissolution and also the effect of pH.

RESULTS AND DISCUSSION

Preparation of alkyl xanthic anhydrides

The most convenient method for the preparation of xanthic anhydrides is the reaction between the appropriate alkyl dixanthogen and potassium cyanide in ethanolic solution described by Whitby and Greenberg [2]:

$$(ROCS_2)_2 + CN^- \rightarrow (ROCS)_2S + SCN^-$$

Other methods have been proposed which involve reaction of an alkyl xanthate with chemicals which are either difficult to obtain such as alkyl chlorothioformates [12]:

$$ROCS_2K + ClC(S)OR \rightarrow (ROCS)_2S + KCl$$

or hazardous such as phosgene [3]:

$$2ROCS_2K + COCl_2 \rightarrow (ROCS)_2S + 2KCl + COS$$

Whitby and Greenberg [2] gave no details of the yields obtained but it is unlikely that 100% yields were obtained because of the simultaneous hydrolysis of dixanthogen [10]:

$$2(ROCS_2)_2 + 6OH^- \rightarrow 2ROCS_2^- + 2ROCSO^- + H_2O_2 + S^0 + S^{2-} + 2H_2O$$

When the method of Whitby and Greenberg [2] was tested, yields of about 50% were achieved for ethyl and isopropyl xanthic anhydrides which is similar to the 57% yield obtained for ethyl xanthic anhydride prepared from potassium ethyl xanthate and ethyl chloroformate [13] but was less than the 80—85.8% yield of methyl xanthic anhydride prepared from phosgene and methyl xanthate [14].

Several attempts were made to prepare the crystalline methyl derivative (m.p. 54.5—56°C [6, 12, 14]) but in this work a yellow oil was always obtained. In some attempts, the pH of the potassium cyanide solution was reduced to about 7 before reaction but no crystalline product was obtained. The purity of the methyl dixanthogen used in the preparation was not evaluated by elemental analysis, but the u.v. absorption spectrum in ethanol had absorption maxima and molar absorptivities close to literature values [15].

Furthermore, the absorption spectrum of the product in ethanol was not greatly different from that of methyl dixanthogen, indicating that little reaction had taken place.

With ethyl and isopropyl dixanthogens, yellow crystalline products were obtained which were readily purified by recrystallization from ethanol. Table 1 gives details of melting points and elemental data.

The isobutyl, sec-butyl, and n-amyl xanthic anhydride products were red-yellow or orange oils which could not be crystallized by ice/salt mixtures. Elemental data for the liquid products were not obtained because it was believed that they contained unreacted dixanthogen (see below).

Liquid chromatography of the reaction products of alkyl dixanthogen and potassium cyanide

The difficulty experienced with the preparation of methyl xanthic anhydride as well as the shape of the u.v. absorption spectrum of the product suggested that a similar incomplete reaction might occur with other dixanthogens where a water-insoluble oil was a product.

Figure 1 shows the liquid chromatograms obtained for the five alkyl xanthic anhydrides prepared. With ethyl or isopropyl xanthic anhydride, there was only one major component, but there were at least two components in the isobutyl, sec-butyl, and n-amyl xanthic anhydrides (which are liquid). Good separation of the two major components of the sec-butyl product was achieved but there was a slight overlap with the isobutyl product and an even greater overlap with the n-amyl product.

The u.v. absorption spectra of the two major fractions showed that with the liquid xanthic anhydrides, unreacted dixanthogen was still present.

Ethyl and isopropyl xanthic anhydrides were found to decompose very slowly in methanol/water mixtures to yield a small amount of the corresponding dixanthogen as shown by the appearance of a small second peak on the chromatogram of solution samples which were 5 days old. Because all the chromatograms in Fig. 1 were obtained immediately after dissolution in methanol/water, the dixanthogen detected in the three liquid products is considered to be unreacted dixanthogen rather than any formed by decomposition.

Although elemental data are often quoted as a measure of purity, a single element determination is of little use in discriminating between compounds of similar composition. For example, the n-hexyl xanthic anhydride "obtained in almost quantitative yield" by Cambron and Whitby [16] could have contained as much as 10.3% of n-hexyl dixanthogen on the basis of the quoted sulphur result (30.5% found, 29.8% calculated). Lack of product purity was also deduced from the λ_{max} and log ϵ values quoted for dibutyl dixanthogen and dibutyl xanthogen monosulphide [15]. The values for both compounds are sufficiently similar to suggest substantial contamination of the monosulphide with dixanthogen.

TABLE 1

Melting point and elemental data for ethyl and isopropyl xanthic anhydride

	Ethyl	Isopropyl
M.p. (° C) this work	52.5	54—55
literature values	55 [1], 52 [2], 52—53 [12], 53—54 [14]	54 [2], 55 [6]
Carbon (%) found[a]	34.4 (34.3)	40.8 (40.3)
Hydrogen (%) found[a]	4.85 (4.8)	5.8 (5.9)
Sulphur (%) found[a]	46.0 (45.7)	40.1 (40.35)

[a]Theoretical values are given in parentheses.

Spectrophotometric determination of xanthic anhydrides

Analytical wavelengths and molar absorptivities. The absorption spectrum of a 20 mg l^{-1} solution of ethyl xanthic anhydride in iso-octane is shown in Fig. 2. The absorption spectra of ethyl xanthic anhydride in chloroform and of isopropyl xanthic anhydride in iso-octane and chloroform were very similar to that shown in Fig. 2. Analytical wavelengths for ethyl and isopropyl xanthic anhydride in iso-octane and chloroform were determined and are given in Table 2. The molar absorptivities of both compounds in both solvents were calculated from a regression analysis of 21 pairs of values from three separate calibration runs and are also given in Table 2.

The small difference in λ_{max} between the two compounds is real and was confirmed by examination of the u.v. absorption spectrum of fractions collected during chromatography with methanol/water. A similar variation in λ_{max} was observed with alkyl dixanthogens [17]. The molar absorptivities listed in Table 2 were used to calculate the following equations, which relate the concentration of the alkyl xanthic anhydride to the absorbance in chloroform or iso-octane:

$$C_{EXA}\,(CHCl_3) = 11.5A_{305};\ C_{EXA}\,(\text{iso-octane}) = 33.4A_{247} = 11.7A_{303};$$

$$C_{IPXA}\,(CHCl_3) = 34.3A_{254} = 13.2A_{306};\ C_{IPXA}\,(\text{iso-octane}) = 36.3A_{251} = 13.2A_{305}$$

where C_{EXA} in chloroform and C_{IPXA} in iso-octane etc., are the concentrations (mg l^{-1}) of ethyl xanthic anhydride (EXA) and isopropyl xanthic anhydride (IPXA) in the specified solvent and A_{305}, etc. are the absorbances at 305 nm, etc., in a 1-cm cell.

The ratio of the absorbances at the two analytical wavelengths (about 2.8:1) can be used as an approximate check of the purity or for establishing the presence of u.v.-absorbing impurities. A value of 2.7 was obtained for the ratio of the molar absorptivities at 302 and 249 nm of ethyl xanthic anhydride in ethanol [13].

Liquid-liquid extraction from aqueous solution. Ethyl xanthic anhydride was found to be readily extracted from the filtrate from an aqueous suspension

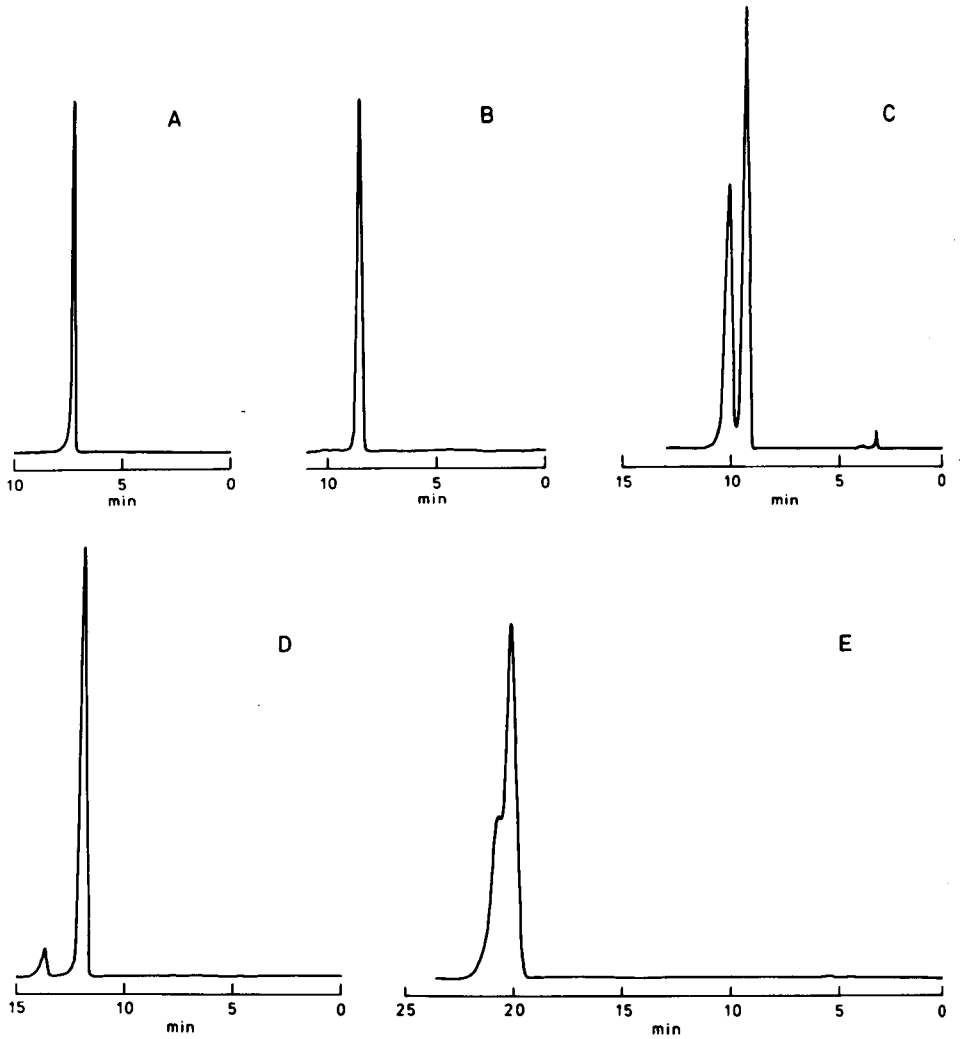

Fig. 1. Liquid chromatograms of alkyl xanthic anhydrides with detection at 303 nm (mobile phase 85:15 methanol/water): (A) ethyl; (B) isopropyl; (C) isobutyl; (D) sec-butyl; (E) n-amyl.

(prepared at pH 1.5 or 7.3) by shaking with either iso-octane or chloroform for 2 min. Examination of the u.v. absorption spectrum of the raffinate from an extraction using either extractant, at 1:1 phase ratio, showed that extraction was virtually quantitative. The absorbance of the raffinate at 300 nm ranged from <0.0005 to 0.004 indicating an extraction of $>99\%$ for iso-octane and $>98\%$ for chloroform.

At more alkaline pH levels the xanthic anhydride is decomposed, as shown earlier. Obviously in alkaline solutions, measurements should be made as soon

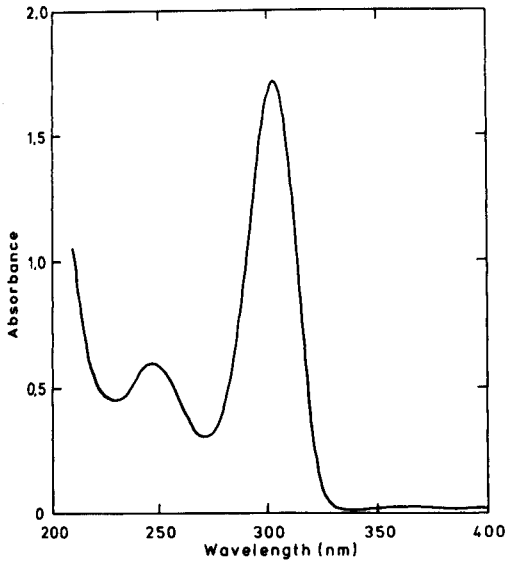

Fig. 2. Ultraviolet absorption spectrum (1-cm cell) of 20 mg l^{-1} ethyl xanthic anhydride in iso-octane.

TABLE 2

Analytical wavelengths and molar absorptivities of ethyl and isopropyl xanthic anhydride

	In chloroform		In iso-octane	
	λ_{max} (nm)	ϵ^a (l mol^{-1} cm^{-1})	λ_{max} (nm)	ϵ^a (l mol^{-1} cm^{-1})
Ethyl xanthic anhydride	n.d.	n.d.	247	6290 ± 60
	305	18 360 ± 60	303	18 010 ± 70
Isopropyl xanthic anhydride	254	6950 ± 90	251	6570 ± 70
	306	18 110 ± 240	305	18 120 ± 140

[a]95% confidence limits. n.d., not determined (too close to u.v. cutoff of chloroform).

as practicable after sampling. Alternatively, the pH could be adjusted to less than 7 if storage before analysis is required.

The extraction would provide the basis of an analytical method for flotation liquors.

Interferences. Similar non-polar compounds such as dixanthogen would also be extracted by organic solvents such as iso-octane or chloroform [17] and would therefore interfere. In such cases, the u.v. absorption spectrum of the organic extract should be examined between 210 and 400 nm for iso-octane or 250 and 400 nm for chloroform. As discussed earlier, the ratio of the absorbances of about 302 and 250 nm (2.8:1) and also the presence of

absorption minima at 230 and 274 nm (in iso-octane) can serve as an invaluable guide to the presence of other u.v.-absorbing species. In a solution of unknown composition, iso-octane would be the preferred extractant because absorbances can be measured down to 210 nm.

Perxanthic acid also interferes because the u.v. absorption spectrum in chloroform is very similar to that of ethyl xanthic anhydride with an absorption maximum at about 302 nm and an absorption minimum at about 265 nm [18]. In iso-octane, however, the absorption maximum at 233 nm can be used to determine whether any perxanthic acid is present [8].

Solubility and decomposition in aqueous solution

It was found that the xanthic anhydrides were reasonably stable in acidic solution but decomposed in alkaline solution. The solubility could therefore only be measured in acidic solution. The decomposition of ethyl xanthic anhydride was studied in alkaline solution.

Solubility. The changes in the u.v. absorption spectrum of the filtrate from a suspension of ethyl xanthic anhydride in aqueous solutions of pH 1.5, 7.3, 9.4, and 12.1 as a function of time are shown in Fig. 3. At pH 1.5 and 7.3 (Fig. 3A and B), the solid slowly dissolved and there was a gradual increase in the absorbance with absorption maxima appearing at about 250 and 300 nm. The ratio of the absorbances at these wavelengths remained approximately constant, indicating that little or no decomposition had taken place. The amount of isopropyl xanthic anhydride dissolved at pH 1.5, as measured by the absorbance at 300 nm, was much less. Longer contact times might have dissolved more of each compound but could also have resulted in decomposition. Similar behaviour was observed with dixanthogens in acidic and neutral solution [10].

From the similar molar absorptivities in iso-octane and chloroform, and the likelihood that the values in aqueous solution would be similar, it was considered not unreasonable to assume an apparent molar absorptivity of 18 000 $l\ mol^{-1}\ cm^{-1}$ at 300 nm in water. This value was then used to estimate the solubility at 20°C at pH 1.5 and at 7.3. The values were estimated to be about 1.5 mg l^{-1} for ethyl xanthic anhydride and about 0.4 mg l^{-1} for isopropyl xanthic anhydride (7.2×10^{-6} and 1.7×10^{-6} mol l^{-1}, respectively).

Decomposition. Decomposition studies were concentrated on the ethyl homologue because of its greater solubility. At pH 9.4 and 12.1, ethyl xanthic anhydride appeared to dissolve much more rapidly (as measured by the increase in absorbance at 300 nm, Fig. 3C and D). This was not the case, however, because there was no corresponding increase in the absorbance at 250 nm. Instead, a new absorption maximum was found at about 224 nm, indicating that the ethyl xanthic anhydride was decomposing as well as dissolving. Welde [1], by qualitative and quantitative tests, showed that hydroxide decomposed xanthic anhydride to xanthate and monothiocarbonate:

$$(ROCS)_2S + 2OH^- \rightarrow ROCS_2^- + ROCSO^- + H_2O$$

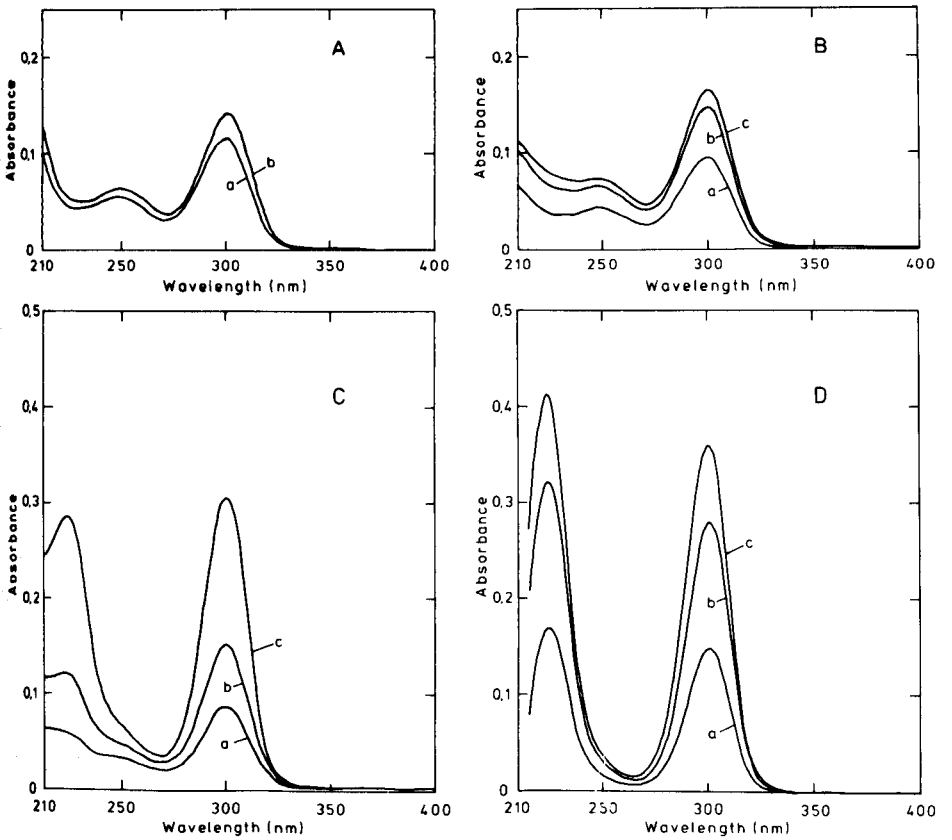

Fig. 3. Ultraviolet absorption spectra (1-cm cell) of filtrate from a suspension of 0.01 g of ethyl xanthic anhydride in 50 ml of aqueous solution, after reaction at different pH values for different times. (A) pH 1.5 (1% HCl):(a) 120 min; (b) 180 min. (B) pH 7.3 (phosphate buffer):(a) 60 min; (b) 120 min; (c) 180 min. (C) pH 9.4 (0.05 M borax):(a) 30 min; (b) 60 min; (c) 120 min. (D) pH 12.1 (0.01 M NaOH):(a) 60 min; (b) 100 min; (c) 120 min.

The decomposition products, at pH 12.1, were confirmed by calculating the xanthate and monothiocarbonate concentrations from the molar absorptivities for xanthate of 17 660 l mol^{-1} cm^{-1} at 301 nm and 9060 l mol^{-1} cm^{-1} at 226 nm [19], and for monothiocarbonate of 10 300 l mol^{-1} cm^{-1} at 222 nm [20]. Approximately equimolar concentrations of ethyl xanthate and ethyl monothiocarbonate were produced by hydrolysis at pH 12.1 (the actual values ranged from 1.06 to 1.10 mol of monothiocarbonate per mole of xanthate). At pH 9.4 the decomposition was much slower and much less monothiocarbonate (MTC) appeared to be formed. Calculated values ranged from about 0.3 mol of MTC per mole of xanthate at the beginning of the test to 0.6 mol of MTC per mole of xanthate after agitation for 2 h. The formation of less MTC than that expected from the above equation was attributed to the lower stability of MTC in the less alkaline solution [10].

At both pH 9.4 and 12.1, although reasonable stoichiometries could be calculated, at least one secondary reaction was taking place. A small amount of perxanthate (as shown by the appearance of an absorption maximum at 348 nm [8]) was observed in both test solutions when they were allowed to stand overnight. The mechanism by which the perxanthate was formed is uncertain. In 95% ethanol solution, ethyl xanthate and ethyl xanthic anhydride slowly form *O*-ethyl *S*-ethyl xanthate ($C_2H_5OCS_2 \cdot C_2H_5$) [21], which has absorption maxima at 221 and 278 nm in cyclohexane; the molar absorptivities at these wavelengths are 8780 and 13 200 l mol^{-1} cm^{-1}, respectively [22]. No evidence was found for the formation of this compound in any of the aqueous systems examined here.

The solubility and decomposition behaviour of ethyl xanthic anhydride in aqueous solution is very similar to that of ethyl dixanthogen [10, 23].

The authors thank Dr I. C. Hamilton of Footscray Institute of Technology for the use of the liquid chromatograph.

REFERENCES

1 H. Welde, J. Prakt. Chem., 15 (1877) 42.
2 G. S. Whitby and H. Greenberg, Trans. R. Soc. Can., Sect. 3, 23 (1929) 21.
3 A. H. Fischer, Brit. Pat. 284 198, Jan. 24 (1927) 3 pp. (Chem. Abstr., 22 (1928) 4449.)
4 CHEMNAME, file 301, in DIALOG Database Catalog, DIALOG Information Services, Palo Alto, CA, 1985, p. 15.
5 D. Guggenheim, M. Guggenheim, S. R. Guggenheim, S. Guggenheim, J. K. MacGowan and E. A. C. Smith, Brit. Pat. 275 563, Apr. 29 (1927) 3 pp. (Chem. Abstr., 22 (1928) 2136.)
6 E. E. Reid, Organic Chemistry of Bivalent Sulfur, Vol. IV, Chemical Publishing, New York, 1962, p. 150.
7 K. Kobayashi and S. Fujita, Jpn. Kokai Tokkyo Koho 78 120 763, Oct. 21 (1978) 4 pp. (Chem. Abstr., 90 (1979) 88582h.)
8 M. H. Jones and J. T. Woodcock, Int. J. Miner. Process., 5 (1978) 285.
9 M. H. Jones and J. T. Woodcock, Int. J. Miner. Process., 8 (1981) 125.
10 M. H. Jones and J. T. Woodcock, Int. J. Miner. Process., 10 (1983) 1.
11 I. A. Kakovskii, Obogashch. Rud (Leningrad), 24(2) (1979) 8 (Chem. Abstr., 92 (1980) 132513d).
12 S. M. Gurvich, R. I. Moiseeva, I. V. Sarychev and I. B. Zalesnik, Zh. Prikl. Khim., 40(8) (1967) 1858.
13 G. Barany, B. W. Fulpius and T. P. King, J. Org. Chem., 43 (14) (1978) 2930.
14 S. V. Zhuravlev and M. I. Galchenko, Zh. Prikl. Khim., 20 (1947) 1038.
15 M. L. Shankaranarayana and C. C. Patel, Acta Chem. Scand., 19 (5) (1965) 1113.
16 A. Cambron and G. S. Whitby, Can. J. Res., 2 (1930) 144.
17 M. H. Jones and J. T. Woodcock, Anal. Chem., 58 (1986) 588.
18 M. H. Jones and J. T. Woodcock, Talanta, 26 (1979) 815.
19 J. Garbacik, J. Najbar and A. Pomianowski, Rocz. Chem., 46 (1972) 85.
20 C. N. Murphy and G. Winter, Aust. J. Chem., 26 (1973) 755.
21 E. A. Castro, B. Meneses, J. G. Santos and J. C. Vega, J. Org. Chem., 50 (1985) 1863.
22 M. J. Janssen, Recl. Trav. Chim. Pays-Bas, 79 (1960) 464.
23 I. C. Hamilton and R. Woods, Aust. J. Chem., 32 (1979) 2171.

Analytica Chimica Acta, 193 (1987) 51—60
Elsevier Science Publishers B.V., Amsterdam — Printed in The Netherlands

INTEGRATED SCHEME FOR MICRO-DETERMINATION OF IRON OXIDATION STATES IN SILICATES AND REFRACTORY MINERALS

E. KISS

Research School of Earth Sciences, The Australian National University, G.P.O. Box 4, Canberra, A.C.T., 2600 (Australia)

(Received 29th September 1986)

SUMMARY

A micro-analytical scheme incorporating four methods is described for the determination of iron(II) and iron(III) in both hydrofluoric acid-soluble and refractory minerals. The acid-soluble minerals are analyzed for FeO by direct constant-current potentiometric titration with potassium dichromate, and a separate solution is titrated similarly after Zn/Hg reduction to give total iron. The micro-determination of FeO in chromite and other refractory minerals involves dissolution in a cerium(IV)/phosphoric acid mixture and constant-current potentiometric and indirect titration of excess of cerium(IV) (phosphatocerate) with iron(II). Lithium tetraborate micro-fusion is required for measurement of total iron by atomic absorption spectrometry or spectrophotometry. The average relative standard deviation ranged between 0.73 and 1.08%.

The oxygen fugacity of the earth's upper mantle, and also some meteorites, can be estimated by applying the reaction to the widespread assemblage olivine + orthopyroxene + spinel:

$$3Fe_2SiO_3 + O_2 \rightarrow 2Fe_3O_4 + 3SiO_2$$

In order to do this, the activity of Fe_3O_4 in naturally occurring, complex Mg-Fe(II)-Al-Cr-Fe(III) spinels must be known. There are now methods available to relate oxygen fugacity to the mole fractions of the various components in these complex spinel solid solutions, and so the problem essentially reduces to that of finding the Fe(II) and Fe(III) content of the spinels. Total iron can be measured by an electron microprobe, and while it is possible to obtain estimates of Fe(II)/Fe(III) from these microprobe analyses by assuming stoichiometry, the results are uncertain because of the low Fe(III) contents which are typical of the spinels of interest. It has also been argued that there is sufficient non-stoichiometry in these spinels to invalidate the method. Thus a direct and independent measurement of the Fe(II)/Fe(III) ratio is important.

The accurate determination of iron(II) (and hence the oxidation state) in very small quantities of minerals (often hand-picked single crystals) by micro-analytical techniques has been both a considerable problem and an important requirement in analytical geochemistry for many years. This circumstance is

0003-2670/87/$03.50

further complicated by some minerals exhibiting extreme resistance towards acid attack and requiring vigorous dissolution (or fusion) conditions. The original oxidation state of iron in the crystal lattice can be irreversibly disturbed by such a dissolution method, thus erasing some essential redox signatures. Methods for micro-scale determination of FeO have been widely used by geoanalytical laboratories; almost all of these depend upon hydrofluoric/sulphuric acid digestion of sample for the spectrophotometric measurement of the iron(II) chelate formed. Riley and Williams [1] described a micro-analytical procedure using a sealed teflon bomb; oxidation was prevented by a very small headspace of acid vapour generated, and spectrophotometric measurement of the α,α'-bipyridine chelate formed ensured good precision. Kiss [2] eliminated aerial oxidation by the in situ chelation of the liberated Fe(II) ions using a highly sensitive ferroin-type reagent added to the mixed acids. In a later paper [3], he described another reagent with an even higher acid tolerance (ensuring rapid chelation in strong acids) which also permitted shorter digestion times. Although these procedures were effective in the decomposition of more resistant silicates, they were limited to minerals soluble in hydrofluoric acid.

Refractory minerals (staurolite, spinels and aluminosilicates) are extremely resistant to acid attack and sample fusion in an inert atmosphere is often necessary. In 1934 Rowledge [4] described a successful attack on most of these minerals by sodium fluoride/boron trioxide fusion in a sealed tube at 900°C and Hey [5] developed a scaled-down technique for the fusion of ca. 10-mg samples in sealed tubes under vacuum. Air oxidation during slow dissolution of the crushed fusion cake was prevented by the presence of iodine monochloride. Bower [6] also succeeded in preventing oxidation of liberated iron(II) ions by the presence of iodine monochloride in strong hydrochloric acid.

Spinels (especially chrome spinels) represent some of the most resistant minerals which are almost entirely unaffected by normal hydrofluoric/sulphuric acid attack. In this laboratory, the micro-fusion of chrome spinel and other resistant minerals (in milligram quantities) was investigated for iron(II) with various fluxes, but no reliable data could be obtained [7]. The dual requirement of quantitative dissolution and the retention of the original iron oxidation state on the micro-scale represented an almost insurmountable difficulty. It was concluded [7] that any solubilizing agent or flux which contains structural oxygen will cause an appreciable oxidation of available Fe(II) ions, irrespective of any careful counter-measures or the most stringent precautions being taken to prevent oxidation.

Thus, attention was focussed on indirect methods in which a measured excess of a thermally stable oxidant was allowed to react with the liberated Fe(II) ions in situ and the excess was back-titrated by a reducing agent, usually iron(II) sulphate. Hannaker and Qing-Lie [8] reported the effective dissolution of a large number of refractory minerals in phosphoric acid and a mixture of phosphoric/perchloric acids but they were not concerned with iron(II). It

was noted that although phosphoric acid effectively dissolved chromite (5 mg) at 300°C under an atmosphere of nitrogen, some 17% of available FeO was lost because of oxidation. Schafer [9] in his excellent review summarized methods in which phosphoric acid decomposition is used in the presence of an added oxidant. Chromite (chrome ore, chrome-magnesite refractories and ferrites) were decomposed by phosphoric/sulphuric acids in the presence of a measured excess of vanadium pentoxide [10—17]. Goswami [18] used cerium(IV) sulphate. Nagato [19] used Mn_2O_3 and measured the excess of manganese(III) by spectrophotometry. Cheng [20] dissolved ferrites in phosphoric acid containing Ce(IV) (phosphatocerate(IV) oxidant) and titrated the excess of cerium(IV) with iron(II) sulphate. None of these methods, however, was concerned with micro-scale analysis in which a relatively minor disadvantage on a macro-scale can be amplified to such an extent that performance at the milligram sample level is quite unacceptable. Thus in this work, the method of Cheng [20] utilizing phosphatocerate(IV) was assessed and the possibility of developing a micro-analytical method for FeO determination was explored. The scaling down of an earlier constant-current potentiometric method [21] for micro-analysis was also successfully evaluated; this offered both an alternative to spectrophotometric methods, and a much simpler methodology with improved analytical precision.

This paper describes an integrated micro-analytical scheme for the precise determination of the iron oxidation state in hand-picked single-crystal minerals (milligram quantities). Depending on the chemical resistance, two categories can be identified: (a) hydrofluoric acid-soluble minerals, and (b) hydrofluoric acid-insoluble or refractory minerals. Group (a) minerals are analyzed by direct constant-current potentiometric titration of dissolved minerals with potassium dichromate. Group (b) minerals are analyzed for Fe(II) by phosphoric acid dissolution in the presence of cerium(IV) as a thermally stable oxidant. The unreacted excess is then back-titrated. Total iron can be determined by atomic absorption spectrometry (a.a.s.) after micro-fusion with lithium tetraborate or by electron microprobe [22].

Preliminary investigations

Stability of phosphatocerate(IV) and iron(II) ammonium sulphate solutions. Cheng [20] prepared 0.1 M phosphatocerate(IV) solution by heating ceric ammonium nitrate in concentrated phosphoric acid:

$$Ce(NO_3)^{2-} + H_3PO_4 \xrightarrow{\Delta\ 300°C} Ce(PO_4)^{2-} + 6HNO_3$$

The light yellow solution polymerized on standing within a few hours and it was necessary to stabilize it by adding sulphuric acid and water. However, the presence of sulphuric acid was undesirable because of the formation of SO_2 and SO_3 at higher digestion temperatures. It was found that by omitting the addition of sulphuric acid and water, the phosphatocerate(IV) solutions (0.006 M) prepared in concentrated phosphoric acid were stable for long

periods of time. Further stabilization was achieved by pre-conditioning the total volume of phosphoric acid required for sample digestion with cerium (IV). The single dose of oxidant/solvent was accurately weighed for each sample digestion. The stability of this titration system (0.006 M phosphatocerate(IV)/0.002 M iron(II) ammonium sulphate) was enhanced by this approach, resulting in an average relative standard deviation (RSD) of 1.13% for 6 measurements over 21 days (see Table 1).

Decomposition of refractory minerals by phosphoric acid. In order to test the range and scope of the proposed method, garnet, rutile, topaz, magnetite, staurolite, kyanite, monazite, tourmaline, ilmenite, pyrite and kaersutite were also analyzed for FeO by phosphoric acid decomposition in the presence of a known excess of cerium(IV). All minerals dissolved adequately (2—8 mg quantities), but some precipitates were formed, such as titanium hydroxide in diluted ilmenite solutions, aluminium phosphate in alumina-rich minerals, rare-earth phosphates in monazite solutions and elementary sulphur in pyrite. Iron(II) could not be determined in pyrite because cerium(IV) was totally consumed by oxidizing sulphur at the same time. The iron oxidation state in sulphide minerals (pyrrhotite, pyrite and chalcopyrite) could be determined by Steger's method [23]. The precision was variable: for some minerals (e.g., kaersutite) precision was very high but for others (staurolite, monazite), reproducibility was quite poor.

Excellent precision (RSD = 1.08%) was obtained when stabilized phosphoric acid/phosphatocerate was added as a single reagent compared to Cheng's procedure [20] (RSD = 3.56%) (see Table 3). Digestion time for the standard was 30 min whereas for the chrome spinel it was necessary to heat samples for 55—60 min at 300—350°C. Curiously, ilmenite decomposed after only 7 min of heating, whereas rutile remained only partially decomposed even after 220 min. In some earlier experiments, borosilicate beakers were

TABLE 1

Stability of phosphatocerate(IV) (0.006 M) and iron(II) ammonium sulphate (0.002 M)[a] titrants

Date of calibration	No. of titrations	FeO equivalent (mg ml^{-1})	RSD (%)
26.6.86	7	0.1409[b]	—
3.7.86	4	0.1530[c]	0.61
8.7.86	4	0.1476[b]	1.95
9.7.86	4	0.1450[b]	1.18
10.7.86	4	0.1449[b]	2.95
16.7.86	4	0.1480[b]	2.36

[a]Calibrated against hedenbergite internal laboratory reference mineral for Fe(II)/Fe(III). [b]Stabilized phosphatocerate reagent solution. [c]Previous stock of the iron(II) titrant. Theoretical value of 0.002 M $Fe(NH_4)_2(SO_4)_2$: 0.1437 mg ml^{-1} FeO. Empirical value found (average of four measurements): 0.1464 mg ml^{-1} FeO.

used and the cloudiness in sample digests indicated appreciable attack on glass but the results did not appear to be adversely affected. However, to attain high chemical resistance and low iron contamination, transparent silica beakers were used for all digestions.

Thermal stability of phosphatocerate(IV). Accurately weighed portions of phosphatocerate solution (0.006 M) were heated at 340°C for specified periods. The cooled solutions were titrated (constant-current potentiometry) with iron(II) ammonium sulphate (0.002 M). This test showed a loss of Ce(IV) concentration as follows: 1.08% (10 min); 3.16% (16 min); 4.46% (30 min); 4.95% (40 min); 5.37% (55 min) and 10.33% (75 min). The thermal degradation of Ce(IV) highlights the necessity of processing blanks with every batch of sample decomposition. However, potassium dichromate decomposes to a much greater extent than the cerium(IV)/phosphoric acid complex.

EXPERIMENTAL

Reagents and apparatus

Phosphatocerate(IV) solution, 0.006 M. Weigh 1.6447 g of ammonium cerium(IV) nitrate (analytical-reagent grade) in a quartz beaker, add ca. 50 ml of concentrated phosphoric acid and heat to 300°C. The nitrogen dioxide evolved is expelled by a nitrogen stream. The reaction takes about 30 min. After all the acidic vapours have been expelled, cool the solution somewhat and make up the volume to 500 ml with concentrated phosphoric acid in a teflon bottle. Allow ca. 2 days for any oxidizable impurities in the phosphoric acid to react with Ce(IV). This solution is stable almost indefinitely, without any tendency to polymerize and its oxidizing potential is closely reproducible on a day-to-day basis.

Iron(II) ammonium sulphate, 0.002 M. Initially prepare a 0.1 M stock solution in 0.5 M sulphuric acid and dilute further to the working concentration, as required, with 0.5 M sulphuric acid. Because both the oxidizing acid and the titrant are calibrated simultaneously with each batch of samples, no deterioration in titratable species is of any consequence. The phosphatocerate (IV)/iron(II) ammonium sulphate titration system showed good stability during daily calibrations.

Potassium dichromate, 1 ml = 0.1 mg FeO. Weigh 68.3 mg of the finely ground, dry substance, dissolve in distilled water and dilute to 1000 ml. Calibrate for FeO equivalency against an appropriate standard; hedenbergite internal laboratory standard was used here.

Hydrofluoric acid/sulphuric acid mixture. Mix 2200 ml of water with 800 ml of concentrated (95% w/v) sulphuric acid in a polypropylene bottle, add 1000 ml of concentrated (ca. 48% w/v) hydrofluoric acid and mix thoroughly.

Metallic reductors were milled from a cylindrical cast of pure zinc ingot (99.995%) in 4-mm thick discs of diameter ca. 1.7 cm. Eight of these discs were perforated for easy flow-through and treated with mercury(II) chloride solution acidified with hydrochloric acid, to give a lustrous surface coating.

These discs were mounted on the inlet tube of the decomposition vessel [21] for total iron runs. Stored discs were re-activated before use by immersion in acidified mercury(II) chloride solution.

All titrations were done with a Metrohm potentiograph (Type E-435) equipped with a synchronized piston burette assembly. The Pt/Pt-Rh(20%) bimetallic electrode [21] was used for all titrations.

Micro-fusions were done in a Leco high-frequency dual-mode furnace model 523. Platinum fusion crucibles (capacity 1 ml), Leco silica vacuum-jacketed graphite fusion crucibles and silica inserts were used.

Recommended procedures

Hydrofluoric acid-soluble silicate rocks and minerals. For the micro-determination of iron(II) (method A; for further details see the previously described method [21]), grind the sample under acetone to 200 mesh BSS. After drying in an oven at 110°C, weigh 3—10 mg of material (Cahn electro-balance), transfer directly to the PTFE vessel (use polonium-210 α-emitter to control static charge) and wash down the sides with ca. 20 ml of water. Within the first set of digestions, weigh also 2—4 portions of hedenbergite laboratory reference mineral (20.912% FeO; ca. 5 mg) to standardize the potassium dichromate solution. Add 20 ml of the HF/H_2SO_4 mixture, mix thoroughly, reassemble the digester and attach to the nitrogen manifold. Connect the side tube to the monitor flask and put the vessel into the heating block preheated to 140°C. Continue digestion for 15—30 min (depending on the ease of sample decomposition; generally sheet silicates require the shortest and orthosilicates the longest duration of heating). Transfer the digested sample to the titration stand and titrate with potassium dichromate (1 ml = 0.1 mg FeO) with the burette tip fully immersed, under a steady nitrogen flow at a +5-μA polarization current (+200-mV compensation potential; 250-mV measuring range). The very sharp peak may require zero off-setting for some types of samples in order to keep the curves on the chart paper. Calculate the results using the standardization data. Typical results obtained are presented in Table 2.

For the micro-determination of total iron (method B), weigh accurately 3—10 mg of finely ground sample (see method A) directly into the PTFE vessel (use polonium-210 static eliminator) and proceed as in the iron(II) determination in every detail except that the digestion is carried out in the presence of a fully-immersed mercury-coated zinc reductor disc [21]. Digestion time is similar to that of method A. Titrate the reduced sample solution as for iron(II). The titration peak values correspond to the total amount of iron present. The results obtained by this method are also presented in Table 2.

Refractory minerals (insoluble in hydrofluoric acid). For the micro-determination of iron(II) (method C), weigh 5—7 mg of spinel (chromite, etc.) and ca. 5 mg hedenbergite reference samples at least in duplicate (20.912% FeO), into 50-ml transparent silica beakers to ±0.0001 mg accuracy. Prepare

TABLE 2

Micro-determination of iron oxidation state in HF-soluble minerals by titration with potassium dichromate[a]

Sample	No. of titrations	FeO (%)	Fe_2O_3 (%)	Total Fe (as Fe_2O_3) (%)	Fe(II)/Fe(III)
BCR-1 Basalt	3	8.76 ± 0.02	—	—	—
Hedenbergite	6	20.89 ± 0.33	—	—	—
Chlorite JW-1	2	11.99 ± 0.04	1.33	14.66 ± 0.17	10.006
Chlorite JW-2	2	10.00 ± 0.02	0.96	12.07 ± 0.00	11.624
Chlorite JW-3	2	10.23 ± 0.01	1.95	13.32 ± 0.02	5.829
Chlorite JW-4a	2	26.57 ± 0.01	4.01	33.50 ± 0.02	7.351
Chlorite JW-5	2	35.33 ± 0.13	5.03	44.29 ± 0.28	7.808
Chlorite JW-6	2	38.00 ± 0.08	4.11	46.33 ± 0.10	10.286
Chlorite JW-7	2	30.62 ± 0.12	10.36	44.39 ± 0.15	3.284
Chlorite JW-17	2	18.98 ± 0.00	0.19	21.84 ± 0.06	116.36
Chlorite JW-22	2	24.36 ± 0.01	1.24	28.31 ± 0.03	21.846
Biotite J1	2	18.60 ± 0.02	2.08	22.76 ± 0.09	9.919
Biotite IB	2	12.25 ± 0.02	5.55	19.16 ± 0.09	2.454
Biotite B1 10	2	21.16 ± 0.11	1.86	25.37 ± 0.05	12.669
Magnetite (ex W.A.)	2	29.74 ± 0.004	—	—	—
Fayalite, synthetic	2	69.51 ± 0.32	—	—	—

[a]Sample size 2—6 mg; Zn/Hg reductor used for total Fe dissolutions.

four blanks also by weighing 5 ml of the phosphatocerate(IV) solution (using a transfer pipette) to 0.0001 g accuracy. (Two blank tests are required for the hedenbergite standard titration because of the much shorter digestion times, and the remainder are set aside for the chrome spinels.) Add to the samples 5 ml of 0.006 M phosphatocerate(IV) solution (transfer pipette) and weigh to ±0.0001 g accuracy. Transfer the covered beakers to a hot plate pre-heated to 300—325°C and allow water vapour to escape by covering the beakers only partially. The chromite dissolution commences after 15—20 min. Continue heating until all visible sample grains are dissolved (45—55 min is usually sufficient), cool to room temperature and place a teflon-coated magnetic bar in the syrupy digest. Dilute the solution to ca. 30 ml with distilled water, transfer to the titration stand, and immerse both the Pt/Pt-Rh(20%) bimetallic electrode [21] and the tip of the capillary delivery tube of the piston burette. Commence the titration of the residual oxidant by delivering iron(II) ammonium sulphate titrant (0.002 M) at a +1.0-μA polarizing current with 250-mV compensation potential (moderate titration speed). Titrate the solution on the I_{pol} function setting with automatic tracing of the titration curve. The end-point is indicated by a sharp depolarization peak. Determine the blank and calibrate against hedenbergite standard at the same time.

It is essential to run blanks with each set of digestions for the same duration because of the slight thermal degradation of cerium(IV) during 45—55 min heating. The calibration of 0.002 M iron(II) ammonium sulphate may

also be checked against potassium dichromate (1 ml = 0.1 mg FeO) in phosphoric acid medium (5 ml) by first differential (dE/dT) end-point detection. However, the standardized mineral hedenbergite is preferred. Table 3 shows results obtained on chrome ore (i.e., chrome spinel) and other refractory minerals. It can be seen that a fairly broad range of resistant minerals can be decomposed by phosphoric acid in the presence of cerium(IV).

No further information for total iron can be extracted from the titrated sample solution (such as total iron) because of the strong chelating effect of the phosphoric acid medium and because iron(II) is used as titrant. Total iron can be determined by electron microprobe analysis (as part of a complete analysis) or by lithium tetraborate microfusion and atomic absorption spectrometry. In either case, the iron oxidation state can be determined from the microtitration data (above) and the total iron data.

Microfusion procedure for the a.a.s. determination of total iron (and chromium). (Chromium can also be determined sequentially if desired.) Weigh ca. 50 mg of dried anhydrous lithium tetraborate in a pre-weighed 1-ml platinum fusion crucible. Weigh the finely ground mineral on a micro-balance (ca. 5 mg to ±0.0001 mg accuracy) and transfer it to the fusion crucible. Mix it with a thin platinum wire as homogeneously as possible and cover this mixture with a 50-mg layer of the flux (without mixing). Transfer the platinum crucible

TABLE 3

Micro-determination of iron(II) in refractory minerals

Reference/minerals	No. of detns.	FeO found (%)	RSD	Other values/remarks
BCS 308 Chrome ore	15	14.03	3.96	Unstabilized H_3PO_4
	10	14.41	1.08	Stabilized H_3PO_4
USGS BHVO-1 Basalt	4	8.35	1.51	Unstabilized H_3PO_4
USGS DTS-1 Dunite	4	7.36	5.28	Unstabilized H_3PO_4
Ilmenite[a]	2	42.63 ± 0.03	—	Clear solution
Monazite[a]	2	1.54 ± 0.13	—	REE-PO_4 precipitated
Garnet[a]	2	8.05 ± 0.39	—	Partial dissolution
Rutile[a,c]	2	1.80 ± 0.32	—	Partial dissolution
Kyanite	2	0.66 ± 0.11	—	$AlPO_4$ precipitated
Kaersutite[b]	2	11.19 ± Nil	—	11.21[b]; clear diss.
Staurolite	2	12.80 ± 0.5	—	$AlPO_4$ precipitated
Topaz	2	2.39 ± 0.02	—	Clear solution
Tourmaline[d]	1	13.80	—	Difficult to dissolve
Zircon[a]	2	1.49 ± 0.03	—	Very difficult to dissolve
Pyrite	2	Cannot be determined (H_2S interference)		

[a]From Rutile and Zircon Mines (Newcastle), beach sand heavy mineral. [b]Kaersutite 44 ex basalt (Glenn Innes, N.S.W., Australia); alkaline basalt-hosted "xenocrysts" (see P. Jakeš, PhD Thesis, Australian National University, 1970). Electron probe analysis: FeO = 11.21%. [c]Rutile was extremely insoluble; 5.6 mg (ground in agate mortar) was partially dissolved after 220 min at 320—350°C. [d]Possibly Fe-rich schorl (black).

to the quartz insert tube of the graphite/quartz cup and lock this assembly in the quartz-tube r.f. furnace. Adjust the nitrogen flow to 2.5 l min^{-1} (air would be also suitable). Commence induction heating by setting the timer on a 20-min cycle and the plate current to 250 mA initially. Increase the plate current by 50-mA increments after each minute and heat the charge at the maximal permissible setting of 500-mA plate current for the remaining time. Cool the furnace assembly at the end of the heating cycle for 10 min. Monitor the cooling rate by measuring the temperature at the nitrogen exit of the quartz tube furnace. When the temperature of 30—40°C is reached, transfer the fusion crucible to a pre-weighed 60-ml FEP-teflon bottle and add ca. 10 ml of 2% hydrochloric acid. Hasten the disintegration of the fusion cake by ultrasonic vibration for about 15 min. Dilute the sample solution to full capacity. Prepare chemical blanks also by fusion of 100-mg flux charges and proceed as for the sample fusions. Measure the atomic absorption of Fe and Cr at 248.3 nm and 357.2 nm with deuterium background correction in an acetylene/air flame against standard solutions containing similar concentrations of flux and matrix elements and reagent blank reference.

RESULTS AND DISCUSSION

Interferences are seldom encountered in the constant-current potentiometric determination of FeO (method A) in most rocks and minerals, even in the presence of acid-soluble sulphides and organic matter. In method B, the use of the Zn/Hg reductor may be too energetic for high titanium-bearing minerals, because of production of co-titratable Ti(III) species, but a Ni/Hg reductor will overcome this problem. The phosphatocerate(IV) solution in method C is susceptible to errors during prolonged heating if airborne dust particles, organic matter (such as camel hair brush, woollen fibres) or anything oxidizable is present. A laminar-flow fume hood is an asset for this type of micro-digestion. Because of the slight thermal decomposition of the oxidant, several blanks must be heated with each batch of mineral digestion to match different dissolution rates.

The main purpose of the integrated micro-analytical scheme described in this work was to permit the determination of iron valency states by a suitable method in as broad a range of minerals as possible. Within this frame of reference, two groups of minerals were identified according to their chemical reactivities: HF-soluble and HF-insoluble (refractories and oxide minerals). Chrome spinel represented one of the most refractory minerals, which was almost completely unaffected by conventional digestion methods. Methods C and D can be used routinely for the micro-determination of FeO and total iron in chromites. The average relative standard deviation (RSD) was 1.08% for FeO (Table 3).

In addition, it can be concluded that the overwhelming majority of rock-forming and accessory minerals can be analyzed by one of the methods described in this scheme. The exceptions include rutile (extremely insoluble

in phosphoric acid), staurolite, tourmaline and zircon which require lengthy digestions (small sample sizes and very fine grinding are essential). Rutile and garnet are attacked more efficiently by stronger hydrofluoric/sulphuric acid mixtures according to methods A and B. Some acid-soluble sulphide minerals may be analyzed by this mixed-acid digestion. However, the FeO content in sulphides cannot be determined by digestion in hot condensed phosphoric acid (method C). In addition to chrome-bearing spinels, lithium tetraborate fusion (method D) would allow the determination of total iron in sulphides or almost any other refractories.

The author is grateful to Mr. R. Rudowski (Mineral Separation Laboratory, R.S.E.S.), who kindly supplied some of the important minerals for this work and to Dr. Joyce Fildes for reading the manuscript. Dr. H. O'Neill and Dr. M. McCulloch (Petrochemistry and Geochronology, R.S.E.S.) showed a keen interest and made constructive suggestions thoughout this project.

REFERENCES

1 J. P. Riley and H. P. Williams, Microchim. Acta, 4 (1959) 516.
2 E. Kiss, Anal. Chim. Acta, 72 (1974) 127.
3 E. Kiss, Anal. Chim. Acta, 161 (1984) 231-244.
4 H. P. Rowledge, J. R. Soc. Western Australia, 20 (1934) 165.
5 M. H. Hey, Mineral. Mag., 26 (1941) 116; 39 (1974) 895.
6 N. W. Bower, Geostd. Newslett., 8 (1) (1984) 231.
7 E. Kiss, Anal. Chim. Acta, 193 (1987) 315.
8 P. Hannaker and Hou Qing-lie, Talanta, 31 (1984) 1153.
9 H. N. S. Schafer, Analyst, 91 (1966) 755.
10 A. V. Shein, Zavod. Lab., 6 (1937) 1199.
11 S. T. Balyuk and V. M. Mirak'yan, Zavod. Lab., 15 (1949) 1004.
12 H. B. Samanta and N. B. Sen, Trans. Indian Ceram. Soc., 5 (1946) 97.
13 T. Nagaoka and S. Yamazaki, Jpn. Anal., 3 (1954) 408.
14 H. Sasuga and Y. Iida, Jpn. Anal., 7 (1958) 7, 248.
15 E. G. Kondrakhina, L. G. Egorova, O. A. Songina, Izv. Akad. Nauk. Kazakh. SSR., 1 (1957) 45.
16 P. Dippel, Silicattechnik, 13 (1962) 51.
17 E. B. T. Cook and T. W. Steele, National Institute for Metallurgy, Randburg, South Africa, Report No. 1088, 1970.
18 N. Goswami, Sci. Cult., 22 (1957) 398.
19 H. Nagato, Jpn. Anal., 10 (1961) 985.
20 K. L. Cheng, Anal. Chem., 36 (1964) 1666.
21 E. Kiss, Anal. Chim. Acta, 89 (1977) 303.
22 N. G. Ware, R.S.E.S., Australian National University, personal communication, 1986.
23 H. F. Steger, Talanta, 24 (1977) 251.

Analytica Chimica Acta, 193 (1987) 61—69
Elsevier Science Publishers B.V., Amsterdam — Printed in The Netherlands

CARBON FIBRE ELECTRODES IN FLOW POTENTIOMETRIC STRIPPING ANALYSIS

HUANG HUILIANG, CHI HUA, DANIEL JAGNER* and LARS RENMAN

Department of Technical Analytical Chemistry, Chemical Center, University of Lund, P.O. Box 124, S-221 00 Lund (Sweden)

(Received 29th July 1986)

SUMMARY

The construction of carbon fibre flow electrodes suitable for use in connection with potentiometric and constant-current stripping is described, and the fibre electrodes are compared with a glassy carbon disc thin layer cell. The signal-to-background ratio is approximately 1.6 times higher for an 8—10 μm carbon fibre compared to the glassy carbon disc electrode. If an Ag/AgCl tube is used as both counter and reference electrode, the signal-to-noise ratio of the fibre electrode is approximately five times better than for a glassy carbon disc electrode with a calomel reference; the latter electrode design, however, gives slightly better precision. The dead volume and internal potential drop of the fibre electrodes are more than one order of magnitude smaller than for the glassy carbon disc electrode. Because of the simplicity of the manufacturing process and low material cost, the fibre cells can be used as disposable electrodes and the polishing process necessary in connection with glassy carbon disc electrodes can be omitted.

As indicated in a recent review by Edmonds [1], carbon fibres now have extensive usage in electrochemical measurements. Carbon fibre electrodes have been introduced for various reasons, one being to exploit the minute dimensions of the fibres in the analysis of very small samples or for *in vivo* measurements. Another advantage of fibre electrodes is the non-linear diffusion conditions applicable to micro-electrodes [2]. These make the fibre electrodes less sensitive to fluctuations in hydrodynamics, thus often increasing the sensitivity.

The use of fibre electrodes for the determination of metal ion concentrations by means of current-measuring techniques such as amperometry and voltammetry often leads to instrumental problems because of the very low currents to be monitored. This problem does not apply to potentiometric stripping analysis because the technique is independent of the surface area of the working electrode. For this reason, it was recognised early on that carbon fibre electrodes might be suitable as working electrodes in potentiometric stripping analysis. Preliminary experimental results were reported by Jennings and Morgan [3]; later, Schulze and Frenzel [4] and Baranski and Quon [5] demonstrated the possibility of using carbon fibres as sensors in potentiometric stripping analysis. These studies, however, were solely concerned with

0003-2670/87/$03.50

batch analysis and the advantages inherent in the flow potentiometric stripping method [6] were not exploited. For this reason, it was decided to attempt to construct and evaluate carbon fibre electrodes suitable for flow potentiometric stripping. The ultimate aim was to construct very inexpensive, and thus disposable, electrodes with increased sensitivity, small dead volume, negligible internal-resistance potential drop and highly reliable non-leakage behaviour, even when very viscous solutions were sucked through the electrodes.

THEORY

The stripping time, t_s, in flow potentiometric stripping with electrodes based on linear diffusion, i.e., the diffusion layer thickness is much less than the electrode radius, is proportional [7] to

$$t_s \propto D_{M^{n+}}[M^{n+}]_s \delta_{el} t_d / \sum_{i=1}^{k} (n/m) D_i [ox]_i \delta_{strip} \quad (1)$$

where D denotes diffusion coefficients, $[M^{n+}]_s$ the sample concentration of analyte, t_d electrolysis time, and δ_{el} and δ_{strip} the diffusion-layer thickness during electrolysis and stripping, respectively. The concentrations of the k different oxidants present in the stripping solution are denoted by $[ox]_i$ and the number of electrons involved in the oxidation of M(Hg) is denoted by m.

Equation 1 is valid, irrespective of the size and shape of the working electrode, provided that the mass transport to the working electrode is diffusion-controlled during both electrolysis and stripping. This is normally the case on the time scales used in potentiometric stripping analysis [7]. The diffusion-controlled mass transport at a fibre electrode is, however, enhanced compared to that of a linear-diffusion disc electrode. The magnitude of this enhancement can be estimated from a comparison of the diffusion-layer volume per working electrode surface area for the two kinds of electrodes. For a fibre electrode, where the length of the fibre is much greater than the diameter of the fibre, the enhancement, E, is

$$E = 1 + \delta / d \quad (2)$$

where d is the electrode diameter and δ the thickness of the diffusion layer for both electrode types. Equation 2 can thus be used to estimate the improvement in signal-to-background ratio when fibre electrodes are used, compared with linear-diffusion electrodes for the same diffusion-layer thickness. For the comparison to be relevant it is, of course, also necessary that the electrochemical properties of the two surfaces are identical.

EXPERIMENTAL

Preparation of flow fibre electrodes

Polyvinyl tubing (outer diameter 2 mm, inner diameter 0.5 mm) was rinsed by sucking acidified ethanol through the tubing for 1 h. An injection needle (outer diameter 0.4 mm, inner diameter 0.2 mm) was then inserted through the centre of a 25-mm piece of the tubing inclined at approximately 30° to the length of the tube. A carbon fibre (Sigri Elektrographit, Meitingen, F.R.G.; diameter 8—10 μm; the fibres were a gift from W. Frenzel and the same as those used earlier [4]) was inserted, under a microscope, into the injection needle which was then removed from the tubing, leaving the fibre behind. The tube was then covered with a cylindrical layer of silver glue (Allied Products Corp., New Haven, Conn.) as shown in Fig. 1. This layer made electrical contact with the two ends of the carbon fibre and also protected the tube from being bent during handling. Because of the minute dimensions of the fibres, it was not possible to be absolutely certain that only a single carbon fibre was used in each flow electrode.

Flow cells

The three different flow cells shown in Fig. 2 were investigated. In all cells, the inlet side of the fibre electrode was connected to the platinum tube (length 8 mm, inner and outer diameters 0.7 and 0.4 mm, respectively) originating at the solution mixing point. This tube was connected to instrumental earth during stripping measurements in order to protect the electrode from noise carried by the electrolytes [8]. In the first cell (Fig. 2a), a platinum tube with the same dimensions as the inlet tube mentioned above was used as counter electrode, and the calomel electrode of a thin-layer cell described elsewhere [8] was used as a reference. In the second cell (Fig. 2b), the calomel electrode was replaced by a silver tube (length 8 mm, inner and outer

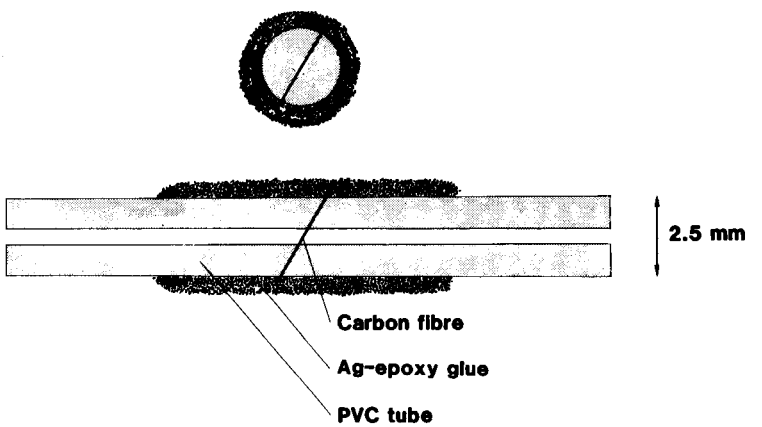

Fig. 1. Carbon fibre flow electrode. The carbon fibre diameter is approximately 10 μm.

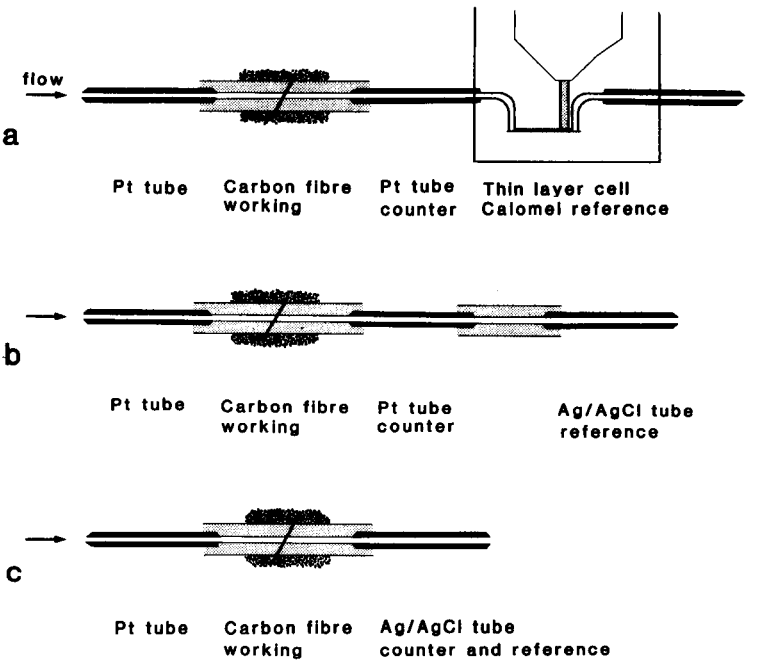

Fig. 2. The three different flow cell designs investigated. The inlet platinum tube was connected to instrumental earth during potential measurements in order to discriminate against noise carried by the electrolytes.

diameters 1.0 and 0.6 mm, respectively) lined with silver chloride. In the third cell (Fig. 2c), the silver/silver chloride tube was used both as reference and counter electrode. The fibre electrodes were compared with the 2-mm diameter glassy carbon electrode in the thin-layer cell arrangement [8].

Instrumentation and electrode test procedure

The automated potentiometric and constant-current stripping analyzer described elsewhere [8] was used in connection with the flow fibre cells. All fibre electrodes produced were subjected to the same test procedure. In this procedure, the fibre electrodes were first coated with a thin film of mercury by means of electrolysis at −1.0 V vs. SCE (when Ag/AgCl was used as reference, the values of the potentials were recalculated to those corresponding to SCE) for 30 s in a 3.5 M calcium chloride solution containing 50 mg l^{-1} mercury(II) and at a flow rate of 0.5 ml min^{-1}. Subsequently, a solution containing 10 μg l^{-1} each of cadmium(II) and lead(II) and 5 μg l^{-1} each of copper(II) and bismuth(III) in 0.1 M hydrochloric acid was electrolyzed for 60 s at −1.00 V vs. SCE at a flow rate of 0.5 ml min^{-1}. Finally a stripping solution containing 4.5 M calcium chloride solution was sucked into the cell for 15 s at a flow rate of 0.5 ml min^{-1} prior to recording of the stripping and background curves.

The stripping curves and background-corrected stripping curves were displayed on the printer/plotter, using an averaging filter width of 20 mV and a Savitzky-Golay filter width of 15 mV, the potential resolution being 1 mV and the data acquisition rate 25.6 kHz.

RESULTS AND DISCUSSION

Signal-to-background ratio

A background-corrected potentiometric stripping curve obtained according to the test procedure above is shown in Fig. 3. Of one hundred electrodes tested, forty electrodes did not yield any response at all. This was attributed to failure in the manufacturing process, the most common failure being fracture of the fibre in the 0.5-mm flow channel of the polyvinyl chloride tube. Apart from yielding no potentiometric stripping curve, failure of an electrode was always indicated by no current passing through the fibre during electrolysis.

The sixty electrodes without failure yielded very similar responses, the relative standard deviations for bismuth(III), copper(II), lead(II) and cadmium(II) from fibre to fibre being 20, 20, 25, and 30%, respectively. This shows that the surface of the fibres is very homogeneous.

The signal-to-background ratio was calculated from non-background-corrected stripping curves. The mean value obtained from the sixty fibre electrodes was approximately 1.6 times better than that obtained from the corresponding number of measurements on freshly polished glassy carbon electrodes. This improvement was obtained for all four elements studied.

The diffusion-layer thickness around a fibre electrode is difficult to calculate because it is not likely that all fibres pass through the centre of the flow channel. An estimate based on calculations for tubular electrodes [9, 10] indicates, however, that the diffusion-layer thickness in the electrode test

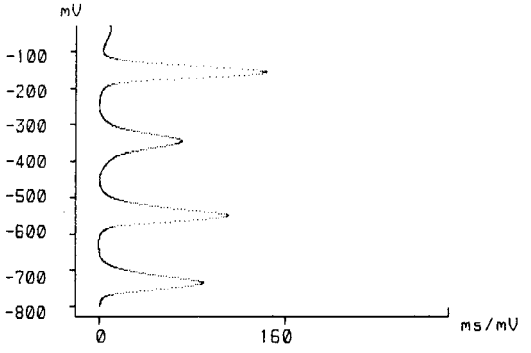

Fig. 3. Results obtained with the flow cell in Fig. 2c. Sample solution, 10 $\mu g\ l^{-1}$ each of cadmium(II) and lead(II) and 5 $\mu g\ l^{-1}$ each of copper(II) and bismuth(III); stripping medium, 4.5 M calcium chloride; electrolysis for 60 s at −1.20 V prior to stripping; reference electrode Ag/AgCl ($[Cl^-]$ = 9 M).

procedure is approximately 10—20 μm. Thus according to Eqn. 2, a signal-to-background improvement of 2—3 ought to be obtained. This is in reasonable agreement with the experimental results, considering that the electrochemical surface properties of the two electrodes are probably very different.

Signal-to-noise ratio

Because of their small surface area, fibre electrodes are more sensitive to electrical noise than are macro-electrodes. The three different flow cells in Fig. 2 were compared with respect to signal-to-noise ratio with the thin-layer cell by means of the electrode test procedure specified above. In order to simplify the measurement of the noise levels, the stripping curves were displayed with an averaging filter of 2 mV and no Savitzky-Golay filtration. No consistent results were obtained because the noise levels were highly dependent on the conditions in surrounding laboratories, and in particular, on experiments that required instrumentation with high power demands. It could, however, be concluded that the noise level of the fibre electrode when calomel was used as reference was approximately five times higher than the noise level of the thin-layer glassy carbon cell [8]. Furthermore, the cell arrangement in Fig. 2(c) where the Ag/AgCl tube was used both as counter and reference electrode yielded noise levels approximately five times lower than the thin-layer cell. In fact, on only one occasion was it possible to measure any noise level at all with this cell arrangement. The cell arrangement of Fig. 2(b) yielded noise levels similar to that of the thin layer cell.

From the point of view of noise level, the use of a Ag/AgCl tube as both counter and reference electrode is obviously highly advantageous. This cell arrangement does, however, have several disadvantages, the most serious being that the potential of the reference electrode is dependent on the chloride concentration of the solution being sucked through the tube. Nor is it possible to attain a stable reference potential in solutions with very low chloride concentrations. Furthermore, if the solutions used contain high concentrations of, e.g., bromide or iodide, the reference electrode is transformed into an Ag/AgBr or an Ag/AgI electrode. Even so, the cell arrangement of Fig. 2(c) can be used in most potentiometric stripping applications because the sample matrix modifier normally contains chloride ions (e.g., hydrochloric acid), as does the stripping medium.

Dead volume and internal potential drop

One distinct advantage of fibre electrodes is the small dead volume between the solution mixing point and the fibre sensor. In the flow cells shown in Fig. 2, this dead volume is approximately 4 μl. This corresponds to a dead time of 0.25 s when going from one solution to another at a flow rate of 1 ml min^{-1}. This is one order of magnitude better than that which can be achieved with a thin-layer cell [8]. This small dead volume is, of course, of particular importance when it is necessary to replace a solution completely (99%) by the next solution as is normally the case when going from the

sample solution to the stripping medium. Under such circumstances, solution corresponding to at least ten dead volumes must be sucked through the cell.

Another advantage of the flow fibre electrodes is the low internal-resistance potential drop during electrolysis. When electrolysis is done at −1.0 V vs. SCE in 0.10 M hydrochloric acid, the typical current is 100 nA, most of it being due to the reduction of dissolved oxygen. From this, it can be estimated that the internal potential drop in the flow cells of Fig. 2 is less than 1 mV as long as the conductivity of the solutions is equal to or higher than that of 0.1 M hydrochloric acid.

Reproducibility, long-term stability and influence of organic matter

The reproducibility of the fibre electrodes was tested by running the electrode test procedure twenty-five times on five different randomly selected fibre electrodes in the cell arrangement of Fig. 2(c). The relative standard deviations were found to be 7—10% for cadmium(II) and lead(II), and 5—8% for copper(II) and bismuth(III). Corresponding values for the thin-layer glassy carbon cell were 6—8% and 7—9%, respectively. Obviously the precision of the fibre electrodes is slightly less than that of the glassy carbon disc electrode. This might be due to inherent differences in the surface properties of the two materials, or simply to lack of knowledge of how to treat the surface of the fibre electrodes in an optimal way prior to use. Moreover, mercury droplets hanging on the carbon fibre are more likely to fall off than those sitting on the glassy carbon disc. The use of other carbon fibres or a more sophisticated surface treatment might well improve the precision. Alternatively, the use of multi-fibre electrodes, i.e., tubes containing several single fibres separated from each other by a distance of at least five times the diffusion-layer thickness, and connected to the same external lead, might result in improved precision.

The surface of the glassy carbon discs normally used as substrates for mercury-film electrodes is frequently regenerated by means of polishing. For obvious reasons, fibre electrodes cannot be polished. When a fibre electrode fails, it has to be replaced by a new electrode. For this reason, the long-term stability of the fibre electrode is of utmost importance. The long-term stability of fibre electrodes as well as that of glassy carbon disc electrodes is highly dependent on the sample composition. Generally, the higher the organic matter content, the more rapidly the electrode deteriorates. Consequently, it is not possible to give any unambiguous number stating how many hours a fibre electrode can be used before it is necessary to replace it, or how many hours a glassy carbon electrode will operate without the need for repolishing. It is, however, possible to compare the two electrodes in the same medium. Such a comparison was done by means of continuously repeating the electrode test procedure overnight on new carbon fibre electrodes and freshly polished glassy carbon discs. In some experiments, the test solution was replaced by a urine sample diluted 1:10 with 2 M hydrochloric acid. Both experiments showed that the long-term stability of the carbon

fibre electrodes was almost one order of magnitude better than that of the glassy carbon disc. This difference was particularly noticeable in the urine samples. In these samples, the lead signal typically decreased to half its initial value after ten hours of operation when a carbon fibre electrode was used. The corresponding value for the glassy carbon electrode was one hour. It should be noted that if a standard addition procedure is used to evaluate the lead content, it is still possible to use the method even if the signal has decreased to one-half of its original value, because the decrease between consecutive electrolysis/stripping cycles is small.

The reason for the improved long-term stability of the fibre electrodes is not known. One explanation might be that the geometry of the fibre favours the growth of many small mercury droplets rather than a few large droplets thus resulting in a more complete surface coverage by mercury. On glassy carbon disc electrodes, the formation of large mercury droplets is often observed and it is generally assumed that the uncovered glassy carbon surface is more sensitive to adsorption of organic matter than are the mercury droplets.

Constant-current stripping

The automated stripping analyzer used in this investigation was constructed both for potentiometric and for constant-current stripping. In contrast to the potentiometric stripping signal, the magnitude of the constant-current stripping signal is dependent on the surface area of the working electrode. Consequently, it can be assumed that carbon fibre electrodes are inferior to glassy carbon disc electrodes in constant-current stripping analysis. Preliminary investigations on the possibility of adopting the cathodic stripping voltammetry procedure for the determination of selenium to constant-current stripping in a flow system do, however, indicate that fibre electrodes yield similar, if not better, results than glassy carbon discs. So far, surface adsorption techniques such as the determination of nickel(II) and cobalt(II) as their dimethylglyoxime complexes [11] have, however, not been investigated.

Conclusions

Several important advantages of the flow fibre electrodes have been demonstrated. They can be produced in large numbers at low material cost. Once the manufacturing procedure has been refined, the failure rate can probably be kept very low. Consequently, fibre electrodes can be used as disposable electrodes and the polishing procedure necessary for glassy carbon electrodes can be omitted. Furthermore, changing of electrodes is simple and rapid and the design of the flow fibre almost eliminates the risk of electrode cell leakage. The small dead volume of the flow fibre cells often decreases the time for one electrolysis/stripping cycle. In computerized flow potentiometric stripping analysis, the sensitivity is normally so high that the time for sample electrolysis is less than ten seconds. Thus the most time-consuming

part of an analysis is the complete replacement of the sample solution by the stripping medium. The time needed for this is proportional to the dead volume of the flow cell. So far, only one kind of fibre electrode has been investigated. Even if this fibre turns out to be the most suitable and no further progress can be obtained, the change from glassy carbon discs to carbon fibre electrodes seems to be well justified.

The performance of these flow fibre electrodes can almost certainly be improved. One obvious direction is towards electrodes of smaller diameters which would yield improved signal-to-background ratios. The practical obstacles to manufacturing such electrodes might, however, prove insurmountable. Another possible direction is the use of fibres with other surface treatments; condensed information on fibres available on the world market is available [12]. A third direction would be the use of multifibre electrodes.

REFERENCES

1 T. W. Edmonds, Anal. Chim. Acta, 175 (1985) 1.
2 K. R. Wehmeyer and R. H. Wightman, Anal. Chem., 57 (1985) 1989.
3 V. J. Jennings and J. E. Morgan, Anal. Proc., 20 (1983) 276.
4 G. Schulze and W. Frenzel, Anal. Chim. Acta, 159 (1984) 95.
5 A. S. Baranski and H. Quon, Anal. Chem., 58 (1986) 407.
6 D. Jagner, Trends Anal. Chem., 2 (1983) 53.
7 D. Jagner, Analyst, 107 (1982) 593.
8 L. Renman, D. Jagner and R. Berglund, Anal. Chim. Acta, 188 (1986) 137.
9 A. Hussam and J. F. Coetzee, Anal. Chem., 57 (1985) 581.
10 H. B. Hanekamp and H. J. van Niewkerk, Anal. Chim. Acta, 121 (1980) 13.
11 H. Eskilsson, D. Jagner and C. Haraldsson, Anal. Chim. Acta, 175 (1985) 79.
12 Carbon and High Performance Fibres, 3rd edn., Pammac Directories, Loudwater, High Wycombe, England.

Analytica Chimica Acta, 193 (1987) 71—79
Elsevier Science Publishers B.V., Amsterdam — Printed in The Netherlands

AUTOMATED DETERMINATION OF CADMIUM AND LEAD IN WHOLE BLOOD BY COMPUTERIZED FLOW POTENTIOMETRIC STRIPPING WITH CARBON FIBRE ELECTRODES

LENA ALMESTRAND, DANIEL JAGNER* and LARS RENMAN

Department of Technical Analytical Chemistry, Chemical Center, University of Lund, P.O. Box 124, S-221 00 Lund (Sweden)

(Received 26th September 1986)

SUMMARY

A sample pretreatment involving only the dilution (1 + 19) of two 0.2—0.4 ml sample aliquots with 0.5 M hydrochloric acid, with a standard addition to one of the aliquots, precedes the injection of each sample. The computer-controlled flow system used automatically executes a pre-programmed number of cycles on each sample pair before presenting the final result. Each cycle, which has a duration of 80 or 135 s for lead(II) and cadmium(II), respectively, involves the display of the derivative stripping signal on a printer/plotter and integration of the stripping peaks generated. For lead(II), stripping is done in 0.5 M hydrochloric acid, which eliminates interferences from copper, though at the cost of a relatively high stripping rate, compared to the 5 M calcium chloride used for cadmium(II). The flow cell consists of a silver chloride-lined silver tube which acts as both reference and counter electrode, and a disposable carbon-fibre working electrode mounted in a PVC tube, which normally will operate for 50—200 cycles. The method was verified for whole blood reference standards and by comparison with results obtained by atomic absorption spectrometry.

Cadmium and lead in whole blood are normally determined by atomic absorption spectrometry, either with the Delves cup or the graphite-furnace technique [1]. The elements can, however, also be determined electrochemically, after wet mineralization, by using differential-pulse anodic stripping voltammetry [2—5]. Morrell and Ghiridhar [6] have described the determination of lead in whole blood by means of anodic stripping voltammetry using the Metexchange reagent instead of acid mineralization. Oehme and Lund [4] pointed out, however, that this reagent cannot completely eliminate ghost peaks originating from electroactive constituents in the sample. Because potentiometric stripping analysis [7, 8] is capable, unlike the anodic stripping techniques, of operating in solutions containing high concentrations of electroactive substances (e.g., dissolved oxygen), this technique was exploited early on for the determination of trace metals in whole blood [9]. It was shown that twelve samples could be analysed for cadmium and lead per hour by means of computerized potentiometric stripping in a batch mode, the limit of detection being 25 nM for both elements [9]. Since then, considerable

0003-2670/87/$03.50

progress has been made in the potentiometric stripping technique, including construction of a flow system enabling improved stripping potential resolution and ease of automation [10]. The use of strong electrolytes as stripping media [11] has increased the sensitivity, as has the introduction of the flow carbon fibre electrode [12]. The latter has also simplified handling of the flow system in that problems associated with cell leakage and internal potential drop have been eliminated. Improvements have also been made in the microcomputer system controlling the flow system, which, apart from being able to control electrolysis potential, flow rates, magnetic inlet valves and autosamplers, is also capable of searching for stripping peaks and of integrating and evaluating the final results, either by standard addition or by calibration plot procedures [13].

In this paper, a highly automated method is described for the determination of cadmium and lead in whole blood in which the only manual operations required are dilution of the sample with a matrix modifier, and addition of a standard addition aliquot of suitable magnitude to a subportion of the sample.

EXPERIMENTAL

Instrumentation, electrode system and reagents

A flow potentiometric stripping analyser, operated by an ABC-806 (Luxor, Sweden) personal computer and described elsewhere [13], was used. In this system, six different solutions can be sucked into the flow cell by computer-controlled random-order opening and closing of magnetic valves. The computer also controls flow direction and flow rate at seven discrete levels between approximately 0.1 and 2 ml min^{-1} and electrolysis potential between −2.047 and +2.047 V vs. the reference electrode, with a potential resolution of 1 mV.

A carbon fibre (Sigri Elektrographit, Meitingen, F.R.G.) with a diameter of 10 μm, inserted into polyvinyl tubing (inner diameter 0.5 mm) as described elsewhere [12], was used as the working electrode. A silver tube lined with silver chloride was used as both counter and reference electrode.

All reagents used were of analytical grade, except the mineral acids, which were of Suprapur grade (Merck). The standard reference samples BCR 194–196 were obtained from the Commission of the European Communities, Community Bureau of Reference (BCR), Brussels, and diluted according to instructions. Samples analyzed previously by means of graphite-furnace atomic absorption spectrometry were obtained from the Department of Occupational Health, University of Lund. These samples were haemolyzed with heparin and stored deep-frozen.

Procedure for the determination of lead

A 200-μl subportion of the whole-blood sample was added to 3.8 ml of 0.5 M hydrochloric acid and another 200-μl subportion was added to 3.8 ml of 0.5 M hydrochloric acid containing 25 μg l^{-1} lead(II). The two solutions were mixed ultrasonically, or by swirling, and placed in different solution

inlets of the flow system. The other four solution inlets were connected to 0.1 M hydrochloric acid in 95% ethanol, 0.5 M hydrochloric acid, distilled water, and a mercury pre-plating solution containing 100 mg l^{-1} mercury(II) in 2.5 M calcium chloride respectively.

Prior to the first analytical run each day, the fibre electrode, which was either a new electrode or an electrode previously used, was washed with the acidified ethanol solution for 5 s at a flow rate of 1 ml min^{-1}, in the absence of an applied potential. The mercury pre-plating sequence (Fig. 1a) was started by admitting the mercury pre-plating solution and applying a potential of —0.60 V vs. Ag/AgCl ($[Cl^-]$ = 5 M) for 1 s and then disconnecting the potential for 1 s. The potential was then decreased to —0.61 V for 1 s and disconnected for 1 s. The procedure was repeated in steps of —0.01 V until a potential of —0.85 V was reached, the electrode being held at this potential for 15 s. The cell was then rinsed for 10 s with 0.5 M hydrochloric acid to remove the mercury pre-plating solution and to prevent coagulation of the blood sample.

The unspiked sample was sucked into the cell at 1 ml min^{-1} (Fig. 1b). Electrolysis was done at —0.90 V vs. Ag/AgCl ($[Cl^-]$ = 0.5 M) for 20 s after which the 0.5 M hydrochloric acid was again allowed into the cell. After 10 s, the flow rate was reduced to 0.4 ml min^{-1} and after a further 10 s the stripping potential gradient was recorded at a real-time potential sampling rate of 19.2 kHz in the interval —0.90 to —0.10 V vs. Ag/AgCl ($[Cl^-]$ = 0.5 M). The electrolysis potential of —0.90 V was then applied again for 5 s, after which the background was recorded. Finally, the acidified ethanol was allowed into the cell at —0.1 V vs. Ag/AgCl ($[Cl^-]$ = 0.1 M in 95% ethanol) for 5 s. In all subsequent runs, the mercury pre-plating procedure was replaced by a mercury-film renewal procedure in which the surface of the mercury film was renewed by means of electrolysis in the mercury plating solution at —0.90 V vs. Ag/AgCl ($[Cl^-]$ = 5 M) for 10 s at a flow rate of 0.4 ml min^{-1}.

In the second run, also following the pattern shown in Fig. 1(b), the spiked sample was allowed into the cell instead of the sample. These first two runs were regarded as electrode-conditioning runs and were not used in the evaluation procedure. During these runs, the sample solution inlets were also rinsed from previous samples.

After the first two runs, the sample and sebsequently the spiked sample were sucked in. After background correction and digital filtration using an averaging filter of 30 mV and Savitzky-Golay filter of 15 mV, the computer program located the lead stripping peaks, searching the interval from —0.52 to —0.40 V vs. Ag/AgCl ($[Cl^-]$ = 0.5 M). Finally, the program integrated the peaks in the region ±0.065 V around the peak potential value and calculated the lead(II) concentration in the sample by using the pre-programmed standard addition value. Simultaneously, the program displayed the stripping curves on the printer/plotter. The analysis of the sample and of the spiked sample can be repeated any pre-programmed number of times, the evaluation program then giving the mean value and the standard deviation for the result.

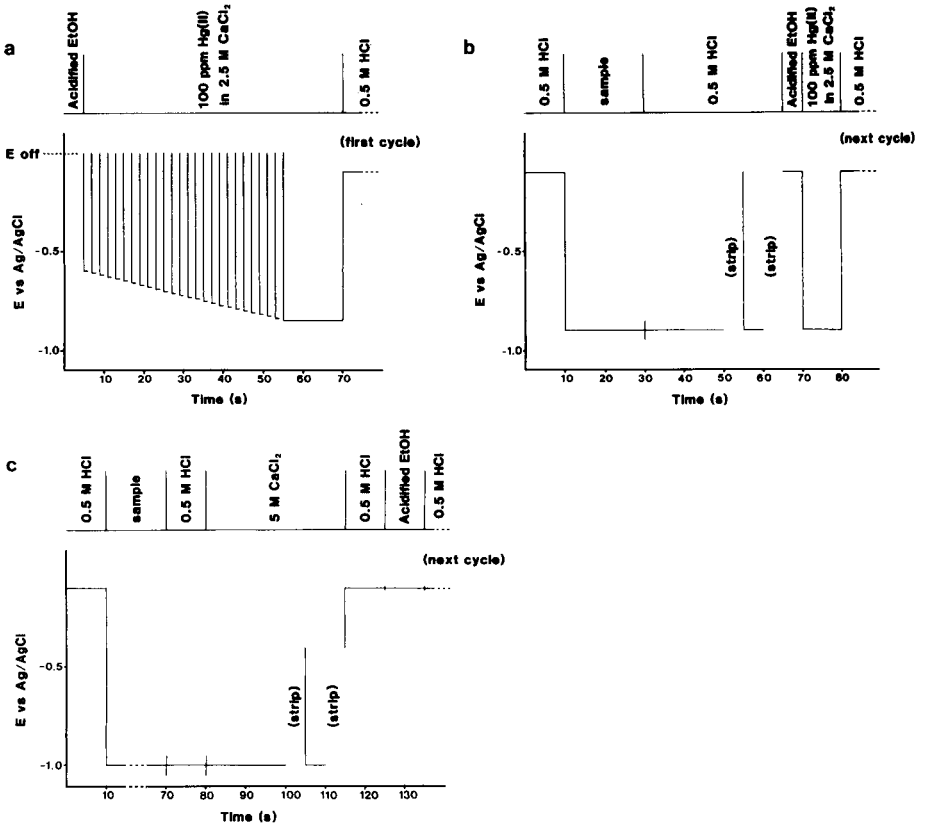

Fig. 1. Procedures used: (a) for mercury pre-plating; (b) for determination of lead(II); (c) for determination of cadmium(II). Flow rates were 1 ml min^{-1} in all cases except during stripping in lead(II) determinations, when the flow rate was decreased to 0.4 ml min^{-1}. Stripping is indicated by discontinuities in the plots showing the electrolysis potential.

After processing of the sample(s), a washing sequence was initiated in which 0.5 M hydrochloric acid and then distilled water were back-flushed into the magnetic valves in order to prevent salt crustation.

Procedure for the determination of cadmium

A 400-μl subportion of the whole-blood sample was added to 7.6 ml of 0.5 M hydrochloric acid and another 400-μl subportion was added to 7.6 ml of 0.5 M hydrochloric acid containing 1 $\mu g\ l^{-1}$ cadmium(II). The two solutions were mixed ultrasonically, or by swirling, and placed in different solution inlets of the flow system. The other inlets contained the same solutions as for lead(II) above, except that the inlet used for distilled water was connected to 5 M calcium chloride containing 10 mg l^{-1} mercury(II).

Irrespective of whether it was a new electrode or one used previously, the carbon fibre was pre-plated with mercury as described for lead(II) above (Fig. 1a). Subsequently, 0.5 M hydrochloric acid was sucked into the flow cell for 10 s at a potential of −0.1 V vs. Ag/AgCl ($[Cl^-]$ = 0.5 M) and the sample was electrolysed for 60 s at −1.0 V vs. Ag/AgCl at a flow rate of 1 ml min^{-1} (Fig. 1c). The flow cell was then washed with 0.5 M hydrochloric acid for 10 s at −1.0 V vs. Ag/AgCl, after which 5 M calcium chloride was allowed into the cell for 20 s at a flow rate of 1 ml min^{-1} prior to recording of the stripping curve in the region −1.00 to −0.40 V vs. Ag/AgCl ($[Cl^-]$ = 10 M), at a real-time measuring rate of 19.2 kHz. After electrolysis for 5 s at −1.0 V vs. Ag/AgCl, the background was recorded. The flow cell was then washed with 0.5 M hydrochloric acid and acidified ethanol for 10 s each, at a flow rate of 1 ml min^{-1} and a potential of −0.1 V vs. Ag/AgCl prior to the next run, in which the spiked sample was examined.

As for lead(II), the first two runs were discarded, and the sample and the spiked sample can be analysed any pre-programmed number of times. The same washing sequence was used as for lead(II), the distilled water step being, however, omitted.

After background correction and digital filtration using an averaging filter of 30 mV and Savitzky-Golay filter of 15 mV, the program located the cadmium stripping peak, searching the potential range −0.65 ± 0.1 V and, finally, evaluated the stripping signal by integration at ±0.06 V around the stripping peak. Simultaneously, the stripping curve was displayed on the printer/plotter.

RESULTS AND DISCUSSION

Matrix-modifying solution

The purpose of the matrix-modifying solution is to convert the trace metal analytes into well-defined, reducible species and, at the same time, to avoid coagulation of the whole-blood samples. It has been shown previously, by means of potentiometric stripping analysis [9] and by using the Metexchange reagent [6], that both lead(II) and cadmium(II) are easily released from the sample on dilution in acidic solution. Hydrochloric acid is the most suitable of the mineral acids and, if the concentration is below 0.7 M, the mixture will not coagulate, provided that the blood sample is diluted at least fifteen times. Experiments showed, however, that if the hydrochloric acid concentration is kept above 8 M, the whole-blood sample does not have to be diluted more than four times to avoid coagulation. In this way, the detection limit for a given electrolysis time can be decreased approximately three times compared with dilution with 0.5 M hydrochloric acid. The lifetimes of the carbon fibre electrodes are, however, reduced dramatically in the strongly acidic solutions, and the fumes from these solutions make it necessary to use a fume hood. For these reasons, the use of concentrated hydrochloric acid as the sample-modifying solution was abandoned during the course of this investigation.

Composition of stripping solutions for the determinations of lead(II) and cadmium(II)

The main purpose of the stripping solution is to resolve the analyte stripping peaks from any overlapping stripping peaks. Preferably, this solution should contain only low concentrations of oxidants (e.g., dissolved oxygen) so that a decrease in stripping rate and thus an increase in signal-to-noise ratio is obtained. The main problem in the determination of lead(II) in whole blood is the high copper concentration in the sample. For this reason, solutions with high chloride concentrations are not suitable as stripping media. If the chloride concentration is higher than ca. 1 M, the amalgamated copper will be oxidized to copper(I) chloride species. Consequently, copper yields a broad stripping peak, and, moreover, on increasing the chloride complexation by increasing the chloride concentration, the copper peak moves in the cathodic direction by 60 mV decade^{-1} while the lead peak moves by only 30 mV decade^{-1}.

Stripping in high chloride concentrations is illustrated in Fig. 2(a), for which a whole-blood sample containing 50 μg l^{-1} lead was diluted and analysed, as described above, with the difference that the electrolysis time was 120 s and that 5 M calcium chloride was used as stripping medium. The signal was displayed on a high-impedance input strip-chart recorder, as is normally the case in non-computerized potentiometric stripping [8]. From Fig. 2(a), it can be seen that the two stripping peaks are not fully resolved. It can also be seen that non-computerized flow potentiometric stripping can be used to estimate the lead content in whole blood if 5 M calcium chloride is used as stripping medium. Preliminary experiments showed that linear calibration plots were obtained in the concentration range 50—500 μg l^{-1}. Further investigation is, however, required to evaluate the potential of this technique.

Nitrate and hydroxide are other ligands which are capable of resolving copper and lead while being highly soluble in water. This is illustrated in Fig. 2(b) and 2(c) where 5 M calcium nitrate and 15 M sodium hydroxide were used as stripping media, using the same procedure as for calcium chloride in Fig. 2(a). Both these media resolve copper and lead well, the copper peak in the calcium nitrate solution being hidden in the baseline. The main disadvantage of these media is that, unlike calcium chloride, they contain appreciable concentrations of lead(II). In order to obtain accurate results in either the computerized or non-computerized mode, a somewhat complicated electrolytic purification procedure would seem necessary.

The stripping curve in Fig. 2(d) was obtained using the same procedure as in Fig. 2(a—c) but with 0.5 M hydrochloric acid as stripping medium. Owing to the high oxygen content of this solution, the stripping plateaux for lead and copper are not discernible when operating in the non-computerized mode. Deoxygenation of the stripping medium by inert gas bubbling results in plateaux of similar magnitudes to those shown in Fig. 2(a—c).

In chloride media, the stripping peak for cadmium is well separated from peak-overlapping interferents present in blood samples, i.e., zinc and lead.

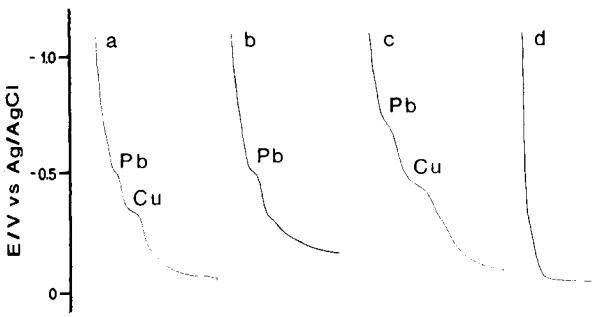

Fig. 2. Effect of different stripping media on the determination of lead(II): (a) 5 M calcium chloride; (b) 5 M calcium nitrate; (c) 1.5 M sodium hydroxide; (d) 0.5 M hydrochloric acid.

Moreover, because the cadmium(II) concentration in whole blood is considerably lower than that of lead(II), a concentrated solution of calcium chloride is the obvious choice as stripping medium.

Results obtained for lead and cadmium in whole blood

The results obtained for lead in standard samples BCR 194—196 and in the samples analysed previously by means of atomic absorption spectrometry are summarized in Table 1. The printer/plotter graphs obtained during the analysis of sample 4 are shown in Fig. 3. As can be seen from Table 1, the values obtained by potentiometric stripping agree satisfactorily with the certified values for the standard samples and with the results obtained by atomic absorption spectrometry (a.a.s.). It is also apparent that the relative standard deviations for the potentiometric stripping results are rather high, typically 15%. This is mainly due to the single-point standard addition technique chosen to evaluate the results.

The results obtained for cadmium in the analysis of standard samples BCR 195 and 196 are also shown in Table 1. The potentiometric stripping curves obtained on the printer/plotter in the analysis of sample BCR 196 are shown in Fig. 4. As can be seen, the results obtained for cadmium in standard samples BCR 195 and 196 agree well with the certified values, but, as for lead, the standard deviations are rather high. Potentiometric stripping results for sample BCR 194 are not reported, because the cadmium content is very close to the detection limit of the technique. It is also close to the blank values obtained from the reagents and from sample handling in a typical laboratory environment.

Conclusions

Computerized flow potentiometric stripping analysis provides a highly automated way of determining lead and cadmium in whole blood. The only manual operation required is the dilution of two subportions of the sample with spiked and unspiked matrix-modifying solutions. After that the computer

TABLE 1

Results obtained for lead and cadmium in standard samples and for lead in previously analysed samples

Sample	Pb or Cd content ($\mu g\ l^{-1}$)		Number of determinations
	Reference or a.a.s. value	p.s.a. value ± stand. dev.	
Lead			
BCR 194	126	113 ± 21	10
BCR 195	416	392 ± 61	10
BCR 196	772	779 ± 120	10
1	195	194 ± 30	5
2	270	241 ± 40	5
3	220	183 ± 40	5
4	370	354 ± 50	5
5	270	293 ± 35	5
6	260	297 ± 30	5
Cadmium			
BCR 195	5.37	5.33 ± 1.1	10
BCR 196	12.4	12.6 ± 1.6	10

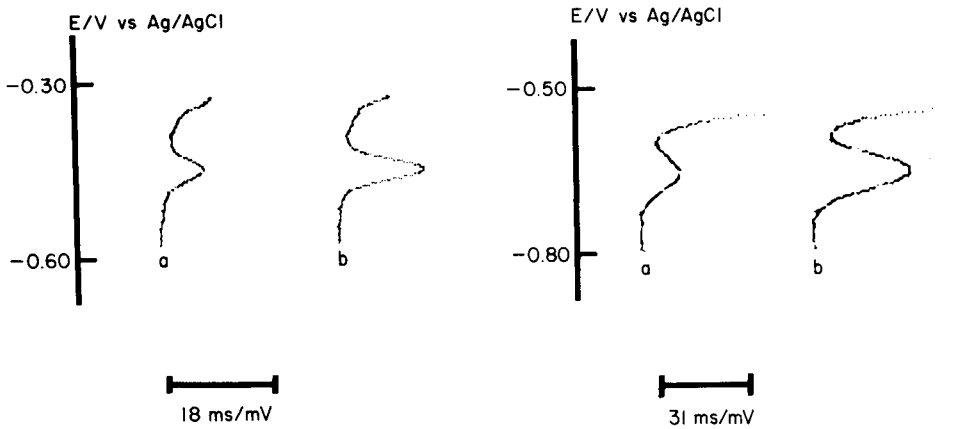

Fig. 3. Printer/plotter display of the derivative analytical signals (after background subtraction and digital filtration) from the determination of lead(II) in blood sample no. 4 (see Table 1): (a) sample diluted (1 + 19) with 0.5 M hydrochloric acid; (b) sample diluted (1 + 19) with 0.5 M hydrochloric acid spiked with 25 $\mu g\ l^{-1}$ lead(II).

Fig. 4. Printer/plotter display of the derivative analytical signals (after background subtraction and digital filtration) from the determination of cadmium(II) in reference blood sample BCR 196 (see Table 1): (a) sample diluted (1 + 19) with 0.5 M hydrochloric acid; (b) sample diluted (1 + 19) with 0.5 M hydrochloric acid spiked with 1 $\mu g\ l^{-1}$ cadmium(II).

controls the pretreatment of the working electrode, the performance of any pre-chosen number of electrolysis/stripping cycles, graphical and digital evaluation, presentation of the results with relevant standard deviations, and finally, cleaning of the system prior to the next analysis. A carbon fibre electrode can be stored for several days and probably for several weeks between analyses, and the same fibre can be used for 50—200 electrolysis/stripping cycles. It would thus seem that flow potentiometric stripping analysis is best suited to laboratories with a limited number of samples, where the object of the analysis is to detect elevated lead or cadmium concentrations. In cases where a large number of samples is to be analysed, a calibration plot procedure is recommended. This would not only increase the sample through-put, but also decrease the relative standard deviation from the present level of 15% to 7—8%.

We are indebted to Andrejs Schütz of the Department of Occupational Medicine, University of Lund, for valuable discussions and for supplying reference blood samples. This work was supported by grants from the Carl Trygger Research Foundation and the Swedish Work Environment Fund.

REFERENCES

1 R. L. Boeckx, Anal. Chem., 58 (1986) 274A.
2 R. Copeland, R. A. Osteryoung and R. K. Skogerboe, Anal. Chem., 46 (1974) 2093.
3 P. Valenta, H. Rützel, H. W. Nürnberg and M. Stoeppler, Fresenius' Z. Anal. Chem., 285 (1977) 25.
4 M. Oehme and W. Lund, Fresenius' Z. Anal. Chem., 298 (1979) 260.
5 J. Wang, J. Electroanal. Chem., 139 (1982) 225.
6 G. Morrell and G. Ghiridhar, Clin. Chem., 22 (1976) 221.
7 D. Jagner and K. Årén, Anal. Chim. Acta, 100 (1979) 375.
8 D. Jagner, Anal. Chem., 51 (1979) 342.
9 D. Jagner, M. Josefson, S. Westerlund and K. Årén, Anal. Chem., 53 (1981) 1406.
10 L. Anderson, D. Jagner and M. Josefson, Anal. Chem., 54 (1982) 1371.
11 H. Eskilsson, C. Haraldsson and D. Jagner, Anal. Chim. Acta, 175 (1985) 79.
12 H. Huiliang, C. Hua, D. Jagner and L. Renman, Anal. Chim. Acta, 193 (1987) 61.
13 L. Renman, D. Jagner and R. Berglund, Anal. Chim. Acta, 188 (1986) 137.

Analytica Chimica Acta, 193 (1987) 81—86
Elsevier Science Publishers B.V., Amsterdam — Printed in The Netherlands

SQUARE-WAVE VOLTAMMETRIC DETERMINATION OF DAMINOZIDE

ROBERT M. IANNIELLO

GAF Chemicals Corporation, Analytical Research and Development, 1361 Alps Road, Wayne, NJ 07470 (U.S.A.)

(Received 18th August 1986)

SUMMARY

A novel electrochemical method is described for the determination of the growth regulator, daminozide. Daminozide is hydrolyzed in alkaline aqueous media to form 1,1-dimethylhydrazine (UDMH). The UDMH is oxidized at −0.38 V vs. Ag/AgCl at the hanging mercury drop electrode and detected by square-wave voltammetry. The sensitivity is about 2.3 nA l mg^{-1} and the standard deviation (n = 8) for different standard solutions is 2.9 nA. Results obtained with apples after steam distillation agreed well with results obtained with a previously published method.

Daminozide, butanedioic acid mono(2,2-dimethylhydrazide) is a widely used farm chemical which is applied on a variety of crops (e.g., apples, tomatoes, peanuts) to help promote ripening and uniform size. Recently [1], the U.S. Environmental Protection Agency announced the imposition of a number of interim regulatory measures as a condition for the continued use of daminozide. This announcement was made in response to concerns over the potential risk of cancer from lifetime exposure to daminozide and its decomposition product, 1,1-dimethylhydrazine (UDMH). Reliable methods are therefore needed to determine daminozide at the newly proposed limit of 20 mg kg^{-1}.

Current methods utilize the alkaline hydrolysis of daminozide to form UDMH. The hydrazine adduct is then separated from the sample mixture by steam distillation followed by derivatization with a color-forming agent [2, 3]. Detection by spectrophotometry can be subject to interference by other amino-type pesticides [3]. In addition, color development may be time-consuming.

This report describes the development of a method for the determination of daminozide in aqueous solution by square-wave voltammetry. In this method, daminozide is hydrolyzed by heating in 2 M sodium hydroxide, followed by electrochemical oxidation of the UDMH product at the hanging mercury drop electrode. The technique is fast and highly selective for UDMH. In addition, a preliminary investigation, based on the proposed method, is presented, demonstrating the removal of daminozide from aqueous solution by crospovidone (cross-linked polyvinylpyrrolidone).

0003-2670/87/$03.50

EXPERIMENTAL

Apparatus and materials

All square-wave voltammetric measurements were obtained by using a BAS-100 Electrochemical Analyzer (Bioanalytical Systems, West Lafayette, IN) which was interfaced to a PAR Model 303A static mercury drop electrode with Model 305 stirrer (EG&G Princeton Applied Research, Princeton, NJ). All measurements were made at 20° C. The Ag/AgCl reference electrode was fitted with a porous polyethylene frit obtained from Princeton Applied Research; this material was found to have superior resistance to strongly alkaline solutions compared to the porous glass frit normally supplied with the instrument. All voltammograms were recorded with a DMP-40 digital plotter (Houston Instruments, Austin, TX). The system was interfaced to an Apple IIe microcomputer with a 15-Mbyte Winchester hard disk which allowed for both experimental control and data storage via software obtained from Bioanalytical Systems. A Reacti-Therm heating/stirring module (Pierce Chemical Co.) was used for sample hydrolysis.

Daminozide (99%; Standards Grade) was obtained from Chem Service (West Chester, PA). Unsymmetrical dimethylhydrazine (99+%) was obtained from Aldrich Chemical Co. Sodium hydroxide pellets (97%, reagent) were obtained from EM Science (Cherry Hill, NJ). Crospovidone (known as Polyclar AT) was a production grade of cross-linked polyvinylpyrrolidone obtained from GAF Corporation. All solutions were prepared from HPLC grade water (J. T. Baker, Phillipsburg, NJ) having a specific conductance of 0.6 μmho cm^{-1}.

Procedure

Stock solutions (1000 or 10 000 mg l^{-1}) of daminozide in distilled, deionized water were used to prepare working standards by serial dilution. Working standards (10-ml aliquots) were then pipetted into 4-dram glass vials containing ca. 0.8 g of sodium hydroxide pellets and a teflon stirring bar. The vials were tightly capped and hydrolyzed with stirring at 70° C for 15 min. Solutions were rapidly cooled to room temperature and adjusted to 10 ml with distilled water. For the adsorption study with crospovidone, the polymer was soaked in distilled water for 24 h to obtain maximum swelling. Daminozide stock standard was added to the stirred slurries of crospovidone and allowed to mix for a specified period of time. Aliquots were then removed, filtered through 0.22-μm Nylon-66 syringe filters, mixed with sodium hydroxide, and treated as described above.

Measurements were made on aliquots of the treated samples which had been deoxygenated by purging for 10 min with electrolyte-saturated argon. Square-wave voltammograms of argon-blanketed solutions were recorded using the following conditions: initial potential, —0.60 V; final potential, —0.20 V; square-wave frequency, 15 Hz; square-wave amplitude, 25 mV; step size, 4 mV; large drop size (0.025 cm^2); stirring rate, 400 rpm (slow).

RESULTS AND DISCUSSION

The hydrolysis of daminozide under acidic or alkaline conditions to form succinic acid and 1,1-dimethylhydrazine is the basis for most quantitative methods for daminozide. The electrochemical behavior of hydrazine and its derivatives in acid and alkali has been reported previously [4—7]. UDMH has been reported to yield a well-defined polarographic wave in 0.1 M KOH/2% sodium sulfite with a half-wave potential of —0.38 V vs. SCE [4]. In addition, it is generally accepted that the unsymmetrical dialkylhydrazines obey an ECC mechanism [8] with generation of a cation radical followed by dimer formation and subsequent decomposition. Thus, the use of aqueous alkali allows for both the formation of UDMH from daminozide and voltammetric detection under conditions favorable for optimum electro-oxidation of UDMH.

The electrochemical behavior of daminozide before and after heat treatment with alkali is shown in Fig. 1. Before heating, daminozide shows no evidence of hydrolysis as the voltammogram is essentially identical to that of the supporting electrolyte. After heating, a well-defined oxidation peak is observed at —0.38 V vs. Ag/AgCl which is similar to that for a UDMH standard solution (Fig. 2). Cyclic voltammetry of the hydrolyzed solution and UDMH yielded voltammograms which indicate quasi-reversible behavior. These observations confirm that UDMH is the electroactive product present after hydrolytic treatment of daminozide. It should be noted, however, that the UDMH standard and hydrolyzed daminozide do not give peak currents of the same magnitudes for roughly equivalent concentrations. As the boiling point of UDMH is ca. 64°C, it was initially suspected that the UDMH product was being volatilized during the hydrolysis treatment. Examination of the peak current of a 50 mg l^{-1} daminozide solution which was heated at various temperatures is shown in Fig. 3. It is evident that the maximum current is obtained at $\geqslant$70°C. In addition, higher temperature does not yield

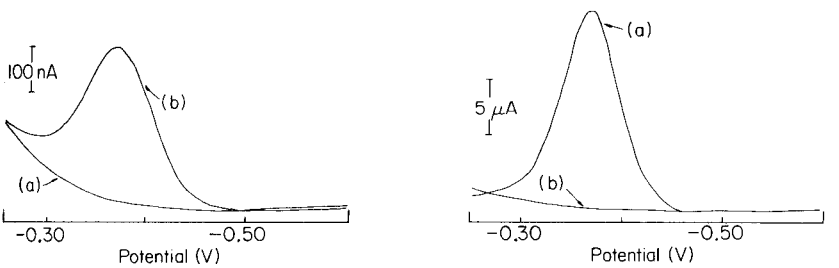

Fig. 1. Square-wave voltammograms of 98 mg l^{-1} daminozide in 2 M NaOH: (a) before heating; (b) after heating at 70° C for 15 min.

Fig. 2. Square-wave voltammogram of: (a) 30 mg l^{-1} UDMH (1,1-dimethylhydrazine) in 2 M NaOH; (b) blank electrolyte.

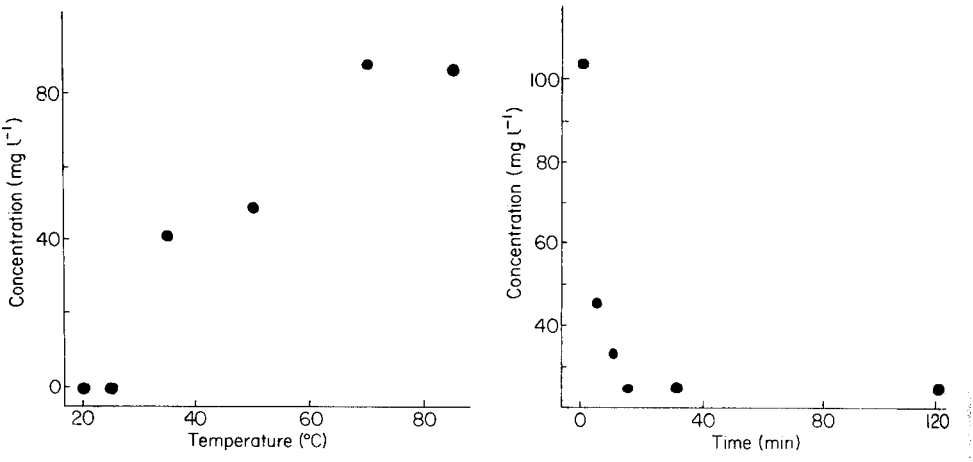

Fig. 3. Dependence of peak current of 50 mg l^{-1} daminozide in 2 M NaOH on hydrolysis temperature. All samples were heated for 15 min at the specified temperature.

Fig. 4. Time-dependent concentration of daminozide in contact with 0.5%(w/w) crospovidone. Initial concentration was 104.2 mg l^{-1}.

a lower peak current but rather a fairly constant response. This indicates that volatilization does not take place to any appreciable degree under the experimental conditions. It was discovered that addition of succinic acid to standard solutions of UDMH in 2 M sodium hydroxide resulted in a drastic decrease in peak current. For example, addition of 60 mg l^{-1} succinic acid to 30 mg l^{-1} UDMH yielded a peak current ca. 60 times less than that of the original UDMH solution. Additionally, the peak width and magnitude of baseline current were significantly larger. This experiment confirmed the inhibitory effect of succinic acid on the UDMH peak current.

The linearity of response was examined for daminozide standard solutions under the optimal hydrolysis conditions. The response, found to be linear in the 5—200 mg l^{-1} range, obeyed the following equation:

$$i_p = (2.34 \pm 0.02)C - (1.46 \pm 2.13)$$

with current in nanoampère and concentration in mg l^{-1}. The correlation coefficient and standard error of estimate were 0.997 and 3.82 nA, respectively. The detection limit, defined as the analyte concentration which yields a peak current twice that of the noise level, was found to be ca. 2 mg l^{-1}. While variation of the square-wave frequency can be used to increase sensitivity in reversible and quasi-reversible systems [9], increase of the frequency did not significantly increase the resulting peak current in this case. This was due to the presence of succinic acid which reduced the anodic electrolysis limit and gave a baseline current with steeper slope. Thus, 15 Hz represented a compromise between somewhat lower sensitivity and superior noise and baseline characteristics.

The precision of response was examined for two different situations. First, a single solution (20 mg l^{-1} daminozide) was hydrolyzed and scanned eight times. The average current was 49.13 ± 2.1 nA. All uncertainties are reported at ±2 standard deviations. For the second case, the average current for eight separate solutions containing 21 mg l^{-1} daminozide was 57.12 ± 5.8 nA.

Unlike various spectrophotometric methods currently used to quantify daminozide, the proposed method does not suffer from interferences caused by species which contain amino or nitro functional groups. However, hydroxylamine, some substituted hydrazines, and various hydrazides have similar oxidation potentials [6] and will cause interference. Hydroxylamine is a particularly strong interferent because of its high diffusion constant.

Assay of daminozide in apples

The proposed method was adapted for the assay of daminozide in apples. Initial attempts to quantify daminozide in alkaline extracts of pulverized apple samples were unsuccessful because of interference from the matrix components. It was therefore necessary to use steam distillation of the hydrolysis mixture in order to separate and concentrate UDMH. Locally purchased apples were prepared and processed by the method of Edgerton et al. [3] and by the proposed procedure. Values obtained for Red Delicious apples with the present method (2.0 and 2.1 mg kg^{-1}) agreed well with those obtained with the published method [3] (2.2 and 2.2 mg kg^{-1}). The latter is based on reaction with 12-molybdophosphoric acid, with absorbance measurements at 825 nm, and has a limit of detection of 1.0 mg kg^{-1}. The content of daminozide in McIntosh apples was below the limit of detection of either method. Typical recovery of daminozide from spiked samples (at the 3 mg kg^{-1} level) was 85—89%. Although the proposed method cannot be used for such samples without steam distillation, very low detection limits are possible because of the removal of succinic acid and the matrix components. Signal enhancement (by increasing the square-wave frequency to 100 Hz) provided a detection limit of 0.1 mg kg^{-1} daminozide in apples.

Once the proposed method had been validated, it was used to measure the removal of daminozide from aqueous solution by crospovidone. Crospovidone is commonly used in the beer and wine industries as a clarifying agent. Examination of the structure of daminozide suggested that there was a strong possibility of adsorption by crospovidone. Initially, solutions containing 117 mg l^{-1} daminozide and various quantities of crospovidone were stirred for 2 min and sampled. In this experiment, it was observed that daminozide could be reduced to undetectable levels by crospovidone levels of $\geqslant$1%(w/w). In order to evaluate the capacity of crospovidone for daminozide, 0.5%(w/w) slurries of crospovidone in 104.2 mg l^{-1} daminozide solution were sampled over a 2-h period. The removal of daminozide with time is shown in Fig. 4. The initial concentration of daminozide was reduced to ca. 24 mg l^{-1} at times $\geqslant$15 min. From these data, the adsorption capacity was calculated to be 16.2 mg of daminozide per gram of crospovidone. The surface loading can

be estimated by determining the surface area occupied by one daminozide molecule and the available surface area (BET) of the adsorbate. The surface area of the daminozide molecule, using CPK space-filling models, was estimated to be 56.2 $Å^2$. Considering the low surface area of crospovidone (ca. 1 $m^2 g^{-1}$), the calculated coverage is 34 times greater than a monolayer. This calculation assumes a close-packing model at the adsorbate/solution interface. The result suggests multilayer adsorption where physical adsorption of daminozide takes place on top of a strongly adsorbed (chemisorbed) primary layer [10]. This is certainly possible considering the likelihood of daminozide undergoing hydrogen bonding with the adsorbate and itself.

The author thanks A. M. Yacynych for use of the CPK space-filling model and for helpful discussions, and K. Ianniello for assistance in sample preparation.

REFERENCES

1 Environmental News, United States Environmental Protection Agency, Office of Public Affairs (A-107), Washington DC, January 22, 1986.
2 Daminozide Method 1(a), Pesticide Analytical Manual, Vol. II, Pesticide Reg. Sec. 180.246, 1975.
3 L. J. Edgerton, M. L. Rockey, H. Arnold and D. J. Lisk, J. Agric. Food. Chem., 15 (1967) 812.
4 P. E. Iversen and H. Lund, Anal. Chem., 41 (1969) 1322.
5 S. Karp and L. Meites, J. Am. Chem. Soc., 84 (1962) 906.
6 J. A. Harrison and Z. A. Khan, J. Electroanal. Chem., 28 (1970) 131.
7 U. Eisner and E. J. Gileadi, J. Electroanal. Chem., 28 (1970) 81.
8 L. Meites and P. Zuman, CRC Handbook of Organic Electrochemistry, Vol. II, CRC Press, Cleveland, OH, 1977, p. 106.
9 E. J. Zachowski, M. Wojciechowski and J. Osteryoung, Anal. Chim. Acta, 183 (1986) 47.
10 A. W. Adamson, Physical Chemistry of Surfaces, 3rd edn., Wiley, New York, 1976, p. 395.

Analytica Chimica Acta, 193 (1987) 87—96
Elsevier Science Publishers B.V., Amsterdam — Printed in The Netherlands

GLUCOSE SENSOR BASED ON A FIELD-EFFECT TRANSISTOR WITH A PHOTOLITHOGRAPHICALLY PATTERNED GLUCOSE OXIDASE MEMBRANE

Y. HANAZATO*, M. NAKAKO, M. MAEDA and S. SHIONO

Central Research Laboratory, Mitsubishi Electric Corporation 1-1, Tsukaguchi-Honmachi 8-Chome, Amagasaki, Hyogo 661 (Japan)

(Received 27th August 1986)

SUMMARY

A photopolymer solution consisting of polyvinylpyrrolidone and 2,5-bis(4'-azido-2'-sulfobenzal)cyclopentanone is used to make a patterned glucose oxidase membrane for a FET-glucose sensor by photolithography. A small patterned glucose oxidase membrane, 0.2 mm wide and 1 mm long, is made on the gate surface of an ISFET by developing a photocross-linked glucose oxidase membrane with aqueous 1—3% glutaraldehyde solution. The optimum composition of the enzyme/photopolymer solution is described. The sensor with the patterned membrane showed linear response to glucose concentration from 0.3 to 2.2 mM and useful response up to 5 mM.

Increasing interest has been shown in biosensors based on semiconductor technology, because of the possibility of producing cheap, small and multifunctional sensors. A hydrogen ion-sensitive field-effect transistor (FET) is most widely used as the electronic device for signal transduction for this type of sensor. In general, an enzyme membrane is placed over the gate surface of an ion-selective FET (ISFET) which senses a change in hydrogen ion concentration caused by an enzyme-catalyzed reaction. Enzyme-modified ISFETs have been proposed for the determination of some organic compounds, e.g., penicillin [1], urea [2—4] and glucose [5—7].

It is only recently that multifunctional FET sensors, made by depositing different enzyme membranes on an integrated ISFET having several hydrogen ion-sensitive FET elements, have been shown to provide simultaneous determinations of several compounds. Advances in semiconductor technology have made it possible to fabricate a miniature and/or integrated ISFET, but the methods for depositing an immobilized enzyme membrane so far developed still have problems: the procedures are expensive and time-consuming, and there is considerable practical difficulty in forming a small membrane on a definite area of an integrated ISFET. Miyahara et al. [8] and Kimura et al. [9] formed micropools with photoresist over ISFET gates by using a photolithographic technique, and injected enzyme-immobilizing solutions into these pools from microsyringes.

0003-2670/87/$03.50

Wen et al. [10] proposed a new method for making a small patterned ion-sensitive membrane on a chemically-sensitive semiconductor device in order to produce an ion sensor. They used a commercially available negative photoresist to deposit an ion-conducting polymer membrane doped with an organic ion-carrier (valinomycin) by this photolithographic technique. This photodefinability was thought to be suitable for producing a miniaturized, multifunctional ion-sensing device.

Attempts have been made to apply this photodefinability to immobilized enzyme membranes. Because enzymes may be denatured by organic solvents, a water-soluble photopolymer is preferable for making patterned immobilized enzyme membranes. In previous work [4], photosensitive poly(vinyl alcohol) (PVA) bearing stilbazolium groups (negative photopolymer) [11–13] was used to form immobilized glucose oxidase and urease membranes over the gate surface of an ISFET; these membranes were made without using the photolithographic technique.

In this report, a water-soluble photocross-linkable polymer was used to make a patterned glucose oxidase membrane on the ISFET by photolithography. This photopolymer is more promising than the photosensitive PVA because the preparation of a photopolymer solution and optimization of the composition of the photopolymer mixture are easier. The optimum conditions for making a patterned glucose oxidase membrane and its performance as a glucose sensor are described.

EXPERIMENTAL

Materials

Glucose oxidase (type IX, from *Aspergillus niger*, 29.3 U mg^{-1}) and bovine serum albumin (BSA) were obtained from Sigma Chemical Co. Glutaraldehyde was used as a 25% solution in water (Ishizu Pharmaceutical Co., Osaka, Japan). Polyvinylpyrrolidone (PVP); m.w. ca. 360 000; extra-pure reagent grade) was purchased from Nakarai Chemicals (Kyoto, Japan), and 2,5-bis(4′-azido-2′-sulfobenzal)cyclopentanone (BASC) was obtained from Tokyo Ohka Kogyo Corp. (Kanagawa, Japan). All other reagents were of analytical grade and were used as received. Distilled/deionized water was used throughout for the preparation of samples, buffer and other solutions.

Sensor construction

An integrated ISFET with a chip size of 5.0 × 6.5 mm was fabricated on epitaxially grown silicon wafers [10-mm diameter; *p*-type epitaxial layer, 8–12 ohm cm, ca. 10 μm thick, *n*-type substrate, 5–7 ohm cm with (100) orientation] by using a conventional *n*-channel MOS process. The gate insulator was composed of a thermally grown silicon oxide layer, 50 nm thick, and a silicon nitride layer deposited by low-pressure chemical-vapour deposition. The silicon nitride layer, which also acted as the proton-sensitive gate material, was 70 nm thick. The ISFET had a lightly-doped *n*-channel

(0.04 X 1 mm) produced by a phosphorus ion-implant before the growth of the gate oxide layer to provide depletion-mode operation. The sensitivity of this ISFET was ca. 50 mV per decade.

The structure of the FET glucose sensor is illustrated in Fig. 1. An integrated ISFET chip was mounted on an epoxy laminate board with gold-plated copper tracks. After electrical connections had been made between the contact pads on the chip and the gold-plated copper tracks with an ultrasonic wire bonder (West Bond, Anaheim, CA; type 7400), the chip was encapsulated with an epoxy resin to provide electrical insulation for the bonding wires and the exposed-side silicon region of the ISFET chip. The composition of the epoxy resin was 100 parts of DER-332 (Dow Chemical Japan Corp., Tokyo), 88 parts of an acid anhydride HN-5500 hardener (Hitachi Chemical, Tokyo), 0.4 parts of 2,4,6-tris(dimethylaminoethyl)-phenol as catalyst (Wako Pure Chemicals, Osaka), and 10 parts of fine silicon oxide powder (Japan Aerosol, Tokyo). A gold electrode as a pseudo-reference electrode was formed on the reverse of the epoxy laminate board. The ISFET surface was silanized with 3-aminopropyltriethoxysilane to improve the adhesion between the surface and the enzyme-containing membrane by the aqueous silanization technique [14].

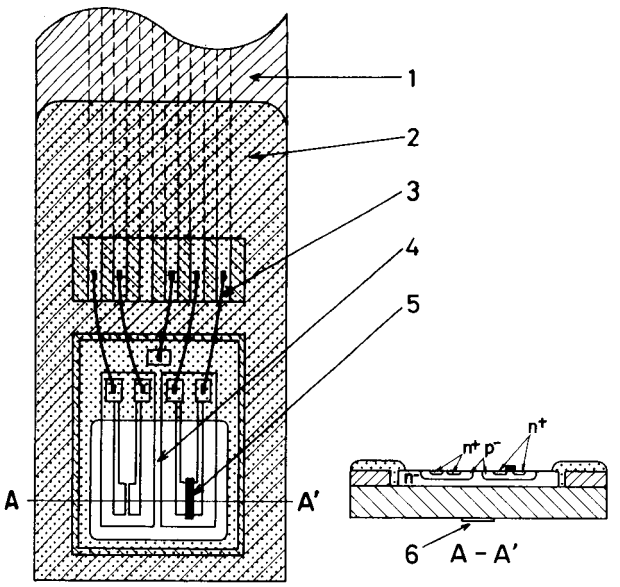

Fig. 1. Structure of the FET-glucose sensor: (1) epoxy laminate board; (2) epoxy resin; (3) aluminium wire; (4) integrated ISFET chip; (5) patterned glucose oxidase membrane; (6) gold electrode.

Glucose oxidase membrane

Glucose oxidase (10 mg) and 10 mg of BSA were dissolved in 0.2 ml of a photopolymer solution (100 parts by volume of water, 10 parts of PVP and 1 part of BASC). This solution was placed dropwise over the exposed gate area of the ISFET electrode illustrated in Fig. 1. The solution-covered area of the ISFET was placed 2 cm away from the rotational centre of the spinner (Kyowa-Riken, Tokyo; type K359SD-270). The whole ISFET shown in Fig. 1 was then spun at 2000 rpm for 2 min to make a thin membrane over the gate surface. The membrane was exposed to ultraviolet irradiation (250 W) on a limited area (0.2 × 1 mm) around the gate surface through a Hoya UV-34 filter with exposure equipment (Union Optical Co., Tokyo; Type ST) for 5 s. The treated ISFET was immersed in aqueous 3% (w/w) glutaraldehyde solution for 5 min at room temperature to form the glucose oxidase membrane. After the electrode had been washed with water, it was immersed in 0.1 M glycine for 15 min to terminate the cross-linking reaction by glutaraldehyde.

Apparatus

The flow-through system described in detail earlier [4] was used for evaluating the performance of the glucose sensor. A sensor was set up at the end of the water jacket thermostated at 34°C for all experiments. Washing solutions of 10 mM acetate buffer (pH 5.5) and sample solutions prepared by dissolving the required amounts of glucose in 10 mM acetate buffer were pumped alternately past the sensor by a peristaltic pump at intervals of several minutes. The flow rate was 6 ml min^{-1}.

The drain-source voltage of each ISFET element was set at 3.0 V and the gate voltage at −1.0 V. The substrate silicon was biased at 4.0 V. Each differential output voltage between the ISFETs without and with the enzyme membrane was measured by the source-follower mode circuit (constant drain-source voltage and constant drain-current mode) as depicted in Fig. 2. The enzyme-membrane thickness was measured with a stylus instrument (Tencor Instruments, Mountain View, CA; type Alpha-Step 100).

RESULTS AND DISCUSSION

Glucose oxidase/photopolymer composition

The PVP/BASC photopolymer was insoluble in water after it had been exposed to u.v. irradiation. The photopolymerized membrane was transparent and showed good adhesion to the surface of the silicon oxide layer of the silicon wafer. However, when glucose oxidase was added to this polymer solution, the dried membrane over the silicon wafer obtained after spin-coating was found to have an uneven surface and was not transparent. Additionally, the photopolymerized membrane spontaneously peeled away from the silicon oxide surface; this might be caused by the swelling of the photocross-linked membrane in aqueous solution. Thus it

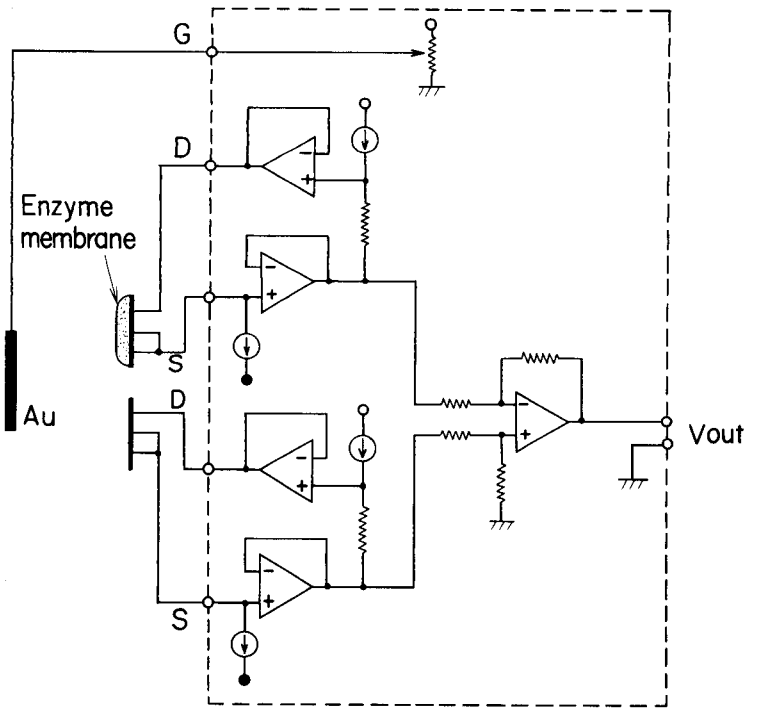

Fig. 2. Measuring circuit for the FET-glucose sensor; the output voltage is obtained as the differential output voltage of each ISFET element.

was found to be impossible to make a photocross-linked glucose oxidase membrane on a silicon oxide layer by the sole use of this photopolymer. As in the case of photosensitive PVA, glucose oxidase was immobilized by use of a PVP-BASC photopolymer which showed good adhesion to the silicon oxide layer when the chemical cross-linking reaction of glucose oxidase and BSA with glutaraldehyde was used in addition to the photo-cross-linking reaction by BASC.

A glucose sensor with two discrete ISFET chips, as illustrated in Fig. 3, was used in preliminary experiments to establish the optimum composition of the enzyme solution, without photolithographic patterning of the enzyme membranes. A glucose oxidase membrane was formed over the whole surface of one ISFET by several methods. In the first, enzyme solution was coated on the ISFET surface by the method described in the Experimental section. In the second, the coated membrane was photopolymerized by u.v. irradiation over the whole surface of one ISFET. In the third, the membrane was immersed in 25% glutaraldehyde solution for chemical cross-linking of glucose oxidase and BSA with glutaraldehyde. In the fourth, after the membrane had been washed by water, it was immersed in 0.1 M glycine to terminate the cross-linking reaction.

It has been shown [4] that at least 10 mg of BSA in 0.2 ml of photopoly-

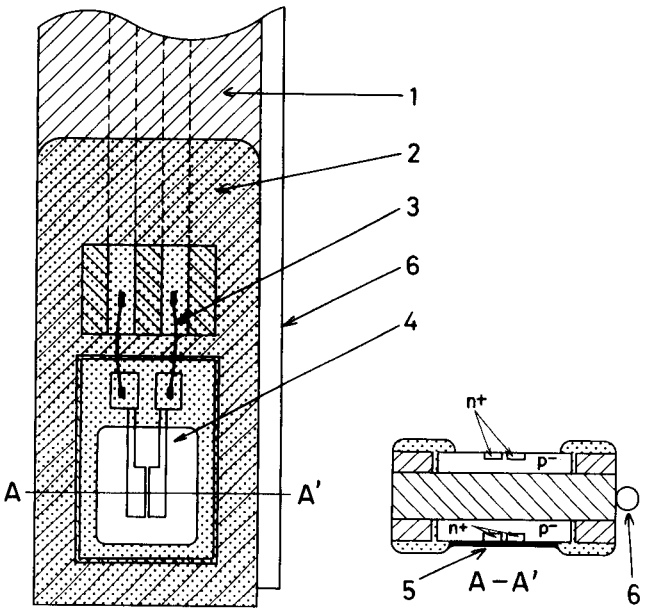

Fig. 3. Structure of the discrete type of glucose sensor used in preliminary experiments to establish the optimum composition of enzyme/photopolymer solution: (1) epoxy laminate board; (2) epoxy resin; (3) aluminium wire; (4) ISFET chip; (5) glucose oxidase membrane; (6) platinum electrode.

mer solution is necessary to make an immobilized glucose oxidase membrane. The concentration of BSA was therefore held at 10 mg in 0.2 ml of the PVP/BASC photopolymer solution in all experiments. The response of the glucose sensor increased with increase in the content of glucose oxidase. Solutions containing $\leqslant$10 mg of glucose oxidase in 0.2 ml of photopolymer solution provided thin uniform membranes on spin-coating, but solutions containing >10 mg of glucose oxidase were too viscous to be coated uniformly over the ISFET surface. The upper limit of glucose oxidase was concluded to be 10 mg in 0.2 ml of photopolymer solution.

The effect of the concentration of BASC on the response of the glucose sensor was also investigated. For solutions consisting of 100 parts of water, 10 parts of PVP and x parts of BASC (with 10 mg each of glucose oxidase and BSA per 0.2 ml), the responses when 1.7 mM glucose was passed through the cell for 5 min at 34°C were 1.94, 5.35 and 10.4 mV for x = 0.2, 0.5 and 1.0, respectively. For $x \geqslant 1.5$, the enzyme/photopolymer solution separated into two phases. Thus the photopolymer solution containing 1 part of BASC was best for making the glucose oxidase membrane.

The enzyme/photopolymer solution described in the Experimental section was used to prepare a discrete glucose sensor, and its performance was evaluated. The calibration graph is shown in Fig. 4. The sensor is suitable for determining glucose between 0.3 and 3 mM. The long-term stability of the sensor is depicted in Fig. 5. The sensor was stored in 10 mM acetate

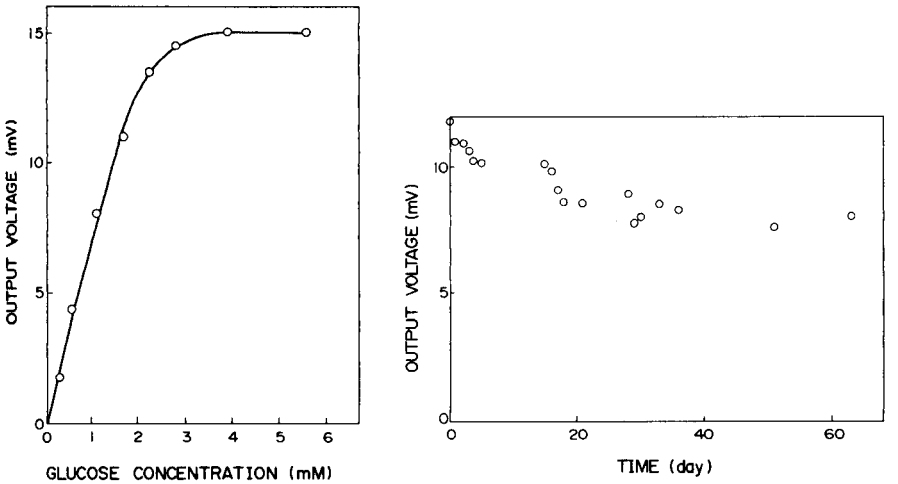

Fig. 4. Calibration graph for discrete glucose sensor prepared without use of photolithography (34°C, pH 5.5).

Fig. 5. Long-term stability of discrete glucose sensor used in Fig. 4. The output voltage indicates the response to 1.7 mM glucose (for conditions, see text).

buffer (pH 5.5) in a refrigerator when not in use. The responses gradually decreased over the first 20 days and then became reasonably constant at ca. 60% of the initial response. The initial decrease is presumably due to enzyme leakage from the membrane.

Photolithographically-patterned glucose oxidase membrane

After u.v. irradiation of the limited area of the dried enzyme membrane which was obtained from spin-coating of the enzyme/photopolymer solution described above on the silicon oxide layer of a silicon wafer, water was first tested as the developer to obtain photolithographically-patterned glucose oxidase membranes. A patterned membrane could be formed, but the membrane thus obtained often peeled off, partially or completely from the surface. To overcome this problem, glutaraldehyde solutions (1—25% w/w) in water were examined as the developer, and were found to be suitable. Strong adhesion was achieved by using 1—3% glutaraldehyde solutions as developer. Typical patterned membranes obtained after development in 2% glutaraldehyde solution are shown in Fig. 6. The membranes are observed as black rectangular shapes in the photograph. This improved adhesion was thought to be due to the higher cross-linking density of the membrane given by the chemical cross-linking reaction of proteins with glutaraldehyde. When the membrane was developed by >5% glutaraldehyde solutions, even membranes which had not been exposed to u.v. irradiation became insoluble in water, and a thin membrane was observed under the microscope over the whole silicon oxide layer on the silicon wafer. The development of the membrane

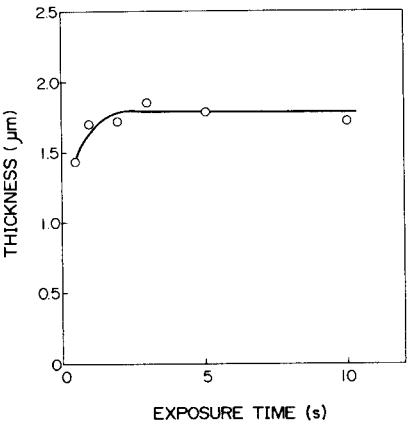

Fig. 6. Photograph of typical patterned glucose oxidase membranes. Widths are 0.1 mm (right side) and 0.2 mm (left side). The membranes were developed with 2% glutaraldehyde solution at room temperature.

Fig. 7. Effect of exposure time on membrane thickness.

with 1—3% glutaraldehyde solution was also thought to give rise to a thin layer containing glucose oxidase over the whole surface of the ISFET, but the response of the reference ISFET to 1.7 mM glucose was found to be negligible.

The effect of the exposure time on the membrane thickness is depicted in Fig. 7. The membrane thickness was measured from the profile of a patterned glucose oxidase membrane with a stylus instrument. This figure indicates that an exposure time longer than 2 s gives a patterned membrane of constant thickness. However, a rectangular-patterned membrane tended to have halation at its side edge after u.v. irradiation for >10 s. The effect of the exposure time on the response of the glucose sensor with a patterned membrane was also examined; the results indicated that at least a 2-s exposure time is desirable for obtaining a constant response and that glucose oxidase is not inactivated by u.v. irradiation for <10 s. Accordingly, an exposure time of 5 s is recommended for making a patterned glucose oxidase membrane.

The performance of the FET-glucose sensor

Figure 8A shows the calibration graph obtained for glucose. The steady-state response was achieved after 2 min. The output voltage shows a linear response to glucose concentration up to 2.2 mM but it saturates at glucose concentrations exceeding 5 mM. Because the oxidation reaction catalyzed by glucose oxidase requires dissolved oxygen, the concentration of dissolved oxygen influences the output voltage of the glucose sensor. The influence of the dissolved oxygen concentration on the output voltage of the sensor is

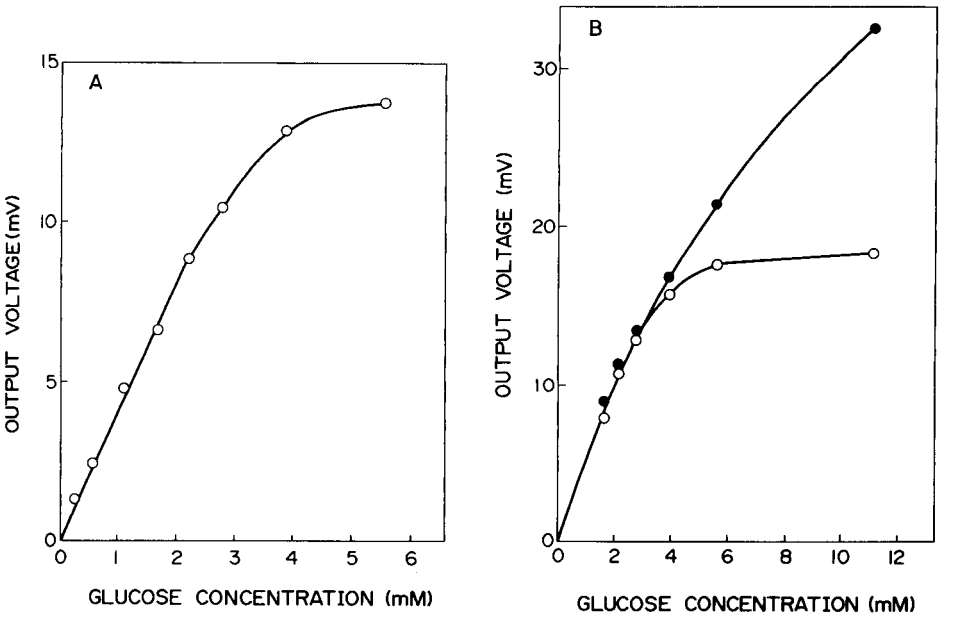

Fig. 8. Calibration graphs for the FET-glucose sensor prepared with use of photolithography: (A) 0—6 mM glucose; (B) 1.7—11 mM glucose. (○) Air-saturated conditions; (●) pure oxygen-saturated conditions. (34°C, pH 5.5.)

depicted in Fig. 8B. Almost the same responses are obtained up to 3 mM glucose for air- or oxygen-saturated solutions. However, above 3 mM, the responses under oxygen-saturated conditions are larger. These results suggest that insufficient dissolved oxygen restricts the response at ca. $\geqslant 5$ mM glucose, when this type of sensor is used under air-saturated conditions.

Compared with the calibration graph in Fig. 4, the graph for the sensor with a patterned membrane (Fig. 8A) shows lower sensitivity but a higher glucose concentration before the response becomes saturated. These differences between the two calibration graphs are mainly due to the amount of glucose oxidase immobilized in the membranes. The thickness of the photo-cross-linked membrane decreased during development in the dilute glutaraldehyde solution, therefore the amount of glucose oxidase immobilized in the developed membrane also decreased in comparison with that immobilized in an undeveloped membrane.

The long-term stability is shown in Fig. 9. The FET-glucose sensor was stored in a water jacket thermostated at 34°C, with 10 mM acetate buffer (pH 5.5) flowing through at 6 ml min^{-1} (under the same conditions as those used to measure the glucose concentration). The response to 2.2 mM glucose gradually decreased to 50% of the initial response after 15 days. Peeling of the patterned glucose oxidase membrane from the ISFET surface was not

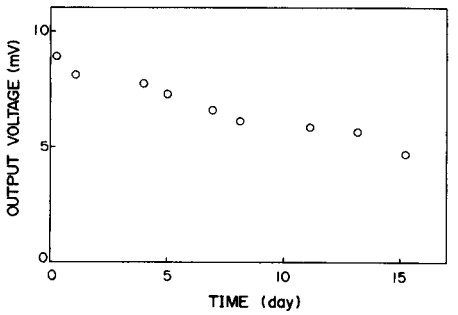

Fig. 9. Long-term stability of the FET-glucose sensor used in Fig. 8 (for conditions, see text).

observed, so the decrease in sensitivity could have been due to thermal or bacterial degradation of glucose oxidase or leakage from the membrane.

The authors are grateful to Mr. Miyazawa for supplying the BASC and for valuable discussions.

REFERENCES

1 S. Caras and J. Janata, Anal. Chem., 52 (1980) 1935.
2 Y. Miyahara, F. Matsu, T. Moriizumi, H. Matsuoka, I. Karube and S. Suzuki, Proc. Int. Meeting Chem. Sensors, Fukuoka, September 19—22, 1983, p. 501.
3 J. Anzai, Y. Ohki, T. Osa, H. Nakajima and T. Matsuo, Chem. Pharm. Bull., 33 (1985) 2556.
4 Y. Hanazato, M. Nakako and S. Shiono, IEEE Trans. Electron Devices, (1986) 47.
5 Y. Hanazato and S. Shiono, Proc. Int. Meeting Chem. Sensors, Fukuoka, September 19—22, 1983, p. 513.
6 M. J. Eddowes, D. G. Pedley and B. C. Webb, Sensors and Actuators 7 (1985) 233.
7 S. D. Caras, D. Petelenz and J. Janata, Anal. Chem., 57 (1985) 1920.
8 Y. Miyahara, T. Moriizumi and K. Ichimura, Sensors and Actuators, 7 (1985) 1.
9 J. Kimura, T. Kuriyama and Y. Kawana, Third Int. Conf. on Solid-State Sensors and Actuators (Transducers '85), Philadelphia, PA, 1985, Digest of Technical Papers, p. 152.
10 C. C. Wen, I. Lauks and J. N. Zemel, Thin Solid Films, 70 (1980) 333.
11 K. Ichimura and S. Watanabe, J. Polym. Sci. Polym. Chem. Ed., 18 (1980) 891.
12 K. Ichimura and S. Watanabe, Polym. Sci. Polym. Chem. Ed., 20 (1982) 1419.
13 K. Ichimura, J. Polym. Sci. Polym. Chem. Ed., 22 (1984) 2817.
14 S. P. Colowick and N. O. Kaplan, in K. Mosback (Ed.), Methods in Enzymology, Academic Press, New York, Vol. 44, 1976, p. 139.

Analytica Chimica Acta, 193 (1987) 97—105
Elsevier Science Publishers B.V., Amsterdam — Printed in The Netherlands

FREQUENCY PROPERTIES OF A PIEZOELECTRIC QUARTZ CRYSTAL IN SOLUTIONS AND APPLICATION TO TOTAL SALT DETERMINATION

YAO SHOU-ZHUO* and MO ZHI-HONG

Institute for New Material Research, Department of Chemical Engineering, Hunan University, Changsha (People's Republic of China)

(Received 21st May 1986)

SUMMARY

For an integrated circuit oscillator, the slope of the linear portion of the frequency shift/electrolyte concentration plot for an AT-cut quartz piezoelectric crystal immersed in a solution is dependent on the circuit capacitance, decreasing from positive to negative values with increasing capacitance. The slope does not vary significantly with the kind of salt. A method based on the frequency measurement is suggested for the rapid determination of the total salt content of natural waters.

Piezoelectric quartz crystals are mostly used for determining minute amounts of substances in gaseous media. Recently, they have also been used for determinations in liquids, for which quantitative knowledge of crystal behavior in solutions is required. Nomura and Nagamune [1] reported the frequency shift in potassium chloride solutions up to 2 mM and showed that, for an oscillator constructed with an integrated circuit (i.c.), the frequency shift decreased with increasing specific conductance of the solution, whereas it increased when a transistorized oscillator was used. The dependence of frequency shift on salt concentration, specific conductance and temperature was also reported recently by Nomura and Watanabe [2]. It was of interest to establish if their results are generally valid and to find the reasons for such a fundamental difference between these two oscillators in the same electrolyte. The results are reported in this present paper.

EXPERIMENTAL

Apparatus and reagents

The piezoelectric quartz crystals used were 9-MHz AT-cut crystals (12.5-mm diameter) having silver electrodes (6-mm diameter) on each side (JA-5 model; Peking Factory No. 707). The crystal holder was directly connected to an oscillator constructed with the integrated circuit shown in Fig. 1. The oscillator supply was a d.c. voltage regulator (JY-30B model; Shijiazhong Electronic Factory No. 4); the i.c. working voltage was set at 5 V. Crystal, crystal

0003-2670/87/$03.50

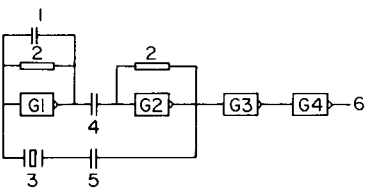

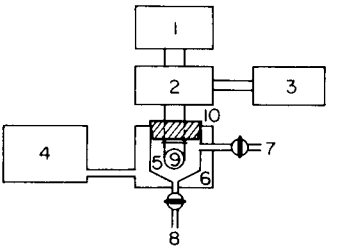

Fig. 1. Oscillator circuit: (1) 8.2 pF; (2) 470 Ω; (3) piezoelectric crystal (9 MHz, AT-cut, JA-5 model); (4) 1 nF; (5) C_{sc}, 10—120 pF; (6) outlet; (G1—G4) SN 7400 integrated circuit.

Fig. 2. Schematic diagram of the measuring assembly: (1) d.c. voltage regulator; (2) oscillator; (3) digital counter; (4) thermostat; (5) detection cell; (6) water bath; (7) sample solution inlet; (8) waste; (9) piezoelectric quartz crystal; (10) rubber cap.

holder and detection cell (volume 10 ml) were placed in a thermostated water bath (25.0 ± 0.5°C) except where otherwise stated. The frequency change was monitored by a digital frequency counter (SS-3320 model; Shijiazhong Electronic Factory No. 4) as shown in Fig. 2. A conductivity meter (DDS-11 model; Shanghai Analytical Instrument Factory No. 2) was used to measure the specific conductance of the aqueous solution.

All chemicals used were of analytical-reagent grade. Double-distilled water was used throughout.

Procedures

Frequency shift/electrolyte concentration measurement. The crystal, previously washed with water, ethanol and dried, was immersed in water thermostated at 25.0 ± 0.5°C, and the oscillation frequency was measured (F_1). The crystal was next immersed in an electrolyte solution, and the frequency again measured (F). The frequency shift, $\Delta F = F - F_1$, was measured 2 or 3 times, and the mean value was calculated. For all electrolytes, the measurements were made in sequence from more dilute to more concentrated solutions. The procedure was repeated for different capacitance values for capacitor C_{sc} (Fig. 1).

Frequency shift/temperature measurement. The crystal was wholly immersed in a solution heated to ca. 45°C. The detection cell was allowed to cool, and the frequency was recorded at regular temperature intervals over this period. The same procedure was used for a crystal immersed in water. The difference between the frequencies in the solution and in water at the same temperature was calculated, and the mean value obtained from 2 or 3 measurements was plotted against temperature.

Determination of the total salt content in waters. Various waters (river, pond and tap) were tested directly for their salt content using the procedure described for the frequency shift/electrolyte concentration measurement. The salt content was obtained from a calibration graph obtained for salt concentrations of 0.5—4.5 mmol l^{-1}.

RESULTS AND DISCUSSION

Frequency behavior of the crystal in electrolyte solutions

The effect of the concentration of various salts (NaCl, KCl, $NaNO_3$, $KHCO_3$; Na_2SO_4, Na_2CO_3; $CaCl_2$ and $MgSO_4$) on the oscillation frequency of the piezoelectric quartz crystal was investigated at constant temperature and equal depth of immersion with the oscillator built with the integrated circuit. Typical frequency shift vs. concentration plots are shown in Fig. 3. The oscillation behavior of the crystal immersed in hydrochloric acid and sodium hydroxide solutions was also studied. The results showed that, for a given value of the capacitance of C_{sc} and over a certain concentration range, the frequency shift varied linearly with electrolyte concentration. This linearity ranged up to 3—4 mmol l^{-1} for most C_{sc} values and salts tested, while hydrochloric acid and sodium hydroxide solutions yielded smaller linear ranges (up to 0.7—1 mmol l^{-1} for hydrochloric acid and 1.5—2 mmol l^{-1} for sodium hydroxide). Some of the regression equations for the frequency shift vs. concentration relation in the linear range was listed in Table 1.

For all salts tested, the linear slope $d\Delta F/d(\text{conc.})$ did not vary significantly

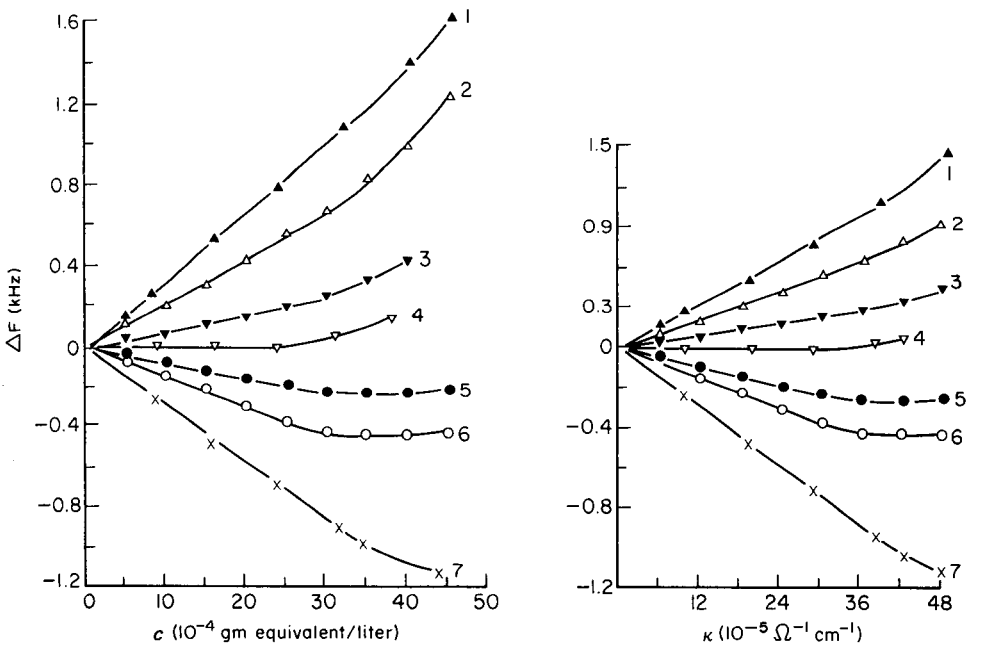

Fig. 3. Frequency shift/concentration dependence for aqueous solutions of sodium chloride at different capacitances of C_{sc}: (1) 10; (2) 12; (3) 14; (4) 15.5; (5) 17; (6) 20; (7) 24 pF.

Fig. 4. Frequency shift/specific conductance dependence for aqueous solutions of sodium chloride at different capacitances of C_{sc}: (1—7) as in Fig. 3.

TABLE 1

Dependence of frequency shift on concentration[a]

Electrolyte		Capacitance C_{sc} (pF)			
		10	12	20	24
NaCl	c	0—40	0—30	0—30	0—35
	ΔF	$35.45c - 31.7$	$21.98c - 6.95$	$-14.05c + 1.79$	$-28.35c - 19.2$
	r	0.9984	0.9510	0.9921	0.9987
$NaNO_3$	c	0—23	0—41	0—32.5	0—32.5
	ΔF	$34.25c - 14.7$	$24.63c - 13.5$	$-18.27c - 17.4$	$-27.98c$
	r	0.9979	0.9959	0.9968	0.9990
Na_2SO_4	c	0—35	0—40	5—20	2.5—25
	ΔF	$38.86c - 26.3$	$23.70c - 14.4$	$-17.50c - 33.5$	$-30.04c - 26.4$
	r	0.9954	0.9939	0.9994	0.9999
$CaCl_2$	c	0—40	0—40	0—30	0—35
	ΔF	$34.91c + 6.13$	$22.34 - 13.0$	$-13.35c - 12.9$	$-29.07c - 17.8$
	r	0.9993	0.9944	0.9971	0.9999
$MgSO_4$	c	0—40	0—28	0—30	0—30
	ΔF	$33.72c + 9.7$	$23.59c - 9.4$	$-16.49c - 23.6$	$-27.00c - 17.8$
	r	0.9938	0.9746	0.9916	0.9973
$KHCO_3$	c	0—30	0—30	0—30	0—30
	ΔF	$34.14c$	$22.98c - 0.5$	$-14.30c - 0.9$	$-28.95c - 1.1$
	r	0.9982	0.9850	0.9970	0.9999
Average slope[b]		35.22 ± 1.88	23.21 ± 0.96	−15.65 ± 2.04	−28.55 ± 1.03
HCl	c	0—7	0.5—7	1—10	1—7
	ΔF	$117.8c + 1.4$	$66.88c - 21.4$	$-47.83c + 31.2$	$-81.38c + 37.0$
	r	0.9995	0.9961	0.9995	0.9989
NaOH	c		0—15		0—15
	ΔF		$56.78c - 51.6$		$-61.38c + 42.9$
	r		0.9925		0.9985

[a] c: concentration range ($\times 10^{-4}$ mol l^{-1}) for the linear regression. ΔF: frequency shift (Hz). r: correlation coefficient (5 points). [b] $\Delta F/dc$ in Hz/10^{-4} mol l^{-1}.

with different kind of salts, e.g. it was 232.1 ± 9.6 Hz/mmol l^{-1} when C_{sc} = 12 pF, or −285.5 ± 10.3 Hz/mmol l^{-1} when C_{sc} = 24 pF. However, hydrochloric acid and sodium hydroxide yielded much greater slopes. This was found to be true for different oscillators, with different values of capacitance for C_{sc}. Nevertheless, the capacitance of C_{sc} significantly affected the value and even the sign of the linear slope for a given electrolyte. All electrolytes tested yielded a series of linear plots with different slopes which decreased from positive through zero to negative values with increasing capacitance. The frequency shift increased with increasing electrolyte concentration when the capacitance of C_{sc} was smaller than a critical value (in this case ca. 16 pF, Fig. 5) whereas it decreased when C_{sc} had a greater value. At the

TABLE 2

Dependence of frequency shift on specific conductance[a]

Electrolyte		Capacitance C_{sc} (pF)			
		10	12	20	24
NaCl	κ	0.13—29.4	0.13—30.5	0.13—36.6	0.13—39.0
	ΔF	$26.71\kappa - 3.4$	$18.07\kappa - 9.6$	$-11.56\kappa + 2.1$	$-23.33\kappa - 5.0$
	r	0.9998	0.9905	0.9921	0.9989
$NaNO_3$	κ	0.13—28.2	0.13—48.9	5.3—48.9	5.3—48.9
	ΔF	$27.88\kappa - 11.0$	$20.96\kappa - 8.5$	$-13.58\kappa - 19.3$	$-23.37\kappa + 3.0$
	r	0.9986	0.9964	0.9848	0.9989
Na_2SO_4	κ	0.13—32.7	0.13—7.2	6.9—43.4	6.9—37.2
	ΔF	$28.39\kappa - 24.1$	$16.22\kappa - 2.1$	$-12.28\kappa - 4.2$	$-23.78\kappa - 5.7$
	r	0.9989	0.9930	0.9985	0.9994
$CaCl_2$	κ	0.13—44	0.13—44	0.13—23	0.13—23
	ΔF	$27.72\kappa - 8.5$	$17.68\kappa - 4.8$	$-11.36\kappa - 6.7$	$-24.20\kappa + 5.6$
	r	0.9993	0.9957	0.9969	0.9975
$MgSO_4$	κ	0.13—30.5	0.13—30.5	0.13—30.5	5.4—30.5
	ΔF	$28.31\kappa + 8.9$	$19.28\kappa - 13.3$	$-12.83\kappa - 10.6$	$-24.26\kappa - 17.3$
	r	0.9953	0.9976	0.9704	0.9987
$KHCO_3$	κ	0.13—22.8	0.13—22.8	0.13—22.8	0.13—22.8
	ΔF	$28.66\kappa - 3.6$	$17.71\kappa - 1.7$	$-11.77\kappa + 1.5$	$-23.82\kappa + 8.9$
	r	0.9991	0.9899	0.9965	0.9997
Average slope[b]		27.95 ± 0.70	18.32 ± 1.62	−12.09 ± 0.62	−23.79 ± 0.39
HCl	κ	2.13—29.5	2.13—42.1	4.25—42.1	4.25—42.1
	ΔF	$27.90\kappa + 1.1$	$18.33\kappa - 6.3$	$-11.37\kappa + 3.9$	-20.15κ
	r	0.9994	0.9918	0.9995	0.9983
NaOH	κ		0.13—24.2		12.2—48.7
	ΔF		$20.60\kappa + 7.2$		-26.13κ
	r		0.9949		0.9999

[a] κ: specific conductance. The range given (in 10^{-5} Ω^{-1} cm^{-1}) corresponds to the linear regression (r measured from 5 results). [b] $\Delta F/d\kappa$ in $Hz/10^{-5}$ Ω^{-1} cm^{-1}.

critical capacitance, the frequency shift did not vary significantly with electrolyte concentration over the initial linear range, but it tended to increase with increasing electrolyte concentration beyond this range.

The variation of the frequency shift with the specific conductance of the electrolyte solution over the linear range of the frequency shift/specific conductance (κ) relation is summarized in Table 2. It is seen that hydrochloric acid and sodium hydroxide yield $d\Delta F/d\kappa$ slopes which do not differ significantly from those of the salt electrolytes. This indicates that the variation of frequency shift with electrolyte concentration is mainly due to its variation with the specific conductance, and the above conclusions derived for the frequency shift/concentration relations are largely also valid for the frequency

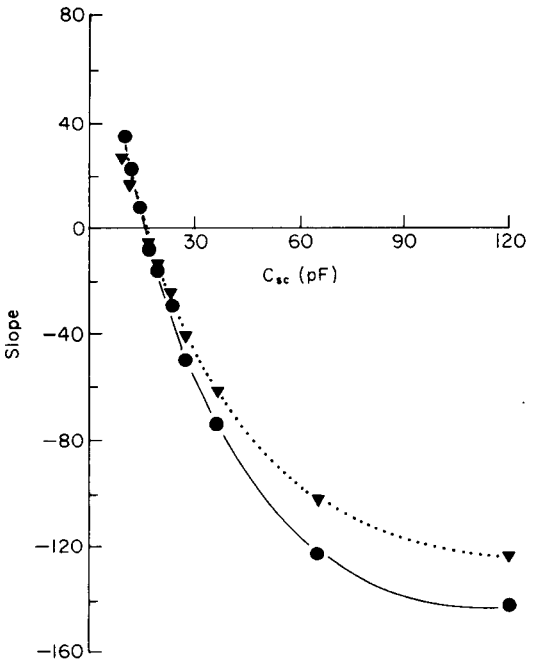

Fig. 5. Influence of the capacitance of C_{sc} on the slope of the linear dependences for electrolyte solutions: (1) $d\Delta F/d(\text{conc.})$ (Hz/10^{-4} mol l^{-1}); (2) $d\Delta F/d\kappa$ (Hz/10^{-5} Ω^{-1} cm^{-1}).

shift/specific conductance dependences. Typical frequency shift/specific conductance plots are shown in Fig. 4.

Figure 5 shows the plots of linear slope for $d\Delta F/d(\text{conc.})$ and $d\Delta F/d\kappa$ vs. capacitance of C_{cs}. They are all parabolic, and there is a critical value of C_{sc} of ca. 16 pF where the slope $d\Delta F/d(\text{conc.})$ or $d\Delta F/d\kappa$ is zero. The slopes shown in Fig. 5 were taken from average values calculated by linear regression for the different electrolytes mentioned above.

The results obtained by Nomura and co-workers [1, 2] for potassium chloride solutions, therefore, only indicate what occurs when the capacitance of C_{sc} is greater than the critical value, where the integrated circuit gives different results from the transistorized circuit. When C_{sc} has a value below the critical value, no such difference is likely to be observed.

Effect of temperature

The above results were obtained at constant temperature, and it was of interest to check the influence of temperature on the crystal frequency in water and electrolyte solutions. It was found that the frequency shift was significantly influenced by the temperature and increased linearly with increasing temperature, e.g., 67 ± 2 Hz/°C for 0.01 mol l^{-1} hydrochloric acid.

When the temperature of the liquid in which the crystal was immersed decreased to a definite critical temperature, the oscillation frequency of the crystal abruptly doubled. This was observed for both pure water and electrolyte solutions. The critical temperature was found to vary with the capacitance of C_{sc} but not with the type and concentration of the salt. For example, for a crystal immersed in pure water and C_{sc} of 10, 12 and 14 pF, the critical temperatures were 11.0, 5.5 and 0.1°C, respectively, while for a 10-pF capacitor, the critical temperature of the same crystal immersed in 1—4 mmol l^{-1} sodium chloride or magnesium sulfate was in the region 10.9—11.2°C. Therefore, it is important if the crystal is to operate properly that it should be used at a temperature higher than the critical temperature.

Determination of salt content

Preliminary experiments showed that the main ions in the natural waters tested were Ca^{2+}, Na^{+}, Mg^{2+}, K^{+}, Cl^{-}, SO_4^{2-}, HCO_3^{-}, and/or CO_3^{2-}, and NO_3^{-} in lesser amounts. The specific conductance was 50—400 $\mu\Omega^{-1}$ cm^{-1}, equivalent to 0.4—3.3 mmol l^{-1} sodium chloride, which is within the linear range of the frequency shift/concentration plot. As the value of the calibration slope does not vary significantly for different salts, and it would be rare for the water to contain a strong acid or base, which does not behave in the same way as the salts, it is possible to determine the salt content of natural waters by measuring the frequency shift. Tests with mixtures of the main ions contained in natural waters at a constant total concentration of salts showed the feasibility of such a suggestion. At a given total (equivalent) concentration of salts, a frequency shift was obtained which varied insignificantly with the relative proportions of the individual salts. Results for a total salt concentration of 2 mmol l^{-1} are listed in Table 3. For all the C_{sc} capacitances tested, the relative error ranged from 2.9 to 7.8% (calculated in terms of sodium chloride).

Natural waters from different sources were analyzed for their total salt content, with a calibration graph based on sodium chloride, which had the following equation (C_{sc} = 24 pF):

$$c_{NaCl}\ (\text{mmol}\ l^{-1}) = -0.35\ \Delta F(\text{Hz}) + 6.77$$

The total salt concentration was calculated from the frequency shift measured. The results (Table 4) were in good agreement with the conductance method for which the following equation was derived:

$$c_{NaCl}\ (\text{mmol}\ l^{-1}) = 8.306\kappa\ (10\ \mu\Omega^{-1}\ cm^{-1}) - 1.39$$

In order to check the accuracy of the method, standard sodium chloride solution was added to the sample solution; the recovery was found to be 99.4—100.9%.

As the crystal can oscillate continuously in electrolyte solutions, it can be expected to be useful for the continuous survey of the salt content of water.

TABLE 3

Additivity test for various salt mixtures and C_{sc} capacitances of 10—14 pF

Sample No.	Salts added (10^{-4} mmol l^{-1})						ΔF(Hz), for C_{sc} (pF)			
	$NaNO_3$	KCl	$KHCO_3$	Na_2CO_3	$MgSO_4$	$CaCl_2$	10	14	20	24
1	5	—	5	—	5	5	650 ± 3	—	—	−639 ± 4
2	—	5	—	5	5	5	—	136 ± 5	−320 ± 2	—
3	2.5	—	5	—	2.5	10	650 ± 3	—	—	−627 ± 5
4	—	2.5	—	2.5	5	10	—	134 ± 8	−316 ± 4	—
5	2.5	—	10	—	2.5	5	630 ± 3	—	—	−613 ± 6
6	—	2.5	—	10	2.5	5	—	128 ± 6	−322 ± 4	—
7	5	—	2.5	—	10	2.5	651 ± 3	—	—	−632 ± 5
8	—	2.5	—	5	10	2.5	—	138 ± 5	−317 ± 5	—
9	10	—	2.5	—	5	2.5	676 ± 3	—	—	−667 ± 4
10	—	10	—	2.5	2.5	5	—	157 ± 5	−297 ± 5	—
Average ± 95% confidence limits							651 ± 20	139 ± 13	−314 ± 12	−636 ± 25
Total salt content, calculated as NaCl[a]							19.3 ± 0.6	18.5 ± 1.5	22.5 ± 0.9	21.6 ± 0.9

[a]From the equations: $c(10^{-4}$ mol $l^{-1}) = 0.0282\Delta F$(Hz) + 0.894 (for C_{sc} = 10 pF); $c = 0.1119\Delta F + 2.944$ (for C_{sc} = 14 pF); $c = -0.0712\Delta F + 0.127$ (for C_{sc} = 20 pF); $c = -0.035\Delta F - 0.677$ (for C_{sc} = 24 pF).

TABLE 4

Determination of salt content of natural waters (C_{sc} = 24 pF)

Sample		Sampling date	κ (10^{-5} Ω^{-1} cm^{-1})	ΔF (Hz)	Conc. found[a] (10^{-4} mol l^{-1})	
					Conduct.	Freq. shift
Pond	1	25 Dec.	17.3	−401 + 5	11.8	14.2
water	2	28 Dec.	21.8	−590 + 5	17.2	18.0
River	1	24 Dec.	36.0	−1071 + 8	30.6	29.8
water	2	28 Dec.	34.1	−990 + 5	28.5	28.2
Tap	1	27 Dec.	28.4	−782 + 5	22.6	23.4
water	2	28 Dec.	28.3	−780 + 3	22.5	23.4
	3	29 Dec.	28.9	−795 + 4	23.0	23.9

[a]Calculated as NaCl.

This work was supported by the National Science Fund.

REFERENCES

1 T. Nomura and T. Nagamune, Anal. Chim. Acta, 155 (1983) 231.
2 T. Nomura and M. Watanabe, Anal. Chim. Acta, 175 (1985) 107.

Analytica Chimica Acta, 193 (1987) 107—118
Elsevier Science Publishers B.V., Amsterdam — Printed in The Netherlands

FORMATION OF TWO REACTION ZONES IN FLOW-INJECTION SYSTEMS FOR KINETIC DETERMINATIONS OF COBALT AND NICKEL

ALFONSO FERNANDEZ, M. DOLORES LUQUE DE CASTRO and MIGUEL VALCÁRCEL*

Department of Analytical Chemistry, Faculty of Sciences, University of Córdoba, Córdoba (Spain)

(Received 4th April 1986)

SUMMARY

The injection of a large sample volume (ca. 1 ml) into a single-channel flow-injection system was studied with a dye (to examine physical dispersion) and with chemical systems having easily-controlled reaction rates (to examine chemical kinetics). With the dye, the response curve has a central plateau caused by non-mixing of carrier and sample. When a chemical reaction takes place, two peaks are obtained with a central minimum corresponding to little or no mixing and reaction. Comparison of these two types of response provides relationships of analytical interest between response parameters and variables in the flow-injection system. The configuration is used for individual kinetic determinations of cobalt and nickel (2.5—30 μg ml^{-1}) based on the rate of their complex formation with 2-hydroxybenzaldehyde thiosemicarbazone. Sample injection rates were 15 h^{-1} for cobalt and 40 h^{-1} for nickel. Differential kinetic determinations of cobalt and nickel in mixtures are based on the increment in peak height (or area) between the two peaks obtained for each injection; sample throughput is 7 h^{-1}.

Among the different methods of flow injection analysis (f.i.a.) described for obtaining several plugs or reaction zones which reach the detection point at different times, the simplest is possibly that which utilizes a multiple injection system. The units making up this system can be located in parallel or in series in the flow configuration. In the first examples, different lengths of channels into which each solution is injected and the confluence of such channels prior to the detector are needed to achieve sequential detection [1—4]. When the injection loops are located in series, the length of the channel linking then fulfills the same function [5]. When a single injection technique is applied, greater ingenuity in designing the configuration is required in order to obtain several signals. This may or may not require splitting of the injected sample. If the sample is split, two peaks are obtained provided that there is a confluence point for two channels (with different geometric characteristics) prior to the detector [6—8], or two flow cells aligned in the same optical path [9, 10] or if the reference and sample cells in a double-beam spectrophotometer are used [7, 9]. A cyclic

0003-2670/87/$03.50

flow-injection system which produces one signal each time the sample zone passes through the detector, until it has mixed homogeneously with the carrier [11—13], is an example of a system with a single injection and no splitting point.

The injection of an analyte into a single-channel system through which a reagent is being pumped results in the formation of two reaction zones at the two sample/reagent interfaces, which normally evolve as the sample passes through the system in such a way that on passing through the detector they provide a typical peak. If a very large sample volume is used, however, it is possible to obtain two separate reaction zones, and so two peaks, as the sample plug passes through the detector, because little or no reagent/sample mixing has occurred at the center of the sample zone. This simple way of generating sequential peaks which involves neither a splitting point nor a cyclic system and which is described in this paper, has been considered only by Painton and Mottola [12] to study the rate of double peak formation, but these authors did not exploit this phenomenon for analytical purposes. Previously the phenomenon had been observed in the normal flow-injection mode [13, 14] and, especially, on injection of reagent into a sample stream [15]. Here, the physical behavior of this system is studied by using a dye, and the comparative influences of dispersion and reaction rate are then discussed. The usefulness of this configuration is demonstrated by applying it to the individual kinetic and differential kinetic determinations of cobalt and nickel, based on the formation of their complexes with 2-hydroxybenzaldehyde thiosemicarbazone (HBAT). The different formation rate constants for these complexes (0.092 s^{-1} and 0.221 min^{-1} for nickel and cobalt, respectively [7]) allows the applicability of the system to be demonstrated over a wide range of reaction rates as well as to the resolution of mixtures by differential kinetic measurements.

EXPERIMENTAL

Reagents

A bromocresol green stock solution was prepared by dissolving 0.400 g of the dye in 25 ml of 95% ethanol and diluting to 100 ml with 0.01 M sodium tetraborate. The working solution was prepared by mixing exactly 1 ml of the stock solution with 199 ml of the 0.01 M borate. The carrier stream for the dispersion studies was 0.01 M sodium tetraborate.

A stock ethanolic solution of HBAT (0.05%) and stock (1.00 g l^{-1}) cobalt and nickel standards were prepared. The carrier stream (pH 5.2) for studying the nickel/cobalt system was a mixture of the stock solution of HBAT, 0.1 M acetic acid + sodium acetate buffer solution, pH 5.1, and distilled water (1:1:3 by volume).

Apparatus

A Perkin-Elmer Lambda-1 spectrophotometer equipped with a Hellma 178.12-QS flow cell (inner volume 18 μl) was used. A Perkin-Elmer 575

spectrophotometer, equipped with flow cells of the same type and with a Peltier system for control of the temperature, was used when temperature control was important, as in the kinetic measurements. Gilson Minipuls-2 and Ismatec S-840 peristaltic pumps, a Tecator L100-1 injection valve, Beckman 3500 pH meter, and Selecta-S 382 thermostat were also used.

A Hewlett-Packard HP-85 microcomputer with built-in tape cartridge drive was equipped with an HP-IB interface with which an HP-3478 multimeter was connected to the spectrophotometers. The integrator used was a Hewlett-Packard 3392A. The methods of data collection and treatment provides a print-out of the characteristic parameters of the responses, as shown in Fig. 1 and defined in Table 1. The criteria adopted for writing the program were as follows: (1) the travel time, t_A, is obtained from the first point at which the absorbance, A, exceeds $Y = 0.05$ (Y being the mean of the first ten absorbance values measured after injection); and (2) the T_1 and T_2 values correspond to the first point at which the absorbance is greater or smaller than 98% A_{max}.

RESULTS AND DISCUSSION

The single-channel manifold used requires only the simple components depicted in Fig. 2. The injection of a large sample volume into this configuration gives the concentration profile shown in Fig. 2, consisting of two mixing (reaction) zones in the leading and tailing regions of the injected samples and a central non-mixing zone (where no reaction occurs).

Two clearly different behaviors can be observed depending on whether or not there is a chemical reaction between the carrier and sample. The

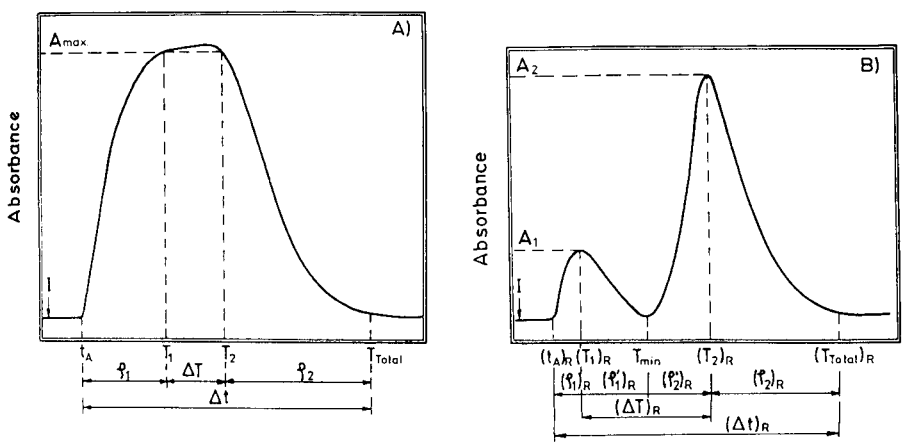

Fig. 1. Recordings obtained from the concentration profile of a very large sample, together with the characteristic parameters: (A) without chemical reaction (injection of a dye); (B) with chemical reaction (formation of a colored complex).

TABLE 1

Definitions of the important characteristic parameters of the responses in f.i.a.

Symbol	Definition
Without chemical reaction	
t_A	travel time
T_1, T_2	time at the onset and end of the plateau
T_{total}	time elapsed from injection to the return to the baseline
ρ_1, ρ_2	intervals between t_A and T_1 and between T_2 and T_{total}, respectively
ΔT	plateau width (interval between T_1 and T_2)
Δt	baseline-to-baseline time
With chemical reaction	
$(t_A)_R$	travel time
$(T_1)_R$, $(T_2)_R$	residence time for the first and second peak, respectively
T_{min}	interval from injection to the minimum
$(T_{total})_R$	time elapsed from injection to the return to the baseline after the second peak
ρ_1, ρ_1', ρ_2', ρ_2	interval between $(t_A)_R$ and $(T_1)_R$, $(T_1)_R$ and T_{min}, T_{min} and $(T_2)_R$ and $(T_2)_R$ and $(T_{total})_R$, respectively
$(\Delta T)_R$	interval between the appearance of the maxima ($(\Delta T)_R = T_2 - T_1$)
$(\Delta t)_R$	baseline-to-baseline time
$(A_{max})_1$, $(A_{max})_2$	absorbance at the maximum of the first and second peaks.

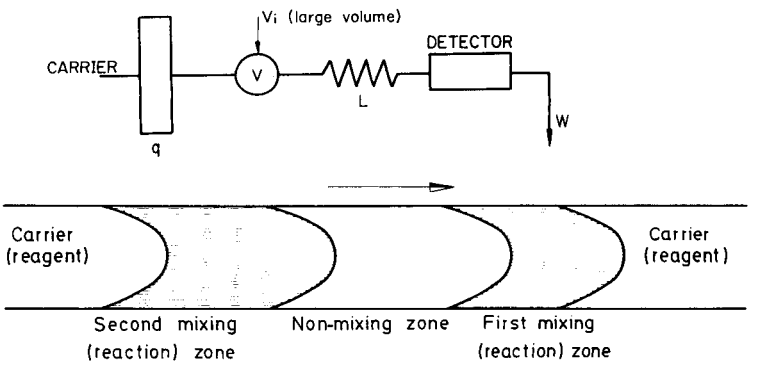

Fig. 2. Manifold used, and profile obtained for the injected sample on its passage through the detector.

injection of an inert dye simply results in the formation of two zones of varying absorbance at the head and tail of the plug, with the non-mixing zone yielding a plateau of constant absorbance (Fig. 1A). If the injected sample reacts with the carrier and the product formed is suitably monitored, the above mixing zones yield two peaks in the initial and final regions and a minimum in between (Fig. 1B). The characteristic parameters which define the response are shown in Fig. 1B and are defined in Table 1.

Physical behavior of the system

The behavior of a dye (bromocresol green) in the manifold shown in Fig. 2 was first studied by changing the injection volume, V_i, between wide limits (127—3354 μl). Later, other variables (flow rate, q; reactor length, L; dye and ethanol concentrations; temperature, etc.) were investigated for two injection volumes (2027 and 527 μl) which yielded responses with or without well-defined plateaux, respectively.

The results showed that the influence of the reactor length, flow rate, and dye and ethanol concentrations were similar for both sample volumes. Changes in the injected volume or temperature and the use of a single-bead-string reactor [16] had different effects. As would be expected, the travel time, t_A, increased linearly with the reactor length and the reciprocal of the flow rate; it also increased, but only slightly, on inserting a single-bead-string reactor, and was unaffected by the injected volume, temperature and ethanol concentration. Because t_A does not change with injected volume, previously described equations [17, 18] can be applied to this flow-injection system for calculating t_A. The baseline-to-baseline time, Δt, remained virtually constant with the reactor length but increased with the reciprocal of the flow rate and injected volume. It is noteworthy that the changes in dye concentration only affect the absorbance parameters of the recording, while the temporal parameters are unchanged.

Because the most important feature of this configuration is that it provides a central unmixed zone, data treatment was aimed at evaluating the conditions required for its formation (a minimum injected volume, V_{min}, which is influenced by the flow rate). Figure 3 shows the effect of the flow-injection variables V_i and q on the plateau time, ΔT. It varies linearly with the injected volume and with the reciprocal of the flow rate, but does not change with the coil length, L. The increase in plateau width can be expressed by

$$\Delta T_1 - \Delta T_0 = k_1 [(V_i)_1 - (V_i)_0] / q \quad (1)$$

where ΔT_0 is the plateau time corresponding to the injection of V_0, and ΔT_1 that corresponding to the injection of V_1. The value of k_1, which is the product of the slope of the straight lines $m = \Delta T / \Delta V$ and flow rate, expressed as μl s^{-1}, was calculated to be 0.644 ± 0.015 (where 0.015 is the standard deviation for 15 measurements).

For a volume $V_0 = V_{min}$ with $\Delta T_0 = 0$, Eqn. 1 becomes

$$\Delta T = k_1 [V_i - V_{min}] / q \quad (2)$$

The V_{min} value (μl) is linearly dependent on the flow rate. The equation representing this behavior was found to be $V_{min} = 845 + 9.75\ q$, where q is expressed in μl s^{-1}; the regression coefficient (r^2) was 0.990.

The study of the regions before and after ΔT (ρ_1 and ρ_2, respectively) provides interesting information on the behavior of the system ρ_1 is always smaller than ρ_2 (this is also true for their relative responses to changes of the

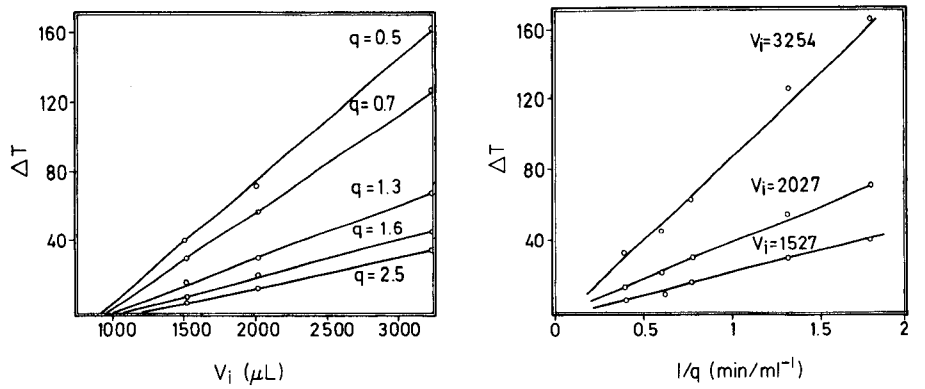

Fig. 3. Influence of the injected volume, V_i, and reciprocal of the flow rate, $1/q$, on the plateau width, ΔT, for the response obtained without chemical reaction.

different variables). The variable which exerts the strongest influence on these parameters is the flow rate; its effect was found to be governed by the expressions

$$\rho_1 = 3.67 + 57.00\, q \quad (r^2 = 0.997)$$

$$\rho_2 = 47.90 + 70.98\, q \quad (r^2 = 0.980)$$

where q is expressed in ml min^{-1}.

Effect of a chemical reaction

When the formation of a reaction product is monitored in the present flow-injection system, two peaks are obtained corresponding to the two mixing zones, where reaction can occur, and a minimum where there is little or no mixing and reaction. Figure 1B shows the profile and parameters defining such a response. Parameters similar to those in Fig. 1A are denoted by subscript R.

The chemical systems chosen for study were the formation of the complexes of nickel and cobalt with 2-hydroxybenzaldehyde thiosemicarbazone (HBAT), which occur at different rates, but which can both be monitored at 400 nm. The formation of the cobalt complex is slow because it is preceded by oxidation of cobalt(II) to cobalt(III), which is a slow step with a rate influenced by pH [7].

In order first to study the diffusion of the complexes, so that this can be distinguished from chemical effects, previously prepared solutions of cobalt and nickel complexes with HBAT were injected. Figure 4 shows the response under such conditions (dashed line) for cobalt compared to the system involving chemical reactions at different rates (continuous lines). Because the concentration of the monitored product did not influence the temporal parameters, an arbitrary concentration of the complex was used in the comparison.

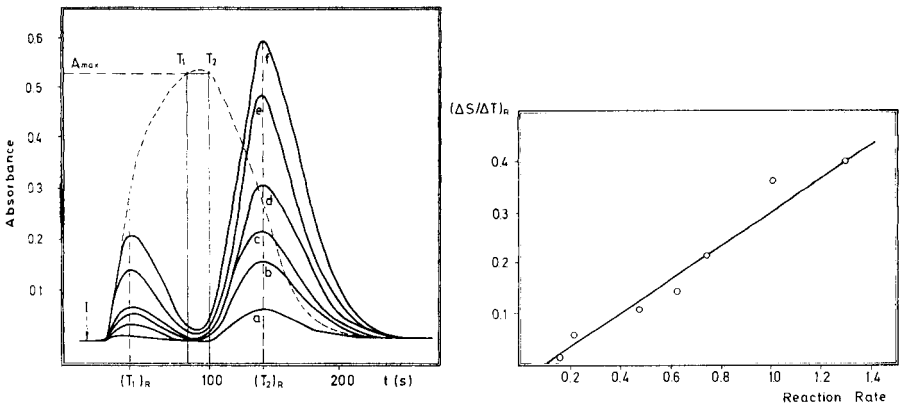

Fig. 4. Influence of the reaction rate on the response from the cobalt—HBAT system. The dashed line corresponds to the system without chemical reaction (injection of the complex). Curves: (a) pH 4.8 (apparent rate constant 0.215 min^{-1}); (b) pH 5.0 (0.475 min^{-1}); (c) pH 5.2 (0.632 min^{-1}); (d) pH 5.4 (0.735 min^{-1}); (e) pH 5.6 (1.050 min^{-1}); (f) pH 5.8 (1.300 min^{-1}).

Fig. 5. Relation between the apparent overall rate, $(\Delta A/\Delta T)_R$ with T in $minutes^{-1}$, and the reaction rate of a chemical system obtained with the proposed configuration.

It is essential to know the value of $(\Delta T)_R$, the time between peak maxima, when a chemical reaction occurs, because its value provides information on peak separation or overlap and, hence, on the measurement time for every peak. The fact that this parameter is unaffected by changes in the reaction rate or in the reagent/sample concentration ratio or temperature, is the key to the use of the flow-injection configuration in kinetic determinations. There is a linear variation of $(\Delta T)_R$ with V_i and $1/q$; however, it scarcely varies with L. The relationship may be expressed as:

$$(\Delta T)_{R_1} - (\Delta T)_{R_0} = k_2[(V_i)_1 - (V_i)_0]/q \quad (3)$$

When $(V_i)_0 = (V_{min})_R$, $(\Delta T)_{R_0}$ becomes zero and Eqn. 3 simplifies to

$$(\Delta T)_R = k_2[V_i - (V_{min})_R]/q \quad (4)$$

The value of the proportionality constant, k_2, calculated as in the preceding section, was 1.072 ± 0.040.

The apparent overall rate, defined as the ratio between the increase in absorbance between the two peaks and the interval between their maxima $(\Delta A/\Delta T)_R$, is directly derived from the parameters of the response. It is of practical interest because it is linearly related to the reaction rate, as shown in Fig. 5. The $(\Delta A/\Delta T)_R$ ratio increases with increasing pH, reagent concentration, temperature, injected volume and flow rate (in the last case because of the sharper decrease in ΔT than in ΔA with q). Changes in length L do not modify the apparent overall rate.

A qualitative comparison between the responses obtained in the presence

and absence of a chemical reaction allows several conclusions to be drawn. First, $(V_{min})_R < V_{min}$, because the plateau is obtained only if there is a non-mixing zone, whereas the formation of the two peaks requires only less mixing in the central region than at some points at both ends (Fig. 6). V_{min} coincides with the $(V_i)_R$ value needed to obtain zero absorbance at the minimum. Secondly, for identical experimental conditions, the responses obtained show that the plateau width, ΔT, does not coincide with the interval between peaks, $(\Delta T)_R$, that the plateau overlaps with the zone of the minimum in which the absorbance is zero, and that part of the second peak obtained when a reaction takes place, lies outside the envelope of the response obtained in the absence of chemical reaction, owing to the increase in the dispersion as a result of concentration changes caused by the reaction. The initial slope and t_A, however, are virtually identical with and without reaction.

Individual kinetic determinations of cobalt and nickel

One of the applications of this approach is the development of kinetic determinations based on the direct relationship between the apparent reaction rate $(\Delta A/\Delta T)_R$ and the analyte concentration. In this way reaction

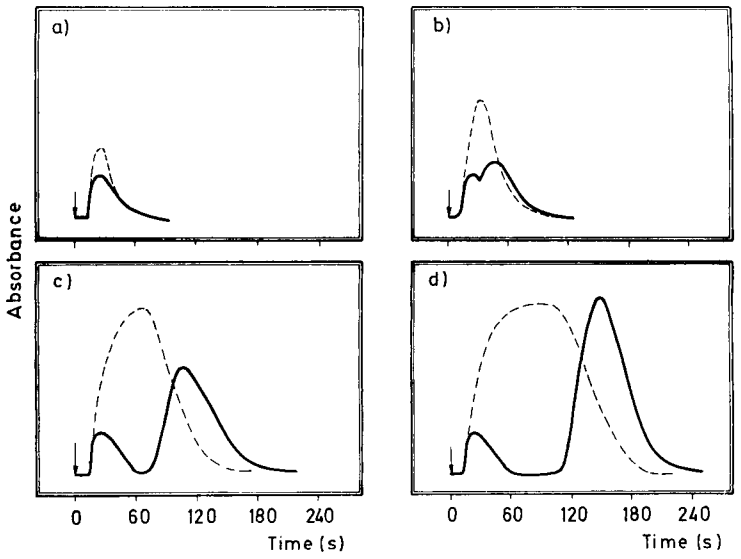

Fig. 6. Influence of the injected volume on the response from the system with (—) and without (---) chemical reaction. In every case, $V_{min} > (V_{min})_R$. $(V_{min})_R$: (a) 227; (b) 527; (c) 1527; (d) 2527 µl.

rates are exploited without use of more complex configurations. The only disadvantage of this methodology is the increased sample consumption.

The cobalt and nickel complexes of HBAT were chosen to establish the precision and reliability of this method of kinetic determinations, in view of their different formation rate constants and the great potential for manipulating the overall reaction rate through the effect of pH on the cobalt reaction.

With the aid of the modified simplex method [19] and the configuration outlined in Fig. 2, the chemical variables were optimized by use of the following response function:

$$F = (\Delta A/\Delta T)_R = [(A_2) - (A_1)]/[(T_2)_R - (T_1)_R]$$

where A_2 and A_1 are the maximum absorbance of the last and first peak, respectively. The optimum values found are shown in Table 2. The sample was identical in ethanol and buffer composition, and in temperature, with the carrier.

The calibration graphs obtained under the optimum conditions are linear between 2.5 and 35.0 $\mu g\ ml^{-1}$ cobalt and 2.5 and 30.0 $\mu g\ ml^{-1}$ nickel. Calibrations were through an exhaustive statististical study in which eleven different samples per concentration were prepared and each was injected in triplicate. Peak heights and areas were measured. Table 3 shows the main results of this study. The results indicate that the measurement of peak height is to be preferred to that of peak area as it provides an increased sensitivity parameter [20]. The sampling frequency was 15 h^{-1} and 40 h^{-1} for the cobalt and nickel systems, respectively.

Differential kinetic determination of cobalt/nickel mixtures

Another application of this configuration, and perhaps the most important, is the resolution of mixtures based on differential kinetics. The modified simplex method was again applied to the chemical variables (reagent concentration and pH) and flow injection variables (reactor length, injection volume, and flow rate). The temperature and ethanol concentration were kept constant at 25°C and 20%, respectively. The development of the five-variable simplex provided the optimal values listed in Table 2, the response

TABLE 2

Optimal values of variables for cobalt and nickel determinations

	pH	HBAT conc. (%, w/v)	V_i (μl)	L (cm)	q (ml min^{-1})
Individual determination					
Cobalt	5.8	0.018	1.024	275	2.4
Nickel	5.2	0.015	1.024	80	1.0
Differential determination	5.0	0.008	1.224	70	0.6

TABLE 3

Individual kinetic determinations of cobalt and nickel[a]

Peak height measurement		Peak area measurement	
Cobalt			
$\Delta A = (9.25 \pm 2.08\ t) + (13.25 \pm 0.10\ t)\ [Co^{2+}]$		$\Delta Area = (15.12 \pm 60.87\ t) + (11.50 \times 10^2 \pm 15.12\ t)\ [Co^{2+}]$	
$r^2 = 0.997$		$r^2 = 0.991$	
$\mu g\ ml^{-1}$	% r.s.d.	$\mu g\ ml^{-1}$	% r.s.d
2.5	5.5	2.5	5.5
5.0	1.9	5.0	4.4
15.0	1.7	15.0	4.1
25.0	2.1	25.0	4.6
35.0	1.6	35.0	1.6
$\sigma xy = 9.23; S = m/\sigma xy = 1.43$		$\sigma xy = 1.37 \times 10^3; S = m/\sigma xy = 0.84$	
Nickel			
$\Delta A = (31.5 \pm 1.82\ t) + (10.00 \pm 0.11\ t)\ [Ni^{2+}]$		$\Delta Area = (0.78 \pm 0.04\ t) + (0.27 \pm 0.002t)\ [Ni^{2+}]$	
$r^2 = 0.994$		$r^2 = 0.995$	
$\mu g\ ml^{-1}$	% r.s.d.	$\mu g\ ml^{-1}$	% r.s.d.
2.5	3.2	2.5	2.3
5.0	2.8	5.0	4.2
15.0	2.3	15.0	2.2
25.0	2.3	25.0	2.3
35.0	1.1	35.0	1.6
$\sigma xy = 8.16; S = m/\sigma xy = 1.22$		$\sigma xy = 0.185; S = m/\sigma xy = 1.42$	

[a] ΔA in mV; ΔArea in mV s; Student's parameter $t = 2.23$ for $P = 0.05$, $n = 11$. For r.s.d., $n = 11$; σxy is the standard deviation of the mean. S is the sensitivity [20] with m in absorbance/$\mu g\ ml^{-1}$.

function used being $(A_1/A_2)_{Ni}/(A_1/A_2)_{Co}$, which takes into account the kinetic behavior of the two analytes (maximum development of the nickel reaction and minimum for that of cobalt in the first peak and vice versa for the second peak). The data obtained in each experiment were collected on-line and suitably treated.

Calibration graphs for both metals were obtained under the optimal conditions and the additivity of the signals for the two analytes was checked. It was also found that the insertion of a single-bead-string reactor between the injector and detector produced better sample/reagent mixing, which improved the reproducibility and sensitivity by increasing the ratio $m_1^{Ni}\ m_2^{Co}/m_2^{Ni}\ m_1^{Co}$ for the calibration graphs for the analytes at each peak (the linear range was 5.0—50.0 $\mu g\ ml^{-1}$ for each analyte). The additivity of the absorbances allowed the equations listed in Table 4 to be used for the mixture resolution. Results for mixtures also appear in Table 4.

The reproducibility of the method was studied with mixtures of equal and extreme ratios of both analytes, for eleven similar samples in each case.

TABLE 4

Differential kinetic determination of cobalt and nickel
(The equations are: $A_1 = 0.873$ [Co] + 3.49 [Ni] + 1.96
$A_2 = 4.359$ [Co] + 8.35 [Ni] + 12.95.)

Added (μg ml^{-1})		Found[a] (=g ml^{-1})		Error (%)	
Cobalt	Nickel	Cobalt	Nickel	Cobalt	Nickel
5.00	5.00	5.27	5.28	5.4	5.6
10.00	10.00	11.95	9.34	19.5	−6.6
20.00	20.00	18.29 (3.7)	20.64 (2.8)	−8.6	3.2
30.00	30.00	31.92	28.97	6.4	−3.4
40.00	40.00	39.75	39.62	−0.6	−1.0
50.00	50.00	48.54	49.16	−2.9	−1.7
5.00	50.00	5.43	49.63	8.6	−0.8
10.00	40.00	11.04 (2.2)	39.63 (0.9)	10.4	−0.9
20.00	30.00	18.86	30.52	−5.7	1.7
30.00	20.00	28.79	20.30	−4.0	1.5
40.00	10.00	38.56 (3.7)	10.42 (5.9)	−3.6	4.2
50.00	5.00	48.74	5.58	−2.5	11.6

[a]For some mixtures, % r.s.d. (n = 11) is given in parentheses.

The values of the relative standard deviations obtained are also given in Table 4. The sampling frequency was 7 h^{-1}.

Conclusions

The present research is an example of a previously unexplored methodology of f.i.a., implemented in a simple single-channel configuration. It makes use of the intrinsic kinetic-physical character of f.i.a., which has been little exploited for analytical purposes [21]. The simultaneous study of the physical dilution and the chemical kinetics has allowed the behavior of the system in these aspects to be clarified. It has also provided a novel approach to reaction-rate methods, especially for simultaneous differential determinations, which has significant advantages over other continuous-flow procedures designed for the same purpose (stopped-flow, use of several detection points, etc.). The lessening of interferences resulting from kinetic discrimination is another advantage over conventional flow-injection procedures.

This work was supported by the CAICyT under Grant No. 2012-83.

REFERENCES

1 H. Kagenow and A. Jensen, Anal. Chim. Acta, 114 (1980) 227.
2 F. Lázaro, M. D. Luque de Castro and M. Valcárcel, Fresenius' Z. Anal. Chem., 320 (1985) 128.
3 P. Linares, M. D. Luque de Castro and M. Valcárcel, Talanta, 33 (1986) 889.

4 E. A. G. Zagatto, M. F. Giné, E. A. N. Fernandes, B. F. Reis and F. J. Krug, Anal. Chim. Acta, 173 (1985) 289.
5 A. Fernández, M. D. Luque de Castro and M. Valcárcel, Analyst, 111 (1986), in press.
6 A. Fernández, M. A. Gómez-Nieto, M. D. Luque de Castro and M. Valcárcel, Anal. Chim. Acta, 165 (1984) 217.
7 A. Fernández, M. D. Luque de Castro and M. Valcárcel, Anal. Chem., 56 (1984) 1146.
8 P. Linares, M. D. Luque de Castro and M. Valcárcel, Anal. Chem., 57 (1985) 2101.
9 J. W. B. Stewart and J. Růžička, Anal. Chim. Acta, 82 (1976) 137.
10 J. Ruz, A. Ríos, M. D. Luque de Castro and M. Valcárcel, Anal. Chim. Acta, 186 (1986) 139.
11 A. Ríos, M. D. Luque de Castro and M. Valcárcel, Anal. Chem., 57 (1985) 1803; J. Chem. Educ., 63 (1986) 552; Anal. Chim. Acta, 179 (1986) 463.
12 C. C. Painton and H. A. Mottola, Anal. Chim. Acta, 158 (1984) 67.
13 F. J. Krug, J. Růžička and E. H. Hansen, Analyst, 104 (1979) 47.
14 B. Karlberg, P. Johansson and S. Thelander, Anal. Chim. Acta, 104 (1979) 21.
15 A. G. Fogg, Analyst, 111 (1986) 859.
16 J. M. Reijn, W. E. van der Linden and H. Poppe, Anal. Chim. Acta, 123 (1981) 229.
17 J. T. Vanderslice, K. K. Stewart, A. G. Rosenfeld and D. J. Higgs, Talanta, 28 (1981) 11.
18 M. A. Gómez-Nieto, M. D. Luque de Castro, A. Martín and M. Valcárcel, Talanta, 32 (1985) 319.
19 J. A. Nelder and R. Mead, Comput. J., 78 (1965) 308.
20 I. M. Kolthoff and P. J. Elving, Treatise on Analytical Chemistry, 2nd edn., Vol. 1, Part I, Wiley, New York, 1984.
21 H. L. Pardue and B. Fields, Anal. Chim. Acta, 124 (1981) 39.

Analytica Chimica Acta, 193 (1987) 119—125
Elsevier Science Publishers B.V., Amsterdam — Printed in The Netherlands

SIMULTANEOUS DETERMINATION OF METALS IN TWO-COMPONENT MIXTURES WITH 5-SULFO-8-QUINOLINOL BY USING PHASE-RESOLVED FLUORIMETRY

KEITH R. VITENSE and LINDA B. McGOWN*
Department of Chemistry, Oklahoma State University, Stillwater, OK 74078 (U.S.A.)
(Received 15th September 1986)

SUMMARY

Determinations of metals in two-component mixtures are described in which 5-sulfo-8-quinolinol is used to produce fluorescent chelates of the metals. The metal chelates have broad, overlapping fluorescence spectra but the fluorescence lifetimes (τ) of the chelates are sufficiently different to permit phase-resolved fluorimetric determinations in which the fluorescence contributions of the two chelates can be resolved. Average determination errors ranged from —4.1% to 2.1% for each metal chelate in mixtures of zinc and cadmium ($\Delta\tau$ = 1.0 ns), gallium and indium ($\Delta\tau$ = 1.7 ns) and aluminum and gallium ($\Delta\tau$ = 5.3 ns). Limits of detection and determination for each individual metal chelate were found to be three times and five times greater, respectively, for the phase-resolved measurements relative to steady-state measurements under the same experimental conditions. Effects of pH on the fluorescence lifetimes and intensities of the metal chelates were studied.

Most metals are non-luminescent, but many can be determined fluorimetrically via the formation of fluorescent complexes with organic ligands. The wide variety of chelating agents that have been used for the fluorimetric determination of metals has been recently reviewed [1]. Simultaneous multicomponent determinations of metal chelates are often difficult because of the very similar, broad fluorescence spectra obtained for different metals with a given chelating agent. Therefore, the emission- and excitation-wavelength parameters do not provide sufficient selectivity for multicomponent determinations. Fluorescence lifetimes of the metal chelates can, however, be significantly different. A study by Hiraki et al. [2] has demonstrated the use of pulsed-source, time-resolved fluorimetry for the simultaneous determination of metal 5-sulfo-8-quinolinolates. The applicability of fluorescence lifetime selectivity for multicomponent determinations of other metal chelate systems has also been studied, as discussed recently [1].

In recent years, phase-resolved fluorimetry has been used as an alternative to pulsed excitation for multicomponent fluorimetric determinations based on fluorescence lifetime selectivity [3]. In the work described here, phase-resolved fluorimetry was used for the determination of two-component

0003-2670/87/$03.50

mixtures of aluminum and gallium, indium and gallium and zinc and cadmium, using 5-sulfo-8-quinolinol (SQ) as the chelating agent. Phase resolution was accomplished by using a sinusoidally-modulated excitation beam in conjunction with phase-sensitive detection, as has been described elsewhere [3–6].

Phase-resolved fluorescence intensities of mixtures and standards were measured at different sets of wavelength and detector phase-angle conditions to generate an overdetermined series of linear equations which are solved for the concentrations of the two metal-chelate components in the mixtures. This approach has been previously applied to multicomponent determinations of organic compounds [7–9].

The pH and chelating-agent concentration dependences of the steady-state fluorescence intensities and the fluorescence lifetimes of the metal chelates were studied. Limits of detection and quantitation for the individual metal chelates were found for both the steady-state and phase-resolved measurement systems.

EXPERIMENTAL

Materials and solutions

Zinc sulfate (gold label), cadmium sulfate (gold label) and 5-sulfo-8-quinolinol (SQ) were purchased from Aldrich. The perchlorate salts of aluminum, gallium and indium were purchased from G. Frederick Smith Chemicals. Dimethyl-POPOP [1,4-bis-2-(4-methyl-5-phenyloxazol-2-yl) benzene; scintillation grade; Aldrich] was used as the reference fluorophore for fluorescence lifetime determinations (τ_{ref} = 1.45 ns) [10]. Distilled, demineralized water was used for all solutions. Stock solutions of the metal ions (150 μM) were prepared by dissolution and dilution of the appropriate weight of the metal salt with water. A fresh stock solution of SQ (1.25 mM) in water was prepared daily. (Poor results were obtained when older solutions were used.)

Standard solutions of the metal chelates (containing 10.0 μM of the metal) and two-component mixtures of metal chelates were prepared in the cuvette by the addition of the appropriate amounts of metal and SQ stock solutions and of buffer (phosphate or acetate). A buffer concentration of 0.085 M was used in all experiments. It was found that the order in which the reagents were added to the cuvettes was very important. Addition of metal to a solution already containing SQ led to non-linear increases in intensity with analytical concentration of metal. Therefore, reagents were added in the order of buffer, metal, and then SQ.

A series of five solutions was used for each two-component system, with cuvette concentrations of 1.25, 2.50, 5.00, 7.50 and 8.75 μM of one metal and the concentration of the other metal required to bring the total metal concentration to 10.0 μM in each solution. The total SQ concentration in each mixture was 0.100 mM in the cuvette. Six solutions, containing 0, 53.2, 160, 266, 532 and 1060 nM of the metal and 0.100 mM SQ in the cuvette, were used to estimate the detection and quantitation limits.

Data collection

Disposable polyethylene cuvettes (Precision Cells) were used for all fluorescence measurements. Solutions were not deoxygenated prior to measurement. Fluorescence measurements were made with an SLM 4800S phase-modulation spectrofluorimeter (SLM/Aminco, Urbana, IL), as previously described [7—9]. Each intensity measurement was the average of ten samplings performed internally by the instrument over a period of ca. 3 s. Fluorescence-lifetime measurements and phase-resolved intensity measurements were made at an excitation modulation frequency of 30 MHz, with excitation at 373 nm, and slit settings of 16, 0.5 and 0.5 nm for the excitation monochromator entrance and exit and the modulation tank compartment exit, respectively. A 520-nm interference filter (Oriel) was used in the emission beam. The temperature of the fluorimeter sample compartment was maintained at 25° ± 0.1°C with a Haake A81 temperature-control unit.

Procedure for two-component determination

The phase-resolved fluorescence intensities, $F(\phi_D)$, of standards and mixtures were measured at eight detector phase angles (0° to 315°, in 45° intervals). The metal standards (10.0 μM metal and 0.100 mM SQ in acetate buffer) were used to find the molar phase-resolved intensity values, $\bar{I}(\phi_D)$, of the chelates at each detector phase angle. The concentrations (C_1 and C_2) of the two metal chelates in the mixtures were found from the overdetermined series of eight equations (one per detector phase angle) of the form:

$$F(\phi_D)_{mixture} = F(\phi_D)_1 + F(\phi_D)_2 = \bar{I}(\phi_D)_1 C_1 + \bar{I}(\phi_D)_2 C_2 \quad (1)$$

in which the measured $F(\phi_D)$ of the mixture is the sum of the values for the two chelates at the wavelength, detector phase angle and modulation frequency used to generate that particular equation. The raw phase-resolved intensity data were used directly in the eight equations for each determination. As an alternative, a least-squares fit to a cosine function was used to smooth the raw data, and the intensity values for the equations were taken from the smoothed cosine curve. The set of eight linear equations for each determination was solved by a non-negative least squares (NNLS) routine [11], using a Hewlett-Packard 9920U computer which provided solutions to the equations almost instantaneously.

RESULTS AND DISCUSSION

Fluorescence spectra and lifetimes

The steady-state fluorescence emission and excitation spectra of the metal-SQ chelates are broad, relatively featureless, and very similar for the different metals. The excitation and emission maxima for the metal chelates are listed in Table 1.

The fluorescence lifetimes calculated from phase-shift are shown as a function of pH for the SQ chelates of indium, aluminum and gallium in Fig. 1

TABLE 1

Fluorescence characteristics of the metal-SQ chelates

Metal[a]	Maxima (nm)		Relative intensity[b]	Lifetimes (ns)	
	λ_{ex}	λ_{em}		τ_p	τ_m
Al	367	500	1.00	5.80 ± 0.02	9.28 ± 0.04
Ga	370	515	0.78	0.53 ± 0.003	1.18 ± 0.07
In	375	520	1.01	2.23 ± 0.01	2.59 ± 0.04
Cd	373	522	0.59	3.31 ± 0.03	3.73 ± 0.02
Zn	374	525	1.00	2.32 ± 0.02	2.43 ± 0.02

[a]Solutions at pH 4.5 for Al, Ga and In, and pH 5.5 for Cd and Zn. [b]Steady state.

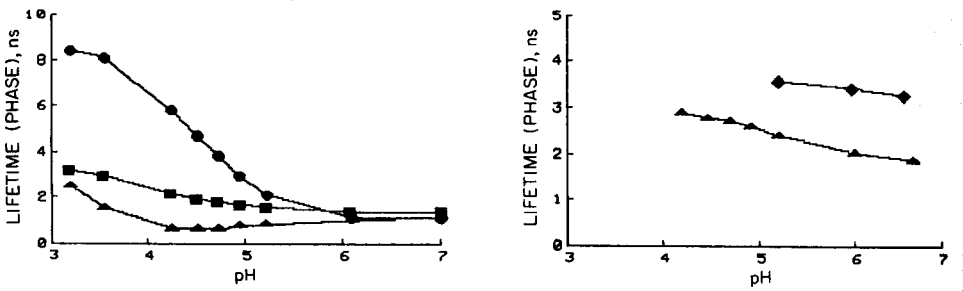

Fig. 1. Fluorescence lifetime (τ_p) as a function of pH for the In (■), Al (●) and Ga (▲) chelates.

Fig. 2. Fluorescence lifetime (τ_p) as a function of pH for the Zn (▲) and Cd (♦) chelates

and of cadmium and zinc in Fig. 2. The Cd-SQ intensities at pH <5 were too low to permit lifetime determinations. The lifetimes calculated from demodulation were within 1—2 ns of those calculated from phase-shift for all of the metal complexes except Al-SQ (see below).

The fluorescence lifetimes calculated from phase-shift (τ_p) and from demodulation (τ_m) of the metal chelates at the pH conditions used for the two-component determinations are listed in Table 1 with standard deviations. The τ_m value of Al-SQ is much longer than the τ_p value at pH 4.5, indicating ground-state heterogeneity, i.e., the presence of more than one fluorescent component. At both lower and higher pH values, the phase and modulation lifetimes tend to converge (at pH 3.21, τ_p = 8.37 ± 0.51 ns and τ_m = 9.9 ± 0.17 ns; at pH 7.00, τ_p = 1.04 ± 0.02 ns and τ_m = 2.14 ± 0.11 ns). Therefore, the heterogeneity at pH 4.5 indicates a mixture of the longer-lived low pH component and the shorter-lived high-pH component.

Fluorescence intensities

The steady-state fluorescence intensities of the SQ chelates as a function of pH in acetate buffer are shown for Al, Ga and In in Fig. 3A and for Zn and Cd in Fig. 3B. The intensities increase with increasing pH except for Al-SQ which has a peak intensity near pH 4.2. The pH effect on intensity is especially pronounced for zinc and cadmium, for which the intensities are very close to zero at low pH.

The fluorescence intensities as a function of the analytical concentration ratio of SQ to metal, were found to level off at ratios in the range of 2—4. For the determination of metals in two-component mixtures, the concentration of SQ was ten times the total metal concentration to ensure an excess of the ligand.

Two-component determinations

The pH used for each two-component system was chosen to combine effectively three factors, including maximum difference in fluorescence lifetime between the components, high intensity and buffering capacity. For Ga/In and Al/Ga mixtures, pH 4.5 was used as a compromise between large lifetime differences at low pH and high intensities at high pH. The Zn/Cd mixtures were used at pH 5.5, some intensity being sacrificed in order to remain in a good buffering range for the acetate buffer. The difference between lifetimes for the Zn and Cd chelates was relatively constant over the pH range studied. Phosphate buffer was tested in early studies to broaden the pH range, but complexation was very sluggish and results were much poorer for phosphate than for acetate buffer, probably because of complexation of these metals with phosphate.

Relative errors with and without signs taken into account are shown in Table 2 for two-component mixtures of Zn and Cd, In and Ga, and Al and Ga. The errors (including signs) for aluminum and gallium are similar to those reported by Hiraki et al. [2] for the same concentration range, but their errors without signs included were approximately three times larger. They were not

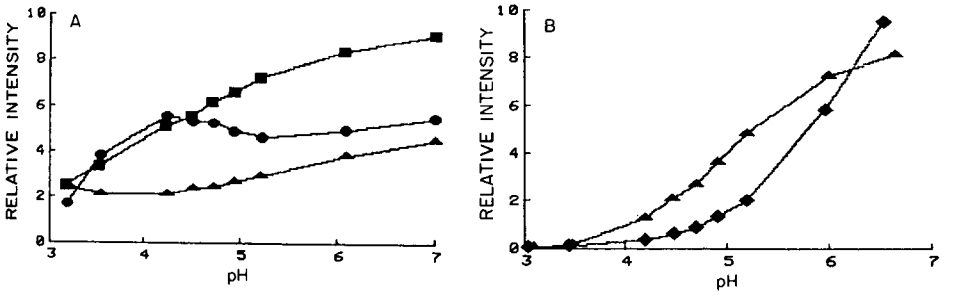

Fig. 3. Steady-state fluorescence intensity as a function of pH: (A) for the In (■), Al (●) and Ga (▲) chelates; (B) for the Zn (▲) and Cd (◆) chelates. The intensity scales are different for each metal.

TABLE 2

Average errors with (E) and without ($|E|$) signs taken into account for two-component mixtures[a]

System	Metal	Errors (%)		$\Delta\phi$[b]
		E	$\|E\|$	
Zn/Cd	Zn	2.1	2.6	11°
	Cd	−1.9	3.3	
Ga/In	Ga	−4.1	4.3	19°
	In	−1.4	1.5	
Al/Ga	Al	−0.9	1.0	44°
	Ga	−1.5	2.1	

[a]Five mixtures per two-component system. [b]Phase difference between components at 30-MHz modulation frequency.

able to obtain simultaneous determinations of Zn/Cd and Ga/In, which have smaller lifetime differences, because of the time-resolution limitations of their instrument. The results shown in Table 2 were obtained by using the raw (unsmoothed) phase-resolved intensity data. No significant improvement was observed when the intensity values were taken from curves fitted with a least-squares cosine fit.

Limits of detection and determination

The limits of detection and determination for the metal chelates of Ga, In and Al were calculated from calibration curves obtained with six solutions (see Experimental). Limits for zinc and cadmium were not examined. The limit of detection was calculated as the concentration of metal chelate required to produce a signal S: $S = S_b + 3s_b$, where S_b is the mean blank signal and s_b is the standard deviation of the blank signal ($n = 16$). The limit of determination was found similarly from $S = S_b + 10s_b$. The limits were calculated both for steady-state and phase-resolved fluorimetry using the pH conditions and wavelength maxima shown in Table 1. The phase-resolved limits were found from phase-resolved intensity measurements at the phase-angle maxima of the chelates ($\phi_D = \phi_{chelate}$). The limits, shown in Table 3, were evaluated in order to compare the inherent loss of signal that occurs in going from steady-state to phase-resolved measurements. Phase-resolved measurements at detector phase angles other than the maximum of the emitter will give intensities that are attenuated by a factor equal to $\sin(\phi_D - \phi_{chelate})$, thereby increasing the detection and determination limits by the same factor. The phase-resolved fluorimetric detection and determination limits were approximately three and five times higher than the steady-state counterparts, but two-component determinations are not feasible with steady-state measurements.

TABLE 3

Limits of detection (LOD) and of quantitation (LOQ) for the metal-SQ chelates

Metal	Concentration limits (nm)			
	Steady-state		Phase-resolved	
	LOD	LOQ	LOD	LOQ
Al	12	18	36	95
Ga	16	25	48	125
In	6	12	20	50

This work was supported by the United States Army Research Office.

REFERENCES

1 A. Fernandez-Gutierrez and A. M. de la Pena, in S. G. Schulman (Ed.), Molecular Luminescence Spectroscopy Methods and Applications: Part 1, Wiley, New York, 1985, Ch. 4.
2 K. Hiraki, K. Morishige and Y. Nishikawa, Anal. Chim. Acta, 97 (1978) 121.
3 L. B. McGown and F. V. Bright, Anal. Chem., 56 (1984) 1400A.
4 T. V. Veselova, A. S. Cherkasov and V. I. Shirokov, Opt. Spectrosc. (U.S.S.R), 29 (1970) 617.
5 J. R. Mattheis, G. W. Mitchell and R. D. Spencer, in D. Eastwood (Ed.), New Directions in Molecular Luminescence, ASTM Special Technical Publication 822, Baltimore, MD, 1983, p. 50.
6 J. R. Lakowicz and H. Cherek, J. Biochem. Biophys. Methods, 5 (1981) 19.
7 L. B. McGown and F. V. Bright, Anal. Chim. Acta, 169 (1985) 117.
8 F. V. Bright and L. B. McGown, Anal. Chem., 57 (1985) 55, 2877.
9 K. Nithipatikom and L. B. McGown, Anal. Chem., 58 (1986) 2469; Appl. Spectrosc., 41 (1987) 395.
10 J. R. Lakowicz, H. Cherek and A. Balter, J. Biochem. Biophys. Methods, 5 (1981) 131.
11 C. L. Lawson and R. J. Hanson, Solving Least-Squares Problems, Prentice-Hall, Englewood Cliffs, NJ, 1974, Ch. 23 and App. C.

Analytica Chimica Acta, 193 (1987) 127—135
Elsevier Science Publishers B.V., Amsterdam — Printed in The Netherlands

INDIRECT ATOMIC ABSORPTION SPECTROMETRIC DETERMINATION OF MIXTURES OF CHLORIDE AND IODIDE BY PRECIPITATION IN AN UNSEGMENTED FLOW SYSTEM

P. MARTÍNEZ-JIMENEZ, M. GALLEGO and M. VALCÁRCEL*

Department of Analytical Chemistry, Faculty of Sciences, University of Córdoba, Córdoba 14004 (Spain)

(Received 16th June 1986)

SUMMARY

Chloride and iodide are injected into a carrier silver nitrate and the precipitates formed are retained on a stainless-steel filter, so that total chloride and iodide can be determined by the decrease in the atomic absorption signal for silver. The silver chloride precipitate is subsequently dissolved with ammonia and chloride only is determined. Iodide is determined by difference. Mixtures of these anions at $\mu g\ ml^{-1}$ levels can be determined for chloride/iodide ratios from 7.5:1 to 1:60, with a sampling frequency of ca. 10 h^{-1}. Applications to the determination of chloride in foodstuffs and wines are described. Up to 10 samples per hour can be handled and 50—100 samples can be run before the filter must be cleaned.

The analysis of halide mixtures is a classic problem arising from the similarity in the chemical properties of these ions. However, such determinations are possible by using differential reactions. Thus, some methods are based on sequential oxidation with appropriate reagents such as manganese dioxide (which oxidizes iodide), or lead peroxide (which oxidizes iodide and bromide) [1]. Other methods involve the conversion of the halides to, for example, alkyl halides prior to their separation and determination by gas chromatography [2]. It is also worth mentioning the simultaneous determination of halide mixtures by potentiometric titration with silver or mercury nitrate as titrant [3].

Flow injection analysis (f.i.a.) has proved to be a suitable technique for simultaneous determinations [4]; however, it has only been used for the individual determination of halides, not for the resolution of their mixtures. Flow-injection determinations of chloride are commonly based on the mercury(II) thiocyanate spectrophotometric method [5—12] or on potentiometric methods [13—17]. Several methods have been proposed for the determination of microgram amounts of iodide by f.i.a., which include potentiometric [17, 18], amperometric [19], enthalpimetric [20] and spectrophotometric [21] procedures.

The indirect determination of chloride and iodide by atomic absorption spectrometry (a.a.s.) involves precipitation with silver, and either measure-

0003-2670/87/$03.50

ment of residual silver or determination in the precipitate after dissolution [22]. Other indirect determinations for these ions by a.a.s. have been reviewed by Hassan [22]. In addition, a.a.s. and f.i.a. have been used in conjunction with a continuous precipitation system in this laboratory for several indirect determinations [23, 24], including chloride.

This paper describes a simple and accurate method for the sequential determination of chloride and iodide in mixtures, based on the precipitation of these anions with silver nitrate. First, chloride and iodide are precipitated, so that both anions are determined from the decreased silver a.a.s. response. Next, the silver chloride is dissolved and chloride is determined by the silver signal generated. The iodide content is found by difference.

EXPERIMENTAL

Reagents and equipment

A 1.00 g l^{-1} silver solution was prepared by dissolving 1.574 g of silver nitrate in 1 l of 1% (v/v) nitric acid. Chloride and iodide standard solutions (1.000 g l^{-1}) were prepared from their potassium salts (dried at 110°C) in distilled water. All other reagents were of analytical grade. Working solutions were prepared daily by appropriate dilution.

An atomic absorption spectrometer (Perkin-Elmer 380) equipped with a silver hollow-cathode lamp was used. The wavelength was set at 328.1 nm and the spectrometer and air/acetylene flame were adjusted following standard recommendations. The spectrometer output was connected to a Radiometer REC-80 recorder. The peristaltic pump was a Gilson Minipuls-2, furnished with PVC pump tubing. Rheodyne 5041 and 5301 selecting valves, and a Tecator L-100-1 injection valve were used. All connecting tubing was of teflon (0.5 mm i.d.) A Scientific System (type 0.5—105) column provided with a removable screen-type stainless-steel filter (pore size 0.5 μm, chamber inner volume 580 μl, filtration area 3 cm^2) which was originally designed as a cleaning device for h.p.l.c., was used for filtration purposes. A potentiograph (E-536, Metrohm), equipped with an automatic burette (E-535, Metrohm), a silver indicator electrode and a calomel reference electrode, were used to provide comparative results for real samples.

Procedure

The manifold described in Fig. 1 and the optimum instrumental conditions (see below) were used. Solutions (pH 1.3—6.2) of chloride and iodide (5—90 and 10—300 μg ml^{-1}, respectively) were injected into a carrier containing an excess of the precipitant (80 μg Ag ml^{-1}) at pH 1.4—7.1. Precipitation took place in the coil (200 cm, 0.5 mm i.d., 10-mm diameter per turn) and the precipitate formed was retained on the filter. Because the concentration of the silver (continuously monitored) decreases as the precipitate is formed, its absorbance diminishes and yields a negative peak, the height of which is directly proportional to the chloride plus iodide concentration in the sample.

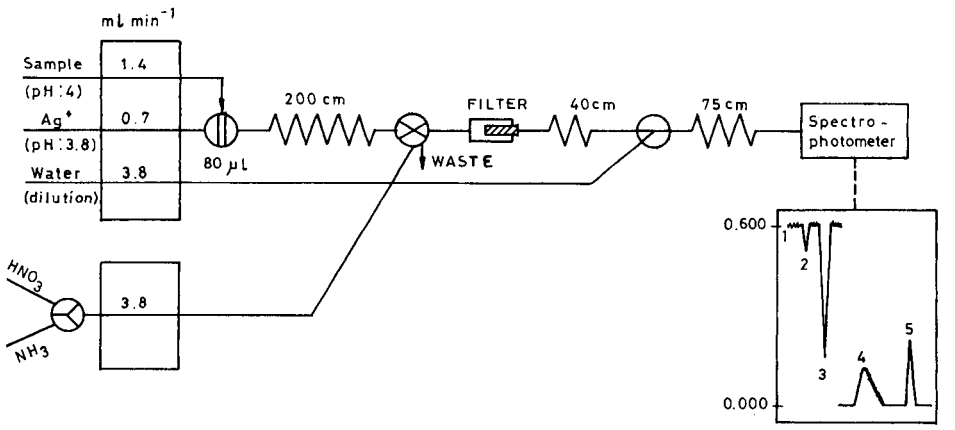

Fig. 1. Manifold used for the determination of chloride/iodide mixtures. Recorder output: (1) silver carrier; (2) water blank injection; (3) sample injection; (4) washing of precipitate; (5) dissolution of silver chloride.

Distilled water was used as a blank. A water stream was incorporated into the flow system to dilute the silver solution prior to nebulization, because the concentration of the excess of precipitant fell above the linear range of the a.a.s. calibration.

The precipitate was washed with 5×10^{-3} M nitric acid and then dissolved in 6 M ammonia. The peak height of the signal yielded by dissolved silver chloride is directly proportional to the chloride concentration in the sample solution. The difference between the silver concentrations obtained in the two steps is directly proportional to the iodide concentration in the sample. No water dilution stream is necessary in the step involving the dissolution of the precipitate.

The filter must be washed in an ultrasonic bath with 6 M ammonia at intervals depending on the concentration of the anions in the injected sample (between 50 and 100 samples).

Procedure for food decomposition

An accurately weighed amount of food (2–16 g depending on its chloride content) was mixed with 20 ml of 5% sodium carbonate solution in a porcelain crucible, evaporated to dryness on a sand bath, and ashed at $\leqslant 500°C$ for 2–10 h, depending on the type of food (the longer time for cheese and eggs). The ash was extracted with 2 ml of 2 M nitric acid, filtered, and washed with distilled water. Finally, the filtrate was diluted to 100 ml with water and transferred to a teflon beaker for the flow-injection procedure.

RESULTS AND DISCUSSION

The classical indirect method for determination of chloride by a.a.s. involves precipitation with silver ion [22]. This method has been adapted to a

continuous flow-injection system [24]; two unsegmented flow configurations, with normal and reversed flow-injection modes, were proposed. These offer several advantages over the conventional manual method, e.g., lower detection limit, wider determination range and higher selectivity and sampling frequency.

Iodide can be determined by injection of the sample into a silver carrier. The amount of silver nitrate required to achieve complete precipitation of iodide was studied on samples containing 60 or 240 $\mu g\ ml^{-1}$ iodide. Figure 2A shows the effect of silver concentration on the response to iodide. As can be seen, less than 65 $\mu g\ ml^{-1}$ silver drastically decreases the response to 240 $\mu g\ ml^{-1}$ iodide. In order to ensure complete precipitation of iodide, 80 $\mu g\ ml^{-1}$ silver ion was chosen. Similar behaviour can be observed in Fig. 2B for the determination of chloride. At concentrations above 80 $\mu g\ ml^{-1}$ silver ion, the signal for chloride or iodide remains constant; however, the smoothness of the baseline deteriorated. The effects of other chemical variables and the flow-injection variables were the same as for the indirect determination of chloride described previously [24].

The silver chloride precipitate is a coagulated colloid which adsorbs silver ions on its surface. Therefore, it is necessary to remove adsorbed silver prior to dissolving the precipitate in order to avoid systematic errors; 5×10^{-3} M nitric acid was used as a wash solution. The precipitate was washed until no signal for silver was obtained (ca. 4 min). The dissolution of the precipitate is more complicated because this should be immediate in order to obtain a transient peak rather than a plateau. Several experiments demonstrated that the dissolution of the silver chloride precipitate was complete and rapid at

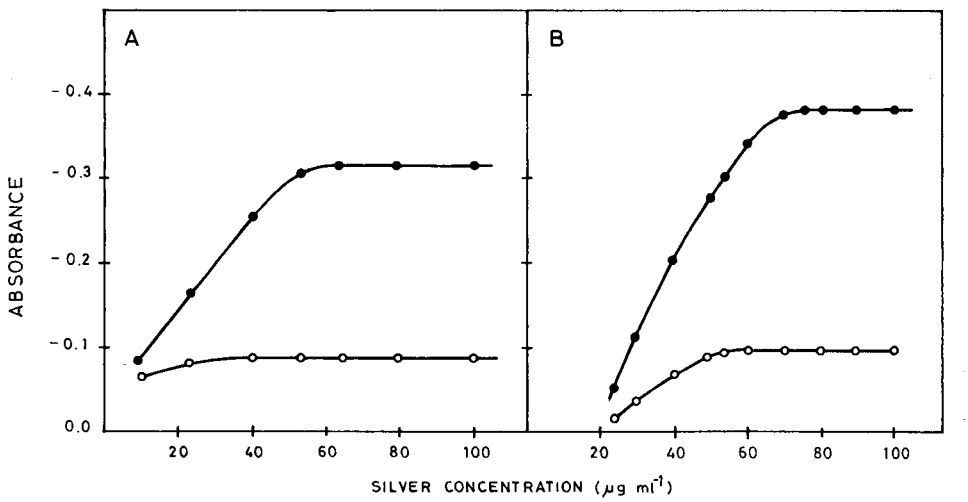

Fig. 2. Effect of silver concentration on the responses for iodide and chloride. (A) Iodide: (○) 60, (●) 240 $\mu g\ ml^{-1}$. (B) Chloride: (○) 20, (●) 80 $\mu g\ ml^{-1}$.

ammonia concentrations above 5 M, so 6 M was chosen [23]. A further experiment demonstrated that the silver iodide did not dissolve in 6 M ammonia for iodide concentrations in the range 10–320 $\mu g\ ml^{-1}$.

Determination of chloride/iodide mixtures

Under the optimum conditions indicated above, three linear calibration graphs were obtained, for chloride and iodide by precipitation, and chloride by dissolution. Table 1 gives the characteristics of these plots, which are also the analytical features of the methods for the individual determination of chloride or iodide. From Table 1, the following equations can be used for the simultaneous determination of chloride and iodide

$$A_1 = -0.003 - 0.005\ [Cl^-] + 0.005 - 0.0014\ [I^-]$$

$$A_2 = -0.006 + 0.006\ [Cl^-]$$

where A_1 and A_2 are the peak absorbances obtained for the complete precipitation of chloride and iodide mixtures, and for dissolution of silver chloride, respectively, and the concentrations are given in $\mu g\ ml^{-1}$.

The applicability of the method was tested by resolving various synthetic mixtures of chloride and iodide (Table 2). Mixtures can be determined with chloride/iodide ratios from 7.5:1 to 1:60. At the limits, the relative error is $\leqslant 7\%$.

Ten consecutive determinations per hour could be made on a sample containing chloride and iodide. When the recommended procedure was applied to a series of eleven samples of 40 $\mu g\ ml^{-1}$ chloride and 100 $\mu g\ ml^{-1}$ iodide, the relative standard deviation (r.s.d.) found was 6.5% for chloride and 4.9% for iodide.

The influence of various amounts of other ions on the indirect determination of 40 $\mu g\ ml^{-1}$ chloride/100 $\mu g\ ml^{-1}$ iodide was investigated. Foreign ions were added at a maximum level of 4 $g\ l^{-1}$. The tolerance limits were taken as the largest amounts yielding an error of less than ±6% in the peak absorbance. The results (Table 3) indicate that the most significant interferences were

TABLE 1

Characteristics of the calibrations and detection limits for the individual determinations of chloride and iodide

Species	Slope[a] (A ml μg^{-1})	Intercept (A)	Corr. coeff. (n = 7)	Range ($\mu g\ ml^{-1}$)	R.s.d. (%)	Detection limit ($\mu g\ ml^{-1}$)
Chloride[b]	−0.005	−0.003	0.998	3–100	2.0	1.3
Chloride[c]	0.006	−0.006	0.997	3–100	5.2	2.1
Iodide[b]	−0.0014	0.005	0.998	10–320	2.3	6.0

[a]A, Absorbance. [b]Without precipitate dissolution. [c]With precipitate dissolution.

TABLE 2

Resolution of chloride/iodide mixtures

Amount added ($\mu g\ ml^{-1}$)		Amount found ($\mu g\ ml^{-1}$)		Amount added ($\mu g\ ml^{-1}$)		Amount found ($\mu g\ ml^{-1}$)	
Iodide	Chloride	Iodide	Chloride	Iodide	Chloride	Iodide	Chloride
300	5.0	298	5.0	40	20.0	41.3	19.4
300	7.5	304	7.4	30	30.0	30.6	29.5
240	10.0	245	9.7	30	60.0	32.1	63.4
200	20.0	192	20.7	30	90.0	29.1	95.4
120	20.0	115	20.9	10	50.0	9.5	51.8
60	20.0	58.1	19.2	10	75.0	9.3	78.2

TABLE 3

Tolerance limits for foreign ions on the simultaneous determination of 40 $\mu g\ ml^{-1}$ chloride and 100 $\mu g\ ml^{-1}$ iodide

Tolerance limit ($\mu g\ ml^{-1}$)	Ion added
4000	SO_4^{2-}, PO_4^{3-}, NO_3^-, NO_2^-, CO_3^{2-}, AsO_2^-, AsO_4^{3-}, $C_2O_4^{2-}$, ClO_3^-, Ca^{2+}, Mg^{2+}, Cu^{2+}, Mn^{2+}
2000	BrO_3^-
1000	IO_3^-
600	Fe^{3+}
100	$Fe(CN)_6^{4-}$
40	Br^-
<40	CrO_4^{2-}, ClO^-, CN^-, $Fe(CN)_6^{3-}$

caused by species yielding precipitates with silver ion such as bromide, cyanide, thiocyanate, hexacyanoferrate(III), chromate and hypochlorite (because hypochlorite is decomposed to chloride). Anions forming silver salts soluble in slightly acidic media (carbonate, phosphate, arsenate and oxalate) did not interfere.

Determination of chloride (and iodide) in foodstuffs

The procedure for chloride and iodide described above was applied to several foodstuffs. Because these foodstuffs contained much more chloride than iodide, iodide was added to the samples, in order to test whether the method could be applied under such circumstances.

For most samples, the AOAC-recommended ashing procedure [25] was used. Wines, however, required no pretreatment. In order to avoid loss of chloride during the lengthy heating (especially for samples with large carbohydrate contents) sufficient sodium carbonate must be present during ignition and the temperature must not be too high.

TABLE 4

Chloride found and recovery of iodide added to white wines

Wine	Aliquot taken[a] (ml)	Chloride found ($\mu g\ ml^{-1}$)	Iodide ($\mu g\ ml^{-1}$)		Iodide recovery (%)
			Added	Found	
1	6.3	9.8	60	57.5, 59.0, 60.5	98.4
	6.3	9.8	140	139.8, 143.2, 140.8	100.9
	10.0	15.6	60	60.0, 59.0, 61.0	100.0
	10.0	15.6	140	138.9, 141.6, 140.9	100.3
2	6.5	10.0	60	62.5, 65.0, 61.0	104.7
	6.5	10.0	140	138.7, 139.0, 140.1	99.5
	10.0	15.4	60	63.1, 60.8, 62.0	103.3
	10.0	15.4	140	137.9, 138.0, 139.2	98.8
3	6.1	10.0	60	62.5, 65.0, 61.0	104.7
	6.1	10.0	140	135.0, 139.0, 140.0	98.6
	10.0	16.4	60	61.5, 63.0, 59.5	102.2
	10.0	16.4	140	137.4, 141.0, 141.5	100.0
4	5.7	10.2	60	59.5, 65.0, 62.5	103.9
	5.7	10.2	140	139.0, 140.0, 139.0	99.5
	10.0	17.9	60	60.2, 62.5, 59.5	101.2
	10.0	17.9	140	135.0, 139.0, 143.0	99.3
5	6.3	10.0	60	59.5, 60.0, 61.0	100.3
	6.3	10.0	140	139.2, 141.0, 143.0	100.8
	10.0	16.0	60	60.2, 65.0, 61.0	103.4
	10.0	16.0	140	139.0, 141.0, 143.0	100.7
6	5.5	12.2	60	61.5, 63.5, 58.5	101.9
	5.5	12.2	140	138.5, 142.0, 139.0	99.9
	10.0	22.1	60	63.5, 61.5, 62.0	103.9
	10.0	22.1	140	139.5, 141.0, 143.0	100.8

[a]Diluted to 25 ml with water.

The amounts of chloride found and the recoveries obtained for iodide added to foodstuffs are shown in Tables 4 and 5. All the sample aliquots taken and the iodide standard solutions added were diluted to 25 ml (10 ml for coffee) with distilled water prior to injection; the pH of the samples was ca. 4. The iodide concentrations added in all cases were 60 and 140 $\mu g\ ml^{-1}$. Recoveries ranged from 97.2 to 104.7% for iodide. Table 6 shows the results obtained for the determination of chloride in these samples compared with those obtained by the standard potentiometric method [3].

Conclusions

The precipitation of chloride and iodide with silver ion is suitable for their simultaneous determinations by using a filter chamber coupled to an a.a.s./flow-injection system. This approach is faster and simpler than conventional procedures and is the first description of a simultaneous determination of

TABLE 5

Chloride found and recovery of iodide added to foodstuffs

Sample	Aliquot taken[a] (ml)	Chloride found (μg ml^{-1})	Iodide (μg ml^{-1})		Iodide recovery (%)
			Added	Found	
Milk	1.8	9.9	60	58.5, 59.0, 57.5	97.2
	1.8	9.9	140	140.0, 141.0, 140.8	100.4
	3.6	19.8	60	60.5, 59.0, 58.5	98.9
	3.6	19.8	140	140.0, 142.0, 139.0	100.2
Cheese	1.0	12.9	60	60.0, 61.5, 60.0	100.8
	1.0	12.9	140	140.0, 142.5, 143.0	101.3
	2.0	25.8	60	59.0, 59.5, 58.5	98.3
	2.0	25.8	140	139.0, 137.5, 141.0	99.4
Bread	1.0	10.0	60	61.5, 62.0, 60.2	102.0
	1.0	10.0	140	139.7, 139.0, 141.0	99.9
	2.0	20.0	60	60.0, 61.5, 60.5	101.1
	2.0	20.0	140	139.0, 138.0, 140.0	99.3
Coffee[b]	2.0	11.0	60	61.5, 62.0, 60.5	102.2
	2.0	11.0	140	143.0, 142.5, 141.0	101.5
	4.0	22.0	60	60.5, 62.0, 58.5	100.6
	4.0	22.0	140	139.0, 142.0, 143.0	100.9
Egg yolk	1.5	13.5	60	62.0, 62.0, 60.5	102.5
	1.5	13.5	140	139.0, 139.0, 137.5	98.9
	3.0	27.0	60	61.5, 60.0, 62.0	101.9
	3.0	27.0	140	143.0, 141.0, 140.5	101.1
Egg white	1.5	12.5	60	62.0, 62.0, 60.0	102.2
	1.5	12.5	140	137.5, 140.0, 141.0	99.6
	3.0	25.0	60	61.0, 60.0, 58.5	99.7
	3.0	25.0	140	137.0, 139.5, 140.5	99.3

[a]From the diluted solution of the ash; aliquot then diluted to 25 ml with water. [b]Diluted to 10 ml with water.

TABLE 6

Determination of chloride in foodstuffs by the flow-injection and potentiometric methods

Sample	Chloride found[a] (mg l^{-1})		Sample	Chloride found (g kg^{-1})	
	F.i.a.	Potentiometric		F.i.a.	Potentiometric
Wine 1	39.0 ± 1.1	40.5 ± 1.3	Milk	1.23 ± 0.01	1.25 ± 0.02
Wine 2	38.5 ± 1.1	39.0 ± 0.9	Cheese	16.13 ± 0.04	16.15 ± 0.04
Wine 3	40.9 ± 0.6	41.3 ± 0.5	Bread	5.01 ± 0.02	5.04 ± 0.02
Wine 4	44.7 ± 0.6	43.8 ± 0.4	Coffee	0.34 ± 0.01	0.34 ± 0.01
Wine 5	40.1 ± 0.4	40.6 ± 0.5	Egg yolk	2.25 ± 0.01	2.26 ± 0.02
Wine 6	55.2 ± 0.6	54.8 ± 0.9	Egg white	2.08 ± 0.02	2.07 ± 0.02

[a]Average of four individual determinations with standard deviation.

both anions by f.i.a. The results reported show the advantages of simplicity, rapidity and versatility of f.i.a. Additional advantages include small sample volume, low reagent consumption, ease of automation, and high precision and sampling frequency (no decantation or centrifugation is needed).

The authors are grateful to the CAICyT (Project No. 2012/83) for financial support.

REFERENCES

1 F. D. Snell, Photometric and Fluorimetric Methods of Analysis. Nonmetals, Wiley, New York, 1981.
2 J. A. Rodriguez-Vazquez, Anal. Chim. Acta, 73 (1974) 1.
3 W. J. Williams, Handbook of Anion Determination, Butterworths, London, 1979.
4 M. D. Luque de Castro and M. Valcárcel, Analyst, 109 (1984) 413.
5 J. Růžička, J. W. B. Stewart and E. A. G. Zagatto, Anal. Chim. Acta, 81 (1976) 387.
6 E. H. Hansen and J. Růžička, Anal. Chim. Acta, 87 (1976) 353.
7 H. Bergamin F°, B. F. Reis and E. A. G. Zagatto, Anal. Chim. Acta, 97 (1978) 427.
8 J. Slanina, F. Bakker, A. Bruyn-Hes and J. J. Möls, Anal. Chim. Acta, 113 (1980) 331.
9 W. D. Basson and J. F. Van Staden, Water Res., 15 (1981) 333.
10 F. J. Krug, L. C. R. Pessenda, E. A. G. Zagatto, A. O. Jacintho and B. F. Reis, Anal. Chim. Acta, 130 (1981) 409.
11 R. Karlicek, Chem. Listy, 77 (1983) 100.
12 P. C. Thijssen, L. T. M. Prop, G. Kateman and H. C. Smit, Anal. Chim. Acta, 174 (1985) 27.
13 H. Müller, 3rd Symposium on Ion-Selective Electrodes, Matrafured, Hungary, 1980.
14 H. Müller, Anal. Chem. Symp. Serv., 8 (1981) 279.
15 R. Virtanen, Anal. Chem. Symp. Serv., 8 (1981) 375.
16 M. Trojanowicz and W. Matuszenski, Anal. Chim. Acta, 77 (1983) 151.
17 P. W. Alexander, P. R. Haddad and M. Trojanowicz, Anal. Chem., 56 (1984) 2417.
18 J. Slanina, W. A. Lingerak and F. Bakker, Anal. Chim. Acta, 117 (1980) 91.
19 K. W. Pratt and D. C. Johnson, Anal. Chim. Acta, 148 (1983) 87.
20 J. M. Elvecrog and P. W. Carr, Anal. Chim. Acta, 121 (1980) 135.
21 K. Fujiwara and K. Fuwa, Anal. Chem., 57 (1985) 1012.
22 S. S. M. Hassan, Organic Analysis using Atomic Absorption Spectrometry, Horwood, Chichester, 1984.
23 P. Martínez-Jimenez, M. Gallego and M. Valcárcel, Anal. Chem., 59 (1987) 69.
24 P. Martínez-Jimenez, M. Gallego and M. Valcárcel, J. Anal. At. Spectrom., (1987) in press.
25 W. Horwitz, (Ed.), Official Methods of Analysis of the Association of Official Analytical Chemists, Thirteenth edn., Washington, DC., 20044, 1980, p. 39.

Analytica Chimica Acta, 193 (1987) 137—146
Elsevier Science Publishers B.V., Amsterdam — Printed in The Netherlands

AUTOMATED DIRECT DETERMINATION OF CHROMIUM IN BLOOD AND URINE BY ELECTROTHERMAL ATOMIC ABSORPTION SPECTROMETRY

J. J. McAUGHEY[a] and N. J. SMITH*

Health and Safety Executive, Occupational Medicine and Hygiene Laboratory, 403 Edgware Road, London NW2 6LN (Great Britain)

(Received 12th June 1986)

SUMMARY

A simple direct procedure for the determination of chromium in whole blood and urine by graphite-furnace atomic absorption spectrometry is described. Whole blood samples are diluted with 0.1% Triton-X solution before injection, whereas urine samples are injected directly. Calibration is done by direct comparison against matrix-matched standards. Between-run precision is 5.4% at 154 nmol l^{-1} for urine and 3.6% at 142 nmol l^{-1} for blood. The detection limits are 3.8 nmol l^{-1} for urine and 11.5 nmol l^{-1} for blood, each for a 20-μl sample. The calibration range extends up to 770 nmol l^{-1} for both blood and urine. This allows the determination of chromium in both occupationally exposed and unexposed groups. The graphite-furnace conditions for each matrix are similar. Elimination of sample pretreatment minimizes the risk of contamination and allows a rapid sample throughput of 50—60 samples per day. The methods described are particularly suited for the screening and surveying of populations occupationally exposed to chromium.

Chromium and its compounds find widespread use throughout industry. The major processes involving exposure to chromium(VI) are chromate production, chromate pigment production, chrome electroplating and stainless-steel welding. It has long been recognized that occupational exposure to chromium(VI) may cause serious acute and chronic health effects [1]. The most important of these is a well-documented increase in the incidence of lung cancer, although the specific carcinogenic compounds have not been identified [2].

It has been suggested that recent uptake of chromium(VI) may best be measured by post-shift urinary chromium concentration, or by an increase in urinary chromium over the shift [3, 4]. In these studies, a rise in urinary chromium concentration was seen during the shift followed by a rapid washout overnight. It is also known from animal studies [5] that chromium(VI) is taken up into red blood cells and binds to haemoglobin. It is possible,

[a]Present address: AERE Harwell, Oxfordshire (Great Britain).

therefore, that blood chromium may better reflect long-term exposure to chromium(VI), while urinary chromium reflects recent uptake.

The screening of large working populations for chromium exposure and uptake by the measurement of blood and urinary chromium requires fast, simple, automated procedures. Of the methods available for the determination of chromium in biological fluids, neutron activation analysis, isotope-dilution mass spectrometry and graphite-furnace atomic absorption spectrometry (a.a.s.) have been most widely used. Graphite-furnace a.a.s. has proved most popular because of its speed, the lack of sample preparation required, and the ease by which methods may be automated.

Many of the early problems associated with the use of graphite-furnace a.a.s. for the determination of chromium in biological fluids have largely been overcome. Re-adsorption and retention of chromium within the graphite tube during atomization have been eliminated by the use of pyrolytically coated carbon tubes and controlled gas flows during atomization [6]. The indequacy of deuterium background correction at the wavelength used for chromium measurement has been overcome by the introduction of the tungsten-iodide background correction lamp [7], a modification of which is now commercially available, although recent work has shown that chromium in urine can be determined without significant interference, by careful adjustment of various instrumental parameters [8]. A recently published method for the determination of chromium in urine at concentrations found in clinical work involved standard addition, and decreased gas flow during atomization to overcome matrix effects [6]. However, methods involving standard addition for either blood or urine analysis are relatively time consuming in terms of analysis and quality control procedures. To survey large occupational groups, rapid sample preparation or direct determination is preferred. The direct determination of chromium in blood has so far been confined to serum chromium, which is of interest in nutritional studies; the absence of direct methods for whole blood analysis may reflect the more complex nature of the whole blood matrix.

In the method proposed here, chromium in urine is determined directly, and only a simple dilution is needed for quantifying chromium in whole blood. Matrix interferences in urine and blood are overcome by peak integration and the use of matrix-matched standard materials. The methods use similar instrument programs for a.a.s., except that blood analysis requires an additional ashing step for the removal of carbonaceous material. The absolute detection limit for chromium in urine is of the same order as that quoted when pooled urine samples from occupationally unexposed subjects were analyzed [6]. The absolute sensitivity and detection limits for both procedures are the same. The methods described here lend themselves readily to automated sampling and the use of on-line data collection allows unattended operation.

EXPERIMENTAL

Apparatus

The Perkin-Elmer model 4000 atomic absorption spectrometer used was fitted with a Perkin-Elmer HGA-500 graphite furnace, with an optical temperature sensor for maximum power heating. Samples were introduced into the furnace by a Perkin-Elmer AS-40 autosampler. A Perkin-Elmer model 056 twin-pen recorder was used to monitor simultaneously the analyte and background absorbance. Data output was recorded remotely via an RS232C interface board to a Trivector Trilab microcomputer system. Pyrolytically coated graphite tubes were used for all determinations after initial temperature calibration with an optical pyrometer (Minolta/Land Cyclops 52). Standards and samples were prepared with use of a Hamilton Microlab-M programmable dispenser/diluter or Oxford P-7000 series pipettes. All preparation work for standards, quality control materials, and samples was done in an Envair laminar-flow, filtered-air cabinet.

Materials and standard solutions

The only reagents used were deionized, double-distilled water, Triton X-100 (Fisons scintillation grade) and 1000 mg l^{-1} chromium (as chromium(III) nitrate) solution (BDH Spectrosol grade). Nitric acid (Fisons Primar grade) was used only for the cleaning of glass and plastic ware.

All glassware used was Grade A and was prepared by soaking in 5% nitric acid followed by two rinses with deionized double-distilled water before use. All disposable pipette tips were rinsed, immediately prior to use, three times with deionized, double-distilled water, and once with the sample to be dispensed. All AutoAnalyzer cups were prepared by soaking in (1 + 9) nitric acid overnight, rinsed twice with deionized double-distilled water, and air-dried before use.

Aqueous solutions of 0.0, 4.8, 9.6, 19.2, 38.5, and 77.0 μmol l^{-1} chromium were prepared directly from the 1000 mg l^{-1} chromium standard solution and were used for spiking the matrix-matched calibration series.

Preparation of blood and urine standards and sample collection

For preparation of blood standards, human whole blood (250 ml) was collected in an acid-washed polypropylene bottle from a volunteer and 1.5 g l^{-1} dipotassium-EDTA was added as anticoagulant. The blood was tested for hepatitis-B surface antigen and for antibody to human T-cell lymphotropic virus Type III before laboratory use. The blood was sonicated with three 45-s bursts from a soniprobe (80 W) with mixing between each burst. Six 25-ml portions of the haemolyzed blood were dispensed into chromium-free polypropylene bottles, and each was spiked with 250 μl of an aqueous standard, giving a calibration series of 0, 48, 96, 192, 385, and 770 nmol l^{-1} added chromium in whole blood. Each of the bottles was mixed for 3 h before 500 μl portions were dispensed into polyethylene

tubes, capped, and stored at −20°C until required. Quality-control samples were prepared by the same procedure by spiking an aliquot of whole blood with an aqueous chromium standard prepared at the required concentration.

Blood samples were collected by venepuncture using a batch of syringes, glass bottles containing dipotassium-EDTA as anticoagulant and stainless-steel needles, all checked for chromium contamination. Although it has been shown that the use of stainless-steel needles can lead to contamination of the sample [9], this was not found to be the case for a single pass through the needles used, either in blood collection or in contamination checks with the EDTA solution.

For preparation of urine standards, urine was collected in an acid-washed glass bottle and allowed to stand for 3 days at 4°C, before filtration to remove any suspended solids. A portion (1 ml) of each chromium standard solution was diluted to 100 ml with the filtered urine, giving a calibration series of 0, 48, 96, 192, 385 and 770 nmol l^{-1} added chromium in urine. Each standard was mixed for 3 h before 500-μl aliquots were dispensed directly into acid-washed AutoAnalyzer cups. These cups were capped and stored at −20°C until required. Quality-control samples were prepared by the same procedure by spiking an aliquot of urine with an aqueous chromium standard prepared at the required concentration.

Urine samples were collected directly in chromium-free polycarbonate bottles.

Blood and urine standards and quality control materials showed no evidence of concentration change over a 12-month period.

Procedures

Blood. Frozen blood standards and quality-control samples were thawed and mixed thoroughly. Standards (100 μl) were diluted (1 + 2) with 0.1% (v/v) Triton X-100 solution (200 μl). The 0.1% Triton X-100 solution was used as the blank. The diluted calibration series was then injected in triplicate.

Blood samples and quality controls were also diluted in duplicate (1 + 2) with 0.1% Triton-X solution, and single firings were used. Quality-control samples were run before and after every eight samples. Any blood sample which had a concentration exceeding the calibration range was appropriately diluted with 0.1% Triton-X solution and re-injected.

Urine. Frozen urine standards and quality-control samples were thawed and mixed thoroughly. The thawed standards were injected directly, in triplicate, with deionized double-distilled water used as the blank. Urine samples and quality controls were analyzed by single firings of duplicate samples. Quality-control samples were run before and after every eight samples. Any urine sample with a concentration exceeding the calibration range was re-analyzed after appropriate dilution with deionized, double-distilled water. Any urine sample repeatedly giving poor agreement between duplicates was filtered by passing the sample through a 0.45-μm filter

(Schleicher and Schuell). This removed any suspended solids which may have caused unrepresentative sampling by the autosampler. No adsorption of chromium on the filter or contamination with chromium by the filter was observed.

Conditions for a.a.s. Samples of 20 μl were injected; the furnace parameters are listed in Table 1. The chromium hollow-cathode lamp wavelength was 357.9 nm and the spectral bandwidth was 0.7 nm. The lamp current chosen was 18 mA rather than the 25 mA recommended by the manufacturer, as both the hollow-cathode lamp and the tungsten-iodide background lamp were found to burn out more rapidly at 25 mA. Absorbance was measured with tungsten-iodide background correction by peak integration (2.0 s) during atomization. The chart recorder was set at 10-mV full scale deflection; the purge gas was argon.

RESULTS

Ashing and atomization techniques and temperatures

Urine. A suitable ashing temperature was selected from a plot of ashing temperature against absorbance for 20-μl injections of urine, and from a plot of ashing temperature against background absorbance for the same urine sample. Background absorbance decreased steadily from 1000°C upwards. No losses of the chromium signal were seen at ashing temperatures below 1250°C. The ashing temperature chosen was 1200°C to allow for any variations in furnace temperature over the day.

The HGA-500 furnace was used in the maximum power-heating mode, and the atomization temperature was plotted against the absorbance produced by 20-μl injections of urine. Although the maximum signal was found at an atomization temperature of 2700°C, subsequent experience showed

TABLE 1

Graphite-furnace parameters for chromium determination in blood and urine

Step	Urine			Blood		
	Temp. (°C)	Ramp time (s)	Hold time (s)	Temp. (°C)	Ramp time (s)	Hold time (s)
Dry	—	—	—	70	5	2
Dry	120	30	30	110	25	20
Ash[a]	—	—	—	800	30	35
Ash[b]	1200	20	20	1200	20	20
Atomize[c]	2500	0	5	2500	0	5
Clean	2700	1	4	2700	1	4

[a]Internal argon flow, 20 ml min^{-1}. [b]Automatic baseline correction after 25 s. [c]Internal argon flow, 50 ml min^{-1}.

improved reproducibility and a 2—3-fold increase in tube lifetime at an atomization temperature of 2500°C.

Blood. The optimum ashing and atomization conditions for urine were used as a basis for optimization of the procedure for blood. The use of these conditions, however, led to a build-up of carbonaceous material within the graphite tube owing to incomplete ashing of protein in the blood. To overcome this, Triton X-100 was used for haemolysis of the blood sample, and the argon flow was decreased during the ashing step at 800°C, which serves to remove organic components of the matrix before final ashing at 1200°C to remove residual inorganic salts. This completely eliminated any carbon build-up and extended the lifetime of the graphite tube, compared with the acid deproteinization and oxygen ashing techniques previously described [10, 11]. The long-term reproducibilities of the results achieved by ashing in oxygen or in a decreased argon flow are compared in Fig. 1.

Analytical performance

Calibration graphs for blood chromium standards were linear up to 770 nmol l^{-1} and those for urine chromium standards were linear up to 385 nmol l^{-1}. Calibration to 770 nmol l^{-1} for urine was possible by using a curve-fitting algorithm (a second-order unweighted least-mean-squares regression) in the microcomputer system. The absolute sensitivity of the

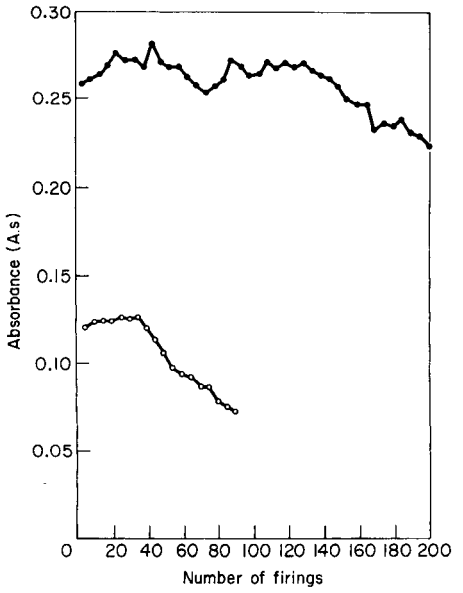

Fig. 1. Effect of ashing in oxygen and in a decreased argon flow on reproducibility (○) 50 ml min^{-1} oxygen with ashing at 600°C; (●) 20 ml min^{-1} argon with ashing at 800°C.

method, calculated as the amount of chromium in a 20-μl sample that produced 1% absorption (or 0.0044 absorbance s), was 6.4 pg for blood and 8.2 pg for urine. The detection limit, defined as three times the standard deviation of the response for a 20-μl matrix blank, was 3.8 nmol l^{-1} for urine and 11.5 nmol l^{-1} for blood, each for an undiluted sample. This gives an absolute detection limit of 4 pg in both cases. The recovery was calculated by spiking samples obtained from an occupationally unexposed person at two levels and running duplicate determinations. The average recoveries for blood (n = 4) at 38.5 and 96.0 nmol l^{-1} added chromium were 102.0% and 101.0% and for urine (n = 6) at 96.0 and 192 nmol l^{-1} were 101.4% and 105.4%, respectively.

The precision of the method for within-run and between-run determinations is shown in Table 2. The data are those obtained from internal quality-control samples, analyzed in routine use. The additional data from freeze-dried material were obtained from the analysis of several samples distributed during the second IUPAC Interlaboratory Survey for the determination of cadmium in urine. These samples had been spiked simultaneously with several additional elements, including 20 μg l^{-1} (385 nmol l^{-1}) chromium.

An assessment of overall accuracy is difficult to obtain because of the scarcity of certified reference materials available for the determination of metals in biological fluids. Assessment of individual sample accuracy is particularly important for urine, because the wide differences in matrix composition encountered produced interferences which differ from sample to sample. To try to overcome this, two approaches were adopted. First, a number of samples was analyzed by the proposed method, and by the method of standard additions for which 1 ml of urine was added to 250-μl portions of 0, 192, 480 and 961 nmol l^{-1} chromium in 0.1% nitric acid, giving a standard addition series of 0, 38.5, 96 and 192 nmol l^{-1} chromium. The concentrations for 32 samples obtained by direct calibration (X) were compared with those obtained by standard addition (Y) by Deming's method,

TABLE 2

Precision of chromium measurements in blood and urine

Sample	Within run			Between run		
	Measured conc. (nmol l^{-1})	n	R.s.d.[a] (%)	Measured conc. (nmol l^{-1})	n	R.s.d.[a] (%)
Blood	142	8	3.7	143	30	3.6
Urine	150	12	3.4	153	42	5.4
	407[b]	4	1.0	418[b]	9	3.7

[a]Relative standard deviation. [b]Freeze-dried urine (Nycomed batch no. 108) with a preliminary recommended value of 423 nmol l^{-1}.

as described by Davidson and Williamson [12]. The regression line was $Y = 1.07X - 1.9$ ($r = 0.99$), showing good agreement. The concentration of the samples ranged from 4 to 275 nmol l^{-1}.

In the second procedure, urine samples were injected directly, and after (1 + 1) dilution with deionized double-distilled water, in order to test for any matrix effects from the urine. The results are shown in Table 3, with each result representing the mean of duplicate determinations on separate days. No significant differences were found.

An NBS reference material (SRM 2670: Toxic Metals In Urine) was also analyzed. The results are included in Table 3. Owing to the high level of chromium in the sample, this sample required a (1 + 1) dilution with deionized, double-distilled water before injection. Consequently a (1 + 3) dilution was also run to test any effect of the urine matrix.

Discussion

The acute and chronic toxicity of chromium(VI) salts has long been established. There is a wide range of industries in which occupational exposure to chromium(VI) compounds can occur. The number and differing physical properties of these compounds makes it important that indicators of uptake and elimination of chromium be established. There is therefore a need for rapid methods for the accurate determination of chromium in biological fluids. It is only recently, however, that a consensus on chromium concentrations in persons not occupationally exposed has been achieved, with the accepted "normal" concentrations of chromium falling by three orders of

TABLE 3

Comparison of urinary chromium results by direct injection and after (1 + 1) dilution

Sample	Urine chromium concentration (nmol l^{-1})			
	Direct		(1 + 1) Dilution	
	Day 1	Day 2	Day 1	Day 2
1	192	189	192	201
2	125	126	—	121
3	391	399	386	388
4	95	96	101	101
5	195	188	196	182
6	272	274	285	256
7	164	158	155	153
8	335	359	361	353
9	494	486	512	465
SRM 2670[a]			1740	1745 1730[b]

[a]Certified value = 85 ± 6 μg l^{-1} (1635 ± 115 nmol l^{-1}). [b]After (1 + 3) dilution.

magnitude over the past two decades to levels less than 20 nmol l^{-1} in both blood and urine [13]. This has been due to a greater awareness of the potential for contamination and the use of "clean-room" facilities but also, more importantly, to improvements in instrumentation; microprocessor control in particular has led to greater reproducibility, especially at lower levels. This is certainly true of graphite-furnace a.a.s. with regard to control over temperature and gas flow, allowing more complex samples to be analyzed.

In the present approach, methods have been adopted which avoid the need for sample pretreatment and rely solely on the controlled selection and optimization of instrumental conditions to minimize interference effects. This avoids the possibility of analyte loss or contamination when pre-instrumental wet- or dry-ashing procedures are used. Any residual matrix interferences when the sample is atomized are overcome by the use of decreased argon flow to prevent re-adsorption of chromium at the cooler ends of the graphite tube, and by the use of peak area rather than peak height for measurement. The matrix may affect the appearance temperature of chromium and, therefore, the residence time of chromium atoms in the furnace. Although this may cause variation in the peak width, and consequently the peak height, the peak area should remain unaffected [14]. This use of peak-area measurement is particularly important in the determination of urinary chromium where a wide variation in matrix composition can be encountered.

Although these measures allow the reproducible determination of urinary chromium, the determination of chromium in whole blood presents further problems because the matrix, although more consistent between samples, is more complex. The most significant problem encountered can be ascribed to protein in the matrix which can lead to the build-up of a carbonaceous residue within the graphite tube if ashing is incomplete. Various techniques have been developed previously to attempt to overcome this carbon build-up. The simplest approach is to dilute the blood sample approximately ten-fold; this has been used successfully for a number of metals, most notably lead in blood [15]. The determination of chromium in whole blood, however, is not sufficiently sensitive for this approach to be used. For other blood analyses, where the sensitivity also limits dilution, two approaches have been adopted: deproteinization by precipitation with 1 M nitric acid, followed by centrifugation and injection of the supernatant liquid [10], or by pre-ashing at 600°C with the introduction of oxygen [11]. However, attempts to apply both these techniques to the present chromium determination led to rapid deterioration of the graphite tube and a falling-off in sensitivity. This could occur after as few as 35 firings when the oxygen ashing technique was used. Use of acid deproteinization also gave rise to significant blanks (20—40 nmol l^{-1} chromium).

In this work, Triton X-100 was used at low concentrations for haemolysis of the blood sample, and ashing at 800°C in a decreased argon flow was used to remove organic components of the matrix, before the further ashing step at 1200°C to remove residual inorganic salts. This allows the additional

ashing to be done at a higher temperature than if oxygen is used, the temperature then being limited to 600°C. The validity of ashing in the decreased argon flow for the determination of chromium in blood is borne out by the absolute sensitivity and detection limit of the method being identical to those of the urine method (after correction for the dilution step used), suggesting that matrix interferences were overcome.

The methods described involve minimal sample handling and allow rapid screening of populations occupationally exposed to chromium(VI). Automated sampling and remote data handling allow unattended operation. The accuracy of the urine method at levels that follow occupational exposure was demonstrated by the use of an NBS Standard Reference Material (2670: Toxic Metals In Urine). Although the two methods described are more directly relevant to occupational levels, clinically relevant levels may also be determined.

REFERENCES

1 NIOSH: Criteria for a Recommended Standard. Occupational Exposure to Chromium(VI). Washington D.C., 1975.
2 IARC: Monographs on the Evaluation of Carcinogenic Risk of Chemicals in Humans. Vol. 23, IARC, Lyon, 1980, pp. 205—323.
3 A. Mutti, A. Cavatorta, C. Pedroni, A. Borghi, C. Giaroli and I. Franchini, Int. Arch. Occup. Environ. Health, 43 (1979) 123.
4 S. Tola, J. Kilpio, M. Virtamo and K. Haapa, Scand. J. Work Environ. Health, 3 (1977) 192.
5 H. J. Wiegand, H. Ottenwalder and H. M. Bolt, Toxicol. Lett., 22 (1984) 273.
6 C. Veillon, K. Y. Patterson and N. A. Bryden, Anal. Chim. Acta, 136 (1982) 233.
7 F. J. Kayne, G. Komar, H. Laboda and R. E. Vanderlinde, Clin. Chem., 24 (1978) 2151.
8 D. J. Halls and G. S. Fell, J. Anal. At. Spectrosc., 1 (1986) 135.
9 J. Versieck and R. Cornelis, Anal. Chim. Acta, 116 (1980) 217.
10 M. Stoeppler and K. Brandt, Fresenius' Z. Anal. Chem., 300 (1982) 372.
11 H. T. Delves and J. Woodward, At. Spectrosc., 2 (1981) 65.
12 D. F. Davidson and J. Williamson. Lab. Pract., 31 (1982) 992.
13 J. Hubert, in D. Shapcott and J. Hubert (Eds.), Chromium In Nutrition and Metabolism, Elsevier, Amsterdam, 1979, pp. 15—30.
14 F. J. Fernandez, M. M. Beaty and W. B. Barnett, At. Spectrosc., 2 (1981) 16.
15 F. J. Fernandez, Clin. Chem., 21 (1975) 588.

Analytica Chimica Acta, 193 (1987) 147—156
Elsevier Science Publishers B.V., Amsterdam — Printed in The Netherlands

RAPID DETERMINATION OF COPPER, NICKEL, LEAD AND CADMIUM IN SMALL SAMPLES OF ESTUARINE AND COASTAL WATERS BY LIQUID/LIQUID EXTRACTION AND ELECTROTHERMAL ATOMIC ABSORPTION SPECTROMETRY

S. C. APTE and A. M. GUNN*

Water Research Centre, Medmenham Laboratory, P.O. Box 16, Medmenham, Marlow, Bucks, SL7 2HD (Great Britain)

(Received 4th July 1986)

SUMMARY

A rapid liquid/liquid extraction of 1.25-ml samples is used with graphite-furnace atomic absorption spectrometry for the determination of dissolved trace metals in saline waters. The metals are chelated with ammonium pyrrolidine dithiocarbamate and extracted into 1,1,1-trichloroethane; 20—40 μl of extract is injected into the furnace. Sample manipulation and overall time are greatly decreased compared to other similar large-scale extraction methods; all the chemical steps are done in the sample cups of an auto-sampler for graphite-furnace a.a.s. Detection limits (Cu 0.3 $\mu g\ l^{-1}$, Cd 0.02 $\mu g\ l^{-1}$, Pb 0.7 $\mu g\ l^{-1}$, Ni 0.5 $\mu g\ l^{-1}$) are low enough for applications in routine monitoring of filterable trace metal concentrations in coastal and estuarine waters to check for compliance with Environmental Quality Standards that apply in the European Community.

Routine monitoring of trace metal concentrations in estuarine and coastal waters is now required in countries of the European Community. The Environmental Quality Standards (EQS) for coastal and estuarine waters are as follows: copper 5 $\mu g\ l^{-1}$, nickel 30 $\mu g\ l^{-1}$, lead 25 $\mu g\ l^{-1}$ and cadmium 2.5 $\mu g\ l^{-1}$. The determination of heavy metals in such waters poses serious analytical problems because of interference effects arising from the high salt content of the matrix. The choice of analytical approach for most laboratories is limited to electrochemical techniques (e.g., anodic stripping voltammetry [1, 2] or, more popularly, graphite-furnace atomic absorption spectrometry (a.a.s.) used in conjunction with a matrix separation/analyte preconcentration step such as chelation and liquid/liquid extraction [3—8], ion exchange [4, 9] or co-precipitation [10, 11].

One extraction a.a.s. method that has proved effective for the determination of a group of trace metals in saline waters relies on chelation of metals by a dithiocarbamate ligand followed by extraction of the complexes into an organic solvent. The metals are back-extracted into an acidic solution (in which they are stable) prior to graphite-furnace a.a.s. determination [4, 5]. An organic solvent that has a low miscibility with water and high affinity for the complexes is preferred. Popular examples are 1,1,2-trichlorotrifluoroethane

0003-2670/87/$03.50

(Freon) [5, 6, 8, 12], chloroform [4] and methyl isobutyl ketone [13, 14]. The efficacy of the graphite-furnace methods has been demonstrated by the determination of trace metals at low ng l^{-1} levels in open ocean water [3, 4]. A great drawback to the routine application of such methods, however, is that they are necessarily very time-consuming. Lengthy sample manipulations are required and stringent practices have to be adopted in order to decrease contamination. Ideally, for routine monitoring purposes, a quicker method that involves fewer sample manipulations and preparation steps would be desirable.

In this work, such improvements have been made by developing and extending a semimicro-scale dithiocarbamate extraction procedure described by Sperling [15, 16]. Reagent additions and extraction are done within commercially available graphite furnace autosampler sample cups (Fig. 1). The need for a back-extraction step is eliminated by introducing the organic extract directly into the furnace. An organic solvent that is denser than water is used in order to decrease evaporation losses that would otherwise affect accuracy. Such modifications are made possible by the small sample volume required for this a.a.s. method (typically <50 μl per determination). A new solvent for dithiocarbamate extraction, 1,1,1-trichloroethane, is also reported. Metal dithiocarbamate complexes are more soluble in this solvent than in Freon and the solutions are more suitable for direct introduction into the graphite furnace. The method is intended for trace metal determinations in estuarine and coastal waters (e.g., as part of EQS monitoring requirements). It is not sufficiently sensitive for accurate determinations in unpolluted coastal waters and open ocean water.

EXPERIMENTAL

Reagents and equipment

1,1,1-Trichloroethane (Aristar, BDH) was stored in a refrigerator prior to use. Chilling of the solvent was found to improve pipetting behaviour. Concentrated hydrochloric acid (Aristar, BDH) was used for sample preservation. Metal concentrations in both of these reagents were generally low, although purification can be achieved by distillation (preferably sub-boiling) if required.

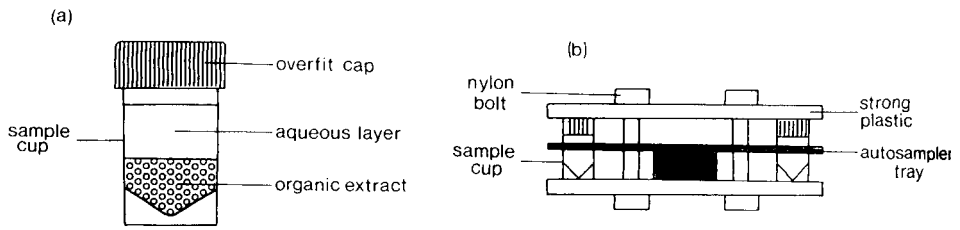

Fig. 1. Schematic diagrams: (a) in-cup liquid-liquid extraction; (b) the assembly used to clamp the cups and autosampler tray during manual shaking.

The pH adjustment/chelating reagent was prepared daily by dissolving 2 g of ammonium pyrolidinedithiocarbamate (APDC) and 5 g of sodium hydrogencarbonate (both analytical-reagent grade) in 100 ml of deionized water. This reagent was purified by addition of 10 ml of 1,1,1-trichloroethane and shaking for 2 min. The solution was allowed to stand for 5 min in order to allow complete phase separation.

Commercially available 2-ml polyethylene sample cups and overfit caps were used for the analysis (Elkay, Shrewsbury, MA). Cups and caps were first soaked in diluted (1 + 9) detergent solution (Decon 90) for 24 h, rinsed thoroughly with deionized water and soaked in diluted (1 + 9) hydrochloric acid for at least 24 h. This was followed by rinsing thoroughly with deionized water, soaking in 2% (w/v) APDC solution for a few minutes, rinsing with distilled water, and finally washing with 1,1,1-trichloroethane. To make this procedure easier, all cleaning steps were applied to batches of cups and caps contained in 1-l polyethylene sample bottles. With some batches of autosampler cup, unacceptably high blanks were obtained even after rigorous cleaning. The authors are at present designing screw-cap polytetrafluoroethylene (PTFE)/fluorinated ethylenepropylene (FEP) autosampler vials which should overcome these periodic problems. As an alternative, however, the extraction can be done satisfactorily in small screw-cap vials or bottles (preferably PTFE or FEP) having good closures, followed by transfer of the contents to PTFE autosampler cups (Perkin-Elmer) prior to spectrometry.

Polyethylene bottles for sample collection and storage were soaked in (1 + 9) detergent solution for at least 3 h, rinsed with water, soaked for at least 3 days in diluted (1 + 9) hydrochloric acid and rinsed with copious quantities of deionized water before use.

Wherever possible, sample manipulations were done in a Class 100 laminar flow hood. It cannot be overstressed that the adoption of such cleaning procedures and rigorous efforts to minimize contamination are crucial to successful use of the method.

Atomic absorption spectrometric procedures

A Perkin-Elmer 4000 atomic absorption spectrometer equipped with an HGA-400 graphite furnace, an AS-40 autosampler and Data System 10 data station was used throughout the work. The instrument was operated with deuterium-lamp background correction. Furnace tubes were not pyrolytically coated and were replaced after ca. 150 firings. Recommended a.a.s. conditions and furnace settings are given in Table 1. The autosampler was adjusted so that the sampling probe would penetrate the upper aqueous layer of the sample and take the sample from just above the base of the cup (i.e., from the lower organic phase). This adjustment was checked daily. New furnace tubes were conditioned by repeated injections of an extracted mid-range standard until a reproducible signal was obtained (ca. 3% relative standard deviation (RSD)). Conditioning was usually complete within 10 injections.

TABLE 1

Operating conditions for graphite-furance a.a.s.

Metal	Pb	Cu	Ni	Cd
Wavelength (nm)	283.3	324.7	232.0	228.8
Bandpass (nm)	0.7	0.7	0.2	0.7
Injection volume (μl)	40	20	40	20
Furnace programs				
Drying temp. (°C)[a]	110	110	110	110
Ashing temp. (°C)[a]	700	900	900	250
Atomization temp. (°C)[b,c]	1750	2200	2200	1750
Clean-out temp. (°C)[d]	2700	2700	2700	2700

[a]Ramp and hold times were 10 s and 10 s. [b]Ramp and hold times were 0 s and 3 s. [c]Argon purge was stopped during the atomization step. [d]Ramp and hold times were 1 s and 3 s.

Recommended procedure

Samples collected in the field are filtered (0.45-μm membrane or similar), preserved by addition of 1 ml l^{-1} concentrated hydrochloric acid and stored in pre-cleaned polyethylene containers. Prior to further treatment, the organic content of the sample can be destroyed (if desired) by ozonolysis [17] or u.v. photo-oxidation [18].

A 1250-μl sample aliquot is accurately pipetted into a sample cup (positioned in the autosampler tray) followed by the addition of 25 μl of the chelating/pH adjustment reagent and 250 μl of 1,1,1-trichloroethane. The use of good-quality dispensing micro-pipettes that are frequently calibrated is recommended for these steps. For samples in which the acidity is different from that recommended, the amount of neutralizing solution to be added to bring the sample pH within the optimum extraction pH range (i.e., pH 4–7) is established on a separate sample aliquot and the composition of the neutralizing/chelating solution is adjusted accordingly. After reagent additions are complete, the sample cups are capped and the autosampler tray is clamped into a purpose-built hand-held shaker (Fig. 1). The tray is shaken vigorously for 10 min. If a mechanical shaker is used for this step, the shaking time should be optimized for the type of shaker used. Samples are then allowed to stand for 5 min, the rig is unclamped and the cups uncapped. The tray is loaded into the autosampler and injections are begun. The elements are determined sequentially on the batch of samples. Standards are prepared in 0.1% (v/v) hydrochloric acid and are extracted in exactly the same manner as the samples.

RESULTS

Solvent introduction into the furnace

The direct introduction of organic solvent extracts into an atom cell such as an air/acetylene flame has been widely used (e.g., see [19]). Direct intro-

duction of such extracts into the graphite furnace, despite reported success by some authors [15, 16, 20], has not been favoured. Difficulties have been reported in dispensing small volumes of organic solvents accurately [5], and interference effects arising from the organic solvent have been encountered [21]. Additionally, the volatility of metal-APDC complexes is reported to cause loss of the analyte during the sample drying and ashing steps of the furnace cycle [22, 23].

During the initial stages of the development work, the above effects were investigated. Atomization profiles were recorded by use of a commercially available software graphics package (Perkin-Elmer) for use with the a.a.s. data station. This allowed the monitoring of atomization profiles during the furnace cycle with a much shorter data-acquisition time than permitted by the conventional spectrometer.

Experiments showed that complexation of metals with APDC did not exert a marked effect on the atomization profile in aqueous media (Fig. 2). The only important effect was a suppression of the lead signal. Atomization profiles from organic solvents, however, were in some cases different from those obtained from aqueous media (Fig. 2). Such effects were presumed to arise from interference effects caused by residual solvent [21] or solvent pyrolysis products present during the atomization step. Extraction into Freon caused a signal enhancement for copper but severe signal suppression for

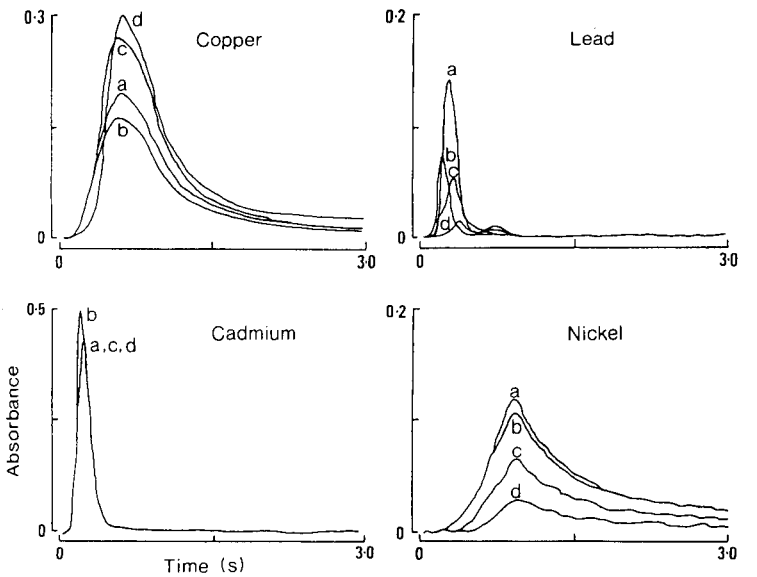

Fig. 2. Atomization profiles for Cu, Pb, Ni (each at 40 $\mu g\ l^{-1}$) and Cd (4 $\mu g\ l^{-1}$): (a) in deionized water; (b) in deionized water containing 0.02% APDC; (c) 1:1 extract of APDC complex into 1,1,1-trichloroethane; (d) 1:1 extract of APDC complex into Freon. Furnace programs were as given in Table 1 except that the argon flow was 50 ml min^{-1} during atomization.

nickel and lead. The use of this solvent, therefore, was abandoned. As a solvent denser than water, and of low toxicity, was required, 1,1,1-trichloroethane was selected as an alternative. Results indicated that this solvent affected atomization profiles in a similar manner to Freon (Fig. 2) but the degree of suppression for nickel and lead was much less severe and, by using the optimized furnace conditions reported in Table 1, adequate sensitivities were obtained.

The accuracy with which volumes of organic solvent were dispensed by the AS-40 autosampler was checked by replicate injections of standards extracted into 1,1,1-trichloroethane. Results showed that the RSD for 20-μl aliquots of extracted standards near the top of the linear calibration ranges was $\leqslant 3\%$, which was only slightly worse than that obtained with aqueous standards of similar concentration.

The carry-over of salt water droplets originating from the upper aqueous sample layer into the furnace was thought to be a potential source of interference. In practice, salt carry-over was found to be a problem only when the underlying organic layer was near depletion. This effect was characterized by a high background signal. Otherwise, the hydrophobic nature of the PTFE sampling probe seemed to prevent the pick-up and transfer of water droplets to the furnace.

Optimization of the extraction procedure

In order to obtain the required detection limits and to enable all four elements to be quantified in one extract, the extraction step was designed to give a 5-fold preconcentration (1250 μl of sample extracted into 250 μl of solvent). Sample cup dimensions limited the application of higher concentration factors.

In some previously developed large-scale extraction procedures [5, 24], workers have recommended the use of a dithiocarbamate reagent for metal chelation consisting of a mixture of sodium diethyldithiocarbamate and ammonium pyrolidine dithiocarbamate (APDC). The mixed reagent was reported to give improved extraction efficiency (for certain elements) over a wide pH range compared to APDC alone. In the present study, it was found that for the metals of interest, the addition of sodium diethyldithiocarbamate was unnecessary to achieve adequate extraction efficiency ($>95\%$) over a wide pH range. The high extraction efficiency was confirmed by examination of the overlying aqueous layer after extraction. The effect of pH on extraction was evaluated; in the pH range 3—8 there was little variation in extraction efficiency (Fig. 3).

The manual shaking time for the cups in the hand-held tray was studied over the range 1—20 min. Cadmium was fully extracted within 2 min and the other three metals within 3—4 min. Absorbances were unaffected by further shaking up to 20 min. For safety, vigorous shaking for 5 min was used to give quantitative extraction of all four metals.

The effect of sample salt concentration on the procedure was checked by

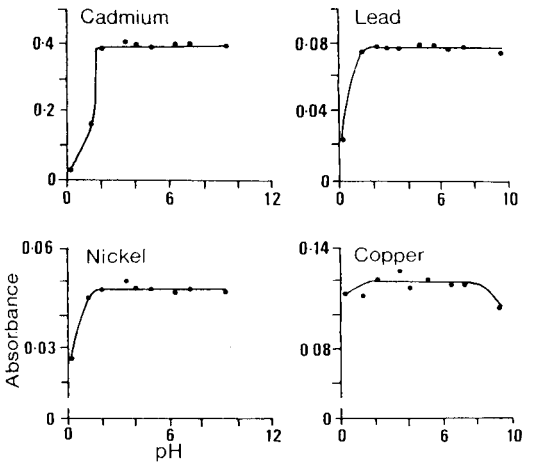

Fig. 3. Effect of pH on extraction efficiency.

comparing the calibration graphs for standards made up in deionized water and in sea water and later by measuring the recoveries of the metals from sea water during routine performance testing. In both cases, it was found that the responses from sea water and deionized water matrices were equivalent. The absence of any appreciable salt error allowed calibration of the method against standards prepared in deionized water and extracted in the same manner as the samples.

Control of pH prior to extraction

Prior to extraction, it is necessary to adjust the pH of acidified samples to within the optimum range for extraction. In previous methods, adjustment of pH was usually achieved by the addition of an alkali such as ammonia solution [3] and/or a buffer [5, 12]. When small volumes are used, as in this method, accurate pH adjustment with a strong base is difficult. A method for pH adjustment that is both robust and simple is preferable. Thus sodium hydrogencarbonate solution (previously recommended by Sperling [16]) was used to adjust the pH. As the reagent is only mildly alkaline (a concentrated solution has a pH similar to that of sea water itself), an excess will not shift the sample pH to above the optimum range for extraction. The amount of neutralizing solution added to acidified samples was adjusted so that even with quite large inaccuracies in sample acidification, the pH would still be within the optimum range for extraction. Samples acidified (to ca. pH 2) with 1 ml l^{-1} hydrochloric acid gave a pre-extraction pH of ca. 5.7, but even with a 20% error in acidification the pH was still in the optimum range for extraction (e.g., 1.2 ml l^{-1} acid added to the sample gave a pre-extraction pH of 4.93 whereas 0.8 ml l^{-1} acid added gave pH 6.01). The pH adjustment solution was combined with the APDC solution in order to produce a single reagent. This also allowed their purification in one step.

Extract stability

For the purpose of this method, it was desirable that extracts were stable for the duration of a working day. In order to assess stability, extracted samples were analyzed, allowed to stand at room temperature (20°C) for 5 h, stored overnight at 10°C and re-analyzed. At all times, the signal was compared to that from stable aqueous standards. There was little detectable change in signal over this period.

Detection limits, precision and accuracy

Data on precision, limits of detection and recoveries were evaluated during a rigorous performance test designed to take into account between-batch as well as within-batch variations in analytical performance [25]. Test solutions were prepared in triplicate by spiking deionized water and sea water (from the Solent, U.K., filtered and ozonolyzed) to the metal concentrations given in Table 2. The samples were analyzed on five days. In order to take into

TABLE 2

Precision and recovery data

Metal	Sample[a]	Metal ($\mu g\ l^{-1}$)		RSD[b] (%)			Recovery[c] (%)
		Added	Found	s_w	s_b	s_t	
Ni	SSW	—	0.70	—	—	—	—
	SSW	2	2.82	6.0	0.0	6.0	106.1 ± 7.4 (8)
	SSW	8	8.52	4.8	0.0	4.8	97.9 ± 2.6 (13)
	DIW	—	0.00	—	—	—	—
	DIW	8	7.89	5.3	1.9	5.7	— (13)
Cd	SSW	—	0.035	—	—	—	—
	SSW	0.25	0.279	6.5	0.0	6.5	97.7 ± 3.8 (13)
	SSW	0.50	0.533	5.4	0.0	5.4	99.6 ± 1.4 (12)
	SSW	0.75	0.754	7.2	0.0	7.2	95.9 ± 1.2 (13)
	DIW	—	0.000	—	—	—	—
	DIW	0.75	0.745	4.3	2.8	5.2	— (10)
Pb	SSW	—	0.25	—	—	—	—
	SSW	2	2.61	5.0	0.0	5.0	118.0 ± 6.8 (12)
	SSW	8	8.19	3.3	1.9	3.9	99.3 ± 2.8 (11)
	DIW	—	0.02	—	—	—	—
	DIW	8	7.95	3.0	4.1	5.2	— (6)
Cu	SSW	—	1.64	—	—	—	—
	SSW	2	3.71	5.1	0.0	5.1	103.8 ± 2.2 (13)
	SSW	8	9.22	3.4	4.3	5.5	94.8 ± 5.5 (6)
	DIW	—	−0.10	—	—	—	—
	DIW	8	7.83	4.1	5.4	6.8	— (6)

[a]SSW, sea water from the Solent; DIW, deionized water.
[b]s_w, within batch; s_b, between batch; s_t, total.
[c]Mean ± 95% confidence limits (degrees of freedom).

account the effect on performance of sample carry-over and calibration drift, samples within each batch were analyzed in a random order. Such a test, conducted over a relatively long period, gives a better indication of likely performance during routine use than a test involving a single batch. This should be borne in mind when the performance data are compared with those of other methods.

Statistically derived limits of detection [25], which were calculated as 4.02 times the within-batch standard deviation of the blank (the mean of two blanks was used for blank correction), were 0.46 $\mu g\ l^{-1}$ Ni, 0.31 $\mu g\ l^{-1}$ Cu, 0.018 $\mu g\ l^{-1}$ Cd and 0.66 $\mu g\ l^{-1}$ Pb. Calibrations were linear up to at least 10 $\mu g\ l^{-1}$ for copper, lead and nickel and up to at least 1.0 $\mu g\ l^{-1}$ for cadmium. The RSD for results for spiked solutions ranged from 4 to 7%; there was no indication that precision varied significantly between sea water and deionized water solutions. Recoveries from spiked sea water solutions were generally excellent (see Table 2), confirming that this method, in common with the larger-scale extraction methods, is essentially free from interference when used during the analysis of saline waters. One exception, however, was the anomalously high recovery (118%) obtained for a low-level lead spike; the reason for this result is unclear and it may conceivably have arisen from a spiking error or sample contamination during preparation of test solutions.

Conclusions

The method described allows the relatively rapid determinations of copper, cadmium, lead and nickel in estuarine and coastal waters. The extraction of a batch of 25 samples (plus standards) takes ca. 90 min. This permits the determination of the four elements in a batch of samples within one day. In spite of the relative simplicity of the technique, limits of detection are comparable to those obtained with a Freon/dithiocarbamate large-scale extraction method for which the performance data have been rigorously evaluated [12]. The cost of the greatly shortened working time appears to be only a slight loss in precision.

The authors thank M. J. Gardner, D. T. E. Hunt and D. A. Winnard of the Water Research Centre, Medmenham, U.K., for their helpful advice during the course of this work.

REFERENCES

1 G. Scarponi, G. Capdaglio, P. Cescon, B. Cosma and R. Frache, Anal. Chim. Acta, 135 (1982) 263.
2 P. W. Balls, Est. Coastal Shelf Sci., 20 (1984) 717.
3 P. J. Statham, Anal. Chim. Acta, 169 (1985) 149.
4 K. W. Bruland, R. P. Franks, G. A. Knauer and J. H. Martin, Anal. Chim. Acta, 105 (1979) 233.
5 L.-G. Danielsson, B. Magnusson and S. Westerlund, Anal. Chim. Acta, 98 (1978) 47.
6 L.-G. Danielsson, B. Magnusson, S. Westerlund and K. Zhang, Anal. Chim. Acta, 144 (1982) 183.

7 H. M. Kingston, I. L. Barnes and T. C. Rains, Anal. Chem., 50 (1978) 2064.
8 B. Magnusson and S. Westerlund, Anal. Chim. Acta, 131 (1981) 63.
9 J. H. Martin and G. A. Knauer, Earth Plan. Sci. Lett., 51 (1980) 266.
10 R. Boniforti, R. Ferraroli, P. Frigieri, D. Heltai and G. Queirazza, Anal. Chim. Acta, 162 (1984) 33.
11 E. A. Boyle and J. M. Edmond, Anal. Chim. Acta, 91 (1977) 189.
12 J. A. Campbell, S. J. Cowling and A. M. Gunn, Water Research Centre Technical Report TR227, Water Research Centre, Medmenham (1985).
13 R. E. Sturgeon, S. S. Berman, A. Desaulnier and D. S. Russel, Talanta, 27 (1980) 85.
14 R. R. Brooks, B. J. Presley and I. R. Kaplan, Talanta, 14 (1967) 809.
15 K. R. Sperling, Fresenius' Z. Anal. Chem., 292 (1978) 113.
16 K. R. Sperling, Fresenius' Z. Anal. Chem., 299 (1979) 103.
17 J. Yates, Water Research Centre Technical Report TR 181, Water Research Centre, Medmenham (1982).
18 G. E. Batley and Y. J. Farrar, Anal. Chim. Acta, 99 (1978) 283.
19 M. S. Cresser, Solvent extraction in flame spectroscopic analysis, Butterworths, London, 1978.
20 R. P. Mitcham, Analyst, 105 (1980) 43.
21 K. R. Sperling, Fresenius' Z. Anal. Chem., 310 (1982) 254.
22 G. Volland, G. Kolblin, P. Tschopel and G. Tolg, Fresenius' Z. Anal. Chem., 284 (1977) 1.
23 R. W. Dabeka, Anal. Chem., 51 (1979) 902.
24 J. D. Kinrade and J. C. Van Loon, Anal. Chem., 46 (1974) 1894.
25 R. V. Cheeseman and A. L. Wilson, Manual on Analytical Quality Control for the Water Industry, Water Research Centre Technical Report TR 66, (1982).

Analytica Chimica Acta, 193 (1987) 157—167
Elsevier Science Publishers B.V., Amsterdam — Printed in The Netherlands

ELECTROTHERMAL ATOMIC ABSORPTION SPECTROMETRY OF ELEMENTS AFTER ELECTROCHEMICAL DEPOSITION ON GRAPHITE ELECTRODES

M. VEBER, S. GOMIŠČEK* and V. STREŠKO[a]

Department of Chemistry and Chemical Technology, Faculty of Natural Sciences, E. Kardelj University, 61001 Ljubljana (Yugoslavia)

(Received 6th July 1986)

SUMMARY

The application of electrochemical deposition on graphite rods for separation and preconcentration prior to electrothermal atomic absorption spectrometry (a.a.s.) is examined. The metals to be determined are electrolyzed onto a graphite rod which is then transferred to a cup atomizer for a.a.s. Although only some of the element present in the solution is deposited on the surface of the graphite rod, favorable preconcentration rates are obtained. The method was tested on the determination of cadmium in aqueous solution. The precision is satisfactory for concentrations down to 5×10^{-8} g l^{-1} cadmium, and the detection limit is 4×10^{-9} g l^{-1}.

Interferences that may occur in electrothermal atomic absorption spectrometry (a.a.s.) can be avoided in different ways. Besides suitable chemical pretreatment such as separation of the analyte from the matrix by the use of liquid-liquid extraction, ion exchange, coprecipitation and modification of the matrix, specific modes of atomization can also be applied.

The most widely utilized is atomization from different metallic or non-metallic surfaces which enables the analyte vaporization to be controlled during the atomization step and the signal characteristics to be improved, especially when suitable temperature regulation is applied. Frequently, graphite inserts of the platform type are used for this purpose, and the sample solution is placed directly on them. Nevertheless, the application of different preconcentration techniques in combination with the use of these inserts can be even more efficient and will also contribute to the elimination of interferences usually occurring in electrothermal a.a.s. Among the preconcentration techniques applied nowadays, electrochemical deposition can be regarded as most promising owing to its suitability for the separation of low concentrations of metals, its selectivity and versatility.

Several authors have proposed and reported on the use of electrochemical deposition for the separation and preconcentration of particular ions prior to

[a]On leave from Geological Institute, Komensky University, Bratislava, Czechoslovakia.

0003-2670/87/$03.50

atomic absorption spectrometric measurements. According to the literature, the electrodeposition of metal ions has proved satisfactory on mercury drop electrodes [1, 2], metal wires of high melting point [3—9], or directly on the internal surface of the graphite furnace [10]. Metals have also been deposited on a graphite rod, which was then ground and homogenized, and portions of the graphite powder were inserted directly into a graphite-tube furnace [11].

In previous work from this laboratory [12, 13], the electrochemical deposition of Ag(I), Cd(II), Cu(II) and Pb(II) ions on graphite electrodes at controlled cathode potential was reported. The metals were subsequently atomized in graphite atomizers for a.a.s. This paper reports the further development of this technique, as well as some phenomena taking place during the electrodeposition of metal ions on graphite electrodes from aqueous solutions, and the subsequent atomization of metal deposits in graphite atomizers.

EXPERIMENTAL

Apparatus and chemicals

The Perkin-Elmer 2280 atomic absorption spectrometer used was equipped with a Varian CRA-90 graphite atomizer.

Standard metal solutions (1 mg ml^{-1}) were prepared by dissolving the required amount of metal salt in twice-distilled water. For the preparation of supporting electrolytes, analytical-grade chemicals were used.

Electrodeposition cell

Two types of electrolytic cells were applied for the deposition of metal ions (Fig. 1). Cell A consisted of a 50-ml glass vessel, PTFE cover, and magnetic stirrer. The cover served also as a holder for a reference (SCE), a platinum counter, and four working electrodes. Each of the working electrodes consisted of a carbon rod with a hole bored at the tip, into which a spectroscopic carbon electrode (Ringsdorff RW-O, 3.05-mm diameter) was inserted tightly in order to ensure good electrical contact. The carbon rod (holder) was insulated with a layer of paraffin wax. The working surface of the carbon insert was ground and polished with fine sand paper and alumina on a filter paper, respectively. The inserts were preheated for 3 s at 2500°C in the atomizer. Afterwards, the insert body was insulated with PTFE tape, leaving only the working surface free for metal deposition. Cell B, which was used for work with smaller volumes of analyte (1—3 ml), was equipped with only one working electrode, a platinum counter electrode and the SCE.

Procedures

The entire procedure includes preheating of the graphite insert at 2000°C, electrolysis at 25°C, transfer of the insert with the deposit to the graphite cup of the atomizer, and atomization of the metal at 2000°C.

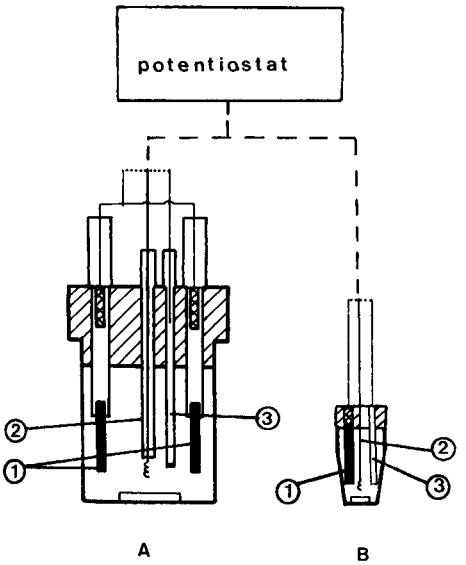

Fig. 1. The electrodeposition cells: (A) for 25 ml of solution; (B) for 5 ml of solution. (1) Working electrode; (2) counter electrode; (3) reference electrode.

Electrolysis. The analyte solution was transferred to the electrolytic cell and the electrolysis was done at controlled cathode potential. The potential of the working electrode was adjusted between −0.6 and −1.2 V vs. SCE, depending on the element under consideration. After the electrolysis, the electrodes were removed from the holders, the insulation tape was removed and the electrodes were used for absorption measurement.

Atomization. The graphite insert was mounted into the graphite cup of the Varian CRA-90 atomizer. The position of the insert is shown in Fig. 2C. The working surface with the deposit must be placed as close as possible to the optical axis of the spectrometer, i.e., towards the opening of the graphite cup. The absorption measurements were done under the conditions listed in Table 1.

RESULTS AND DISCUSSION

The atomizers for electrothermal a.a.s. available commercially are designed primarily for the atomization of solutions, with little consideration given to powdered samples. Up to the present, the techniques applied have been based on modification of wall atomization; the use of platform-type inserts represents an improvement for this type of atomization. It minimizes some of the interferences but cannot eliminate them completely. In spite of the improved sensitivity of the determination, a main drawback of this technique remains its inability to allow speciation of the forms of metal ions under consideration.

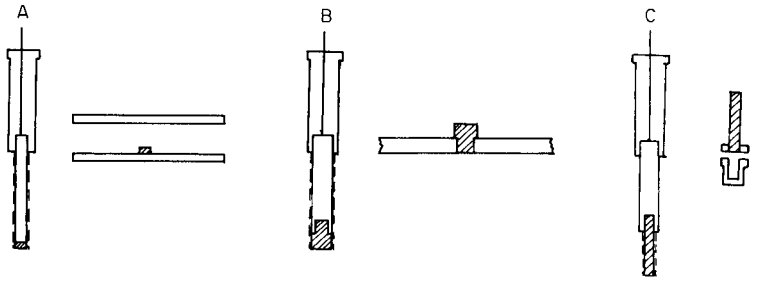

Fig. 2. Techniques for atomization of metals deposited on the graphite rods: (A) HGA-70 (Perkin-Elmer); (B and C) CRA-90 (Varian).

TABLE 1

Experimental conditions for the a.a.s. measurements[a]

Element	Wavelength (nm)	Ashing		Atomization	
		Temp. (°C)	Time (s)	Temp. (°C)	Time (s)
Cu	324.8	600	10	2500	3
Pb	217.0	400	10	2200	3
Cd	228.8	300	10	1900	3

[a]In all cases, the slit width was 0.7 nm and the drying step lasted 15 s at 100° C.

The combination of a suitable separation and preconcentration technique could contribute to solving the problem of speciation and simultaneously make it possible to determine even very low concentrations of species under consideration as a result of the preconcentration. Preconcentration of ions by electrolysis at controlled potential of the working electrode, done in such a way that the electrode later serves as a platform or part of the atomizer for electrothermal a.a.s., seems to be very promising.

Because commercial instrumentation does not allow work with large inserts on which the metals have been deposited electrochemically, some unconventional approaches are necessary to introduce the sample. There are four possible ways: (1) crush the electrode after the electrolysis and insert the powder into the atomizer [11]; (2) cut off the part of the electrode with the deposit in the form of a thin disc and insert it into the graphite tube; (3) incorporate the electrode into the atomizer as a rod or tube; or (4) conduct the electrolysis with an electrode of suitable shape for direct insertion into the graphite cup or the graphite tube of the atomizer. The techniques which were used in this work and in preliminary investigations are shown in Fig. 2. The technique involving insertion of a disc into the graphite tube (Fig. 2A) had the disadvantage of many additional operations which can increase the blank, although the sensitivities obtained by this technique were

favorable. The use of the electrode with deposit as part of the atomizer (Fig. 2B) suffered from lack of sensitivity because of the undefined and larger absorption volume. Therefore, work was concentrated on the systems with electrodes of suitable dimensions and shape for insertion into the graphite cup or tube of the atomizer (Fig. 2C).

The work with an additional graphite insert in the CRA showed that the thermal characteristics of the CRA and consequently its atomization properties were changed. The increased heat capacity of the system influenced the heating rate as well as the temperature distribution across the graphite cup or tube. This was reflected in differences in the atomization in comparison with wall atomization and consequently in the form and height of absorption peaks.

When a standard aqueous solution (5—10 μl) of the element under consideration was pipetted into the graphite cup, and atomization was done under conditions similar to those presented in Fig. 3C, i.e., graphite cup covered with graphite insert, double absorption pulses were observed (Fig. 3). This phenomenon can be explained by two-step atomization. The first step corresponds to the atomization of metal vapours resulting from thermal dissociation, which condensed on the colder insert surface and were again evaporated when the insert reached the vaporization temperature. The ratio of the two absorption signals depends on the conditions of atomization and on the properties of the element under consideration. The absorption peaks

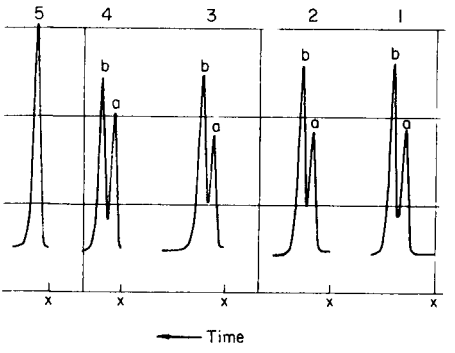

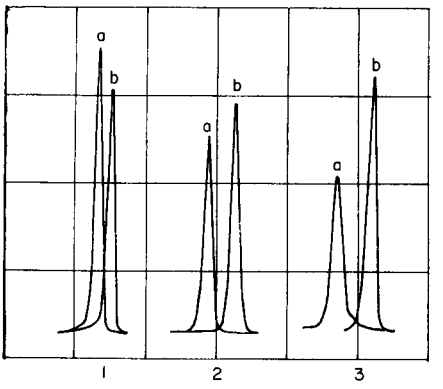

Fig. 3. Atomization of Cd^{2+} solution from a cup covered with a graphite rod in dependence on heating rate. Peaks: (a) atomization from the cup; (b) atomization from the rod. Heating rates: (1) 400° C s^{-1}; (2) 600° C s^{-1}; (3) 700° C s^{-1}; (4) 800° C s^{-1}. Peak 5: atomization from the cup without insert at a heating rate of 700° C s^{-1}. Points X indicate the start of atomization.

Fig. 4. Atomization of Cd^{2+} solution previously pipetted on the carbon rod in dependence on the rod position in the atomization cup. Distance of insertion of carbon rod into the cup for peaks a: (1) 2 mm; (2) 1 mm; (3) 0.5 mm. Peaks b correspond to wall atomization of the same amount of Cd^{2+} solution.

obtained by the technique are shown in Fig. 4; signals (a) correspond to wall atomization whereas signals (b) can be ascribed to atomization from the surface of the insert. The delay in the appearance of signals corresponding to atomization from the graphite insert is the consequence of the temperature distribution in the atomizer. The graphite insert reaches the temperature necessary for evaporation of the sample later than does the graphite cup. But when the atomization does occur under isothermal conditions, the peak heights are higher, i.e., the sensitivity of the measurement is increased. Although this mode of introducing the sample solution into the atomizer was used only for better understanding of some relationships during the atomization in the graphite cup equipped with the insert, it could be of use for aqueous samples because it exhibits quite satisfactory precision (Fig. 5). The relative standard deviation for the peak-height signals was below 5% and the technique can therefore be used in the direct electrothermal a.a.s. of solutions.

The situation in the atomization of elements deposited electrolytically on the electrodes is similar to that described in the above experiments. The only difference is that the origin of the solid metal deposited on the electrode is related to the electrochemical reaction (reaction A) whereas in the case of direct atomization from the solution, thermal dissociation of the compound investigated is responsible for the production of the metal atoms which are afterwards deposited on the inserted electrode in the elemental form, or in the form of the corresponding compound (reaction B). But in this case also, the proportion of the elemental form is greater relative to the amount of compounds. In both cases, the production of free atoms can be ascribed to the melting and subsequent evaporation of metal atoms from the inserted electrode surface (reaction C), which is confirmed by the similar shape of absorption peaks obtained. Therefore the same atomization mechanisms can

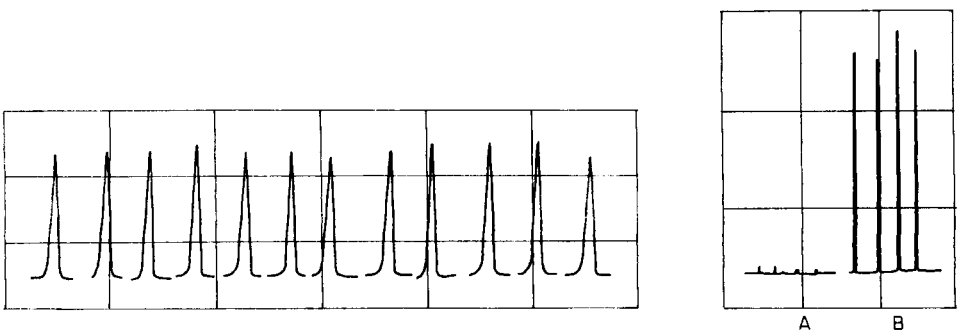

Fig. 5. Reproducibility of measurements by atomization from inserts (0.01 ng of Cd^{2+} was previously pipetted on the rods, which were dried and placed on the cup atomizer).

Fig. 6. Effect of electrochemical preconcentration on the sensitivity of the measurement (0.04 $\mu g\ l^{-1}$ Cd): (a) direct sampling (10 μl); (b) deposit after 10 min of electrolysis. (Electrolyte 0.1 M KCl, pH 7, E_c = —0.8 V vs. SCE; all other experimental conditions as in Table 1.)

be presumed. Consequently, the following schemes can be proposed for the atomization of cadmium:

A: $Cd^{2+}(aq) + 2e^- \rightarrow Cd(s)$

B: $Cd^{2+}(aq) + 2Cl^-(aq) \rightleftharpoons CdCl_2(s) \rightleftharpoons CdCl_2(l) \rightleftharpoons CdCl_2(v) \rightleftharpoons$

$Cd(v) + 2Cl(v) \rightleftharpoons Cd(s) + Cl_2(v)$

$\Downarrow$

or $CdCl_2(s)$

C: $Cd(s) \rightleftharpoons Cd(l) \rightleftharpoons Cd(v)$

Here s, l and v indicate the solid, liquid and vapour phases.

Additionally for the case of atomization from $CdCl_2$, the following mechanism is also likely:

$$CdCl_2(aq) \rightleftharpoons CdCl_2(s) \rightleftharpoons CdCl_2(l) \rightleftharpoons CdCl_2(v) \rightleftharpoons \begin{cases} Cd \\ Cd^* + Cl_2(v) \\ Cd^{2+} \end{cases}$$

This scheme is also valid for normal wall atomization. The study and comparison of these systems can therefore be of value for better understanding of processes and reaction mechanisms in electrothermal atomizers, as well as for practical analytical applications because the determinations involving electrolytic preconcentration are free of matrix interferences in the final measurement step.

As was mentioned above, electrolysis at controlled cathode potential is an excellent technique for the successive removal of metals and their species from solution. However, the experimental conditions (electrolyte, electrolysis current, time of electrolysis, etc.) must be carefully controlled; the quantity and quality of the metal deposit are strongly dependent on these conditions, as are the preconcentration, separation efficiency and reproducibility. These are especially critical for electrodeposition on non-metallic electrodes from solutions of low concentrations of metal ions [14]. Table 2 shows the influence of the electrolyte and applied potential on the amount of the deposited metal.

In addition to the parameters mentioned above, the selection of graphite electrodes and preparation of their surfaces are important because they also influence the reproducibility of results. As is shown in Table 3, the porosity of the graphite depends on the producer (origin) and on the exposure to higher temperatures. High porosity is detrimental to reproducibility because of uncontrolled sorption processes. However, the same electrode can be used for several successive electrolyses without additional treatment if the quality of the graphite is satisfactory. Usually, after the fifth run the working surface should be renewed, i.e., it must be repolished.

Although only a small part of the element present is deposited from the solution, high preconcentration rates are obtained. The amount of metal

TABLE 2

The influence of the pH of the 0.1 M KCl electrolyte and the potential, E_c, of the working electrode on the amount of cadmium deposited

pH	E_c vs. SCE (V)	Absorbance (peak height)	pH	E_c vs. SCE (V)	Absorbance (peak height)
3	−0.7	0.299	7	−1.0	0.419
	−0.8	0.342		−1.2	0.433
	−1.0	0.364	9	−0.7	0.056
	−1.2	0.423		−0.8	0.226
7	−0.7	0.319		−1.0	0.350
	−0.8	0.360		−1.2	0.349

TABLE 3

Absorption properties of different types of carbon after successive exposures to high temperatures during atomization[a]

Run	Ringsdorff		Karbon-Topolčany	
	A	B	C	D
1	0.015	0.032	0.040	0.038
2	0.023	0.030	0.122	0.070
3	0.040	0.038	0.100	0.070
4	0.020	0.015	0.089	0.066
5	0.028	0.035	0.099	0.082
6	0.060	0.040	0.081	0.079
7	0.030	0.028	0.951	0.266
8	0.045	0.042	0.848	0.998
9	0.060	0.035	—	—

[a]Rods A, B, C and D were soaked for 3 min in a 2.5 μg l^{-1} solution of cadmium. (The absorbance for direct measurement of 10 ml of the same solution was 0.105.) After each soaking, the rods were rinsed with distilled water and exposed to the atomization temperature.

deposited on the electrode obviously depends on the time of deposition. For example, for 0.08 μg l^{-1} cadmium deposited at −0.8 V vs. SCE, the absorbance peak heights obtained were rectilinearly related to the deposition time up to at least 5 min. However, it should be noted that the electrolyses were done under conditions such that the metal ions to be deposited were not depleted to any great extent in the solution. The use of this technique can be extended to a wide range of concentrations in the solution.

The selection of the potential of the working electrode is very important. If the analyte solution is complicated, the presence of possible complex-forming ligands must be considered because the potential is defined by the

ligand present in the solution, in accordance with the stability of the metal complex formed (Table 4)

$$M^{n+} + nL^{-} \rightleftharpoons ML_n^{m-n};\ K = [ML_n^{m-n}]/[M^{n+}][L^{-n}]$$

and can be calculated on the basis of the relationship

$$E_c = E^0_{M^{n+}/M} - \log K_{(ML_n^{m-n})} - (0.059/n) \log [L^{-n}]/[ML_n^{m-n}]$$

The potential should be as negative as possible when high preconcentration rates are desirable. Of course, the evolution of hydrogen must be avoided, because the evolution of gas causes the reproducibility of the deposition to deteriorate (Table 5). Under such conditions, the deposit on the surface is likely to be inhomogeneous. Therefore, experimental testing of the calculated cathode potential is advisable. Selection of the proper potential of the working electrode is especially critical when different species of an element in the solution are to be determined.

The dependence of the absorption on the concentration was found to be rectilinear over wide concentration ranges. This range is primarily dependent on the duration of the electrolysis. For example, with a 5-min electrolysis time, but otherwise under the conditions used for Fig. 6, the calibration was rectilinear for the range 0.04—0.20 $\mu g\ l^{-1}$ cadmium. The technique allows reliable results to be obtained. The precision of the whole procedure is satisfactory; relative standard deviations are in the range 7—15% at concentrations

TABLE 4

The influence of EDTA and the potential of working electrode on the amount of deposited cadmium

Electrolyte	Absorbance (peak height)		
	−0.70[a]	−0.80[a]	−0.90[a]
0.1 M KCl	0.049	0.069	0.071
0.1 M KCl/EDTA (pH 7)[b]	0.049	0.069	0.070
0.1 M KCl/EDTA + NH_3 (pH 9)[b]	0.020	0.029	0.023

[a] E_c vs. SCE (V) for deposition. [b] For a 0.5 $\mu g\ l^{-1}$ Cd^{2+} solution with 1:1 mole ratio of Cd^{2+} to EDTA.

TABLE 5

The influence of the potential of working electrode on the amount of cadmium deposited[a]

E_c vs. SCE (V)	−0.70	−0.75	−0.80	−0.85	−0.90	−0.95	−1.00
Absorbance	0.409	0.413	0.438	0.441	0.481	0.485	0.501
s_r (%)[b]	17.7	16.0	8.5	14.2	15.2	18.0	16.3

[a] Conditions: 20 ml of 1 $\mu g\ l^{-1}$ Cd^{2+} solution (0.1 M KCl) electrolyzed for 10 min. Absorbances are the mean of four measurements. [b] Relative standard deviation.

TABLE 6

Results obtained in the analysis of water samples

Sample	Cadmium found ($\mu g\ l^{-1}$)		
	This method	s_r (%)	A.s.v.
Sea water	0.13	3.3	–
Mineral water	0.05	30.1	0.03
Spring water	0.03	18.5	0.03
River Sava	0.06	30.6	–
River Ljubljanica	0.04	10.1	–
River Gradaščica	0.04	15.7	–
River Drava	0.20	9.0	0.20

down to 0.05 $\mu g\ l^{-1}$ for aqueous solutions. The detection limit for cadmium was 4×10^{-9} g l^{-1} for a 20-min electrolysis time. The proposed design of the electrolysis cell enables several electrolyses to be done simultaneously from the same sample solution, which contributes to the reliability of the final result.

Electrochemical preconcentration on graphite electrodes can be advantageous in a.a.s. determinations of some elements in materials like pure reagents, biological materials, environmental samples, etc. The technique was tested for the determination of cadmium in water samples. Some of the results obtained are presented in Table 6. They are comparable with those obtained by anodic stripping voltammetry (a.s.v.). However, it is necessary to consider the fact that the ionic strength, composition and character of the sample can influence the efficiency of electrodeposition. Therefore, the use of the standard addition method for the evaluation of results is advisable.

The authors thank M. Strle for her help in the experimental work. Financial support from the Research Community of Slovenia is gratefully acknowledged.

REFERENCES

1 C. Fairless and A. J. Bard, Anal. Lett., 5 (1972) 433.
2 F. O. Jensen, J. Dolezal and F. J. Langmyhr, Anal. Chim. Acta, 72 (1974) 245.
3 W. Lund and B. V. Larsen, Anal. Chim. Acta, 70 (1974) 299.
4 W. Lund and B. V. Larsen, Anal. Chim. Acta, 72 (1974) 57.
5 M. P. Newton, J. V. Chauvin and D. G. Davis, Anal. Lett., 6 (1973) 89.
6 M. P. Newton and D. G. Davis, Anal. Chim. Acta, 47 (1975) 2003.
7 E. J. Czobic and J. P. Matousek, Spectrochim. Acta, Part B, 25 (1980) 741.
8 G. E. Batley and J. P. Matousek, Anal. Chem., 49 (1977) 2031.
9 G. Volland, P. Tschöpel and G. Tölg, Anal. Chim. Acta, 90 (1977) 15.
10 W. Lund, Y. Thomassen and P. Døvle, Anal. Chim. Acta, 93 (1977) 53.
11 Y. Thomassen, B. V. Larsen, F. J. Langmyhr and W. Lund, Anal. Chim. Acta, 83 (1976) 103.

12 M. Veber and S. Gomišček, Proceedings of 6th Yug. Conference on Pure and Applied Spectroscopy, Bled, 1976, Vol. I, p. 238.
13 M. Veber and S. Gomišček, Vestn. Slov. Kem. Drus., 31 (1984) 313.
14 J. L. Andersen and R. E. Sioda, Talanta, 30 (1983) 627.

Analytica Chimica Acta, 193 (1987) 169—178
Elsevier Science Publishers B.V., Amsterdam — Printed in The Netherlands

QUELQUES INTERFERENCES SUR LE DOSAGE DU PLOMB DANS LES EAUX ALIMENTAIRES PAR SPECTROSCOPIE D'ABSORPTION ATOMIQUE SANS FLAMME

J. VANDEGANS*, P. ROSSEELS, W. VERPLANCKEN et J.-C. HAUREZ

Service de Chimie Analytique, Institut des Industries de Fermentation — Institut Meurice Chimie, C.E.R.I.A., Avenue Emile Gryzon 1, 1070 Bruxelles (Belgique)

(Reçu le 14 Juillet 1986)

SUMMARY

Interferences in the determination of lead in potable water by graphite-furnace atomic absorption spectrometry are examined. The peak-height signal and the pyrolysis/atomization curves are studied as a function of the nature and concentration of the interferent. Some interferences are caused not by the cation or anion, but by the salt. Magnesium chloride interferes most extensively not only by decreasing the signal but also by changing the pyrolysis curve. Interferences are more pronounced in hydrochloric than in nitric acid medium. Frequently, stabilization of an interfering effect from a defined interferent concentration was observed in nitric acid medium whereas in hydrochloric acid medium the signals continued to change.

RÉSUMÉ

La spectroscopie d'absorption atomique avec four en graphite a été utilisée en vue de montrer les interférences sur le dosage du plomb dans les eaux alimentaires. Cette étude s'est portée sur la variation de la hauteur du signal et sur les courbes de pyrolyse/atomisation en fonction de la nature et de la concentration de l'interférent. Nous avons pu mettre en évidence un certain nombre d'interférences non pas de cations ou d'anions mais plutôt de sels. Parmi ceux-ci, le $MgCl_2$ produit les effets les plus marqués non seulement par une diminution importante des signaux mais encore par une modification des courbes de pyrolyse. De plus, la manière dont $MgCl_2$ interfère dépend de sa concentration. Les interférences sont beaucoup plus marquées en milieu chlorhydrique qu'en milieu nitrique. A plusieurs reprises, nous avons observé une stabilisation du phénomène à partir d'une certaine concentration en interférent en milieu HNO_3 alors qu'en milieu HCl le signal continue à évoluer.

Etant donné la présence fréquente de canalisations en plomb dans de nombreuses installations domestiques de distribution d'eau, le contrôle de la teneur de cet élément dans les eaux alimentaires reste un problème d'actualité. La technique la plus utilisée est sans conteste la spectrométrie d'absorption atomique avec four en graphite. Le plomb est malheureusement un élément dont le dosage est rendu difficile à cause du nombre très élevé d'interférences auxquelles il est sensible. Une littérature considérable traite de ce sujet, soit dans le but de comprendre ces interférences [1—4], soit d'y

0003-2670/87/$03.50

remédier au moyen de correcteurs chimiques (nitrate [3, 5—8], agent complexant [9—11], phosphate [4, 12], l'oxygène [3]), de correcteurs spectrométriques (lampe au D_2, correcteur Zeeman [13]) ou de modifications du four en graphite (plate-forme de L'vov [8]).

Dans la majorité des cas, les travaux portent essentiellement sur l'influence de la concentration d'un élément sur le signal d'absorbance du plomb et plus rarement sur l'étude des courbes de pyrolyse et d'atomisation. Notre travail aborde surtout cette deuxième partie du problème. Nous nous sommes intéressés à l'influence des principaux ions que l'on rencontre dans les eaux alimentaires à savoir Na^+, K^+, Ca^{2+}, Mg^{2+}, Cu^{2+}, Zn^{2+}, Fe^{3+}, SO_4^{2-} et PO_4^{3-} en comparant les milieux nitriques et chlorhydriques.

PARTIE EXPERIMENTALE

Toutes les mesures sont effectuées sur un spectrophotomètre d'absorption atomique Perkin-Elmer, modèle 360, équipé d'un four en graphite HGA-74. La source est une lampe à décharge sans électrode au plomb (Perkin-Elmer). La raie excitatrice utilisée est à 283,3 nm. Aucun système de correction des absorptions non spécifiques n'a été utilisé. Les injections sont réalisées manuellement au moyen de micropipettes Eppendorf de 20 μl. Chaque mesure a été répétée au minimum quatre fois. Des tests de reproductibilité ont été réalisés sur vingt mesures. Le courant gazeux (N_2) est coupé pendant l'étape d'atomisation (gas stop).

Nous avons vérifié si les températures mesurées (T_m) correspondaient aux températures programmées (T_p) (Fig. 1). Pour ce faire, nous avons introduit dans le four en graphite, par l'ouverture réservée à l'introduction de l'échantillon, un thermo-couple chromel-alumel. Les températures ont été mesurées pendant l'étape d'atomisation, dans les trois modes de balayage du gaz inerte (gas stop, mini flow et gas flow). Le thermo-couple a été placé soit au centre soit contre la paroi du tube de graphite. La Fig. 1 présente les résultats comparés aux valeurs théoriques. Toutes les températures données sont les températures mesurées et non celles programmées (les températures supérieures à 1300°C sont extrapolées (Fig. 1)). Les températures mesurées au centre et contre la paroi interne sont identiques aux erreurs de mesure près. Le programme de température est présenté au Tableau 1.

Tous les réactifs sont de qualité pour analyse (Merck). En milieu nitrique les interférents sont ajoutés sous forme de nitrates tandis qu'en milieu chlorhydrique ils le sont sous forme de chlorures. Les solutions de plomb contiennent toujours 50 ng ml^{-1}. Dans les graphiques, h_0 représente la hauteur du signal d'absorbance (cm) en l'absence d'interférent et h, le signal en présence de l'interférent, blanc déduit.

RÉSULTATS

Influence de la nature des anions

Lors de la prise d'un échantillon d'eau, il est nécessaire d'additionner une certaine quantité d'acide, généralement 1%, afin d'éviter les adsorptions sur

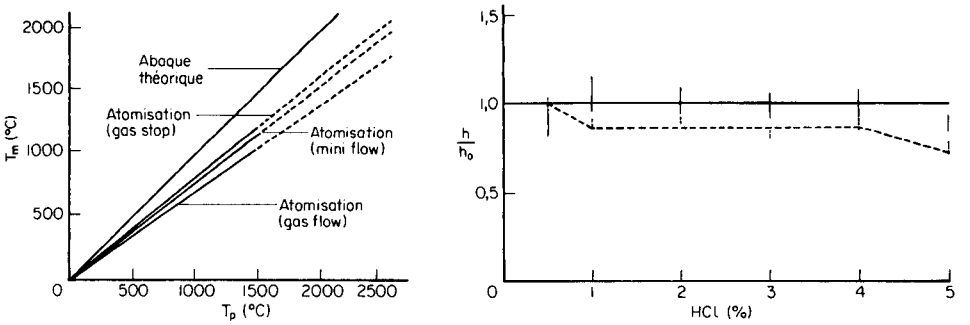

Fig. 1. Comparaison des températures programmées (T_p) avec les températures mesurées (T_m) dans le four en graphite.

Fig. 2. Influence de la concentration en HCl (%) sur le signal relatif d'atomisation du Pb: (——) milieu HCl pur; (- - -) milieu HNO_3 1% + HCl x%. Température de pyrolyse 450°C, température d'atomisation 2 000°C.

TABLEAU 1

Programme de températures

Séchage		30 s	130°C
Pyrolyse		20 s	450°C
	ou	20 s	T variable[a]
Atomisation		6 s	2000°C
	ou	6 s	T variable[b]
Nettoyage		3 s	T maximum

[a]Pour l'établissement de la courbe de pyrolyse. [b]Pour l'établissement de la courbe d'atomisation.

les parois du récipient ou les précipitations de certains cations. L'acide nitrique étant le milieu le plus souvent conseillé pour l'analyse du plomb, nous le prendrons comme milieu de référence.

Dans les conditions de pyrolyse et d'atomisation utilisées (450°C et 2000°C) la présence d'HCl, en lieu et place d'HNO_3, ne modifie guère le signal d'absorbance du plomb (Fig. 2). Par contre en milieu mixte (HNO_3 1% + HCl x%, Fig. 2) une atténuation du signal, de l'ordre de 20%, se marque. L'apparente inactivité de HCl peut paraître contradictoire avec de nombreux travaux [2, 4—9, 11, 12] mais dans ces études, les chlorures sont le plus souvent ajoutés sous forme de sel et pas d'acide (voir ci-dessous).

Si l'action de HCl par rapport à HNO_3 est nulle sur le signal dans les conditions de pyrolyse et d'atomisation précitées, elle est loin d'être négligeable sur les courbes de pyrolyse/atomisation comme nous pouvons le constater sur la Fig. 3. Cette action se marque surtout sur la courbe de pyrolyse. Les pertes par volatilisation lors de la pyrolyse apparaissent dès 450°C en milieu HCl contre 760°C en milieu HNO_3 1%. En milieu chlorhydrique l'entité présente en phase vapeur, serait PbCl [2, 4]. L'addition d'acide nitrique à

une solution chlorhydrique fournit une courbe de pyrolyse fort semblable à celle obtenue en milieu nitrique seul (Fig. 3), preuve du déplacement de HCl par HNO_3, le plomb se retrouvant finalement sous la forme PbO. Nous observons simplement une légère dégradation de la reproductibilité des mesures. Nous notons en outre une différence de température par rapport aux travaux de Pinta et Riandey [14] et qui signalent la volatilisation de l'oxyde dès 600° C.

Nous avons également recherché l'action des ions sulfates et phosphates additionnés sous forme d'acide sulfurique et phosphorique. Les sulfates et les phosphates entraînent une légère exaltation du signal du plomb (Fig. 4). Maney et Luciano [12] constatent également cette action positive des phosphates, qui ont d'ailleurs été proposés comme suppresseur d'interférences [4, 8]. Par contre, Bertenshaw et al. [6] signalent une action négative importante des sulfates, mais leurs conditions opératoires ne sont pas identiques aux nôtres. Ils ajoutent du Na_2SO_4 au lieu de H_2SO_4 et travaillent à 217 nm contre 283,3 nm.

Contrairement à ce que l'on pourrait croire, les sulfates et les phosphates ne stabilisent pas le plomb lors de la pyrolyse (Fig. 5) comme le fait l'acide nitrique. La courbe de pyrolyse commence à chuter rapidement. D'autre part, les phosphates provoquent une augmentation de la température d'atomisation maximale, la portant presque à 2100° C contre 1800° C en milieu nitrique et 1700°C en milieu chlorhydrique (Fig. 3). Nous observons également une dégradation de la reproductibilité.

Influence de la nature des cations en milieu nitrique

Afin de ne pas observer d'influences mixtes, les cations sont ajoutés sous forme de nitrates. Le signal h_0 est celui obtenu en milieu nitrique 1% pur. Les Ca, Cu, Zn et Fe n'agissent pratiquement pas tandis que Na, K et Mg

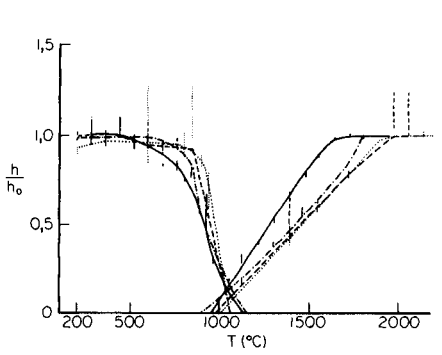

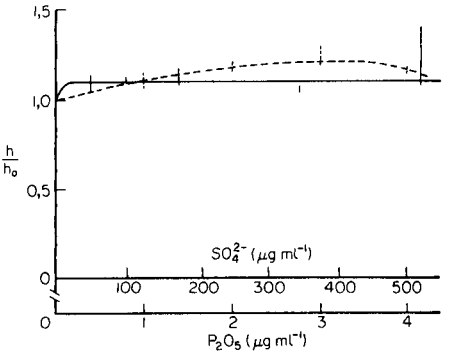

Fig. 3. Courbes de pyrolyse/atomisation (50 ng ml^{-1} Pb): (—·—) HNO_3 1%; (——) HCl 1%; (- - -) HNO_3 + HCl 1%; (· · ·) HNO_3 + HCl 2%.

Fig. 4. Influence de la concentration en acide sur le point d'atomisation du Pb: (——) H_2SO_4 ; (- - -) H_3PO_4. Température de pyrolyse 450°C, température d'atomisation 2000°C.

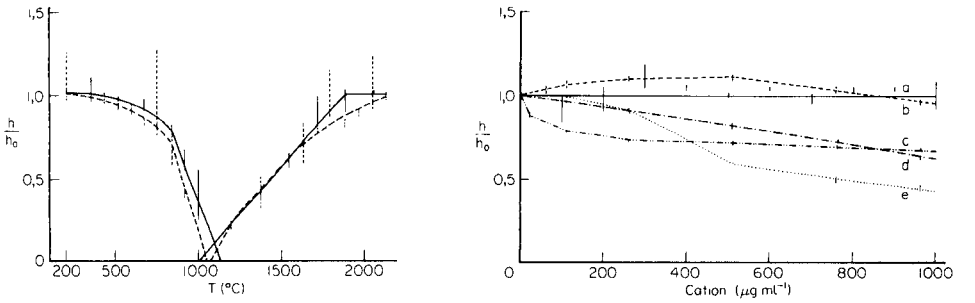

Fig. 5. Courbes de pyrolyse/atomisation (50 ng ml^{-1} Pb): (—) 175 $\mu g\ ml^{-1}$ SO_4^{2-}; (- - -) 4 $\mu g\ ml^{-1}$ P_2O_5.

Fig. 6. Influence de la concentration en cation sur le signal relatif d'atomisation du Pb en milieu HNO_3 1%: (a) Ca^{2+}, Cu^{2+} et Zn^{2+}, droites confondues à celle du Ca^{2+}; (b) Fe^{3+}; (c) K^+; (d) Na^+; (e) Mg^{2+}. Température de pyrolyse 450°C, température d'atomisation 2000°C.

atténuent le signal du plomb de 30% pour les deux premiers et de 50% pour le troisième (Fig. 6).

Nous comparons les courbes de pyrolyse/atomisation à celles obtenues en milieu HNO_3 pur (Fig. 3). Le calcium ne modifie guère la courbe de pyrolyse (Fig. 7). Quelle que soit la concentration en Ca^{2+} (100, 200, 300 et 500 $\mu g\ ml^{-1}$) les courbes sont identiques. Le magnésium agit de la même manière alors que le potassium favorise la volatilisation (Fig. 8), celle-ci débutant de nouveau dès 450°C. La courbe d'atomisation en présence de l'un ou l'autre de ces trois éléments est peu ou pas influencée (Fig. 8).

Influence de la nature des cations en milieu chlorhydrique

Toujours afin de ne pas observer d'influences mixtes, les sels utilisés sont des chlorures. La hauteur h_0 dans ces essais-ci, est celle obtenue en milieu HCl 1% pur. Il est bien connu que le milieu chlorhydrique est plus sujet aux interférences que le milieu nitrique. Nos expériences confirment la chose mais font aussi apparaître un certain nombre de points nouveaux. Tous les éléments étudiés (Ca, Mg, Na, K, Zn, Cu, Fe) en milieu chlorhydrique provoquent une diminution de la sensibilité du plomb (Fig. 9), diminution qui peut atteindre 80%. Quand l'interférence apparaît déjà en milieu nitrique, elle est beaucoup plus forte en milieu chlorhydrique (Na, K).

Les courbes pyrolyse/atomisation sont également fort perturbées (Figs. 10 et 11). En examinant les courbes de pyrolyse nous constatons que le palier avant le début de volatilisation se réduit fortement et disparaît même totalement en présence de magnésium (Fig. 10). D'autre part, la pente de la courbe de pyrolyse, qui dépend notamment du ΔH de vaporisation est moins raide qu'en milieu nitrique ce qui entraîne souvent une température de volatilisation complète plus élevée qu'en milieu nitrique. De même la tempér-

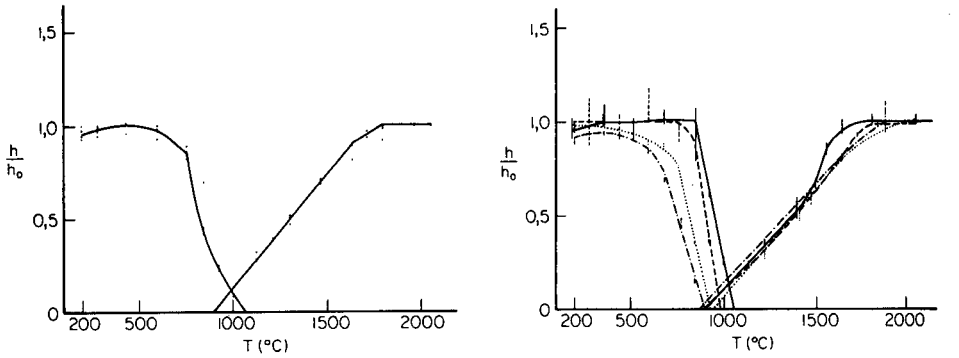

Fig. 7. Courbe de pyrolyse/atomisation (50 ng ml^{-1} Pb) en présence de Ca^{2+} et de HNO_3 1%.

Fig. 8. Courbe de pyrolyse/atomisation (50 ng ml^{-1} Pb) en milieu HNO_3 1% en présence d Mg^{2+} et de K^+: (—·—) 100 μg ml^{-1} K^+; (···) 5 μg ml^{-1} K^+; (- - -) 50 μg ml^{-1} Mg^{2+}; (— 30 μg ml^{-1} Mg^{2+}.

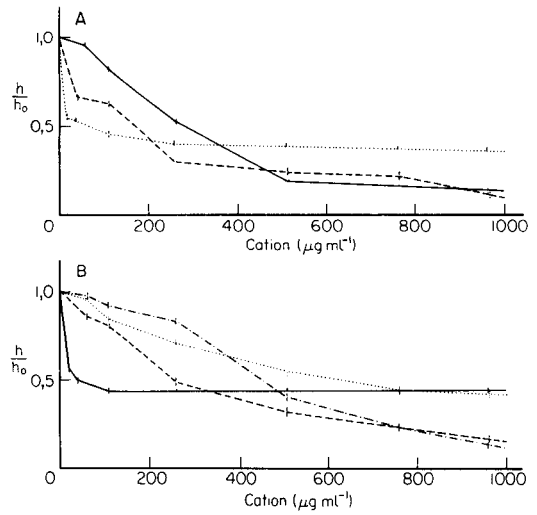

Fig. 9. Influence de la concentration en cation sur le signal d'atomisation du Pb en milieu HCl 1%. (A) (···) Na^+; (—) Mg^{2+}; (- - -)Ca^{2+}. (B) (—) K^+; (—·—) Fe^{2+}; (- - -) Cu^{2+}; (···) Zn^{2+}. Température de pyrolyse 450°C; température d'atomisation 2000° C.

ature de début d'atomisation est plus élevée. Ce ne sont cependant pas les deux seuls points qui ont été observés et nous prendrons le cas du magnésium pour étudier la troisième influence. Il s'agit d'une dégradation de la reproductibilité. En milieu simple, la déviation standard relative estimée sur 20 mesures est de 3% avec l'acide nitrique et de 4% avec l'acide chlorhydrique ce qui est tout à fait acceptable. Nous avons observé, et ceci de façon systématique une moins bonne reproductibilité des mesures lorsque

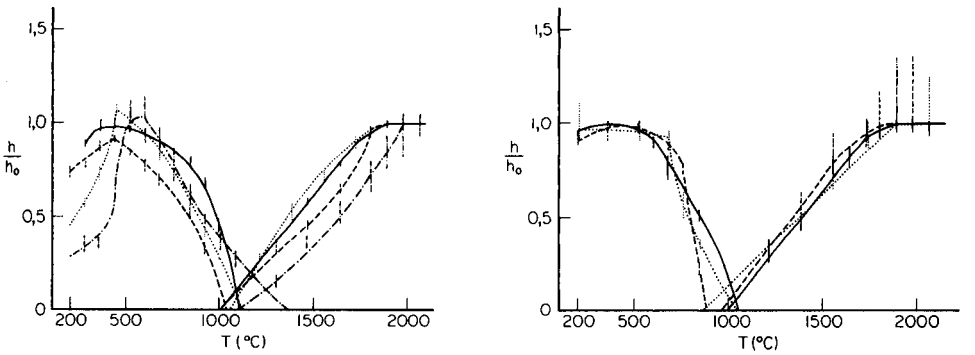

Fig. 10. Courbes de pyrolyse/atomisation (50 ng ml^{-1} Pb) en milieu HCl 1% en présence de Mg^{2+} à différentes concentrations: (——) 10; (- - -) 30; (· · ·) 50; (— · —) 250 $\mu g\ ml^{-1}$.

Fig. 11. Courbes de pyrolyse/atomisation (50 ng ml^{-1} Pb) en milieu HCl 1%: (- - -) 20 $\mu g\ ml^{-1}$ Na^+; (· · ·) 50 $\mu g\ ml^{-1}$ K^+; (——) 40 $\mu g\ ml^{-1}$ Ca^{2+}.

les solutions contiennent au moins 250 $\mu g\ ml^{-1}$ de magnésium. La déviation standard oscille alors entre 15 et 20% (Fig. 10).

Il est bien connu que si les solutions deviennent trop concentrées en sel, la reproductibilité diminue. Ce fait a été attribué à une mauvaise désagrégation des cristaux entraînant des occlusions de l'élément à doser [6, 15]. L'interférence du $MgCl_2$ a déjà été étudiée de nombreuses fois en absorption atomique [3, 7, 8] tout comme en émission atomique [16]. Comme nous avons travaillé sans système de correction des absorptions non spécifiques, nous pourrions croire que c'est à ce niveau qu'il faut chercher l'explication. Le fait de brancher un correcteur au D_2, comme nous l'avons fait un moment donné, ne réduit pas cette interférence. Allain et Mauras [3] ont d'ailleurs montré que le $MgCl_2$ moléculaire en phase vapeur n'absorbe pratiquement pas. L'action du $MgCl_2$ est triple: le signal d'absorption du plomb est fortement réduit; la courbe de pyrolyse ne présente presque plus de palier, et dans certains cas, la reproductibilité est très aléatoire. Ces trois points nous paraissent indissociables. Lorsque la courbe de pyrolyse ne présente plus de palier, la reproductibilité des températures de pyrolyse n'est plus suffisante ce qui peut entraîner un manque de reproductibilité des mesures et/ou des pertes considérables pendant l'étape de pyrolyse.

DISCUSSION

L'examen de l'abondante littérature relative aux interférences montre, à quelques exceptions près, que les auteurs ont souvent tendance à attribuer une interférence à l'un ou l'autre cation ou anion sans nécessairement tenir compte de l'ion qui accompagne ce cation ou cet anion. D'après nos résultats et ceux obtenus dans d'autres travaux, nous pensons que l'anion et le cation agissent conjointement. Prenons quelques exemples précis. Nous avons constaté que l'acide sulfurique ne modifie pratiquement pas le

signal jusqu'à 500 μg ml^{-1} (Fig. 4) alors que Na_2SO_4 réduit considérablement le signal [8] dans le même domaine de concentration. On pourrait croire que c'est le sodium qui est en cause et l'on devrait par conséquent s'attendre à ce que le NaCl produise un effet similaire ce qui n'est pas le cas selon Sthapit et al. [8]. Si nous comparons l'effet que nous avons observé en présence de fer, nous constatons qu'il est différent avec $Fe(NO_3)_3$ (Fig. 6) et $FeCl_2$ (Fig. 9B), alors que HCl et HNO_3 donnent les mêmes résultats.

A ce stade, nous pouvons nous poser deux questions: les correcteurs chimiques sont-ils toujours adéquats et les résultats obtenus sur un appareil sont-ils transposables à un autre? La réponse à ces deux questions dépend avant tout de la précision que l'on attend de son dosage, mais nous avons plutôt envie de répondre par non. Slavin et al. [7] proposent notamment d'utiliser l'acide sulfurique pour corriger l'interférence des chlorures. L'idée paraît évidemment tout à fait pertinente dans la mesure où l'acide sulfurique déplace les chlorures encore mieux que l'acide nitrique bien que la courbe de pyrolyse en milieu sulfate soit moins favorable (Fig. 5), mais d'autre part si l'échantillon contient une certaine quantité de Na^+, même seulement 100 μg ml^{-1}, le Na_2SO_4 formé risque d'encore plus perturber la mesure. Schmid et Krivan [4] proposent quant à eux l'addition de $NH_4H_2PO_4$. Ici c'est une action conjuguée avec K^+ qui est à craindre [8]. Il y a par conséquent de fortes chances qu'avec certains échantillons l'acide sulfurique, ou le phosphorique, convienne, alors que dans d'autres cas les résultats soient complètement faussés.

Il arrive souvent que l'action d'un sel sur l'absorbance du plomb varie avec la concentration de ce sel et ceci parfois de façon très importante. Le rôle du correcteur, qui est normalement de niveler l'action de la matrice, peut être complètement détruit par de légères fluctuations d'un des ions de la matrice d'un échantillon à l'autre. Rappelons enfin que les études d'interférences sont généralement réalisées ion par ion ou sel par sel mais nous ne savons presque rien sur les actions conjuguées de plusieurs cations et anions.

Les transpositions directes des résultats d'un appareil à l'autre nous paraissent également hasardeuses. Sthapit et al. [8] ne signalent aucune interférence du $Mg(NO_3)_2$ jusqu'à 500 μg ml^{-1} alors que nous avons observé une diminution du signal d'environ 30% à 500 μg ml^{-1} (Fig. 6). C'est aussi le seul cas énoncé par ces auteurs où l'usage d'une plate-forme de L'vov est défavorable par rapport au four classique. Toujours selon les mêmes auteurs, NaCl n'agit presque pas jusqu'à 500 μg ml^{-1}. Dans notre étude, dès 20 μg ml^{-1}, le signal a chuté de 40% (Fig. 9A). Legret et al. [17] montrent que l'influence du potassium ne fait que croître avec la concentration en K^+ alors que dans notre travail nous observons une stabilisation dès 100 μg ml^{-1} (Figs. 6 et 9B). Nous pourrions multiplier les exemples presque indéfiniment.

Nous pensons que ces divergences sont dues à l'appareillage. En effet, les températures qui règnent dans le four ne sont pas, du moins avec notre installation, celles programmées sur la console de commande. Les différences

peuvent être considérables (Fig. 1). Lorsque les paliers de pyrolyse sont fortement réduits, de très légères différences d'un appareil à l'autre, peuvent entraîner des conséquences énormes. La vitesse avec laquelle la température augmente lors de l'étape d'atomisation joue un rôle important comme l'ont montré Schmid et Krivan [4] et des différences non négligeables peuvent également apparaître d'un appareil à l'autre. Tous ces facteurs peuvent influencer considérablement les résultats d'une analyse. Du point de vue chimique, il semble que l'acide nitrique soit malgré tout le meilleur acidifiant. C'est avec lui que les interférences sont les moins prononcées. Une concentration de 1% en acide nitrique nous paraît être un bon compromis entre une action chimique efficace d'une part et une bonne conservation du four en graphite d'autre part. L'usage de la droite de calibrage n'est pas à conseiller et nous lui préférons nettement la méthode de l'addition standard, à condition bien entendu d'être tout à fait certain de la linéarité parfaite de la résponse avec la concentration en plomb. L'étalonnage en température du four et l'établissement des courbes de pyrolyse/atomisation dans la matrice à analyser sont deux précautions indispensables à prendre avant toute analyse. Bien qu'on ne puisse nier l'existence des interférences chimiques, nous pensons que bon nombre de résultats sont faussés suite à un choix insuffisamment rigoureux des conditions de programmation.

Conclusions

Cette étude nous a permis de mettre en évidence un certain nombre d'interférences non pas de cations ou d'anions mais plutôt de sels, sur le signal d'absorbance du plomb. Parmi les sels étudiés, le $MgCl_2$ est celui qui produit les effets les plus marqués non seulement par une diminution importante des signaux mais encore par une modification considérable des courbes de pyrolyse et une dégradation importante de la reproductibilité. De plus, la manière dont le $MgCl_2$ interfère dépend de la concentration de celui-ci.

Les interférences sont beaucoup plus marquées en milieu chlorhydrique qu'en milieu nitrique. A plusieurs reprises, nous avons observé une stabilisation du phénomène à partir d'une certaine concentration en interférent en milieu HNO_3 alors qu'en milieu HCl le signal continue à évoluer. Dans des travaux ultérieurs, nous rechercherons quelles sont les influences mixtes par addition de deux, trois ou plusieurs sels en proportions variables.

BIBLIOGRAPHIE

1 R. E. Sturgeon, C. L. Chakrabarti et C. H. Langford, Anal. Chem., 48 (1976) 1792.
2 W. Frech et A. Cedergren, Anal. Chim. Acta, 88 (1977) 57.
3 P. Allain et Y. Mauras, Anal. Chim. Acta, 165 (1984) 141.
4 W. Schmid et V. Krivan, Anal. Chem., 57 (1985) 30.
5 S. Yasuda et H. Kakiyama, Anal. Chim. Acta, 89 (1977) 369.
6 M. P. Bertenshaw, D. Gelsthorpe et K. C. Wheatstone, Analyst, 107 (1982) 163.

7 W. Slavin, G. R. Carnrick et D. C. Manning, Anal. Chem., 56 (1984) 163.
8 P. R. Sthapit, J. M. Ottaway, D. J. Halls et G. S. Fell, Anal. Chim. Acta, 165 (1984) 121.
9 M. Tominaga et Y. Umezaki, Anal. Chim. Acta, 139 (1982) 279.
10 K. Matsusaki, T. Yoshino et Y. Yamamoto, Anal. Chim. Acta, 144 (1982) 189.
11 K. Matsusaki, Anal. Chim. Acta, 141 (1982) 233.
12 J. P. Maney et V. J. Luciano, Anal. Chim. Acta, 125 (1981) 183.
13 G. Wibetoe et F. J. Langmyhr, Anal. Chim. Acta, 165 (1984) 87.
14 M. Pinta et C. Riandey, Analusis, 3 (1975) 86.
15 J. A. Krasowski et T. R. Copeland, Anal. Chem., 51 (1979) 1843.
16 J. Marshall, S. K. Giri, D. Littlejohn et J. M. Ottaway, Anal. Chim. Acta, 147 (1983) 173.
17 M. Legret, D. Demare, P. Marchandise et D. Robbe, Anal. Chim. Acta, 149 (1983) 107.

Analytica Chimica Acta, 193 (1987) 179—191
Elsevier Science Publishers B.V., Amsterdam – Printed in The Netherlands

ORGANOPHOSPHORUS ACID INTERFERENCES IN FLAME ATOMIC ABSORPTION SPECTROMETRY

A. M. MAITRA

School of Chemistry, Macquarie University, North Ryde, N.S.W. 2113 (Australia)

E. PATSALIDES*

Department of Inorganic Chemistry, Sydney University, Sydney N.S.W. 2006 (Australia)

(Received 18th July 1986)

SUMMARY

The interference of the organophosphorus acids, 1-hydroxyethane-1,1-bisphosphonic acid, aminotris(methylenephosphonic acid), ethylenediaminetetrakis(methylenephosphonic acid) and hexamethylenediaminetetrakis(methylenephosphonic acid) on the determination of eighteen metal ions by flame atomic absorption spectrometry is reported. Comparisons with the effect of orthophosphoric acid reveal similarities and distinct differences in their interfering effects. In the air/acetylene flame, depressive interferences are attributed to the formation of phosphates, $M_3(PO_4)_2$, or hydroxyapatite-like compounds, $M_5(OH)(PO_4)_3$, in the flame aerosol particles for Mg, Ca, Sr, Ba, Mn, Co and Ni. Iron(III) and chromium(III) appear to form stable oxide phosphates, $M_2O_3 . MPO_4$ or $M_3O_4 . MPO_4$. Evidence for the formation of stable molybdenum carbides, MoC and MoC_2, is also presented. In the nitrous oxide/acetylene flame, serious interferences persisted only for molybdenum but were eliminated by the addition of sodium sulphate.

Organophosphorus acids I—IV and related compounds containing the C—$PO(OH)_2$ functional group [1] are increasingly being used in industrial water systems, principally boiler and cooling waters. These additives contribute, in synergy with other additives (e.g., hydroxide, zinc salts and polyacrylates), to scale and corrosion control, dispersion and deflocculation [2—5]. The stability, multifunctional properties and low toxicity of these chemicals make them attractive alternatives to older additives such as polyphosphates and chromate. Typical effective concentrations in treated systems are 1—10 mg l^{-1} [2]. The compounds here are 1-hydroxyethane-1,1-bisphosphonic acid (I), aminotris(methylenephosphonic acid) (II), ethylenediamine-

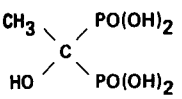

I

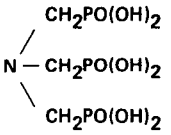

II

0003-2670/87/$03.50

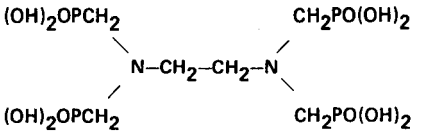

III

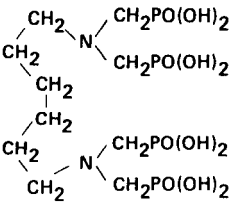

IV

tetrakis(methylenephosphonic acid) (III) and hexamethylenediaminetetrakis (methylenephosphonic acid) (IV).

There is a need for improved methods for the determination of organophosphorus compounds in water. Methods currently available [6, 7], with the possible exception of ion chromatography [8], are prone to interference. Another problem, on which little had been reported, is the interference of these additives in the determination of traces of other species. Such interferences can result from the sequestering and threshold-inhibiting properties of the organophosphorus acids. Methods based on complexiметry, turbidimetry and ion chromatography may be seriously affected if the organophosphorus acids are not decomposed prior to measurement steps. For example, in the turbidimetric determination of sulphate [9], the formation of colloidal barium sulphate may be prevented by these acids [6]. Similarly, strong complexation of the alkaline-earth and other metal ions may seriously affect their determination by EDTA titrations [9] or ion chromatography.

A further type of interference of the organophosphorus acids, which is the subject of this paper, arises in atomic absorption spectrometry (a.a.s.). This problem is related to the well-known depressive interference of orthophosphate in alkaline-earth and other metal determinations which occurs in the air/propane and air/acetylene flames [10—13]. Though interferences of phosphorus-containing species other than orthophosphate have not been much studied, results for glycerophosphate [14] and phosphine [15] indicate that they produce very similar effects to orthophosphate, at least for calcium.

In this paper, the interferences of organophosphorus acids I—IV on the a.a.s. determination of various metals are examined. The metals studied are those usually found in process waters, i.e., alkali metals (Li, Na, K), alkaline earths (Mg, Ca, Sr, Ba), other main-group metals (Zn, Cd, Pb) and transition metals (V, Cr, Mn, Fe, Co, Ni, Cu, Mo). The aim of this study was to identify interferences under various flame conditions, gain some insight into the interference processes and to find conditions for their elimination.

EXPERIMENTAL

Chemical and solutions

Organophosphorus acids I—IV were obtained from Monsanto Australia and Catoleum Pty. Dequest-2010 (I) and Dequest-2000 (II) were supplied as

aqueous 60% and 50% (w/w) solutions, respectively. Dequest-2041 (III) and Dequest-2051 (IV) were solids of nominal purity 95% and 97%, respectively. Nitrate salts were utilized except for vanadium(V) and molybdenum(VI) where the ammonium salts were used.

Stock solutions (1000 mg l^{-1}) of organophosphorus acids and other reagents were prepared in distilled water and stored in sealed polyethylene bottles. Working solutions (100 mg l^{-1}) were prepared immediately before use. All solutions were prepared with distilled water. Where necessary, the pH was adjusted with 15 M, 1 M or 0.1 M ammonia and/or nitric acid to values between 1 and 10.

Instrumentation and measurements

Varian-Techtron atomic absorption spectrometers (models 1200 and AA6) were used. Measurements, without background correction, were made at the most sensitive spectral lines (nm) and with the bandpasses (nm) recommended by the manufacturer: Li 670.8 (1.0), Na 589.0 (0.5), K 766.5 (1.0), Mg 285.2 (0.5), Ca 422.7 (0.5), Sr 460.7 (0.2), Ba 553.5 (0.5), Pb 217.0 (0.5), Zn 213.9 (1.0), Cd 228.8 (0.5), V 318.5 (0.2), Cr 357.9 (0.2), Mn 279.5 (0.2), Co 240.7 (0.2), Fe 248.3 (0.2), Cu 324.7 (0.5), Ni 232.0 (0.2), Mo 313.3 (0.5).

Flame conditions and viewing heights were varied as required. Instrument-grade acetylene (CIG Australia) was used as received. The specified phosphine content of this gas was 1—5 ppm (v/v).

Dual nebulization system. For the Varian AA6 instrument, a dual nebulizer was constructed by machining a polypropylene cap similar to that of the instrument nebulizer system. The cap was drilled to accommodate two Varian AA6 nebulizers and glass impact beads. A 3-cm polyethylene baffle was fixed between the nebulizers to prevent early mixing of the aerosol streams. In operation, one of the nebulizers, a variable type, was adjusted to give the same uptake (5.5 ml min^{-1}) as the fixed nebulizer. This system was used to distinguish between condensed-phase and vapour-phase interferences [16]. This technique was also used to study the mode of action of the releasing agents.

Molar metal/phosphorus ratios. Where interferences were stoichiometric i.e., interference plots consisted of two nearly linear curves, the first usually having a negative slope and the second an approximately zero slope), metal/phosphorus ratios were evaluated by interpolating the curves to the equivalence point and calculating the ratio of the molar concentration of metal to phosphorus.

RESULTS AND DISCUSSION

Alkali metals (Li, Na, K)

No serious interferences were observed for the determination of these metals in the air/acetylene flame. Relatively high concentrations of orthophosphoric or organophosphorus acids (100 mg l^{-1}) produced very small (ca. 2%) enhancements for 5 mg l^{-1} lithium.

Magnesium and alkaline earth metals

In this group, interferences produced by the organophosphorus acids I—IV strongly resembled those of orthophosphoric acid and were not markedly affected by pH in the range 1—10. For example, at low observation heights in the fuel-lean air/acetylene flame (0—5 mm above the tip of the inner blue cone), depressive stoichiometric interferences were obtained (Fig. 1). No interferences were observed at higher positions (10 mm or above) in this flame nor, as expected, in the hotter nitrous oxide/acetylene flame. In the fuel-rich air/acetylene flame, depressions were again observed at low heights. However, whereas for strontium and barium these effects persisted higher in the flame, clear enhancements were observed for magnesium and calcium at these heights. The nature of these interferences was examined in dual-nebulizer experiments (Table 1). The data show that interferences produced by compounds I—IV and orthophosphoric acid in the fuel-lean flame are of the condensed-phase type, resulting from the formation of refractory compounds in the flame aerosol particles. From the absorbance/height profiles in Fig. 2, it is apparent that such particles vaporize or decompose during their ascent in the flame; the interference diminishes with height, eventually becoming zero. The reason for the enhancing effect is not clear; it is not due to a condensed-phase effect because enhanced absorbance was obtained even when the analyte and interferent were introduced into the flame from separate nebulizers. The enhancement effects are therefore assigned to flame reactions involving phosphorus species.

Metal/phosphorus ratios calculated from interference curves like Fig. 1 further characterize the interferences. Table 2 summarizes the data for various metals. For magnesium and the alkaline earths, the ratios were in the range 1.50—1.81 for the organophosphorus acids and 1.50—1.65 for orthophosphoric acid, with an average standard deviation of 0.15. From these data it is concluded that for each element the same refractory species forms in the flame irrespective of whether the interferent is I, II, III, IV or orthophosphoric acid. Furthermore, because the ratios are similar for all the four metals tested, the same type of species is involved in each case. This can arise if rapid pyrolysis and combustion of organophosphorus acids occurs in the aerosol particles, forming phosphoric acid. The latter would then react with the metal ions in the usual way to produce a refractory phosphate. Because the metal/phosphorus ratios did not alter with flame height, this is further evidence for condensed-phase interference. Earlier workers [11, 12, 16] dealing with the composition of the refractory calcium species proposed the formation of $Ca_3(PO_4)_2$, $Ca_5(OH)(PO_4)_3$ or $Ca_2P_2O_7$. Only the first two of these species give ratios (1.50 and 1.65, respectively) consistent with the values obtained here. Further distinction between these two possibilities on the basis of the ratios is uncertain; therefore either phosphates or hydroxyapatite compounds or both are formed in the flame.

From the analytical viewpoint, all the above interferences can readily be avoided. In the air/acetylene flame this can be achieved, albeit with loss of

TABLE 1

Dual-nebulizer data for calcium (10 mg l^{-1}) and magnesium (2 mg l^{-1}) in air/acetylene flames in the presence of interferent (10 mg l^{-1})

Nebulizer[a]		Absorbance		
1	2	Ca	Mg	
		Fuel-rich[b]	Fuel-lean[b]	Fuel-rich[c]
M	DW	0.06	0.58	0.37
M + H_3PO_4	DW	0.04	0.42	0.40
M	H_3PO_4	0.06	0.59	0.39
M + I	DW	0.04	0.38	0.39
M	I	0.06	0.58	0.40
M + II	DW	0.04	0.34	0.39
M	II	0.06	0.57	0.38
M + III	DW	0.04	0.36	0.39
M	III	0.06	0.56	0.39
M + IV	DW	0.04	0.40	0.37
M	IV	0.06	0.58	0.40

[a]M is Ca or Mg; DW, distilled water; I—IV are the organophosphorus acids. [b]Measured 3 mm above inner blue cone. [c]Measured 12 mm above inner blue cone.

TABLE 2

Molar metal/phosphorus ratios for magnesium and alkaline earth metals in the fuel-lean air/acetylene flame and first-row transition metals in the fuel-rich flame. (Absorbance measurements were made 4 mm above the tip of the inner blue cone)

Metal ion	Metal/phosphorus ratio[a]				
	H_3PO_4	I	II	III	IV
Mg^{2+}	1.65	1.61	1.69	1.73	1.74
Ca^{2+}	1.55	1.58	1.71	1.60	1.81
Sr^{2+}	1.60	1.58	1.60	1.72	1.74
Ba^{2+}	1.50	1.52	1.54	1.50	1.58
Co^{2+}	1.55	1.35	1.55	1.48	1.45
Mn^{2+}	1.59	1.40	1.74	1.41	1.26
Ni^{2+}	1.74	1.46	1.53	1.57	1.64
Cu^{2+}[b]	0	0	0	0	0
Fe^{3+}	4.4	3.10	4.6	3.50	3.4
Cr^{3+}	1.51	4.0[c]	3.8	4.2	4.5[c]

[a]Standard deviations of the ratios were 0.10—0.15 for the first four metal ions and 0.15—0.25 for the rest. [b]No stable species were indentified for copper. [c]Difficult to extrapolate owing to curvature of interference plot.

sensitivity, by using a fuel-lean flame and measuring at a sufficiently high position in the flame. The use of releasing agents (e.g., lanthanum chloride) or a nitrous oxide/acetylene flame with ionization suppressant (e.g., potassium chloride) were shown, in earlier unpublished work, to be effective for removing these interferences.

Lead, zinc and cadmium

No interferences were detected for these metals in the fuel-lean air/acetylene flame or the nitrous oxide/acetylene flame. In the fuel-rich air/acetylene flame, phosphoric acid and the organophosphorus acids interfered seriously. For example, for 5 mg l^{-1} (Zn, Cd or Pb in the presence of 100 mg l^{-1} **IV**), absorbance enhancements of 5, 10 and 40%, respectively, were obtained for one set of conditions utilized. As for the alkaline earths, these effects had a vapour-phase origin. No depressive interferences could be found by varying the flame composition or height.

First-row transition elements (V, Cr, Mn, Co, Fe, Cu, Ni)

No significant interferences were found in the fuel-lean air/acetylene flame or in the nitrous oxide/acetylene flame (vanadium was examined in the nitrous oxide/acetylene flame only). The presence of compounds **I**—**IV** or related compounds therefore is unlikely to affect the determination of these elements by flame a.a.s. Complications, however, can be caused by pH changes and the "threshold-inhibiting" effect, both of which can result in precipitate formation. Thus, solutions containing both chromium(III) (5 mg l^{-1}) and compound **IV** (0—400 mg l^{-1}) aged for four days gave large decreases in absorbance (in both flames) corresponding to the "turbidity region" of the chromium(III)/compound **IV** (50—150 mg l^{-1} **IV**). At lower and higher concentrations of **IV**, corresponding to the "threshold" and "sequestration" regions, respectively, absorbances tended to the value of untreated chromium(III) solutions. For this ion, also, there was a strong pH dependence of the absorbance of aged solutions, with maximum decrease occurring at pH ca. 3 for all Dequests (e.g., **IV** gave an 80% decrease). Below pH 1 and above pH 10, limiting values were again obtained. Untreated chromium(III) solutions, or chromium(III) solutions treated with orthophosphate, however, gave progressively smaller absorbances with increasing pH. Effects with other elements of this group were not examined.

Pronounced interferences, different from those described above, were encountered in the fuel-rich air/acetylene flame. This flame should therefore be avoided despite the increased sensitivity that can be achieved for some metals, e.g., chromium and molybdenum. These interferences were, in some cases, also different from those exhibited by orthophosphoric acid, as is evident in Figs. 3—5. At relatively low observation heights in the fuel-rich flame (0—5 mm above the inner blue cone tip), depressive, stoichiometric interferences were observed with both orthophosphric acid and the organophosphorus acids. Under these conditions, the shapes of the interference

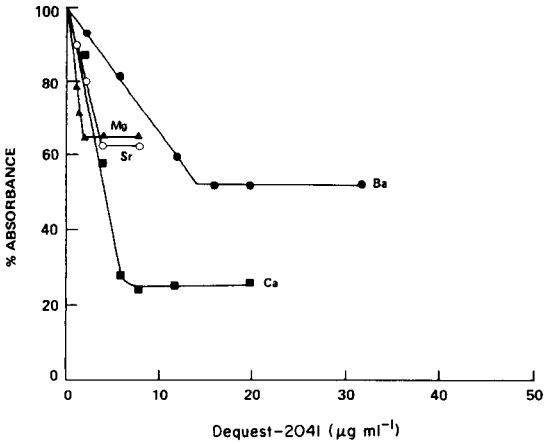

Fig. 1. Effect of organophosphorus acid III (Dequest-2041) on the absorbance of magnesium and the alkaline earth metals in the fuel-lean air/acetylene flame; (▲) Mg, 1 mg l^{-1}; (■) Ca, 5 mg l^{-1}; (○) Sr, 10 mg l^{-1}; (●) Ba, 50 mg l^{-1}. Similar curves were obtained for compounds I, II, IV and orthophosphoric acid.

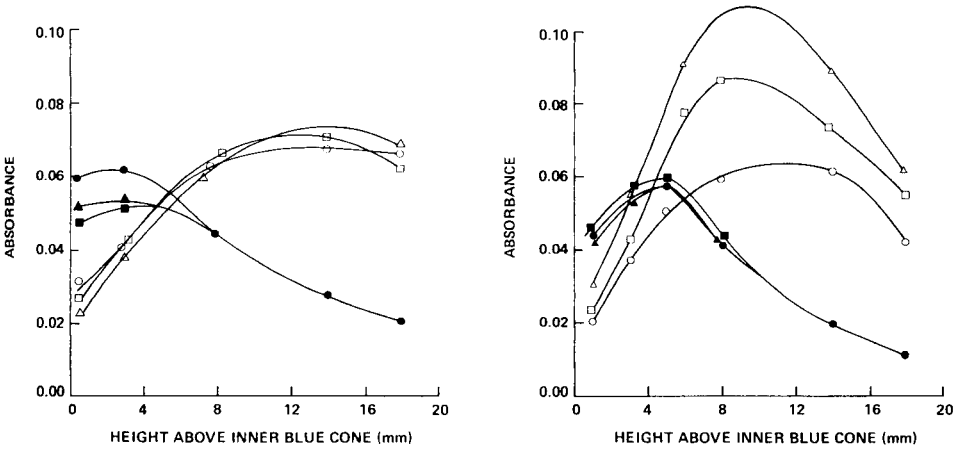

Fig. 2. Absorbance/height profiles for calcium (10 mg l^{-1}) in the fuel-lean (filled symbols) and fuel-rich (open symbols) air/acetylene flames: (○, ●) Ca; (□, ■) Ca + 10 mg l^{-1} H_3PO_4; (△, ▲) Ca + 10 mg l^{-1} III.

Fig. 3. Absorbance/height profiles for chromium (5 mg l^{-1}) in air/acetylene flames: (○, ●) Cr; (□, ■) Cr + 300 mg l^{-1} H_3PO_4; (△, ▲) Cr + 300 mg l^{-1} III. Open and filled symbols as for Fig. 2.

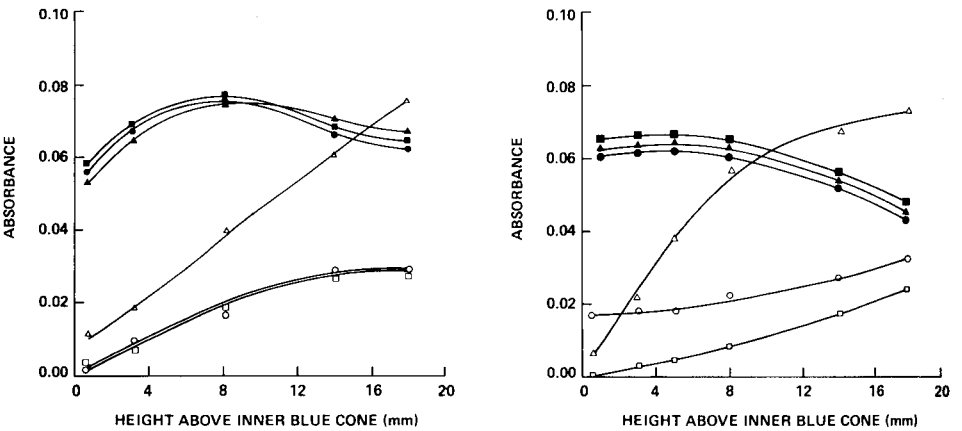

Fig. 4. Absorbance/height profiles for iron (5 mg l^{-1}) in air/acetylene flames: (○, ●) Fe; (□, ■) Fe + 200 mg l^{-1} H_3PO_4; (△, ▲) Fe + 200 mg l^{-1} III. Open and filled symbols as for Fig. 2.

Fig. 5. Absorbance/height profiles for nickel (5 mg l^{-1}) in air/acetylene flames: (○, ●) Ni; (□, ■) Ni + 200 mg l^{-1} H_3PO_4; (△, ▲) Ni + 200 mg l^{-1} III. Open and filled symbols as for Fig. 2.

curves for the two groups of interferents were generally similar (cf. Fig. 6) although the organophosphorus acids gave curves with more rounded "heels", particularly for chromium. The cobalt and nickel curves, in addition, demonstrated anomalous humps at lower interferent concentrations. Dual-nebulizer studies confirmed these interferences to be of the condensed-phase type.

Metal/phosphorus ratios evaluated from the above plots (Table 2) indicate the formation of interesting flame aerosol species. First, cobalt(II), nickel(II) and manganese(II) seem to produce stable phosphates or hydroxyapatite-like compounds [17] similar to those for the alkaline earths. Because these compounds were detected only in the cooler flame, it is concluded that they are less thermally stable than those of the alkaline earth metals. With copper, no stable species could be detected in the fuel-rich flame, which is consistent with an even lower stability of its phosphates. For iron(III) and chromium(III), the expected MPO_4 species were not obtained. The metal/phosphorus ratios, with one exception, were 3.1—4.6, which suggests the formation of oxide phosphates $M_2O_3.MPO_4$, $M_3O_4.MPO_4$ or $2M_2O_3.MPO_4$. Indeed, refractory species of this type are known [18—21] although their formation in flames does not appear to have been recognized previously. An exception to this trend was chromium with orthophosphoric acid, where a metal/phosphorus ratio of 1.51 was obtained, suggesting the possible formation of $Cr_3(PO_4)_2$ or an oxide phosphate $Cr_2O_3.4CrPO_4$.

At relatively high positions in the fuel-rich air/acetylene flame (>10 mm above the inner blue cone tip) significant enhancements in absorbance were

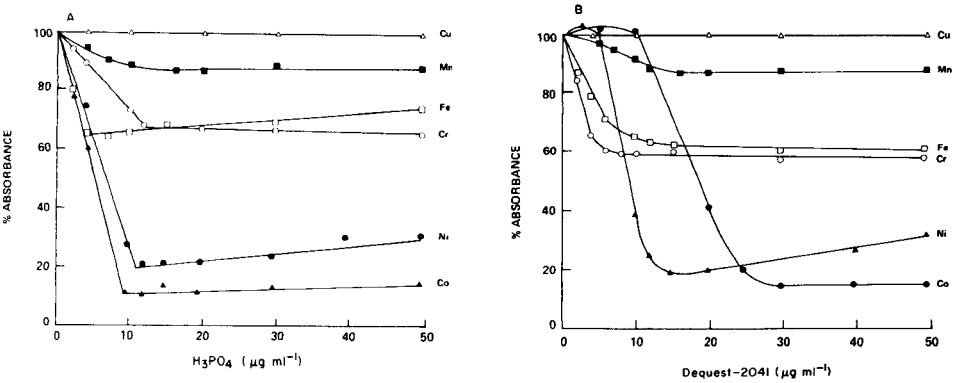

Fig. 6. Effect of orthophosphoric acid (A) and Dequest-2041 (B) on the absorbance of some first-row transition metals in the fuel-rich air/acetylene flame. Curves: (▲) Cu; (■) Mn; (□) Fe: (○) Cr; (●) Ni; (▲) Co. Metal ion concentrations were 10 mg l^{-1}, except for 20 mg l^{-1} Co in B. Curves obtained for compounds I, II and IV were similar to those for Dequest-2041 (compound III).

caused by the organophosphorus acids, but not by orthophosphoric acid (cf. Figs, 3—5). Again, these interferences were shown to be of vapour-phase origin though the flame reactions involved remain obscure.

Molybdenum

The organophosphorus acids produced severe depressions of the molybdenum absorbance, both in the fuel-rich air/acetylene flame and the hotter nitrous oxide/acetylene flame. This is clearly seen in Fig. 7. These effects were independent of pH in the range 1—10. The absorbance changed little with height, quite different to the effect of orthophosphoric acid. Thus, while compounds I—IV caused severe depressions, orthophosphoric acid had little or no effect in the fuel-rich air/acetylene flame and produced an enhancement in the nitrous oxide/acetylene flame. Dual-nebulizer studies indicated the interferences to be of condensed-phase and vapour-phase origin for the organophosphorus acids and phosphoric acid, respectively. Although interference curves like those in Fig. 7 were difficult to interpolate accurately, it was possible to calculate approximate values for the ratios Mo/P, Mo/O and Mo/C in the fuel-rich air/acetylene flame. The data listed in Table 3 can be interpreted in several ways. Thus, $MoPO_4$, MoO_3 or MoC/MoC_2 correspond to the tabulated ratios, although other species may fit these data. Carbide formation (MoC and/or MoC_2) is considered the most likely cause. This is supported by the fact that the degree of interference increases with the % carbon in the ligand, i.e., in the order of orthophosphoric acid < I < II < III < IV (Fig. 7). Also, it is difficult to see why phosphates or oxide phosphates should form in the flame when orthophosphoric acid itself does not produce a similar interference. Further support for carbide formation is that low μg ml^{-1} levels

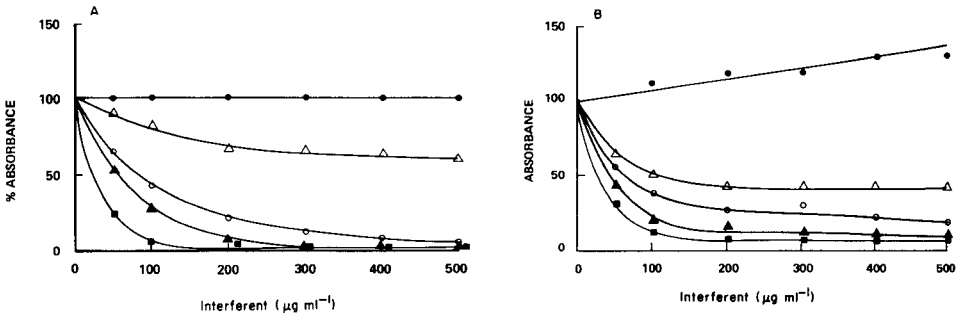

Fig. 7. Effect of orthophosphoric and organophosphorus acids on the absorbance of molybdenum (20 mg l^{-1}) in the fuel-rich air/acetylene flame (A) and in the nitrous oxide/acetylene flame (B). Acid used; (△) I; (○) II; (▲) III; (■) IV; (●) orthophosphoric.

TABLE 3

Mole ratios for molybdenum to compounds I—IV in the fuel-rich air/acetylene flame

Interferent	Mole ratio			
	Mo/ligand	Mo/P	Mo/O	Mo/C
I	3.1	1.0	0.33	1.0
II	2.3	1.1	0.33	1.0
III	4.3	1.0	0.33	0.7
IV	5.0	1.3	0.42	0.5

of many seemingly unrelated involatile organic compounds (sucrose, dextrin, humic acid, EDTA, glycine, etc.) depressed the molybdenum absorbance in a similar way to the organophosphorus acids. Thus, the depressive effects of organophosphorus acids on molybdenum are attributed to the ability of the compounds to generate carbonaceous material in the flame aerosol particles. This carbonaceous material would react with molybdenum at elevated temperatures to produce refractory carbides. Consistent with this hypothesis, many volatile or readily pyrolyzed organic compounds (e.g., ethanol, glycerol, Triton-X, urea, oxalic acid, succinic acid) produced no detectable interference at low $\mu g\ ml^{-1}$ levels.

Flame conditions could not be adjusted to eliminate interferences on molybdenum, therefore several additives were tested for their releasing action on this element. The results, with compound IV as the interferent, are shown in Fig. 8. Other reagents tested (lanthanum nitrate, thorium nitrate and EDTA) aggravated the suppression in the air/acetylene flame, probably because of the formation of stable spinels [22], or carbides in the case of EDTA. The most effective additive, in terms of both dose effectiveness and the degree of signal enhancement produced was sodium sulphate. Similar results were obtained in the nitrous oxide/acetylene flame. In that flame, however, borax showed complex behaviour, with severe depressions observed above about

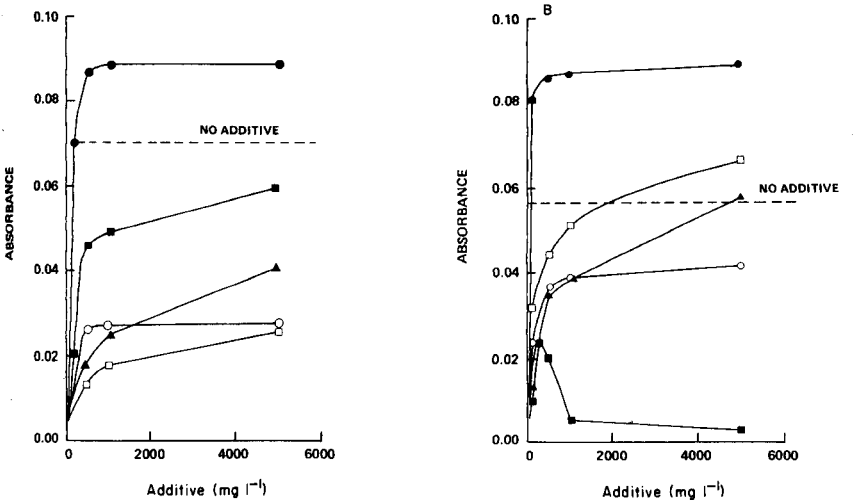

Fig. 8. Effect of various releasing agents on the interference of compound IV (100 mg l^{-1}) on molybdenum (20 mg l^{-1}) in the fuel-rich air/acetylene flame (A) and in the nitrous oxide/acetylene flame (B). Additive: (•) Na_2SO_4; (▪) $Na_2B_4O_7$; (▲) $LaCl_3$; (○) $(NH_4)_2SO_4$; (□) H_3PO_4.

TABLE 4

Dual-nebulizer data showing the releasing action of various additives (0—5000 mg l^{-1}) on molybdenum (20 mg l^{-1}) in the presence of compound IV (50 mg l^{-1}) in a fuel-rich air/acetylene flame and a nitrous oxide/acetylene flame

Nebulizer		Absorbance	
1	2[a]	Air/acetylene	Nitrous Oxide/acetylene
Mo	DW	0.21	0.11
Mo + IV	DW	0.02	0.03
Mo + IV + Na_2SO_4	DW	0.26	0.28
Mo + IV	Na_2SO_4	0.10	0.08
Mo + IV + $(NH_4)_2SO_4$	DW	0.06	0.07
Mo + IV	$(NH_4)_2SO_4$	0.02	0.03
Mo + IV + borax	DW	0.19	0.01
Mo + IV	Borax	0.05	0.03
Mo + IV + $LaCl_3$	DW	0.09	0.12
Mo + IV	$LaCl_3$	0.02	0.07
Mo + IV + H_3PO_4	DW	0.09	0.12
Mo + IV	H_3PO_4	0.03	0.04

[a]DW, distilled water.

100 mg l^{-1}. Elevated temperatures may promote the formation of a refractory molybdenum/boron species.

Dual-nebulizer experiments showed interesting variations in the behaviour of the additives (Table 4). Ammonium sulphate was found to be active solely in the condensed phase. Its mode of action may therefore be restricted to being an inert, volatile dispersant. Other additives active solely in the condensed phase were lanthanum chloride (air/acetylene flame only) and borax (nitrous oxide/acethylene flame only). Other reagents appeared to have a releasing action in both the condensed and vapour phases. The particular effectiveness of sodium sulphate may largely be due to its thermal properties and the effect of these on the dispersion of aerosol particles in the flame.

Conclusions

Interferences, both depressive and enhancing, were indentified for the organophosphorus acids with different metal ions. Depressive interferences are attributed to condensed-phase reactions and are prominent at the base of the flame. Depending on the metal, stable phosphates, oxide phosphates or carbides are thought to be formed. Enhancing interferences are attributed to vapour-phase reactions involving phosphorus species and are prominent higher in the fuel-rich air/acetylene flame. All these interferences can be avoided by careful selection of flame conditions, or, for molybdenum, by the addition of sodium sulphate.

REFERENCES

1 M. I. Kabachnik, T. Ya Medved, N. M. Dyatlova and M. V. Rudomino, Russ. Chem. Rev., 43 (1974) 733.
2 A. D. F. Toy, Phosphorus Chemistry in Everyday Living, Am. Chem. Soc., Washington, DC, 1974, Ch. 14.
3 M. J. Collie (Ed.), Industrial Water Treatment Processes, Developments Since 1978, Noyes data corp., Park Ridge, NJ, 1983.
4 G. B. Hatch and P. H. Ralston, Mat. Perform., 11 (1972) 39.
5 F. N. Kemmer (Ed.), The Nalco Water Handbook, McGraw-Hill, New York, 1979.
6 Monsanto Chemical Co. St Louis, MO, Special Reports 7158, 7256, 7666, 7917 and 8097, and Technical Bulletins IC/WT 101 and IC/SCS-321.
7 S. S. Sloat and M. Buck, Combustion, 51 (1979) 10.
8 D. R. Eubanks and J. R. Stillian, Pittsburg Conference, Atlantic City, NJ, U.S.A., Marci 1984.
9 Standard Methods for the Examination of Water and Wastewater, Amer. Public Health Assoc., Washington DC, 16th edn., 1985, Method 426c, p. 467; Method 311c, p. 199.
10 C. Rocchiccioli and A. Townshend, Anal. Chim. Acta, 41 (1968) 93 (and reference therein).
11 E. Pungor, Pure Appl. Chem., 23 (1970) 51.
12 J. Spitz, G. Uny, M. Roux and J. Besson, Spectrochim. Acta, Part B, 24 (1969) 399.
13 W. B. Barnett, Anal. Chem., 44 (1972) 695.
14 P. S. Chen and T. Y. Toribara, Anal. Chem., 25 (1953) 1642.
15 G. L. Long and C. B. Boss, Anal. Chem., 54 (1982) 624.
16 C. T. J. Alkemade and R. Herrman, Fundamentals of Analytical Flame Spectroscopy Wiley, New York, 1979.
17 W. Rathje, Ber., 74B (1941) 342, 357.

18 G. P. Romanova, L. L. Koshlyak and O. S. Grum-Grzhimailo, Steklo Keram., 9 (1976) 23; Chem. Abstr. 86, 33308k.
19 T. V. Kalinskaya, O. Kh. Chakhalyan, Yu. P. Tarlakov and N. A. Novoselova, Zh. Prikl. Khim. (Leningrad), 49 (1976) 2212; Chem. Abstr. 86, 91820g.
20 T. V. Kalinskaya, I. S. Krasotkin and L. B. Lobanova, Zh. Prikl. Khim. (Leningrad), 52 (1979) 1003; Chem. Abstr. 91, 58745s.
21 I. V. Tananaev, E. V. Maksimchuk, Yu. G. Bushuev and S. A. Shestov, Izv. Akad. Nauk SSR, Neorg. Mater., 14 (1978) 719; Chem. Abstr. 89, 31573f.
22 A. M. Abdallah, M. M. El-Defrawy, M. A. Mostafa and A. B. Sakla, Anal. Chim. Acta, 174 (1985) 347.

Analytica Chimica Acta, 193 (1987) 193—207
Elsevier Science Publishers B.V., Amsterdam — Printed in The Netherlands

COUPLING OF NARROW-BORE LIQUID CHROMATOGRAPHY TO THIN-LAYER CHROMATOGRAPHY
Part 2. Application of Fluorescence-based Spectroscopic Techniques for Off-line Detection

J. W. HOFSTRAAT*, M. ENGELSMA, R. J. VAN DE NESSE, U. A. Th. BRINKMAN, C. GOOIJER and N. H. VELTHORST

Department of General and Analytical Chemistry, Free University, De Boelelaan 1083, 1081 HV Amsterdam (The Netherlands)

(Received 27th August 1986)

SUMMARY

The effluent from a narrow-bore liquid chromatographic (l.c.) separation can be immobilized on thin-layer chromatographic (t.l.c.) plates with little loss of resolution. The deposited compounds are then available for further inspection. For off-line detection, direct fluorescence emission, fluorescence excitation emission spectra, and fluorescence line-narrowing spectroscopy are investigated with tetracene and benz[k]fluoranthene as model compounds. Detection based on direct emission measurements and on measurements for which complete spectra are obtained for the separated compounds, is suitable for identification and determination. Detection limits are of the same order of magnitude as those for on-line detection in narrow-bore l.c. The fluorescence spectra of immobilized compounds can be obtained with a conventional fluorescence spectrometer equipped with a solid-sample accessory. No other special apparatus is needed. The immobilized chromatogram is also suitable for techniques incompatible with flow systems, e.g., fluorescence line-narrowing spectroscopy, which yields fluorescence spectra via laser excitation of low-temperature solid samples. Very selective narrow-line fluorescence spectra were obtained for tetracene deposited on t.l.c. plates in amounts down to the low picogram level.

In Part 1 of this series [1] it was shown that the effluent from a narrow-bore liquid chromatography (l.c.) column can be deposited on a thin-layer chromatographic (t.l.c.) plate without serious loss of chromatographic resolution. Storage of the chromatogram proved to be satisfactory for some polynuclear aromatic hydrocarbons (PAHs) after both normal-phase and reversed-phase l.c. separations. Silica as well as alkyl-modified silica t.l.c. plates were used for deposition. The interface was a fused silica capillary which connected the l.c. column outlet with the spray jet assembly of a slightly modified Linomat applicator for t.l.c. The various factors, e.g., migration of the deposited compounds on the t.l.c. plate, l.c. flow rate and Linomat table speed, influencing the storage process have been discussed [1].

Immobilization of the l.c. separation is useful in two important ways. First, when the separated compounds have been stored on a t.l.c. plate, the

0003-2670/87/$03.50

separation efficiency can be improved by the application of a second chromatographic technique. Secondly, the detection potential can be increased. As the chromatogram remains conserved, a point that will be considered separately, several detection principles can be combined and, in addition, techniques that are not compatible with or too slow for l.c. flow systems become feasible.

In this paper, the applicability of direct fluorescence emission spectrometry, fluorescence emission/excitation spectrometry and fluorescence line-narrowing spectroscopy will be discussed for the off-line detection of chromatograms immobilized on t.l.c. plates.

The application of direct fluorescence emission spectrometry as off-line detection method (i.e., straightforward scanning along the deposited trace while recording one emission region only) does not offer any advantages over conventional on-line fluorescence detection. However, this study was begun with this detection principle to investigate aspects that influence the sensitivity of the detection, such as background luminescence, scattering and surface irregularities of various t.l.c. materials.

Complete fluorescence emission spectra of compounds separated in the l.c. system, so that intensity values are obtained for the whole spectral range of interest, can be recorded on-line only with difficulty and at significant cost. In conventional fluorescence detectors, the scanning of a spectrum takes too much time to be feasible in a flowing system. Only by application of optical image devices, which allow for simultaneous detection over a large spectral region, can spectra be obtained [2, 3]. Such devices, especially linear photodiode arrays, are presently available in a number of commercial l.c. absorption detectors [4]. They offer similar sensitivities to photomultiplier-based detectors because absorption techniques are based on ratioing two signals. At present, multichannel absorption detection is widely applied in l.c. In contrast, parallel detection of fluorescence spectra in l.c. is little used, the most important reason probably being that no commercial equipment is available yet. As only the very expensive intensified linear photodiode arrays can detect similarly low levels of light as photomultiplier tubes, the introduction of commercial systems seems to be hampered by the large investment required to reach acceptable sensitivities [5, 6]. However, when the liquid chromatogram has been immobilized on a t.l.c. plate, fluorescence emission spectra can be easily recorded with a densitometer used for the examination of t.l.c. plates, or with a conventional fluorescence spectrometer equipped with an accessory for handling solid samples. In addition, the recording of fluorescence excitation spectra becomes feasible.

Fluorescence line-narrowing spectroscopy cannot be applied as on-line detection method in l.c., as it requires low-temperature solid samples. The technique provides very selective detection that enables one to measure vibrationally resolved fluorescence spectra, thus combining the inherent sensitivity of fluorescence spectrometry with the selectivity of infrared and Raman spectroscopy. The technique is based on the fact that inhomogeneous broadening in luminescence spectra can be removed to a

great extent via selective laser excitation of analytes at low temperatures ($T < 30$—50 K, depending on the system under study) [7, 8]. Recently it has been shown that such spectra can also be measured for compounds on t.l.c. plates [9, 10].

Finally, attention will be paid to a feature that may occasionally impede the application of t.l.c. plates as the buffer memory for l.c. It has been observed that, on some t.l.c. materials, PAHs decompose fairly rapidly [11, 12]. Adequate precautions to circumvent this problem will be indicated.

EXPERIMENTAL

Instrumentation

Chromatography. In the chromatographic set-up, extensively described in Part 1 [1], normal-phase (eluent n-hexane) narrow-bore l.c. effluent was deposited on t.l.c. plates by using a modified Camag (Muttenz, Switzerland) Linomat III line applicator. For the experiments described below, an eluent flow rate of 30 μl min^{-1} and a Linomat table speed of 6.8 mm min^{-1} were used. Both bare silica and alkyl-modified silica t.l.c. plates were used.

Spectrometry. The t.l.c. plates were scanned with a Zeiss (Oberkochen, F.R.G.) chromatogram spectrophotometer operated in the fluorescence mode. For excitation, the light from a 48-W high-pressure mercury arc lamp was passed through a M4Q-III prism monochromator and focussed on the plate so that a rectangular spot, with a width varying from 0.2 to 0.7 mm and 2.1 mm long, was illuminated. Two mercury lines (254 nm and 313 nm) were used. The total emission from the plate was recorded by using suitable filters followed by a RCA (Lancaster, PA) 1P28 photomultiplier. The instrumental parameters for the two model compounds are summarized in Table 1.

Fluorescence emission and excitation spectra of the separated compounds were recorded with a Perkin-Elmer MPF-44A fluorescence spectrometer equipped with a DCSU-2 differential corrected spectra unit. A special t.l.c. accessory (Hitachi, Tokyo) was used. A 2 × 2 mm^2 area was illuminated on the t.l.c. plate. The spectral resolution was 5 nm on the emission side and 10 nm on the excitation side in the emission experiment and 5 nm on the excitation side and 10 nm on the emission side in the excitation experiment. To detect weak signals, optical filtering was necessary to remove stray light. In the emission experiment, a short wavelength cut-off filter was placed before the emission monochromator and a bandpass or interference filter after the excitation monochromator. For excitation measurements, of course, only the cut-off filter for the emission monochromator was used (see Table 1). In addition, a correction for the emission of the blank t.l.c. plate could be obtained with the DCSU-2.

The fluorescence line-narrowing spectra were recorded at approximately 9 K in a Cryodyne model 21 closed-cycle helium refrigerator (CTI Cryogenics; Waltham, MA). The samples were excited with the 457.9-nm and

TABLE 1

Experimental conditions for room-temperature fluorescence measurements

Material	Carl Zeiss		Perkin-Elmer MPF-44A			
	λ_{ex} (nm)	λ_{em} (nm)	λ_{ex} (nm)	Filters	λ_{em} (nm)	Filter
Benz[k]fluoranthene	313	>390	307	Schott UG11 (u.v. bandpass) Schott GG375 (375-nm cut-off)	431	Schott GG375
Tetracene	280[a]	>390	414	416-nm interference Schott GG435 (435-nm cut-off)	510	Schott GG495 (495-nm cut-off)

[a]In this experiment, a deuterium lamp was used for excitation.

476.5-nm lines of a Coherent (Palo Alto, CA) CR-10 argon-ion laser. Non-lasing plasma lines were removed with a laser filter monochromator (Applied Photophysics, London). With a lens (f = 30 cm), the laser light was focussed to a spot with a diameter of about 1 mm on the sample. The fluorescence was detected at an angle of 30° from the excitation light and projected onto the entrance slit of a Jeol JRS-400D double monochromator with a quartz lens (f = 10 cm). The resolution of the monochromator was 0.1 nm. The signal was processed by a RCA-31034A photomultiplier tube cooled to −20°C and a Jeol photon-counting system.

All experiments were done within a short time after deposition of the compound to avoid photodegradation effects. When necessary, special precautions were taken (e.g., storage in the dark).

Materials

The model compounds tetracene (Eastman Kodak, Rochester, NY) and benz[k]fluoranthene (Joint Research Center of the European Economic Communities, Petten, the Netherlands, reference compound) were used as received. The eluent n-hexane (J. T. Baker; h.p.l.c. quality, distilled from sodium) was deaerated before use. In some experiments, a glycerol/water (1:1, v/v) mixture was added to the sample holder to improve the thermal contact of the t.l.c. plate with the cold tip of the helium refrigerator. Several types of plates were used, i.e., precoated t.l.c.-quality (DC Alufolien Kieselgel 60-H and Fertigplatten Kieselgel 60) and h.p.t.l.c. plates (HPTLC-Fertigplatten Kieselgel 60) from Merck. The backing materials were aluminum foil and glass for the Alufolien and Fertigplatten, respectively. Several types of alkyl-modified silica plates were also used, i.e., precoated t.l.c. quality (KC_{18}; Whatman), and h.p.t.l.c. quality (HPTLC-Fertigplatten RP18; Merck) C_{18}-modified plates, and a conventionally coated C_2-modified plate (DC-Fertigplatten Kieselgel 60 silanisiert; Merck). All the alkyl-modified plates had glass backing.

RESULTS AND DISCUSSION

Direct fluorescence emission detection

For straightforward detection of the immobilized chromatogram, single-wavelength fluorescence emission was recorded along the deposited trace. A Carl Zeiss densitometer, equipped with a prism monochromator to select one of the excitation lines from a mercury arc lamp and a cut-off filter before the photomultiplier to select the emission light, was used for this purpose. As the configuration at the emission side permits the measurement of total luminescence, very sensitive detection is expected. As an example, Fig. 1(a) shows the band measured for 4 pg of benz[k]fluoranthene on a RP_{18} silica plate by scanning along the trace. The log-log calibration plot found under such conditions was linear over three decades, from 5 ng down to the detection limit of 3 pg, corresponding to 2×10^{-8} M of benz[k]fluoranthene injected. The standard deviation was 6% ($n = 9$) at 1 ng of benz[k]fluoranthene.

It is interesting to note that the detection limit in this experiment was not governed by the level of statistical noise. Most probably, the surface composition of the t.l.c. plate is irregular, leading to a humpy outlook of the blank trace because of irregular scattering and luminescence background effects. Surface irregularity is inherent to the commercial t.l.c. plates used here. Table 2 shows a comparative survey of the surface irregularity of these plates. An estimate was taken from the variation in the intensity of the emission light recorded in scanning a bare t.l.c. plate with the Carl Zeiss densitometer. It appeared that the irregularity of the plates used did not differ much except for the Whatman C_{18}-modified silica plate, which is more irregular than the others, and the aluminum-backed silica plate which is less irregular. However, the non-uniformity of the surface composition is

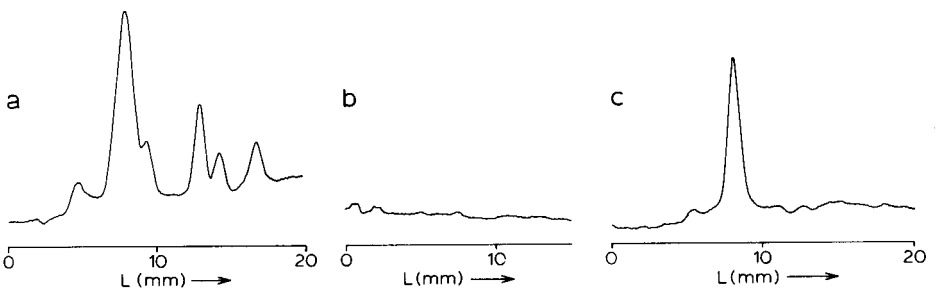

Fig. 1. (a) Densitometer scan along the trace for 4 pg of benz[k]fluoranthene deposited on an untreated RP_{18} plate. (b) Densitometer scan obtained for a bare RP_{18} plate. (c) Densitometer scan along the trace for 4 pg of benz[k]fluoranthene deposited on a purified RP_{18} plate. Experimental conditions: eluent flow rate, 30 μl min^{-1}; Linomat table speed, 6.8 mm min^{-1}; excitation and emission wavelengths as in Table 1. The illuminated area on the t.l.c. plate was 0.7 × 2.1 mm.

TABLE 2

Comparative survey of the characteristics of several t.l.c. plates[a]

Material	Background luminescence	Surface irregularity	Fluorescence peak height[b]	Relative bandwidth[b]
KC_{18}	720	400	50	130
RP_{18}	100	100	100	100
C_2-silica	160	100	30	100
Silica-on-aluminum	300	50	50	60
Silica-on-glass	150	100	20	60
H.p.t.l.c. silica-on-glass	140	100	12	80

[a]All measurements were done with the Carl Zeiss densitometer with 254-nm mercury arc excitation; illuminated area 0.7 × 2.1 mm. All values are indicated with respect to the result obtained for RP_{18} = 100. [b]For 2.5 ng of benz[k]fluoranthene deposited on the t.l.c. plate.

probably enhanced as a consequence of the deposition process, mainly because of migration of any luminescent impurities that are present in the surface layer of the plate. An important reduction of the enhancement of the surface irregularity caused by deposition was achieved by removing the impurities; this could be done by overnight elution of the plates with, for instance, methanol. The impurities were then found as a broad band at the top of the plate. When such a purified plate was used for deposition, a 10-fold improvement in detection limit was obtained compared to the unpurified plate.

The irregularity of the surface measured after purification was of about the same order of magnitude as that observed for the t.l.c. plate before deposition (Fig. 1b) so that the effect of the deposition process was completely eliminated. Figure 1(c) shows the band obtained for 4 pg of benz[k]-fluoranthene on the purified plate. The log-log calibration plot measured under these conditions was linear over concentration 4 decades, from 5 ng to 0.3 pg. At amounts above 5 ng, deviation from linearity occurred because of the high local concentration of the compound on the t.l.c. plate. The relative standard deviation was 7% (n = 8) at 40 pg.

Improvements in the detection limit would require t.l.c. plates with a completely regular surface. For such ideal plates, an ultimate limit of detection of about 40 fg or 3×10^{-10} M injected may be estimated for benz[k]fluoranthene in this experimental set-up, if 3 times the (statistical) noise were taken as criterion. This value would be as good as the limits of detection obtainable in on-line single-wavelength fluorescence detection in micro-l.c. with conventional light sources [13].

The material of the t.l.c. plate has some effect on the peak height of the fluorescence signal. Such data obtained for 2.5 ng of benz[k]fluoranthene deposited on a number of t.l.c. materials are surveyed in Table 2. The alkyl-

modified plates, especially the RP_{18} plate, gave the highest values, even though the observed bandwidths were somewhat larger than those for the unmodified silica plates. Several explanations might be given for this observation. The main reason for the lower fluorescence intensity observed with silica plates is probably that the strong adsorption of the PAHs on such materials enhances nonradiative processes [14]. The strength of the interaction on the silica t.l.c. materials is clearly demonstrated by the relatively fast rate at which the photodegradation proceeds (see below). Another factor that may play a role is the influence of the polarity of the solvent on fluorescence and especially absorption spectra [15]. The intensity for the aluminum-backed silica plate is substantially higher than for the glass-backed silica plates. Probably, part of the emission and/or excitation radiation is reflected by the aluminum backing material so that the emitted radiation can be more efficiently detected and/or more efficient use can be made of the exciting radiation.

Fluorescence emission and excitation spectra

Fluorescence emission and excitation spectra can be conveniently recorded for compounds immobilized on t.l.c. plates after separation in a l.c. system. Figure 2 shows the fluorescence spectra obtained for benz[k]fluoranthene in methanol solution (Fig. 2a) and on a silica plate (Fig. 2b). No sophisticated instruments were required to obtain the off-line l.c. spectra; a simple, conventional fluorimeter system equipped with a t.l.c. accessory was used. The similarity of the spectra is clear, demonstrating the excellent capability of the t.l.c. material to serve as an inexpensive means of increasing the detection potential in l.c. The spot on the plate can be identified quite confidently as benz[k]fluoranthene on the basis of this spectral information. Nevertheless, there is a major difference between the two spectra shown in Fig. 2. The fluorescence excitation spectrum in Fig. 2(a) shows the influence of scattering of the excitation radiation by the t.l.c. plate; such scattering is rarely a problem with solutions. The scattered radiation measured by the emission monochromator has two origins: (a) Rayleigh scattering of the excitation radiation; and (b) the excitation monochromator leaks radiation at other wavelengths than the one used for excitation, which is also efficiently scattered by the t.l.c. plate. As the xenon lamp used in the Perkin-Elmer MPF-44A does not have a smooth spectral intensity distribution, this can be troublesome, especially in the 450—550-nm region where several fairly intense, narrow xenon emission lines occur. Apart from the scattering processes, the luminescent background of the t.l.c. plates can also complicate the recording of spectra for immobilized compounds although such effects can be reduced by using the facility for blank emission subtraction in the DCSU-2.

The spectrum shown in Fig. 2(a) was recorded for a 2.5-ng spot of benz[k]fluoranthene. When no precautions were taken to remove the above scattering effects, useful spectra were obtained down to about 0.1 ng (i.e.,

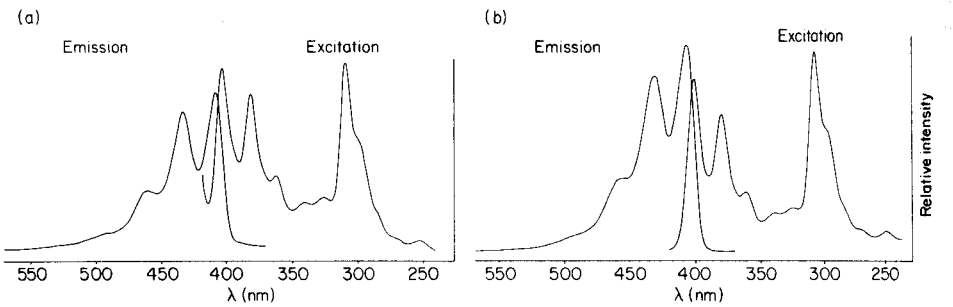

Fig. 2. Room-temperature fluorescence emission and excitation spectra of benz[k]-fluoranthene: (a) on a silica-on-aluminum plate (2.5 ng); (b) in methanol solution (1.0 X 10^{-6} M). Experimental conditions are given in Table 1.

7×10^{-7} M benz[k]fluoranthene injected). However, under these conditions, no spectra were obtained for tetracene which emits in the 480–530-nm range, where the scattering problems with the xenon lamp are most severe. In addition, the fluorescence quantum yield for tetracene is much lower than that for benz[k]fluoranthene. When suitable filters were used, scattering effects were reduced. In the emission experiment, a band filter was placed on the excitation side to remove light leaking from the excitation monochromator and a cut-off filter for the emission monochromator was used to remove scattered excitation light. The excitation spectra were measured with a cut-off filter in front of the emission monochromator only. The filter combinations used for the two model compounds are given in Table 1.

With filtering, the scattering effects were reduced by a factor of about 10 in the emission experiment. The detection limit (3 times the peak-to-peak noise) for benz[k]fluoranthene after reduction of the scatter was ca. 2×10^{-8} M injected (3 pg). This value is of the same order of magnitude as reported for several PAHs in microcolumn l.c. with intensified photodiode-array detection to obtain fluorescence emission spectra [16]. Compared to direct fluorescence measurements, the limit of detection observed for fluorescence spectra was less dependent on the irregularity of the plate surface. The spectra were recorded without movement of the plate so that the background gave a relatively constant contribution to the emission spectrum of the analyte; also, the area of the plate observed was larger (2×2 mm^2) yielding some averaging of any irregularities, and background correction with the DCSU-2 was used. Under these conditions, fluorescence emission spectra could be obtained for tetracene down to concentrations of about 2×10^{-5} M injected (or 2.5 ng). Fluorescence emission and excitation spectra obtained for tetracene on a silica-on-aluminum plate are shown in Fig. 3.

The fluorescence emission spectra were also used for quantitative purposes. For benz[k]fluoranthene, the log-log calibration curve was linear over

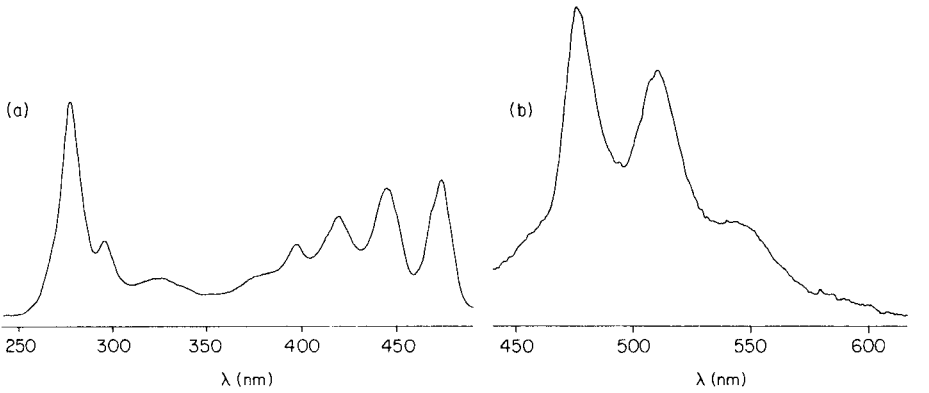

Fig. 3. Room-temperature fluorescence excitation (a) and emission (b) spectra of tetracene; 13 ng of tetracene was deposited on a silica-on-aluminum plate. Experimental conditions are given in Table 1.

decades (from about 5 ng to the detection limit of 3 pg) when based on the intensity of the 431-nm emission. The slope of the plot obtained was 0.97 (s.d. 0.016) with a correlation coefficient of 0.9993 (n = 6). The relative standard deviation was 1% (n = 6) for 76 pg of benz[k]fluoranthene.

Fluorescence line-narrowing spectroscopy

Fluorescence line-narrowing spectroscopy can only be applied at extremely low temperatures; therefore, it cannot be used as an on-line detection method. In the present study, the feasibility of applying this technique for off-line detection in l.c. was investigated after immobilization of the column effluent on a t.l.c. plate. Tetracene was used as model compound; the S_1—S_0 (fluorescence) 0—0 transition occurs in the 475-nm region and so is very suitable for excitation with the argon-ion laser lines at 457.9 nm and especially 476.5 nm. Excitation at 476.5 nm (in the 0—0 transition area) produces emission with the laser line as the origin of the spectrum so that only the vibrational part of the fluorescence spectrum is observed. When the 457.9-nm line is used, tetracene is excited to the vibrationally excited part of the S_1 state, ca. 750 cm^{-1} above the 0—0 transition; radiationless deactivation of the excess of vibrational energy to the S_1 vibrational ground-state then precedes the emission. The whole fluorescence spectrum, including the 0—0 transition area, can then be recorded.

Part of the spectrum of tetracene (13 ng) deposited on a silica plate obtained with 5-mW 457.9-nm laser excitation at 9.3 K is shown in Fig. 4(a). The 0—0 transition at 474.1 nm and a number of vibronic emission bands can be discerned. It was not necessary to insert filters to remove scattered light in this case; any Rayleigh scattering was removed by the double monochromator used for detection. The background emission of the t.l.c. plate, however, was much stronger with laser excitation than with a conventional lamp source because even compounds with very low fluorescence quantum

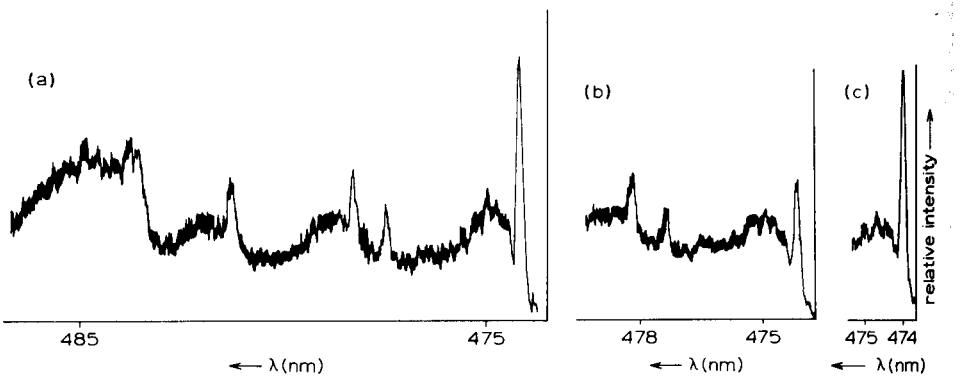

Fig. 4. Fluorescence line-narrowing spectra for 13 ng of tetracene on a silica-on-aluminum plate (λ_{ex} = 457.9 nm at 5 mW; T = 9.3 K). Spectrum recorded: (a) immediately after commencing laser irradiation; (b) after 1.5 h of laser irradiation; (c) after 1.5 h of laser irradiation and annealing to 80 K.

yields fluoresced. The luminescent background observed in Fig. 4(a) has about the same intensity as the strongest peak in the spectrum, but tends to be broad and structureless. Amounts of tetracene well below the limit of detection of 5 ng for room-temperature fluorescence can therefore be observed.

An important advantage of t.l.c. materials as matrices in fluorescence line-narrowing spectroscopy compared with glassy solvents, is the relative slowness of non-photochemical hole burning [17]; this burning causes the intensity of the narrowed lines to decrease with time under the influence of laser irradiation, possibly owing to irreversible site interconversion of the solute molecules in the excited state. As shown in Fig. 4(b) for tetracene on a silica plate, the intensity of the narrow lines was about halved after 1.5 h of irradiation. For comparison, in low-temperature glasses with similar laser powers and temperatures for tetracene, typical half-lives were 5—10 min [17]. The original fluorescence intensity was restored by annealing the sample to 80 K (Fig. 4c). The green background emission from the t.l.c. plate also decayed (by about 30%) on prolonged irradiation but annealing did not restore its original intensity (Fig. 4c), probably because of some irreversible photochemical process. Thus, background emission can be reduced by annealing after prolonged laser irradiation. This was also observed for other t.l.c. materials.

Figure 5 shows the spectrum obtained for tetracene on a Whatman KC_{18} plate with excitation at 476.5 nm; the spectrum was recorded from 483 nm. The first part of the spectrum cannot be recorded, because of Rayleigh scattering of the intense laser light, unless time-resolved detection is used. The first strong line observed in the spectrum, at 483.8 nm, relates to a vibronic emission band at 314 cm^{-1} from the origin; the intensity of this band is about a quarter of the intensity of the 0—0 transition (cf. Fig. 4a). Several other strong transitions in the 1100—1500 cm^{-1} region from the origin can be assigned by comparison with vibrational data [18, 19].

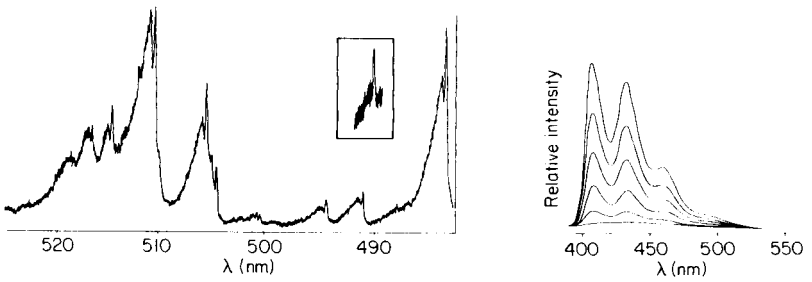

Fig. 5. Fluorescence line-narrowing spectra of 3.1 ng of tetracene on a KC_{18} t.l.c. plate (λ_{ex} = 476.5 nm at 1 mW; T = 9.3 K). Inset shows the 483.8-nm emission line recorded for 31 pg of tetracene.

Fig. 6. Room-temperature fluorescence emission spectra of benz[k]fluoranthene (2.5 ng) on a silica-on-aluminum plate. Spectra were recorded after 0, 10, 20, 45, 80 and 200 min of irradiation at 254 nm.

The spectrum shown in Fig. 5 was obtained for 3.1 ng of tetracene at a laser power of 1 mW (cf. Fig. 4). Clearly, the 476.5-nm excitation provides a better signal-to-noise ratio. Several causes are plausible. First, excitation with the 476.5-nm laser line will yield spectra with 5—20 times stronger intensity than when the 457.9-nm line is used, the exact value depending on the matrix material. Only relatively weak bands of tetracene are situated in the region 400—900 cm^{-1} above the origin [18]. Secondly, the intensity of the narrow lines for tetracene on alkyl-modified silica plates appears to be one order higher than on bare silica; only 10% of this loss on silica can be attributed to photochemical degradation of the sample during the lengthier preparation (see below). A main reason for the difference found with the two matrix materials is the fixed excitation wavelength. Solvent-induced shifts in the absorption spectrum of the analyte affect the efficiency of excitation; a tunable dye laser would enable the most efficient excitation wavelength to be selected. The intensities of individual emission lines may also be influenced by solvent interactions [10]. Finally, any aggregates of tetracene, which would give broad features to the spectrum rather than line-narrowing, would be less likely to form on the apolar material.

With the experimental set-up used here, the lowest limit of detection for tetracene was obtained for excitation with the 476.5-nm line and an alkyl-modified t.l.c. plate. The emission line obtained for 31 pg of tetracene on a KC_{18}-silica plate is shown as an inset in Fig. 5. Even lower detection limits would be possible with higher laser powers or a tunable dye laser. The very narrow bands obtained with the line-narrowing method are obviously suitable for identification purposes; comparison of the spectra in Figs. 3—5 emphasizes this point. For quantification, however, internal standards are needed, as discussed earlier [10]. For quantitative work, a new experimental set-up based on a helium bath cryostat is being constructed, to improve reproducibility.

Stability of PAHs on t.l.c. plates

The suitability of t.l.c. plates as storage devices for l.c. effluents obviously depends on the stability of the deposited compounds. Stability during several hours is needed if the stored compounds are to be used for quantification. However, if several detection techniques are to be applied or the chromatogram is to be stored, stability for days or even weeks is necessary. Seifert [11] and Hellman [12] observed relatively fast decay times for several PAHs on silica t.l.c. plates; e.g., benz[a]pyrene fluorescence intensity was reduced to <10% of its original value within 30 min on h.p.t.l.c. silica plates.

The stability of benz[k]fluoranthene on the t.l.c. plates applied here was examined. Preliminary tests showed that the instability of PAHs on these plates can be ascribed primarily to a photo-oxidation process. Compounds on plates kept in the dark under nitrogen remained intact for several weeks. To ensure reproducible experimental conditions, decay curves were recorded for benz[k]fluoranthene on various t.l.c. plates by continuously irradiating the sample with the 254-nm mercury line from the Carl Zeiss densitometer. The fluorescence emission spectra recorded at regular time intervals on the Perkin-Elmer MPF-44A instrument showed a steady decrease of signal (Fig. 6). No increase in emission was found at other wavelengths, even with different excitation wavelengths.

The temporal decay was also monitored by recording the total benz[k]-fluoranthene fluorescence on the densitometer while continuously irradiating the sample at 254 nm. The curves recorded were of two types. Figure 7(a) shows a typical single exponential curve obtained for silica plates, which represents a first-order reaction. The alkyl-modified plates all gave a curve of the type shown in Fig. 7(b). The slight increase in intensity in the first 50—60 min also occurred when blank alkyl-modified plates were irradiated. This initial increase in intensity was common to all types of plates studied, but was not observed on loaded silica plates because the relatively rapid decrease of the benz[k]fluoranthene signal predominated. The KC_{18} plate was unusual in that the (relatively high) background fluorescence decreased on prolonged irradiation; for long irradiation times the recorded fluorescence intensity became "negative" but when the curve was corrected for the blank background effect, single exponential decays were also obtained for benz[k]fluoranthane on alkyl-modified plates. The rate constants of the photo-oxidation process on the various t.l.c. plates are listed in Table 3. In contrast to the observations of Seifert [11], there was no significant variation in the decay behaviour of the repeated experiments; the average rate constants (Table 3) are precise within 2—10%. Possibly the t.l.c. plates used here were more homogeneous than those used by Seifert; and Seifert did not irradiate the plates continuously, but made repeated scans at intervals. In general, however, the present results agree with Seifert's. The benz-[k]fluoranthene signal decays quite quickly on silica plates. Thus the plates must be kept in the dark after deposition and, for quantitative work, the

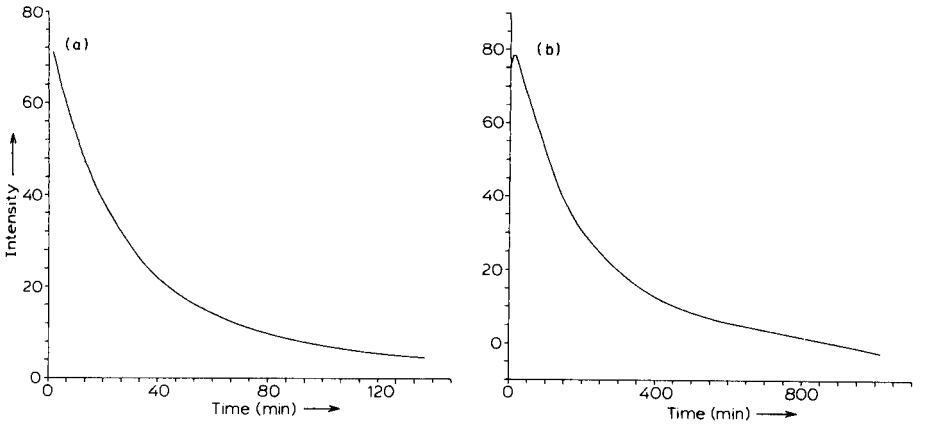

Fig. 7. Decay curves of the total fluorescence intensity of 2.5 ng of benz[k]fluoranthene: (a) on a silica-on-aluminum plate; (b) on a KC_{18} plate.

TABLE 3

Stability of benz[k]fluoranthene on various t.l.c. plates[a]

T.l.c. material	Rate constant[b] (s^{-1})	T.l.c. material	Rate constant (s^{-1})
KC_{18}	6.2×10^{-5}	Silica-on-aluminum	5.9×10^{-4}
RP_{18}	1.6×10^{-4}	Silica-on-glass	6.2×10^{-4}
C_2-silica	7.4×10^{-5}	H.p.t.l.c. silica-on-glass	7.8×10^{-4}

[a]2.5 ng of benz[k]fluoranthene was deposited on the plate and continuously irradiated at 254 nm in the Carl Zeiss densitometer. [b]Rate constant k for the intensity decay $I = I_0 \exp(-kt)$ observed for benz[k]fluoranthene fluorescence. The decay curves were subjected to a least-squares fit; the values given are the means of 3—4 experiments.

mode of working must be reproducible. On alkyl-modified plates, the decay is generally 10 times slower, so that fewer precautions are needed. The faster decay observed on h.p.t.l.c. plates than on t.l.c. plates is probably due to the smaller particle size of such plates, i.e., larger effective surface area.

The alkyl-modified plates are clearly more suitable for storage and quantitative purposes than silica plates. Even when the C_{18} plates were stored without any precautions for 6 days, the intensity of the benz[k]fluoranthene signal decreased only by 30%; with plain silica plates no emission was observed after that time. In practice, however, silica plates are useful for quantitative purposes, when the measurements are made within 2—3 h after deposition, and for conservation purposes, when the plates are kept in the dark under nitrogen. Some compounds (e.g., tetracene) are more prone to photochemical decomposition than benz[k]fluoranthene and require careful testing for stability on storage.

Conclusion

The usefulness of t.l.c. plates as a l.c. buffer memory for fluorescence emission and excitation experiments has been clearly demonstrated. The immobilized compounds remain available for quantitative and qualitative evaluation for several days or longer when adequate precautions are taken. In this respect, PAHs on alkyl-modified t.l.c. plates are much less susceptible to photodegradation than on silica plates. For immediate (i.e., within hours) inspection of the deposited compounds, no extra precautions are usually required unless unstable compounds such as tetracene are involved.

Room-temperature fluorescence emission measurements with a cut-off filter to detect total fluorescence or a monochromator to record the spectrum are both feasible and can be used for quantitative purposes. Calibration plots for benz[k]fluoranthene are linear over 3—4 orders, from about 5 ng to the limit of detection. Detection limits are around 1 pg for single-wavelength detection when the t.l.c. plates are purified and in the low pg range for detection via fluorescence spectra. Immobilization offers additional advantages. Fluorescence emission and excitation spectra can be recorded for the separated compounds without having to stop the l.c. flow and without specialized equipment. In principle, detection limits could be improved by methods such as signal-averaging, blank subtraction and repetitive scan procedures which would be impossible to apply on-line. The usefulness of fluorescence emission and excitation spectra for identification requires no further comment.

For qualitative purposes, the line-narrowing technique is clearly useful. This low-temperature method, which is obviously incompatible with dynamic systems, provides highly-resolved fluorescence spectra and is very sensitive: detection of tetracene, a compound with a much lower fluorescence quantum yield than benz[k]fluoranthene, is possible down to the low picogram range.

REFERENCES

1 J. W. Hofstraat, M. Engelsma, R. J. van de Nesse, C. Gooijer, N. H. Velthorst and U. A. Th. Brinkman, Anal. Chim. Acta, 186 (1986) 247.
2 Y. Talmi (Ed.), Multichannel Image Detectors, Vol. 1, ACS Symposium Series 102, American Chemical Society, Washington, DC, 1979.
3 Y. Talmi (Ed), Multichannel Image Detectors, Vol. 2, ACS Symposium Series 236, American Chemical Society, Washington, DC, 1983.
4 D. G. Jones, Anal. Chem., 57 (1985) 1057A, 1207A.
5 Y. Talmi, Appl. Spectrosc., 36 (1982) 1.
6 J. W. Hofstraat, M. Engelsma, J. H. de Roo, C. Gooijer and N. H. Velthorst, Appl. Spectrosc., in press.
7 R. I. Personov, in V. M. Agranovich and R. M. Hochstrasser (Eds.), Spectroscopy and Excitation Dynamics of Condensed Molecular Systems, North-Holland, Amsterdam, 1983, pp. 555—619.
8 L. A. Bykovskaya, R. I. Personov and Yu. V. Romanovskii, Anal. Chim. Acta, 125 (1981) 1.
9 J. W. Hofstraat, M. Engelsma, W. P. Cofino, G. Ph. Hoornweg, C. Gooijer and N. H. Velthorst, Anal. Chim. Acta, 159 (1984) 359.

10 J. W. Hofstraat, H. J. M. Jansen, G. Ph. Hoornweg, C. Gooijer and N. H. Velthorst, Anal. Chim. Acta, 170 (1985) 61; J. Mol. Struct., 142 (1986) 279.
11 B. Seifert, J. Chromatogr., 131 (1977) 417.
12 H. Hellman, Fresenius Z. Anal. Chem., 295 (1979) 24.
13 P. Kucera, in P. Kucera (Ed.), Microcolumn High-performance Liquid Chromatography, Elsevier, Amsterdam, 1984, p. 39.
14 A. Alak, E. Heilweil, W. L. Hinze, H. Oh and D. W. Armstrong, J. Liq. Chromatogr., 7 (1984) 1273.
15 A. Nakajima, Bull. Chem. Soc. Jpn., 44 (1971) 3272.
16 J. C. Gluckman, D. C. Shelley and M. V. Novotny, Anal. Chem., 57 (1985) 1546.
17 J. W. Hofstraat, M. Bobeldijk, G. Ph. Hoornweg, C. Gooijer and N. H. Velthorst, J. Mol. Struct., 141 (1986) 301.
18 N. J. Kruse and G. J. Small, J. Chem. Phys., 56 (1972) 2985.
19 W. P. Cofino, J. W. Hofstraat, G. Ph. Hoornweg, C. Gooijer, N. H. Velthorst and C. MacLean, Chem. Phys. Lett., 89 (1982) 17.

Analytica Chimica Acta, 193 (1987) 209—217
Elsevier Science Publishers B.V., Amsterdam — Printed in The Netherlands

3,4-DIHYDRO-6,7-DIMETHOXY-4-METHYL-3-OXO-QUINOXALINE-2-CARBONYL AZIDE AS A HIGHLY SENSITIVE FLUORESCENCE DERIVATIZATION REAGENT FOR PRIMARY, SECONDARY AND TERTIARY ALCOHOLS IN HIGH-PERFORMANCE LIQUID CHROMATOGRAPHY

MASATOSHI YAMAGUCHI, TETSUHARU IWATA and MASARU NAKAMURA*

Faculty of Pharmaceutical Sciences, Fukuoka University, Nanakuma, Jonan-ku, Fukuoka 814-01 (Japan)

YOSUKE OHKURA

Faculty of Pharmaceutical Sciences, Kyushu University 62, Maidashi, Higashi-ku, Fukuoka 812 (Japan)

(Received 11th June 1986)

SUMMARY

3,4-Dihydro-6,7-dimethoxy-4-methyl-3-oxo-quinoxaline-2-carbonyl azide is a highly sensitive fluorescence derivatization reagent for primary, secondary and tertiary alcohols for high-performance liquid chromatography. Reaction conditions are optimized with benzyl alcohol, n-hexanol, cyclohexanol and 2-methyl-2-butanol. The reagent reacts with the alcohols in benzene to produce the corresponding fluorescent carbamic acid esters, which can be separated on a reversed-phase column YMC Pack C_8 with aqueous methanol as eluent. The detection limits for the alcohols are 2—5 fmol per 10-μl injection. The reagent also reacts with hydroxysteroids with primary, secondary and/or tertiary alcoholic group(s) to form fluorescent derivatives. Hydroxycarboxylic acids and phenols do not give any chromatographic peaks.

Various fluorescence derivatization reagents have been reported for the determination of primary and secondary alcohols by high-performance liquid chromatography (h.p.l.c.), e.g., 4-dimethylamino-1-naphthoylnitrile [1], (+)- and (−)-2-methyl-1,1′-binaphthalene-2′-carbonyl nitriles [2], 2-dansylethyl chloroformate [3], 1- and 9-anthroylnitriles [4], 3- and 4-chloroformyl-7-methoxy- [5], 7-[(chlorocarbonyl)methoxy]-4-methyl- [6] and 4-diazomethyl-7-methoxycoumarins [7], and 7-methoxycoumarin-3- and 4-carbonyl azides [8]. In contrast, only a few reagents, 2-(4-isocyanatophenyl)-6-methylbenzothiazole [9, 10] and naphthyl- [11] and anthryliso-cyanate [12] have been developed for the derivatization of alcohols including tertiary alcohols. However, the methods based on these reagents are not very sensitive.

It has been shown that 3,4-dihydro-6,7-dimethoxy-4-methyl-3-oxo-quinoxaline (DMOQ) derivatives fluoresce intensely in aqueous methanol and acetonitrile [13], and DMOQ-2-carbonyl chloride (DMOQ-COCl) has

0003-2670/87/$03.50

been developed as a highly sensitive fluorescence derivatization reagent for primary and secondary alcohols in h.p.l.c. [14]. However, DMOQ-COCl did not react with tertiary alcohols.

The purpose of this study is to develop a highly sensitive fluorescence derivatization reagent which also reacts with tertiary alcoholic hydroxyl groups. It is known that the carbonyl azide group reacts with alcohols, including tertiary alcohols, to form carbamic acid esters [8, 15, 16]. Therefore, DMOQ-2-carbonyl azide (DMOQ-CON_3; Table 1) was synthesized. In order to investigate its reactivity with alcohols, benzyl alcohol, n-hexanol, cyclohexanol and 2-methyl-2-butanol were used as model primary, secondary and tertiary alcohols; DMOQ-CON_3 reacts with these alcohols in benzene to produce the corresponding fluorescent carbamic acid esters. The esters can be separated by reversed-phase h.p.l.c. with aqueous methanol. The reactivity of DMOQ-CON_3 with various other alcohols (hydroxysteroids and hydroxycarboxylic acids) is also reported.

EXPERIMENTAL

Reagents and materials

All chemicals were of analytical reagent grade, unless noted otherwise. Deionized-distilled water was used. Organic solvents were distilled and dried in the usual manner. DMOQ-COCl was prepared as described previously [14].

Synthesis of DMOQ-CON_3. To DMOQ-COCl (0.5 g, 1.8 mmol) dissolved in 200 ml of dry acetone was added activated sodium azide (0.16 g, 2.5 mmol; Wako, Osaka, Japan). The mixture was stirred at 0°C for 2 h and the reaction mixture was then poured into ice water (100 ml). The resulting precipitate was collected by filtration and recrystallized from benzene/hexane (1:1, v/v).

The DMOQ-CON_3 obtained was stable in the crystalline state for at least 3 months when kept dry in the dark at room temperature. The reagent dissolved in benzene can be used for two days when stored at 4°C in the dark in a refrigerator.

Preparation of the fluorescent compounds from benzyl alcohol, n-hexanol, cyclohexanol and 2-methyl-2-butanol

The DMOQ-CON_3 (200 mg, 0.7 mmol) and the alcohol (0.7 mmol) were dissolved in 10 ml of benzene. The solution was placed in a screw-capped test tube (20 ml), heated at 80°C for 1 h and then cooled. The reaction mixture was evaporated to dryness under reduced pressure. The residue was dissolved in 5 ml of chloroform and chromatographed on a silica gel-60 column (25 cm × 2.7 cm i.d.; ca. 130 g, 70—230 mesh; Japan Merck) with n-hexane/ethyl acetate (2:1, v/v). The main fraction was evaporated to dryness under reduced pressure and the residue was recrystallized from methanol. The properties of the four products are summarized in Table 1.

TABLE 1

Analytical data for DMOQ-CON_3 and its derivatives with the four alcohols[a]

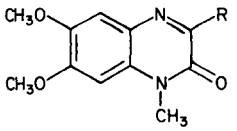

Compound	R	Yield (%)	M.p. (°C)	Formula	Elemental data (%) Calc. (Found)		
					C	H	N
DMOQ-CON_3	CON_3	78	272	$C_{12}H_{11}N_5O_4$	49.8 (50.0	3.8 3.8	24.2 22.4)
I	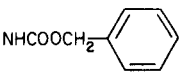	20	194	$C_{19}H_{19}N_3O_5$	60.8 (61.05	4.8 5.1	11.8 11.6)
II	$NHCOOC_6H_{13}$	15	101	$C_{18}H_{25}N_3O_5$	59.5 (59.4	6.9 7.2	11.6 11.4)
III	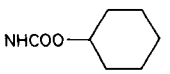	8	155	$C_{18}H_{22}N_3O_5$	59.8 (59.85	6.4 6.6	12.0 11.9)
IV	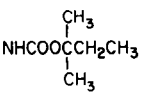	5	181	$C_{17}H_{22}N_3O_5$	58.4 (58.1	6.6 6.9	11.9 12.0)

[a]All compounds were pale yellow needles; DMOQ-CON_3 was somewhat more intensely colored than the derivatives.

Apparatus and h.p.l.c. conditions

Uncorrected fluorescence spectra and intensities were measured with a Hitachi 650-60 spectrofluorimeter in 10 × 10-mm quartz cells; spectral bandwidths of 10 nm were used for both the excitation and emission monochromators. Fluorescence quantum yields were obtained by the method of Parker and Rees [17]. Ultraviolet (u.v.) spectra and absorbances of acetonitrile solutions were measured with a Hitachi 200-20 spectrophotometer in 10-mm quartz cells. Infrared (i.r.) spectra were recorded in potassium bromide pellets with a Shimadzu IR-430 spectrophotometer. ^{1}H-nuclear magnetic resonance (n.m.r.) spectra were obtained with a Hitachi R-90H spectrometer at 90 MHz using a ca. 5% (w/v) solution of [$^2H_6$]dimethylsulfoxide containing tetramethylsilane as the internal standard. Field desorption mass spectra (m.s.) were taken with a JEOL DX-300 spectrometer. Uncorrected melting points were measured with a Yazawa melting point apparatus.

For the h.p.l.c. separation of the DMOQ derivatives, a Waters 510 high-performance liquid chromatograph equipped with a U6K universal injector

(10-μl loop) was used with a Hitachi F1100 fluorescence spectrophotometer equipped with a 12-μl flow cell, operated at an excitation wavelength of 360 nm and an emission wavelength of 440 nm. The column was a YMC Pack-C_8 (150 × 6 mm i.d.; particle size 10 μm; Yamamura Chemical Labs., Kyoto). The column can be used for more than 1000 injections with only a small decrease in the number of theoretical plates, provided that it is washed with methanol every day after use. The mobile phase used for the separation of the DMOQ derivatives of the examined alcohols was 70% (v/v) methanol in water at a flow rate of 2.0 ml min^{-1} (ca. 140 kg cm^{-2}). The column temperature was ambient (15–25°C).

Derivatization procedure

To 0.1 ml of a test solution of alcohols in benzene (12 pmol–15 nmol ml^{-1} each) placed in a PTFE screw-capped reaction vial (2 ml) was added 0.9 ml of 3 mM DMOQ-CON_3 in benzene. The vial was tightly closed and heated at 130°C for 60 min in the dark. After cooling, 20 μl of the reaction mixture was diluted with 100 μl of methanol, and an aliquot (10 μl) of the resulting solution was injected into the chromatograph. For the reagent blank, 0.1 ml of benzene in place of a test solution was subjected to the same procedure.

RESULTS AND DISCUSSION

Fluorescent products of reaction between alcohols and DMOQ-CON_3

Because acyl azides react with alcohols in an inert solvent such as benzene to form carbamic acid esters [8, 15, 16], the reaction products from benzyl alcohol, n-hexanol, cyclohexanol and 2-methyl-2-butanol should be the corresponding DMOQ-carbamic acid esters, which were confirmed as compounds **I**, **II**, **III** and **IV**, respectively, from the elemental data (Table 1) and i.r., m.s. and ^{1}H-n.m.r. spectral data (Table 2).

The fluorescence properties of the DMOQ derivatives were examined in methanol, acetonitrile and water, which are widely used as components of mobile phases in reversed-phase h.p.l.c. (Table 3). The DMOQ derivatives of the alcohols (compounds **I**–**IV**) showed almost the same fluorescence excitation and emission maxima; the maxima were almost independent of the kinds of the alcohols and the solvents. The fluorescence intensities (quantum yields) in water were slightly smaller than those in methanol and acetonitrile.

H.p.l.c. and derivatization conditions

The separation of DMOQ derivatives of benzyl alcohol, n-hexanol, cyclohexanol and 2-methyl-2-butanol was studied on a reversed-phase column, YMC Pack C_8, with aqueous methanol. At methanol in water concentrations higher than 75% (v/v), the peak for the cyclohexanol derivative partially overlapped with the peak for the 2-methyl-2-butanol derivative whereas methanol concentrations of 60–65% caused a delay in elution with peak broadening. Optimum separation was attained with 70% (v/v) methanol. Figure 1 shows a typical chromatogram obtained with the alcohol derivatives.

TABLE 2

Spectral data for DMOQ-CON_3 and its derivatives with alcohols

Compound	U.v. λ_{max} (nm)	I.r. ν_{max} (cm^{-1})				M.s. *m/z* (M^+)	^{1}H-n.m.r.[a] (δ, ppm)
		C=O	Arom. C=C and/or C=N	NH	N_3		
DMOQ-CON_3	363 (4.15)	1750 1645	1615	—	2150	289	7.37 and 6.71 (1H each, s each, aromatic H) 4.07 and 4.02 (3H each, s each, OCH_3) 3.79 (3H, s, NCH_3)
I	370 (4.17)	1740 1645	1625	2900	—	369	8.70 (1H, s, NH) 7.52—7.20 (5H, m, aromatic H) 7.37 and 6.68 (1H each, s each, aromatic H) 5.27 (2H, s, $COOCH_2$) 3.97 and 3.93 (3H each, s each, OCH_3) 3.72 (3H, s, NCH_3)
II	358 (4.20)	1730 1645	1625	2900	—	363	8.53 (1H, s, NH) 7.35 and 6.69 (1H each, s each, aromatic H) 4.27 (2H, t, J = 3.3 Hz, $COOCH_2$) 3.98 and 3.92 (3H each, s each, OCH_3) 3.75 (3H, s, NCH_3) 1.88—1.00 (11H, m, $(CH_2)_4CH_3$)
III	360 (4.52)	1740 1640	1620	2800	—	361	8.51 (1H, s, NH) 7.35 and 6.69 (1H each, s each, aromatic H) 5.02—4.68 (1H, m, COOCH) 3.98 and 3.92 (3H each, s each, OCH_3) 3.75 (3H, s, NCH_3) 2.12—1.04 (10H, m, $(CH_2)_5$)
IV	359 (4.24)	1735 1650	1610	2950	—	349	8.46 (1H, s, NH) 7.37 and 6.69 (1H each, s each, aromatic H) 3.98 and 3.92 (3H each, s each, OCH_3) 3.74 (3H, s, NCH_3) 4.90 (2H, q, J = 7.5 Hz C-CH_2-) 1.44 (3H, t, J = 7.5 Hz, -CH_2-$C\underline{H}_3$)

[a] s = singlet; d = doublet; t = triplet; q = quartet; m = multiplet.

TABLE 3

Fluorescence properties of DMOQ-CON_3 and its derivatives with alcohols in methanol (M), acetonitrile (A) and water (W)

Compound	Excitation maximum (nm)			Emission maximum (nm)			RFI[a]			Quantum yield		
	M	A	W	M	A	W	M	A	W	M	A	W
DMOQ-CON_3[b]	—	373	—	—	434	—	—	55	—	—	0.39	—
I	362	360	364	441	432	448	100	98	83	0.68	0.59	0.54
II	362	359	363	443	431	447	86	91	60	0.62	0.58	0.45
III	362	359	363	443	430	447	82	86	71	0.64	0.58	0.57
IV	361	358	363	440	429	447	97	96	78	0.62	0.61	0.53

[a]Relative fluorescence intensity. The fluorescence intensity was measured at the excitation and emission maxima. The intensity of compound I in methanol was taken as 100.
[b]DMOQ-CON_3 reacted partly with methanol to produce DMOQ-$NHCOOCH_3$ even at room temperature, and was decomposed by water.

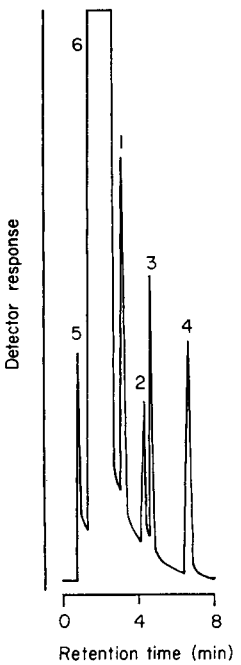

Fig. 1. Chromatogram of DMOQ derivatives. Peaks: (1) benzyl alcohol; (2) cyclohexanol; (3) n-hexanol; (4) 2-methyl-2-butanol; (5, 6) unknown products, probably decomposition products of DMOQ-CON_3. An aliquot (0.1 ml) of a mixture of the alcohols (0.5 nmol ml^{-1} each) was treated as in the described procedure.

Benzene used as a solvent for the derivatization reaction provided the most intense peaks for the alcohols examined; toluene gave less intense peaks (ca. 60% of those in benzene). The reaction proceeded only slightly or not at all in chloroform, dimethylsulfoxide, dimethylformamide, tetrahydrofuran, ethyl acetate, acetonitrile, acetone and 1,4-dioxane. Water interfered with the reaction because of the decomposition of DMOQ-CON_3. Thus, benzene was chosen for use in the procedure.

The derivatization reaction with benzyl alcohol, cyclohexanol and n-hexanol occurred more rapidly with increasing reaction temperature. The effects for cyclohexanol are shown in Fig. 2A; the reaction was complete within 60 min at 100°C or within 40 min at 130°C. The reaction with 2-methyl-2-butanol was slower (Fig. 2B), and peak heights became maximal and constant only after heating at 130°C for 55 min. Thus, heating for 60 min at 130°C was used tentatively in the procedure for the simultaneous derivatization of all the alcohols examined.

DMOQ-CON_3 gave the most intense peaks at concentrations greater than 2.5 mM for 2-methyl-2-butanol, 0.2 mM for cyclohexanol and 0.14 mM for benzyl alcohol or n-hexanol in the solution. Therefore, a 3 mM reagent solution was used in the procedure for the simultaneous derivatization of the four alcohols. The efficiency of conversion of the four alcohols to the DMOQ derivatives was examined by comparing the peak heights obtained under the reaction conditions with those given by the pure reaction products (compounds I, II, III and IV); the extents of conversion (%, mean ±s.d., n = 6) were 68.6 ± 2.2 (benzyl alcohol), 76.0 ± 0.5 (n-hexanol), 74.9 ± 0.4 (cyclohexanol) and 41.4 ± 2.4 (2-methyl-2-butanol). The DMOQ derivatives in the final mixture were stable for at least 72 h in daylight at room temperature.

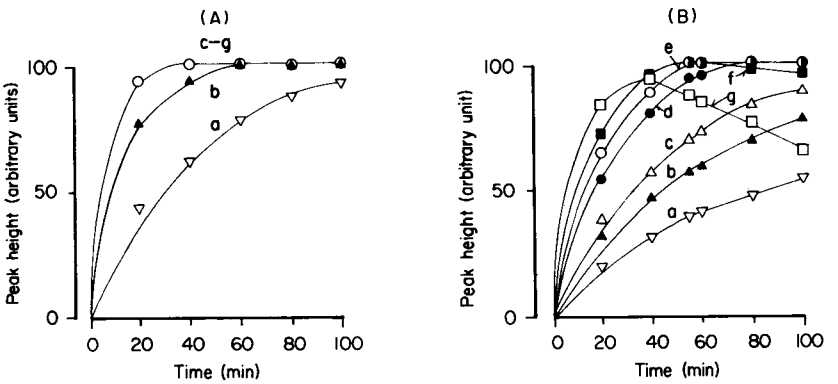

Fig. 2. Effect of reaction time and temperature on peak height: (A) cyclohexanol; (B) 2-methyl-2-butanol. Reaction temperature: (a) 80°; (b) 100°; (c) 110°; (d) 120°; (e) 130°; (f) 140°; (g) 150°C. Aliquots (0.1 ml) of the alcohol (0.5 nmol ml^{-1} each) were treated as in the recommended procedure apart from time and temperature.

Calibration graphs, precision and detection limits

The plots of peak heights versus the amounts of the individual alcohol were linear from 2 fmol to at least 2.5 pmol per 10-μl injection volume (corresponding to 1.2 pmol—1.5 nmol in 0.1 ml of test solution). The precision was established by repeated complete determinations (n = 10) of a mixture of the four alcohols (15 nmol ml^{-1} each). The relative standard deviations were 2.4% (benzyl alcohol), 0.5% (n-hexanol), 0.4% (cyclohexanol) and 2.6% (2-methyl-2-butanol). The detection limits (fmol per 10-μl injection, signal/noise = 2) were 2 (benzyl alcohol), 2.5 (n-hexanol), 3 (cyclohexanol) and 5 (2-methyl-2-butanol). The sensitivity for the primary and secondary alcohols is similar to that of the methods based on DMOQ-COCl [14] and 7-methoxycoumarin-3-carbonyl azide [8], and is much higher than that of the methods with the other fluorescence derivatization reagents [1—7]. In addition, the reagent is the first to allow tertiary alcohols to be detected at femtomole levels.

Reaction of DMOQ-CON_3 with other substances

Many hydroxysteroids and tertiary alcohols reacted with DMOQ-CON_3 under the derivatization conditions recommended, to form fluorescent derivatives. The retention times and detection limits for the DMOQ derivatives of these compounds are shown in Table 4. Hydroxycarboxylic acids (lactic and malic acids) did not give fluorescent products. Other substances such as carboxylic acids, 17 L-α-amino acids, aldehydes, ketones, phenols and sulfhydryl compounds gave no peaks on the chromatogram. Amines (n-butyl-, cyclohexyl- and benzyl-amines) may react with DMOQ-CON_3, but no peaks were detected on the chromatogram obtained under the present h.p.l.c. conditions.

TABLE 4

Retention times and detection limits for DMOQ derivatives of hydroxysteroids and other tertiary alcohols

Compound	Mobile phase Aqueous methanol (%, v/v)	Retention time (min)	Detection limit[a] (fmol)
4-Pregnen-21-ol-3,11,20-trione (11-dehydrocorticosterone)	70	3.7	6
4-Pregnen-21-ol-3,20-dione (deoxycorticosterone)	70	7.4	6
5-Pregnen-3β-ol-20-one (pregnenolone)	70	40.6	13
5-Androsten-3β-ol-17-one (dehydroisoandrosterone)	70	18.2	6
5-Cholesten-3β-ol (cholesterol)	100	4.3	3
5α-Cholestan-3β-ol (cholestanol)	100	4.7	3
4-Androsten-17α-ethinyl-17β-ol-3-one (ethisterone)	70	11.5	45
2-Methyl-2-propanol	60	6.8	20
2-Methyl-2-pentanol	70	7.9	7

[a]The amount in the injected volume (10 μl) giving a signal/noise ratio of 2.

Conclusions

The new reagent has excellent properties as regards reactivity and sensitivity for the derivatization of alcohols. It permits highly sensitive detection of tertiary alcohols, which cannot be attained with the fluorescence derivatization reagents reported previously. Thus, DMOQ-CON_3 should be useful as a fluorescence derivatization reagent in h.p.l.c. of primary, secondary and tertiary alcohols.

REFERENCES

1 J. Goto, S. Komatsu, N. Goto and T. Nambara, Chem. Pharm. Bull., 29 (1981) 899.
2 J. Goto, N. Goto and T. Nambara, Chem. Pharm. Bull., 30 (1982) 4597.
3 A. Takadate, M. Iwai, H. Fujino, K. Tahara and S. Goya, Yakugaku Zasshi, 103 (1983) 962.
4 J. Goto, N. Goto, F. Shamsa, M. Saito, S. Komatsu, K. Suzaki and T. Nambara, Anal. Chim. Acta, 147 (1983) 397.
5 C. Hamada, M. Iwasaki, N. Kuroda and Y. Ohkura, J. Chromatogr., 341 (1985) 426.
6 K. E. Karlsson, D. Wiesler, M. Alasandro and M. Novotny, Anal. Chem., 57 (1985) 229.
7 A. Takadate, T. Tahara, H. Fujino and S. Goya, Chem. Pharm. Bull., 30 (1982) 4120.
8 A. Takadate, M. Irikura, T. Suehiro, H. Fujino and S. Goya, Chem. Pharm. Bull., 33 (1985) 1164.
9 R. Wintersteiger, G. Gamse and W. Pacha, Fresenius Z. Anal. Chem., 312 (1982) 455.
10 O. S. Wolfbeis and H. Marhold, Monatsh. Chem, 114 (1983) 599.
11 R. Wintersteiger, G. Wenninger-Weinzierl and W. Pacha, J. Chromatogr., 237 (1982) 399.
12 R. Wintersteiger, J. Liq. Chromatogr., 5 (1982) 897.
13 M. Yamaguchi, S. Hara, R. Matsunaga, M. Nakamura and Y. Ohkura, J. Chromatogr., 346 (1986) 227.
14 T. Iwata, M. Yamaguchi, S. Hara, M. Nakamura and Y. Ohkura, J. Chromatogr., 362 (1986) 209.
15 T. Curtius, J. Prakt. Chem., 91 (1915) 1.
16 H. Lindemann and W. Schultheis, Justus Liebigs Ann. Chem., 464 (1982) 237.
17 C. A. Parker and W. T. Rees, Analyst (London), 85 (1960) 587.

Analytica Chimica Acta, 193 (1987) 219—229
Elsevier Science Publishers B.V., Amsterdam — Printed in The Netherlands

DETERMINATION OF METHYLARSENIC COMPOUNDS IN AIRBORNE PARTICULATE MATTER BY GAS CHROMATOGRAPHY WITH ATOMIC ABSORPTION SPECTROMETRY

HITOSHI MUKAI* and YOSHINARI AMBE

Chemistry and Physics Division, National Institute for Environmental Studies, Yatabe, Tsukuba, Ibaraki 305 (Japan)

(Received 6th June 1986)

SUMMARY

A sensitive method is described for the determination of mono-, di- and tri-methylarsenic compounds in airborne particulate matter by hydride-generation and gas-liquid chromatography with atomic absorption spectrometric detection. Interferences of various species are discussed. Absolute detection limits are 70, 80 and 100 pg As, respectively for the mono-, di- and tri-methylarsenic species. Recoveries of methylarsenic compounds added to airborne particulate matter are almost 100%. An iron/nitrate mixture interfered strongly but this was overcome by adding EDTA.

The biomethylation of arsenic in various media such as river water, sea water, sediment and soil has been reported [1—5]. Trimethylarsine and dimethylarsine are well known as volatile forms in these methylated products. They are liberated from various media containing arsenic to the air by fungi and molds [6—11]. Johnson and Braman [12] found trimethyl- and dimethyl-arsenic compounds in both gas and particulate matter in the air. Thus speciation of arsenic in air samples is important for the evaluation of natural sources of arsenic compounds in the air.

Many methods for determining methylarsenic compounds have been published but applications to airborne particulate matter are rarer. A sensitive hydride-generation method for inorganic and methylarsenic compounds was described by Braman et al. [13]. The arsines produced were trapped by a glass-bead column cooled in liquid nitrogen, and were released in the order of their increasing boiling points by heating; they were detected by d.c.-discharge atomic emission spectrometry. Andreae [3] and Howard and Arbab-Zavar [14] used a similar hydride-generation method and atomic absorption spectrometry for detection of methylarsenic compounds. Talmi and Bostick [15] used cold toluene as an arsine trap, gas chromatographic separation and microwave emission spectrometric detection. Odanaka et al. [16] determined inorganic and methylarsenic compounds in animal urine by using a similar heptane trap followed by gas chromatography/mass spectrometry.

0003-2670/87/$03.50

This paper describes a method for determination of methylarsenic compounds in airborne particulate matter by gas chromatography and atomic absorption spectrometry. Because arsines released to the air are considered to be oxidized and exist as dimethylarsinic acid and trimethylarsine oxide in airborne particulate matter [17], these compounds are extracted from the filter sample with a solvent and reduced with sodium tetrahydroborate. Unlike samples such as river water, samples of airborne particulate matter are generally very small, various elements (Fe, Ca, Al, etc.) are present which interfere with the reduction of methylarsenic compounds, and there is more than ten times as much inorganic arsenic as methylarsenic compounds. Therefore, selection of the extraction method and reduction conditions to prevent interferences were studied in detail. In order to decrease the amount of sample necessary, direct injection of reduced arsenic compounds into the gas chromatograph from a glass-bead column cooled by liquid nitrogen was attempted. Arsenic was detected by a sensitive atomic absorption system with a heated alumina tube as proposed by Ebdon et al. [18].

EXPERIMENTAL

Apparatus

The apparatus consisted of a reduction system and a detection system. The reduction system had a three-way cock for injection of reduction reagent, and a reduction vessel (volume ca. 30 ml) connected to a U-tube trap cooled by liquid nitrogen by teflon tubing (0.5 mm i.d.). Sodium tetrahydroborate was injected from a syringe and was pushed into the reduction vessel by helium carrier gas (40 ml min^{-1}). Silanized glass beads (60/80 mesh) were packed in the latter half of the glass U-tube trap (20 cm × 3 mm i.d.), so that water vapor from the reduction vessel would be trapped at the front of the U-tube and not block the later packing [13]. This trap was fitted with a four-way cock to allow the carrier gas to flow through the trap or to bypass it. A nichrome wire heater (0.5 mm thick) was used to heat the trap, to transfer the arsines to the chromatograph with the helium carrier still at 40 ml min^{-1}.

The detection system consisted of a gas chromatograph (Shimadzu GC-5A) and an atomic absorption spectrometer (Jarrel-Ash AA-781). The trap was connected to the injector of the gas chromatograph by a stainless-steel capillary inserted through a septum. The gas chromatographic column was of glass (1.5 m × 3 mm i.d.) packed with 5% PEG-20M on 60/80-mesh Chromosorb 101. The effluent from the column was led to a quartz T-piece (1.6 mm i.d) by a glass-lined stainless-steel transfer line (0.7 mm i.d.), mixed with hydrogen (30 ml min^{-1}; and thence to a 11-cm long ceramic alumina tube (6 mm o.d., 4 mm i.d.) through a hole (4-mm diameter) at the center of the side of the tube. The tube was supported at both ends by stainless-steel V fixtures, and was heated by an air/acetylene flame to 900—1000°C. The atomic absorbance was recorded by a Yanaco (YR-110) strip-chart recorder

and a Hitachi D-2000 Chromato-integrator. The conditions used for gas chromatography and atomic absorption spectrometry are summarized in Table 1.

TABLE 1

Instrumental parameters used for the determination of methylarsenic compounds

Gas chromatograph		Atomic absorption spectrometer	
Injection temp.	175°C	Arsenic hollow-cathode lamp	10 mA
Column temp.		Wavelength	193.7 nm
initial temp.	25°C	Spectral bandwidth	0.2 nm
ramp rate	20°C min^{-1}	Background correction	no
final temp.	180° C (3 min.)	Flame	Air/acetylene
Transfer line temp.	160°C		(6/1.75 l min^{-1})
Helium carrier gas	40 ml min^{-1}	Additional H_2	30 ml min^{-1}

Reagents

Sodium tetrahydroborate tablets for hydride generation, high-grade EDTA and hydrochloric acid (all from Wako Pure Chemical Co.) were used. Each tetrahydroborate solution (10% in distilled water) was used only for half a day. Disodium methanearsonate ($CH_3AsO_3Na_2 \cdot 6H_2O$, 99%) was donated by Merck. Sodium dimethylcacodylate [$(CH_3)_2AsO_2Na \cdot 3H_2O$, 97.0%] was from Wako Pure Chemical Co. Solutions of ca. 1 μg ml^{-1} arsenic of these compounds were prepared.

Trimethylarsine oxide was synthesized from dimethylarsenic iodide. The latter was prepared from sodium dimethylcacodylate (ca. 20 g in 70 ml of water) and potassium iodide (30 g) in the presence of sodium hydrogensulfite (20 g) by adding concentrated hydrochloric acid until a yellow layer of dimethylarsenic iodide was produced. The crude dimethylarsenic iodide was purified by vacuum distillation to give ca. 10 ml of product.

The diethyl ether solvent of the commercial methyllithium product (5%, 100 ml; Merck) was replaced by dibutyl ether in a three-necked flask, so that the solvent and the trimethylarsine produced could be separated easily. Dimethylarsenic iodide (10 ml) was added slowly to form trimethylarsine, which was distilled off and condensed in a test tube cooled in ice. About 1 ml of crude trimethylarsine was obtained, from which a ca. 50 mg As l^{-1} trimethylarsine solution was prepared in dibutyl ether; 25 ml of this solution was mixed with 7.5 ml of 10% hydrogen peroxide and shaken in a separating funnel for several minutes to oxidize trimethylarsine to trimethylarsine oxide [19]. After residual trimethylarsine in the water layer had been removed by two extractions with dibutylether, the arsenic content of the water layer was determined by inductively-coupled plasma/atomic emission spectrometry. Finally, an aqueous 3.74 mg As l^{-1} solution of trimethylarsineoxide containing only a small concentration of dimethylarsinic acid (0.303 mg As l^{-1}) was prepared from this solution.

Procedure

Airborne particulate matter was collected on a quartz-fiber filter (20 cm × 25 cm, 2500 QAST; Pallflex, Putnam, CT) for 3 days with a high volume air sampler (1000 or 500 l min^{-1}). Prior to use, this filter was heated (300°C) for over 20 h in a vacuum drying oven.

A disk (3-cm diameter) was cut from the loaded filter with a punch; it was then cut into small pieces and put into a centrifuge tube (10 ml). After addition of 1 ml of 0.02 M EDTA, 1 M hydrochloric acid was added to give a total volume of 10 ml. Methylarsenic compounds were extracted from the filter by keeping this tube in an ultrasonic cleaner for 10 min. After centrifuging at 3000 rpm for 10 min, the supernatant liquid (0.4 ml) was put into the reduction vessel. A further 1 ml of 0.02 M EDTA and 9 ml of 1 M hydrochloric acid were added to this vessel. The air in this solution and in the vessel was purged by helium (40 ml min^{-1}) for 5 min.

Aqueous sodium tetrahydroborate solution (10%, 6 ml) was injected by syringe into the reductor and the arsines formed were purged with helium for 5 min, whilst heating at ca. 50°C with a hot air blower. Released arsines were trapped in the half-packed U-tube immersed in liquid nitrogen. After trapping was complete, the trap was detached from the reduction system with the four-way cock adjusted so that U-tube was closed. The inlet and outlet of the trap were connected to the helium supply line (40 ml min^{-1}) and the gas chromatograph, respectively. The four-way cock was opened and carrier gas was passed through the trap. The trap was heated by a nichrome wire heater (40 V) for 2 min and by a hot air blower, as soon as it had been taken out of the liquid nitrogen. Heating by the hot air blower was stopped when the ice in the front of the trap had melted, in order not to inject water vapor to the column. Arsines thus released were concentrated at the front of the gas chromatographic column, which was at room temperature (25°C). After all arsines had been released from the trap, the trap was detached from the gas chromatograph, and the chromatographic column was heated as shown in Table 1. Separated arsines were detected by the atomic absorption system (conditions as in Table 1) and their peak areas were calculated by chromato-integrator.

For calibration, standards of each methylarsenic compound corresponding to ca. 30 ng of arsenic were put into 10-ml centrifuge tubes, 1 M hydrochloric acid was added until the total volume was 10 ml, and the solutions were treated exactly as described above.

RESULTS AND DISCUSSION

Reduction conditions

The production of arsines is influenced by the acidity of the solution and the concentration of reductant [13, 15, 16]. Figure 1 shows the influence of acidity on the signals given for mono-, di- and tri-methylarsine. The signals from dimethylarsine decreased somewhat lower when the acidity was

low, but trimethylarsine gave a higher signal under these conditions. This agrees with the results obtained by Odanaka et al. [16]. The production of monomethylarsine was constant over the range of acidity used. The pH of the final solution is also indicated in Fig. 1. It shows that the production of trimethylarsine appears to be better in slightly alkaline conditions.

The best compromise for the acid concentration was considered to be 1 M. The effect of changing the volume of 10% sodium tetrahydroborate solution from 3 to 6 ml was studied at this acidity. The signals of mono- and di-methylarsine did not change, but there was a 20% increase of the signal for trimethylarsine, probably because of the increased alkalinity.

Molecular rearrangement of arsines during reduction has been reported, particularly when oxygen is left in the solution [15]. When a solution of the three methylarsines (ca. 1.4 ng As each) was purged with helium for 5 min, however, the amounts of other arsines produced by rearrangement during reduction (1 M HCl, 6 ml of 10% $NaBH_4$) were below their detection limits (70, 80 and 100 pg (S/N = 2), respectively). Therefore, for practical purposes, this effect can be ignored. However, it was found that inorganic arsenic, contained in airborne particulate matter in 10—20-fold weight excess compared to methylarsenic compounds, gave rise to small amounts of mono- and

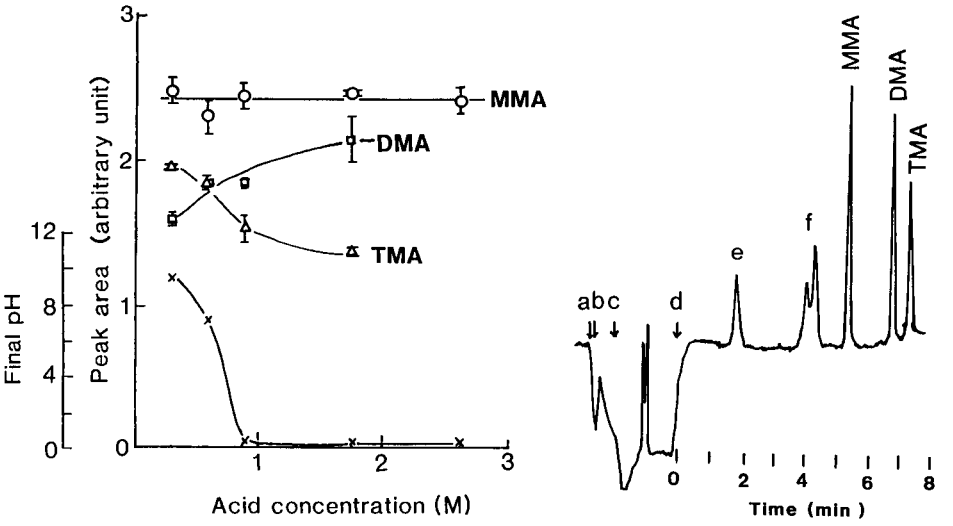

Fig. 1. Influence of the acidity on the production of arsines: (○) MMA; (□) DMA; (△) TMA. (×) pH of the solution after reduction. (3 ml of $NaBH_4$ in all cases.)

Fig. 2. Typical chromatogram of methylarsenic compounds. Each peak corresponds to ca. 1 ng As as a methylarsenic compound. Points a—d indicate the injection of the U-tube needle opening the four-way cock, removal of liquid nitrogen and heating of U-tube, and starting to heat the gas chromatograph column, respectively. Peak e indicates the arsine produced by the blank inorganic arsenic. Peak f may be due to blank CO_2.

tri-methylarsines, i.e., 0.3—0.4% of the inorganic arsenic for each. The amounts of inorganic arsenic which gave rise to a signal corresponding to the detection limits for mono- and tri-methylarsine were both ca. 20 ng. When the amount of inorganic arsenic is above this value, the measured concentrations of mono- and tri-methylarsine must be corrected.

Sensitivity

A typical chromatogram is shown in Fig. 2. The detection limit for each methylarsenic compound and the relative standard deviations (RSD) for measurement of each are listed in Table 2. These absolute detection limits were somewhat higher than those (20—30 pg) obtained by gas chromatography/mass spectrometry [16] and by gas chromatography/microwave emission spectrometry [15]. However, in those methods, more sample was needed than in the present method, because cold toluene or heptane was used to trap the arsines and only a portion of the trap solution was injected into the gas chromatograph; in the present method, all the arsines trapped in the U-tube were transported to the chromatograph.

Relative sensitivities based on the peak area of the monomethyl compound (=1) were 0.80—0.86 (dimethyl) and 0.65—0.87 (trimethyl). These values varied somewhat with column conditions. Peak areas were linear up to ca. 3 ng of arsenic.

Extraction method and recovery of added standard

Four extraction solvents (0.05 M NaOH, 1 M HCl, 0.05 M NaOH/0.02 M EDTA (9 + 1) and 1 M HCl/0.02 M EDTA (9 + 1)) were examined. A standard solution of methylarsenic compounds (20.0 ng As in the monomethyl form, 22.0 ng in the dimethyl form and 26.3 ng in the trimethyl form) were added to a sample of airborne particulate matter (3-cm diameter disk) cut from a filter sampled in February or August. This filter was air-dried, and the methylarsenic compounds were extracted by each solvent. Methylarsenic compounds in each extract were reduced under various conditions (acidity and amount of reductant) and the recoveries were evaluated. The results are shown in Table 3. The four solvents gave almost complete recoveries of the monomethyl form, while for the di- and tri-methyl forms, hydrochloric acid gave better extraction than sodium hydroxide. Adding EDTA to the acid appeared to improve the extraction efficiency for the trimethyl form; EDTA was considered to block adsorption of arsenic compounds by species of aluminum, iron, etc. under acidic conditions.

Investigation of the effect of reduction conditions on the recovery showed that 6 ml of 10% sodium tetrahydroborate in 1 M hydrochloric acid in the presence of EDTA gave the best recoveries and a reasonable reproducibility for the two different samples. Added standards were recovered almost completely from the filter. Therefore extraction with hydrochloric acid and EDTA and reduction with 6 ml of reductant with 1 M hydrochloric acid and EDTA were chosen for general use.

TABLE 2

Detection limits and reproducibility for the determination of methylarsenic compounds

Arsenic species	Detection limit[a] (pg)	RSD[b] (%)
Monomethylarsinic acid (MMAA)	70	6.1 (0.72)
Dimethylarsinic acid (DMAA)	80	7.8 (0.79)
Trimethylarsine oxide (TMAO)	100	6.0 (0.94)

[a]For signal/noise = 2. [b]n = 5 (peak area); the weight of arsenic (ng) found is given in parentheses.

TABLE 3

Effect of extraction solvent and reduction conditions on the recoveries of methylarsenic compounds[a]

Case no.	Sample[b]	Extraction	Reduction[c]		Recovery[d] (%)		
			Acidity (M)	$NaBH_4$ (ml)	MMAA	DMAA	TMAO
1	F	NaOH	1	3	103 ± 2	81 ± 5	69 ± 13
2	F	NaOH/EDTA	1	3	95 ± 5	90 ± 10	68 ± 20
3	A	NaOH/EDTA	1	3	94 ± 1	78 ± 3	77 ± 4
4	F	HCl	1	3	98 ± 9	95 ± 7	69 ± 2
5	F	HCl/EDTA	1	3	101 ± 9	94 ± 7	112 ± 10
6	A	HCl/EDTA	1	3	101 ± 1	102 ± 2	84 ± 9
7	A	HCl/EDTA	0.67	3	93 ± 6	114 ± 8	115 ± 38
8	A	HCl/EDTA	1	6	98.9 ± 2	100 ± 6	97 ± 12
9	F	HCl/EDTA	1	6	105 ± 4	99 ± 1	98 ± 10

[a]Methylarsenic compounds (20 ng As as MMAA, 22 ng As as DMAA, 26.3 ng As as TMAO) were added to each filter. The amounts of methylarsenic compounds (ng As) estimated to be already present on the filter were: (F) MMAA, 0.28; DMAA, 0.74; TMAO, 1.97; (A) MMAA, 1.0; DMAA, 5.1; TMAO, 58.2. [b]Samples collected in February (F) or August (A). [c]20 μmol EDTA added during reduction in all cases. [d]Obtained from the difference between the amounts (peak areas) with and without standard addition; mean ± SD for 2 results (3 results for 8 and 9).

Interferences

Many species are present in extracts from airborne particulates. Iron(III), aluminum, sulfate and nitrate are present as the main ions, and small amounts of antimony, tin, nickel and chromium, which may interfere with the reduction of arsenic compounds, are also present. Table 4 shows the influence of these ions on the reduction after addition of 20 μmol of EDTA. The concentrations shown (except nitrate and sulfate) were chosen to be similar to the usual concentrations in airborne particulate matter in Japan [20] with the sampling volume used here. Individual interferences were

TABLE 4

Interferences of various species on the determination of MMA, DMA and TMAO

Species[a]	Conc. ($\mu g\ ml^{-1}$)	Recovery[b] (%)		
		MMAA	DMAA	TMAO
Al	2	110	103	110
Fe(III)	2	92.9	94.8	88.2
Ca	2	98.9	99.5	107
Sb(III)	0.02	96.9	98.7	103
Sn(II)	0.02	87.4	95.3	99.2
Ni	0.01	108	101	114
Cr(VI)[c]	0.01	97.9	101	105
NO_3^-	3	109	95.3	87.1
SO_4^{2-}	10	123	109	98.2
Fe+Ca	1+1	98.1	100	101
Fe+Sb+Sn+Ni+Cr	1+0.01+0.01+0.005+0.005	101	102	93.7
Fe+Al	1+1	97.8	106	105
Al[d]+NO_3^-	2+13.8	99.4	84.1	76.7
Fe[d]+NO_3^-	1+3.4	64.0	42.3	31.0
Fe+NO_3^-	1+3	75.1	50.7	39.9
Fe+NO_2^-	1+3	43.4	22.2	1.0
NO_2^-	3	31.7	6.6	1.3
NO_2^-	0.3	80.1	50.7	73.3
Fe+NH_4	1+1	101	93.5	103
Fe+SO_4^{2-}	1+8	85.8	81.9	87.3
Al[d]+NO_3^-+Ca	1+6.9+1	105	98.8	81.3
Al[d]+NO_3^-+Fe	1+6.9+1	81.6	59.0	37.6
Al[d]+NO_3^-+Fe+Ca	1+6.9+1+1	83.3	47.9	52.1
Al+NO_3^-+Fe+Ca+Sb +Sn+Ni+Cr[e]	1+6.9+1+1 . . + citric acid (10 μmol)	83.1	68.6	39.5
	0.5+3.5+0.5 + citric acid (10 μmol)	92.4	63.0	65.8
Al+NO_3^-+Fe+Ca+Sb +Sn+Ni+Cr[e]	0.5+3.5+ . . +tartaric acid (10 μmol)	91.5	67.4	85.8
	0.5+3.5+ . . +tartaric acid (30 μmol)	99.6	75.0	73.2
Al+NO_3^-+Fe+Ca+Sb +Sn+Ni+Cr[e]	0.5+ . . . +EDTA (20 μmol)	98.0	86.5	89.4

[a]Except where noted, the ions were added as their chlorides or sodium salts; charges on cations omitted. [b]EDTA (20 μmol) was always added to the reducing solution. [c]Added as potassium dichromate. [d]Added as nitrate salt. [e]Mixed at the same concentration ratio as shown for single ions except NO_3^-. The ratio of NO_3^- to Fe^{3+} was closer to that found in real samples; Al^{3+} and NO_3^- were added as $Al(NO_3)_3$.

masked by 20 μmol of EDTA, as reported by Howard and Arbab-Zavar [14]. Strong interference was observed from a mixture of iron and nitrate, which interfered with the reduction of the dimethyl and trimethyl forms, and has not been reported previously. As nitrite was also found to interfere strongly with the reduction of these compounds, as shown by Howard and Arbab-Zavar [14], it was considered that nitrate was reduced to nitrite in the presence of iron during the reduction with tetrahydroborate.

In order to eliminate this interference, the effects of adding citric acid, tartaric acid and EDTA were studied; EDTA improved the recovery of the three arsenic compound most. Figure 3 shows the effects of EDTA on the recovery of the three forms of arsenic from the mixture of elements listed in the final lines of Table 4, which have relative concentrations similar to those from real airborne particulate matter (except sulfate). These results indicate that over 20 μmol of EDTA must be added when the iron concentration in the solution for reduction is over 0.3 μg ml^{-1} although 20 μmol of EDTA masked up to 0.5 μg ml^{-1} iron in ambient airborne particulate matter extracts.

Applications

The procedure developed was applied to several samples of airborne particulates collected in rural areas. Figure 4(a) shows a typical chromatogram obtained from a sample taken in summer; the trimethyl form predominated, the dimethyl form was only about 10% of the trimethyl form, and the monomethyl form was hardly detected, except in an unusual sample (Fig. 4b). The tri- and di-methylarsenic compounds were considered to originate from biological methylation, but the monomethyl form may have arisen from iron methanearsonate, which is a pesticide spread on rice fields

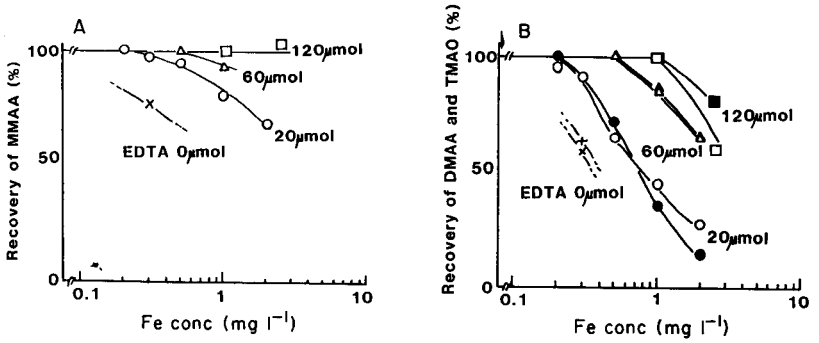

Fig. 3. Effect of adding EDTA on the interference of the mixed solution with the determination of the mono-, di- and tri-methylarsenic compounds. (A) All symbols refer to MMAA; (B) open symbols refer to DMAA and filled symbols to TMAO. The iron concentration on the horizontal axes represents the mixed ions listed in the final lines of Table 4 (see text).

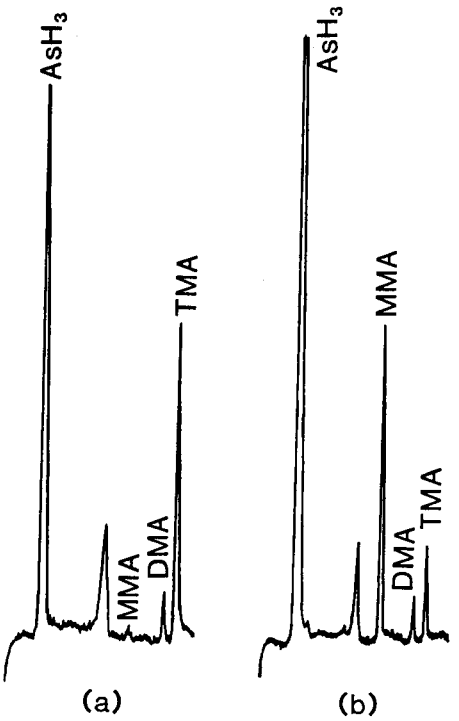

Fig. 4(a) Typical chromatogram obtained from airborne particulate matter collected on August 26—30, 1985; (b) sample collected on July 9, 1985.

TABLE 5

Concentration of methylarsenic compounds in air particulates[a]

Place	Date[b]	Concentration (pg As m^{-3})		
		Monomethyl	Dimethyl	Trimethyl
Tsukuba	26—30 Aug.	<10	53	604
	9 July	485	45	162
	5—8 Feb.	ND	11	29
	25—26 March	ND	6	25
	26—28 March	ND	10	66
Ooarai[c]	25 March (cold day)	ND	8	6
Katsuura[c]	27 March (wind from the sea)	ND	3	20
Iioka[c]	28 March (wind from the land)	ND	17	57

[a]Samples were taken during July/August 1985 and during February/March 1986. [b]ND, not detected. [c]Sea shore.

nearby [21]. In winter, the concentration of methylarsenic compounds decreased (Table 5), indicating that methylation of arsenic is influenced by the temperature.

It is known that seaweeds concentrate arsenic [22] and that trimethylarsine is produced when seaweed is decomposed. The concentration of methylarsenic compounds was measured at a beach with much seaweed (Katsuura) but it was not high compared to data obtained inland (Tsukuba) on the same day (Table 5).

The authors are sincerely grateful to Dr. T. Uehiro and Dr. M. Morita for much useful advice.

REFERENCES

1 R. S. Braman and C. C. Foreback, Science, 182 (1973) 1247.
2 J. U. Lakso and S. A. Peoples, J. Agric. Food Chem., 23 (1975) 674.
3 M. O. Andreae, Anal. Chem., 49 (1977) 820.
4 M. O. Andreae, Limnol. Oceanogr., 24 (1979) 440.
5 T. Takamatsu, R. Nakata, T. Yoshida and M. Kawashima, Jpn. J. Limnol., 46 (1985) 93.
6 J. M. Wood, Science, 183 (1974) 1049.
7 D. P. Cox and M. Alexander, Bull. Environ. Contam. Toxicol., 9 (1973) 84.
8 B. C. McBride and R. S. Wolfe, Biochemistry, 10 (1971) 4312.
9 M. B. Akins and R. J. Lewis, Soil Sci. Soc. Am. J., 40 (1976) 655.
10 D. P. Cox, in E. A. Woolson (Ed.), Arsenical Pesticides, American Chemical Society, Symposium Series 7, Washington, DC, 1975, p. 81.
11 R. S. Braman, in E. A. Woolson (Ed.), Arsenical Pesticides, American Chemical Society, Symposium Series 7, Washington, DC, 1975, p. 108.
12 D. L. Johnson and R. S. Braman, Chemosphere, 6 (1975) 333.
13 R. S. Braman, D. L. Johnson, C. C. Foreback, J. M. Ammons and J. L. Bricker, Anal. Chem., 49 (1977) 621.
14 A. G. Howard and M. H. Arbab-Zavar, Analyst, 106 (1981) 213.
15 Y. Talmi and D. T. Bostick, Anal. Chem., 47 (1975) 2145.
16 Y. Odanaka, N. Tsuchiya, O. Matano and S. Goto, Anal. Chem., 55 (1983) 929.
17 G. E. Parris and F. E. Brinckman, Environ. Sci. Technol., 10 (1976) 1128.
18 L. Ebdon, R. W. Ward and D. A. Leathard, Analyst, 107 (1982) 1271.
19 A. Merijanian and R. A. Zingaro, Inorg. Chem., 5 (1966) 187.
20 T. Mamuro and A. Mizohata, J. Jpn. Soc. Air Pollution, 13 (1978) 357.
21 H. Mukai and Y. Ambe, Atmos. Environ., 21 (1987) 185.
22 A. Yasui, C. Tsutsumi and S. Toda, Agric. Biol. Chem., 42 (1978) 2139.

Analytica Chimica Acta, 193 (1987) 231—238
Elsevier Science Publishers B.V., Amsterdam — Printed in The Netherlands

AQUEOUS SIZE-EXCLUSION CHROMATOGRAPHY OF HUMIC ACIDS ON A SEPHADEX GEL COLUMN WITH DILUTED PHOSPHATE BUFFERS AS ELUENTS

SADAO MORI*

Department of Industrial Chemistry, Faculty of Engineering, Mie University, Tsu, Mie 514 (Japan)

MASATAKA HIRAIDE and ATSUSHI MIZUIKE

Faculty of Engineering, Nagoya University, Chikusa-ku, Nagoya 464 (Japan)

(Received 18th March 1986)

SUMMARY

The elution behavior of humic acids on a Sephadex gel column is sensitive to the composition, concentration, and pH of the eluent. The concentrations of the eluent in the literature are too high to obtain the correct molecular size distribution of humic acids. By reducing the concentration of phosphate buffer eluents to about a hundredth of conventional concentrations, the correct distribution is obtained. In the proposed method, 1 ml of 0.1% sample solution is introduced into a Sephadex G-50 column (2.2-cm diameter, 55 cm long) and humic acids are eluted with a 10^{-3} M phosphate buffer solution (pH 7—9) at a flow rate of 1 ml min^{-1}.

Humic substances in river and sea waters, sediments and soils are formed from biological substances. They are assumed to be polymeric, complex organic acids having many carboxylic and hydroxylic groups attached to aromatic rings and to have molecular weights ranging from a few hundred to a few hundred thousand daltons. Among humic substances, materials which are soluble in dilute alkaline solutions but insoluble in dilute acid solutions (below pH 1) are called humic acids and those which are soluble in both dilute alkaline and acid solutions are called fulvic acids.

Humic substances stain natural waters yellow, increase the solubility of heavy metals such as iron and copper by forming stable complexes [1, 2], increase the solubility of phthalic acids and pesticides in water [3], and yield chloroform by their reaction with chlorine [4]. Because humic substances can affect a variety of chemical, physical, and biological reactions in natural waters, their characterization is very important in environmental sciences.

Size-exclusion chromatography (s.e.c.) has often been applied to the fractionation of macromolecules to estimate molecular weight averages. Size-exclusion chromatography of humic acids with dextran gel (Sephadex gel), so-called gel-filtration or gel chromatography, has been reported by several

0003-2670/87/$03.50

workers. Among recent reports are the separation of humic acids in river waters with pure water as eluent and estimation of the distributions of heavy metals in humic acids [5], the use of 0.01 M sodium hydroxide/0.1 M sodium chloride as the eluent and the estimation of heavy metals distributions in humic and fulvic acids [6, 7], and the use of 0.05 M Tris-chloride (pH 9.0) as the eluent [8]. Other packing materials have also been used for the s.e.c. of humic acids: TSK-GEL G-3000-SW with 0.1 M sodium chloride as eluent [9] and μ-Bondagel E-125 with water (pH 5) or 0.1 M sodium sulfate/0.1 M sodium acetate (pH 5) [10].

Humic acids are anionic macromolecules and dextran gels include a small number of carboxylic groups. Therefore, when humic acids are fractionated on dextran-gel columns, humic acids are not likely to be fractionated according to molecular size because of interactions, such as ionic repulsion and adsorption, with the gel; these interactions are affected by the concentration of humic acids and the ionic strength and pH of the eluent used [11]. To reduce these interactions, a method was proposed using ion-pairs of humic acids with tris(hydroxymethyl)aminomethane and borate buffer eluents [11]; this procedure gave a continuous molecular-size distribution rather than a discontinuous distribution grouped around several molecular weights.

Different elution behavior of humic acids was observed on a dextran-gel column in our laboratories when the composition, concentration, and pH of eluents were changed and it was almost impossible to obtain the correct molecular-size distribution. Most of the methods proposed so far [5—10] do not seem to give the correct distribution, either. Only ion-pair chromatography seems to give the correct distribution but unfortunately, humic acids not attached to ion-pair reagents are needed for the characterization.

In the present work, to establish experimental conditions for obtaining the correct molecular-size distribution of humic acids, systematic experiments were conducted with several kinds of eluents. By reducing the ionic strength of phosphate buffer in the eluents, humic acids could be fractionated according to molecular size.

EXPERIMENTAL

Column

The dextran gel, Sephadex G-50 (Pharmacia Fine Chemicals) was used without further screening. The dry gel (20 g) was suspended in distilled water overnight and then packed into a glass tube of 2.2-cm i.d. by the usual method [12]. The height of the gel bed was 48 cm, the total column volume, V_t, was 182 ml, and the void volume, V_0, was 75 ml (including dead volume); this was obtained with Blue Dextran 2000 (Pharmacia). The inner volume, V_i, was about 100 ml according to the manufacturer's data.

Samples and elution

Humic acid powder from Wako Pure Chemicals was used unless otherwise stated. Humic acid from Aldrich Chemical Company was also used. A humic

acid extracted from black soil and fulvic acid [13] was obtained from Drs. Arai and Kumada at Nagoya University. A 50-mg portion of humic acids was dissolved in 5 ml of a 0.1 M potassium hydroxide solution and then diluted to 50 ml with water. The pH of this solution was about 9.

Eluents examined here were distilled water, sodium chloride solutions, citrate buffers (citric acid/sodium hydrogenphosphate, pH 2.2, 3.0), Walpole buffers (acetic acid/sodium acetate, pH 4.0), phosphate buffers (sodium hydrogenphosphate/potassium dihydrogenphosphate, pH 5.0, 6.0, 7.0, 8.0, and 9.0), and glycine buffers (glycine/sodium chloride/sodium hydroxide, pH 10.0).

A 1-ml aliquot of sample solution was introduced onto the column and elution proceeded under gravitational force at a flow rate of 1 ml min^{-1}. The eluate was fractionated every 5 or 10 ml and the ultraviolet (u.v.) absorption of each fraction was measured at 230 nm on a u.v. absorption spectrophotometer Model UV-200 (Shimadzu Seisakusho).

RESULTS AND DISCUSSION

Influence of composition and concentration of constituents in eluents and sample solutions

The elution behavior of humic acids with eluents such as water and sodium chloride solutions was investigated systematically. The effects of sodium chloride in the sample solution was also examined.

Elution of humic acids with water or with sodium chloride solutions as eluent. As shown in Fig. 1(a), most humic acids were eluted at the exclusion limit (void volume, V_0) with water as eluent. The cation-exchange capacity of Sephadex G-25 was reported to be 2.2 ± 0.2 μeq g^{-1} of dry gel [14]. Therefore, the elution at V_0 is easily assigned to be due to ion exclusion.

The addition of neutral salts such as sodium chloride or sulfate to the mobile phase is supposed to reduce ion exclusion and other ionic interactions. Most mobile phases proposed in the literature for s.e.c. of humic acids also include these salts [6—10]. However, as shown in Fig. 1(b)—(d), the peak at V_0 decreased at a sodium chloride concentration of 1×10^{-4} M and broad small bands were obtained when the sodium chloride concentration was between 2.5×10^{-4} and 10^{-3} M. Above 10^{-3} M, no peak appeared except for a small peak near the total permeation limit ($V_0 + V_i$). Below 10^{-4} M, most humic acids appeared at V_0, and at 10^{-5} M, the chromatogram was identical to that obtained with water as eluent.

When sodium chloride solutions are used as mobile phases, acidic groups in the gel matrix and in humic acids might be surrounded by sodium cations, resulting in the reduction of ionic repulsion. Therefore, humic acids might adsorb on the gel by hydrophobic or other interactions. They are more strongly adsorbed on the gel with increasing sodium chloride concentration.

Effects of addition of sodium chloride to sample solution. In order to reduce the salt effect shown in Fig. 1(b)—(d), an attempt was made to

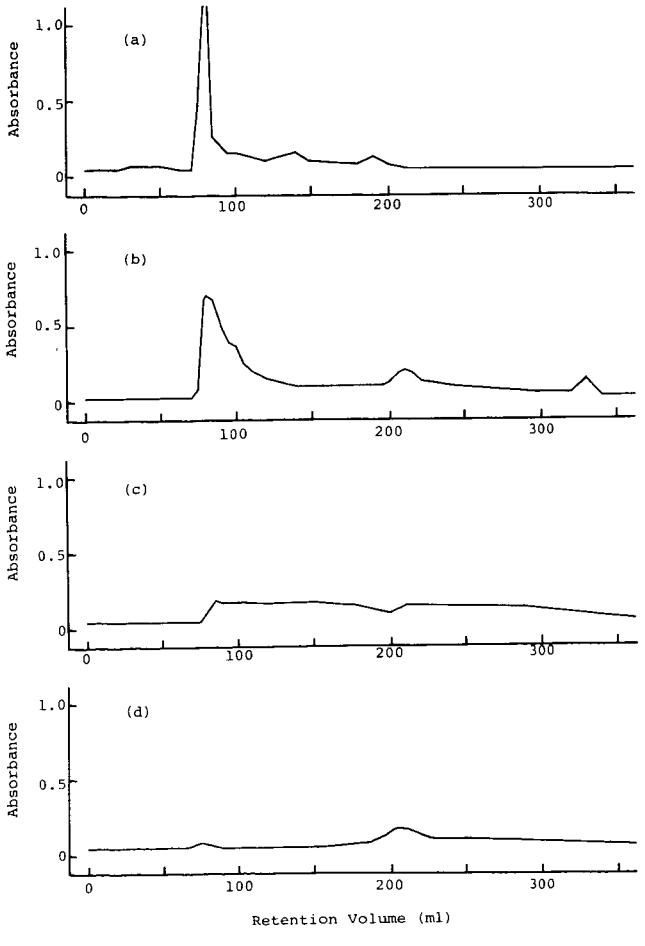

Fig. 1. Chromatograms of humic acids (Wako Pure Chemicals) with water and sodium chloride solutions as eluents. Eluents: (a) water; (b) 1.0×10^{-4} M NaCl; (c) 2.5×10^{-4} M

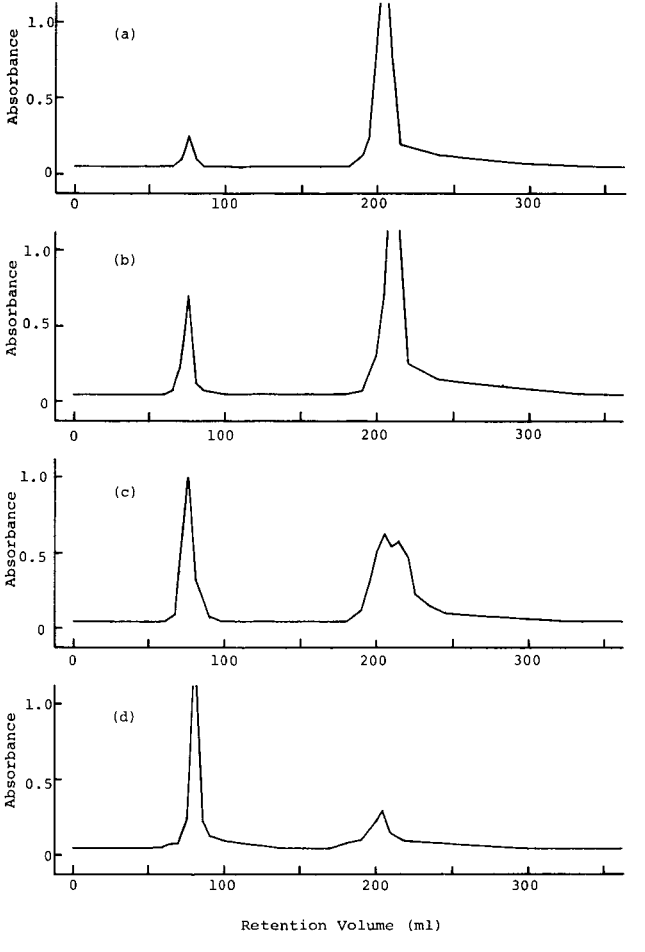

Fig. 2. Chromatograms of humic acids after addition of sodium chloride to sample solutions, with water as eluent. Sodium chloride in sample solutions: (a) 1.0 M; (b) $1.0 \times$

decrease the total salt content during elution. Sodium chloride was added to the sample solutions and the elution was done with water. The results are shown in Fig. 2. The chromatograms had two peaks; one was eluted at V_0 indicating ion exclusion and the other just beyond $V_0 + V_i$, indicating adsorption. The latter peak increased with increasing salt concentration in the sample solution. The reason why the second peak appeared near $V_0 + V_i$ is still not clear.

Elution of humic acids with pH-regulated eluents. In s.e.c. of ionic solutes, the pH of the mobile phase is also important, because ionization of the ionic solutes in addition to the gel is regulated by it. Several 0.1 M buffer solutions ranging from pH 2.2 to 10.0 were examined as eluents. The results are shown in Fig. 3. The chromatogram at pH 2.2 was similar to that at pH 3.0 (Fig. 3a).

As ionization of both humic acids and ionic groups on the gel was suppressed below pH 3.0, humic acids were adsorbed on the gel. With increasing pH, humic acids started to elute. Above pH 7.0, all solutes seem to be eluted giving broad chromatograms with peak maxima around 200 ml near $V_0 + V_i$. Under these conditions, size exclusion and adsorption effects probably appeared together.

Elution of humic acids with buffer solutions of low concentrations (proposed elution conditions)

As humic acids are assumed to be macromolecules having a broad molecular-size distribution, none of the chromatograms in Figs. 1—3 can represent the correct distribution. If the chromatogram appears between V_0 and $V_0 + V_i$, then fractionation would be more effective, and though there are some adsorption effects, molecular-size distribution can be obtained. As shown in Fig. 1, a decrease in the salt concentration of the eluent seems to be effective in moving the peak position of humic acids to smaller retention volume. Moreover, Fig. 3 indicates that an appropriate pH of the mobile phase is required to elute humic acids from the column. These results, therefore, suggest that a decrease in the buffer concentration at pH 7—9 would be appropriate for obtaining reasonable chromatograms.

Figure 4 shows the chromatograms obtained with 10^{-2} and 10^{-3} M phosphate buffer eluents of pH 8.0; the peaks moved to smaller elution volumes with decreasing salt concentration. At 10^{-3} M, the chromatogram appeared between V_0 and $V_0 + V_i$. The same results were obtained with buffer solutions of pH 7.0 and 9.0. Ion-pair chromatography of humic acids with tetrabutylammonium bromide also provided chromatograms similar to those shown in Fig. 4(b). Therefore, it can be concluded that, with 10^{-3} M phosphate buffer solutions of pH 7.0—9.0, molecular-size distribution of humic acids can be obtained effectively.

Other types of humic acids, obtained from Aldrich Chemical Company or extracted from black soil, and fulvic acids were also separated by the proposed elution conditions, with the results shown in Fig. 5.

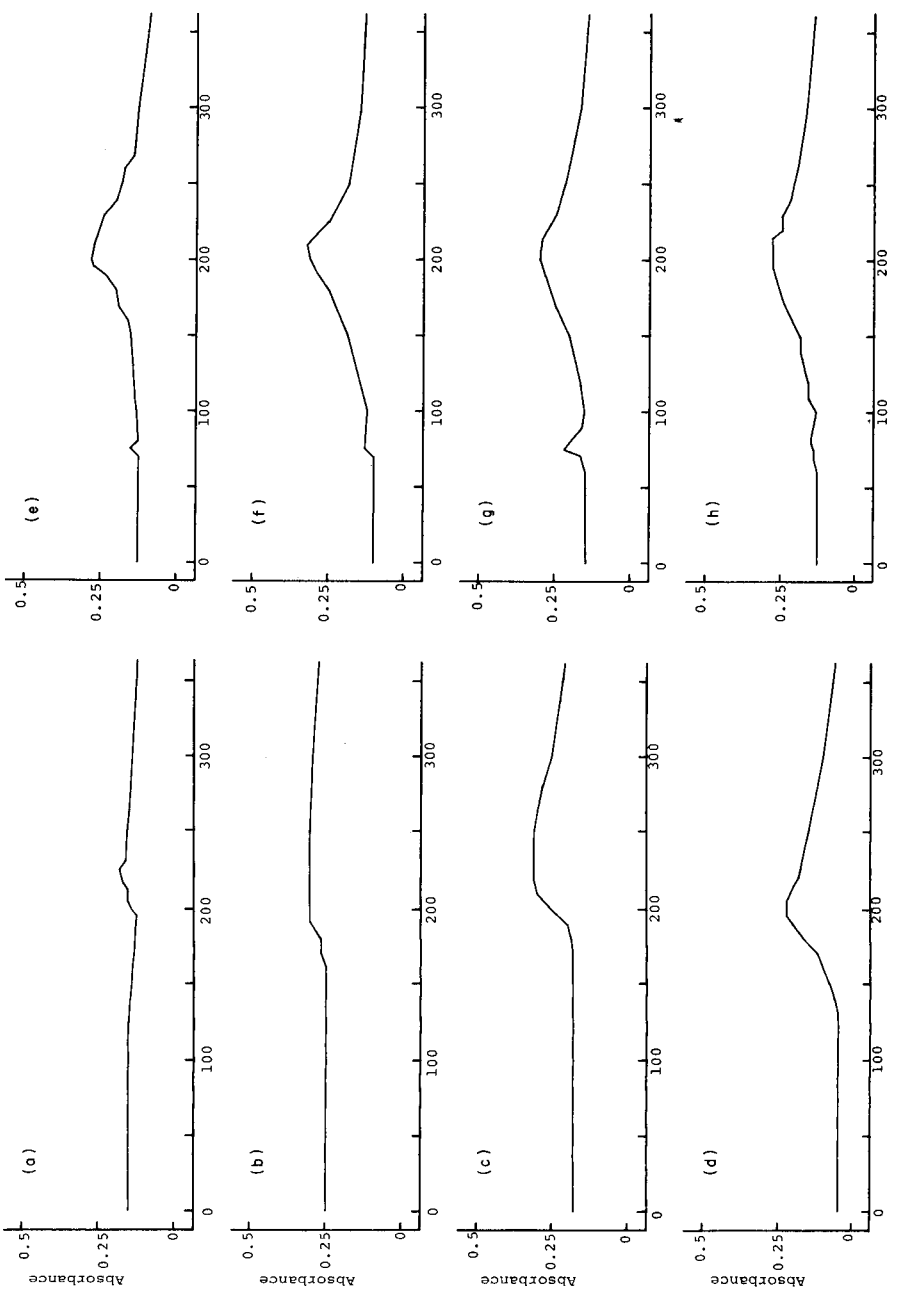

Fig. 3. Chromatograms of humic acids (Wako Pure Chemicals) with 0.1 M buffer solutions at different pH as eluents. pH of eluent: (a) 3.0; (b) 4.0; (c) 5.0; (d) 6.0; (e) 7.0; (f) 8.0; (g) 9.0; (h) 10.0.

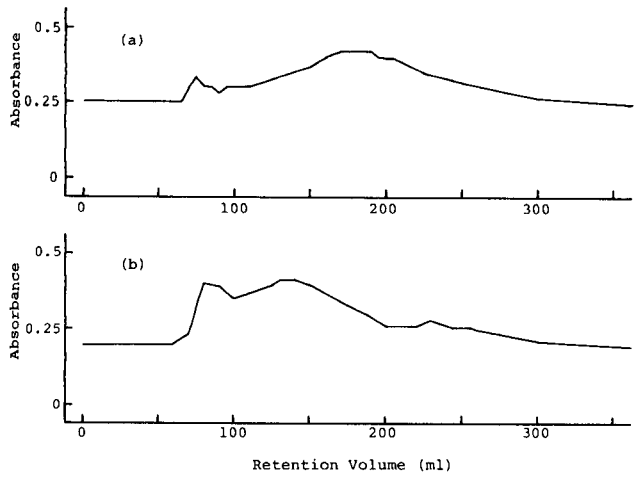

Fig. 4. Chromatograms of humic acids (Wako Pure Chemicals) with phosphate buffer solutions of low concentrations at pH 8.0 as eluents. Concentration of eluent: (a) 1.0×10^{-2} M; (b) 1.0×10^{-3} M.

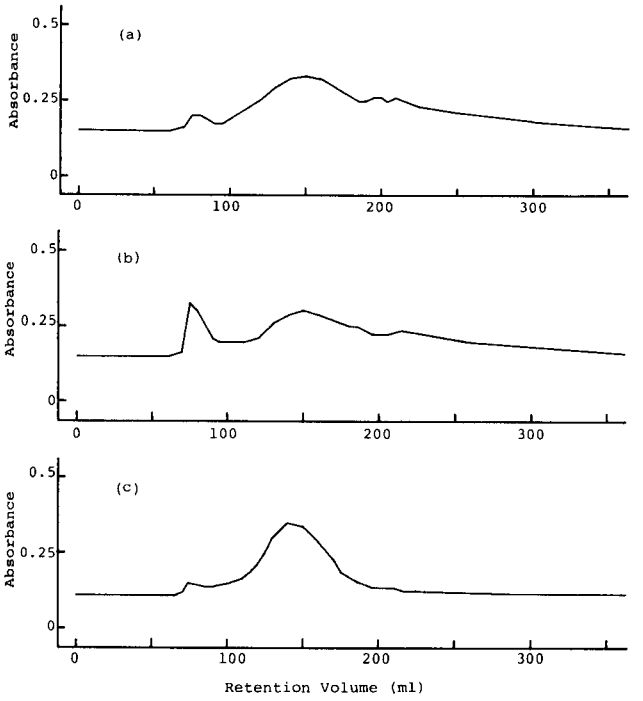

Fig. 5. Chromatograms of other humic and fulvic acids: (a) humic acids from Aldrich Chemical Company; (b) humic acids extracted from black soil; (c) fulvic acids. Eluent: 1.0×10^{-3} M phosphate buffer.

The effects of salt concentration in a solution of humic acid (Wako Pure Chemicals) were also examined. The eluent was 1×10^{-3} M phosphate buffer. A peak appeared at a retention volume of 240 ml, when sodium chloride was added to the sample solution (0.1% humic acid solution). This peak decreased with decrease in the added concentration of sodium chloride, from 0.1 to 0.01 M, and disappeared below 4×10^{-3} M. Therefore, the salt concentrations in sample solutions must be controlled below this value.

This work was supported by Grants in Aid for Scientific Research, Special Research Project on Environmental Science No. 59035027 from the Ministry of Education, Culture and Science, Japan.

REFERENCES

1 W. T. Bresnaham, C. L. Grant and J. H. Weber, Anal. Chem., 50 (1978) 1675.
2 B. Brady and G. K. Pagenkopf, Can. J. Chem., 56 (1978) 2331.
3 R. L. Wershaw, P. J. Burcar and M. C. Goldberg, Environ. Sci. Technol., 3 (1969) 271.
4 J. W. Moore and S. Ramamoorthy, Organic Chemicals in Natural Waters. Applied Monitoring and Impact Assessment, Springer, Berlin, 1984, p. 26.
5 J. L. Means, D. A. Crerar and J. L. Amster, Limnol. Oceanogr., 22 (1977) 957.
6 S. Hirata, J. Chem. Soc. Jpn., (1979) 1316.
7 S. Hirata, J. Oceanogr. Soc. Jpn., 39 (1983) 203.
8 N. More de Gonzalez, M. Castagnola and D. Rossetti, J. Chromatogr., 209 (1981) 421.
9 Y. Saito and S. Hayano, J. Chromatogr., 177 (1979) 390.
10 C. J. Miles and P. L. Brezonik, J. Chromatogr., 259 (1983) 499.
11 R. S. Swift and A. M. Posner, Soil Sci., 22 (1971) 237.
12 S. Mori, M. Furusawa and T. Takeuchi, J. Chromatogr., 49 (1970) 230.
13 S. Arai and K. Kumada, Soil Sci. Plant Nutr. (Tokyo), 29 (1983) 543.
14 S. Kadokura, T. Miyamoto and H. Inagaki, Polym. J., 14 (1982) 993.

Analytica Chimica Acta, 193 (1987) 239—245
Elsevier Science Publishers B.V., Amsterdam — Printed in The Netherlands

SELECTIVE SUBSTOICHIOMETRY FOR INORGANIC ARSENIC(V) BY ION-PAIR EXTRACTION WITH PYROGALLOL/TETRAPHENYLARSONIUM CHLORIDE AND ITS APPLICATION IN THE ANALYSIS OF SEAWEED

NOBUO SUZUKI*, FUMIHARU JITOH, HISANORI IMURA and YUKIO KANDA[a]
Department of Chemistry, Faculty of Science, Tohoku University, Sendai, 980 (Japan)
(Received 8th July 1986)

SUMMARY

Arsenic(V) is substoichiometrically extracted from 0.4—3 M sulfuric acid solutions into 1,2-dichloroethane with 1.0×10^{-5} M tetraphenylarsonium chloride in the presence of 2.0×10^{-1} M pyrogallol. Reproducibility of the substoichiometric extractions with a constant amount of tetraphenylarsonium chloride is high (0.5% RSD). This substoichiometric extraction is very selective for arsenic(V) from arsenic(III), monomethylarsonic acid, and dimethylarsinic acid. The extraction combined with the isotope dilution principle was applied to the determination of arsenic(V) in an acid-digested solution of a seaweed sample (*Laminaria religiosa* Miyabe) and to the determination of total arsenic in this sample.

In environmental samples, arsenic occurs in different chemical forms which have different toxicity and biological activity. Recently, much attention has been focused on the speciation of arsenic in different valence states as well as inorganic and organic states. Various techniques have been introduced to determine the different arsenic species such as arsenic(V), arsenic(III), monomethylarsonic acid, and dimethylarsinic acid: hydride generation/gas chromatography [1, 2], gas chromatography of volatile complexes [3, 4], and ion-exchange chromatography followed by polarography [5] or atomic absorption spectrometry [6, 7]. In these instrumental methods, it is always necessary to separate and recover each arsenic species quantitatively.

Substoichiometry combined with isotope dilution has the following advantages: the quantitative recovery of the species in question is not required, and the final determination is made by simple measurement of the radioactivity of the substoichiometric extract. Therefore, this analytical method is considered to be suitable for the speciation. Several papers on the substoichiometric determination for arsenic(III) have been reported [8—12], but none at all for arsenic(V). The extraction behavior of the above four arsenic species in various extraction systems was recently investigated; it was

[a]Present address: National Laboratory for High Energy Physics, Tsukuba, Japan.

0003-2670/87/$03.50

found that the ion-pair extraction with pyrogallol and tetraphenylarsonium was effective for arsenic(V) [13].

In the present paper, a highly selective substoichiometric determination of arsenic(V) is developed. The optimum conditions of the substoichiometric extraction of arsenic(V) are investigated for the pyrogallol/tetraphenylarsonium system, and the selectivity of arsenic(V) from other arsenic species is examined. The method is applied to the determination of arsenic(V) in an acid digest from a seaweed sample and to the determination of total arsenic after complete acid decomposition of this sample.

EXPERIMENTAL

Materials and apparatus

A radioactive arsenic(V) solution labelled with ^{74}As was prepared in the same manner as that described previously [13]. The carrier concentration was determined accurately by the substoichiometric isotope dilution method developed here.

Pyrogallol, tetraphenylarsonium (TPA) chloride, and 1,2-dichloroethane were of guaranteed reagent grade. Pyrogallol was dissolved in 2 M sulfuric acid. TPA was dissolved in 1,2-dichloroethane.

Other reagents and apparatus were the same as those used previously [13].

Procedures

Preparation of the seaweed sample. A seaweed sample of brown algae (*Laminaria religiosa* Miyabe) was collected in Onagawa Bay, Miyagi during June 1985 and immediately stored at below −20°C after washing with filtered sea water. It was dried by lyophilization for 48 h, powdered in a ball mill made of high-purity alumina, and stored in a refrigerator. The sample was dried for 2 h at 85°C before use.

Acid digestion and preseparation. A 0.5-g portion of seaweed sample was weighed out and placed in a teflon decomposition vessel (Uniseal, 70 ml). An aliquot of the radioactive arsenic(V) solution and 10 ml of concentrated nitric acid were added, and the sealed vessel was heated for 2 h at 150°C. After cooling, the resulting solution was transferred to a beaker and evaporated to dryness. For complete decomposition of organic arsenic species, 3 ml of concentrated sulfuric acid was added and heated for 3 h at about 240°C. Then water and a sodium iodide solution were added to the sulfuric acid solution to give 5—6 M sulfuric acid and 1 M iodide concentrations. The mixture was shaken with benzene for 5 min to extract arsenic(V). It was back-extracted with 0.5 M sulfuric acid, heated with 30% (w/v) hydrogen peroxide for 1 h at about 80°C, and evaporated to dryness. The residue was dissolved in a small amount of water and used for the substoichiometric extraction.

Substoichiometric extraction. The concentrations of pyrogallol and sulfuric acid in the aqueous sample solution were adjusted to 0.2 M and 1.6 M, respectively, and the mixture was shaken for 5 min with a 1,2-dichloroethane

solution containing a substoichiometric amount of tetraphenylarsonium chloride (usually 1×10^{-5} M). The γ-radioactivity of an aliquot of the organic phase was measured by using a NaI(T1) well-type scintillation counter.

RESULTS AND DISCUSSION

Optimum conditions for substoichiometric extraction

Figure 1 shows the effect of sulfuric acid concentration of the aqueous phase on the substoichiometric extraction of arsenic(V) with 9.96×10^{-6} M and 1.99×10^{-6} M TPA in the presence of 0.2 M pyrogallol. A constant amount of arsenic(V) was extracted over a wide range of acidity (0.4—3 M). The concentrations of arsenic(V) extracted into the organic phase were in good agreement with those expected from the quantitative reaction of 1:1 ion pair formation between an arsenic(V)/pyrogallol complex and a substoichiometric amount of TPA. This substoichiometric extraction equilibrium was rapidly achieved within 2 min.

Figure 2 shows the effect of the pyrogallol concentration on the substoichiometric extraction of arsenic(V) with 9.96×10^{-6} M TPA. When the concentration of pyrogallol is only 0.02 M, only 20% of the arsenic(V) expected from the quantitative reaction of a substoichiometric amount of TPA is extracted, but in the presence of more than 0.1 M pyrogallol, a substoichiometric amount of TPA reacts quantitatively with an arsenic(V)/pyrogallol complex and a constant amount of arsenic(V) is extracted without any undesirable extraction of arsenic(V) with a large excess of free pyrogallol.

Reproducibility of substoichiometric extraction

To examine the reproducibility of substoichiometric extraction of arsenic(V), the substoichiometric extraction with 9.96×10^{-6} M TPA in the presence of 0.2 M pyrogallol was applied to a series of solutions (5 ml) containing various amounts of radioactive arsenic(V). Figure 3 shows that the radioactivity of the organic phase increases with increase in the amount of arsenic(V) but beyond the equivalence point of TPA corresponding to 3.7 μg of arsenic(V) in 5 ml of solution, a constant amount of arsenic(V) is extracted. The precision of these substoichiometric extractions is very high; the relative standard deviation (RSD) for the radioactivities of the organic extracts in the plateau region of Fig. 3 is 0.52% (5 extractions), and arsenic(V) at the ca. 0.8 μg ml^{-1} level in the sample solution can be accurately determined under the proposed substoichiometric conditions. Reproducibility of the substoichiometric extractions from five independent test solutions and of five successive substoichiometric extractions from a single test solution was very good. For example, when the substoichiometric extraction was done from each of five 5-ml portions of 0.2 M pyrogallol in 3 M sulfuric acid containing 7 μg of As(V) with 2.0×10^{-6} M TPA in 1,2-dichloroethane, the mean activity of the organic phase was 17895 ± 119 cpm with RSD of 0.7%. When the substoichiometric extraction was done successively five times from the same

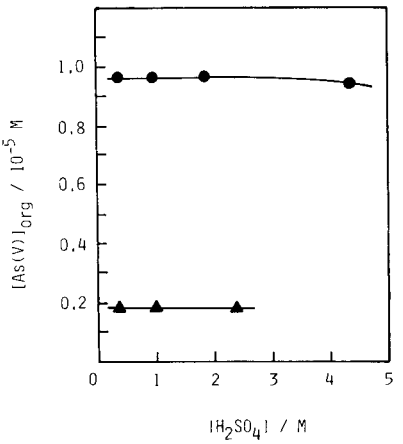

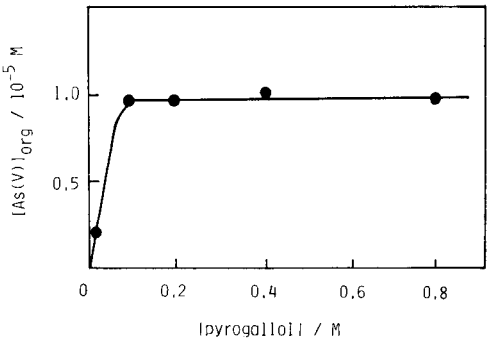

Fig. 1. Effect of sulfuric acid concentration of the substoichiometric extraction ([pyrogallol], 0.2 M; shaking time, 5 min): (•) [As(V)], 1.03×10^{-4} M; [TPA], 9.96×10^{-6} M; (▲) [As(V)], 3.43×10^{-5} M; [TPA], 1.99×10^{-6} M.

Fig. 2. Effect of pyrogallol concentration on the substoichiometric extraction. Conditions: [As(V)], 1.03×10^{-4} M; [TPA], 9.96×10^{-6} M; [H_2SO_4], 1.6 M; shaking time, 5 min.

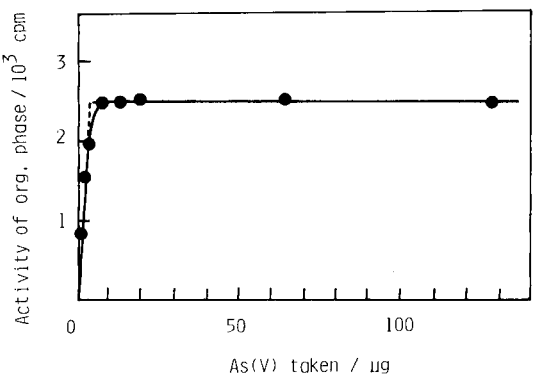

Fig. 3. Precision of substoichiometric extraction of As(V). Conditions: [TPA], 9.96×10^{-6} M; [pyrogallol], 0.2 M; [H_2SO_4], 1.6 M; shaking time, 5 min.

aqueous medium containing 15 μg As(V)/5 ml, the mean activity of the organic phase was 18014 ± 139 cpm with RSD of 0.8%.

Selectivity for arsenic(V)

The selectivity of the present method for arsenic(V) was investigated by the substoichiometric extraction from an aqueous solution containing 29.1 μg of radioactive arsenic(V) in the presence of a large amount of inactive arsenic

TABLE 1

Selectivity of substoichiometric extraction of As(V)[a]

Diverse arsenic species			Activity of extract (cpm)
	Taken (mg)	Mole ratio[b]	
—	—	—	6173
As(III)	3.87	101	6017
MMA	9.97	99.5	6158
DMA	5.53	103	6353

[a]Organic phase, 9.96×10^{-6} M TPA; aqueous phase, 0.2 M pyrogallol in 1.6 M sulfuric acid; As(V) taken, 29.10 μg/5 ml. [b][Diverse arsenic species]/[As(V)].

species, i.e., arsenic(III), monomethylarsonic acid (MMA), and dimethylarsinic acid (DMA). The radioactivities of the substoichiometric extracts obtained in the presence or absence of these species are compared as shown in Table 1. As could be expected from large difference in extraction behavior of these different arsenic species [13], no significant interference was observed in the presence of large amounts of arsenic(III), MMA, and DMA. The present substoichiometric extraction system is thus highly selective for arsenic(V) species. In addition, these results demonstrate that no isotopic exchange takes place between radioactive arsenic(V) and inactive arsenic(III), MMA, or DMA. Many common diverse ions do not give any interference, as is summarized in Table 2.

However, an interference from iodine which is contained in seaweeds at fairly high levels was observed; the relative amount of arsenic(V) extracted with a substoichiometric amount of TPA decreased to 92% in the presence of a large amount (about 36-fold over arsenic(V)) of sodium iodide. The preseparation of arsenic(V) by liquid-liquid extraction from an acidic iodide solution was introduced [13], but to avoid transfer of iodide into the final sample solution, a careful back-extraction of arsenic(V) was made as mentioned in the Experimental section.

Determination of arsenic(V) in an acid digest of seaweed

The seaweed sample, composed of soft tissues, appeared to be easily decomposed by an ordinary acid digestion with concentrated nitric acid in a teflon decomposition vessel. Arsenic(V) in this acid digest was determined by the substoichiometric method, but the value found was only 5.89 μg g^{-1} (No. 1, Table 3), which must be compared with the total arsenic content of 68.0 μg g^{-1}. The effect of additional digestion with concentrated sulfuric acid after the nitric acid digestion was then examined. It is clear from Table 3 that the value found for arsenic increases with increased heating temperature and time of the sulfuric acid treatment. Because the proposed substoichiometric extraction shows high selectivity for inorganic arsenic(V), these results mean that

TABLE 2

Effect of diverse ions in the substoichiometric extraction of arsenic(V)[a]

Diverse ions	Activity of organic phase (cpm)	Diverse ions	Activity of organic phase (cpm)	Diverse ions	Activity of organic phase (cpm)
None	19978	Cd^{2+}	20526	SeO_4^{2-}	20396
Fe^{3+}	20355	Mn^{2+}	20453	WO_4^{2-}	19365
Cr^{3+}	20398	Hg^{2+}	19958	VO_4^{3-}	18843
Sb^{3+}	19571	PO_4^{3-}	20550	GeO_3^{2-}	19452
Zn^{2+}	19261	MoO_4^{2-}	19774	SiO_3^{2-}	19972
Cu^{2+}	19851	SeO_3^{2-}	19679		

[a]Organic phase, 2.0×10^{-6} M TPA; aqueous phase, 0.2 M pyrogallol in 3 M sulfuric acid; 0.1 mg of ion was added to 5 ml of aqueous phase containing 7 μg of As(V).

TABLE 3

Decomposition conditions for arsenic determinations in a seaweed[a]

No.	Conditions of further conc. H_2SO_4 treatment	As(V) found ($\mu g\ g^{-1}$)	Ratio of As(V) to total As (%)
1	—[b]	5.89 ± 0.34	8.66
2	170°C, 2 h	10.5 ± 0.05	15.4
3	170°C, 20 h	65.1 ± 1.1	95.7
4	240°C, 2 h	69.9 ± 1.9	102.8

[a]*Laminaria religiosa* Miyabe, arsenic content 68.0 ± 2.1 $\mu g\ g^{-1}$ (cf. Table 4). [b]Acid digestion with nitric acid.

TABLE 4

Substoichiometric determination of total arsenic in the same seaweed

Sample weight (W_x) (g)	Activity from spike solution[a] (a_s) (cpm)	Activity from sample solution (a_x) (cpm)	Concentration of As (C_x)[b] ($\mu g\ g^{-1}$)
0.5232	4951	2159	71.9
		2207[c]	69.2
		2261	66.2
0.5227	3841	1762	65.7
		1737	67.5
		1736	67.5
	Mean value ± standard deviation		68.0 ± 2.1

[a]As(V) in spike (M_s): 29.10 μg. [b]Calculated from $C_x = M_s\,(a_s/a_x - 1)/W_x$. [c]Successive substoichiometric extraction (see text).

most of the arsenic species occur as very stable organic forms in seaweed and are gradually converted to inorganic arsenic(V) with the sulfuric acid treatment at higher temperature.

Table 4 shows the total arsenic content in the seaweed sample solution, which was obtained by the proposed procedure involving the sulfuric acid treatment at high temperature. In the substoichiometry, only a substoichiometric amount of arsenic(V) is extracted in the first substoichiometric extraction, hence the same substoichiometric extraction can be made successively for the remaining sample solution. As shown in Table 4, the results obtained by the first and the second substoichiometric extractions are consistent. The overall mean value, 68.0 ± 2.1 $\mu g\ g^{-1}$, is in good agreement with that obtained by non-destructive photon activation analysis in this laboratory, 67.1 ± 1.7 $\mu g\ g^{-1}$ [14].

REFERENCES

1 M. O. Andreae, Anal. Chem., 49 (1977) 820.
2 Y. Odanaka, N. Tsuchiya, O. Matano and S. Goto, Anal. Chem., 55 (1985) 929.
3 B. Beckermann, Anal. Chim. Acta, 135 (1982) 77.
4 S. Fukui, T. Hirayama, M. Nohara and Y. Sakagami, Talanta, 30 (1983) 89.
5 F. T. Henry and T. M. Thorpe, Anal. Chem., 52 (1980) 80.
6 G. R. Ricci, L. S. Shepard, G. Colovos and N. E. Hester, Anal. Chem., 53 (1981) 610.
7 W. A. Maher, Anal. Chim. Acta, 126 (1981) 157.
8 A. Zeman, J. Růžička, J. Stary and E. Kleckova, Talanta, 11 (1964) 1143.
9 A. Zeman, J. Stary and K. Kratzer, Radiochem. Radioanal. Lett., 4 (1970) 1.
10 T. Braun, L. Ladanyi, M. Marothy and I. Osgyani, J. Radioanal. Chem., 2 (1969) 263.
11 Y. Kanda and N. Suzuki, Radiochem. Radioanal. Lett., 39 (1979) 221.
12 Y. Kanda and N. Suzuki, J. Radioanal. Chem., 54 (1979) 7.
13 N. Suzuki, K. Satoh, H. Shoji and H. Imura, Anal. Chim. Acta, 185 (1986) 239.
14 Y. Iwata, M. Sc. Thesis, Tohoku University, 1985.

Analytica Chimica Acta, 193 (1987) 247—254
Elsevier Science Publishers B.V., Amsterdam — Printed in The Netherlands

EXTRACTION OF SELECTED TERVALENT LANTHANIDES WITH *N*-PHENYLACYLHYDROXAMIC ACIDS

TED CECCONIE, MASSOUD HOJJATIE and HENRY FREISER*

Strategic Metals Recovery Research Facility, Department of Chemistry, University of Arizona, Tucson, AZ 85721 (U.S.A.)

(Received 4th September 1986)

SUMMARY

The extraction behavior of certain tervalent lanthanides into chloroform solutions containing various *N*-phenylacylhydroxamic acids is reported. The ligands include *N*-*o*-methylphenyl-*m*-trifluoromethylbenzohydroxamic acid (MPFBHA), *N*-*m*-trifluoromethylphenyl-*o*-methylbenzohydroxamic acid (FPMBHA), *N*-*o*-methylphenylbenzohydroxamic acid (MPBHA), *N*-phenyl-*o*-methylbenzohydroxamic acid (PMBHA), *N*-*o*-methylphenyl-*p*-tert-butylbenzohydroxamic acid (MPBBHA), and *N*-phenyl-*p*-tert-butylbenzohydroxamic acid (PBBHA). Of the *N*-phenylacylhydroxamic acids mentioned, only PBBHA was found suitable to extract the lanthanides under the experimental conditions used. The selected lanthanides, namely La, Pr, Eu, Ho, and Yb, were all found to extract with PBBHA as self-adducts of the form $LnL_3 \cdot 2\,HL$, where L and HL denote the ligand anion and neutral ligand, respectively. The extraction constants and separation factors for the lanthanides with PBBHA were evaluated. It is possible that steric hindrance prevents the lanthanides from extracting with MPFBHA, FPMBHA, MPBHA, PMBHA, or MPBBHA.

This work is part of a systematic study of separation of individual lanthanide ions by using carefully chosen ligand families, including 8-quinolinol and its derivatives [1—6], acylpyrazolones [7—9], *N*-phenylacylhydroxamic acids [10], and acidic phosphorus extractants [11, 12], both alone or in combination with neutral adductants or ion-pairing reagents, and focuses on the behavior of *N*-phenylacylhydroxamic acids.

Arylhydroxamic acids have been used as extractants [13], as precipitating reagents for niobium and tantalum [14], and reagents for the spectrophotometric determination of several metal ions [15]. As regards the extraction of the lanthanides, both *N*-phenylbenzohydroxamic acid (PBHA) [16—19] and *N*-phenyl-*m*-trifluoromethylbenzohydroxamic acid (PFBHA) [10] have been studied. Results obtained with these ligands have shown that the lanthanides will extract as self-adducts. The number of adducting molecules changes, however, from the unsubstituted hydroxamic acid PBHA to the substituted hydroxamic acid PFBHA. In the case of PBHA, the extracted chelates were found to have stoichiometries of $LnL \cdot HL$ whereas with PFBHA, the chelates were described by $LnL_3 \cdot 2\,HL$. With the addition of 1,10-phenanthroline (phen) to these systems, the lanthanides were found to extract as mixed

0003-2670/87/$03.50

chelates with both extractants. The formulas of these mixed chelates were $LnL_3 \cdot$ phen for all metals with PBHA and for Pr and Eu with PFBHA, and $LnL_3 \cdot 2$ phen for Eu and Yb with PFBHA. The overall selectivity of lanthanide extraction was found to be greater for the substituted hydroxamic acid PFBHA over that of the unsubstituted PBHA.

In the present study, the role of alkyl substituents was further investigated to establish if other substitutions would also affect the extractibility and selectivity of the *N*-phenylacylhydroxamic acids toward the lanthanides.

EXPERIMENTAL

Apparatus and reagents

An Eberbach box-type shaker was used to equilibrate the solutions. An Orion Research model 701-A digital Ionalyzer was used for equilibrium pH measurement. A Cary 219 spectrophotometer was used in determining the K_{DR} of PBBHA. A Gilford model 240L spectrophotometer was used in determining the pK_a of PBBHA. A Perkin-Elmer 6500 ICP spectrometer was used for the determination of the metal concentrations after extraction.

The *N*-*o*-methylphenyl-*m*-trifluoromethyl- (MPFBHA), *N*-*m*-trifluoromethylphenyl-*o*-methyl (FPMBHA), *N*-*o*-methylphenyl- (MPBHA), *N*-phenyl-*o*-methyl- (PMBHA), *N*-*o*-methylphenyl-*p*-tert-butyl- (MPBBHA), and *N*-phenyl-*p*-tert-butyl- (PBBHA) derivatives of benzohydroxamic acid were synthesized by the reaction of an appropriate β-phenylhydroxylamine with an appropriate acyl chloride in the presence of sodium bicarbonate [20]. The β-phenylhydroxylamines were prepared by the reduction of an appropriate nitrobenzene with zinc dust [21]. These general procedures were modified to give significantly higher yields than those reported previously [22]. The hydroxamic acids were recrystallized from ethanol until the compounds gave constant melting ranges. The hydroxamic acids were protected from light and dissolved in chloroform just prior to their use.

Stock solutions which contained 100 mg l^{-1} La, Pr, Eu, Ho or Yb were prepared from their chloride salts (Alfa Inorganics; 99.9%). Buffer solutions containing 0.425 M sodium tartrate/0.120 M tris(hydroxyamino)methane (Tris) were prepared to cover the pH range 6.8—9.2. Chloroform (analytical-reagent grade) was washed three times with deionized water just prior to its use.

All other reagents were analytical grade and used without further purification.

Procedures

Determination of the distribution constant for PBBHA. The distribution constant, K_{DR}, for PBBHA distributed between water and chloroform was evaluated by equilibrating aqueous phases (pH values between 3 and 7; ionic strength = 0.1 (KCl); 23 ± 1°C) with an equal volume of a 1.00×10^{-2} M PBBHA solution in chloroform for 1 h. The amount of PBBHA which distributed into the aqueous phase was measured from its absorbance at 300 nm.

Determination of the pK_a of PBBHA. The acidity constant of PBBHA was determined spectrophotometrically because its solubility in water is too low for potentiometric determination. In this experiment, the absorbance of aqueous solutions of PBBHA (ionic strength = 0.1 (KCl); 23 ± 1°C) having pH values ranging from 2.0 to 11.0 was monitored at 300 nm. The absorbance increased at this wavelength with increasing pH, indicating the formation of the ligand anion; this was used to evaluate the pK_a.

Extraction equilibrium. A 25.0-ml volume of a lanthanide ion solution (10.0 mg l^{-1} initial concentration for La, Pr, Eu, Ho, or Yb), buffered with sodium tartrate/Tris (0.0425 M and 0.0120 M, respectively), was equilibrated with a 25.0-ml volume of a chloroform solution containing the *N*-phenylacylhydroxamic acid in a 125-ml glass bottle covered with aluminum foil and fitted with a plastic cap equipped with a polyethylene liner. Equilibration was achieved by shaking the mixture in a box-type shaker for a time found adequate for equilibrium to be reached. It was found necessary to cover the bottles with foil because the *N*-phenylacylhydroxamic acids were photosensitive; a chloroform solution of the material would darken if exposed to light for more than 3—4 h. The equilibrium pH of the aqueous phase was measured after phase separation. The concentration of lanthanide both extracted and unextracted was determined by inductively-coupled plasma/atomic emission spectrometry (ICP/AES), with the instrument conditions shown in Table 1. The concentration of metal extracted into the organic phase was determined by back-extraction into 10^{-2} M hydrochloric acid and quantifying the lanthanide concentration in the resulting aqueous solution. The concentration of unextracted metal was determined in the aqueous phase by ICP/AES; manganese was used as internal standard to correct for aerosol transport differences which were found to exist between the sample and standard solutions. The concentration values which were obtained were used to find the distribution ratio, D, defined as $D = C_{Ln(o)}/C_{Ln(aq)}$.

RESULTS AND DISCUSSION

Extraction of the lanthanides with PBBHA

It was found that only PBBHA was effective for the extraction of the lanthanides. The other alkylated arylhydroxamic acids did not extract any of

TABLE 1

Instrumental conditions for ICP/AES

PMT voltage 360—500 V	Viewing height 15 mm
Plasma power 1250 W	Integration time 0.2 s
Reflected power < 5 W	Plasma Ar flow rate 15 l min^{-1}
Slit 0.02 nm	Nebulizer Ar flow rate 0.7 l min^{-1}

Auxiliary Ar flow rate 0.3 l min^{-1} for back-extraction, 0.5 l min^{-1} for direct aqueous phases
Wavelengths (nm) La 379.478, Pr 390.844, Eu 381.967, Ho 345.600, Yb 328.937, Mn 257.610

the lanthanide ions tested. The values of log K_{DR} and pK_a for PBBHA obtained from the spectrophotometric experiments are indicated in Table 2 along with the values for PBHA [19] and PFBHA [10] found previously. The addition of the *p*-tert-butyl group to the acyl ring increases both the log K_{DR} and pK_a of the hydroxamic acid, as would be expected based on the hydrophobic and electron-releasing natures of the tert-butyl group. The pK_a value of 8.44 is in good agreement with that which would be expected from the Hammett equation with σ(*p*-tert-butyl) = −0.20, but the log K_{DR} is not as high as the hydrophobic factor for the tert-butyl would predict (π = 1.98) [23]. A smaller log K_{DR} value for PFBHA than expected from its hydrophobic factor [$\pi(CF_3)$ = 0.88] has also been observed [10].

The stoichiometries and the extraction constants for the PBBHA system were obtained from the relationships of log D vs. pH, log D − 3 pH vs. log [PBBHA], and log D − 3 pH − 5 log [PBBHA] vs. log [Ln] where [Ln] is lanthanide concentration. Plots of these relationships are shown in Figs. 1—3. From these figures, slopes of 3 with respect to pH, 5 with respect to PBBHA concentration, and zero with respect to Ln concentration were observed within experimental error. Least-squares results for these plots are presented in Table 3.

These results indicate that the following extraction equilibrium holds:

$$LnT_{2(aq)}^{-} + 5\ HL_{(o)} \rightleftharpoons LnL_3 \cdot 2\ HL_{(o)} + 3\ H_{(aq)}^{+} + 2\ T_{(aq)}^{2-} \quad (1)$$

where T^{2-} is the tartrate dianion, LnT_2^- is the tartrate complex of the lanthanides which exists in solution [1], and the subscripts (o) and (aq) refer to the organic and aqueous phases, respectively. The distribution ratio, D, for this situation would be described by the following equation:

$$D = \beta_3 K_{DC} K_a^3 \beta_{2HL} [HL]_o^5 / K_{DR}^3 \beta_2 C_T^2 [H]^3 = K'_{ex} \beta_{2HL} [HL]_o^5 / [H^+]^3 \quad (2)$$

$$\text{or: } \log D = \log K'_{ex} \beta_{2HL} + 3\ pH + 5 \log [HL]_o \quad (3)$$

where K_a is the acidity constant of PBBHA, $10^{-8.44}$, K_{DR} is the distribution constant, $10^{3.45}$, β_3 is the overall formation constant of LnL_3, K_{DC} is the distribution constant for the metal complex, and β_{2HL} is the overall adduct formation constant for the reaction

$$LnL_{3(o)} + 2\ HL_{(o)} \rightleftharpoons LnL_3 \cdot 2\ HL_{(o)} \quad (4)$$

TABLE 2

Physical properties of *N*-phenylacylhydroxamic acids

Compound	Melting point (° C)	pK_a[a]	log K_{DR}[b]
PBHA	121—122	8.15 ± 0.01	2.33 ± 0.01
PFBHA	80—81	7.96 ± 0.02	2.93 ± 0.02
PBBHA	136—137	8.44 ± 0.04	3.45 ± 0.02

[a] Acidity constant in water. [b] Distribution constant between chloroform and water.

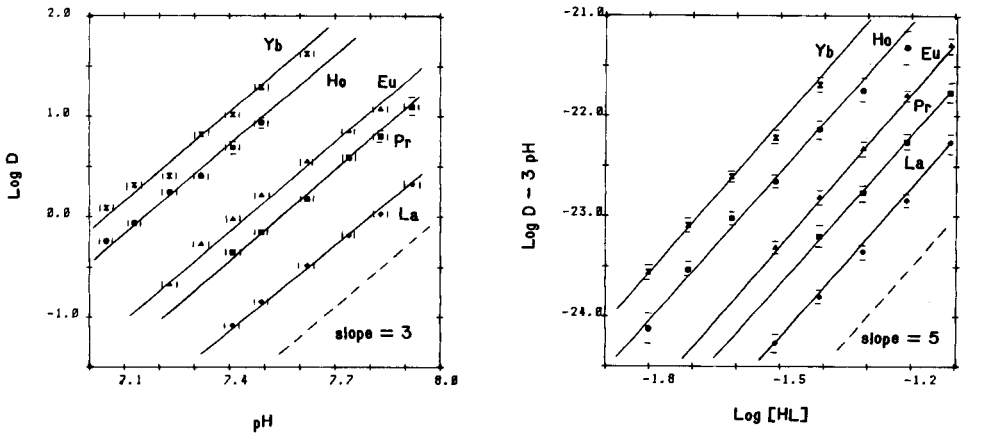

Fig. 1. Dependence of the metal distribution on pH. [PBBHA] = 0.0500 M in chloroform; $[Ln]_{initial} = 10.0\ mg\ l^{-1}$.

Fig. 2. Dependence of the metal distribution on the PBBHA concentration. $[Ln]_{initial} = 10.0\ mg\ l^{-1}$; pH = 7.70 ± 0.03.

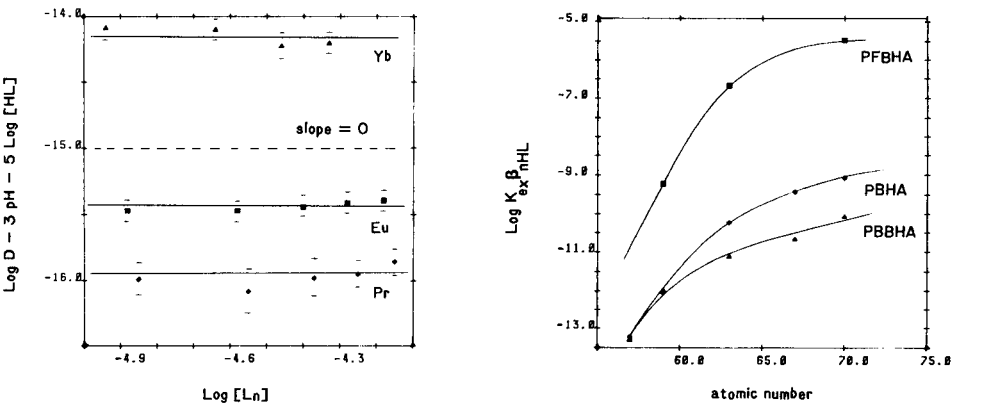

Fig. 3. Dependence of the metal distribution on the metal concentration. [PBBHA] = 0.0500 M in chloroform; pH = 7.49 ± 0.07.

Fig. 4. Selectivity trends of the *N*-phenylacylhydroxamic acids for the extraction of the lanthanides.

The conditional extraction constant, K'_{ex}, is related to the extraction constant, K_{ex}, in the following manner:

$$K_{ex} = K'_{ex}\beta_2 C_T^2 = \beta_3 K_{DC} K_a^3 / K_{DR}^3 \qquad (5)$$

where β_2 is the overall formation constant for the reaction of Ln^{3+} with T^{2-} to form LnT_2^-, and C_T is the total tartrate dianion concentration. The values

TABLE 3

Extraction results with PBBHA

Plot	Metal	Slope	Corr. coeff.	No. of points
log D vs. pH	La	2.70 ± 0.06	0.9991	6
	Pr	2.87 ± 0.07	0.9994	6
	Eu	2.81 ± 0.12	0.996	7
	Ho	2.65 ± 0.09	0.999	6
	Yb	2.75 ± 0.14	0.993	7
log D − 3 pH vs. log [HL]	La	4.94 ± 0.14	0.999	5
	Pr	4.82 ± 0.10	0.9997	4
	Eu	5.06 ± 0.05	0.9999	5
	Ho	4.65 ± 0.15	0.997	7
	Yb	4.70 ± 0.13	0.999	5
log D − 3 pH − 5 log [HL] vs. log [Ln]	Pr	0.08 ± 0.12	0.63	5
	Eu	0.12 ± 0.03	0.94	5
	Yb	−0.22 ± 0.09	0.86	4

of log $K_{ex}\beta_{nHL}$ for PBBHA are given in Table 4 along with the values obtained for PBHA and PFBHA [10]. Also given are the separation factors, defined as the difference in log $K_{ex}\beta_{nHL}$, for the Pr/Eu, Eu/Yb, and Pr/Yb couples.

The stoichiometry of the extracted chelates with PBBHA is the same as that obtained with PFBHA but different from that obtained using PBHA. This may be attributed to the increased residual Lewis acidity of the Ln-PFBHA and Ln-PBBHA complexes over that of the Ln-PBHA complexes and/or the stronger adducting ability of the less acidic PBBHA molecule.

The extraction constants for PBBHA are smaller than those obtained for PBHA or PFBHA [10]. This signifies that higher solution pH would be required for the extraction of the lanthanides with PBBHA over that required for PFBHA or PBHA given that the same ligand concentrations were used.

A more interesting comparison which can be made from the results in Table 4 is of the separation factors. The results show that all of the hydroxamic acids have similar selectivity for the Eu/Yb pair, with separation factors of about 1.2. However, the selectivity behaviors of the compounds are dramatically different for the lighter lanthanides as represented by the Pr/Eu pair. It is observed that PFBHA possesses the highest selectivity (SF = 2.54), with PBHA showing the next highest (SF = 1.22), and PBBHA showing the lowest selectivity (SF = 0.88). This trend in selectivity parallels the trend of pK_a values. A similar trend of increased selectivity for lanthanide extraction with decreasing pK_a was observed for 8-quinolinol [1] and 5,7-dibromo-8-quinolinol [3].

A plot of log $K_{ex}\beta_{nHL}$ vs. atomic number (Fig. 4) reveals the selectivity trends shown by the hydroxamic acids.

TABLE 4

Extraction constants and separation factors

Compound	log $K_{ex}\beta_{nHL}$[a]					Separation factor		
	La	Pr	Eu	Ho	Yb	Pr/Eu	Eu/Yb	Pr/Yb
PBHA	−13.21	−12.05	−10.23	−9.42	−9.07	1.82	1.16	2.98
PFBHA	—	−9.22	−6.68	—	−5.46	2.54	1.22	3.76
PBBHA	−13.30 (±0.08)	−12.00 (±0.05)	−11.12 (±0.06)	−10.68 (±0.11)	−10.07 (±0.08)	0.88	1.05	1.93

[a] $n = 1$ for PBHA; $n = 2$ for PFBHA and PBBHA.

Extraction results with MPFBHA, FPMBHA, MPBHA, PMBHA, and MPBBHA

The feasibility of extraction with these compounds was tested by equilibrating 1.00×10^{-1} M chloroform solutions of the compounds with aqueous phases containing the lanthanides, 0.100 M sodium perchlorate, and buffer (pH 9.21 ± 0.01; 0.0425 M sodium tartrate/0.0120 M Tris) for 16 h. The ICP/AES results indicated that no detectable amount of any of the lanthanides was extracted ($\log D < -2$). Although these compounds were found unsuitable for lanthanide extraction, they were capable of extracting nickel(II) and copper(II) ions from mildly acidic solutions (pH ≈ 3); MPBHA can also extract zinc ions under these conditions.

The most likely cause of the inability of these compounds to extract the lanthanides is steric hindrance because all of the compounds in question contain an *o*-methyl substituent on either the phenyl or acyl ring.

Conclusions

The *p*-tert-butyl-substituted hydroxamic acid, PBBHA, was found useful for the extraction of the lanthanides. When compared to other *N*-phenylacylhydroxamic acids which have been studied, PBBHA was found to have comparable selectivity for the extraction of the Eu/Yb pair but less selectivity for the extraction of the Pr/Eu pair.

o-Methyl-substituted hydroxamic acids such as MPFBHA, FPMBHA, MPBHA, PMBHA, and MPBBHA were found to be unsuitable for the extraction of the lanthanides. The most likely cause for this is the decrease in the overall formation constant of the metal chelate owing to the steric hindrance of the *o*-methyl substituent.

This research was supported by a grant from the United States Department of Energy.

REFERENCES

1 T. Hori, M. Kawashima and H. Freiser, Sep. Sci., 15 (1980) 861.
2 M. Kawashima and H. Freiser, Anal. Chem., 53 (1981) 284.
3 O. Tochiyama and H. Freiser, Anal. Chem., 53 (1981) 874.
4 E. Yamada and H. Freiser, Anal. Chem., 53 (1981) 2115.
5 S. Taguchi and H. Freiser, Solv. Ext. Ion Exch., 4 (1986) 275.
6 S. Taguchi and H. Freiser, Solv. Ext. Ion Exch., 4 (1986) 1139.
7 O. Tochiyama and H. Freiser, Anal. Chim. Acta, 131 (1981) 233.
8 Y. Sasaki and H. Freiser, Inorg. Chem., 22 (1983) 2289.
9 C. Huang and H. Freiser, Solv. Ext. Ion Exch., 4 (1986) 41.
10 S. Inoue, F. Ordonez and H. Freiser, Solv. Ext. Ion Exch., 3 (1985) 839.
11 S. Motomizu and H. Freiser, Solv. Ext. Ion Exch., 3 (1985) 637.
12 K. Li and H. Freiser, Solv. Ext. Ion Exch., 4 (1986) 739.
13 J. Stary and H. Freiser, IUPAC Equilibrium Constants of Liquid-Liquid Distribution Reactions, Part IV, Chelating Extractants, Pergamon, Oxford, 1978.
14 S. Agrawal, B. Chandravanshi and V. Gupta, Croat. Chem. Acta, 51 (1978) 279.
15 A. K. Majumdar, *N*-Benzoylphenylhydroxylamine and its Analogues, Pergamon, Oxford, 1972.
16 D. Dyrssen, Acta Chem. Scand., 10 (1956) 353.
17 T. Sekine and D. Dyrssen, Talanta, 11 (1964) 867.
18 A. Reidel, J. Radioanal. Chem., 6 (1970) 75.
19 N. Poluektov, R. Lauer and V. Mishchenko, Zh. Analit. Khim., 24 (1969) 1665.
20 S. Sandler and W. Karo, Organic Functional Group Preparations, Vol. III, Academic Press, New York, 1972, p. 427.
21 O. Kamm, Org. Synth., 4 (1925) 57.
22 M. Hojjatie, T. Cecconie and H. Freiser, Anal. Chim. Acta, in press.
23 C. Hansch and A. Leo, Substituent Constants for Correlation Analysis in Chemistry and Biology, Wiley, New York, 1979.

Analytica Chimica Acta, 193 (1987) 255—268
Elsevier Science Publishers B.V., Amsterdam — Printed in The Netherlands

STEPWISE DELETION: A TECHNIQUE FOR MISSING-DATA HANDLING IN MULTIVARIATE ANALYSIS

JAN B. HEMEL*

Central Laboratory for Clinical Chemistry, University Hospital Groningen, P.O. Box 30001, NL-9700 RB Groningen (The Netherlands)

HILKO VAN DER VOET

Research Group Chemometrics, Pharmaceutical Laboratories, State University of Groningen, A. Deusinglaan 2, NL-9713 AW Groningen (The Netherlands)

FRANS R. HINDRIKS and WILLEM VAN DER SLIK

Central Laboratory for Clinical Chemistry, University Hospital Groningen, P.O. Box 30001, NL-9700 RB Groningen (The Netherlands)

(Received 8th July 1986)

SUMMARY

Multivariate data sets often contain gaps in the data matrix. Especially with medical data, missing values are not always avoidable. Most techniques of data analysis do not allow for data gaps; a brief overview is given of the methods currently used to cope with this problem. There are two major groups of missing-data handling techniques: preprocessing techniques used before the data analysis, and techniques integrated into the data analysis. Preprocessing techniques can involve deletion of incomplete objects or variables, which loses existing values, or replacement of missing data by estimates, which introduces pseudo-information and bias. Integrated methods are not usually satisfactory. To avoid most of these disadvantages, a new preprocessing technique is proposed for deleting missing data. The algorithm comprises a stepwise deletion of both variables and objects, which retains as much of the data as possible. It is demonstrated on several artificially constructed problem data sets and on some real clinical data collections. It is shown to retain considerably more of the original data sets than other deleting procedures.

Multivariate data collections, especially medical ones, often suffer from a large proportion of missing data. Data gaps can originate from various causes, including *differences in aim* between the originator and user of the data, *impossible cases*, and *accident*. If multivariate analysis is a secondary goal of data collection, as is usually the case in (retrospective) medical research, differences in objective between the primary data user (e.g., the physician) and the researcher may cause missing data to occur. Measurements may have been omitted deliberately by the primary user, because other measurements had already provided the desired information. Although desirable from the point of view of efficiency, the trend to make only "useful" measurements leaves the researcher with a data set having a composition highly dependent on the kind of object. In medical data sets, for example, kidney-function

0003-2670/87/$03.50

test results will often not be known if a liver disease is tentatively diagnosed. As this is a common property for the class of liver patients, much classifying information lies in the selection of tests. This selection was made by an expert who knew or made educated guesses about the class of the patient. If classification of patients is to be done without this medical know-how, the information that is represented by the variable selection of an expert should not be used. This arises when test patients are to be classified without variable selecting medical expertise. In these cases, such data are difficult to use for statistical modelling of the classes.

Another cause of data gaps is that measurements may have been impossible to make because of a special condition of the object. Some measurement techniques impose certain requirements on the sample, e.g., a maximum serum opacity or viscosity tolerable for the instruments used. If the object exceeds these boundaries, and a good alternative assay is not available, the result will be missing. A different kind of impossibility as a cause of a data gap occurs if some objects fundamentally do not possess the property to be measured, e.g., the length of the menstrual cycle for a man. As when difference in aim is the cause of missing values, here too there will be a strong dependence of the composition of the data set on the class of the object. A third cause is that measurements may have failed incidentally. If data gaps are caused by accidental failure, this does not imply that missing values are randomly distributed all over the data set. Some measurements may be more prone to failure than others; some may be repeatable, others not. In these cases, the data-set contents will depend (slightly) on the class of the object.

As most standard multivariate analysis techniques require completeness of the data, these gaps must be removed. So far, no single best solution has been found for missing-data handling in multivariate analysis. Many methods have been devised, all with their specific advantages and disadvantages. They can be divided into two major groups. The first group consists of preprocessing techniques which modify the data before the real multivariate analysis. This group can be subdivided into two classes of procedures. In the first such class, missing values are removed by deletion; these procedures result in a reduction of the data set. In removing missing values, information in present values is unavoidably destroyed also. The deletion of all objects presenting missing values is one way to delete missing values; this is the default way of missing data handling used in many procedures of SPSS (listwise deletion) [4]. In data sets with many variables there is a relatively large probability for an object to have at least one missing value, thus especially small classes can be deleted completely. The second class of preprocessing is deletion of all variables presenting missing values. In data sets with many objects, there is a substantial chance for every variable to be missing at least once. In many cases, this technique leads to complete destruction of the data set.

A second subgroup of handling techniques for missing data consists of those in which missing data are removed by substitution. Such procedures invariably introduce pseudo-information into the data. Differences between

classes may become illusively masked or marked, depending on the distributional pattern of the missing values. A biased sample from the object population is then obtained. Some examples of frequently used procedures are: (a) substituting the mean of the variable; (b) substituting the mean of the variable in the class of the object; (c) estimation of data gaps by regression of the variable presenting the missing value on the other variables; (d) estimation by iteratively fitting a principal component model, e.g., the INPCFI routine in ARTHUR [2]; (e) estimation by solving a set of linear equations according to the procedure by Yates [3] as referenced and extended by Haseman and Gaylor [1]; (f) substitution by a randomly selected value from the variable in the class of the object; (g) substitution by a random value from a fitted multivariate normal distribution (here, the gaussian distributional assumption is crucial). Procedure (b) is inapplicable to data from an unknown class such as test samples or routinely processed samples in future. Therefore, procedure (a) is normally used in test sets. As for procedure (b) it is not possible to evaluate procedure (f) with future data from an unknown class; in test sets the substitution value must be selected randomly from the entire data set.

The other major group of handling techniques for missing data consists of selecting methods which are tolerant to missing data. Some techniques for this purpose need model assumptions, and thus may introduce bias; in others bias is removed at the cost of increased variance. In these cases, missing-data handling is part of the analysis itself. Mostly, the holes in the data matrix are just skipped in the process. The use of this way of missing-data handling is of course restricted to the methods that use the resulting intermediate matrices. There are four main procedures. In the first, a covariance matrix is calculated by using for every term all objects that present both variables involved (pairwise deletion). This procedure is offered by statistical computer packages like SPSS [4]. Haitovsky [5] showed in simulation studies that this method can perform very poorly. In the second, a covariance matrix is fitted by postulating a multivariate normal model. Different techniques have been reviewed and discussed by Beale and Little [6]. In the third, a principal component model is fitted by iteratively estimating eigenvectors [7]. The refined algorithm proposed [7] ends with principal component analysis on the data matrix that is completed by using the estimates from the principal component model. With this refinement this algorithm in fact is a preprocessing method. In the fourth procedure, the PLS algorithm by H. Wold [8], which is called NIPALS in the multivariate classification SIMCA method by S. Wold et al. [9], is used to skip data gaps.

In a very clear paper, Donner [10] discusses, for a simple regression problem, the procedures of deleting objects, substitution of the overall mean of the variable, estimation by regression, and pairwise deletion in the calculation of the covariance matrix. Bias and variance of the estimators of the regression coefficients are calculated and pairwise deletion for the calculation of a covariance matrix is found to yield estimators with large mean squared errors (MSE). Substitution of the mean of the variable turns out to be a

weak method if data are strongly correlated. Estimation of the missing values by regression is concluded to be effective if it is based on enough cases to provide stability. However, because not all data sets contain linear relations between the variables, it is not clear how far these results are relevant to environments other than simple regression.

Substitution of missing values, although often applied, can introduce too much pseudo-information to make the class models reliable or discriminating. For instance, if a class misses an observation completely, as is often the case in medical data sets, the substituted values are based entirely on objects of other classes, thus masking differences between the classes. If, however, the value of a variable is known only for a few objects in a class, these objects often determine the substitution values for all objects in their class, thus making uniformity in the class often illusively great compared to other classes. In these cases, the discriminatory power of the variable will also be exaggerated. If one does not want to make prior model assumptions, deletion of variables or objects that present "too many" missing values is usually chosen. The remaining data gaps are often filled by substitution techniques, thus reducing the adverse effects of both methods.

In the next section, a procedure is proposed for deletion of missing values by omitting both variables and objects; the procedure aims at preserving as many present values as possible. Both objects and variables are treated as equivalent. Its application is demonstrated with real data, as well as with some artificially constructed data sets that are known to present difficulties. Finally, the advantages and disadvantages of the proposed procedure are discussed.

The abbreviations used throughout this paper are summarized in Table 1.

STEPWISE DELETION OF MISSING DATA

The principles

In stepwise deletion, missing data are deleted by omitting in each step either an object or a variable, whichever leaves most of the present values, until the remaining data are complete. The solution of the problem of selecting variables to delete to remove missing data is very straightforward: as all variables are mutually independent in this respect, all variables that present data gaps are simply deleted. It is easy, too, to include a ranking in the selection: the variable that has most missing values is deleted first, followed by the next most incomplete, and so on.

In this way, for every variable a deletion efficiency score DE can be defined: $DE = MV/PV$ (for notation, see Table 1). This score can be regarded as the general efficiency of deleting one present value in the variable. The DE expresses the ease with which a variable can be omitted from the data set to leave it as little affected quantitatively as possible. In an analogous way, DE can be defined for deletion of objects. By stepwise deletion of the variable or object with the highest DE, followed by recalculation of all DEs, a ranked deletion of both objects and variables can be achieved.

TABLE 1

Nomenclature used

Abbreviation	Meaning
DE	Deletion efficiency
MV	Number of missing values in the item under consideration
PV	Number of present values in the item under consideration
IGS	Item group size. For variables, the *IGS* is p, the number of variables; for objects, the *IGS* equals the number of objects that are present in the class of the object
Item	Variable or object
n/p ratio	Minimum ratio of number of objects (in a class) to number of variables

In "narrow" data matrices, i.e., data sets with many objects and few variables or with few objects and many variables, equal *DE*s are commonly found, thus some additional rule is useful. Next to the *DE* score, the number of items available for deletion (variables, objects) is important. Deleting an object from a small class affects the data more than from a large one. One variable out of many can be missed more easily than an object from a small group. As a second criterion following the *DE* score, therefore, the item group size (*IGS*, the number of available objects or variables) is used in cases for which the *DE* score does not allow a choice to be made. No attempt is made to integrate *DE* and *IGS* into a new score. Although this would be possible, it would lead to a criterion that is more difficult to understand than the two separate criteria.

Another problem is the possibility of deleting objects or variables twice. An object may be deleted because of missing values while later all variables that had these missing values are deleted separately. In this case, the object should be restored, thus saving its present values for the data set. The same reasoning pertains to "doubly" deleted variables. In this way, the algorithm somewhat resembles the stepwise regression procedure in which at each step a variable may be selected because it adds information, or rejected because the combination of others makes it irrelevant.

The described version of the algorithm includes several refinements. It allows a minimum ratio of objects in a class to variables (n/p ratio) to be specified. As long as this ratio is not exceeded for all classes, only variables are deleted. This prevents small classes from being erased from the data set completely. Furthermore, as a stopping criterion for the deletion, a maximum missing fraction of an item is added. Such a stopping criterion is useful to ensure that the disadvantages of the usual missing-data handling methods (see above) have little impact, while a larger part of the present values is retained than stepwise deletion allows. The remaining gaps can be filled by any conventional procedure.

To assure the maximum n/p ratio, deletion of a variable is preferred if a choice cannot otherwise be made.

The algorithm

The algorithm for stepwise deletion is as follows.

(0) Specify the maximum fraction of an item that may remain missing (default: 0). This is the same as specifying a minimum *DE*. Specify the minimum *n/p* ratio for all items (default: 0).

(1) Delete all items that lack all values. Repeat this step until no item is completely missing.

(2) If the highest missing fraction of an item exceeds the specified maximum then proceed with step 3, else stop.

(3) If the lowest *n/p* ratio exceeds the specified minimum, then calculate the *DE* and the *IGS* for all items, else calculate the *DE* for all variables only.

(4) Find the item(s) with largest *DE*. Stop if the largest *DE* is zero, else proceed with step 5.

(5) If the same maximum *DE* is shared by several items, select the one(s) with highest *IGS*.

(6) If several items share the same *DE* and *IGS*, then select the first variable with that combination if present; if not, select the first object.

(7) Delete the selected item.

(8) If a variable was deleted last, look for already deleted objects for which missing values have been deleted twice, i.e., they have been removed by deletion of the object but also by omitting all variables involved. If such an object is found, restore it. If an object was deleted last, look for doubly deleted variables and restore them if present.

(9) If there are still data left, proceed with step 1.

APPLICATIONS

All calculations were done with the CLAS program [11]. This program was made especially for multivariate classification and the evaluation of performance in practical situations. In the following examples, default values were used for the *n/p* ratio and the stopping criterion, i.e., all missing values were deleted with no guaranteed minimal value of the *n/p* ratio.

Artificial data

To illustrate the technique, some simple data sets are shown in Figs. 1 and 2, together with the remainders after deletion of all incomplete objects, and after deleting all variables that have data gaps. The last column shows the remaining data set after stepwise deletion. The number below each column refers to the percentage of the values that were originally present in the set that survived the procedure (the recovery). It is seen that, in these examples, stepwise deletion retains at least as many values as the best of the other techniques (Fig. 1a—c). In data sets that are affected by randomly distributed gaps (Fig. 2a—b), stepwise deletion may retain a much larger fraction of the data. The sample data matrix in Fig. 2a has 20% missing values; in Fig. 2b, 10% of the data is lacking.

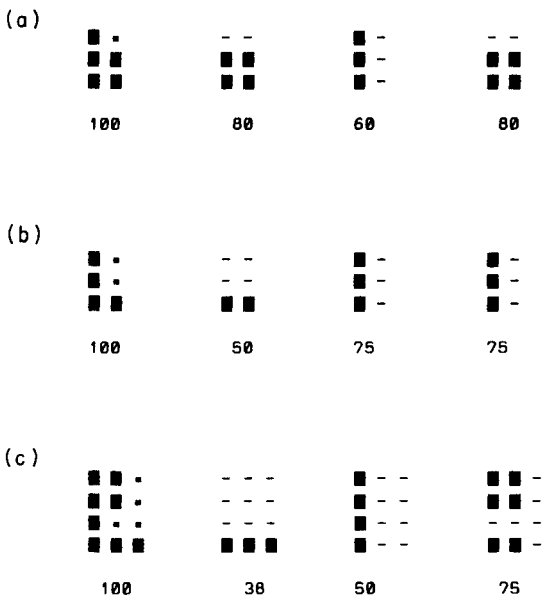

Fig. 1. (a) Stepwise deletion reaches the same result as deletion of objects; (b) stepwise deletion reaches the same result as deletion of variables; (c) stepwise deletion reaches better results than other procedures. (■) Present value; (▪) missing value; (—) deleted value. The numbers indicate the percentage of the present values in the original data set that is retained. The first column is the original data set; the second and third columns are the remainders after deletion of objects and variables, respectively, and the last column shows the data set after stepwise deletion.

Figure 3 shows an example of the restoration of a variable that was previously deleted. The steps in the procedure are shown separately. In the first step (Fig. 3a), variable 5 was found to have the highest *DE* and was deleted. Then all *DE*s were recalculated and four objects turned out to have the same *DE* (Fig. 3b). As the *IGS* was also equal for all of them, the first one was deleted arbitrarily. Because of this deletion, the variable *DE*s changed. Yet another object was selected (Fig. 3c). In this way all incomplete objects were selected for deletion (Fig. 3d, e). After this had been done, the fifth variable appeared to have been deleted uselessly (Fig. 3f). It was restored, yielding 20% extra values (Fig. 3g).

An example of a data set that consists of two classes is shown in Fig. 4. It is seen that arbitrary choices are sometimes made that can have a substantial influence on the final result. Three items (variable 2 and objects 1, 2 and 3) have the same $DE = 0.33$. Based on the difference in *IGS*, the variable and object 1 can be excluded from deletion in the first step. The choice between object 2 and object 3 for deletion is arbitrary but determines the subsequent series of deletions to get a complete set of data. In the end, the preference for object 2 for deletion leaves 72% of the originally present data untouched

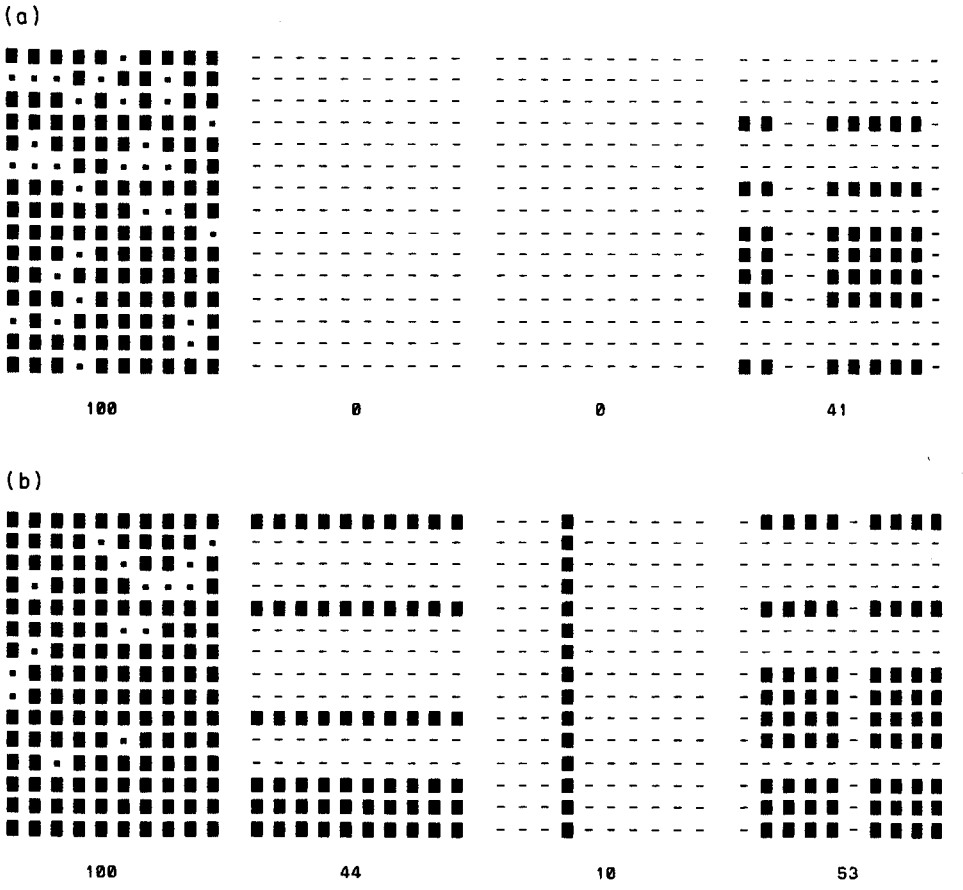

Fig. 2. Two data sets that are randomly disturbed by missing data: (a) 20% of data is missing; (b) 10% of data is missing. In these cases stepwise deletion retains many more present values than the other procedures. Symbols and explanation of numbers and columns as in Fig. 1.

and saves the small class, while the alternative way sacrifices the 1-object class (which is possible because no minimum n/p ratio was requested) and gives a 69% recovery. It is clearly seen that the optimal solution of the deletion problem is not guaranteed; this is characteristic of all stepwise methods.

Real-world data

Table 2 lists the results of a comparison between the three deleting techniques of missing-data handling on real data. These data sets are considered here as consisting of one class only.

The NEURO data set consists of amino acid concentrations measured in serum and spinal fluid of patients from different neurological diseases. It is a large data set with many (42) variables, as well as many (261) objects. All

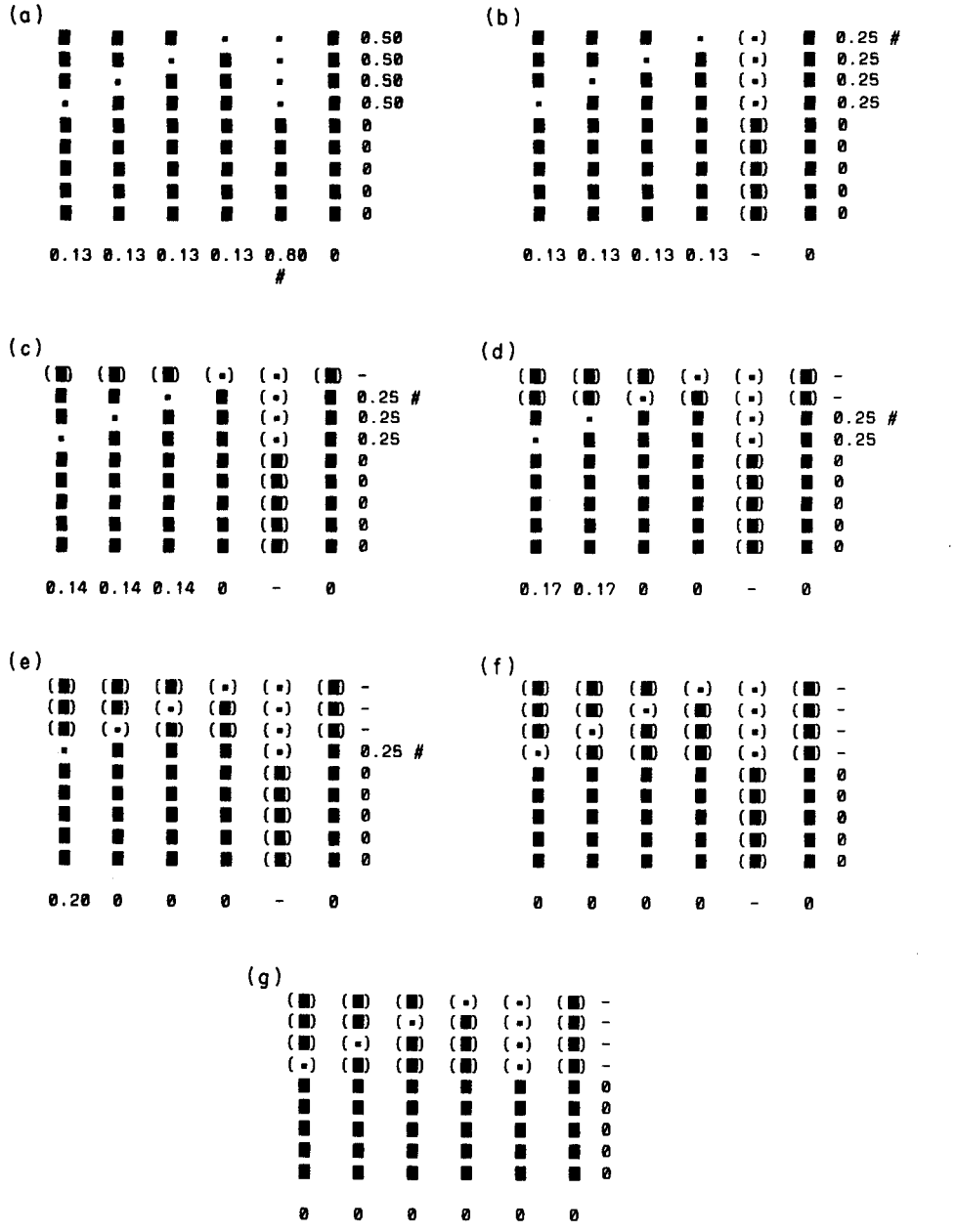

Fig. 3. Restoration of a variable in stepwise deletion; the procedure is shown after each step. The numbers refer to the *DE* scores. *IGS* numbers are not shown, as they are irrelevant in this case. The variable/object that is to be deleted is marked with a #. Deleted values are in parentheses. Symbols as in Fig. 1.

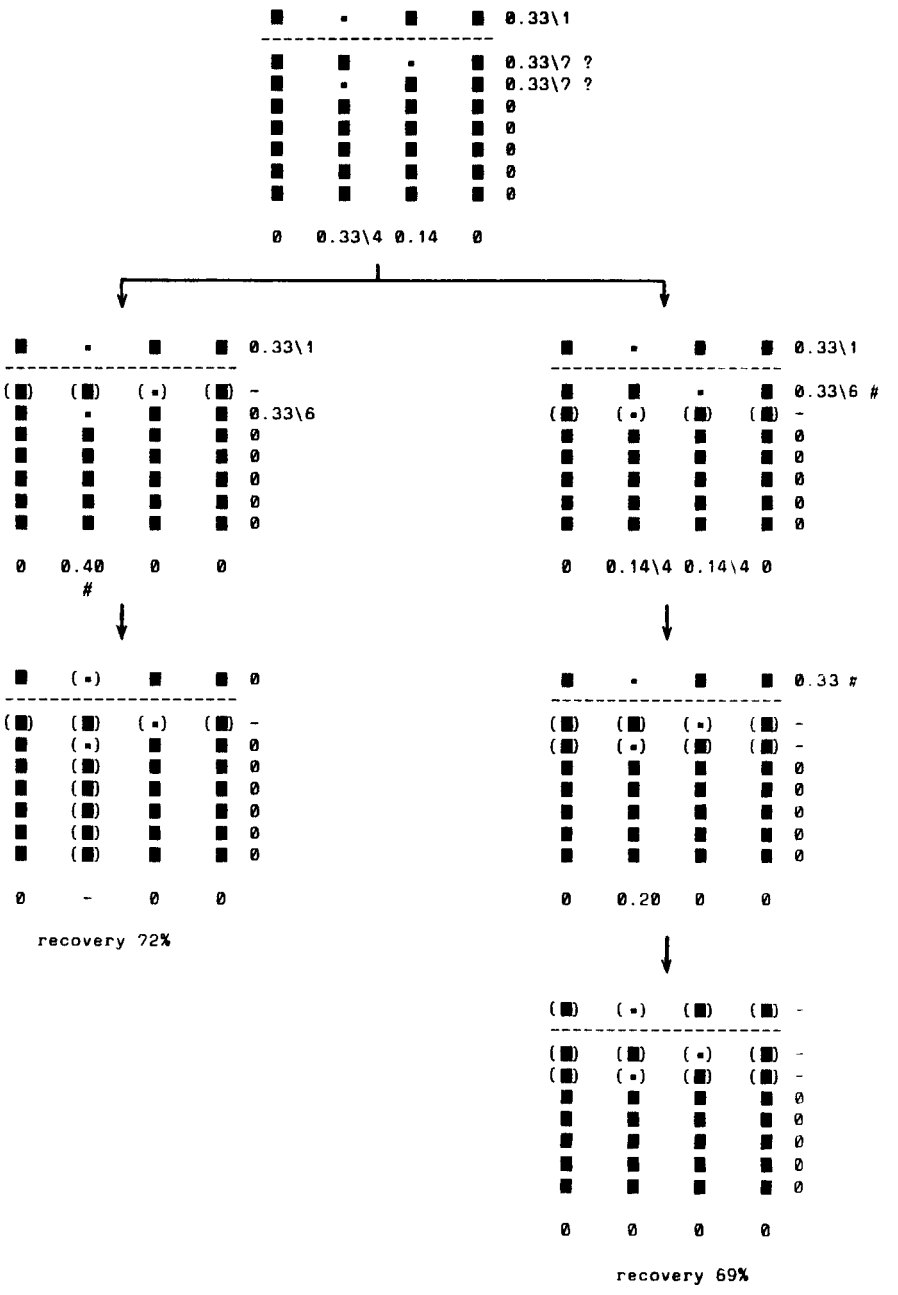

Fig. 4. The use of the *IGS* in stepwise deletion. The first item to delete is based on the *IGS*s to save the small class. The next object is selected arbitrarily and substantially influences the final result. The *IGS* is given after the backslash (\) if relevant. (———) Boundary between classes; other symbols as in Fig. 1. Deleted values are in parentheses.

TABLE 2

Efficiency of deleting missing values

	Data set			
	NEURO	ASTHMA	KILIHR	INTERN
Number of objects (total/incomplete)	261/261	76/61	142/103	127/61
Number of variables (total/incomplete)	42/42	21/8	20/19	20/14
Fraction of values missing (%)	35	10	12	3
Deletion of objects				
Number of objects retained	0	15	39	66
Number of variables retained	0	21	20	20
Present values retained (%)	0	22	31	54
Deletion of variables				
Number of objects retained	0	76	142	127
Number of variables retained	0	13	1	6
Present values retained (%)	0	69	6	31
Stepwise deletion				
Number of objects retained	192	70	78	86
Number of variables retained	21	15	15	18
Present values retained (%)	56	73	47	63

objects miss at least one variable score, and all variables are missing at least once. A total of 35% of the values is missing. Current deleting techniques of missing-data handling will erase the entire data set. Stepwise deletion, however, retains 192 complete objects, each with 21 known variables, i.e., 56% of the values that were present in the data set originally. The ASTHMA data stem from a study on allergic asthma induced by house-dust mites; the data set and its modelling will be described in detail elsewhere. The 21 variables measured are all related to lung function and allergy. The number of patients is 76. Several of the variables have missing data in several of the objects. In this case, both current missing-data handling techniques leave a substantial part of the data untouched. Stepwise deletion, however, retains more.

The KILIHR data set contains 142 objects with 20 variables from a clinical chemical routine package. This package includes determinations of blood levels of sodium, potassium, chloride, urea, creatinine, uric acid, alkaline phosphatase, lactate dehydrogenase, aspartate aminotransferase, alanine aminotransferase, direct and total bilirubin, calcium, inorganic phosphate, total protein, albumin, cholesterol, triglycerides, iron, and γ-glutamyl transferase. It is often used for screening purposes, but part of this package can be ordered for more specific objectives. The patients in this data set came from kidney, liver and heart disease groups; they were not further selected and 12% of the values is missing. Deletion of variables alone leaves 6% of the present values and

deletion of objects retains 31%. Stepwise deletion yields a data set containing 78 objects and 15 variables, thus preserving 47% of the data. The last data set is called INTERN and comprises 127 patients with the same set of 20 variables as in the KILIHR data. The patients came from different diagnostic categories in the Department of Internal Medicine, Groningen University Hospital, and were selected to provide at least 18 out of the 20 measured variables in the routine package. By this selection, the data refer mainly to patients who were screened, as opposed to monitored patients for whom a more restricted set of determinations would normally be ordered.

DISCUSSION

A complete set of data is always preferable to an incomplete one. However, in many cases, a complete data set is not available. If it is known which objects and which variables offer most information, a ranked deletion of variables and/or objects to remove missing values may be viable. This procedure, based on expertise, can ensure that the maximum amount of information is retained in the data. Unfortunately, knowledge about the information content of each object and variable is seldom available. Whenever a knowledge-guided deletion is impossible, some kind of arbitrary procedure must be used. Existing techniques like deletion of all objects or all variables with data gaps is not satisfactory, because many present values will also be deleted. Alternative techniques try to fill the data gaps with estimates, introducing pseudo-information, or to do calculations without them, either postulating statistical models or adding to the variance.

Stepwise deletion is a technique of deleting objects and/or variables that retains more data, which it is hoped will also contain more information. The algorithm with the refinement of restoring doubly deleted objects and variables closely resembles variable selection by stepwise regression. In variable selection, one is interested in an optimal subset of variables to describe the data. Such an optimal subset can in general only be found by trying all possible subsets and choosing the best. Techniques of forward selection, backward elimination or stepwise regression all try to find the optimum subset, but none can guarantee the result. In the problem of missing-data handling, the main concern is to preserve as many present measurement values as possible while deleting all missing ones. The optimal solution can only be found by trying all possible ways of variable and/or object deletion. By repeated omission of the most dispensable object/variable, an overall optimum is sought but only a local optimum may be reached. The possible restoration of objects/variables after each deletion step prevents some errors, but not all.

Another aspect that might be considered non-optimal is that the data reduction is not guided by criteria of dispensability with respect to information content. Very discriminatory variables or characteristic objects may be deleted just because of lack of values. However, extraction of information should be done by data analysis methods and stepwise deletion is intended

primarily as a general and efficient preprocessing method that aims to keep the data free from the contamination that would result from missing data being filled in. The procedure cannot, of course, replace expertise or common sense; if variables or objects are known to be essential for modelling, they must not be subjected to this technique.

If the presence of data gaps depends on the level of the variable (e.g., high levels cannot be measured) or on the type of object (e.g., medication affects the assay), stepwise deletion by selecting only fairly complete objects and variables can yield an uncontrolled biased sample from the population. An advantage that is offered by the techniques of deleting only objects or variables is that the kind of bias can be controlled; deletion of variables only, for instance, does not introduce "object selection" bias. If there exists a strong data dependency on the missing values, there is no way to balance it, and the complete data set that results from whatever technique is used cannot be seen as a random sample from the population.

The data sets ASTHMA and NEURO used for illustration were meant to be complete. All missing values should be caused accidentally or incidentally (see Introduction). Because the probability for failure of an assay is not the same for all variables and objects, there may be a certain dependency on the "type" of patient but this is considered to be only slight. The other sets, INTERN and KILIHR, however, may show a stronger data dependency on the data gaps. Physicians who suppose that a patient has liver disease may order mainly liver function tests, omitting others. If this is the case, only variables that are commonly ordered by all physicians will be least absent. These may be variables that are not very discriminatory between the disease groups, so if these data sets are to be used for classification purposes, stepwise deletion may seriously reduce the information content. However, deletion of variables is even worse in this respect, and deletion of objects may erase entire diagnostic groups. As the patients from the INTERN data had already been selected to provide at least 18 out of 20 variables measured, prior to the missing-data treatment, the risk of encountering only non-informative data was smaller compared to the KILIHR set.

The algorithm proposed above shows the general tendency to delete mainly objects if the majority of objects is complete, but delete preferably variables if most variables are almost always present. Useful properties of the procedure are that: (a) no pseudo-information is introduced except possible selection of a subclass of data because of relative "completeness"; (b) redundant deletion is partly remedied; (c) the procedure of deletion is applicable even if all objects and all variables contain data gaps; and (d) small classes are retained as long as possible (by the usage of *IGS*).

The technique described counts the number of remaining values as information content. The intrinsic information in a variable or object is not rated. If no prior information is available about the usefulness of objects and variables, preserving as many results as possible can be the best guess to approach maximum information content. However, if some objects or variables are

known beforehand to be less useful while containing a considerable number of missing values, it is preferable to drop them before proceeding. After the reduction of the training set and fitting of class models, newly collected test data must be complete. Subclasses of patients that are deleted in the training data because they provide unavoidable missing data (caused by impossibility), should not be included in the test data because their recognition is not sure.

The authors thank J. G. R. de Monchy, A. W. Teelken, J. P. W. F. Lakke and all members of the staff of the Department of Internal Medicine of the Groningen University Hospital for kindly placing their patient data at our disposal.

REFERENCES

1 J. K. Haseman and D. W. Gaylor, Technometrics, 15 (1973) 631.
2 A. W. Harper, D. L. Duewer, B. R. Kowalski and J. L. Fasching, in B. R. Kowalski (Ed.), Chemometrics: Theory and Application, ACS Symposium Series 52, American Chemical Society, Washington DC, 1977, p. 241.
3 F. Yates, Emp. J. Exp. Agric., 1 (1933) 129.
4 N. H. Nie, C. Hadlai Hull, J. G. Jenkins, K. Steinbrenner and D. H. Brent, SPSS, Statistical Package for the Social Sciences, McGraw-Hill, New York, 1975.
5 Y. Haitovsky, J. R. Statist. Soc. B, 30 (1968) 67.
6 E. M. L. Beale and R. J. A. Little, J. R. Statist. Soc. B, 37 (1975) 129.
7 C. L. de Ligny, G. H. E. Nieuwdorp, W. K. Brederode, J. C. van Houwelingen and W. E. Hammers, Technometrics, 23 (1981) 91.
8 H. Wold, in K. G. Jöreskog and H. Wold (Eds.), Systems under Direct Observation, North-Holland, Amsterdam, 1982.
9 S. Wold, C. Albano, W. J. Dunn III, K. Esbensen, S. Hellberg, E. Johansson and M. Sjöström, in J. Martens (Ed.), Proceedings of the IUFOST conference "Food Research and Data Analysis", Applied Science, London, 1983.
10 A. Donner, Am. Stat., 36 (1982) 378.
11 J. B. Hemel and H. van der Voet, Anal. Chim. Acta, 191 (1986) 33.

Analytica Chimica Acta, 193 (1987) 269—276
Elsevier Science Publishers B.V., Amsterdam — Printed in The Netherlands

SOLOMON, A CLASSIFICATION PROGRAM BASED ON A STATISTICAL MULTIVARIATE DISJOINT MODEL

H. STEIGSTRA and A. P. JANSEN

Laboratory for Clinical Chemistry, Sint Radboud Hospital, Geert Grooteplein 8, 6500 HB Nijmegen (The Netherlands)

G. KATEMAN*

Department of Analytical Chemistry, Catholic University of Nijmegen, Toernooiveld, 6525 ED Nijmegen (The Netherlands)

(Received 15th August 1986)

SUMMARY

An algorithm called SOLOMON is presented for classification of patterns in multi-dimensional space. This is achieved by constructing a statistical model based on multivariate analysis of the classes under study. The disjoint multivariate analysis is done by using multi-inductive component analysis which has many advantages compared to techniques such as principal components analysis. A weighting algorithm is described for optimum classification results.

One of the techniques in pattern recognition is the classification of known and unknown objects by using a learning machine. Parametric and non-parametric techniques are the two major types. The advantage of non-parametric methods is the independence of the distribution from the variables. These techniques usually give better results when the distributions do not look Gaussian. Some commonly used techniques are the K-nearest neighbour [1], ALLOC80 [2] and PLANE [3] classification methods. When the distributions are more Gaussian, the choice of a parametric method is preferable. Some frequently used techniques are linear discriminant analysis [4] and SIMCA [5]. The first method optimizes a discriminant function, based on differences in the mean values of the distributions (see Fig. 1A). This approach fails, however, when the difference between the distributions is not caused by differing mean values but by differing correlation coefficients (Fig. 1B) or differing variances (Fig. 1C). SIMCA involves a multivariate analysis of each class. Subsequently, a "confidence box" is constructed for each class, based on the results of the multivariate analysis. The classification results are generally good. However, when the distributions overlap, the performance of the method decreases significantly. The scaling and number of eigenvectors taken into account are experimental factors of great importance and require the knowledge of an expert in pattern recognition.

0003-2670/87/$03.50

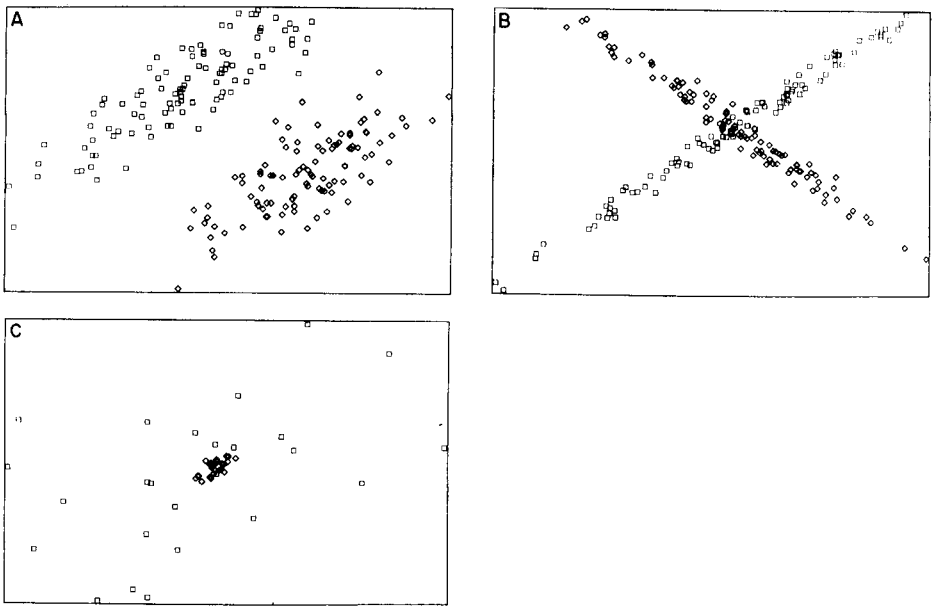

Fig. 1. Simulated examples of (partially) separable distributions: (A) distinctive mean values; (B) distinctive correlation coefficients; (C) distinctive standard deviations.

The authors have recently developed a classification program (learning machine) based on statistical distribution functions and called multi-inductive component analysis, MICA [6]. The multivariate algorithm is used to obtain statistically independent variables. The absence of the experimental factors used in SIMCA is one of the most important advantages of this method.

THEORY

The purpose of classification programs is to classify (un)known objects into one of the classes that have been defined previously. Generally, the characteristics of these classes are unknown, but can be estimated on the basis of properties of a so-called training data set. The way in which these properties are used for classifying an unknown object depends on the algorithm used. However, all algorithms have in common that there is always some uncertainty in the classification, especially when the classes overlap partially. To minimize the chance of classifying an object into a wrong class, a multi-dimensional probability distribution has to be known for each class under study. On the assumption that within each class each variable has a normal distribution and that there are only linear correlations between the variables, a model can be constructed, based on estimated parameters which can be easily calculated from the training data set:

$$D_j = f(x_i, \mu_{ij}, \sigma_{ij}, \rho_{i_1 i_2 j}) \quad (i = 1 \ldots nv; j = 1 \ldots nc) \tag{1}$$

where *nv* is the number of variables and *nc* the number of classes. Figure 2A is an example of a two-class distribution with two variables. To avoid the rather complicated evaluation of this density function, the data must be transformed to obtain scaled, uncorrelated features. The first step of this transformation is the scaling of each vector with respect to its corresponding class mean (μ) and class deviation (σ):

$$z_{ijk}^{(j)} = (x_{ijk} - \mu_{ij})/\sigma_{ij} \tag{2}$$

The second step involves the elimination of correlation between the variables within each class by multiplying each data matrix **Z** with a transformation matrix **V**:

$$U^{(j)} = \mathbf{V}^{(j)} Z^{(j)} \tag{3}$$

Principal components analysis (PCA) is an obvious method to apply. A serious disadvantage, however, is that variables which are not correlated with other variables and which do not discriminate between classes, will still contribute to all eigenvectors, including those with the highest eigenvalues. Consequently, the presence of these variables will veil the separating information.

The MICA transformation [6] is used here to eliminate correlations. In MICA, uncorrelated variables will not appear in linear combinations with other variables and can be easily eliminated by applying well chosen weighting factors. In the MICA approach, each data vector Z is presented as a linear combination of *nv* independent normalized stochastic variables, hence

$$Z^{(j)} = \mathbf{P}^{(j)} U^{(j)} \tag{3a}$$

where **P** is the inverse transformation matrix $\mathbf{V}^{-1}$. One of the options of MICA is rearrangement of the variables. This implies that the variables are ranked in decreasing represented variance (or in terms of MICA, induced variance). This rearrangement will be performed simultaneously for the variables in all classes, based on the correlation matrix of all patterns in the training set.

A special feature of **P** is that the diagonal elements express the amount of independent deviation. The density model of each class can then be written as a product of independent normal distributions:

$$D_j^{(j)} = \prod_{i=1}^{nv} \{[1/\sigma_{ij} p_{ii} (2\pi)^{1/2}] \exp [-(U_i^{(j)})^2/2]\} \tag{4}$$

When applied to the distributions in Fig. 2A, four new distributions can be distinguished. After transformation according to class model 1, the symmetric distribution $D_1^{(1)}$ and the projected distribution $D_2^{(1)}$ (Fig. 2B) are obtained. After transformation according to class model 2, $D_2^{(2)}$ and the projected distribution $D_1^{(2)}$ are obtained (Fig. 2C).

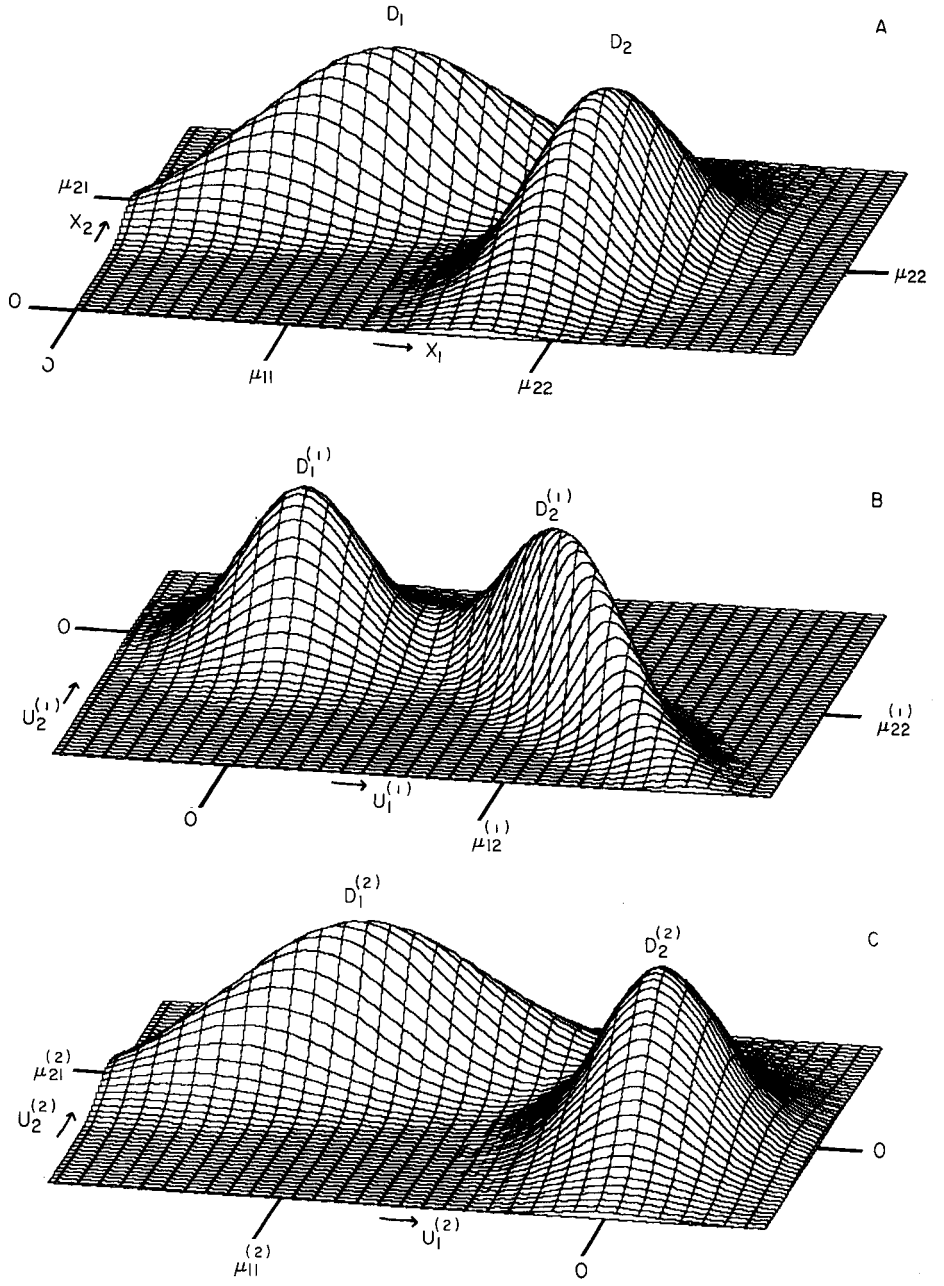

Fig. 2. Three-dimensional representations of two distributions: (A) original distributions; (B) distributions after transformation according to the disjoint model of distribution 1; (C) distributions after transformation according to the disjoint model of distribution 2.

Weight factors

The density models obtained are still descriptions of the classes in nv-dimensional space and are subject to statistical uncertainties. The effect of these uncertainties can be reduced by applying weight factors for each dimension. The choice of these factors is very critical and has to emphasize the differences between the class density functions. Conventional weightings such as Fisher and variance weights only emphasize differences in mean values. A new weighting technique was therefore developed, based on the discriminating power of the features. Figure 3 shows two single parameter distributions, having low Fisher and variance weight, although they are well separated from the statistical point of view. The ordinates X_1 and X_2 are set where the densities of the distributions are equal. A sample taken from distribution 1 will be classified as a member of class 1 when the density of class 1 at this ordinate is higher than the density of class 2. Consequently, this sample will be classified into the wrong class when the sample lies between X_1 and X_2, with a statistical probability of

$$E_{12} = \int_{X_1}^{X_2} [1/\sigma_1(2\pi)^{1/2}] \exp [-(x-\mu_1)^2/2\sigma_1^2]\, dx \tag{5a}$$

In contrast, a sample taken from class 2 will be classified as class 1 with a probability of

$$E_{21} = \int_{-\infty}^{X_1} [1/\sigma_2(2\pi)^{1/2}] \exp [-(x-\mu_2)^2/2\sigma_2^2]\, dx + \int_{X_2}^{\infty} [1/\sigma_2(2\pi)^{1/2}] \exp [-(x-\mu_2)^2/2\sigma_2^2]\, dx \tag{5b}$$

X_1 and X_2 can be calculated by equalizing the density functions. Numerical procedures are available for the calculation of E_{12} and E_{21} [7].

The separation weight factor W_{12} is now defined as

$$W_{12} = 1 - E_{12} - E_{21} \tag{6}$$

and lies between zero (equal distributions) and 1 (perfectly separated distributions). If more than two classes can be distinguished, the weight factor is defined as the arithmetic mean of the separation weight factors for all combinations of classes:

$$W_i = 2 \sum_{k=2}^{nc} \sum_{l=1}^{k-1} (1 - E_{kl} - E_{lk})/nc\,(nc-1) \tag{7}$$

In multidimensional space, this weight factor has to be evaluated for each dimension, hence

$$W_i = 2 \sum_{k=2}^{nc} \sum_{l=1}^{k-1} (1 - E_{ikl} - E_{ilk})/nc\,(nc-1) \tag{8}$$

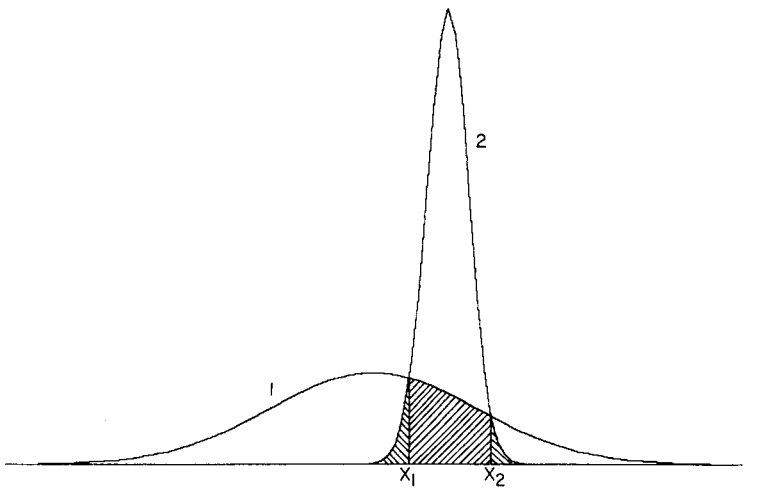

Fig. 3. Misclassification rates with two distributions. The central hatched area corresponds to patterns in distribution 1 classified as class 2. The two outer hatched areas represent patterns in distribution 2 classified as class 1.

The error function E (Eqn. 5a) now becomes a function in the (normalized) transformed multidimensional space:

$$E_{ikl} = \int_{X_1}^{X_2} [1/(2\pi)^{1/2}] \exp(-x^2/2)\, dx \tag{9}$$

The calculation of X_1 and X_2 is now more complicated, because the multidimensional distribution of class 1 has to be projected into model k. The obtained transformed mean value ($\mu_{il}^{(k)}$) and standard deviation ($\sigma_{il}^{(k)}$) of feature i for that class have to be used as parameters in the single variable distribution:

$$[1/(2\pi)^{1/2}] \exp(-x^2/2) = [1/\sigma_{il}^{(k)}(2\pi)^{1/2}] \exp[-(x-\mu_{il}^{(k)})^2/2\sigma_{il}^{(k)^2}] \tag{10}$$

which leads to the final solution for X_1 and X_2:

$$X_1, X_2 = -\mu_{il}^{(k)} \pm \sigma_{il}^{(k)} [\mu_{il}^{(k)^2} + (\sigma_{il}^{(k)^2} - 1)\, 2 \ln(\sigma_{il}^{(k)})]^{1/2}/(\sigma_{il}^{(k)^2} - 1) \tag{11}$$

When the separation weight factors W_i (Eqn. 8) have been calculated, they are used to modify the density function D (Eqn. 4) in such a way that the influence of irrelevant features will be minimized:

$$D_j^{(j)} = \prod_{i=1}^{nv} \{[1/\sigma_{ij}p_{ii}(2\pi)^{1/2}] \exp[-(U_i^{(j)})^2/2]\}^{Wi} \tag{12}$$

It should be emphasized that this density function includes all original (measured) variables and none of them has been eliminated. Only the influence of redundant variables has been reduced by applying separation weight factors,

which are found automatically: the procedures do not contain parameters which have to be tuned manually, such as the number of features or variables.

For the ultimate classification of an unknown object, the density functions for all classes are evaluated and the object is assigned to the class for which the density is maximum.

RESULTS

To evaluate the performance of this SOLOMON classification procedure, a number of data sets was generated. The objects were classified by SOLOMON, SIMCA and by means of linear discriminant analysis (LDA). When the distributions overlap only partially (as in Fig. 1A and B), SIMCA is able to classify 95% to 98% of the patterns correctly. As SIMCA does not give a real statistical description of each class, problems are to be expected when the distributions have severe overlap. The present experiments confirmed this. Patterns with distributions like Fig. 1C were correctly classified only to the extent of 60%. Addition of random variables could reduce this score to about 50%.

When the standard deviations and correlations of the variables of the two distributions are equal, the optimum separation will be theoretically a straight line. The performance of LDA will consequently be good. When correlations (Fig. 1B) or deviations (Fig. 1C) differ, however, the optimum line will be a parabola or a hyperbola. The scores of LDA will not be much better than 75%.

As SOLOMON gives a detailed statistical description of each class, it is capable of classifying 95% to 99% of the patterns correctly in each of the described situations. These results will be described in more detail in a separate paper.

Conclusions

SOLOMON offers an attractive, comprehensive and powerful alternative to commonly used classification techniques. Classification results are good and the absence of experimental factors makes the program accessible to analysts who are inexperienced with pattern recognition techniques. The inherent use of MICA combined with the calculation of separation weight factors gives a clear indication of which variables are responsible for the separation of the classes and which are redundant.

MATHEMATICAL SUMMARY

Let the number of variables be nv, the number of classes nc and the number of patterns within class j be np_j. The estimation for the mean value of variable i of class j will be

$$\mu_{ij} = \sum_{k=1}^{np_j} x_{ijk}/np_j \qquad \text{(M1)}$$

and the estimation of the standard deviation will be

$$\sigma_{ij} = \sum_{k=1}^{np_j} (x_{ijk} - \mu_{ij})^2/(np_j - 1) \quad \text{(M2)}$$

The correlation of variable i_1 with i_2 of class j is then

$$\rho_{i1\,i2j} = \sum_{k=1}^{np_j} (x_{i1jk} - \mu_{i1j})\,(x_{i2jk} - \mu_{i2j})/[\sum_{k=1}^{np_j} (x_{i1jk} - \mu_{i1j})^2 \sum_{k=1}^{np_j} (x_{i2jk} - \mu_{i2j})^2]^{1/2} \quad \text{(M3)}$$

To facilitate calculations, transformation is needed to obtain uncorrelated features. First, the patterns of each class are normalized with respect to the corresponding class parameters:

$$z_{ijk} = (x_{ijk} - \mu_{ij})/\sigma_{ij} \quad \text{(M4)}$$

Next for each class a transformation matrix **P** is calculated having the property:

$$U^{(j)} = \mathbf{P}^{(j)^{-1}} Z^{(j)} = \mathbf{V}^{(j)} Z^{(j)} \quad \text{(M5)}$$

where $U^{(j)}$ is an orthogonal data set and **P** and **V** are transformation matrices. For each class, $\mathbf{P}^{(j)}$ is given by the MICA transformation:

$$p_{il}^{(j)} = [\rho_{ilj} - \sum_{m=1}^{l-1} p_{mi}^{(j)} p_{ml}^{(j)}]/p_{ii}^{(j)} \quad (\text{for } i \leqslant l) \quad \text{(M6a)}$$

$$p_{il}^{(j)} = 0 \quad (\text{for } i > l) \quad \text{(M6b)}$$

When the patterns in class j are then transformed according to the procedure given by Eqns. M4—M6, new features are obtained with the following properties:

$\mu_{ij}^{(j)} = 0$, $\sigma_{ij}^{(j)} = 1$ and $\rho_{i1\,i2j}^{(j)} = 0$ (for $i1 \neq i2$).

Transformation of the patterns in class j according to the model obtained for class k will result in distributions with the following parameters:

$$\mu_{ij}^{(k)} = \sum_{l=1}^{i} v_{li}^{(k)} (\mu_{lj} - \mu_{lk})/\sigma_{lk}$$

$$\sigma_{ij}^{(k)} = [\sum_{l=1}^{i} \sum_{m=1}^{i} v_{li}^{(k)} v_{mi}^{(k)} \sigma_{lj}\, \sigma_{mj}\, \rho_{lmj}/\sigma_{lk}^2]^{1/2}$$

$$\rho_{i1\,i2j}^{(k)} = \sum_{l=1}^{i1} \sum_{m=1}^{i2} (v_{li1}^{(k)} v_{mi2}^{(k)} \sigma_{lj}\, \sigma_{mj}\, \rho_{lmj}/\sigma_{i1j}^{(k)}\, \sigma_{i2j}^{(k)})$$

This study was conducted with support of the Stichting Kwaliteitsbewaking Klinisch Chemische Ziekenhuislaboratoria.

REFERENCES

1 T. M. Cover and P. E. Hart, IEEE Transactions on Information Theory, IT-13 (1967) 21.
2 J. Hermans, J. D. F. Habbema, T. K. D. Kasanmoentalib and J. W. Raatgever, ALLOC80 Discriminant Program, University of Leiden, 1982.
3 A. Ralston and H. S. Wolf, Mathematical Methods for Digital Computers, Wiley, New York, 1966, p. 191.
4 B. R. Kowalski, Anal. Chem., 41 (1969) 695.
5 S. Wold, Pattern Recognition, 8 (1976) 127.
6 H. Steigstra, A. P. Jansen and G. Kateman, Anal. Chim. Acta, 186 (1986) 175.
7 E. Kreizig, Introductory Mathematical Statistics, Wiley, New York, 1970.

Analytica Chimica Acta, 193 (1987) 277—285
Elsevier Science Publishers B.V., Amsterdam — Printed in The Netherlands

INVESTIGATION OF THE RELATIVE MERITS OF SOME *n*-POINT CURRENT APPROXIMATIONS IN DIGITAL SIMULATION
Application to an Improved Implicit Algorithm for Quasi-Reversible Systems

DIETER BRITZ

Department of Chemistry, Aarhus University, Langelandsgade 140, 8000 Aarhus C (Denmark)

(Received 28th July 1986)

SUMMARY

The *n*-point current approximations ($n = 2, 3, \ldots$) in electrochemical digital simulation are examined for accuracy by using two model concentration profiles, both for point and box spacing. The recommendation is $n = 5$. This finding is incorporated in a simplified and generalized implicit flux scheme for simulating quasi-reversible systems.

This paper deals with two studies. The use of the first n concentration points to approximate the concentration gradient at the electrode by an $(n - 1)$-order polynomial is examined. Then, an improved and simplified algorithm is described for simulating quasi-reversible systems, based on the findings of the first part.

n-POINT APPROXIMATIONS

In electrochemical digital simulation [1, 2], what is computed is always a sequence of concentration values, either in a number of boxes [1] or at a number of points [2, 3] to one side of an electrode. What one is usually most interested in, however, is the current flowing across the metal/solution interface; it is proportional to the concentration gradient at the interface, and must be derived from the concentration values. This can be done in several ways, but most workers use the simple two-point approximation, in effect drawing a straight line from the concentration at the electrode to that at the nearest point in the solution. This procedure invariably distorts the true value of the gradient. Some workers have used three-point (parabolic) approximation schemes [4, 5], Stephens and Moorhead [6] used four points, and Amatore and Saveant [7] used a six-point formula, all without explanation.

In the evaluation of a particular digital-simulation technique, there has always been the problem of whether current or concentration should be used. Clearly, current is the desired quantity, but the inherent error in two-point

0003-2670/87/$03.50

formulae presents a problem. As has been shown [2], the error can cancel out concentration errors and give an incorrect impression of accuracy. While there are theoretical indications (see below) that a three-point scheme should be superior to one with two points, experience can seem to show the opposite [2, 8]. The present paper addresses this question. The conclusions reached allow a unification (in terms of accuracy) of current and concentration, removing the problem.

Theory

The argument is restricted to one-dimensional systems. Figure 1 shows the points in space (along coordinate x) at which concentrations c_i ($i = 0, 1, 2, \ldots$) are sampled, for both the point and box spacing [2, 3]. The interval in x is given the symbol h. At the electrode, $x = 0$ and $c = c_0$.

In the following paragraphs, the approximation $g_0 \approx (\partial c/\partial x)_{x=0}$ will often be used for convenience.

If concentration is treated as the continuous function $c(x)$ and Taylor's expansion is used, then

$$c(h) = c(0) + h(\partial c/\partial x)_{x=0} + (h^2/2!)(\partial^2 c/\partial x^2)_{x=0} + \ldots \tag{1}$$

giving

$$(\partial c/\partial x)_{x=0} = [(-c(0) + c(h))/h] - (h/2!)(\partial^2 c/\partial x^2)_{x=0} - (h^2/3!)(\partial^3 c/\partial x^3)_{x=0} - \ldots \tag{2}$$

Neglecting derivative terms of order $\geqslant 2$ and reverting to discrete notation, this gives the familiar two-point formula

$$g_0 \approx -(c_0 + c_1)/h \tag{3}$$

with an error $0(h)$.

For the three-point approximation, the additional equation is used

$$c(2h) = c(0) + 2h(\partial c/\partial x)_{x=0} + (4h^2/2!)(\partial^2 c/\partial x^2)_{x=0} + (8h^3/3!)(\partial^3 c/\partial x^3)_{x=0} + \ldots \tag{4}$$

which, paired with Eqn. 1, can eliminate terms in $(\partial^2 c/\partial x^2)_{x=0}$, giving

$$g_0 = [(-3c(0) + 4c(h) - c(2h))/2h] - (h^2/6)(\partial^3 c/\partial x^3)_{x=0} - \ldots \tag{5}$$

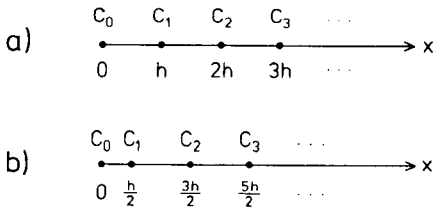

Fig. 1. Distribution of concentration sampling points: (a) for the point method; (b) for the box method.

yielding the approximation

$$g_0 \approx (-3c_0 + 4c_1 - c_2)/2h \tag{6}$$

with an error $0(h^2)$. Similar expressions with errors of the same respective orders are obtained for the box distribution, with different coefficients. Clearly, the three-point approximations should have smaller errors (h being small).

The Taylor expansion can be extended to higher orders by adding further equations (for $c(3h)$, $c(4h)$ ...) and solving each system. An equivalent procedure is to fit an $(n-1)$-order polynomial to the n points:

$$c(x) = p_0 + p_1 x + p_2 x^2 + \ldots \tag{7}$$

Then, $g_0 = p_1$. This is easier to work than the Taylor expansion and the method is readily automated on a computer. For both the box and point methods, the expressions obtained can be generalized as

$$g_0(n) \approx (1/a_n h) \sum_{i=0}^{n-1} b_{n,i} c_i \tag{8}$$

with a_n and $b_{n,i}$ integer coefficients.

Table 1 shows their values for some n. For the box distribution, the values become quite large for larger n, and the computer program was unable to go beyond $n = 5$.

Evaluation of the approximations

To evaluate these expressions, two well-described concentration profiles were used, that for the Cottrell equation and that for diffusion-limited chronopotentiometry. Normalizing the variables in the usual manner [2]

TABLE 1

Coefficients for the n-point g_0 approximation given by Eqn. 8

n	a_n	$b_{n,0}$	$b_{n,1}$	$b_{n,2}$	$b_{n,3}$	$b_{n,4}$	$b_{n,5}$	$b_{n,6}$
(a) *Point distribution* (h, $2h$, $3h$, ...)								
2	1	−1	1					
3	2	−3	4	−1				
4	6	−11	18	−9	2			
5	12	−25	48	−36	16	−3		
6	60	−137	300	−300	200	−75	12	
7	60	−147	360	−450	400	−225	72	−10
(b) *Box distribution* ($\frac{1}{2}h$, $3/2h$, ...)								
2	1	−2	2					
3	3	−8	9	−1				
4	60	−184	225	−50	9			
5	840	−2816	3675	−1225	441	−75		

gives $C = c/c_b$, $X = x/(D\tau)^{1/2}$, and $T = t/\tau$, where τ is an arbitrary experimental time interval, c_b the bulk concentration at large x, and D the diffusion coefficient. Thus for the Cottrell experiment,

$$C(X, T) = \text{erf}\,(X/2T^{1/2}) \tag{9}$$

$$G_0(T) = 1/(\pi T)^{1/2} \tag{10}$$

where $G_0 = (\partial C/\partial X)_{X=0}$.

For chronopotentiometry, setting the transition time equal to τ ($T = 1$), the equations are

$$C(X, T) = 1 - T^{1/2} \exp(-X^2/4T) + (X\pi^{1/2}/2)\,\text{erfc}(X/2T^{1/2}) \tag{11}$$

$$G_0 = \pi^{1/2}/2 \tag{12}$$

Programs were written in Fortran, using double precision (including the routines for erf and erfc), and were run on a VAX 11/780. Values of G_0 computed via Eqn. 8 were calculated from exact C_i ($i = 0, 1, \ldots n-1$) values and the error e, defined as $e = [G_0(\text{approx.})/G_0(\text{anal.})] - 1$, with G_0(anal.) given by Eqn. 10 or 12, was computed over a range of T and the interval X. There were no surprises in the T domain, but the H dependence ($H = h/(D\tau)^{1/2}$) is interesting; Fig. 2 shows these. Figure 2(a) for the Cottrell equation shows that for all H, the simple two-point approximation is slightly better than the three-point one. This has been previously mentioned [2, 8]. For chronopotentiometry, they are in the expected order.

The unexpected behaviour of the Cottrell system can be explained simply. Note that the order (H) (marked in the figures) for $n = 2$ in Fig. 2(a) is 2, not 1 as expected from Eqn. 3. Writing the error function erf(z) as a series expansion and differentiating it, one obtains finite odd-order derivatives but the even-order derivatives approach zero for small z.

Equation 3, for the 2-point approximation, has the error

$$e = -(h/2)(\partial^2 c/\partial x^2)_{x=0} + (h^2/3!)(\partial^3 c/\partial x^3)_{x=0} - \ldots \tag{13}$$

the first term of which approaches zero, leaving the second term of $0(h^2)$ to dominate. For the three-point approximation, the expected $0(h^2)$ is obtained. The "missing" even-order derivatives cause the pairing of $e(h)$ against n seen in Fig. 2.

For chronopotentiometry, the same treatment shows finite even-order derivatives and near-zero odd-order derivatives (except the first). Here, for the two-point g_0, e is $0(h)$ (see Fig. 2b) and the three-point g_0 is $0(h^3)$, paired with the four-point g_0, because the third-order derivative approaches zero. Therefore, to conclude, as the present author has done [2], that the three-point approximation can be inferior to the simple two-point approximation, is wrong; in such (model) cases, the two-point expression happens to be better than it generally should be, and is paired with the three-point expression.

In real simulations, then, one can expect an improvement in g_0 accuracy with increasing n. For a realistic H value, typically about 0.01, n should be

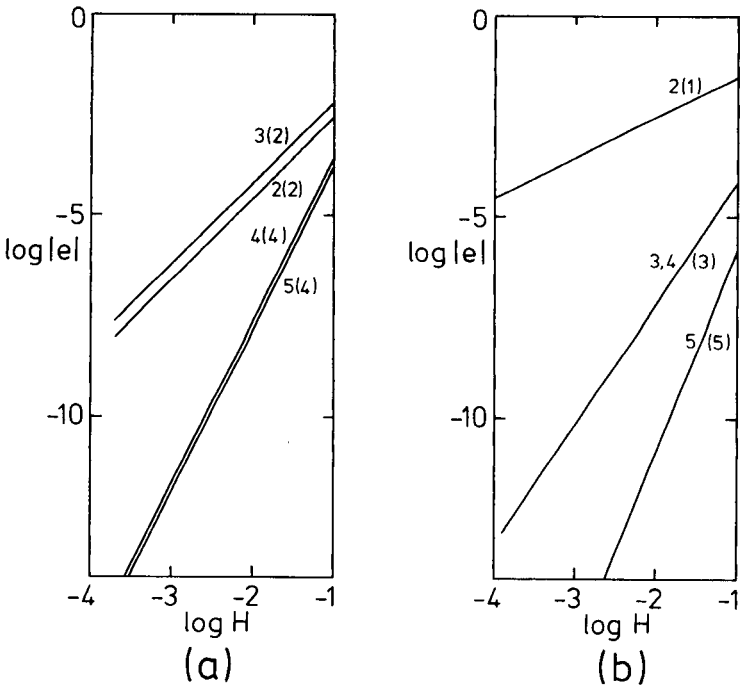

Fig. 2. Logarithmic plot of absolute error e of the G_0 approximation against H, for different values of n and (in parentheses) the error orders (H), as marked. G_0 approximation obtained by fitting Eqn. 8 to the concentration profile for (a) the Cottrell equation, and (b) chronopotentiometry.

chosen so as to match or exceed the accuracy in the simulated concentration values, which will be controlled to around 10^{-4} (by choice of the simulation parameters and method). If the two test profiles used to obtain the results of Fig. 2 are representative, then $n = 4$ fulfils the requirement. Because there is no difficulty in using Eqn. 8, $n = 5$ is recommended, which will then ensure good accuracy for all practical H. Application of the five-point formula does not affect program efficiency, because this calculation is done only at relatively long intervals.

Concentration and current accuracies are thus unified and it is no longer necessary to make an arbitrary choice between them for evaluation of a new digital simulation technique, if the five-point formula is used.

CHRONOAMPEROMETRY OF QUASI-REVERSIBLE SYSTEMS

Simulation of cyclic voltammetry in particular, or quasi-reversible reactions generally (i.e., systems controlled by both diffusion and electron-transfer rates) presents some difficulty: in order to compute the new value c'_0 for the next time ($t + \delta t$) for a given species, one needs to know the flux f' (or

concentration gradient g'_0) of the species at the new time, which in turn depends upon c'_0. Usually, this is handled by using the old flux f (or g_0). This introduces an error which necessitates, even for implicit techniques, a large number of iterations for satisfactory convergence. Recently, a scheme has been proposed [5] for calculating c'_0 and f' implicitly. In what follows, this will be called the HSM scheme. As implemented, it has two weaknesses, which makes it less accurate than it could be: a poor approximation is used, viz., the discretized Fick equation of the electrode surface ($x = 0$); and a fixed three-point current (flux) approximation is built in. These two defects are easily removed, resulting in an improved HSM scheme. Lasia [9] has also examined the problem but misunderstood the HSM scheme in part.

The reaction $A + ne^- \rightleftharpoons B$ is considered; subscripts A and B, or these letters in brackets, denote substances A or B, respectively. The respective diffusion coefficients are D_A and D_B. Here, in contrast to HSM [5], the point spacing as in Fig. 1(a) is used for clearer presentation.

The net molar flux f_A of substance A per unit area is given by $f_A = -D_A(\partial c_A/\partial x)_{x=0}$ and that for B, f_B is equal and opposite to f_A: $f_B = -f_A = -D_B(\partial c_B/\partial x)_{x=0}$. Normalizing and defining $d = D_B/D_A$, these equations become

$$F_A = -(\partial C_A/\partial X)_{X=0} = -G_0(A) \quad \text{and} \quad F_B = -F_A = -dG_0(B)$$

or

$$G_0(B) = -G_0(A)/d$$

Thus, if $G'_0(A)$ (referring now to $T + \delta T$), i.e., the first unknown, is available, the fluxes and the current flowing are known. There are two more unknowns, $C'_0(A)$ and $C'_0(B)$. Three equations can be generated to provide the solutions: for both A and B, G_0 is given by Eqn. 8. This obviously introduces more unknowns via C'_i, but it will be shown below that these can be reduced to just one, either C'_0 or C'_1, by choice. The third equation is given by the Butler-Volmer equation at the electrode potential E' at $T + \delta T$: in dimensionless form, this is

$$G'_0(A) = k'_f C'_0(A) - k'_b C'_0(B) \tag{14}$$

with $k'_f = k^0 \exp[-\alpha P']$ and $k'_b = k^0 \exp[(1-\alpha)P']$, where k^0 is the (normalized) standard heterogeneous rate constant at the standard potential E^0 and P' is the potential expression at time $T + \delta T$,

$$P' = (nF/RT)(E' - E^0) \tag{15}$$

First, Eqn. 8 is reduced to just one C'_i. The Crank-Nicolson discretization [2] of the diffusion equation at point $X = iH$ is

$$C'_{i-1} + aC'_i + C'_{i+1} = b_i \tag{16}$$

with $a = -(2/\lambda)(1 + \lambda)$ where $\lambda = \delta T/H^2$ and

$$b_i = -C_{i-1} + (2/\lambda)(1-\lambda)C_i - C_{i+1}$$

The customary manner of solving for this (which assumes a known C'_0) [2] is to go from left to right (low to high i), reducing recursively from three to two variables until the X limit is reached at $i = n_x$ where $C'_{i+1} = C_b$ (bulk concentration) and then go recursively backwards reducing to one, thus obtaining all new values. Here a start is made at the solution end, $i = n_x$ and using C_b, the system is reduced to two variables in a similar manner. This gives the recursive formula

$$C'_{i-1} + a'_i C'_i = b'_i \tag{17}$$

with $a'_i = a - 1/a'_{i+1}$ and $b'_i = b_i - b'_{i+1}/a'_{i+1}$

and $a'_{n_x} = a$ and $b'_{n_x} = b_{n_x} - C_b$.

The system of n_x two-variable equations (Eqn. 17) can then be used to express any of the C'_i in terms of any other. In particular, $C'_1, C'_2, \ldots$ can be expressed in terms of C'_0 or all (see below for reason) in terms of C'_1, in Eqn. 8. For example, if a two-point approximation is used, and $G'_0 \approx (-C'_0 + C'_1)/H$, then $C'_0 + a'_1 C'_1 = b'_1$ can be used to get

$$C'_0 = b'_1 - a'_1 C'_1 \quad \text{or} \quad C'_1 = (b'_1/a'_1) - (C'_0/a'_1)$$

to get

$$G'_0 \approx [C'_1(1 + a'_1) - b'_1]/H \quad \text{or} \quad G'_0 \approx \{C'_0[1 + (1/a'_1)] + b'_1\}/H$$

The reason for the alternative developments in terms of either C'_0 or C'_1 is that, as mentioned by Heinze et al. [5], in Eqn. 14 one might multiply very large with very small numbers, thus degrading accuracy, because C'_0 may approach zero. Heinze et al. used a trick to overcome this problem, which amounts to replacing C'_0 with C'_1 (although via a different expression). It may be noted that Lasia [9] incorrectly takes this to be an approximation iteration; the expression in terms of C'_1 is in fact exact. Because one should, in any case, work in double precision, this trick is probably not necessary and so Eqn. 14 is used here as it stands.

One must remember that the λ values and thus the a and b_i coefficients are different in Eqn. 16 because (possibly) $D_A \neq D_B$. This implies a separate set of a'_i(A), a'_i(B) and b'_i(A), b'_i(B).

If Eqn. 8 is rewritten for both A and B, using the equation G_0(B) = $-G_0$(A)/d, then some rearrangement yields two equations of the form

$$G'_0 = P_A + QC'_0(A) \tag{18}$$

$$G'_0 = P_B + QC'_0(B) \tag{19}$$

which, together with Eqn. 14, easily solves for all three unknowns. The coefficients P are n-dependent and P and Q are tabulated in Table 2. Once all the a'_i and b'_i coefficients of Eqn. 17 have been generated, all C'_i can be calculated, by a forward recursive process, starting with the now known C'_0 values.

TABLE 2

P and Q coefficients for Eqns. 18 and 19; the a'_i are independent of A or B; $b'_i(\mathrm{A}) \neq b'_i(\mathrm{B})$, giving P_A or P_B

n	P_A or P_B	Q
2	$\frac{1}{h} \times \frac{b'_1}{a'_1}$	$-\frac{1}{h}\left(1 + \frac{1}{a'_1}\right)$
3	$\frac{1}{2h}\left[\frac{4b'_1}{a'_1} - \frac{a'_1 b'_2 - b'_1}{a'_1 a'_2}\right]$	$-\frac{1}{2h}\left[3 + \frac{4}{a'_1} + \frac{1}{a'_1 a'_2}\right]$
4	$\frac{1}{6h}\left[\frac{18b'_1}{a'_1} - \frac{9(a'_1 b'_2 - b'_1)}{a'_1 a'_2} + \frac{2(a'_1 a'_2 b'_3 - a'_1 b'_2 + b'_1)}{a'_1 a'_2 a'_3}\right]$	$-\frac{1}{6h}\left[11 + \frac{18}{a'_1} + \frac{9}{a'_1 a'_2} + \frac{2}{a'_1 a'_2}\right.$
5	$\frac{1}{12h}\left[\frac{48b'_1}{a'_1} - \frac{36(a'_1 b'_2 - b'_1)}{a'_1 a'_2} + \frac{16(a'_1 a'_2 b'_3 - a'_1 b'_2 + b'_1)}{a'_1 a'_2 a'_3}\right.$ $\left. - \frac{3(a'_1 a'_2 a'_3 b'_4 - a'_1 a'_2 b'_3 + a'_1 b'_2 - b'_1)}{a'_1 a'_2 a'_3 a'_4}\right]$	$-\frac{1}{12h}\left[25 + \frac{48}{a'_1} + \frac{36}{a'_1 a'_2} + \frac{1}{a'_1 a'_2}\right.$ $\left. + \frac{3}{a'_1 a'_2 a'_3 a'_4}\right]$

The procedure was tested with a system in which both A and B are initially present at equal concentrations and a jump to potential P is made. The equations are then (see Bard and Faulkner [10] for details)

$$G_0(T) = k_f C_0(\mathrm{A}) \exp(k^2) \operatorname{erfc}(k) \tag{20}$$

with $k = (k_f + k_b)T^{1/2}$. Figure 3 shows the errors against actual computing time for this system. Clearly, the standard explicit method gives a poor result; an attempt to improve on this by using the Crank-Nicolson scheme (but not incorporating the implicit flux algorithm) failed. In contrast, the implicit flux is a great improvement. The original HSM scheme [5] was also programmed, i.e., using the poor approximation

$$C'_0 - C_0 = (\lambda/2)(C'_0 - 2C'_1 + C'_2 + C_0 - 2C_1 + C_2) \tag{21}$$

The results (not shown) were very close to the present three-point case. When the HSM scheme was developed again, by replacing the left side of Eqn. 21 with the more accurate $C'_1 - C_1$, the result exactly matched the three-point result. It can be seen in Fig. 3 that not much is gained by going beyond $n = 3$, which more or less agrees with Fig. 2; evidently, the G_0 accuracy then matches that of the simulated concentrations.

The HSM scheme, as modified here, can thus be recommended in those cases where it can be used. Unfortunately, as has recently been pointed out [11], chronoamperometry (e.g., cyclic voltammetry) finds its greatest application at present in systems with homogeneous chemical reactions; if the reaction kinetics order exceeds unity, the Crank-Nicolson scheme becomes impractical, and one is forced to use the standard explicit technique.

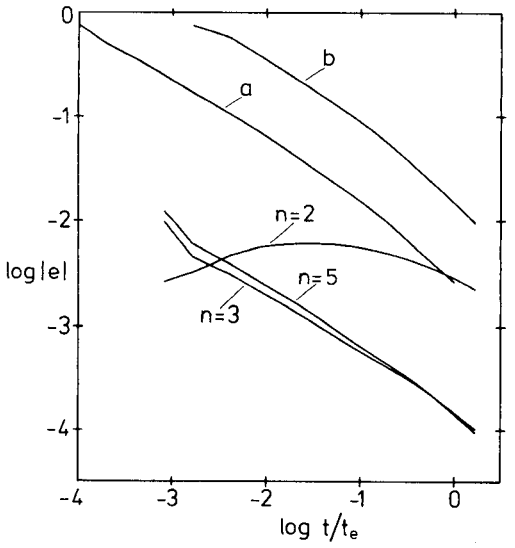

Fig. 3. Logarithmic plot of the absolute error e in G_0 vs. relative CPU time t/t_e for simulation of a potential step to $P = 1$ in a solution of equal starting concentrations of A and B; D_B assumed equal to D_A and k^0 set at unity. Curves: (a) explicit simulation, taking the reference CPU time t_e; (b) for the Crank-Nicolson scheme without implicit flux; the others are the present modified HSM scheme with n as marked.

The author thanks Dr. John Mortensen (Freiburg University), and Dr. Ole Hammerich and Merete Folmer Nielsen (Copenhagen University) for stimulating discussions.

REFERENCES

1 S. W. Feldberg, in A. J. Bard (Ed.), Electroanalytical Chemistry, Vol. 3, M. Dekker, New York, 1969, p. 199 ff.
2 D. Britz, Digital Simulation in Electrochemistry, Springer, Heidelberg, 1981.
3 D. Britz, Anal. Chim. Acta, 122 (1980) 311.
4 M. K. Hanafey, R. L. Scott, T. H. Ridgway and C. N. Reilley, Anal. Chem., 50 (1978) 116.
5 J. Heinze, M. Störzbach and J. Mortensen, J. Electroanal. Chem., 165 (1984) 61.
6 M. M. Stephens and E. D. Moorhead, J. Electroanal. Chem., 164 (1984) 17.
7 C. Amatore and J. M. Saveant, J. Electroanal. Chem., 102 (1979) 21.
8 A. Lasia, J. Electroanal. Chem., 146 (1983) 397.
9 A. Lasia, J. Electroanal. Chem., 191 (1985) 185.
10 A. J. Bard and L. Faulkner, Electrochemical Methods, Wiley, 1980.
11 M. Nielsen (Copenhagen), private communication.

Analytica Chimica Acta, 193 (1987) 287—293
Elsevier Science Publishers B.V., Amsterdam — Printed in The Netherlands

QUANTIFICATION OF A KNOWN COMPONENT IN AN UNKNOWN MIXTURE

HARALD GAMPP, MARCEL MAEDER, CHARLES J. MEYER and ANDREAS D. ZUBERBUEHLER*

Institute of Inorganic Chemistry, University of Basel, Spitalstrasse 51, CH-4056 Basel (Switzerland)

(Received 13th August 1986)

SUMMARY

A method is described for quantifying individual absorbing species in mixtures of unknown composition. The algorithm can be applied to the resolution of chromatographic peaks, to the evaluation of spectrophotometric titrations, and to related methods producing ordered, two-dimensional arrays of data. In contrast to rank-annihilation factor analysis, it is sufficient to know the absorption spectrum of the species in question. All information about the response in the second dimension, e.g., the concentration profile(s), results from the numerical analysis.

Modern instrumentation with multichannel detection systems makes it easy to obtain ordered two-dimensional arrays of data in various fields of analytical chemistry. Examples are video fluorimetry, liquid chromatography (l.c.) monitored by diode-array u.v.-visible detectors, and spectrophotometric titration of equilibrium systems. In the above-mentioned examples, the rank of data matrices corresponding to a mixture of S absorbing species ideally is equal to S.

Several methods have been proposed for quantifying individual components in mixtures, e.g., in overlapped chromatographic peaks. The linear least-squares method [1] suffers from the condition that prior quantitative knowledge of all components is needed. Self-modelling curve resolution is essentially restricted to mixtures of two components [2, 3]. Rank-annihilation factor analysis (RAFA) [4—8] is more general in scope. It can be applied to any data matrix D which has elements $D(i, j)$ obeying the bilinear form

$$D(i, j) = \sum_{k=1}^{S} \beta(k)\, X(i, k)\, Y(j, k) \text{ or } \mathbf{D} = \sum_{k=1}^{S} \beta(k)\, \mathbf{N}_k \qquad (1)$$

provided that the response matrix $\mathbf{N}_k$

$$N(i, j) = X(i, k)\, Y(j, k) \text{ or } \mathbf{N}_k = \mathbf{X}_k\, \mathbf{Y}_k^t \qquad (2)$$

for the species k to be quantified is known. The RAFA method has been successfully tested in excitation/emission fluorescence [4], l.c. with u.v. detection [5] and t.l.c./reflectance imaging spectrophotometry [6].

0003-2670/87/$03.50

Evolving factor analysis (EFA) [9—12] is a rather different approach. Again, it can be applied to any array **D** that obeys Eqn. 1, if the data are ordered in such a way that different continuous ranges of non-zero response N_k in either the x or y direction are present for the individual species. This condition is normally fulfilled for the concentration profiles in l.c. with u.v.-visible detection [11] and in spectrophotometric equilibrium studies [9, 10, 12] for which EFA has been tested and used successfully. In contrast to RAFA, EFA does not need the response of individual components as input; in fact, **X** and **Y** are the primary results of the numerical treatment. Thus EFA can be applied even to problems where the response of the pure components cannot be evaluated independently, the most obvious example being complexation equilibria, where the individual species cannot be separated in general. In l.c. with u.v. detection, the spectra of interesting components can often be measured independently, but if RAFA is to be applied several difficulties have to be overcome, and sophisticated instrumentation is needed to obtain acceptable reproducibility of the concentration profiles for solutions of different concentrations and composition [5].

Here a new algorithm is described. In a way, it combines the ideas behind RAFA and EFA, and may be called rank annihilation by evolving factor analysis, RAEFA. Like RAFA, RAEFA can be used to quantify a given species in an unknown mixture, but only the response in one direction (normally the absorption spectrum) has to be known, thus obviating any need for high chromatographic reproducibility. Alternatively, RAEFA may be used to supplement EFA itself for cases in which some of the absorption spectra are known independently. Despite the intrinsic power of EFA, it is advisable to make use of such information if it is available.

RANK ANNIHILATION BY EVOLVING FACTOR ANALYSIS

Although the analysis is completely independent of the physical significance of **X** and **Y** in Eqn. 1, it is assumed in the following argument that the $M \times W$ data matrix **D** is made up of M spectra obtained at W wavelengths. For S absorbing species, deconvolution into matrices of concentrations, **C** ($M \times S$), and absorptivities, **A** ($S \times W$), $\mathbf{D} = \mathbf{CA}$, is then sought. The general scheme is outlined in Fig. 1.

The species to be quantified by RAEFA has the known spectrum $\mathbf{A}_k$ and the corresponding unknown concentration profile $\mathbf{C}_k$ is calculated by the following series of steps.

(1) EFA is performed on the complete set of data, yielding the "concentration windows" or ranges of species existence as described earlier [9—12]. Correlation of appropriate "windows" with the corresponding species is trivial in equilibrium studies as far as the free metal ion (first species) or the fully formed complex (last species) is concerned. Also, in l.c. with diode-array detection at least the relative order of elution does not generally create severe problems.

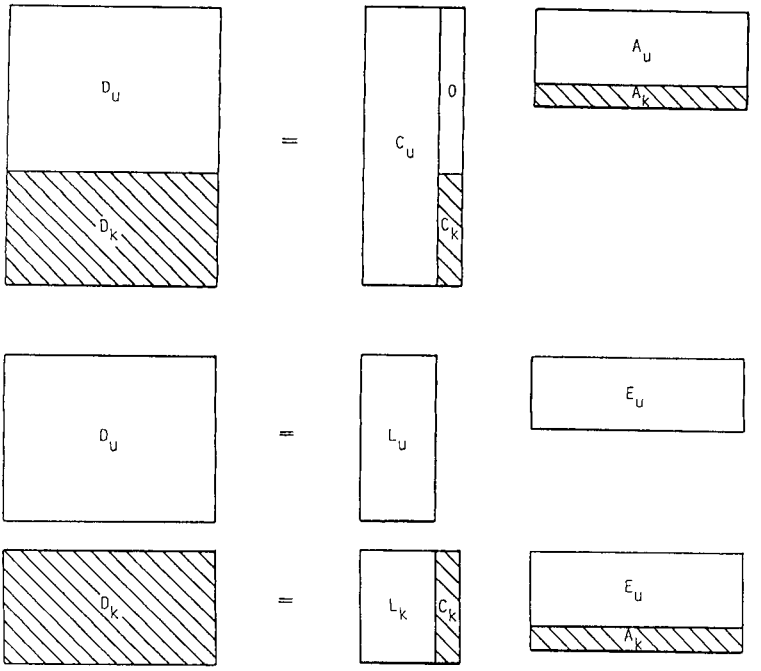

Fig. 1. Schematic diagram of the deconvolution. For explanation, see text.

(2) With the result of (1), **D** can be divided into $\mathbf{D}_k$ and $\mathbf{D}_u$, where the known species only contributes to the shaded parts $\mathbf{D}_k$ (Fig. 1). The other part of **D**, $\mathbf{D}_u$, only contains linear combinations of the unknown spectra $\mathbf{A}_u$; the rank of $\mathbf{D}_u$ therefore is $S - 1$.

(3) Principal component analysis is applied on $\mathbf{D}_u$ yielding an eigenvector representation $\mathbf{E}_u$ of the unknown spectra $\mathbf{A}_u$, spanning the same vector space of dimension $S - 1$.

(4) The complete vector space of spectra is obtained by combining the known spectrum $\mathbf{A}_k$ with the eigenvector representation $\mathbf{E}_u$ of the unknown spectra $\mathbf{A}_u$, giving a combined matrix $\mathbf{A}_c$ with full rank S.

(5) The concentration profile $\mathbf{C}_k$ of the species with a known spectrum is now easily calculated. It is identical with the appropriate column of the concentration matrix $\mathbf{C}_c$ which is obtained by simple linear regression

$$\mathbf{C}_c = \mathbf{D}_k \, \mathbf{A}_c^t \, (\mathbf{A}_c \mathbf{A}_c^t)^{-1} \tag{3}$$

As for $\mathbf{A}_c$, $\mathbf{C}_c$ is a mixed matrix with rank S spanning the complete vector space of concentrations by a combination of the physically meaningful column $\mathbf{C}_k$ and an abstract eigenvector representation $\mathbf{L}_k$ of the unknown concentrations.

As far as species k is concerned, the analysis is then complete and quantification has been obtained without independent knowledge of the concentration profile. Based on EFA, it is then also possible to quantify the other

species with unknown spectra and concentration profiles. This is done in the reduced vector space which is obtained by subtracting the contribution of the known species from the complete set of data.

$$\mathbf{D}_r = \mathbf{D} - \mathbf{C}_k A_k \tag{4}$$

The reduced data matrix $\mathbf{D}_r$ again only has rank $S - 1$ and quantification of the unknown species is possible by applying EFA to $\mathbf{D}_r$ as described in detail previously [9—12].

RESULTS AND DISCUSSION

By using EFA, absorbing species in unknown mixtures can be quantified on a completely model-free basis. Nevertheless, if the spectra of some of the species are known beforehand, this information should not be neglected but used in the analysis. The new RAEFA algorithm for quantifying individual species in unknown mixtures has the advantage over the competing RAFA method that only the spectrum and not the complete response is needed for the species in question. Two different applications of RAEFA are presented below.

The first example pertains to l.c. with a diode-array detector where four strongly overlapping components appear under one chromatographic peak. Model data were used to obtain systems of appropriate complexity and to remove any ambiguities with respect to the quality of the evaluation. Spectra as well as elution profiles were represented by simple Gaussian curves. All spectra were given a maximum absorbance of unity and identical line widths with a resolution of 0.3 between neighbouring peaks. An error of 0.001 absorbance was superimposed on the model data D. Peak concentrations, C_{peak}, of the elution profiles were between 0.2 and 1; the chromatographic resolution was varied between 0.2 and 0.5. The results for some calculations are

TABLE 1

Quantification of the third eluting species from a four-component chromatographic peak by RAEFA

Entry	Resolution	C_{rel}[a]	ΔC_{int} (%)[b]	ΔC_{peak} (%)[b]	σ_C(%)
1	0.5	0.5	0.38	0.01	0.15
2	0.44	0.5	0.98	0.12	0.39
3	0.37	0.5	1.98	0.38	0.88
4	0.31	0.5	3.23	1.02	1.46
5	0.25	0.5	8.76	4.62	4.47
6	0.19	0.5	22.31	18.88	13.80
7	0.31	0.2	5.75	1.82	2.75
8	0.31	1.0	2.85	0.90	1.38

[a]Peak heights were 0.2, 1.0, and 0.8 for species 1, 2, and 4 in all calculations. [b]Difference between model and calculated values, divided by model values.

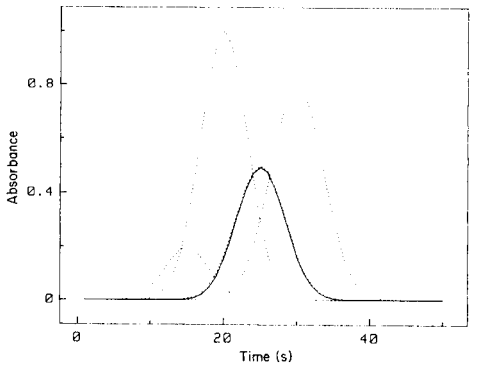

Fig. 2. Quantification of eluting species from a four-component chromatographic peak. Data correspond to entry 4 in Table 1. (. . .) Model data used as input; (—) calculated by using RAEFA.

summarized in Table 1 and a typical example is shown in Fig. 2. As indicated by Fig. 2 and entry 4 of Table 1, a very satisfactory result is obtained with a resolution of 0.3 for both the absorption spectra and the concentration profiles. The peak concentration C_{peak} is identical within 1% and the integrated concentration C_{int} is correct to 3%. More significantly, the complete elution profile is very closely represented by RAEFA as is indicated by the relative standard deviation σ_C of 1.46%:

$$\sigma_C = \left\{ \sum_{i=1}^{M} \sum_{j=1}^{S} [C_{mod}(i,j) - C_{calc}(i,j)]^2 / n \right\}^{1/2} / C_{max} \qquad (5)$$

where n represents degrees of freedom, the number of non-zero values for $\mathbf{C}_{calc}$, and C_{max} is the maximum value of $\mathbf{C}_{mod}$ between the model concentrations $\mathbf{C}_{mod}$ and those calculated by RAEFA, $\mathbf{C}_{calc}$.

As shown in Table 1, the results are improved significantly if the resolution on the concentration profiles (entries 1—3) or the relative contribution of the species to be analyzed (entry 8) is increased. Of course, the opposite is true for calculations with decreasing resolution or contribution (entries 5—7), but in fact the analysis should be considered successful for all the calculations summarized in Table 1, provided that the resolution is better than 0.2.

The second example provides a brief illustration of how RAEFA can support EFA when all species must be quantified. Problems can arise in equilibrium systems when two or more species are present in high amounts from the beginning (i.e., when the concentration windows of two species start at the same point [12]). One example of that type is given in Fig. 3. Obviously, the pure EFA result with σ_C = 8.4% is incorrect. The concentration profiles of the species present at low pH (broken lines) are wrong, as are the corresponding spectra. However, in equilibrium measurements, the absorption spectrum of the free copper ion can be obtained independently, in the absence of ligand. Its concentration profile therefore can be calculated by

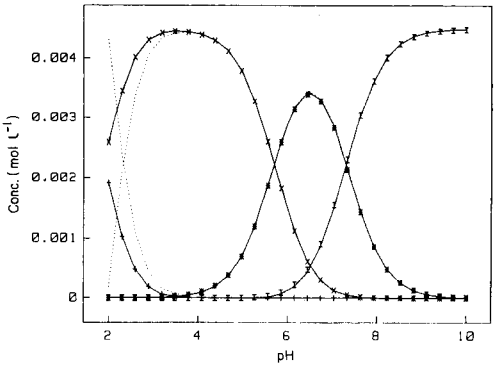

Fig. 3. Calculation of pH/concentration profiles in a four-component equilibrium system. Model data obtained from absorption spectra with log k^{H}_{LH} = 8.40 and log $k^{H}_{LH_2}$ = 6.55 for Cu^{2+} complexes with 3,7-diazanonane diamide (L) [10, 12, 13]. Noise on the data is 0.0002 absorbance. Equilibrium constants used for generation of data: log k^{Cu}_{CuL} = 13.7, log k^{H}_{CuL} = 5.7, log $k^{H}_{CuLH_{-1}}$ = 7.3. Curves: (+) Cu^{2+}; (×) CuL^{2+}; (*) $CuLH^{+}_{-1}$; (I) $CuLH_{-2}$; (...) curves calculated by using EFA [10, 12] alone, with σ_C = 8.4% (cf. Eqn. 5); (—) curves with quantification of Cu^{2+} by RAEFA followed by EFA for the remaining three species, with σ_C = 0.25%.

RAEFA and the model-free EFA can be restricted to the actual complexes. After application of RAEFA in support of EFA, σ_C is reduced to 0.25% and, as shown in Fig. 3, all concentrations can be quantified very well even if complexation is already half complete for the first measured spectrum.

RAEFA is a new powerful algorithm for quantifying a given species in an unknown mixture. In contrast to RAFA, only the absorption spectrum and not the complete two-dimensional response of the species in question is used as input. RAEFA, however, is based on the existence of 'concentration windows' which are not available in the classical RAFA example of excitation/emission experiments [4]. In the case of l.c. with u.v.-visible detection, RAEFA obviates the need for special instrumentation for high reproducibility [5] in obtaining elution profiles and problems related to column overloading or distortion of profiles caused by interaction between eluting species can be avoided. The use of RAEFA instead of RAFA is mandatory in the case of equilibrium studies, where the concentration profiles of the individual absorbing species cannot be determined by independent experiments and prior knowledge of the complete response is impossible.

This work was supported by the Swiss National Science Foundation, Grant No. 2.021-0.83.

REFERENCES

1 J. C. Sternberg, H. S. Stillo and R. H. Schwendeman, Anal. Chem., 32 (1960) 84.
2 W. H. Lawton and E. A. Sylvestre, Technometrics, 13 (1971) 617.

3 M. A. Sharaf and B. R. Kowalski, Anal. Chem., 54 (1982) 1291.
4 C.-N. Ho, G. D. Christian and E. R. Davidson, Anal. Chem., 50 (1978) 1108; 52 (1980) 1071; 53 (1981) 92.
5 M. McCue and E. R. Malinowski, J. Chromatogr. Sci., 21 (1983) 229.
6 M. L. Gianelli, D. H. Burns, J. B. Callis, G. D. Christian and N. H. Andersen, Anal. Chem., 55 (1983) 1858.
7 A. Lorber, Anal. Chim. Acta, 164 (1984) 293; Anal. Chem., 57 (1985) 2395.
8 E. Sanchez and B. R. Kowalski, Anal. Chem., 58 (1986) 499.
9 H. Gampp, M. Maeder, C. J. Meyer and A. D. Zuberbühler, Talanta, 32 (1985) 1133.
10 H. Gampp, M. Maeder, C. J. Meyer and A. D. Zuberbühler, Chimia, 39 (1985) 315.
11 M. Maeder and A. D. Zuberbühler, Anal. Chim. Acta, 181 (1986) 287.
12 H. Gampp, M. Maeder, C. J. Meyer and A. D. Zuberbühler, Talanta, 33 (1986) 943.
13 A. D. Zuberbühler and Th. A. Kaden, Talanta, 26 (1979) 1111.

Analytica Chimica Acta, 193 (1987) 295—307
Elsevier Science Publishers B.V., Amsterdam — Printed in The Netherlands

A RECEPTOR MODEL FOR URBAN AEROSOLS BASED ON OBLIQUE FACTOR ANALYSIS

KRISTIAN KEIDING* and MORTEN S. SØRENSEN

Environmental Engineering Laboratory, University of Aalborg, Box 159, 9100 Aalborg (Denmark)

NIELS PIND

Department of Chemistry, Aarhus University, Langelandsgade 140, 8000 Aarhus C (Denmark)

(Received 22nd July 1986)

SUMMARY

A procedure is outlined for the construction of receptor models of urban aerosols, based on factor analysis. The advantage of the procedure is that the covariation of source impacts is included in the construction of the models. The results are compared with results obtained by other receptor-modelling procedures. It was found that procedures based on correlating sources were physically sound as well as in mutual agreement. Procedures based on non-correlating sources were found to generate physically obscure models.

In studies of air pollution, it is desirable to know the pollutant sources as well as the contributions of the sources to air quality. To obtain this information, models based on the observed air quality have been developed. Two different approaches have been suggested in attempts to develop such receptor models for urban aerosols. One is the chemical element balance, which involves linear regression of source emission profiles upon total suspended particulates (TSP) [1, 2]. This approach has a number of drawbacks because of the high variability of source emission profiles not only with time but also in specific emittants in one source type. Furthermore, it is a prerequisite for this approach that the pollution sources be known, hence the generality of the approach is limited.

The other approach suggested involves the application of procedures based on factor analysis for the construction of receptor models. Such models have the advantage that qualitative identification of the pertinent sources can readily be obtained on the basis of the correlation between the observed variables. Within this approach, the quantification of source profiles and source contributions has been obtained by either Q-mode or R-mode factor analysis. Q-mode factor analysis, in which sample variations are described, was applied in conjunction with target transformation factor analysis [3]. For the present study, R-mode factor analysis, which involves correlation of autoscaled variables, was used [4, 5]. The procedure recently described by

0003-2670/87/$03.50

Keiding et al. [4] has been adapted and further developed. The authors suggested the use of principal factor analysis followed by varimax rotation, so that the autoscaled source contribution was estimated. It was then assumed that the observed TSP is described by the identified sources, and a regression of the autoscaled source contributions upon TSP provided constants for rescaling the derived values back to the absolute values. A necessary assumption for the use of the varimax rotation is that source contributions are not correlated. It is, however, realized that this assumption is not physically reasonable. Correlation between the observed variables will occur either because of common emission characteristics or because of meteorological conditions; for example, it is likely that up to half of the variation in TSP can be ascribed to meteorological conditions. It is therefore essential that a receptor model should allow for these effects, i.e., that correlation amongst the derived sources is considered in the construction of the model.

Correlations between source contributions imply that the factor axis cannot be orthogonal. While the varimax rotation assumes orthogonality, the oblimin rotation (defined in eqn. 7) relaxes that requirement. Therefore, in this paper, the former procedure [4] is expanded by including the oblimin rotation in the factor analysis. The degree of obliqueness for the derived solution was evaluated from the mean correlation of prominent elements in the more distinct sources. After the derivation of autoscaled source contributions, these can be regressed on TSP by multiple regression techniques that allow for the collinearity which has entered the system. Thus, rescaling of the solution is still possible.

For the sake of comparison, the derived model was compared to other procedures based on R-mode factor analysis. These consist of the previously proposed model based on varimax rotation [4], a model in which the mean source contribution is found from unique source elements [6] and by models based on tracer elements [7].

THEORY

General method

The fundamental assumption is a linear model relating ambient elemental concentrations to the contributions of different sources to the suspended particles by a matrix, A, containing the source profiles of the p derived sources:

$$x_t = \mathrm{A}f_t + \epsilon_t \tag{1}$$

The concentration of element i measured at the collection site at time t is given by x_{it}, and f_{jt} is the concentration of suspended particulate from source j; ϵ_t is a stochastic residual which is assumed to have a zero mean. The source profile element a_{ij} is the ratio of the mass element i to the mass of suspended particles at the collection site originating from source j. The

autoscaling of x_t implies that the actual model used in factor analysis is

$$y_t = Bg_t + \delta_t \tag{2}$$

where $y_t = S_x^{-1}(x_t - \bar{x})$ and $g_t = S_f^{-1}(f_t - \bar{f})$. Here S_x and S_f are diagonal matrices containing the standard deviations, and δ_t is a random error term. Next A is given by

$$A = S_x B S_f^{-1} \tag{3}$$

S_f is so far unknown, but by assuming that the sum of f_j equals TSP, S_f can be estimated. If c_j is defined as the coefficients of regression between g_j and TSP, then the diagonal elements of S_f are given by

$$s_{f_j} = s_{TSP} c_j \tag{4}$$

This permits the calculation of each element in the source profile matrix A:

$$a_{ij} = s_{x_i} b_{ij} / (s_{TSP} c_j) \tag{5}$$

Once the A matrix has been established, estimation of the source contributions, f_t, is done by weighted linear regression. The weight matrix is diagonal with elements $w_{ii} = (1 - h_i^2) s_{x_i}^2$, where h_i^2 is the communality of element i. A more detailed description of these calculations is available [4].

For the comparison of different models, the standard estimate of errors is considered. All the uncertainty was ascribed to the estimates of source profiles (Eqn. 5). For the standard error of the standard deviations, s_{x_i} and s_{TSP}, confidence intervals are estimated. For the relative error of the regression constants, $b_{i,j}$, calculated from N cases

$$(\sigma_{b_{i,j}} / b_{i,j})^2 = (N - 2)^{-1}(1 - b_{i,j}^2)/b_{i,j}^2 \tag{6}$$

is applied [8]. Likewise, Eqn. 6 is used for the estimation of the relative error of c_j.

Propagation of errors is used for the final estimate of standard error for the source profiles.

Factor analysis with oblimin rotation

The principal factor solution followed by an oblimin rotation can be used to calculate B. The theory of this method has been described in detail by Harman [9]. This method was chosen in order to introduce a method based on factor analysis involving correlation between factors. The idea of the oblimin criteria is to minimize the cross-product of the primary factor loadings. This is obtained by minimizing the following expression:

$$\sum_{p<q=1} \left(\sum_{j=1} b_{jp}^2 \cdot b_{jq}^2 - \gamma / N \sum_{j=1} b_{jp}^2 \cdot \sum_{j=1} b_{jq}^2 \right) \tag{7}$$

where the b's are the factor pattern loadings, from Eqn. 2, and γ is an empirically set variable, controlling the obliqueness of the solution. If γ is less than ca. —5, the oblique solution is in practice identical to the varimax

solution, i.e., the derived factors are virtually uncorrelated. If γ exceeds +0.5, the factor correlation becomes so high that the dimension of the solution is less than the initial dimension, and for higher values of γ, the dimension decreases to one.

The degree of obliqueness, γ, can be set by comparing calculated factor correlations with the observed source correlations. By calculating factor correlations for various γ values, a value can be chosen which reproduces the observed source correlations. Source correlations are estimated as a mean correlation of elements which are highly representative of the sources chosen. Two criteria must be met when the source correlation is to be estimated from the original element correlation values. The elements used must be uniquely related to one source alone, and the correlations must be significantly different from zero, i.e., the precision of the correlations must be high.

In Harman [9], a detailed procedure for obtaining mean correlations is described on p. 263. Since, as encountered in the present study, the values of factor loadings are high, the mean element correlation can be estimated as the cosine of the angle between source-related vectors defined with reference to the varimax solution (Fig. 1). If the elements Y_i and Y_j are closely connected to factor G_1 from the varimax solution and the elements Y_m and Y_n are similarly associated to factor G_2, the mean points for the pairs of elements can be calculated as the mean factor loadings for each set of variables. Then, the source vectors, S_1 and S_2, are given by the mean factor loadings, and the mean correlation between the two sets of variables is estimated as the scalar

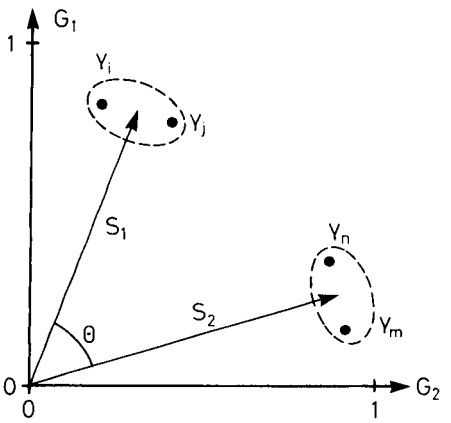

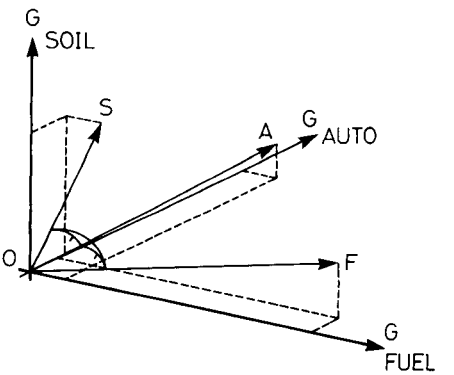

Fig. 1. Estimation of source correlation. Prominent elements of the sources 1 and 2 are plotted against the factor reference axes through the factor loadings. The correlation between source 1 and source 2 is calculated as the cosine to the angle between the source vectors S_1 and S_2 ; $r_{1,2} = \cos\theta$.

Fig. 2. Calculations of mean source correlation. The source correlations are cosine to the angles between the vectors **OA**, **OS** and **OF**.

product of S_1 and S_2. After these calculations, oblique factor analysis is performed with varying γ values. The correlations between the modelled source contributions are calculated, and that γ-value, for which the mean source correlation and the modelled source correlation are identical, is the value of choice for the system.

Comparison methods

The procedure described above, referred to as OBL, was compared to other procedures for the construction of receptor models. These include factor analysis with the application of varimax rotation, unique element procedure and regressive procedures based on tracer elements.

Factor analysis with the application of varimax rotation (VAR) follows the procedure described above as the *general method* [4]. Recently, a procedure, called the unique element method, was proposed by Kronborg et al. [6]. If it is assumed that an element x_i is uniquely related to source f_j (i.e., $b_{i,j} = 1$ and thus $b_{i,k} = 0$ for $k \neq j$), the coefficient of variation for x_i equals that for f_j. Thus, the mean source contribution is estimated from

$$\bar{f}_j = c_j \, s_{\mathrm{TSP}} \, (\bar{x}_i / s_{x_i}) \tag{8}$$

Because the value of c_j is dependent on the choice of rotational criteria, the unique element method is used along with varimax rotation (U-VAR) as well as oblimin rotation (U-OBL). Based on tracer elements chosen from the factor loadings of the varimax-rotated solution, a linear regression approach was suggested by Kneip et al. [7]. In the notation used here, c_j is the correlation between a tracer element and TSP, and b_{ij} is the correlation between element x_i and the tracer element for source j. Two different ways of estimating coefficients of correlations were used. The term conventional linear regression (CLR) covers the use of the empirical coefficient of correlation. Multiple regression (MR) [10] means regression techniques that take multicollinearity, i.e., source correlations, of the independent variables into account.

EXPERIMENTAL

The data used here were obtained from the National Air Pollution Monitoring Program conducted by the National Environmental Protection Agency, Air Pollution Laboratory. During 1983, TSP was sampled daily at a sampling site along an entrance road to the city of Odense (200 000 inhabitants). The elemental composition of TSP was determined by proton-induced x-ray emission spectrometry and TSP was determined by conditioned weighing of filters before and after exposure [11]. The total number of samples used was 322; 15 elements (Al, Si, S, Cl, K, Ca, Ti, V, Mn, Fe, Ni, Cu, Zn, Br and Pb) were present in detectable amounts.

All calculations were done on the original data, i.e., no mathematical screening or weighting was used. The computer was a CDC Cyber 170-730.

For the statistical analysis, the programs were from the SPSS system (ed. 9.0-1984) [12, 13]. For multiple regression, five options are available; however, there was no difference in the results obtained with any of the procedures.

RESULTS AND DISCUSSION

Sources and tracers

The sources identified by factor analysis were qualitatively identical in the two suggested factor-analysis procedures (OBL, VAR). Table 1 shows the sources and the source-related elements along with factor loadings in the varimax-rotated solution. Further discussion of the source identification was given recently [4].

Determination of γ

In order to establish the obliqueness of the oblique factor rotation, elements were chosen according to the previously stated criteria. These criteria are best met by the "automobile-exhaust" factor, characterized by Pb and Br, and by the "fuel-oil-combustion" factor characterized by V and Ni. To a slightly lesser extent, the criteria are met by the "soil" factor, characterized by Si and Ti. In Table 2, the factor loadings of these elements from the varimax solution are listed. The mean loadings for Si and Ti, for Pb and Br, and for V and Ni are termed S, A and F, respectively. The mean source correlation was calculated as the cosine to the angles between the vectors OA, OF and OS (see Fig. 2). The angles are calculated in the 3-dimensional space constituted by the factors mentioned. The influence of the omitted factors ("sea", "straw" and "LRT") is minimal because they are virtually uncorrelated to any other factor in the solution, which implies that the scalar products between the omitted factors and the used factors are close to zero. The following values were obtained: the mean correlation

TABLE 1

Identified sources and prominent source-related elements

Source	Element (loading)		
Soil	Al (0.84)	Si (0.89)	Ca (0.86)
	Ti (0.88)	Mn (0.77)	Fe (0.80)
Fuel oil combustion	V (0.89)	Ni (0.89)	
Automobile exhaust	Pb (0.85)	Br (0.85)	
Sea spray	Cl (0.99)		
Straw burning	K (0.87)		
Long range transport	S (0.86)		

[a]The loading of the varimax-rotated factor solution is given in parentheses. The underlined element was used as tracer for the sources.

TABLE 2

Selected factor loadings from the varimax-rotated factor solution and the mean loadings of prominent elements in the sources

Elements	Factor loading					
	Soil (S)		Auto (A)		Fuel (F)	
	Loading	Mean	Loading	Mean	Loading	Mean
Si	0.89	0.89	0.14	0.24	0.15	0.17
Ti	0.88		0.33		0.19	
Pb	0.32	0.32	0.85	0.85	0.28	0.25
Br	0.32		0.85		0.23	
V	0.24	0.24	0.30	0.29	0.89	0.89
Ni	0.24		0.28		0.89	

between the "auto" source and the "soil" source is 0.60; the mean correlation between the "soil" and "fuel" sources is 0.48, and that between the "auto" and "fuel" sources is 0.60.

By variation of γ in the oblique factor solution, values of factor correlations can be obtained as a function of γ. In Fig. 3, this relationship is depicted for the correlations between the three above-mentioned factors. It can be seen that the estimated source correlations at 0.60, 0.48 and 0.60 all give a preferred γ value at approximately -0.03. A more detailed inspection of this plot shows that for $r_{A,S}$, γ should be -0.04; $r_{S,F}$ gives γ at -0.03 and finally $r_{F,A}$ suggests γ at -0.02. The mean of the three values obtained was chosen; however, there is only a slight difference between the solutions obtained by using any of the γ values found.

Modelling abilities

To describe the modelling abilities of the procedures used, the modelled means were calculated and compared to the corresponding observed values. The correlation between the modelled values and observed values was also calculated. These results are shown in Table 3 for the OBL, VAR and MR procedures. The unique-elements procedures cannot provide such information, and the results of the CLR procedure have been omitted because they were very obscure.

The most striking feature of Table 3 is the identical results obtained by the two procedures based on factor analysis: 97.3% of the total element variation was modelled by OBL and VAR, while MR modelled 95.1%. The average modelled mean values for OBL, VAR and MR are 99.4%, 99.4% and 95.4%, respectively. The tracer elements chosen are identified in Table 3 by a correlation between modelled and observed values equal to unity. It is worth noting that this ideal modelling of the tracer element is inherent in the MR procedure and that the modelling of non-tracer elements in general is poorer for MR than for OBL and VAR. The practically identical modelling power of the procedures reflects the solution of the eigenvalue problem for the

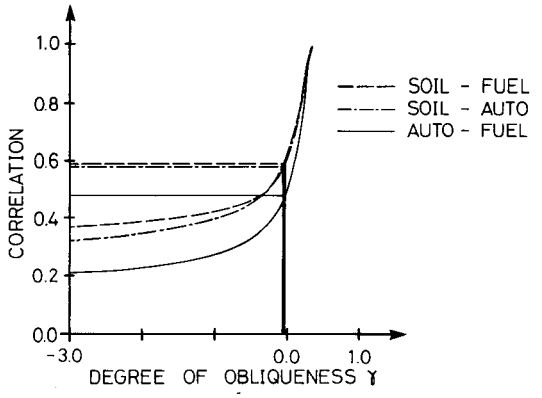

Fig. 3. Correlation amongst model-generated source emissions as a function of the degree of obliqueness γ. From the estimated mean correlation $r_{A,F}$, $r_{S,A}$ and $r_{S,F}$, the mean γ is found at −0.03.

TABLE 3

Comparison of observed and modelled values. Observed and modelled means and correlations between observed and modelled values are shown for three procedures: oblique-factor analysis (OBL), varimax-factor analysis (VAR) and multiple regression by tracer elements (MR). Tracer elements are asterisked

Element	$\bar{x}_{obs}$ (ng m^{-3})	$\bar{x}_{OBL}$ (ng m^{-3})	$\bar{x}_{VAR}$ (ng m^{-3})	$\bar{x}_{MR}$ (ng m^{-3})	r_{OBL}	r_{VAR}	r_{MR}
Al	476.7	494.9	494.9	549.3	0.97	0.97	0.96
Si*	1105.0	940.7	940.7	1105.0	0.94	0.94	1
S*	2038.0	1870.0	1870.0	2038.0	0.99	0.99	1
Cl*	1884.0	1880.0	1880.0	1884.0	1.0	1.0	1
K*	325.0	330.0	330.0	325.0	0.99	0.99	1
Ca	665.7	670.4	670.4	734.6	0.97	0.97	0.88
Ti	64.16	60.36	60.36	63.65	0.99	0.99	0.93
V*	20.01	19.45	19.45	20.01	0.99	0.99	1
Mn	18.71	21.05	21.05	21.02	0.97	0.97	0.90
Fe	703.4	713.7	713.7	699.3	0.99	0.99	0.95
Ni	7.729	7.936	7.936	8.371	0.99	0.99	0.97
Cu	19.29	18.47	18.47	18.18	0.97	0.97	0.93
Zn	89.62	102.5	102.5	101.2	0.90	0.90	0.83
Br	169.3	180.5	180.5	171.6	0.95	0.95	0.90
Pb*	786.4	758.1	758.1	786.4	0.98	0.98	1

correlation matrix. A six-factor solution was chosen, and thus the percentage of the total variance explained equalled the sum of the first six eigenvalues divided by 15. This means that any rotation of the first six eigenvectors will provide solutions with an overall communality of ca. 95% if the rank of the solution is 6. Hence, other criteria must be sought in order to qualify the use of the suggested procedures.

The criterion that the obtained models are physically reasonable implies that source-profile elements (A) as well as source contributions (f_t) must be positive. Table 4 shows the number of calculated negative source contributions for OBL, VAR and MR. As above, such calculations for U-OBL and U-VAR were not possible, and for CLR, the total number of negative source contributions was as large as 732. Table 4 shows that OBL and MR have practically no negative source contributions, i.e., 0.4% and 0% of the values are negative. It was noted that the suggested way of estimating γ also resulted in the least number of negative source contributions. For VAR, 17.0% of the predicted values were negative. Because the mean values in the latter approach compared well with the observed means, the minimum and maximum values were much more extreme in VAR than in OBL and MR. According to the criteria stated by Henry [14], VAR fails to produce a sound model.

For the application of receptor models in air pollution studies, the mean source contribution of suspended particles is of interest. Table 5 shows that the oblique factor procedure provides results virtually equal to the unique-element method based on oblique rotation. Thus, the source variation obtained by the OBL procedure closely resembles the variation of the

TABLE 4

Number of negative source contributions

Method	Negative source contributions						
	Soil	Fuel	Sea	Auto	Straw	LRT	Total
OBL	8	0	0	0	0	0	8
VAR	123	24	60	42	56	24	329
MR	0	0	0	0	0	0	0

TABLE 5

Annual mean values of source contributions from six modelling procedures: oblique- and varimax-factor analysis (OBL and VAR), unique-element method based on either oblique- or varimax-rotations (U-OBL and U-VAR) and regression by tracer elements based on either conventional regression (CLR) or multiple regression (MR). The observed annual mean value of total suspended particulate (TSP) is 65.5 $\mu g\ m^{-3}$

Method	Mean source contribution ($\mu g\ m^{-3}$)						
	Soil	Fuel	Sea	Auto	Straw	LRT	Total
OBL	17.0	8.7	3.1	6.8	3.1	18.9	57.5
U-OBL	20.7	9.0	3.0	7.0	3.7	20.0	63.4
VAR	9.3	9.8	3.3	16.8	3.0	15.7	57.5
U-VAR	30.1	18.5	3.3	22.2	6.7	23.3	104.1
CLR	39.6	35.6	6.4	46.2	19.4	40.3	187.5
MR	12.5	6.5	3.7	14.9	2.5	20.9	61.0

chosen unique elements. This is further emphasized by the resemblance of these results to the results of the MR procedure. However, the source variational patterns obtained by the CLR, VAR and U-VAR procedures are not in mutual agreement. There is no similarity in results between the CLR procedure and the two approaches based on varimax rotation. Further, the CLR procedure fails to describe the observed TSP, and the source contributions deviate dramatically from the results obtained by the other approaches. The failure of the varimax-based approaches and the CLR procedure emphasizes that correlation amongst sources, i.e., correlation among source-specific elements, is a critical property in the construction of receptor models. Left for further inspection are the results of the OBL and MR procedures because the U-OBL method does not permit calculation of daily source contributions.

To compare these two procedures, the standard estimate of errors for the source profile element $a_{i,j}$ was calculated. When the standard estimate of error is ascribed to the A matrix alone, one must be aware that, in principle, it is not possible to assess the distribution of the error function between the A and F matrices. Various approaches to this problem have been reported [15, 16]. In the present study, the estimate of error for the A matrix was maximized by ascribing no errors to the F matrix. The relative errors of s_{xi} and s_{TSP} are about 4%. In the present study, 322 cases were included. Indeed, there is autocorrelation in these data and it must be considered in evaluating the degrees of freedom. However, this was found to be of minor importance here.

The source profiles obtained by the OBL and MR procedures are listed in Table 6. The values are listed with their standard errors; however, when an estimated value was less than twice the standard error, the value was omitted. For the "sea" and "straw" factors, this criterion implies that these factors are not significant, which is due to the low correlation between the source contributions and TSP, implying a high relative error of c_j in these cases. However, because they are pertinent for viewing the element variation, the values of the predominant elements are included. Table 6 shows that the results for the "LRT", "sea-spray" and "straw" sources compare well, while the "soil" and "fuel-oil" sources deviate somewhat. For the "auto" source in general, a fair agreement is obtained, but the important elements Br and Pb differ by a factor of two. Further inspection of the results indicates that the critical parameter in these estimations is c_j in Eqn. 4. Because the values of c_j estimated are often low, the error estimated is high, as recognized in Table 6. If the standard deviation of the source contributions is biased, the estimate of the source profiles will likewise be biased. Because the source contributions are estimated on the assumption that $\bar{x} = A\,\bar{f}$, a low estimate of a source-profile element will imply a high estimate of the mean of the corresponding source contribution. Thus the difference between the two procedures reflects the critical nature of the c_j estimation.

TABLE 6

Estimated source profiles obtained by oblique factor analysis (OBL) and multiple regression by tracer element (MR)

Element	Estimated source contribution[a] (ng μg^{-1})					
	Soil	Fuel	Sea	Auto	Straw	LRT
MR procedure						
Al	20 (3)	—	—	7 (3)	—	6.5 (1.7)
Si	88 (12)	—	—	—	—	—
S	—	—	—	—	—	98 (12)
Cl	—	—	500 (250)	—	—	—
K	—	—	—	—	131 (100)	—
Ca	26 (4)	—	21 (13)	16 (5)	—	—
Ti	2.6 (0.9)	—	—	1.5 (0.5)	—	—
V	—	3.1 (1.5)	—	—	—	—
Mn	0.53 (0.09)	—	—	0.33 (0.12)	—	0.37 (0.07)
Fe	21 (3)	—	—	20 (6)	—	6 (2)
Ni	—	1.2 (0.6)	—	—	—	—
Cu	0.11 (0.05)	—	—	0.9 (0.2)	—	—
Zn	0.9 (0.3)	—	—	2.2 (0.7)	—	—
Br	—	—	—	11 (3)	—	1.7 (0.3)
Pb	—	—	—	52 (12)	—	—
OBL procedure						
Al	18 (2)	—	—	—	—	5 (2)
Si	71 (9)	—	—	—	—	—
S	—	—	—	—	—	103 (17)
Cl	—	—	700 (500)	—	—	—
K	—	—	—	—	87 (47)	—
Ca	28 (4)	—	23 (19)	—	—	—
Ti	2.7 (0.3)	—	—	—	—	—
V	—	2.2 (0.7)	—	—	—	—
Mn	0.62 (0.08)	—	—	—	—	0.39 (0.09)
Fe	21 (3)	—	—	—	—	5 (2)
Ni	—	0.9 (0.3)	—	—	—	—
Cu	0.13 (0.04)	—	—	1.9 (0.9)	—	—
Zn	1.3 (0.3)	2.2 (0.9)	—	—	—	2.3 (0.5)
Br	—	—	—	26 (12)	—	—
Pb	—	—	—	101 (50)	—	—

[a]Standard errors are given in parentheses.

The moderate differences between these two procedures could result from the statistics used or from properties of the original data. The assumption that the differences in the results of the two methods are connected to the data and not the statistical methods was confirmed by using the oblique-factor procedure on the six tracer elements alone. This provided a solution virtually identical to the MR procedure using the same basis for estimation (six tracer elements and TSP) and no difference in results from either statistical estimates was observed. When more elements were added to the data, it

was found that when an element with high correlation to a tracer element alone was added, only a slight change of result was observed with the OBL procedure; this means that the statistical estimate was strengthened. When other elements with a more diffuse correlation pattern were added to the data, a significant change in the OBL results was observed. Indeed, zinc is distributed over all factors (Table 6); this distribution may reflect a statistical concurrence rather than a physicochemical association with the sources. Such an element may distort the factor analysis model.

Conclusion

Various procedures for the construction of receptor models were compared. Elemental composition data for urban aerosols were used and the sources for TSP were found to be soil dust, automobile exhaust, fuel oil, sea spray, straw burning and long-range transport. Given the right number of factors (i.e., the right dimension according to the eigenvalue problem) proper modelling of the element variation and of annual mean can be obtained. This in itself is not sufficient justification of a model. By assuming non-negative source-profile elements and source contributions, it is shown that procedures based on non-correlating sources fail to produce a proper model. Thus, while varimax-based factor analysis can provide a qualitative source identification, it fails to produce a quantitative model.

The oblique-factor procedure developed turned out to be a possible general approach to the construction of receptor models. For the right number of factors, the degrees of obliqueness are determined by a γ value of about zero. This means that the oblimin-rotational criterion is reduced to the first term in Eqn. 7. From the analogy to quantum mechanics, a physical interpretation of the rotation corresponds to that of the minimization of the overlap between the density functions of the sources. This leads to a model with resolution sufficient to satisfy the criterion of good modelling ability and physically meaningful results.

As for the factor analysis model, the same qualifications justify the use of trace elements provided that multicollinearity is considered in the regression techniques used.

The results obtained by either approach are in mutual agreement, and presently no criteria are available to distinguish between the two models. However, it seems that the chemical and physical structure of the observed data are more important for the modelling results than the statistical method used.

We acknowledge the help of Finn Palmgren, Kåre Kemp and Niels Z. Heidam in making the data available to us as well as partaking in valuable discussions.

REFERENCES

1 G. S. Kowalczyk, C. E. Choquette and G. E. Gordon, Atmos. Environ., 12 (1978) 1143.
2 M. S. Miller, S. K. Friedlander and G. M. Hidy, Aerosol and Atmospheric Chemistry, Academic Press, New York, 1972, p. 301.
3 D. J. Albert and P. K. Hopke, Atmos. Environ., 14 (1980) 1137.
4 K. Keiding, F. Palmgren Jensen and N. Z. Heidam, Anal. Chim. Acta, 181 (1986) 79.
5 G. D. Thurston and J. D. Spengler, Atmos. Environ., 19 (1985) 9.
6 D. Kronborg, F. Palmgren Jensen, K. Keiding and N. Z. Heidam, Atmos. Environ., 1987, to be published.
7 T. J. Kneip, R. P. Mallon and M. T. Kleinman, Atmos. Environ., 17 (1983) 299.
8 N. Z. Heidam, MSTLUFT-A31, Risoe Natl. Lab., Denmark, 1980.
9 H. H. Harman, Modern Factor Analysis, 3rd edn., University of Chicago Press, Chicago, 1976.
10 K. Conradsen, Introduction to Statistics, 3rd edn., IMSOR, Lyngby, Denmark, 1979.
11 K. Kemp, MSTLUFT-A100, Risoe Natl. Lab., Denmark, 1985.
12 N. H. Nie, C. H. Hull, J. G. Jenkins, K. Steinbrenner and D. H. Bent, SPSS-Statistical Package for the Social Science, McGraw-Hill, New York, 1975.
13 C. H. Hull and N. H. Nie, SPSS-Update 7-9, McGraw-Hill, New York, 1981.
14 R. C. Henry, Atmos. Environ., 1987, to be published.
15 N. Z. Heidam, Atmos. Environ., 16(8) (1982) 1923.
16 B. A. Roscoe and P. K. Hopke, Anal. Chim. Acta, 132 (1981) 89.

Analytica Chimica Acta, 193 (1987) 309—314
Elsevier Science Publishers B.V., Amsterdam — Printed in The Netherlands

Short Communication

RECORDING THE REAL SAMPLE DISTRIBUTION AND CONCENTRATION/TIME FUNCTIONS IN FLOW INJECTION ANALYSIS

E. A. G. ZAGATTO, O. BAHIA Fº and H. BERGAMIN Fº*

Centro de Energia Nuclear na Agricultura da Universidade de S. Paulo, Caixa Postal 96, 13400 Piracicaba, S. Paulo (Brasil)

(Received 11th June 1986)

Summary. A flow-injection system with zone sampling is proposed which enables images representing the real sample distribution at any time after injection to be obtained, and the concentration/time function to be monitored at any point of the analytical path. These images provide information on the mixing conditions of the system and the interaction between the injected sample and the carrier stream in real situations. It is intended to complement theoretical studies of dispersion in flow injection analysis.

The development of theory for flow injection analysis (f.i.a.) has led to an ever-increasing interest in the exact sample distribution after a given processing time. The pioneering work done on the single-bead-string reactor in f.i.a. by Reijn et al. [1], indicated that images representing the sample zone could be achieved by numerical calculations. In 1984, Betteridge et al. [2] demonstrated the feasibility of the random walk approach for this purpose. Recently, Vanderslice et al. [3] and Wada et al. [4] calculated the shapes of travelling sample zones; the latter group took into account the occurrence of chemical reactions affecting dispersion. Both research groups compared the predicted and experimentally monitored concentration/time functions. Direct comparison between the expected and observed shapes of the sample zones was not possible because of the lack of a flow-injection procedure which could achieve images representing the sample zone in real situations.

The zone-sampling process [5] can be exploited to obtain both the sample distribution and concentration/time functions. With this aliquoting process, any portion of the dispersed sample can be selected, removed from the original analytical path and re-introduced into a second carrier stream to be further processed and quantified [5, 6]. With a very small resampling loop, a scan of the zone-sampling time, t_s [6] enables the measuring unit to record, step by step, the concentration/time function [5—9]. Similarly, a stepwise variation in the length of the first dispersion reactor permits the entire sample zone to be aliquoted, so that the recorded peaks will provide an image representing the real axial distribution of the dispersed sample after a given processing time. It should be emphasized that when the peak heights are expressed in relative units, the recorded functions are almost

0003-2670/87/$03.50

independent of the parameters linked to the second carrier stream. Therefore, they are not subject to the dead-volume and response-time effects associated with the flow-through detector.

The possibility of achieving images of the sample distribution and concentration/time functions by using zone-sampling processes [6] is described in this communication. Images which represent a sample zone passing through a confluence point are presented.

Experimental

All instruments, including the B352 Micronal commutator, were the same as used previously [6]. The R reactor (Fig. 1) consisted of 4.0-cm long polyethylene tubes (i.d. 0.7 mm, o.d. 1.0 cm) connected by means of external tygon bushings. This open tubular reactor, the size of which can be changed at will, was kept as straight as possible. The other components of the flow-injection manifold have already been described [6].

A 300 mg l^{-1} bromocresol green solution, also 0.01 M in sodium tetraborate, was used to simulate the sample, being detected at 517 nm [6]. The 0.01 M sodium tetraborate was also used as carrier stream.

The flow diagram of the system is outlined in Fig. 1, which shows the electronically operated commutator in the sampling position. The sample is aspirated to fill the first sampling loop, L, the excess being discarded. When the commutator is moved to the alternative position, the selected sample volume is introduced into the first carrier stream and the resampling loop, L′, is placed in the same path. After a predetermined time interval, t_s, when the dispersed sample is passing through the resampling loop, the commutator

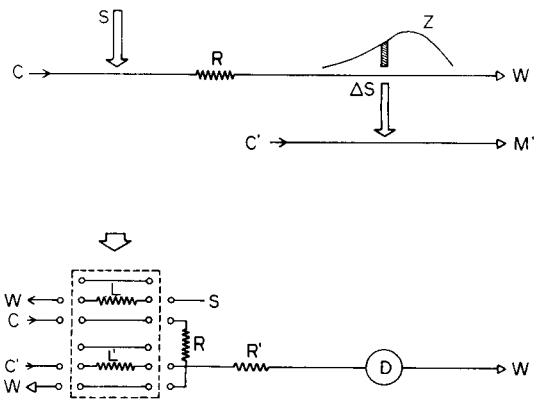

Fig. 1. A general view (upper) and a flow diagram (lower) of the flow-injection system. S, Sample; C, first carrier stream; R, first reactor; Z, sample zone; W, waste; ΔS, sampled aliquot; C′, second carrier stream; M′, measuring unit; L and L′, sampling and resampling loops; R′, second reactor; D, detector. The components within the dashed lines are linked to the movable central bar of the commutator; the direction of movement is indicated by the big arrow on top of it. The sites where pumping is applied are indicated by arrows, and flow directions by triangles.

is switched back to the position specified in Fig. 1, starting another cycle. This introduces the sampled aliquot into the second carrier stream, originating another zone to be thereafter processed and measured. Scans based on different t_s values enable the entire dispersed sample to be transferred stepwise to the second carrier stream, allowing the detector to build up an image representing the temporal variation of the sample concentration at the resampling loop. In this sense, this loop can be regarded as an intermittent monitor which acts as the dispersed sample flows through it [6, 8, 9]. Similarly, stepwise variation in the length of reactor R enables an image of the sample distribution referred to a given t_s value to be obtained. This procedure is equivalent to regular displacement of the sensor along the sample zone with only discrete preselected portions of the dispersed sample being examined.

The resampling loop, L′, should be as small as possible, almost a point sampler. Its length (8.0 cm) was chosen as a compromise between the ideality of the point sampler and the reproducibility of measurements. The other parameters were fixed as follows: first and second carrier stream flow rates, 1.6 and 4.0 ml min^{-1}, respectively; sample aspiration rate, 2.5 ml min^{-1}; first sampling loop, 20 cm; R′ reactor length, 80 cm; total flow injection period, 50 s.

The concentration/time function was obtained by maintaining the length of reactor R at 42 cm and increasing the t_s value (initially 8 s) by 1 s after each commutation cycle. In order to maintain the total residence time, the resting time of the commutator in the injection position was decreased appropriately.

The sample distributions were obtained by maintaining the t_s value at 15 or 25 s and increasing the length of reactor R by 4.0 cm after each cycle. The manifold modifications were made when the commutator rested in the injection position, so that any spurious air bubbles could be discarded. For t_s = 15 s, an image representing a sample zone passing through a confluence point was obtained. The confluent stream flowing at 1.6 ml min^{-1} was added at a point located 20.0 cm downstream from the commutator. For each experiment, the initial length of reactor R was re-adjusted according to preliminary trial and error tests.

Results and discussion

Peak broadening in f.i.a. depends not only on the injection process, but also on the dispersion inside the reactors, connectors, detector and any other device in the analytical path with significant dead volume, as well as the dampening factor of the related electronics. The sample distributions calculated earlier [2—4] were achieved by assuming ideality of the sensor and of the injector, as well as the absence of factors altering the dispersion, such as the roughness of the tube walls, the presence of confluence points, the establishment of secondary flows, and so on. In contrast, the sample distributions shown in Fig. 2 were obtained by using zone-sampling processes,

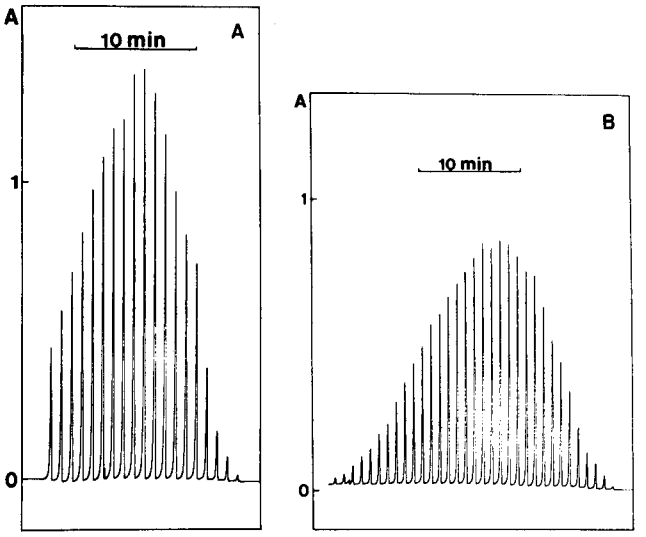

Fig. 2. Sample distribution 15 s (A) and 25 s (B) after injection. From left to right, recorded peaks refer to R lengths of 2, 6, 10, 14, . . . 70 and 74 cm in A and lengths of 2, 6, 10, 14, . . . 126 and 130 cm in B.

so that they were not affected by the dead-volume and response-time effects associated with the detector. Figure 2A represents the real mean sample distribution, 15 s after the injection, and is dependent on all the parameters affecting dispersion in f.i.a. Its two-dimensional character arises from the fact that, with the zone-sampling process, each aliquoted slice is processed as a whole, averaging effects being unavoidable.

Analysis of the dispersed sample distribution as obtained here may provide further insight into mixing processes, allowing detailed study of the boundaries of the dispersed sample and carrier stream. Parallel experiments involving chemical reactions indicated that, with this approach, it is possible to follow the interaction between a reagent carrier stream and a sample injected into it; inverted peaks and/or double peaks were often recorded. In addition, the smoothness of the recorded distribution provides useful information about the mixing conditions. In fact, the smoothness of the sample zone shown in Fig. 2A improved (Fig. 2B) when the time available for mixing was increased by 10 s. Here, it is important to note that, 15 s after the injection, a significant portion of the sample still remains inside the sampling loop. Switching the commutator back to the sampling position directs this diluted sample portion towards waste and is, therefore, an efficient way to improve sampling rate [6].

The sample distributions in Fig. 2 are not fully symmetrical, as predicted by Griffiths in 1911 [10]. However, they are more symmetrical than the concentration/time function (Fig. 3). It should be emphasized that Figs. 2A and 3 are directly comparable as the maxima of the peaks were obtained

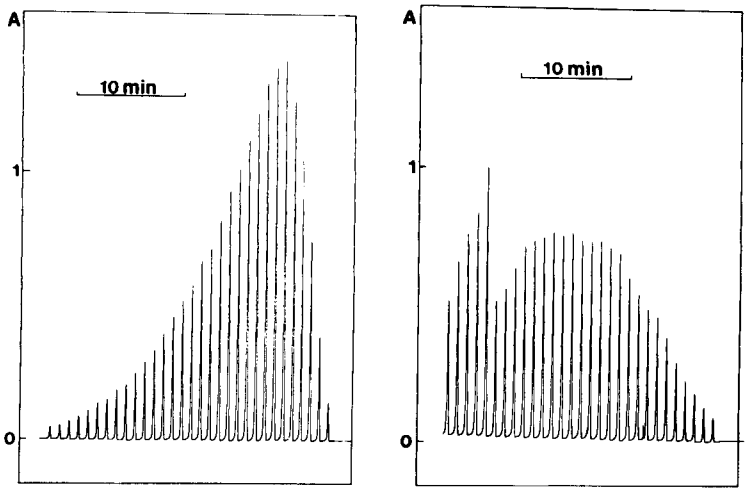

Fig. 3. Concentration/time function monitored by the resampling loop located 42 cm downstream from the commutator. From left to right, recorded peaks refer to t_s values of 38, 37, 36, . . . 10, 9 and 8 s.

Fig. 4. Sample zone passing a confluence point located 20 cm from the commutator. From left to right, recorded peaks refer to total R lengths of 2, 6, 10, 14, . . . 110 and 114 cm.

under identical experimental conditions. The recorded concentration/time function does not represent the sample distribution but the temporal variation of the monitored concentration, usually recorded as a peak. The asymmetry of the recorded peak is explained by the facts that different processing times refer to regions of the initial sample zone situated at its front and tail, and that the concentration gradients along the sample zone decrease as the processing time increases. For large dispersion [11], the asymmetry of the recorded peak decreases because the gradient modifications caused by increased processing times become less relevant.

The proposed approach can be used to obtain the sample zone distribution in the presence of any artifact affecting dispersion. Figure 4 shows a sample zone passing a confluence point. It can be noted that, in less than 4 cm, the predicted amount of the confluent stream was added. The effects of the confluent stream addition on the mean length of the sample zone and on the volumetric fractions [12] are evident.

Partial support of this research by CNPq (Conselho Nacional de Desenvolvimento Científico e Tecnológico) and by FINEP (Financiadora de Estudos e Projetos) is greatly appreciated. The authors express their gratitude to F. J. Krug, M. Martinelli and J. R. Ferreira, for their constructive comments, and to Mrs. D. Athiê for her help with the manuscript.

REFERENCES

1 J. M. Reijn, W. E. van der Linden and H. Poppe, Anal. Chim. Acta, 123 (1981) 229.
2 D. Betteridge, C. Z. Marczewski and A. P. Wade, Anal. Chim. Acta, 165 (1984) 227.
3 J. T. Vanderslice, A. G. Rosenfeld and G. R. Beecher, Anal. Chim. Acta, 179 (1986) 119.
4 H. Wada, S. Hiraoka, A. Yuchi and G. Nakagawa, Anal. Chim. Acta, 179 (1986) 181.
5 B. F. Reis, A. O. Jacintho, J. Mortatti, F. J. Krug, E. A. G. Zagatto, H. Bergamin Fº and L. C. R. Pessenda, Anal. Chim. Acta, 123 (1981) 221.
6 F. J. Krug, H. Bergamin Fº and E. A. G. Zagatto, Anal. Chim. Acta, 179 (1986) 103.
7 A. O. Jacintho, E. A. G. Zagatto, H. Bergamin Fº, F. J. Krug, B. F. Reis, R. E. Bruns and B. R. Kowalski, Anal. Chim. Acta, 130 (1981) 243.
8 M. F. Giné, B. F. Reis, E. A. G. Zagatto, F. J. Krug and A. O. Jacintho, Anal. Chim. Acta, 155 (1983) 131.
9 E. A. G. Zagatto, M. F. Giné, E. A. N. Fernandes, B. F. Reis and F. J. Krug, Anal. Chim. Acta, 173 (1985) 289.
10 A. Griffiths, Proc. Phys. Soc. London, 23 (1911) 190.
11 J. Růžička and E. H. Hansen, Flow Injection Analysis, Wiley, New York, 1981.
12 E. A. G. Zagatto, Doctoral Thesis, Piracicaba, Universidade de S. Paulo, 1986.

Analytica Chimica Acta, 193 (1987) 315—323
Elsevier Science Publishers B.V., Amsterdam — Printed in The Netherlands

Short Communication

MICRO-FUSION AND SPECTROPHOTOMETRIC DETERMINATION OF IRON(II) AND IRON(III) IN CHROME SPINELS AND OTHER REFRACTORIES

E. KISS

Research School of Earth Sciences, The Australian National University, G.P.O. Box 4, Canberra, A.C.T., 2600 (Australia)

(Received 29th September 1986)

Summary. Spectrophotometric determination of FeO in milligram samples of chrome spinels and related refractory minerals after high-frequency micro-fusion with lithium tetraborate in an inert atmosphere is described. Anomalous responses (apparent reduction or oxidation of FeO depending on the ferroïn-type reagent) rendered the procedure highly unreliable. All the fluxes containing structural oxygen, as well as phosphoric acid, acted as oxidants even when atmospheric oxidation was rigorously excluded. However, the method is suitable for micro-determination of total iron in spinels. Spectrophotometric measurements gave an average relative standard deviation of 0.73%.

Exact knowledge of the iron oxidation state in some refractory minerals (chromites and other spinels) has an important rôle in certain geochemical investigations relating to oxygen fugacity studies of the earth's upper mantle. Because these minerals exhibit considerable resistance to normal dissolution processes (with boiling hydrofluoric acid in an atmosphere of nitrogen), a special approach was required for quantitative sample dissolution such as high-temperature fluxing in an inert atmosphere. The retention of the original oxidation state during fusion and subsequent chemical procedures was of paramount importance. Hey [1, 2] developed a micro-scale technique for the sealed-tube vacuum fusion of refractory minerals but the fusion cake required prolonged leaching and protection from oxidation by the addition of iodine monochloride. Schafer [3] and Maxwell [4] summarized the most significant techniques for determining FeO in silicates. However, no suitable procedure is available for milligram quantities of refractory minerals and this investigation was therefore undertaken. The fact that no satisfactory micro-fusion techniques for FeO emerged from this study is indicative of the almost insurmountable difficulties associated with this problem. However, further work showed this technique to be effective for the determination of total iron.

Preliminary investigations

Micro-fusion experiments were conducted with lithium tetraborate ($Li_2O \cdot 2B_2O_3$), lithium metaborate ($Li_2O \cdot B_2O_3$), an equimolar mixture of

0003-2670/87/$03.50

these borates, boron trioxide, boric acid/LiF, potassium fluoride and "condensed" phosphoric acid. Lithium tetraborate was first tested because of its effectiveness for decomposing refractory minerals and because it was considered to be a non-oxidizing flux. It was envisaged that the micro-fusion of various resistant minerals would be effected in a radio-frequency (r.f.) heated furnace under nitrogen flow. Complete decomposition was achieved for the following minerals (the weight, in milligrams, of mineral mixed with 100 mg of flux is in parentheses): zircon (17), chromite (2—10), tourmaline (25), monazite (20), ilmenite (20), rutile (10), staurolite (15), garnet (15), topaz (17), kyanite (15) and pyrite (20). The major cations leached from monazite and rutile fusions with 2% sulphuric acid hydrolyzed on standing, but higher acid concentrations should be more suitable. All sample/flux fusion cakes (containing 100 mg of flux) dissolved completely after 10—20 min of ultrasonic vibration at temperatures ranging from 25°C to boiling. The acidic leachate or pyrite contained a thin film of colloidal sulphur and a strong smell of hydrogen sulphide was evident.

Fusion with boron trioxide was then tested. Although the time and temperature required to dissolve chromite completely was comparable to those with lithium borates, the resultant fusion cake was extremely insoluble even when leached in the ultrasonically agitated acidic reagent. The results showed that that B_2O_3 was strongly oxidizing (see below) and the hue of the Fe(II) complex formed for spectrophotometry [6] was also adversely affected.

To examine the dissolution of chrome spinel in condensed phosphoric acid, 5 mg of the spinel was heated in a quartz test tube with 3 ml of phosphoric acid under nitrogen bubbling. The gently boiling mixture was gradually dehydrated and the condensed acid rapidly dissolved the brown suspension, forming a clear green solution of Cr(III). The cooled sample solution was diluted and titrated potentiometrically [7] in the presence of HF/H_2SO_4 with potassium dichromate as titrant. Although the dissolution was rapid and complete, the FeO values were invariably low. Because the possibility of oxidation during digestion was rigorously excluded, the low results indicated the oxidizing character of the phosphoric acid at ca. 300°C. Thus further work with this type of digestion was abandoned in favour of the direct titration of FeO.

Simultaneous dissolution and chelation was then studied. Chrome spinel was treated with PPDT-TAS (see below) in HF/H_2SO_4 reagent mixture (see below) for 3 days at 110°C in a closed PTFE micro-bomb. (The bomb was sealed in the presence of dry ice to expel air effectively.) However, the acidic reaction products dehydrated almost completely after two days and opening of the bombs was necessary. In another experiment, chrome spinel was fused with lithium tetraborate and leached with a slightly acidic solution of 1,10-phenanthroline. The leaching was extremely slow (even after four days the solids were only partially removed from the fusion crucible) and the long delays before buffering resulted in oxidation of a substantial fraction of Fe^{2+} ions. None of these experiments was successful for a variety of reasons

(e.g., extreme insolubility of chrome spinel in acid solutions and the difficulty of rigorously excluding air from the prolonged digestion operations).

Alkali fluorides (NaF, KF and LiF) and their mixtures were next examined for digestion efficiency. Potassium fluoride was deemed more suitable than other fluorides because of higher solubility (i.e., rapid leaching after fusion) and its relatively lower melting point. Some eutectic fluoride compositions would merit further investigation. All fluorides tested dissolved chrome spinel (5—10 mg) effectively but the slight effervescence and the tendency of the melt to creep over the crucible rim made it difficult to contain samples quantitatively in 1-ml platinum fusion crucibles. Anhydrous potassium fluoride, prepared by heating in a platinum dish at 450—500°C and stored in a desiccator, showed significantly less tendency to effervesce.

Experimental

Reagents and apparatus. The tri-ammonium salt of the trisulphonic acid derivative of 3-(4-phenyl-2-pyridyl)-5,6-diphenyl-1,2,4-triazine (PPDT-TAS), was prepared by the action of fuming sulphuric acid (30% SO_3) on PPDT and isolated as described [5]. PPDT-TAS (2%) was prepared in a mixture of 10% hydrofluoric acid/5% sulphuric acid. Aqueous solutions of PPDT-TAS (0.005 M) and tetra-ammonium 5,6,5′,6′-tetra(4-sulphophenyl)-3,3′-bis-(1,2,4-triazine) (TSBT-TAS; 3 M) and buffer solutions were prepared as described previously [6].

Absorbances were measured with a Unicam SP-500 S-2 spectrophotometer equipped with a digital readout facility. The pH measurements were made with a Metrohm potentiograph type E-436 and micro-weighings were made by a Cahn G-2 electrobalance. Micro-fusions were done in a Leco dual-mode induction furnace model 523; Leco silica vacuum-jacketed graphite fusion crucibles and silica inserts were used. Platinum crucibles (capacity 1 ml) were cleaned by total immersion in molten potassium pyrosulphate, effectively removing iron and other metallic contamination, followed by leaching in boiling hydrochloric acid. It was essential to use platinum crucibles frequently cleaned in this way, otherwise unacceptable levels of iron blank could occur.

Procedure for lithium tetraborate micro-fusion and spectrophotometric determination of iron(II) oxide. The following method was closely reproducible. Weigh ca. 50 mg of dried anhydrous lithium tetraborate (high purity) in a pre-weighed 1-ml platinum fusion crucible. Weigh the finely ground mineral (e.g., chromite) on a micro-balance (ca. 2 mg to ±0.0001 mg accuracy) and carefully transfer it to the fusion crucible. With a thin platinum wire make a homogeneous mixture and cover this with a layer of the flux (50 mg) without mixing. Transfer the platinum crucible to the quartz insert of the graphite/quartz cup and lock the heating assembly in the quartz-tube r.f. furnace. Remove all traces of air by a steady flow of nitrogen (2.5 l min^{-1}) for 10 min. Commence induction heating by setting the timer on a 20-min cycle and the plate current to 250 mA initially. Increase the plate current by 50-mA increments after each minute and heat the sample at 500-mA plate current for the

remaining time. Cool the furnace assembly at the end of the heating cycle for at least 10 min and monitor the cooling rate by taking temperature readings (digital thermometer) at the nitrogen exit of the quartz tube furnace. After an initial reading of ca. 230°C, rapid cooling is observed and the crucible may be removed without the danger of oxidation when a temperature of 25—30°C is reached. Transfer the fusion crucible into a pre-weighed 125-ml FEP-teflon bottle containing 15 ml of a suitable acidic leachate (either 0.033 M TSBT-TAS or 0.5% PPDT-TAS, in 2% sulphuric acid) and rinse the bottle with nitrogen. Hasten disintegration of the fusion cake by ultrasonic vibration for at least 15 min. Observe the crucible by carefully tilting the bottle so that most of the intensely colored solution is drained from it. Additional ultrasonic treatment for a few more minutes at this stage will ensure complete dissolution of the fusion cake. Dilute the solution with ca. 50 ml of water and add 10 ml of 2 M sodium acetate buffer. Dilute to full capacity, record the total weight (±0.001 g accuracy) and after leaving for 2 h in subdued light, measure the absorbance against appropriate reagent blanks in a 10-mm quartz flow-through cell at 450 nm and 550 nm (TSBT-TAS) or 570 nm (PPDT-TAS), respectively. Calculate the concentration of FeO using calibration data previously prepared for the gravimetric-dilution spectrophotometry. The residual solution can be used for the determination of total iron, thus securing the measurement of oxidation state from a single 2-mg sample. Results obtained are summarized in Table 1.

The average values found were 15.27% FeO (TSBT-TAS) or 4.24% (PPDT-TAS).

Determination of total iron. Weigh the FEP-teflon bottle containing the residual solution after the FeO determination, add 10 ml of aqueous 10% (w/v) hydroxylammonium chloride solution, mix thoroughly and weigh again (±0.001 mg accuracy). Allow at least overnight standing in a darkened place for the reduction, and measure the absorbance against appropriate reagent blanks in a 10-mm quartz flow-through cell at 450 nm and 550 nm (TSBT-TAS) or 570 nm (PPDT-TAS), respectively. Calculate the value of total iron first, then the oxidation state of iron.

Alternatively, total iron can be measured by atomic absorption spectrometry (a.a.s.) with deuterium background correction, using calibrating standards which contain the same amount of added spectrophotometric reagents.

The total iron (expressed as FeO) was 14.64% by a.a.s. and 14.88% by spectrophotometry.

Results and discussion

Lithium tetraborate micro-fusion in inert atmosphere. Because chrome spinel is one of the most refractory minerals with respect to chemical dissolution, the standard material Grecian Chrome Ore BCS 308 was used exclusively in this study. The reference material was ground in an agate mortar under acetone (to avoid aerial oxidation).

The ferroin-type reagent PPDT-TAS [5] was initially chosen as chromogen, but in later experiments TSBT-TAS [6] was substituted because of its higher

TABLE 1

Spectrophotometric determination of iron(II)/iron(III) in chromite after inert atmospheric micro-fusion

Sample weight (mg)	FeO found (%)	Remarks
3.0125	4.01	PPDT-TAS, 0.5% in 2% H_2SO_4
3.0620	6.59	
3.3780	4.01	PPDT-TAS, 0.5% in 2% H_2SO_4
3.1995	5.10	All crucibles were cleaned by $K_2S_2O_7$ fusion and HCl
3.5195	15.16[a], 14.89[b]	TSBT-TAS, 0.033 M in 2% H_2SO_4
3.4035	15.20[a], 14.97[b]	Total Fe as FeO by a.a.s.: 14.79
3.4700	15.30	TSBT-TAS, 0.033 M in 2% H_2SO_4
3.2835	15.10	
2.7900	15.41	Total Fe as FeO: 15.37, 15.10 by spectrophotometry with TSBT-TAS
2.2440	15.35	
2.2455	15.39	TSBT-TAS, 0.033 M in 2% H_2SO_4
2.8610	15.22	
2.4015	4.15	PPDT-TAS, 0.5% in 2% H_2SO_4
2.5955	4.05	Total Fe as FeO: 14.53; 14.54 (spectrophotometry)
2.3950	4.71[a], 4.46[b]	Boron trioxide fusion[c] (flux ratio: 2:100)
	5.04[a], 4.85[b]	Reagent: TSBT-TAS in 2% H_2SO_4

[a]Absorbance measured at 450 nm. [b]Absorbance measured at 550 nm. [c]Conditions were strongly oxidizing compared with lithium tetraborate fusion values of 15.27% FeO.

acid tolerance and faster reaction rate, which are essential parameters in preventing aerial oxidation during the slow disintegration of the fusion cake. This resulted in immediate improvements in reproducibility: 8 consecutive fusions of chromite gave 15.23% FeO with a relative standard deviation of only 0.73%.

It was further envisaged that total iron could be measured after the Fe^{2+} absorption measurements by some convenient means such as atomic absorption spectrophotometry (a.a.s.) (or spectrophotometry in the presence of hydroxylammonium chloride). Interestingly, the total iron obtained by either of these methods was less than the FeO found or at most, the excess of iron calculated as Fe_2O_3 was $<0.2\%$. Calculations for the probable mineralogy showed the presence of ca. 2% oxidized iron, assuming that the silica present is in the olivine fraction. Analytical data showed anomalous responses by the PPDT-TAS and TSBT-TAS: with the former reagent, the data indicated an apparent oxidation but TSBT-TAS seemed to suffer from reduction, a condition which proved to be consistently reproducible. This discrepancy required

a closer examination; possible causes may involve such factors as flux chemistry (alkalinity), aerial oxidation, reduction by the macromolecular carbon chemistry of the reagents, interference by the protonating dissolution of the fusion cake under ultrasonic activation, or a combination of all these effects. An examination of factors relating to the possibility of oxidation alone reveals a fairly complex pattern and its implications for the erratic FeO recoveries are summarized in Table 2.

These empirical observations suggest that hitherto unexplained or poorly understood phenomena are involved. Hey [8] observed the reduction of the (1,10-phenanthroline)iron(III) complex in aqueous solutions and referred to spontaneous transformation of Fe(II) to Fe(III) ions, Serpone et al. [9] considered the iron(III) system capable of oxidizing water (also hydroxide) and Nord et al. [10] even suspected that the α,α-diimine heterocyclic compounds are oxidized to the *N*-oxide. Gillard [11] explained this phenomenon in terms of the analogy between quaternization of the ligand and its coordination with iron(II) ions. Because the proton activity varies strongly among reagents containing this type of ligand, it was reasonable to suspect analogous reduction mechanisms to occur for both PPDT-TAS and TSBT-TAS. Also

TABLE 2

Oxidation-related factors involved in erratic FeO recovery

Oxidation caused by	Remedies taken/consequences
1. Flux chemistry	Use only "non-oxidizing" fluxes (lithium borates)
2. Air exposure (impure N_2); seal breakage while sample is still hot	Use only high-purity N_2 and allow gas flow temperature to cool to 20—25° C before opening furnace
3. Post-fusion reaction from excessive heating	The time required for quantitative fusion is variable. This uncertainty may cause the liberated Fe(II) in some minerals to undergo further change
4. Slow dissolution of sample fusion cake	Ultrasonic agitation enhances dissolution. Faster reaction rates of ferroïn lowers oxidation. TSBT-TAS is preferred to PPDT-TAS
5. Anomalous behaviour of the ferriin chelate in the presence of the ferroin chelate [11]	No known remedy; spectrophotometry was replaced by potentiometric titration but other factors (oxidation by flux) lessened its usefulness considerably
6. Iron contamination from the fusion crucible	New platinum crucibles are cleaned with $K_2S_2O_7$ and boiling HCl
7. Auto-oxidation of mineral constituents in molten flux in presence of Mn(III), Cr(VI), V(V)	This factor is unavoidable if fusion is required; non-destructive measurement (Mössbauer spectroscopy of Fe(II)/Fe(III) is unaffected)
8. Entrapped air and moisture in the sample/flux mixture	Use dried anhydrous lithium tetraborate stored in a desiccator
9. Sample oxidation during dry grinding	Grind sample under acetone as finely as possible

the flux alkalinity during fusion and the ultrasonic acidic dissolution of the alkaline fusion cake in the presence of these ligands may have an effect.

In order to obtain a better understanding of these phenomena, another mineral in which most of the iron is present in the iron(III) state was analyzed. A pure hand-picked fraction of the pyroxene group mineral aegirine was selected for further work. A summary of the results is presented in Table 3. The finely subdivided mineral (ground under acetone) was examined for FeO and total Fe(FeO) by spectrophotometry [5, 6] and by constant-current potentiometry [7]. The results obtained showed that the "true value" of FeO (i.e., 0.69% FeO by potentiometry) was enhanced enormously by the fusion/spectrophotometry methods: 5.58 times higher for PPDT-TAS and 36.3 times higher for TSBT-TAS. However, after the hydroxylamine reduction of the excess solution, the value of total Fe(FeO) thus obtained was remarkably reproducible. When PPDT-TAS was used for the sample of chrome spinel (Table 1), the value obtained suggested that oxidation was occurring, whereas in the case of aegirine the reagent appeared to be reducing. TSBT-TAS showed a higher extent of reduction for chrome spinel than for aegirine.

The effect of trace oxygen impurities during fusion. The dual requirements for complete fusion and absolute retention of the original redox chemical structure in refractory minerals present severe experimental difficulties and constraints. For example, because of the prolonged heating necessary for complete fusion, very low levels of oxygen may be scavenged by the mineral sample from the nitrogen flow, with detrimental effects on Fe(II) ions.

TABLE 3

Determination of Fe(II)/Fe(III) in aegirine

Sample weight (mg)	FeO (%)	Fe_2O_3 (%)	Total Fe (% as Fe_2O_3)	Remarks
2.2750	24.28	5.21	29.42	TSBT-TAS
2.1590	25.80		29.41	TSBT-TAS
1.9650	4.54		27.75, 28.63	PPDT-TAS
1.5760	3.16		29.02	PPDT-TAS
2.2960	4.94		28.29	PPDT-TAS[a]
2.2065	3.10		29.51	PPDT-TAS[b]
2.4670	4.29		28.25	4% HF[c]
2.1445	4.14		28.49	4% HF[c]
11.14	0.69		—	Potentiometry[d]
8.00	0.70		—	—

[a]The fusion cake was dissolved by immersion in hot water instead of ultrasonic treatment. [b]The fusion cake was dissolved in a neutral 0.5% solution of PPDT-TAS by immersion in a hot water bath. [c]The chromogen PPDT-TAS was prepared in 4% hydrofluoric acid. [d]Potassium dichromate titrant (1 ml = 0.1 mg FeO) was used.

Further, if the sample charge is inadequately purged before heating commences, air is trapped within the fresh flux volume (typically of 0.5 ml) and this air volume may contribute as much as 4.4×10^{-4} M oxygen, which is almost equivalent to the amount necessary for total oxidation of iron(II) in the mineral sub-sample. To test this proposition further, high-purity nitrogen was de-oxygenated by a copper trap (heated to 425°C) and also ultra-high purity argon was scrubbed by a magnesium trap (heated at 425°C). The residual oxygen molarity of these gases entering in the combustion tube was estimated to be $<10^{-11}$ M. The results obtained on chromite (see Table 4) were inconclusive, mainly because of the additional oxidizing effect of the flux on the sample (ca. 40%). The discolouration of copper in the nitrogen flow and the formation of MgO smoke in a dry ice trap from the argon flow were positive evidence of effective removal of trace oxygen impurities. The use of argon was undesirable because of the frequent formation of powerful plasmas over the sample crucible in the high plate-current r.f. induction furnace.

TABLE 4

Constant-current potentiometry ($Li_2O \cdot 2B_2O_3$ micro-fusion)

Sample	Weight (mg)	FeO found (%)	Remarks/conditions
Hedenbergite standard	11.58	19.69	HF/H_2SO_4 dissolution
	7.59	20.09	Av. = 19.958% FeO
	6.11	19.87	RSD = 1.12%
	6.54	20.18	
	9.285	17.49	$Li_2O \cdot 2B_2O_3$; high-purity N_2
	9.083	15.91	
	8.717	15.97	
	9.165	16.92	
Basalt BHVO-1	12.66	8.75	$HF + H_2SO_4$ dissolution
	18.19	8.76	Av. = 8.759%
	15.40	8.78	RSD = 0.17%
Chrome Ore BCS 308	3.4035	10.28	High-purity N_2
	3.1515	8.15	
	8.206	10.15	15-min fusion: unfused residue (industrial N_2)
	8.532	7.63	30-min fusion: oxidation
	3.3820	11.93	Perfect fusion, Ar, Mg trap (425°C)
	4.048	7.92	Powerful plasma generated and sustained throughout. Dry ice trap collected MgO
	4.333	8.34	
	3.5295	8.37	High-purity N_2; Cu trap (425°C)
	2.6490	9.84	

Conclusion

The micro-fusion of chemically resistant minerals in an inert atmosphere for the determination of FeO (and the oxidation state) is a difficult and challenging problem. None of the exploratory findings produced a satisfactory analytical method for FeO. However, the lithium tetraborate micro-fusion (see above) should be very useful for total iron determinations by a.a.s. A study of sample fusion in an oxygen-free atmosphere showed that rigorous exclusion of air was mandatory. Previously the fluxes and acids used were presumed to be non-oxidizing, but sample oxidation occurred during fusion. It appears that any chemical agent possessing structurally bound oxygen can act as an oxidant in the molten flux chemistry with r.f. induction heating. Oxygen-free fluxes such as alkali fluorides presented their own problems, relating to equipment design. The experimentally defined reduction/oxidation (apparent spontaneous transformation) of iron(II) complexes in the spectrophotometric reactions is an additional uncertainty.

Work is continuing in a new direction, based on phosphoric acid dissolution of chrome-bearing spinels in the presence of cerium(IV). Preliminary results of this micro-analytical approach are very promising.

The author thanks Mr. R. Rudowski for kindly separating some of the important minerals for this work and Dr. Joyce Fildes for reading the manuscript. The keen interest of Dr. H. O'Neill and Dr. M. McCulloch against all odds helped this project to evolve to the present level.

REFERENCES

1 M. H. Hey, Mineral. Mag., 26 (1941) 116.
2 M. H. Hey, Mineral. Mag., 39 (1974) 895.
3 H. N. S. Schafer, Analyst, 91 (1966) 755.
4 J. A. Maxwell, Rock and Mineral Analysis, Wiley-Interscience, New York, 1968, p. 202.
5 E. Kiss, Anal. Chim. Acta, 72 (1974) 127.
6 E. Kiss, Anal. Chim. Acta, 161 (1984) 231.
7 E. Kiss, Anal. Chim. Acta, 89 (1977) 303.
8 M. H. Hey, Mineral. Mag., 46 (1982b) 512.
9 N. Serpone, G. Ponterini, M. A. Jamieson, F. Bolletta and M. Maestri, Coordination Chem. Rev., 50 (1983) 209.
10 G. Nord, B. Petersen and E. Bjergbakke, J. Am. Chem. Soc., 105 (1983) 1913.
11 R. D. Gillard, Mineral. Mag., 49 (1985) 101.

Analytica Chimica Acta, 193 (1987) 325—330
Elsevier Science Publishers B.V., Amsterdam — Printed in The Netherlands

Short Communication

FORMATION AND REDUCTION OF MOLYBDOTHOROPHOSPHORIC ACID

M. BALÓN* and M. A. MUÑOZ

Department of Applied Physical Chemistry, Faculty of Pharmacy, University of Seville, Seville (Spain)

(Received 22nd May 1986)

Summary. The stoichiometry of formation and the kinetics of reduction of molybdothorophosphoric acid in nitric acid solutions were studied spectrophotometrically. The Mo:Th:P ratio in the complex is 12:1:1, assuming that Mo(VI) exists in acid solutions as a dimer. The ternary heteropoly acid is more stable and is reduced more slowly to the heteropoly blue than 12-molybdophosphoric acid. The kinetics of the first stages of the reduction were studied with ascorbic acid and *p*-methylaminophenol as reductants. The experimental rate law is in good agreement with a mechanism involving an equilibrium step in formation of the heteropoly acid followed by the reduction. Under recommended conditions, Beer's law was obeyed up to 40 mg l^{-1} thorium.

Methods have been reported for determining thorium based on the formation [1] and reduction [2] of a thorium molybdophosphoric acid. These methods require strict control of time and pH, and removal of the interference of the simultaneously formed 12-molybdophosphoric acid (12-MPA). The formation of the molybdothorophosphoric acid, MThPA, was investigated [1], but there are no data for the kinetics of the reduction reaction. These kinetics were studied here, to clarify the nature and composition of MThPA and to provide a theoretical basis for improving the existing analytical methods.

Experimental

Reagents. Stock molybdate solutions were prepared from reagent-grade $Na_2MoO_4 \cdot 2H_2O$ and stored in polyethylene bottles. Working solutions were made from the nitrate and used immediately, or prepared in nitric acid to ized nitric acid. Phosphate solutions were prepared from reagent-grade, oven-dried dipotassium hydrogenphosphate. Stock thorium solutions were made from the nitrate and used immediately, or prepared in nitric acid to avoid hydrolysis. Ascorbic acid and *p*-methylaminophenol sulphate were used as reductants. Ascorbic acid solutions were prepared just prior to use. All other reagents were of analytical grade.

Spectrophotometric measurements. Spectrophotometric measurements of the formation of MThPA were made with a Beckman DBGT spectrophotometer, equipped with digital readout, at 350 nm, at which it was shown that

0003-2670/87/$03.50

Beer's law is obeyed. All measurements were made against distilled water as reference.

For the kinetic measurements, the desired solution, without the reductant, was prepared in a standard flask, and a portion was pipetted into an absorption cell. After a wait of a few minutes for temperature equilibration (to 25.0 ± 0.1°C), the reductant was injected into the cell with a micropipette to initiate the reaction. The absorbance of the heteropoly molybdenum blue formed was monitored at 700 nm.

Results and discussion

Addition of thorium to the yellow solution of 12-MPA enhances the colour, and this has been attributed to formation of a ternary molybdothorophosphoric acid [1]. This heteropoly acid can be separated from 12-MPA by extracting the latter with n-butyl acetate. To find the conditions under which 12-MPA is not formed to any appreciable extent, several mixtures of 12-MPA stock solution were prepared with thorium solutions of different concentrations. A small volume of each mixture was extracted with n-butyl acetate, the layers were separated and both phases were examined spectrophotometrically at 350 nm. The results showed that the absorbances of the aqueous phase increased and those of the organic phase diminished with increasing thorium concentration. For Th:P ratios $\geqslant 1$, the ternary heteropoly acid was practically the only complex formed, and therefore, solutions with a slight excess of thorium were used whenever possible.

The formation of MThPA, like that of 12-MPA, is very pH-dependent. Both heteropoly acids are decomposed in very dilute and very concentrated acid solutions. However, MThPA is more stable over a wider pH range, as shown in Fig. 1. Within defined concentration limits, solutions of MThPA behave in accordance with Beer's law. The molar absorptivity is $(7.98 \pm 0.27) \times 10^3$ l mole^{-1} cm^{-1} at 350 nm. This value was obtained by forcing the reaction to completion with a large excess of molybdenum(VI) and thorium(IV), the concentration of MThPA being assumed then to be equal to that of the phosphate taken.

Stoichiometry studies. The binary element ratios in MThPA were studied by preparing a series of solutions isomolar with respect to thorium and phosphorus but containing an excess of molybdate, and a series with various concentrations of molybdate but constant equimolar concentrations of phosphate and thorium. The solutions were extracted with n-butyl acetate and the absorbances of the aqueous layers were measured. The former solutions showed (Fig. 2) that the maximum absorbance corresponded to Th:P = 1:1. Although it is difficult to measure the exact Mo:P ratio in MThPA, because it is so large, the series with equal thorium and phosphorus concentrations showed a maximum at Mo:P = 12 (Fig. 3).

To establish the effect of nitric acid, the procedure used was the same as that used by Crouch and Malmstadt in their study of 12-MPA [3], based on measurement of the concentration of MThPA formed when the reactants are

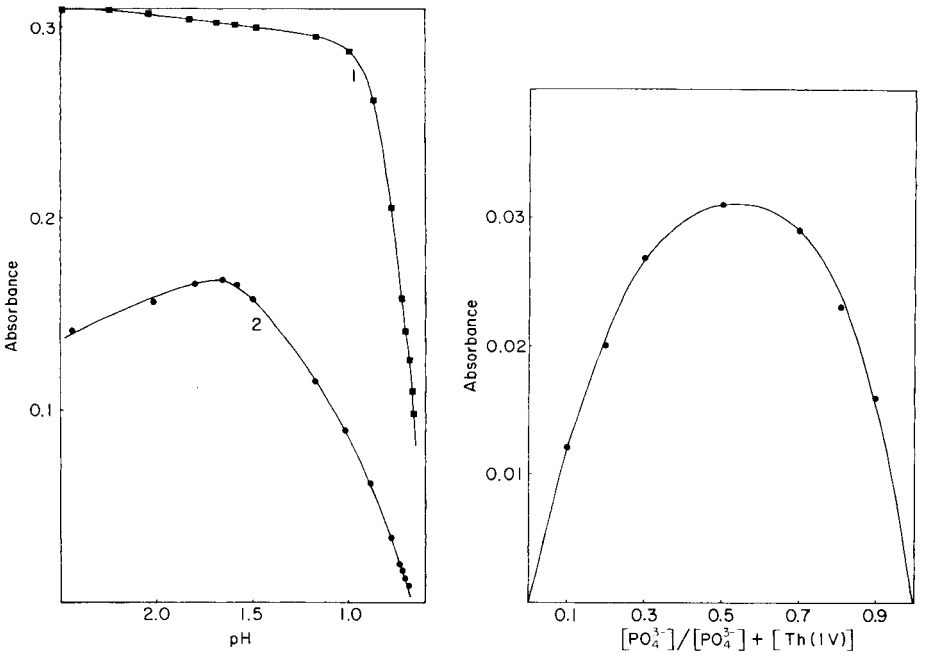

Fig. 1. Influence of pH on the formation of molybdothorophosphoric (1) and molybdophosphoric (2) acids. [Mo(VI)] = 2×10^{-3} M, $[PO_4^{3-}]$ = [Th] = 4×10^{-5} M.

Fig. 2. Th:P ratio in MThPA. [Mo(VI)] = 2×10^{-3} M, $[HNO_3]$ = 0.279 M, $[PO_4^{3-}]$ + [Th] = 5×10^{-5} M.

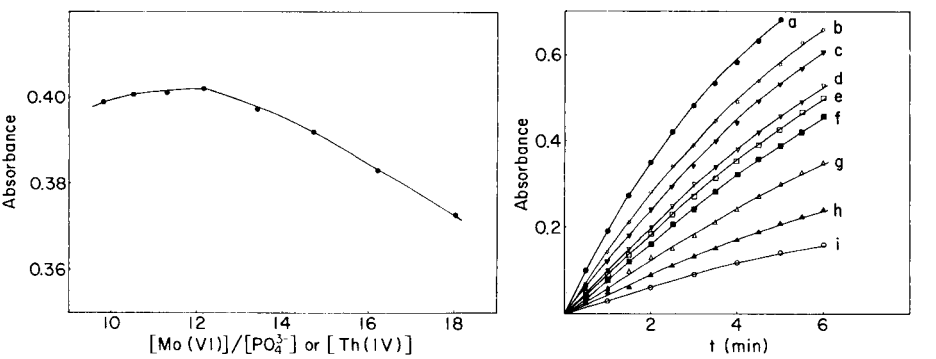

Fig. 3. Mo:P or Th ratio in MThPA. $[HNO_3]$ = 0.248 M, [Th(IV)] = $[PO_4^{3-}]$, [Mo(VI)] + [Th(IV)] + $[PO_4^{3-}]$ = 2.5×10^{-3} M.

Fig. 4. Absorbance vs. time at different phosphate or thorium concentrations. In all cases, [Mo(VI)] = 2×10^{-3} M, $[HNO_3]$ = 0.242 M, [ascorbic acid] = 7.5×10^{-3} M. Thorium concentration (M): (a) 1×10^{-5}; (b) 2×10^{-5}; (c) 3×10^{-5}; (d) 4×10^{-5}; (e—i) 5×10^{-5}. Phosphate concentration (M): (a—e) 5×10^{-5}; (f) 4×10^{-5}; (g) 3×10^{-5}; (h) 2×10^{-5}; (i) 1×10^{-5}.

mixed under conditions such that the extent of reaction is kept small. By varying the concentration of nitric acid while keeping the other concentrations constant, and plotting log absorbance (350 nm) vs. log nitric acid concentration, a straight line with slope of -9.1 ± 0.7 was obtained.

To confirm the stoichiometry of MThPA, some of its salts were prepared and examined. A solution of thorium nitrate was added slowly with stirring to a freshly prepared solution of 12-MPA until a mixture equimolar in phosphorus and thorium was obtained. This resulted in a rapid colour change from orange-yellow to lemon yellow. The mixture was kept for a few minutes at ca. 80°C, filtered and cooled. The caesium and ammonium salts of MThPA were precipitated by adding an excess of concentrated aqueous solutions of caesium nitrate and ammonium molybdate, respectively, to the MThPA. The fine yellow precipitates were filtered off, washed repeatedly with dilute nitric acid and ether, dried in air and then at 110°C, and analysed. Thorium was determined by the arsenazo method [4], phosphate spectrophotometrically as molybdenum blue [5] and molybdate by titration with lead nitrate, with PAR as indicator [6]. The following Th:P:Mo mole ratios were established for the solid salts; 1:1.02:12.2 (caesium salt) and 1:0.96:11.9 (ammonium salt). Because molybdenum exists as a dimeric cation in fairly acidic solutions [7, 8], the following partial equilibrium is likely for MThPA formation:

$$H_3PO_4 + Th(IV) + 6[Mo(VI)]_2 \rightleftharpoons 12\text{-MThPA} + 9H^+$$

The existence of heteropoly anions of zirconium [9] and titanium [10] with similar stoichiometry has been proposed previously.

Kinetic measurements. The rate of reduction of 12-MThPA to a heteropoly blue was investigated in nitric acid media, with ascorbic acid and *p*-methylaminophenol as reductants. Initial reaction rates were measured in experiments for which the reactant concentrations were varied independently. Because the concentrations of the heteropoly blue were unknown, rate constants were expressed as the change in absorbance per unit time ($\Delta A/\Delta t$). In preliminary experiments, it was found that the initial reaction rates diminished with increasing Th:P ratio and approached a constant value for Th:P $\geqslant 1$ (Fig. 4). This is evidence that 12-MThPA is reduced more slowly than 12-MPA.

Reaction orders were obtained by least-squares regression of the slopes of plots of log (initial rate) vs. log (initial concentration of the reagent varied). Table 1 summarizes the conditions used, which were adjusted so that the 12-MThPA concentrations formed prior to reduction were small. The initial concentrations of reactants were thus approximately equal to the analytical initial concentrations. When these conditions were not maintained, the dependence of the reaction rate on the initial phosphate and molybdate concentrations began to deviate from the orders indicated. In kinetic measurements for the determination of reaction order with respect to thorium, the phosphate and thorium concentrations were varied simultaneously, but with Th:P kept constant at 10.

TABLE 1

Reaction orders for 12-MThPA reduction

Variable	$[PO_4^{3-}]$ (10^{-5} M)	[Th(IV)] (10^{-5} M)	[Mo(VI)] (10^{-3} M)	$[HNO_3]$ (M)	[Reductant] (10^{-3} M)	Reaction order[a]
PO_4^{3-}	2.0—5.0	5.0	2.0	0.242	7.5[b]	1.0 ± 0.1
Th(IV)	0.5—3.0	5.0—30	1.0	0.138	7.5[b]	1.0 ± 0.1
Mo(VI)	4.0	4.0	1.4—2.2	0.242	7.5[b]	5.8 ± 0.4
HNO_3	4.0	4.0	2.0	0.501—0.194	7.5[b]	−9 → 0
Ascorbic	10.0	10.0	10.0	0.808	0.1—1.0[b]	0.9 ± 0.1
Ascorbic	4.0	4.0	2.6	0.404	3.0—15[b]	0
p-Methyl	4.0	4.0	2.0	0.250	0.02—0.5[c]	(0.5 ± 0.0) → 0

[a]Ranges given are the confidence limits of the regression coefficient at the 95% confidence level. [b]Ascorbic acid. [c]*p*-Methylaminophenol, to which 7.5 g l^{-1} $NaHSO_3$ was added.

The effect of nitric acid on the rate of reaction was very marked; at high acidities, the reaction rate was inverse ninth order with respect to hydrogen ions, whereas at low acidities the reaction rate was essentially independent of acidity. The experimental results can be expressed according to the following rate equations. At high acidity,

$$d[\text{blue}]/dt = k\,[H_3PO_4]\,[\text{Th}]\,[\text{Mo(VI)}]^6[\text{red}]^n/[H^+]^9$$

At low acidity,

$$d[\text{blue}]/dt = k'[H_3PO_4]\,[\text{Th}]\,[\text{Mo(VI)}]^6$$

where blue represents the reduced heteropoly acid, red the reductant, $n = 1$ for ascorbic acid or $n = 0.5$ for *p*-methylaminophenol, and [Mo(VI)] represents the total molybdenum concentration.

The results expressed in these equations are similar to those obtained by Crouch and Malmstadt [3] for the reduction of 12-MPA. Hence it can be concluded that reductions of 12-MPA and 12-MThPA obey similar kinetics and proceed by a similar mechanism. A standard kinetic derivation, applying a steady-state assumption to 12-MThPA, gives the following rate equation:

$$d[\text{blue}]/dt = k_1[H_3PO_4]\,[\text{Th}]\,[\text{Mo(VI)}]^6/\left\{(k_{-1}\,[H^+]^9/k_2\,[\text{red}]^n) + 1\right\}$$

This equation can be expressed in two limiting forms. At high acidities, $k_{-1}\,[H^+]^9/k_2\,[\text{red}]^n \gg 1$, so

$$d[\text{blue}]/dt = (k_1\,k_2/k_{-1})\left\{[H_3PO_4]\,[\text{Th}]\,[\text{Mo(VI)}]^6\,[\text{red}]^n/[H^+]^9\right\}$$

At low acidities, $k_1\,[H^+]^9/k_2\,[\text{red}]^n \ll 1$, so

$$d[\text{blue}]/dt = k_1\,[H_3PO_4]\,[\text{Th}]\,[\text{Mo(VI)}]^6$$

where k_1 and k_{-1} are the rate constants for formation and dissociation of 12-MThPA and k_2 is the reduction rate constant. These equations agree with

the experimental rate equations obtained above if a dimeric molybdenum species is assumed.

Analytical considerations. The results of the study of stoichiometry and kinetics have several interesting implications for thorium determination based on these reactions. For methods based on formation or reduction of 12-MThPA, a critical problem is the removal of the 12-MPA simultaneously formed under the conditions necessary for thorium determination ([Th] < [P]). Although different procedures based on extraction [1] or destruction [2] of 12-MPA have been proposed, difficulties were encountered in its complete elimination in highly acidic media. Moreover, the solution acidity must be carefully controlled because the equilibria and rates show a marked dependence on acidity. To obtain reproducible and accurate results, the complex should be formed at low acidities (pH > 2), at which 12-MPA formation is less favoured and the reduction proceeds rapidly and is independent of acidity. At pH near to 5, the quantity of 12-MPA formed can be considered negligible even when the ternary heteropoly concentration is appreciable.

Absorbances of standard solutions containing molybdate (1×10^{-2} M), nitric acid (0.07 M), phosphate (1×10^{-3} M), and suitable quantities of thorium, adjusted to pH 5.1 with acetic acid/acetate buffers, were measured at 400 nm. A straight-line calibration graph was obtained up to 40 μg ml^{-1} thorium. The molar absorptivity over this range was $(2.5 \pm 0.1) \times 10^3$ l mole^{-1} cm^{-1}.

The authors are indebted to Prof. Daniel Rosales for the analysis of the caesium and ammonium salts of the ternary heteropoly acids.

REFERENCES

1 K. Murata, Y. Yokoyama and S. Ikeda, Anal. Chim. Acta, 48 (1969) 349.
2 B. L. Madison and J. C. Guyon, Anal. Chem., 39 (1967) 1706.
3 S. R. Crouch and H. V. Malmstadt, Anal. Chem., 39 (1967) 1084.
4 J. Fries and H. Getrost, in E. Merck (Ed.), Organic Reagents for Trace Analysis, Darmstadt, 1977. pp. 360, 361.
5 M. Jean, Anal. Chim. Acta, 14 (1956) 172.
6 I. M. Kolthoff and P. J. Elving, Treatise on Analytical Chemistry, Part II, Vol. 10, Wiley, New York, 1978, p. 337.
7 Y. Sasaki and L. G. Sillen, Acta Chem. Scand., 18 (1964) 1014.
8 P. Souchay, Pure Appl. Chem., 6 (1963) 61.
9 Y. F. Shkaravskii, Russ. J. Inorg. Chem., 11 (1966) 64.
10 A. K. Babko and Y. F. Shkaravskii, Russ. J. Inorg. Chem., 6 (1961) 1068.

Analytica Chimica Acta, 193 (1987) 331—336
Elsevier Science Publishers B.V., Amsterdam — Printed in The Netherlands

Short Communication

SPECTROPHOTOMETRIC DETERMINATION OF CHLORIDE IN NON-POLAR MEDIA BY THE MERCURY(II) THIOCYANATE REACTION

B. VEKIĆ* and D. RAŽEM

Radiation Chemistry and Dosimetry Laboratory, Ruđer Bošković Institute, 41000 Zagreb (Yugoslavia)

(Received 24th June 1986)

Summary. A simple, rapid and accurate method for the spectrophotometric determination of chloride in non-polar media is described. The method is based on the well-known reaction of mercury(II) thiocyanate with chloride to release thiocyanate, which then reacts with iron(III). The optimum concentrations of reagents for the determination of chloride in 2,2,4-trimethylpentane (iso-octane) and cyclohexane are reported. The molar absorptivity of the complex at 505 nm is 5120 ± 200 dm^3 mol^{-1} cm^{-1} for iso-octane and 5340 ± 340 dm^3 mol^{-1} cm^{-1} for cyclohexane. Beer's Law is obeyed in the range 2×10^{-7}—2×10^{-5} mol dm^{-3} (0.01—1 mg l^{-1}) chloride.

Numerous methods are available for determining trace amounts of chloride in aqueous solutions and some other polar media, but none is really suitable for the determination of trace quantities of chloride in non-polar media. Known methods such as the potentiometric determination of chlorides in solutions of chlorobenzene in n-hexane [1], or conductometric determination of chlorides in petroleum [2], as well as other electroanalytical techniques generally lack the required sensitivity and simplicity. Because of this, the work reported here was aimed at developing a simple, rapid and accurate determination of radiolytically produced chloride in solutions of chlorobenzene in iso-octane [3].

Spectrophotometric measurements appeared to be the most convenient for this purpose. Among the spectrophotometric determinations of trace amounts of chloride, one of the best known is the method based on the displacement of thiocyanate from mercury(II) thiocyanate by chloride, and subsequent reaction of the liberated thiocyanate with iron(III) to form a reddish-orange iron(III)-thiocyanate complex [4, 5]. This method has been in widespread use for the determination of chloride in high-purity waters and different aqueous solutions [4—9], corrosion products, concentrated hydrogen peroxide and even polyethylene and naphtha [5]. Application to organic materials, however, usually requires a time-consuming separation or decomposition prior to the final measurement in aqueous solution.

The mercury(II) thiocyanate method has also been used for the determin-

ation of chloride in ethylene glycol and water-soluble alcohols [10] and in ethanol [11, 12]. Ražem et al. [11] made a systematic investigation of the solution variables in ethanol, which were found to be different compared to aqueous media [9]. The most important was that the sensitivity of the method increased significantly in ethanol, and it was reasonable to expect additional increase in sensitivity in less polar media.

Experimental

Apparatus and reagents. A Cary 17 spectrophotometer was used with 5-cm or 10-cm cells for all absorbance measurements and for recording absorption spectra.

All reagents were of analytical-reagent grade and were used as received.

For the iron(III) reagent, 7.55 g of iron(III) nitrate nonahydrate was dissolved in 5.25 mol dm^{-3} perchloric acid to obtain 100 ml of aqueous 0.187 mol dm^{-3} iron(III) nitrate, which was stored in a dark bottle.

A 1.5×10^{-3} mol dm^{-3} solution of mercury(II) thiocyanate was prepared by dissolving 475.15 mg of the salt in 1 l of absolute ethanol. Ultrasonic vibration for 2 h was used to ensure complete dissolution; 200 ml of this solution was diluted to 1 l with absolute ethanol to prepare a 3×10^{-4} mol dm^{-3} solution. This solution was used in the procedure; it was kept in a dark bottle.

For the chloride standard solution (6×10^{-5} mol dm^{-3}) 43.83 mg of sodium chloride (dried at 110°C for 2 h) was dissolved in 500 ml of absolute ethanol (ultrasonic vibration for 2 h) and 20 ml of this solution was diluted to 500 ml with absolute ethanol.

Procedures. Place 5 ml of absolute ethanol in a 25-ml volumetric flask, add 0.55 ml of 72% perchloric acid followed by 0.1 ml of 0.187 mol dm^{-3} iron(III) nitrate, 3.5 ml of 3×10^{-4} mol dm^{-3} mercury(II) thiocyanate, and 5 ml of iso-octane or cyclohexane, in that order. Prepare solutions for measurements by adding appropriate volumes of the chloride-containing hydrocarbons and then dilute to 25 ml with absolute ethanol. Mix well and keep for 5 min to develop the colour. Measurements must be made at 20°C. Fill the 5-cm cells and leave them in the cell compartment of the spectrophotometer for 15 min before taking measurements, to allow sufficient time for thermal equilibrium. Measure the absorbance at 505 nm against a blank which contains all the components as the sample except chloride.

If the concentration of chloride is below 2×10^{-6} mol dm^{-3}, prepare the final solution in a 50-ml volumetric flask. Use double volume of the same standard solutions as above and in the same order. Mix well and develop the colour for 10—15 min. Measure the absorbance against the blank in 10-cm cells after the cells have been in the cell compartment for another 15 min.

Results

The indirect spectrophotometetric determination of trace amounts of chlorides based on the reaction of iron(III) with the liberated thiocyanate

ions in water and ethanol solutions has been well characterized. However, in the application of the method to non-polar media such as iso-octane and cyclohexane, it was necessary to implement considerable modifications. The reagents, especially iron(III) nitrate, are not soluble in non-polar media, and the perchloric acid does not mix with iso-octane or cyclohexane. It was therefore necessary to add a large volume of absolute ethanol and minimal quantities of water (i.e., inorganic acid) to the final solution. The sample containing chloride had to be diluted so that the final solution contained 20% (v/v) of iso-octane or cyclohexane and up to 3% (v/v) of water in absolute ethanol.

Effects of reagent concentrations. Figure 1 shows the effect of mercury(II) thiocyanate concentration in iso-octane and cyclohexane on the determination of 6×10^{-6} mol dm^{-3} chloride. Maximum absorbance was obtained with about 4.2×10^{-5} mol dm^{-3} mercury(II) thiocyanate, and higher concentrations caused a slight but constant decrease in the absorbance. Similar, although less sharp, were the effects of the iron(III) (Fig. 2) and perchloric acid (Fig. 3) concentrations. The optimum concentrations were 7.5×10^{-4} mol dm^{-3} and 0.26 mol dm^{-3} for iron(III) and perchloric acid, respectively.

Absorption spectra and calibration. The absorption spectra of the iron(III)-thiocyanate complex under the conditions recommended showed the usual broad band at around 505 nm. The colour developed within 5 min and was stable for 30 min in normal light and for days if stored in the dark. With solutions of optimal composition, the molar absorptivity for chloride was evaluated at 20°C, which was approximately ambient temperature. Large

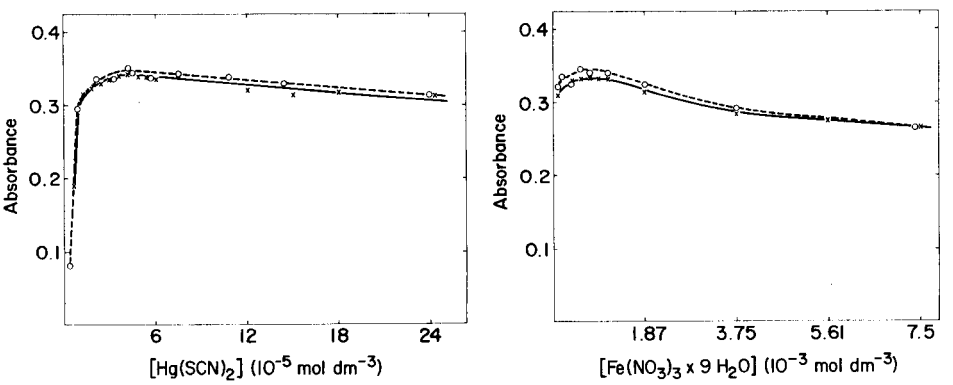

Fig. 1. The effect of mercury(II) thiocyanate concentration on the absorbance of the $FeSCN^{2+}$ complex in iso-octane (×) and cyclohexane (○). Conditions: 6×10^{-6} mol dm^{-3} NaCl, 0.26 mol dm^{-3} $HClO_4$, 7.5×10^{-4} mol dm^{-3} $Fe(NO_3)_3$; 10-cm cells.

Fig. 2. The effect of iron(III) concentration on the absorbance of the $FeSCN^{2+}$ complex in iso-octane (×) and cyclohexane (○). Conditions as for Fig. 1 except for 4.2×10^{-5} mol dm^{-3} $Hg(SCN)_2$ and variable iron(III) content.

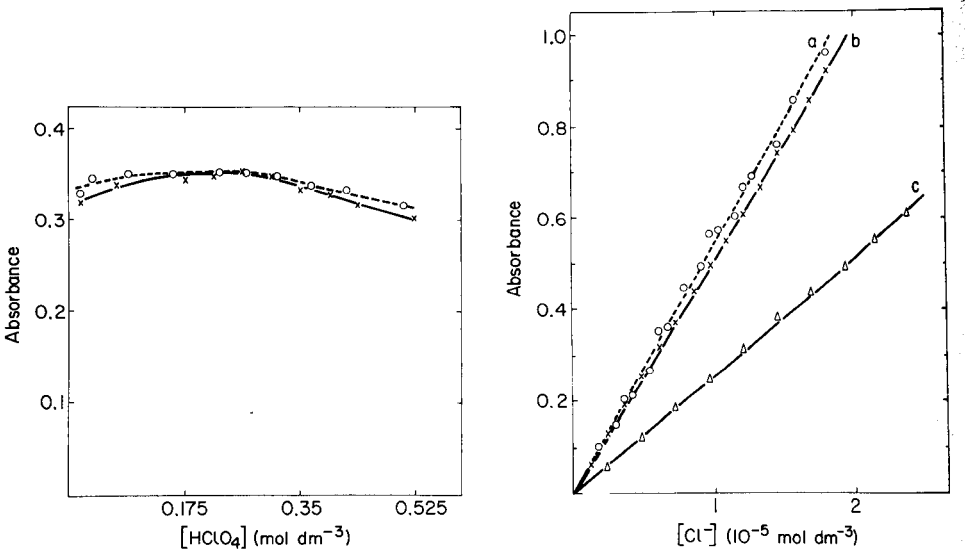

Fig. 3. The effect of perchloric acid concentration on the absorbance of the $FeSCN^{2+}$ complex in iso-octane (×) and cyclohexane (○). Conditions: 6×10^{-6} mol dm^{-3} NaCl, 4.2×10^{-5} mol dm^{-3} $Hg(SCN)_2$, 7.5×10^{-4} mol dm^{-3} $Fe(NO_3)_3$; 10-cm cells.

Fig. 4. Calibration graphs obtained for chloride in different media: (○) cyclohexane (10-cm cells); (×) iso-octane (10-cm cells); (△) iso-octane (5-mm cells). Conditions: 4.2×10^{-5} mol dm^{-3} $Hg(SCN)_2$, 0.26 mol dm^{-3} $HClO_4$, 7.5×10^{-4} mol dm^{-3} $Fe(NO_3)_3$.

variations of temperature affected the absorbance, which decreased with increasing temperature.

The molar absorptivity obtained for iso-octane solutions from 81 measurements in 5-cm cells, and 31 measurements in 10-cm cells, in the concentration range 2×10^{-6}—2×10^{-5} mol dm^{-3} chloride (Fig. 4) was 5120 ± 200 dm^3 mol^{-1} cm^{-1}. The value obtained for cyclohexane from 33 measurements in the same concentration range was 5340 ± 340 dm^3 mol^{-1} cm^{-1}. Beer's law was obeyed and was valid over the range 2×10^{-7}—2×10^{-5} mol dm^{-3} (0.01—1 mg l^{-1}) chloride. The precision of the measurements decreased with decreasing concentration of chloride. At 2×10^{-6} and 5×10^{-7} mol dm^{-3} chloride, the relative standard deviations from 10 measurements were 2.2% and 9.0%, respectively.

Discussion

The reaction between chloride, mercury(II) thiocyanate and iron(III) was first proposed for the determination of chloride in water by Iwasaki et al. [4]. Since then, considerable modifications of the method have been adopted. Acetone, having a low dielectric constant, was shown to intensify the colour [6]. A similar effect was observed in ethanolic media [5, 11, 12]. Lower concentrations of reagents are then required to produce sufficient absorbance. The concentration of iron(III) that gives maximum colouration

TABLE 1

The effect of polarity of the medium on the absorption maximum and molar absorptivity of the iron(III) thiocyanate complex formed

Medium (% v/v)	λ_{max} (nm)	Molar absorptivity ($dm^3\ mol^{-1}\ cm^{-1}$)	Ref.
Water/ethanol, 92/8	460	2600	9
Water/ethanol, 10/90	485	3990 ± 60	11
Water/ethanol/iso-octane, 3/77/20	505	5120 ± 200	This work
Water/ethanol/cyclohexane, 3/77/20	505	5340 ± 340	This work

in ethanol, or in iso-octane or cyclohexane, is about 40 times less than in aqueous solution. The concentration of mercury(II) thiocyanate needed is also much smaller (about a quarter). The absorbance of the complex is sensitive to the type and amount of acid present. Perchloric acid is superior to other inorganic acids [6, 7, 9] and less is needed than in aqueous solutions.

The absorption maximum is displaced from around 460 nm in aqueous solutions and 485 nm in ethanol to 505 nm in iso-octane and cyclohexane. The molar absorptivity is also higher in non-polar media because of displacement of chemical equilibria [12]. Data for absorption maxima and molar absorptivities in different media are given in Table 1. When iron(III) is in large excess, as it is here, published data [13, 14] indicate that $FeSCN^{2+}$ is the only absorbing species. Because of the well-known sensitivity of the metathesis reaction to changes of temperature and reagent concentrations, controlled concentrations of mercury(II) thiocyanate in ethanol are preferred to saturated solutions. In some early work [5, 9, 10], water or ethanol was used instead of a reagent blank in the reference cell. With the non-polar media, it is important to use the same composition of solution in the blank as in the sample (except for chloride) because even spectroscopically pure ethanol may contain some chloride [15]. The method described for determining traces of chloride in solutions of iso-octane or cyclohexane should, with minor modifications, be applicable to other non-polar media.

REFERENCES

1 S. Musić, M. Bonifačić and M. Vlatković, Croat. Chem. Acta, 46 (1974) 89.
2 A. Z. Mitrofanov, Neftepromysl. Delo, No. 2 (1980) 20.
3 B. Vekić, D. Ražem and I. Dvornik, in J. Dobo, P. Hedvig and R. Schiller (Eds.), Proc. 5th Tihany Symp. Radiat. Chem., Akademiai Kiado, Budapest, (1983) 709.
4 I. Iwasaki, S. Utsumi and T. Ozawa, Bull. Chem. Soc. Jpn., 25 (1952) 226.
5 See, e.g., F. D. Snell, Photometric and Fluorimetric Methods of Analysis. Nonmetals, Wiley, New York, 1981, p. 244.
6 D. M. Zall, D. Fisher and M. Q. Garner, Anal. Chem., 28 (1956) 1665.
7 H. N. Elsheimer and R. L. Kochen, Anal. Chem., 38 (1966) 145.
8 Y. Yamamoto, T. Kumamaru, A. Tatehata and N. Yamada, Anal. Chim. Acta, 50 (1970) 433.

9 T. M. Florence and Y. J. Farrar, Anal. Chim. Acta, 54 (1971) 373.
10 R. P. Marquardt, Anal. Chem., 43 (1971) 277.
11 D. Ražem, G. Očić, J. Jamičić and I. Dvornik, Int. J. Appl. Radiat. Isot., 32 (1981) 705.
12 F. J. Krug, L. C. R. Pessenda, E. A. G. Zagatto, A. O. Jacintho and B. F. Reis, Anal. Chim. Acta, 130 (1981) 409.
13 H. E. Bent and C. L. French, J. Am. Chem. Soc., 63 (1941) 568.
14 S. M. Edmonds and N. Birnbaum, J. Am. Chem. Soc., 63 (1941) 1471.
15 R. Belcher, Submicro Methods of Organic Analysis, Elsevier, Amsterdam, 1966, p. 46.

Analytica Chimica Acta, 193 (1987) 337—341
Elsevier Science Publishers B.V., Amsterdam — Printed in The Netherlands

Short Communication

CYCLIC FLOW-INJECTION DETERMINATION OF COPPER WITH HEXADECYLTRIMETHYLAMMONIUM BROMIDE MICELLE-ENHANCED, FLUORESCEIN-SENSITIZED CHEMILUMINESCENCE DETECTION

MASAAKI YAMADA* and SHIGETAKA SUZUKI

Department of Industrial Chemistry, Faculty of Technology, Tokyo Metropolitan University, Setagaya-ku, Tokyo 158 (Japan)

(Received 24th June 1986)

Summary. In the flow-injection system reported, the reagent stream is continuously cycled. The circulating chemiluminescence reagents (β-nitrostyrene/NaOH/hexadecyltrimethylammonium bromide sensitized with fluorescein) allowed 0.1—10 ng of copper(II) to be determined in hundreds of successive injections, even with samples of sea water or a solution of zinc dust.

Flow-injection analysis (f.i.a.) with chemiluminescence detection has received much attention in recent years [1]. This evolves from the attractive features of combining the advantages of chemiluminescence detection (high sensitivity, wide dynamic range, simple instrumentation, etc.) with the rapidity, simplicity, and reproducibility of f.i.a. Nevertheless, the combined system is slow to achieve recognition. The reason seems to lie mostly in the detection itself, i.e., its often poor selectivity and the paucity of usable chemiluminescence systems. Accordingly, the search for new chemiluminescence systems of high selectivity is essential for wider acceptance of the method. Recent efforts have been devoted to seeking new reactions. Several systems have been developed which use organized surfactant molecular assemblies (micelles or bilayer vesicles) [2—6]. During this work, a frequently encountered dilemma was that effective detection of the emission from a fast chemiluminescence reaction required a high flow rate of reagent solution, resulting in considerable reagent consumption. This stimulated attempts to cycle the reagent solution. This would have the advantage of permitting long-running of the flow system without additional supply of reagent solution, although there is a limit in that the system must consist of a single flow line.

This communication reports preliminary investigations on such a cyclic chemiluminescence flow-injection method for the determination of copper(II). A new chemiluminescence system, β-nitrostyrene/NaOH/hexadecyltrimethylammonium bromide (CTAB)/fluorescein, is utilized. Light emission arises from the copper(II)-catalyzed oxidation of β-nitrostyrene by dissolved

0003-2670/87/$03.50

oxygen in the alkaline CTAB micellar solution, to which fluorescein is added as sensitizer.

Experimental

Apparatus. A schematic diagram of the flow system is given in Fig. 1. A CTAB micellar solution (100 ml) containing β-nitrostyrene, sodium hydroxide, and fluorescein is circulated by a peristaltic pump (P). Copper(II) and other species are injected by means of a 20-μl rotary valve injector (S). A spiral flow cell D is assembled as described previously [7]. Teflon tubing (1 mm i.d.) is used for the flow line except for the pump tube and flow cell. The distance between S and D is ca. 5 cm (the minimum distance achieved) for effective detection of the light emission arising from the fast chemiluminescent reaction. The light emitted is observed directly by a photomultiplier tube (Hamamatsu Photonics R453) with no wavelength discrimination.

Reagents. Chemicals of reagent grade were used as received. β-Nitrostyrene was dissolved in CTAB micelles by use of an ultrasonic bath (Bransonic 220). This solution was freshly prepared.

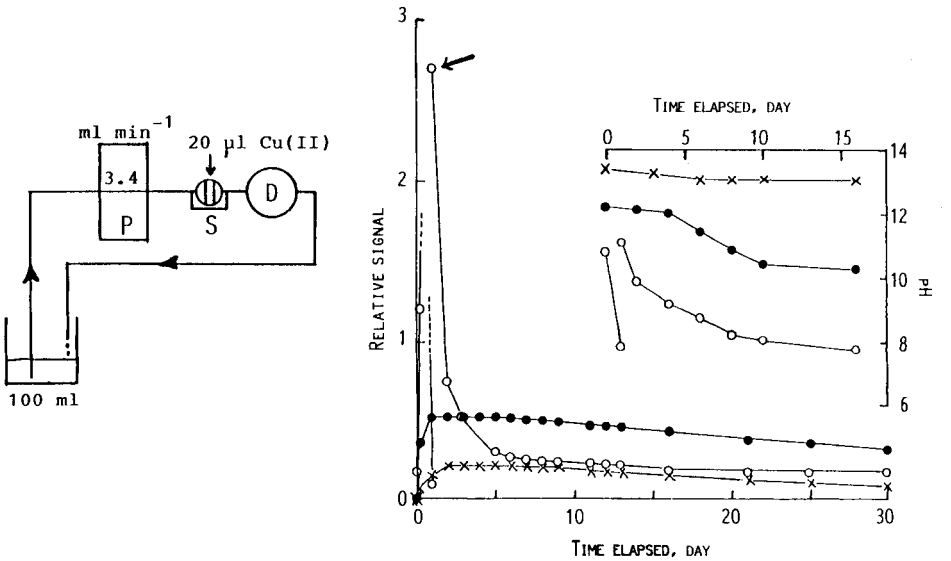

Fig. 1. Diagram of the cyclic flow-injection system with chemiluminescence detection. Operating conditions: 1×10^{-3} M β-nitrostyrene, 1×10^{-2} M NaOH, 5×10^{-3} M CTAB, 4×10^{-5} M fluorescein; flow rate 3.4 ml min^{-1}; 20-μl injections.

Fig. 2. Effect of age of reagent solution on the relative signal for copper. NaOH concentration (M): (○) 1×10^{-3}; (●) 1×10^{-2}; (×) 0.1. Other conditions as in Fig. 1; for explanation of arrow, see text. The relevant pH changes are shown in the inset.

Results and discussion

Stability of the reagent solution. To achieve a satisfactory system, the reagent solution circulated must be stable, so that the chemiluminescence signal will be unchanged when the system runs for a long time. The stability of the reagent solution was examined over a month by monitoring the signal for 1×10^{-6} M copper(II). The results (Fig. 2) indicate that the stability depends strongly on the sodium hydroxide concentration. The higher the alkalinity the greater the stability but the lower the signal. With 1×10^{-3} M alkali, the signal reached a maximum and then decreased rapidly within a day after preparation of the reagent solution. The response was restored to its previous sensitivity on addition of a 1-ml portion of 0.1 M sodium hydroxide (shown by an arrow in the figure) to the solution in the reservoir, but the sensitivity again decreased within a few days. In contrast, the high sodium hydroxide concentrations provided maximum signals within one or two days after preparation. Although the signals were lower than for 10^{-3} M alkali, they remained constant for several days and then decreased gradually over 20 days or more. With 10^{-2} M alkali, the signal after 60 days was ca. 60% of the maximum signal, and this decreased signal could be restored to ca. 90% of the original by addition of 1 ml of 1 M alkali, i.e., decreased sensitivity was improved by addition of more alkali. For further experiments, 1×10^{-2} M sodium hydroxide was chosen because it provided high reagent stability and good sensitivity.

In addition to the stability of the reagent solution itself, its durability to repeated injections of copper(II) solution is also important. The signal for 1×10^{-6} M copper was measured by means of successive injections and 100 injections per day. With successive injections, no signal change was observed during the first 750 injections; the next 250 injections during the following day gave a slightly decreased signal (ca. 90% of the initial value). When 100 injections were made per day, the reagent solution continued to give unchanged signals for 3 days; after 4 days, the signal had decreased to ca. 90% of the initial value, which might have been due partly to the instability of the reagent solution, as shown in Fig. 2. During the experiments, a precipitate of copper(II) hydroxide appeared gradually in the cycling solution.

Characteristics of the β-nitrostyrene chemiluminescence system. Under the conditions specified in Fig. 1, which are not fully optimized for providing the largest chemiluminescence signal for copper, the analytical characteristics of the proposed system were explored. Such operating conditions gave a detection limit (2σ) of 0.1 ng (20-μl injection), the linear (log-log) dynamic range was $>10^2$ above the detection limit, the sample throughput was 200 h^{-1}, and the relative standard deviation (n = 10) was 2.2% for 1 ng of copper. The system is fairly selective for copper. Cobalt(II), the best catalyst after copper(II), gave a signal 4% of that for an equivalent amount of copper; iron(II), chromium(III), nickel(II), iron(III) and manganese(II) provided signals 1, 0.4, 0.4, 0.1, and 0.1%, respectively. Species like chromium(VI), cadmium, zinc and lead gave no emission at submicrogram levels.

Applicability of the cyclic method to real samples. In order to explore the applicability of the method to real samples, sea water and a zinc solution containing copper(II) were injected. The durability of the reagent solution to numerous successive injections of the real samples was examined. The sea-water sample was made 1×10^{-6} M in copper, and was compared with aqueous 1×10^{-6} M copper. The zinc solution (pH 2.7) was prepared by dissolving zinc dust (0.1 g) in hydrochloric acid and diluting to 100 ml; the copper content was found to be 4.8×10^{-6} M by a standard addition method based on the above procedure, a value that was confirmed by flame atomic absorption spectrometry. It was found that the responses from at least 500 injections of the sea-water sample or the aqueous standard were identical and unchanged. For the zinc sample, the signal was unchanged for 400 injections; after 800 injections, the signal had decreased to ca. 60% of its initial value, and the pH of the reagent solution had changed from 12.1 to 11.2. The decrease in signal is probably due to the precipitation of zinc hydroxide; filtration restored the signal to ca. 90% of its initial value. Therefore, during the experiment, a device for removal of any precipitate formed by the matrix element is required.

Mechanism. The chemiluminescence arises from the copper(II)-catalyzed aerobic oxidation of β-nitrostyrene solubilized in CTAB micelles, efficiently sensitized by fluorescein. This was confirmed by the fact that the injection of a 1×10^{-6} M copper(II) solution gave no emission in the absence of β-nitrostyrene but weak emission in the absence of fluorescein. The non-sensitized emission may stem from the chemiluminescent reaction involving the production of superoxide ion. This is supported by the finding that the addition of a superoxide trapper (nitro blue tetrazolium) into the chemiluminescence system completely suppressed the emission. Superoxide ion seems likely to be produced in the alkaline micellar solution during the formation of copper(II) hydroxide, although the mechanistic details are not obvious. No change in light emission was observed on addition of a singlet oxygen trapper (sodium azide or 1,4-diazabicyclo[2.2.2]octane). Therefore, it is likely that singlet oxygen is not involved in the chemiluminescent reaction. However, no satisfactory explanation for the β-nitrostyrene chemiluminescent reaction can be offered.

Conclusions

This preliminary investigation has shown the possibility of cycling a reagent solution in a flow-injection method with chemiluminescence detection. The proposed system is suitable because β-nitrostyrene retains the ability to chemiluminesce over a long period and after numerous sample injections. The reaction products do not interfere in subsequent chemiluminescent reactions. The cyclic system is unusual in that it will run for a long time with no significant consumption of reagent solution. Therefore, it might be very useful in clinical analysis, e.g. for rapid examination of numerous samples and for continuous monitoring during a long surgical operation.

The authors are indebted to Mr. Mikita Ishii, Kyorin University, for the determination of copper(II) in zinc dust by flame atomic absorption spectrometry.

REFERENCES

1 A. Townshend, Anal. Proc., 22 (1985) 370.
2 M. Yamada and S. Suzuki, Anal. Lett., 17 (1984) 251.
3 M. Kato, M. Yamada and S. Suzuki, Anal. Chem., 56 (1984) 2529.
4 M. Yamada, S. Kamiyama and S. Suzuki, Chem. Lett., (1985) 1597.
5 M. Ishii, M. Yamada and S. Suzuki, Bunseki Kagaku, 35 (1986) 373, 379.
6 M. Ishii, M. Yamada and S. Suzuki, Anal. Lett., 19 (1986) 1591.
7 S. Nakahara, M. Yamada and S. Suzuki, Anal. Chim. Acta, 141 (1982) 255.

Analytica Chimica Acta, 193 (1987) 343—347
Elsevier Science Publishers B.V., Amsterdam — Printed in The Netherlands

Short Communication

FLUORIMETRIC DETERMINATION OF NITRATE IN NATURAL WATERS WITH 3-AMINO-1,5-NAPHTHALENEDISULPHONIC ACID IN A FLOW-INJECTION SYSTEM

SHOJI MOTOMIZU*, HIROSHI MIKASA and KYOJI TÔEI

Department of Chemistry, Faculty of Science, Okayama University, Tsushimanaka, Okayama-shi 700 (Japan)

(Received 28th July 1986)

Summary. A rapid, sensitive and precise flow-injection method for the determination of nitrate in natural waters is presented. Nitrate is first reduced in a copperized cadmium column to nitrite, which reacts with 3-amino-1,5-naphthalenedisulphonic acid to form the azoic acid. This acid forms a fluorescent salt in alkaline medium. The injection rate is about 30 h^{-1}, the relative standard deviation for 10 injections of 2×10^{-5} M nitrate is 0.8%, and the detection limit ($S/N = 3$) is 1×10^{-8} M nitrate.

The determination of nitrogen compounds such as nitrate, nitrite and ammonium ions in natural waters is essential in environmental chemistry, geochemistry and limnology. Nitrate in waters has been determined successfully by flow-injection analysis (f.i.a.) [1—7]. Most of the flow-injection determinations of nitrate have been based on the reduction of nitrate to nitrite and spectrophotometry of an azo dye formed by diazotization/coupling reactions.

Previously [8], the authors have reported the spectrofluorimetric determination of nitrite in water by f.i.a., which was based on the formation of the fluorescent azoic acid salt from nitrite and 3-amino-1,5-naphthalenedisulphonic acid (C acid). The method was very sensitive and accurate for the determination of nitrite ion in natural waters. In this communication, the method is adapted for the determination of nitrate in water. The procedure is rapid, sensitive and accurate, and applicable to natural waters.

Experimental

Reagents and solutions. Disodium 3-amino-1,5-naphthalenedisulphonic acid (C acid) (Tokoyo Kasei Kogyo Co.) was used as received. C acid (0.35 g) was dissolved in 100 ml of 0.01 M hydrochloric acid.

For the reagent stream, the solution of C acid (9 ml) was mixed with 3 ml of 0.1 M EDTA, 50 ml of concentrated hydrochloric acid (35% w/w) and 238 ml of distilled water. For the carrier stream, 30 ml of 0.5 M sodium chloride, 3 ml of 0.1 M EDTA and 300 ml of distilled water were mixed and the pH was adjusted to 8.1—8.4 with 6 M sodium hydroxide. The alkali stream was a 20% (w/w) solution of sodium hydroxide.

0003-2670/87/$03.50

A nitrate standard solution was prepared from potassium nitrate, dried at 100—110°C. The stock solution was 1×10^{-3} M. Nitrate working solutions were freshly prepared by diluting the stock solutions.

Apparatus. The fluorescence was measured with a Hitachi 650-10S spectrofluorimeter with an 18-μl flow-through cell, and recorded with a Toa Denpa FBR-251A recorder. Two double-plunger micropumps (Sanuki Kogyo Co.) were used for propelling the reagent, carrier and sodium hydroxide solutions; each stream was at 0.7 ml min^{-1}. The sample was injected by a 6-way injection valve into the carrier stream (sample volume 160 μl). The flow lines were made from teflon tubing (0.5 mm i.d.). The reaction coil (RC_1) was kept in a thermostated bath (90°C). A copperized cadmium reduction column (RC) (particle size of copperized cadmium, 0.5–2 mm) was made from a teflon column (30 cm × 2 mm i.d.), and was installed just behind the sample injection valve.

A diagram of the flow system is shown in Fig. 1.

Results and discussion

Optimum experimental conditions. Concentrations of hydrochloric acid and EDTA in the reagent stream were 2 M and 10^{-3} M, respectively, i.e., the same as those for the determination of nitrite.

In general, nitrate is present in natural waters at concentrations 10—100 times those of nitrite. It is thus necessary to use more concentrated solutions of C acid for nitrate than for nitrite determinations. As nitrate is present in natural waters at concentrations of $\geqslant 10^{-5}$ M, a concentration of 3×10^{-4} M of C acid was chosen for reliability (Fig. 2). When the C acid concentration was 3×10^{-5} M, which is the same as that used for nitrite, nitrate at concentrations below 6×10^{-6} M was quantified with good sensitivity and reproducibility.

The carrier solution contained EDTA and sodium chloride. EDTA promoted the reproducible reduction of nitrate to nitrite. Figure 3 shows the

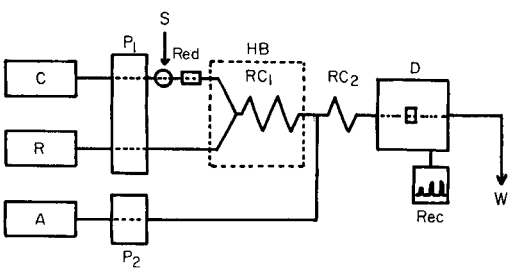

Fig. 1. Schematic diagram of flow system: C, carrier solution (NaCl/EDTA, pH 8.3); R, reagent solution (C acid/HCl); A, alkaline solution (NaOH); P_1 and P_2, plunger type pumps (0.7 ml min^{-1}); S, sample (160 μl); Red, reduction column (Cu/Cd; 2 mm i.d. × 30 cm); HB, heating bath (90°C); RC_1, reaction coil (0.5 mm i.d. × 13 m); RC_2, reaction coil (0.5 mm i.d. × 1 m); D, detector (λ_{ex} = 365 nm, λ_{em} = 470 nm) with 18-μl flow cell; Rec, recorder; W, waste.

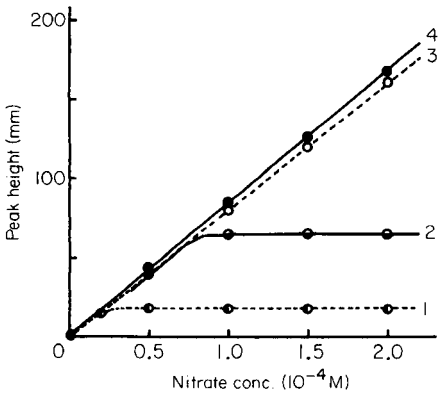

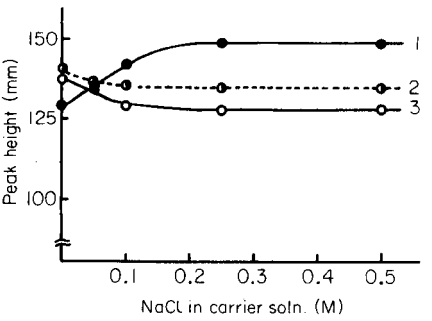

Fig. 2. Effect of C acid concentration on peak heights for nitrate: (1) 10^{-5} M; (2) 3×10^{-5} M; (3) 10^{-4} M; (4) 3×10^{-4} M.

Fig. 3. Effect of sodium chloride in carrier stream on peak heights for nitrate (1.5×10^{-4} M) solutions containing different amounts of sodium chloride: (1) 0; (2) 0.25; (3) 0.50 M.

effect of sodium chloride on the peak heights. With about 0.05 M sodium chloride in the carrier stream, the peak heights for sample solutions of nitrate containing no, 0.25 M and 0.50 M sodium chloride were almost the same as one another; this shows that nitrate in solutions containing $\leqslant 0.5$ M sodium chloride can be quantified accurately by using a carrier stream containing 0.05 M sodium chloride. Thus, nitrate can be determined in both sea water and fresh water.

The length of the reduction column was varied from 10 to 30 cm; a 20-cm length sufficed to reduce nitrate (>98%) to nitrite. For reliability, a 30-cm column was used. The reductor lasted for more than one month when regularly used. Sample injection volumes were 160 μl, which was smaller than that for the determination of nitrite. Other experimental variables such as flow rate, mixing coils, bath temperature, concentration of the alkaline solution and excitation and emission wavelengths were the same as those adopted for nitrite.

Calibration graph, reproducibility and detection limit. The calibration graph was rectilinear up to 2×10^{-4} M nitrate. The relative standard deviation (RSD) of 10 injections of 2×10^{-5} M nitrate was 0.8%, and the detection limit ($S/N = 3$) was about 10^{-8} M nitrate with the recommended sample volume (160 μl) and C acid concentration (3×10^{-4} M). Typical outputs for calibration are shown in Fig. 4. For the determination of smaller amounts of nitrate, a lower concentration of C acid (e.g., 3×10^{-5} M) is used and larger volumes (e.g., 360 μl) of sample solution are injected. With these modifications, the calibration graph was rectilinear up to 5×10^{-5} M and, by using a higher sensitivity on the fluorimeter the detection limit ($S/N = 3$) was 1×10^{-9} M.

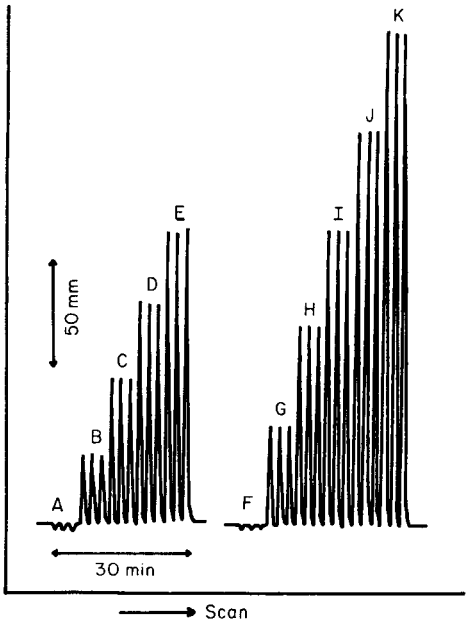

Fig. 4. Calibration outputs for nitrate. Nitrate concentration (10^{-5} M); A, 0; B, 0.4; C, 0.8; D, 1.2; E, 1.6; F, 0; G, 2; H, 4; I, 6; J, 8; K, 10. For peaks A—E, the more dilute reagent solution and larger injection volume were used (see text).

TABLE 1

Effect of co-existing ions

Ion	Tolerable concentration[a] (M)	Ion	Tolerable concentration[a] (M)
Na^+, Cl^-	0.5	NH_4^+, Br^-, HCO_3^-	10^{-3}
Mg^{2+}, SO_4^{2-}	0.05	Cu^{2+}, Al^{3+}, I^-, SiO_3^{2-}	10^{-4}
K^+, Ca^{2+}	10^{-2}	Fe^{2+}, Fe^{3+}	10^{-5}

[a]Maximum tested.

Effect of co-existing ions. The effect of co-existing ions on the determination of nitrate was examined (Table 1). Most cations and anions commonly found in natural waters do not interfere.

Application to natural waters. To examine the applicability of this flow-injection method to natural waters, nitrate was determined in some river and sea waters (Table 2). The results obtained by the proposed method are in good agreement with those obtained by an ion-chromatographic (i.c.) method.

TABLE 2

Determination of nitrate in waters

Sample[a]		Nitrate (× 10^{-5} M)		Sample[a]		Nitrate (× 10^{-5} M)
		Present method	I.c.			Present method
River				*Sea*		
Takahashi	A	1.4	1.2	Yamada	A	0.14
	B	4.4	4.2		B	0.14
Asahi	A	3.6	3.4	Desaki		0.34
	B	3.8	3.6			
Yoshii	A	2.5	2.3			
	B	0.72	0.6			

[a]Samples A and B were taken on different days.

REFERENCES

1 L. Anderson, Anal. Chim. Acta, 110 (1979) 123.
2 M. F. Gine, H. Bergamin F°, E. A. G. Zagatto and B. F. Reis, Anal. Chim. Acta, 114 (1980) 191.
3 K. S. Johnson and R. L. Petty, Limnol. Oceanogr., 28 (1983) 1260.
4 J. Růžička and E. H. Hansen, Anal. Chim. Acta, 114 (1980) 19.
5 J. F. van Staden, Anal. Chim. Acta, 138 (1982) 403.
6 S. Nakashima, M. Yagi, M. Zenki, A. Takahashi and K. Toei, Bunseki Kagaku, 31 (1982) 732.
7 S. Nakashima, M. Yagi, M. Zenki, A. Takahashi and K. Toei, Fresenius' Z. Anal. Chem., 319 (1984) 506.
8 S. Monomizu, H. Mikasa and K. Toei, Talanta, 33 (1986) 729.

Analytica Chimica Acta, 193 (1987) 349—354
Elsevier Science Publishers B.V., Amsterdam — Printed in The Netherlands

Short Communication

SIMULTANEOUS DETERMINATION OF HISTAMINE AND SPERMIDINE BY SECOND-DERIVATIVE SYNCHRONOUS FLUORESCENCE SPECTROMETRY

M. C. GUTIERREZ, S. RUBIO, A. GOMEZ-HENS and M. VALCÁRCEL*

Department of Analytical Chemistry, Faculty of Sciences, University of Córdoba, Córdoba (Spain)

(Received 8th August 1986)

Summary. The method is based on formation of the fluorescent condensation products with *o*-phthaldialdehyde; 0.5—2000 ng ml^{-1} histamine and 3—700 ng ml^{-1} spermidine can be quantified, with relative standard deviations of 2—3%. Histamine/spermidine ratios of 2.5:1—1:30 can be handled. A selectivity study is reported.

Reliable and fast methods for determinations of histamine are of interest because histamine has been implicated in several food poisoning episodes. Fluorimetric methods based on the condensation of histamine with *o*-phthaldialdehyde [1—3] are used routinely to determine histamine in foods; but the interferences found usually require prior separation of histamine from the matrix. The most serious interferences are from histidine and spermidine, which also form fluorescent derivatives with *o*-phthaldialdehyde. Derivative synchronous fluorescence spectrometry [4] was recently applied [5] to improve the sensitivity and selectivity of the conventional fluorimetric method for histamine [1], and to avoid the separation step usually needed for food samples. None of the species tested interfered at the same concentration level as histamine. Spermidine, the most important interference, was tolerated in ten-fold amounts, but this ratio is inadequate for some food samples.

In this communication, the application of derivative synchronous fluorescence spectrometry is extended to the resolution of histamine/spermidine mixtures. The method is optimized to provide good resolution, albeit at the expense of decreased sensitivity.

Experimental

Apparatus. The Perkin-Elmer fluorescence spectrophotometer used, Model MPF-43A, was fitted with a 1-cm quartz cell and a xenon-arc source. The cell compartment was thermostated at 25°C. The spectral bandpass was 5 nm for the excitation and emission monochromators. For synchronous fluorescence measurements, both monochromators were scanned simultaneously at 8 nm s^{-1}. Derivative spectra were obtained by electronic differen-

0003-2670/87/$03.50

tiation of the signal with a Perkin-Elmer derivative accessory (Model H-200-0507). Of the six differential time constants available through the mode switch, position 6 was selected for all measurements. The spectrofluorimeter response time constant was set at 0.3 s. Fluorescent polymer samples were used daily to correct for changes in the source intensity.

Reagents. Twice-distilled water was used throughout. Stock solutions (1 mg ml^{-1}) of histamine dihydrochloride (Aldrich) and spermidine trihydrochloride (Sigma) were prepared in water and stored at 0—4°C. More dilute standards were prepared daily by appropriate dilution with water. An *o*-phthaldialdehyde (OPT) solution (0.1%, w/v) was prepared by dissolving 25 mg of reagent (Merck) in 5 ml of ethanol and diluting to 25 ml with water. All chemicals used were of analytical-reagent grade.

Procedure. To a 10-ml volumetric flask was added an adequate volume of the histamine/spermidine sample to give final concentrations in the range 0.5—2000 ng ml^{-1} histamine, and 3—700 ng ml^{-1} spermidine. Then 6 ml of 0.1 M sodium hydroxide and 0.3 ml of 0.1% OPT solution were added. After 6 min, 0.4 ml of 1 M sulfuric acid was added and the mixture was diluted to the mark with water. The second-derivative synchronous fluorescence spectrum was recorded by scanning both monochromators with a constant 140-nm difference between them. The excitation monochromator was scanned from 220 to 460 nm and the emission monochromator from 360 to 600 nm. Second-derivative peak-to-peak measurements [6] were made. Spermidine measurements were made at 386 nm (maximum peak) and 402 nm (adjacent minimum) ($\Delta I_{386/402}$), and histamine at 504 and 550 nm ($\Delta I_{504/550}$). Each analyte in the mixture was evaluated from the corresponding calibration graphs, obtained previously under the same conditions as those for the mixture. The net fluorescence for each peak was obtained by subtracting the signal from a blank solution with no histamine or spermidine.

Results and discussion

Fluorescence characteristics. Histamine and spermidine react with OPT in alkaline medium, yielding strongly fluorescent compounds; the fluorescence intensity of the histamine derivative is greater than that of the spermidine derivative. Figure 1 shows the conventional excitation and emission spectra of the fluorescent derivatives for solutions containing 10-times more spermidine than histamine. Overlap of the spectral peaks makes the measurement of histamine difficult in the presence of high spermidine concentrations. There is a narrow wavelength range over which only the histamine derivative fluoresces, so that histamine can be quantified in a mixture, but measurements in this region are imprecise because slight variations in the wavelength result in large changes in signal, and sensitivity is lower because the measurements are not made at the fluorescence maximum.

Synchronous scanning provides much narrower bands, the bandwidth depending on the wavelength intervals ($\Delta\lambda$) used, as shown in Fig. 2. However, these spectra do not produce more precise results for either compound.

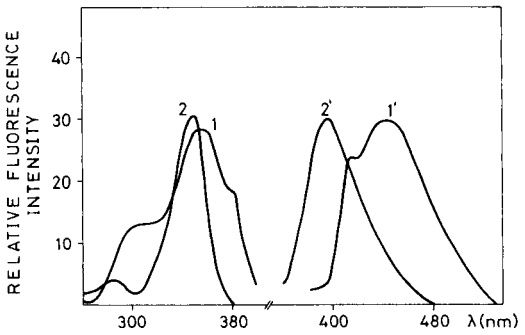

Fig. 1. Excitation (1,2) and emission (1', 2') spectra of the condensation products of OPT with histamine (1,1') and spermidine (2,2'). (10 ng ml^{-1} histamine, 100 ng ml^{-1} spermidine.)

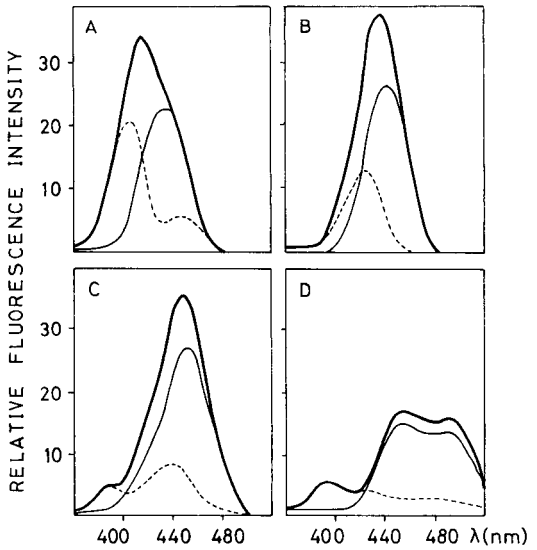

Fig. 2. Synchronous fluorescence spectra of the condensation products of OPT: (-) histamine; (---) spermidine; (—) their mixture. Values of $\Delta\lambda$ (nm): (A) 60; (B) 80; (C) 100; (D) 140. (Concentrations as in Fig. 1.).

In the $\Delta\lambda$ range 60—80 nm (Fig. 2A, B) there is only partial overlap of the synchronous spectra; spermidine can be quantified on the rising portion of the spectrum, and histamine can be quantified on the falling portion, but errors can be very large. When the $\Delta\lambda$ values used are $\geqslant$100 (Fig. 2C, D), spermidine can be quantified directly from the first maximum near 400 nm, but the signals are low so that sensitivity is poor.

Figure 3 shows the second-derivative synchronous fluorescence spectra of the histamine and spermidine derivatives and of their mixture, for $\Delta\lambda$ =

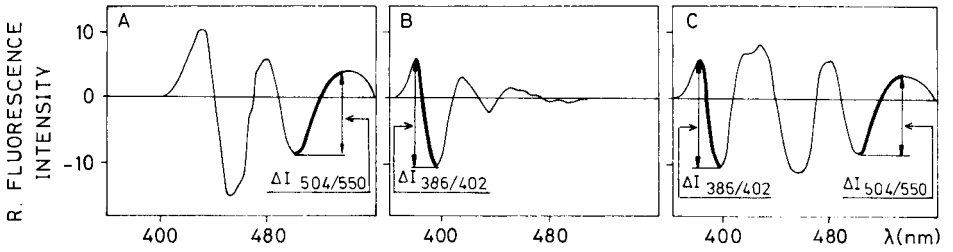

Fig. 3. Second-derivative synchronous fluorescence spectra of the condensation products of OPT: (A) histamine; (B) spermidine; (C) their mixture. ($\Delta\lambda$ = 140 nm; concentrations as in Fig. 1.)

140 nm. Under these conditions, the spermidine concentration correlates very well with $\Delta I_{386/402}$ and the histamine concentration with $\Delta I_{504/550}$. These signals are more intense than those obtained in the normal synchronous spectrum.

Effect of variables. The chemical and instrumental variables were optimized in the univariate manner, the aim being to keep each analyte signal independent of the other analyte signal, while maximizing both fluorescent signals.

The $\Delta\lambda$ value chosen is critical for the resolution of histamine/spermidine mixtures. The maxima and minima of the second-derivative synchronous spectrum undergo bathochromic shifts as the $\Delta\lambda$ value increases. In the $\Delta\lambda$ range tested (60—160 nm), best resolution was obtained at 140 nm. Figure 4

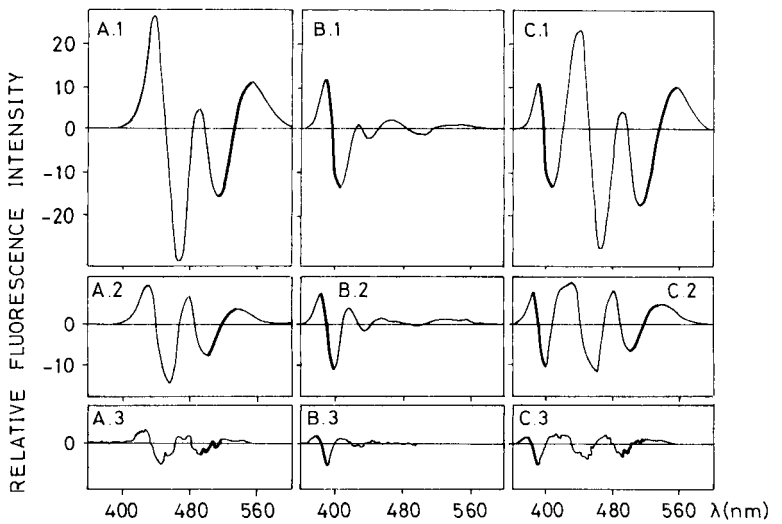

Fig. 4. Effect of wavelength scan rate on the second-derivative synchronous fluorescence spectra ($\Delta\lambda$ = 140 nm) of the condensation products of OPT: (A) histamine; (B) spermidine; (C) their mixture. Scan rate: (1) 8; (2) 4; (3) 2 nm s^{-1}. The bold lines represent the measured signal components.

shows the effect of the wavelength scan rate on the derivative spectra. This variable affects peak height and spectral resolution. As ΔI decreases with decreasing scan rate, a value of 8 nm s^{-1} was chosen. The differentiation constant exerts an effect similar to that described for the scan rate: the analytical signals are maximal and the spectral resolution is adequate when the response speed is lowest. To study the effect of the spectrofluorimeter response, time constants of 0.3, 1.5 and 3.0 were tested; the spectral resolution did not change appreciably, but the relative intensities of all peaks increased as the time constant decreased.

The condensation reaction between histamine and OPT proceeds best in alkaline medium [1], but the pH has no appreciable effect on the reaction of spermidine. At pH 12.2—12.5, both reactions are complete within ca. 6 min. The fluorescence intensity of both condensation products, however, is higher in acidic media; thus, the solutions were adjusted to pH 1.5—5.0 with sulfuric acid for fluorescence measurements. The OPT concentration did not affect the histamine signal above 1.5×10^{-4} M, but the spermidine signal decreased above an OPT concentration of 2.5×10^{-4} M. The fluorescence intensity of both systems was independent of the order of reagent addition. The signal for histamine was not affected by a measurement temperature in the range 15—30°C, but the signal for spermidine increased over the range 15—25°C. Therefore 25°C is recommended.

Characteristics of the method. The plot of $\Delta I_{386/402}$ vs. spermidine concentration was linear in the range 3—700 ng ml^{-1}; the plot of $\Delta I_{504/550}$ vs. histamine concentration was linear in the range 0.5—2000 ng ml^{-1}. The use of these calibration graphs allowed the determination of histamine and spermidine in a single scan. The relative standard deviation (r.s.d.) of the simultaneous method was evaluated for two mixtures of the analytes. For a mixture of 5.0 ng ml^{-1} histamine and 50.0 ng ml^{-1} spermidine, the r.s.d. were 3.0 and 1.7%, respectively. For a mixture of 25.0 ng ml^{-1} histamine and 500 ng ml^{-1} spermidine, the r.s.d. was 1.9% for each analyte ($n = 11$, $P = 0.05$). These values are adequate and are attainable provided that the spermidine concentration is higher than that of histamine, as is the case with some food samples.

The selectivity was examined for various inorganic ions, amines and related compounds that frequently accompany histamine and spermidine in food samples (Table 1). The method is more selective for histamine than for spermidine.

Simultaneous determination of histamine and spermidine. The second-derivative synchronous fluorescence method was applied to the determination of several synthetic mixtures of histamine and spermidine. Results are summarized in Table 2. The proposed method allows the determination of histamine and spermidine in ratios between 2.5:1 and 1:30.

TABLE 1

Effect of various species on the determination of 5 ng ml^{-1} histamine and 50 ng ml^{-1} spermidine

Tolerance wt. ratio species/analyte	Species added	
	Histamine method	Spermidine method
1000:1	1-Methyl-4-imidazoleacetic acid, 3-methylhistidine, putrescine, 1-methylhistidine, cadaverine, spermine, NAD^+, EDTA, Ca^{2+}, Mg^{2+}, Fe^{3+}	
200:1	3-Methylhistamine	
100:1		1-Methyl-4-imidazoleacetic acid, 1-methylhistidine, NAD^+, EDTA, 3-methylhistidine, Ca^{2+}, Mg^{2+}
50:1	Norepinephrine	
25:1		3-Methylhistamine, cadaverine, putrescine, epinephrine
10:1	Epinephrine, histidine	Spermine, Fe^{3+}
5:1	Cu^{2+}	Norepinephrine, histidine, Cu^{2+}

TABLE 2

Resolution of histamine/spermidine mixtures[a]

Histamine (ng ml^{-1})		Spermidine (ng ml^{-1})		Histamine (ng ml^{-1})		Spermidine (ng ml^{-1})	
Taken	Found	Taken	Found	Taken	Found	Taken	Found
25	24.9	10.0	8.3	5.0	5.4	50	49
200	198	100	97	10.0	10.2	100	101
200	195	200	201	5.0	5.2	75	76
10.0	9.8	50	48	5.0	5.1	100	104
50	52	250	252	25	26	750	751
100	98	500	504				

[a] All results are the mean of three determinations.

REFERENCES

1 P. A. Shore, Methods Enzymol., 17 (Pt. B) (1971) 842.
2 R. Hakanson and A. L. Ronnberg, Anal. Biochem., 60 (1974) 560.
3 S. L. Taylor and E. R. Lieber, J. Food Sci., 42 (1977) 1584.
4 P. John and I. Soutar, Anal. Chem., 48 (1976) 520.
5 M. C. Gutiérrez, S. Rubio, A. Gómez-Hens and M. Valcárcel, Anal. Chem., 59 (1987) 769.
6 T. C. O'Haver, Clin. Chem., 25 (1979) 1548.

Analytica Chimica Acta, 193 (1987) 355—360
Elsevier Science Publishers B.V., Amsterdam — Printed in The Netherlands

Short Communication

EMISSION EFFICIENCY FOR PARTICULATE FORMS OF IRON AND ALUMINUM IN RAIN-WATER MEASURED BY INDUCTIVELY-COUPLED PLASMA ATOMIC EMISSION SPECTROMETRY

YOSHINARI AMBE* and MASATAKA NISHIKAWA

National Institute for Environmental Studies, Yatabe-machi, Tsukuba, Ibaraki 305 (Japan)

(Received 10th June 1986)

Summary. The bulk emission efficiency for particulate forms of iron and aluminum in rain-water was evaluated. The efficiencies for iron and aluminum were >80% for particles 0.4—1 μm in diameter and about 17% for particles >8 μm; relative standard deviations were <20%. A procedure is described by which the concentrations of particulate forms of iron and aluminum in rain-water are determined. Fluctuation of particles in rain-water during a rainfall event can be monitored in detail.

Simultaneous determinations of many elements in rain-water can be achieved by inductively-coupled plasma (ICP) atomic emission spectrometry, although in some cases preconcentration is needed. In this way the temporal variation of the concentration of dissolved elements in rain-water has been studied in detail [1—3]. When samples were directly introduced into the ICP spectrometer, a significant difference in the emission intensity of various elements was observed in filtered and unfiltered samples, suggesting that this difference could be applied to estimate particulate forms of elements in rain-water.

Several studies have demonstrated that particulate matter can be analyzed by ICP atomic emission spectrometry [4—11]. Sugimae and Mizoguchi [11] measured iron in airborne particles by dispersing them in an organic solvent and directly introducing the suspension into an ICP. It was shown in these studies that the efficiency of atom formation in the plasma from the elements in the particulate matter depends on the size of the particles. The particle size also influences the efficiency of nebulization in the ICP system. Saba et al. [4] reported that the efficiency of a sample introduction system for the transport of 7—14-μm metal particles was 62%.

In this study, the emission efficiency of several sizes of particulate forms of iron and aluminum in rain-water was examined by direct ICP emission spectrometry. This emission efficiency was used to provide a simple method for estimation of the concentration of particulate matter in rain-water. Temporal fluctuations of the particles during a rainfall event could then be studied in detail.

0003-2670/87/$03.50

Experimental

Each rain-water sample was collected in a polypropylene bottle via a sampler made of a square acrylic resin board (1 m × 1 m × 2 cm) covered with a teflon sheet. The sample (ca. 1 l) was agitated ultrasonically for 10 min and shaken for several minutes to prevent precipitation and aggregation of particles and to keep the sample homogeneous. Immediately afterwards, some of the sample was directly nebulized into the ICP system to measure the total concentration of each element in the dissolved and particulate forms. Another portion of the sample was filtered sequentially by membrane filters (Nuclepore) with pore sizes of 8, 1 and 0.4 μm. As the particles in rain-water have various forms derived from various origins, a clear-cut discrimination of particle size is a difficult practical problem. In this study, the size of particles is defined operationally as follows: the size of particles on the 8-μm filter is described as >8 μm, those on the 1-μm filter as 1—8 μm and those on the 0.4-μm filter as 0.4—1 μm. The filtrate was agitated ultrasonically and examined by ICP emission spectrometry.

The particulate matter on each filter was transferred to a teflon beaker and digested with 2 ml of concentrated nitric acid, 1 ml of 60% perchloric acid and 2 ml of 48% hydrofluoric acid for 2 h on a hot-plate at 200°C. The residue was dissolved in 0.1 ml of (1+1) nitric acid, and diluted with water to 2 ml. This solution was examined by ICP emission spectrometry.

Of the 30 elements that could be quantified in this way, iron and aluminum, which are major components of particulate matter in rain-water, were studied in detail. The working conditions of the ICP system were as follows. The spectrometer was a Plasma Atomcomp Model 975 (Jarrell-Ash). The plasma source unit had a frequency of 27.12 MHz, and a power of 1.1 kW. The coolant argon flow rate was 20 l min^{-1}, and the argon carrier flow rate was 0.5 l min^{-1}. The nebulizer was a cross-flow type, with a sample take-up rate of 1.2 ml min^{-1}. A standard Fassel-type quartz torch was used. The observation height was 18 mm above the work coil.

Results and discussion

The emission efficiency is defined here as $100\,(C_d - C_f)/C_p(\%)$, where C_d is the emission intensity of an element in unfiltered rain-water measured by direct sample introduction into the ICP and expressed as the concentration of the element ($\mu g\ l^{-1}$), C_f is the emission intensity of the element in filtered rain-water, again expressed in $\mu g\ l^{-1}$, and C_p is the concentration of the element in particulate matter measured after digestion ($\mu g\ l^{-1}$). Emission efficiency was calculated for the samples filtered through each pore size of filter. According to this definition, the emission efficiency expresses the total efficiency of the ICP system with regard to the emission of particulate matter, including efficiency of sample introduction, transport of particles in the nebulizer and mixing chamber, the fraction of atomized analyte in the plasma, etc.

Emission efficiency of iron and aluminum in rain-water particulates. Table 1 shows an example of the results obtained. The emission efficiencies of iron

TABLE 1

Concentrations of aluminum and iron in various particle-size forms in rain-water (sample taken on 15/4/1986, cf. Table 2) examined after acid digestion (A), or obtained by difference from the intensities of filtered and unfiltered samples (B)

Element	particle size (μm)	Concentration ($\mu g\ l^{-1}$)[a]		Emission efficiency $100B/A$ (%)
		A	B	
Fe	>8	100	21	21
	1—8	63	51	81
	0.4—1	6.1	6.5	≈100
	⩾0.4[b]	169	79	47
Al	>8	150	16	11
	1—8	97	44	45
	0.4—1	7.3	6.0	82
	⩾0.4[b]	254	66	26

[a] A corresponds to C_p and B to $C_d - C_f$. [b] All particles ⩾0.4 μm.

and aluminum both decreased with increasing particle size. The mean values of emission efficiency of iron and aluminum for different particle sizes measured for several rainfalls are shown in Table 2. The emission efficiency of iron was usually a little higher than that of aluminum for every size of particles. This agrees with the order of ease of atom formation for these elements [12]. This emission efficiency includes, as mentioned above, not only efficiency of atom formation in the plasma but also many other factors, such as the efficiency of the nebulizing process. The combined effects of these processes are considered markedly to decrease the value of emission efficiency for larger size particles. If it is assumed that the values of emission efficiency of each particle size are constant for each rainfall (relative standard deviations measured for six rainfall events were below 20%), an approximate estimation of the concentration of particulate forms of the elements is possible based on this emission efficiency.

Estimation of concentration of iron and aluminum in various sizes of particles in rain-water. From the beginning of a rainfall event, every 0.1 mm of rain-water (100 ml) was collected successively. After ultrasonic agitation, part of the sample was examined as above to evaluate C_d and the other part was immediately filtered sequentially with 8-, 1- and 0.4-μm filters to evaluate C_f. An example of the temporal variations of the metal concentrations for the unfiltered sample water and those filtered through each size of filter is illustrated in Fig. 1. From these data, $C_d - C_f$ was determined for iron and aluminum in particles >8, 1—8 and 0.4—1 μm in each sample. Dividing $C_d - C_f$ for each size by the value of the emission efficiency, the concentrations of the particulate forms of the elements were obtained. The temporal variations thus estimated are illustrated in Fig. 2. In this example, the major proportion of the particulate form of iron and aluminum was in the particles

TABLE 2

Emission efficiencies (%) of different sizes of particulate forms of iron and aluminum in rain-water for several rainfall events

Date	Fe			Al		
	>8 μm	1—8 μm	0.4—1 μm	>8 μm	1—8 μm	0.4—1 μm
17/2/1982	12	78	85	18	61	88
16/7/1982	17	67	91	19	62	71
2/7/1983	17	—	—	19	—	—
20/9/1983	18	—	—	20	—	—
5/7/1984	17	100	100	13	58	100
15/4/1986	21	81	100	11	45	82
Mean	17	82	94	17	57	85
S.d.	2.6	11.9	6.4	3.4	6.8	10.5
R.s.d. (%)	15	15	7	20	12	12

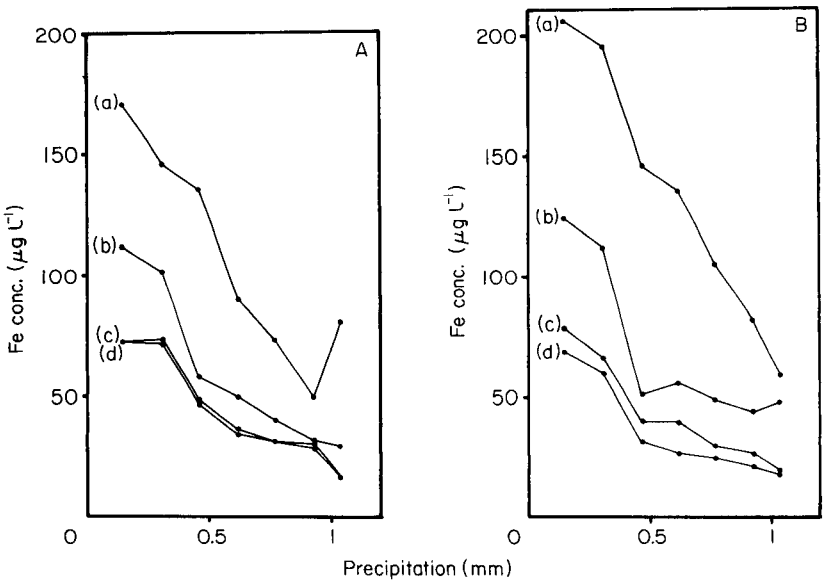

Fig. 1. Temporal variation of concentration of iron (A) and aluminum (B) in rain-water. Filter used: (a) none; (b) 8 μm; (c) 1 μm; (d) 0.4 μm. Sample taken on 16th July 1982.

larger than 8 μm; 5—10% was in the 1—8-μm particles and only a few percent was in the 0.4—1-μm particles. As the range of temporal fluctuation exceeds the relative standard deviation of the emission efficiency, this fluctuation is meaningful, and shows a complicated variation of the washout of atmospheric particulate matter by rain.

If it is assumed that the major origin of particulate matter in rain-water is soil, the concentration of bulk particulate matter can be estimated from the concentration of the particulate forms of iron or aluminum in rain-water

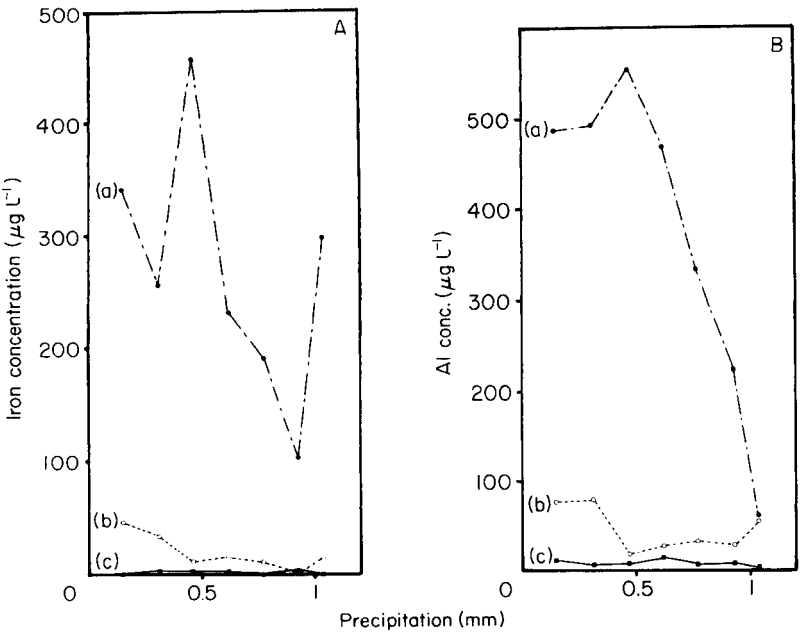

Fig. 2. Temporal variation of concentration of particulate forms of iron (A) and aluminum (B) in rain-water. Particle size: (a) >8 μm; (b) 1—8 μm; (c) 0.4—1 μm. Sample as in Fig. 1.

and its average concentration in the soil particles. As the measurement by ICP spectrometry requires only a few milliliters of sample (which is insufficient to measure the amounts of particles in rain-water by weighing) fluctuations in the particulate concentrations of elements can be measured with higher resolution than by the conventional method. Thus, although the precision of the ICP measurements is not high, measurements of detailed fluctuations of particulate matter in rain-water are easily possible. This will be helpful for elucidating the washout mechanism for atmospheric particulate matter.

The authors thank Dr. N. Furuta for his kind advice.

REFERENCES

1 Y. Ambe and M. Nishikawa, Hydrology, 15 (1985) 2.
2 Y. Ambe and M. Nishikawa, Atmosph. Environ., 20 (1986) 1931.
3 M. Nishikawa, Y. Ambe and T. Mizoguchi, Bunseki Kagaku, 34 (1985) 659.
4 S. S. Saba, W. E. Rhine and K. J. E. Eisentraut, Anal. Chem., 53 (1981) 1099.
5 C. W. Fuller, R. C. Hutton and B. Preston, Analyst, 106 (1981) 913.
6 L. Ebdon and M. R. Cave, Analyst, 107 (1982) 172.
7 J. Y. Marks, D. E. Fornwalt and R. E. Yongk, Spectrochim. Acta, Part B, 38 (1983) 172.
8 A. G. Page, S. V. Godbole, K. H. Madrasbala, M. J. Kulbarni, V. S. Mallapurkar and B. D. Joshi, Spectrochim. Acta, Part B, 39 (1984) 551.
9 A. Aziz, J. A. C. Broekaert, K. Laqua and F. Leis, Spectrochim. Acta, Part B, 39 (1984) 1091.

10 A. Lorber and Z. Goldbart, Analyst, 100 (1985) 155.
11 A. Sugimae and T. Mizoguchi, Anal. Chim. Acta, 144 (1982) 205.
12 R. K. Winge, V. A. Fassel, V. J. Peterson and M. A. Floyd, Inductively-Coupled Plasma Atomic Emission Spectroscopy. Elsevier, Amsterdam, 1985, p. 548.

Analytica Chimica Acta, 193 (1987) 361—365
Elsevier Science Publishers B.V., Amsterdam — Printed in The Netherlands

Short Communication

LOW-TEMPERATURE HYDRIDE FURNACE MODIFIED FOR THE ATOMIC ABSORPTION SPECTROMETRIC DETERMINATION OF METALS WITH LOW APPEARANCE TEMPERATURES

C. BRUHN[a], H. BERNDT* and M. L. TRISTAO[b]

Institut für Spektrochemie und angewandte Spektroskopie, Postfach 7781, D-4600 Dortmund 1 (Federal Republic of Germany)

(Received 1st September 1986)

Summary. The sample is vaporized from tungsten filament coils (150 W) and transported by an argon stream to the cell of a modified hydride furnace for atomic absorption spectrometry (a.a.s.). The system provides almost the same sensitivity for elements with low appearance temperatures (e.g., Bi, Cd, Pb, Tl, Zn) as graphite-furnace a.a.s. The detection limits are between 0.1 and 5 ng ml^{-1}, depending on the element.

The typical temperature range of the quartz cell normally used for the determination of hydrides by atomic absorption spectrometry (a.a.s.) lies between 700 and 1000°C. However, the temperature of the cell can be raised to ca. 1200°C by varying the tube position in the flame or, in the case of an electrically heated cell, the electrical power [1, 2]. This temperature is high enough to allow the determination of elements with low appearance temperatures (e.g., Bi, Cd, Pb, Tl, Zn), so it was expected that these elements could be determined with this type of cell. For the introduction of the sample into the cell, a prevaporization step at higher temperature is required. Normally, a separate sample volatilization step is included, to avoid the low efficiency of pneumatic nebulizers, or for producing an aerosol directly from solids [10]. For this purpose, several approaches have been described [3—10], and prevaporization of samples to produce aerosols for sample introduction is well known.

In this communication, a simple, relatively inexpensive prevaporization device is described for use with a "hydride" furnace as an isothermal absorption cell for the determination of the above elements by a.a.s. A flame or electrically heated quartz tube can be used as an atomization cell. When a flame-heated quartz tube is used, it is possible to introduce part of the flame gas into the tube through holes, thus allowing the determination of elements

[a]Present address: Department of Instrumental Analysis, Faculty of Pharmacy, University of Concepcion, P.O. Box 237, Concepcion, Chile.
[b]Present address: Department of Chemistry, Pont. University Cath., CEP 22453 Rio de Janeiro, Brasil.

0003-2670/87/$03.50

with higher appearance temperatures (e.g., Mn, Cr, Ni, Co) [11]. For more volatile elements, the higher temperature of the flame is unnecessary. In this case, it is possible to work with an electrically-heated furnace system for elemental atomization instead of a flame. Kanipayor et al. [9] used a graphite furnace for the prevaporization step, together with a flame-heated quartz T-tube. In the present work, both the quartz tube and the prevaporization system are electrically heated. The main advantage of this is the use of commerically produced tungsten coils for the prevaporization step. These filaments are normally produced for use in halogen lamps for slide projectors. Therefore, the tungsten wire of the filament is concentrated in a small area (ca. 4 X 2.5 mm) which can support small solution samples (5—50 μl). To heat up such a filament to more than 3000°C (m.p. of tungsten = 3400°C), only a very low power (e.g., 150 W; 15 V, 10 A) is required. With such a filament, it is possible to provide a very rapid increase of temperature (>1000°C s^{-1}).

Experimental

A Perkin-Elmer 3030 atomic absorption spectrometer (double-beam, video screen), a graphics printer and a Perkin-Elmer hydride furnace were used. (The furnace was heated to 1150°C.) Figure 1 shows a schematic diagram of the modified furnace connected to a simple power supply. The original quartz tube of the hydride furnace is replaced by another T-tube containing the prevaporization unit. This is composed of the tungsten filament (Osram) supported by two small stainless-steel electrodes held by a ceramic connector with a central bore for the carrier gas (98% Ar/2% H_2). The carrier gas, which is controlled by a calibrated flow meter, has two functions:

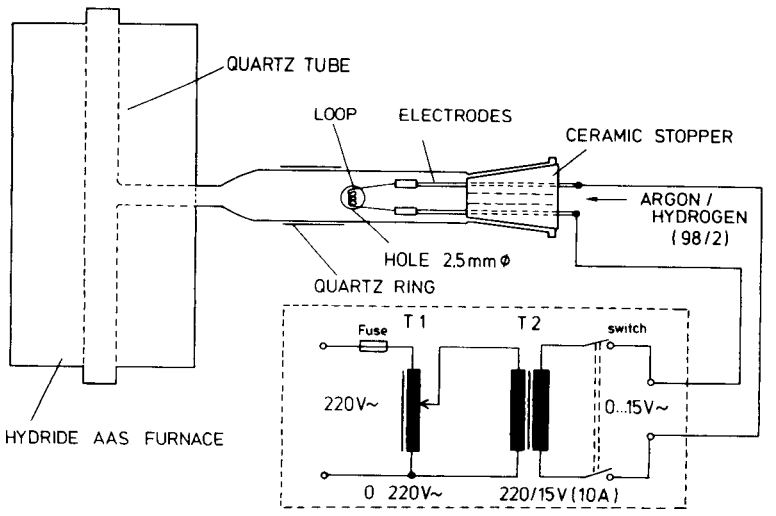

Fig. 1. Schematic diagram of the low-temperature modified hydride furnace with a simple power supply.

it protects the filament against oxidation and transports the volatilized sample to the heated cell for absorption measurements.

The sample is introduced with the aid of a microlitre pipette through a small hole (2.5 mm diameter) bored in the T-tube just above the filament position. The hole is closed by means of an adjustable, movable quartz ring. In the closed position, the whole argon/hydrogen stream passes through the heated part of this T-tube.

The current is provided by a simple, manually-controlled power supply made of two transformers (T1, T2) and a switch (Fig. 1). This supply provides different voltages across the filament: (1) after sample introduction, a low voltage is set to provide a drying step; (2) a mid-range voltage is set for ashing; and (3) a high or full voltage is set for sample vaporization. For better reproducibility in the vaporization with the manually-controlled power supply, it is best to start the third step with a cold loop (open switch). By closing the switch, the vaporization step is accomplished very quickly. Instead of this simple power supply unit, a programmable time-controlled power supply developed in this Institute could be used.

Results and discussion

Optimization studies. Figure 2 shows the influence of the atomic absorbance (peak height) of the carrier gas flow rate. The shapes of the curves for the five elements studied are similar. Between flow rates of ca. 1.6 and 3.2 l min^{-1}, the sensitivity increases but between flow rates of ca. 3.0 and 4.4 l min^{-1} there is no significant change in sensitivity. The explanation for this behaviour could be a compensatory effect between an increasing signal caused by greater sample transport by the increasing gas flow rate, and a decreasing signal caused by dilution of the sample vapor and the lower temperature attained by the filament with increasing gas flow rate. Appreci-

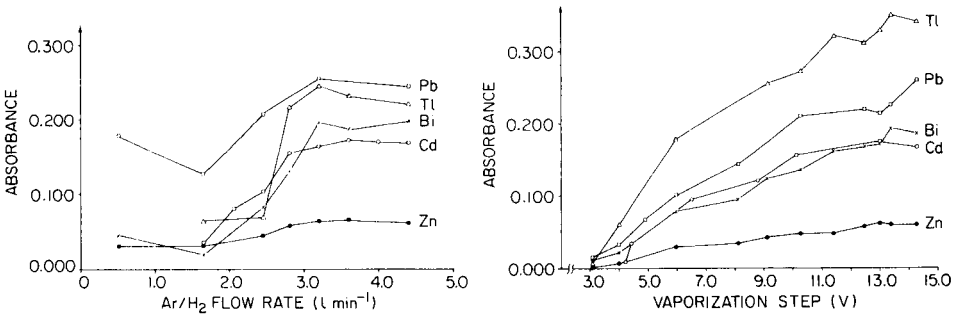

Fig. 2. Effect of gas flow rate (98% Ar/2% H_2) on absorbance peak height (sample volume 20 μl; 0.02 M HNO_3). Metal concentrations: (□) 0.100 μg ml^{-1} Pb; (△) 0.200 μg ml^{-1} Tl, (×) 0.100 μg ml^{-1} Bi; (○) 0.001 μg ml^{-1} Cd; (●) 0.002 μg ml^{-1} Zn.

Fig. 3. Effect of vaporization voltage applied to the tungsten filament (maximum operating voltage 15 V) on the absorbance peak height (sample volume 20 μl; 0.02 M HNO_3). Metal concentrations as in Fig. 2.

able differences in the sensitivities for the elements can be observed in Fig. 2.

Figure 3 shows the influence on the atomic absorbance (peak height) of the voltage used for the vaporization step. As expected, higher voltages produce increased sensitivities. It seems that above 14 V there is no further significant change in sensitivity, except for lead. Depending on the type of filament used, the maximum possible voltage which can be utilized without rapid filament destruction is 15 V. However, for longer filament life, the operating voltage should be kept below this maximum voltage (ie., 12—14 V).

Sensitivity and detection limits. Table 1 shows the characteristic concentrations and masses for the elements studied, evaluated with 20 μl of solution. Also indicated are the equivalent data for a normal graphite-furnace a.a.s. system, as given in the instruction manual. Comparison of the data shows that the modified hydride-furnace system provides nearly the same sensitivity as the normal graphite furnace. The relative standard deviation lies between 3 and 12% depending on the element and the concentration used. For the graphite-furnace system, the reproducibility is normally better than 5%. The absolute detection limits (3σ for the blank, Table 1) lie between 2 and 100 pg. The average lifetime of a tungsten filament ranges from 50 (1—3 M nitric acid) to 150 measurements (0.02 M acids).

The proposed modified hydride a.a.s. furnace system is thus suitable for determinations of elements other than those that form volatile hydrides, with a relatively high sensitivity which is comparable to that of graphite-furnace a.a.s. The sample volume used ranged from 10 to 50 μl. In this investigation only acidified aqueous solutions were examined. Further work should be undertaken to study interferences and spectral background effects, so that the technique can be used for real samples.

TABLE 1

Characteristic data for the determination of Bi, Cd, Pb, Tl and Zn with the low-temperature a.a.s. furnace

Element	Ni	Cd	Pb	Tl	Zn
Characteristic conc. (ng ml^{-1})[a]	2.6	0.2	2.4	2.9	0.1
Characteristic mass (pg)[a]					
low temp. furnace	53	5	47	58	2
graphite furnace[b]	39	1.5	37	37	2.2
R.s.d. (%)[c]	7.0	12	3.4	7.2	5.0
	(200)	(0.5)	(50)	(50)	(6)
Detection limit (ng ml^{-1})	5	0.3	4	2.5	0.1
Absolute (pg)	100	6	80	50	2

[a]Concentration or amount that gives 1% absorption. [b]Manual Perkin-Elmer HGA-500, gas flow = 50 ml min^{-1}, uncoated graphite tube. [c]The numbers in parentheses are the concentrations (ng ml^{-1}) at which the relative standard deviations (r.s.d.) were evaluated (n = 10).

The cooperation between the Institut für Spektrochemie und angewandte Spektroskopie (ISAS), Dortmund, F.R.G. and the Faculty of Pharmacy, University of Concepcion, Concepcion, Chile, is supported by the Deutscher Akademischer Austauschdienst (DAAD) and the University of Concepcion. M. L. Tristao was supported by CNPq (Brazil). This work was done with the financial assistance of the Bundesministerium für Forschung und Technologie and the Ministerium für Wissenschaft und Forschung des Landes Nordrhein-Westfalen.

REFERENCES

1 B. Welz, Atomabsorptionsspektrometrie, 3rd edn., Verlag Chemie, Weinheim, 1983.
2 W. J. Price, Spectrochemical Analysis by Atomic Absorption, Heyden, London, 1979.
3 T. Kantor, L. Polos, P. Fodor and E. Pungor, Talanta, 23 (1976) 585.
4 T. Kantor, E. Pungor, I. Sztatisz and L. Bezur, Talanta, 26 (1979) 357.
5 A. Aziz, J. A. C. Broekaert and F. Leis, Spectrochim. Acta, Part B, 37 (1982) 369.
6 G. F. Kirkbright and S. J. Walton, Analyst, 107 (1982) 276.
7 G. F. Kirkbright and Zhang Li-Xing, Analyst, 107 (1982) 61.
8 T. Kantor, P. Fodor and E. Pungor, Anal. Chim. Acta, 102 (1978) 15.
9 R. Kanipayor, D. A. Naranjit, B. H. Radziuk and J. C. van Loon, Anal. Chim. Acta, 166 (1984) 1121.
10 H. Berndt, Spectrochim. Acta, Part B, 39 (1984) 1121.
11 H. Berndt and M. L. Tristao, 24th Colloquium Spectroscopicum Int., Garmisch-Partenkirchen, Abstracts, Vol. 3, 1985, p. 482.

Analytica Chimica Acta, 193 (1987) 367—371
Elsevier Science Publishers B.V., Amsterdam — Printed in The Netherlands

Short Communication

ENANTIOMER-SELECTIVE MEMBRANE ELECTRODE FOR AMINO ACID METHYL ESTERS

TOSHIO SHINBO*, TOMOHIKO YAMAGUCHI, KOICHIRO NISHIMURA, MASAYOSHI KIKKAWA and MASAAKI SUGIURA

National Chemical Laboratory for Industry, Yatabe, Ibaraki 305 (Japan)

(Received 10th June 1986)

Summary. Polymeric membrane electrodes based on the chiral crown ether, 2,3:4,5-bis-[1,2-(3-phenylnaphtho)]-1,6,9,12,15,18-hexaoxacycloeicosa-2,4-diene, were prepared, and their characteristics were examined. The electrodes showed good enantiomer-selectivity for many amino acid methylesters, the enantiomer-selective factor reaching the high value of 13 for phenylglycine methyl ester. The electrodes responded preferably to the enantiomer forming the more stable complex with the crown ether. The electrodes proved useful for determining the concentrations of each enantiomer. The calculated concentrations from the potential changes of the electrodes were in good agreement with the predicted ones.

One of the current interests in analytical chemistry is the separation and determination of optically active compounds. Simon and co-workers [1—4] have described some enantiomer-selective membrane electrodes based on chiral neutral carriers such as macrocyclic polyethers (crown ethers). They showed that these electrodes had enantiomer-selectivity for optically active amines; the best selectivity factor reported so far is 2.65, which was observed for phenylethylamine [3].

In this communication, an enantiomer-selective membrane electrode is described; it is prepared by incorporating the chiral crown ether, **1** (see Fig. 1), into the sensor membrane. Compound **1** was first synthesized by Lingenfelter et al. [5] and has been shown to have good enantiomer-selectivity for many amino acids and their methyl esters by liquid-liquid extraction and membrane-transport experiments [5, 6]. As expected, an electrode based on **1** exhibited good enantiomer-selectivity for various amino acid methyl esters, and the enantiomer-selectivity factor reached the unusually high value of 13.1 for phenylglycine methyl ester. Some properties of this electrode and its application for determinations of enantiomer concentrations are described below.

Experimental

(R)- and (S)-2,3:4,5-bis[1,2-(3-phenylnaphtho)]-1,6,9,12,15,18-hexaoxacycloeicosa-2,4-diene (abbreviated as R-1 and S-1) were synthesized as described by Lingenfelter et al. [5]. Amino acid methyl esters and amines were used as their hydrochloric salts.

0003-2670/87/$03.50

Membranes were prepared by pouring 10 ml of tetrahydrofuran (THF) containing 200 mg of poly(vinyl chloride) (PVC), 600 mg of *o*-nitrophenyl octyl ether, 4 mg of sodium tetraphenylborate and 8 mg of R-1 or S-1 on a flat Petri dish (6-cm i.d.), and letting the solvent evaporate slowly at room temperature. The membrane electrode was constructed as follows. A piece of the above membrane containing R-1 or S-1 was glued to a PVC tube with THF, and a portion of 2×10^{-2} M D- (or L)-phenylglycine methyl ester (abbreviated as PGM) which was 10^{-1} M in Tris-Cl (pH 7.0) was added as the internal reference solution. This solution and a Ag/AgCl electrode (internal reference electrode) were connected through a small glass tube filled with agar gel containing the same solution as the internal reference solution. The electrode was conditioned for a few days in 10^{-2} M D- (or L)-PGM solution.

The electrode potentials were measured at 25°C with the following cell assembly: enantiomer-selective electrode/sample solution/salt bridge (agar gel, 1 M lithium acetate)/reference electrode (KCl, AgCl/Ag).

Results and discussion

The enantiomer-selective electrodes based on R-1 and S-1 (denoted as the R- and S-electrodes hereafter) exhibited a Nernstian response to D- and L-phenylglycine methyl esters (D- and L-PGM), respectively, in the range above 10^{-4} M. Figure 1 shows typical responses to concentration changes with the S-electrode. The S-electrode showed a greater response

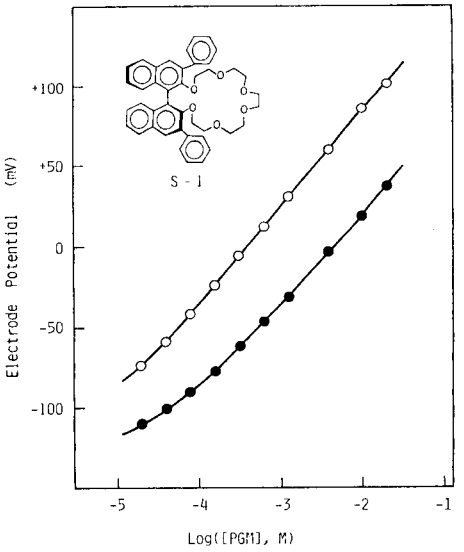

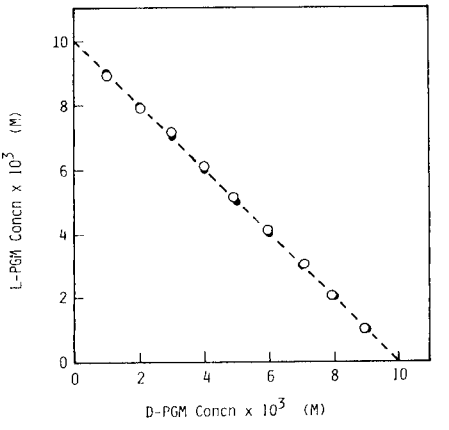

Fig. 1. The response of the enantiomer-selective electrode (S-electrode) to D- and L-enantiomers of phenylglycine methyl ester: (●) D-PGM; (○) L-PGM.

Fig. 2. Comparison of the calculated and actual concentrations of D- and L-PGM: (○) calculated concentration of PGM; (●) true concentration of PGM.

to L-PGM than to D-PGM. The potential difference between the responses to 10^{-2} M L-PGM and D-PGM with the S-electrode reached a high value of 66 mV. When the R-electrode was used, the reverse response was obtained, i.e., the R-electrode responded preferably to D-PGM, and the potential difference between the responses to the two enantiomers was the same as that obtained with the S-electrode. These results indicate that the electrodes respond preferably to the enantiomer forming the more stable complex (R-1 and S-1 are known to form the more stable complexes with D- and L-PGM, respectively [5]). The response time to achieve a steady potential (±1 mV) was about 2 s for a 10-fold increase in concentration from 10^{-4} to 10^{-3} M.

The electrode potentials of the R- and S-electrodes can be represented as

$$E^{R} = E_{o}^{R} + (RT/F) \ln [a_{\overline{G}} + K_{G\overline{G}}^{pot}(R) a_{G} + \Sigma K_{\overline{G}\overline{A}}^{pot}(R) a_{\overline{A}} + \Sigma K_{\overline{G}A}^{pot}(R) a_{A} + \Sigma K_{\overline{G}j}^{pot} a_{j}^{1/Z_j}] \quad (1)$$

$$E^{S} = E_{o}^{S} + (RT/F) \ln [a_{G} + K_{G\overline{G}}^{pot}(S) a_{\overline{G}} + \Sigma K_{G\overline{A}}^{pot}(S) a_{\overline{A}} + \Sigma K_{GA}^{pot}(S) a_{A} + \Sigma K_{Gj}^{pot} a_{j}^{1/Z_j}] \quad (2)$$

where E_o, a and K^{pot} are the standard potential, the activity of the cation and the potentiometric selectivity coefficient, respectively. The subscripts $\overline{G}$ and G refer to D- and L-PGM; $\overline{A}$ and A refer to the D- and L-enantiomers of other optically active monovalent cations, respectively; j represents other interfering ions. From the symmetrical nature of the optical isomers, the following relations for the selectivity coefficients are valid:

$$K_{G\overline{G}}^{pot}(R) = K_{G\overline{G}}^{pot}(S) = K_{G\overline{G}}^{pot} \quad (3)$$

$$K_{G\overline{A}}^{pot}(R) = K_{GA}^{pot}(S) = K_{GA}^{pot} \quad (4)$$

$$K_{GA}^{pot}(R) = K_{G\overline{A}}^{pot}(S) = K_{G\overline{A}}^{pot} \quad (5)$$

As shown by Bussmann and Simon [4], the selectivity coefficients can be correlated to the stability constants (K) of the complexes between compound 1 and the optically active cations in the membrane. Thus $K_{G\overline{G}}^{pot}(R) = K_{GR}/K_{\overline{G}R}$ and $K_{G\overline{G}}^{pot}(S) = K_{\overline{G}S}/K_{GS}$; and $K_{G\overline{A}}^{pot}(R)/K_{GA}^{pot}(R) = K_{AR}/K_{\overline{A}R}$ and $K_{G\overline{A}}^{pot}(S)/K_{GA}^{pot}(S) = K_{\overline{A}S}/K_{AS}$. The following relations are valid because of the symmetrical nature of the optical isomers: $K_{\overline{G}R} = K_{GS}$ and $K_{GR} = K_{\overline{G}S}$; and $K_{\overline{A}R} = K_{AS}$ and $K_{AR} = K_{\overline{A}S}$. From these relationships, the enantiomer-selectivity factor (α where $\alpha > 1$) can be defined as $\alpha = 1/K_{G\overline{G}}^{pot}$ and $\alpha = K_{GA}^{pot}/K_{G\overline{A}}^{pot}$ (or $\alpha = K_{G\overline{A}}^{pot}/K_{GA}^{pot}$).

The selectivity coefficients for the R-electrode towards various inorganic cations are listed in Table 1. The measurements were done by the separate-solutions method. Of course, the S-electrode gave the same selectivity constants for these achiral cations. The selectivity coefficients for alkali metal ions were in the following order: $K^+ > Rb^+ > Cs^+ > Na^+ \gg Li^+$. This order is the same as that obtained with the electrode based on dibenzo-18-

TABLE 1

Selectivity coefficients for various inorganic ions, j, with the R-electrode

Ion	K_{Gj}^{pot}	Ion	K_{Gj}^{pot}	Ion	K_{Gj}^{pot}
H^+	1.9×10^{-4}	Rb^+	8.7×10^{-3}	Ca^{2+}	4.6×10^{-5}
Li^+	6.2×10^{-5}	Cs^+	5.0×10^{-3}	Ba^{2+}	7.4×10^{-5}
Na^+	4.3×10^{-3}	NH_4^+	3.0×10^{-3}	Mn^{2+}	2.1×10^{-5}
K^+	2.1×10^{-2}	Mg_2^{2+}	1.7×10^{-5}	Pb^{2+}	1.4×10^{-4}

crown-6 [7]. Crown ethers form complexes with cations by accommodating the cations within the coordination cavity and the main factor controlling selectivity is the relative sizes of the cations and the cavity. As compound 1 has a cavity size approximately equal to that of dibenzo-18-crown-6, the results in Table 1 are reasonable. It should be noted that the selectivity coefficients for metal ions were usually quite small, i.e., the electrodes developed here showed a good preference for PGM over metal ions.

Table 2 shows the selectivity coefficients for various L-amino acid methyl esters and L-amines. For L-amino acid methyl esters, the selectivity coefficients of the S-electrode were greater than those of the R-electrode, indicating that the electrodes respond preferably to the enantiomers which form more stable complexes with compound 1, as in the case of PGM (described above). The validity of Eqns. 3—5 was confirmed by measuring the selectivity coefficients for the D-antipodes. The order of the selectivity coefficients of the S-electrode for L-enantiomers (all as methyl esters) was: tryptophan > phenylalanine ≥ leucine > methionine > isoleucine > valine > alanine. This order may be governed by two major factors, the lipophilicity of the methyl esters and the stability of the complexes. Table 2 also gives the enantiomer-selectivity factors. The electrodes exhibited good enantiomer-selectivity for many amino acid methyl esters and amines, but the values of enantiomer-selectivity obtained here are a little smaller than those obtained from the liquid-liquid extraction experiments of Lingenfelter et al. [5]. This discrepancy may be due to the difference in the method of measurement and/or the differences in the solvent and temperature used.

To examine the validity of using the present enantiomer-selective electrodes for the determination of the enantiomer concentrations, the concentrations of D- and L-PGM in a sample solution were measured by using both R- and S-electrodes. If the sample solution contains only D- and L-PGM, Eqns. 1 and 2 lead [4] to

$$E^R = E_o^R + (RT/F) \ln (a_{\overline{G}} + K_{G\overline{G}}^{pot} a_G)$$

$$E^S = E_o^S + (RT/F) \ln (a_G + K_{G\overline{G}}^{pot} a_{\overline{G}})$$

From these equations,

$$a_G = \tfrac{1}{2}\{[(p^S + p^R)/(1 + K_{GG}^{pot}) + (p^S - p^R)/(1 - K_{GG}^{pot})]\} \quad (6)$$

TABLE 2

Selectivity coefficients and enantiomer-selectivity factors for amino acid methyl esters and amines

Substance	Selectivity coefficient		Selectivity factor (α)
	R-electrode (K^{pot}_{GA})	S-electrode (K^{pot}_{GA})	
Methyl esters			
L-Phenylglycine	7.6×10^{-2}	1	13.1
L-Alanine	8.5×10^{-3}	2.9×10^{-2}	3.4
L-Valine	7.5×10^{-3}	4.1×10^{-2}	5.5
L-Leucine	6.2×10^{-2}	4.5×10^{-1}	7.3
L-Isoleucine	1.3×10^{-2}	1.5×10^{-1}	11.5
L-Phenylalanine	1.2×10^{-1}	4.9×10^{-1}	4.1
L-Tryptophan	1.4×10^{-1}	5.7×10^{-1}	4.1
L-Methionine	3.7×10^{-2}	2.4×10^{-1}	6.5
Amines			
L-α-Amino-ϵ-caprolactam	3.1×10^{-4}	1.2×10^{-3}	3.9
L-α-Phenylethylamine	1.3	6.9×10^{-1}	1.9

$$a_{\overline{G}} = \tfrac{1}{2}\{[(p^S + p^R)/(1 + K^{pot}_{GG}) - (p^S - p^R)/(1 - K^{pot}_{GG})]\} \quad (7)$$

where

$p^S = \exp[F(E^S - E^S_o)/RT]$ and $p^R = \exp[F(E^R - E^R_o)/RT]$

Figure 2 shows the comparison of the calculated concentrations of D- and L-PGM ($a_{\overline{G}}$ and a_G) from Eqns. 6 and 7 with the true concentrations. The ratio of D- to L-PGM in the sample solution was varied, but the total concentration of D- and L-PGM was kept constant at 10^{-2} M. The calculated values are in good agreement with the true ones. This indicates that the enantiomer-selective electrodes described here are very useful for the determination of enantiomer concentrations of these optically active amines.

REFERENCES

1 A. P. Thoma, Z. Cimerman, U. Fiedler, D. Bedeković, M. Güggi, P. Jordan, K. May, E. Pretsch, V. Prelog and W. Simon, Chimia, 29 (1975) 344.
2 A. P. Thoma, A. Viviani-Nauer, K. H. Schellenberg, D. Bedeković, E. Pretsch, V. Prelog and W. Simon, Helv. Chim. Acta, 62 (1979) 2303.
3 W. Bussmann, J.-M. Lehn, V. Oesch, P. Plumere and W. Simon, Helv. Chim. Acta, 64 (1981) 657.
4 W. Bussmann and W. Simon, Helv. Chim. Acta, 64 (1981) 2101.
5 P. S. Lingenfelter, R. C. Helgeson and D. J. Cram, J. Org. Chem., 46 (1981) 793.
6 T. Yamaguchi, K. Nishimura, T. Shinbo and M. Sugiura, Maku (Membrane), 10 (1985) 178; Chem. Lett., (1985), 1549.
7 M. Mascini and F. Pallozzi, Anal. Chim. Acta, 73 (1974) 375.

Analytica Chimica Acta, 193 (1987) 373—379
Elsevier Science Publishers B.V., Amsterdam — Printed in The Netherlands

Kurze Mitteilung

EXTRAKTIONSVERHALTEN METHYLSUBSTITUIERTER CHINOLIN-8-OLE GEGENÜBER KUPFER†

A. FRIEDRICH, H. BUKOWSKY und E. UHLEMANN*

Pädagogische Hochschule "Karl Liebknecht", DDR-1500 Potsdam (Deutsche Demokratische Republik)

K. GLOE und P. MÜHL

Akademie der Wissenschaften der DDR, Zentralinstitut für Festkörperphysik und Werkstofforschung, DDR-8027 Dresden (Deutsche Demokratische Republik)

(Eingegangen den 2 Juli 1986)

Summary. (Extraction behaviour of methyl-substituted 8-quinolinols towards copper). The distribution of 2-, 5-, and 7-methyl-8-quinolinols and the extraction of their copper chelates are reported for the chloroform/water system. The stability constants for the copper complexes were calculated. From the acidity and distribution constants of the isomeric 8-quinolinols and the stability and extraction constants of the copper chelates, 7-methyl-8-quinolinol provides the highest complex stability and is the best extractant of the series.

Zusammenfassung. Die Verteilung von 2-, 5- und 7-Methyl-chinolin-8-olen sowie die Extraktion ihrer Kupferchelate wurde für das System Chloroform/Wasser untersucht. Die Extraktionsparameter ermöglichten die Berechnung der Stabilitätskonstanten für die Kupferkomplexe. Mit Hilfe der Säure- und Verteilungskonstanten der isomeren Chinolin-8-ole und der Stabilitäts- und Verteilungskonstanten ihrer Kupferkomplexe ist eine Beurteilung der Extraktionseigenschaften möglich. Als Folge der größten Komplexstabilität erwies sich 7-Methyl-chinolin-8-ol als das beste Extraktionsmittel der Reihe.

Das Extraktionsverhalten und die Komplexbildung des Chinolin-8-ols und einiger ausgewählter alkyl- bzw. alkenylsubstituierter Derivate mit verschiedenen Metallen waren das Ziel zahlreicher Utersuchungen [1—3]. Schwerpunkte bildeten dabei die umfassende Charakteristik der Chinolin-8-ole als Chelatbildner sowie grundsätzliche Untersuchungen zu den in 7-Stellung substituierten Derivaten, von denen Kelex-100 als technisches Extraktionsmittel angeboten wird. Neuere Untersuchungen wurden zu der Frage durchgeführt, wie Art und Stellung der Alkenyl- bzw. Alkylsubstituenten Komplexbildung und Extraktionsvermögen des Chinolin-8-ol-Systems zu beeinflussen vermögen [4—8].

Für die Bestimmung der Stabilitätskonstanten von Kupfer mit Chinolin-8-olen bietet sich die Flüssig-Flüssig-Verteilung an. Weiterhin ist es möglich, an

†IX. Mitteilung über Chelate von Chinolin-8-Derivaten. VIII. Mitt. vgl. [8].

0003-2670/87/$03.50

Hand der Dissoziations- und Verteilungskonstanten der Chelatbildner sowie der Verteilung und der Stabilität der Kupferchelate den Einfluß der einzelnen Parameter auf das Extraktionsverhalten der methylsubstituierten Chinolin-8-ole zu ermitteln.

Experimentelles

Bestimmung der Säurekonstanten. Es wurden pH-potentiometrische Titrationen bei 298 K in Wasser unter Stickstoff als Inertgas durchgeführt. Zu Beginn der Messungen enthielten die 50 ml Probelösung 10^{-4} mol Ligand, 10^{-4} mol HNO_3 und KNO_3 zur Erreichung der Gesamtionenstätke 1,0 M. Als Titrationsmittel diente carbonatfreie 0,1 M Natronlauge nach Sörensen [9].

Die Messungen erfolgten mit einer Versuchseinrichtung, in der Thermostatierung, Rührwerke und automatische Dosierung gekoppelt waren. Alle Messungen wurden unter Verwendung einer Meßkette GB-50/Kalomel 20 (Forschungsinstitut Meinsberg) und des Digital-pH-Meters MV-870 (VEB Präcitronic, Dresden) durchgeführt. Die Konstanten wurden mit Hilfe des Programms PKLOGK an einem Rechenautomaten BESEM-6 berechnet.

Bestimmung der Verteilungskonstanten der Liganden. Die Verteilung der Liganden wurde im System Chloroform/Wasser untersucht. Die Ligandkonzentration in der organischen Phase betrug $2 \cdot 10^{-4}$ mol l^{-1}. Als wäßrige Phase dienten Pufferlösungen, deren Ionenstärke mit Kaliumchlorid auf I = 1,0 mol l^{-1} eingestellt war.

Zur Untersuchung der Zweiphasenverteilung wurden in einem 50-ml Schütteltrichter 10 ml der vorgegebenen wäßrigen Phase mit 10 ml der Ligandlösung in Chloroform versetzt und 10 Min geschüttelt. Nach Abtrennung der organischen Phase wurde deren Extinktion bei einer charakteristischen Wellenlänge gegen Chloroform als Blindlösung vermessen.

Die Aufnahme der UV/VIS-Spektren erfolgte mit den Geräten Specord UV-VIS und VSU 2P (VEB Carl Zeiss, Jena). Die Bestimmung des pH-Wertes der jeweiligen wäßrigen Phase wurde mit dem pH-Meßgerät MV 84 (VEB Präcitronic, Dresden) vorgenommen.

Extraktionsuntersuchungen. Zur Bestimmung der Verteilungsverhältnisse wurden radiometrische Messungen mit ^{64}Cu nach der AKUFVE-Technik durchgeführt [10]. Die Untersuchungen erfolgten im System Chloroform/Wasser. Dabei enthielt die wäßrige Phase jeweils 10^{-4} mol l^{-1} $Cu(NO_3)_2$ und die organische Phase 10^{-2} mol l^{-1} Extraktionsmittel. Die Ionenstärke wurde mit KNO_3 auf I = 1,0 mol l^{-1} eingestellt.

Die Ermittlung der Verteilungskonstanten und der Stabilitätskonstanten der Metallchelate erfolgten mit Hilfe des Rechenprogramms MIQUA am Rechner K-1630 (VEB Robotron, Dresden). Das Programm MIQUA basiert auf der Bestimmung der Koeffizienten der Gleichung

$$1/D = (1 + \beta_1 [L^-] + \beta_2 [L^-]^2)/[L^-]^2 K_v(ML_2)\beta_2 \quad (1)$$

für n Wertepaare ($[L^-]$; $1/D$) nach der Methode der kleinsten Fehlerquadrate.

Die Lösung des sich ergebenden Gleichungssystems erfolgt mit dem Gauss-Jordan-Verfahren in der Subroutine GLESYS. Mittels der Subroutine FEGHUS erfolgt für negative Koeffizienten eine Fehlerberechnung nach dem Gauss'schen Fehlerfortpflanzungsgesetz, so daß nur chemisch sinnvolle Ergebnisse ermittelt werden.

Ergebnisse und Diskussion

Säurekonstanten der Chelatbildner. Die berechneten pK_s-Werte sind, gemeinsam mit einigen Vergleichswerten, in der Tabelle 1 dargestellt. Wie am Beispiel des Chinolin-8-ols ersichtlich wird, liegt eine gute Übereinstimmung mit bisherigen Literaturwerten vor. Beim Protonisierungsgleichgewicht am Heterostickstoff ergibt sich durch den Einfluß der Methylsubstituenten erwartungsgemäß eine Erhöhung der pK_{s_1}-Werte auf Grund des induktiven Effektes dieser Gruppe, die einhergeht mit der Entfernung des Substitutionsortes zum Heterostickstoff.

Bei der Deprotonierung an der Hydroxylgruppe treten geringere Differenzen auf, aber auch hier ist erkennbar, daß der Methylsubstituent in der Position 7 auf Grund seiner Nähe zur Hydroxylgruppe die größte Basizitätserhöhung hervorruft.

Verteilung der Chelatbildner. Bei der Verteilung der Chinolin-8-ole zwischen Wasser und organischen Lösungsmitteln ist zu berücksichtigen, daß in wäßriger Lösung verschieden protonierte Formen, im organischen Lösungsmittel aber nur die Neutralformen der Liganden auftreten. Für den Verteilungskoeffizienten gilt dann

$$D = K_v(\mathrm{HL})/\{([\mathrm{H}^+]/K_{s_1}) + 1 + (K_{s_2}/[\mathrm{H}^+])\} \qquad (2a)$$

Abbildung 1 zeigt die $\log D$/pH-Abhängigkeit für den sauren Bereich. Da K_{s_2} unter diesen Bedingungen zu vernachlässigen ist, ergibt sich für $\log D = 0$ (50%ige Extraktion):

$$\log K_v(\mathrm{HL}) = pK_{s_1} - \mathrm{pH} \qquad (2b)$$

Danach sind aus Messungen an den sigmoiden Ästen der Verteilungskurven mit Hilfe der aus potentiometrischen Messungen zur Verfügung stehenden Säurekonstanten die Verteilungskonstanten leicht zugänglich. Prinzipiell gilt dies auch für das allerdings meßtechnisch weniger günstige alkalische Gebiet.

TABELLE 1

Säurekonstanten und Verteilungskonstanten der Chinolin-8-ole

Substituent	pK_{s_1}	pK_{s_2}	$\log K_v$(HL)	Substituent	pK_{s_1}	pK_{s_2}	$\log K_v$(HL)
—	5,03	9,53	2,49	2-Me	—	—	3,22 [14]
—	5,00	9,66	2,66 [11]	5-Me	5,25	10,08	3,19
—	5,03	—	2,63 [12]	5-Me	—	—	3,27 [15]
—	4,92	9,58	2,59 [13]	7-Me	5,21	10,12	3,38
2-Me	5,71	9,88	3,16	7-Eth	5,26	—	4,27

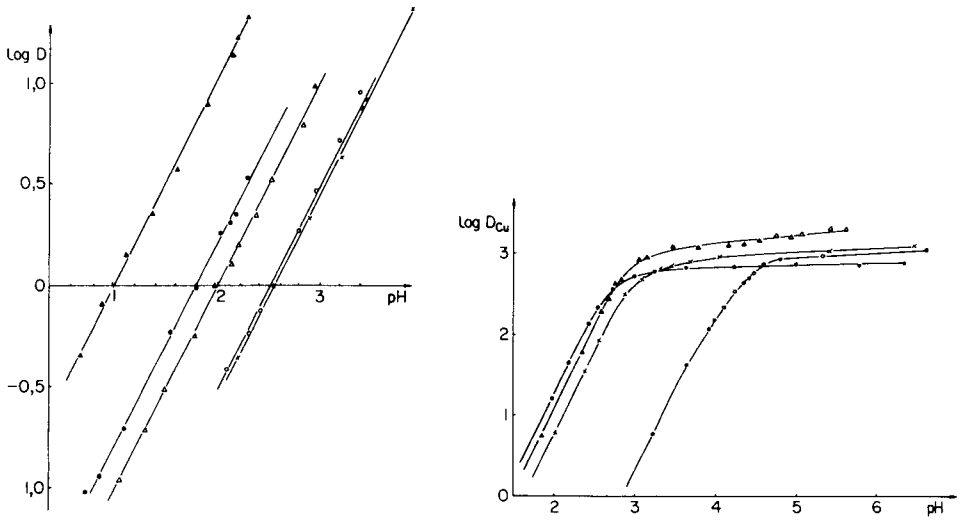

Abb. 1. Log D/pH-Darstellung für die Verteilung von Chinolin-8-olen im System Chloroform/Wasser: (×) Chinolin-8-ol; (○) 2-Methyl-; (△) 5-Methyl-; (●) 7-Methyl-chinolin-8-ol; (▲) 7-Ethyl-chinolin-8-ol.

Abb. 2. pH-Abhängigkeit der Kupferextraktion mit Chinolin-8-olen: (×) unsubstituiert; (○) 2-Methyl; (△) 5-Methyl-; (●) 7-Methyl.

Die Ergebnisse der Untersuchungen sind in Tabelle 1 zusammengefaßt. Ein Vergleich mit Literaturdaten, die unter ähnlichen Bedingungen bestimmt wurden, zeigt eine gute Übereinstimmung. Aus den ermittelten Werten wird ersichtlich, daß eine Methylsubstitution am Chinolin-8-ol zu einer etwa vier- bis fünffach höheren Verteilungskonstante führt und dabei für die 2- und 5-Stellung keine deutlichen Unterschiede auftreten, ein Sachverhalt, den Dyrssen für homologe Serien organischer Chelatbildner beschrieb [16]. Beim 7-Methylchinolin-8-ol kommt es zu einer fast achtfachen Erhöhung der Verteilungskonstante gegenüber dem unsubstituierten Chinolin-8-ol.

Die Ursache könnte im Abschirmungseffekt dieser, der Hydroxylgruppe dicht benachbarten Gruppe liegen. Dann käme es nämlich zu geringeren Wechselwirkungen von Wassermolekülen mit der Hydroxylgruppe, was zwangsläufig zur schlechteren Löslichkeit in der wäßrigen Phase führen sollte. Bei Verlängerung des Substituenten in 7-Stellung um eine CH_2-Gruppe erhöht sich K_v(HL) gegenüber dem 7-Methylchinolin-8-ol wieder fast um den achtfachen Betrag (log K_v(HL) für 7-Ethylchinolin-8-ol = 4,27).

Verteilung und Stabilität der Kupferchelate. Aus den erhaltenen Extraktionsdaten (log $D = f$(pH)) ist nach Kenntnis der Säure- und Verteilungskonstanten der Chelatbildner die Berechnung der Verteilungskonstante des Metallchelates $K_v(ML_2)$ und der Komplexstabilitätskonstanten β_1 und β_2 nach Gleichung 1 möglich. Bei den hier diskutierten Extraktionsmitteln

müssen bei der Berechnung der Ligandanionenkonzentration die beiden Säurekonstanten berücksichtigt werden.

Um $[L^-]$ aus der Konzentration der eingesetzten Verbindung und aus dem pH-Wert der wäßrigen Phase einfach zu erhalten, wählt man einen 100-fachen Ligandüberschuß. Es gelten dann die folgenden Beziehungen für die Berechnung der Ligandanionenkonzentration:

$$[HL]_{ausg.} = [HL]_0 + [HL]_{aq}$$

$$= K_v(HL)\,[HL]_{aq} + [H_2L^+] + [HL] + [L^-]$$

$$= K_v(HL)\,([H^+]\,[L^-]/K_{s_2}) + ([H^+]^2\,[L^+]/K_{s_1}\,K_{s_2}) + ([H^+]\,[L^-]/K_{s_2}) + [L^-]$$

$$[L^-] = ([HL]_{ausg.}\,K_{s_2}/[H^+])\{K_v(HL) + ([H^+]/K_{s_1}) + (K_{s_2}/[H^+]) + 1\}^{-1} \quad (3b)$$

Die auf diesem Wege bestimmten $K_v(ML_2)$, β_1- und β_2-Werte sind in der Tabelle 2 dargestellt.

Abbildung 2 zeigt die log D/pH-Abhängigkeit für die Extraktion des Kupfers mit methylsubstituierten Chinolin-8-olen. Danach kann Kupfer bereits aus stark saurer Lösung extrahiert werden, wobei das 7-Methylchinolin-8-ol die höchsten Verteilungsverhältnisse aufweist, gefolgt von 5-Methylchinolin-8-ol und dem unsubstituierten Vertreter. Gegenüber der Ligandverteilung weicht das 2-Methylchinolin-8-ol deutlich von den anderen Vertretern der Serie ab. Aus dem Anstieg der Geraden im log D/pH-Diagramm ergibt sich erwartungsgemäß das Molverhältnis von 2:1 für Chinolin-8-ol zu Cu(II) im extrahierten Komplex.

Ein Vergleich der berechneten Verteilungskonstanten der Kupferchelate weist beim Bis(2-Methylchinolin-8-olato)-Cu(II) eine Erhöhung gegenüber dem unsubstituierten Vertreter um das 1,5-fache aus, während die $K_v(ML_2)$-Werte der anderen Vertreter absinken. Die früher [14] beschriebene Erhöhung der $K_v(ML_2)$-Werte beim Übergang vom Chinolin-8-ol zum 2-Methylchinolin-8-ol konnte nicht bestätigt werden.

Aus den Säure- und Verteilungskonstanten der Chelatbildner sowie den Stabilitäts- und Verteilungskonstanten der Kupferchelate wurden die Extraktionskonstanten nach folgender Beziehung berechnet:

TABELLE 2

Stabilitätskonstanten und Extraktionsdaten für Kupferkomplexe von Chinolin-8-olen

Substituent	log $K_v(ML_2)$	log β_1	log β_2	K_{ex}	log K_{ex}	
—	3,03	11,85	22,18	14,75	1,17	
—	3,48	12,10	23,00	—	—	[14, 17]
	3,38	11,90	22,83	—	—	[13]
2-Me	3,21	11,28	21,57	0,05	−1,30	
2-Me	4,45	—	—	—	—	[14]
5-Me	2,83	12,42	25,41	15,07	1,18	
7-Me	2,89	12,99	25,90	61,58	1,79	

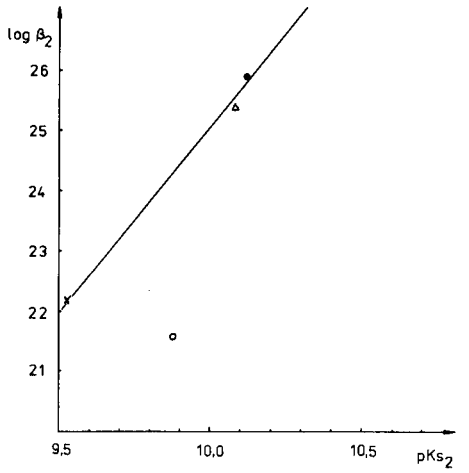

Abb. 3. Korrelationsgerade (log β_2/pK_{s_2}) für die Kupferkomplexe mit Chinolin-8-olen (×) unsubstituiert; (○) 2-Methyl-; (△) 5-Methyl-; (●) 7-Methyl.

$$K_{ex} = K_v(ML_2)\,\beta_2\;K_{s_2}^2/K_v^2(HL) \qquad (4)$$

Die erhaltenen Daten (Tabelle 2) zeigen für das 7-Methylchinolin-8-ol mit $K_{ex} = 61{,}58$ den höchsten Wert.

Während die Differenz zum 5-Methylchinolin noch relativ klein ist, erfolgt zum Chinolin-8-ol und besonders zum 2-Methylchinolin-8-ol eine deutliche Abgrenzung.

Betrachtet man den Einfluß der einzelnen Größen in der Gleichung 4, so ergibt sich folgender Sachverhalt. Die hohen K_{ex}-Werte der in 5- und 7-Stellung substituierten Vertreter resultieren in erster Linie aus den hohen Komplexstabilitäten der Kupferchelate und der höheren Basizität der Liganden gegenüber dem Chinolin-8-ol. Der vergleichsweise niedrige K_{ex}-Wert des 2-Methylchinolin-8-ols liegt vorrangig in der verminderten Komplexstatilität begründet. Die durch den Mathylsubstituenten hervorgerufene Basizitätserhöhung des Liganden geht, wie aus Abb. 3 hervorgeht, nicht einher mit einer Erhöhung des β_2-Wertes. Die Ursachen hierfür liegen vermutlich in der Geometrie des Chelates [18].

LITERATUR

1 J. Stary, The Solvent Extraction of Metal Chelates, Pergamon, Oxford, 1964.
2 Y. Marcus und A. S. Kertes, Ion Exchange and Solvent Extraction of Metal Complexes, Wiley, New York, 1969.
3 H. A. Mottola und H. Freiser, Talanta, 13 (1966) 55.
4 E. Uhlemann und W. Weber, Anal. Chim. Acta, 156 (1984) 201.
5 E. Uhlemann, W. Weber, F. Dietze und W. Kalies, Z. Anorg. Allg. Chem., 510 (1984) 79.
6 E. Uhlemann, B. Opitz, U. Schilde, M. Raab und W. Kalies, Z. Anorg. Allg. Chem., 520 (1985) 167.

7 E. Uhlemann, U. Schilde, R. Kirmse und G. Stach, Z. Anorg. Allg. Chem., 524 (1985) 193.
8 A. Friedrich, U. Schilde und E. Uhlemann, Z. Anorg. Allg. Chem., 534 (1986) 199.
9 S. P. Sörensen, Biochem. Z., 21 (1909) 166.
10 K. Gloe und P. Mühl, Isotopenpraxis, 15 (1979) 236.
11 D. Dyrssen, Sven. Kem. Tidskr. 64 (1952) 213.
12 J. G. Mason und I. Lipschitz, Talanta, 18 (1971) 1111.
13 B. Magyar und P. Wechsler, Talanta, 21 (1974) 539.
14 J. Fresco und H. Freiser, Anal. Chem., 36 (1964) 631.
15 D. Dyrssen, Rec. Trav. Chim. Pays-Bas, 75 (1953) 753.
16 D. Dyrssen, Division of Analytical Chemistry, ACS Summer Symposium, Tucson, AZ, 1963.
17 L. G. Sillén und A. E. Martell, Special Publication No. 25, The Chemical Society, London.
18 H. Nariai, Y. Masuda und E. Sekido, Bull. Chem. Soc. Jpn., 57 (1984) 3077.

Analytica Chimica Acta, 193 (1987) 381—385
Elsevier Science Publishers B.V., Amsterdam — Printed in The Netherlands

Short Communication

PRECONCENTRATION OF ANTIMONY(III) FROM WATER WITH THIONALIDE LOADED ON GLASS BEADS WITH THE AID OF COLLODION

MASAE MATSUI, KEN MATSUMOTO and KIKUO TERADA*

Department of Chemistry, Faculty of Science, Kanazawa University, Kanazawa, Ishikawa 920 (Japan)

(Received 28th July 1986)

Summary. 2-Mercapto-*N*-2-naphthylacetamide (thionalide) loaded on glass beads with the aid of collodion is used for preconcentration of microgram levels of antimony(III) from aqueous solution. Antimony is quantitatively retained on the loaded beads from 0.4—0.8 mol l^{-1} hydrochloric acid solutions; equilibration is achieved within 1 min. The retention capacity of the beads is 0.2 μmol Sb g^{-1} at 0.6 mol l^{-1} hydrochloric acid. The maximum flow rate for quantitative retention is 1.27 ml min^{-1} cm^{-2}. Antimony retained on the column is completely eluted with 10 ml of 6.0 mol l^{-1} hydrochloric acid at flow rates <1.9 ml min^{-1} cm^{-2}.

The concentrations of antimony are very low in natural waters, as little as 0.1—0.5 μg kg^{-1} in seawater [1] and 0.01—0.2 μg kg^{-1} in river water [2]. The detection limit of the most sensitive method, hydride-generation/inductively-coupled plasma atomic emission spectrometry, is only 0.19 μg l^{-1} Sb [2, 3]. Therefore, preconcentration is necessary for its precise determination.

Thionalide (2-mercapto-*N*-2-naphthylacetamide) yields water-insoluble white or pale-coloured precipitates with most of the di- or tri-valent metals which precipitate with sulphide [4—7]. The reagent is insoluble in water but soluble in acetone or tetrahydrofuran. 2-Mercaptobenzothiazole (MBT) loaded on glass beads with the aid of collodion has been found to be an excellent selective collector for μg l^{-1} levels of copper(II) and lead(II) from aqueous solutions [8]. The loaded beads are prepared simply and rapidly, and because the complexing agent is incorporated in the collodion, the reagent is protected from oxidation by air. In the present study, thionalide was chosen as the complexing agent, and its retention behaviour at various acidities, the retention rate of antimony(III), and the preconcentration and recovery of antimony from dilute solutions were investigated.

Experimental

Reagents. Thionalide and tetrahydrofuran (THF) were analytical-reagent grade; the latter was purified by distillation. A standard solution of antim-

0003-2670/87/$03.50

ony(III) (1000 μg ml^{-1}) was prepared by dissolving 0.2790 g of antimony (99.999% purity) in 10 ml of sulphuric acid by heating, evaporating to white fumes, cooling and dissolving in (1 + 1) hydrochloric acid, and then making up to 250 ml with the same acid.

Glass beads (Toshinriko Co., No. 06, 0.49—0.70 mm in diameter) were soaked in (1 + 1) nitric acid for 3 days, washed with deionized water, soaked in hydrofluoric acid (ca. 11.5% w/w) for 10 min with continuous stirring, and washed with deionized water. Finally, the beads were soaked in (1 + 1) nitric acid for 2 days and, after being washed with deionized water, were dried in an oven at 90°C. The purified beads were stored in a desiccator. Used glass beads could be purified as follows: the beads were washed with ethanol and acetone to remove collodion and thionalide, then soaked in (1 + 1) nitric acid for 2 days, washed with deionized water and dried at 90°C for 12 h. The collodion containing 5.0—5.5% cellulose nitrate was extra-pure reagent grade.

Preparation of thionalide loaded on glass beads with the aid of collodion (thionalide/CGB). About 100 g of purified glass beads was placed on a teflon sheet which was spread in a crystallizing dish. A collodion solution containing thionalide (2.0 g of thionalide/16 ml of collodion solution/16 ml of THF) was poured onto the dish and mixed well with the glass beads. Then the solvent was completely removed under reduced pressure. Finally, the dry glass beads adhering to each other on the teflon sheet were gently separated by pressing the sheet.

Apparatus. A Hitachi 170-50 atomic absorption spectrometer was used for the determination of antimony. An Iwaki VS electric shaker was used for batch experiments. A Toyo Model SF-160K balance-operated fraction collector and a Tokyo Rikakikai Model MP-3 peristaltic pump were used for column experiments. The columns were glass tubes (10-mm i.d., 140 mm long) with a coarse sintered glass disc and stopcock at the bottom.

Procedure for batch experiments. To a 50-ml glass stoppered centrifuge tube were added 5 ml of hydrochloric acid, 5 ml of 10 μg ml^{-1} antimony(III) solution and 4 g of thionalide/CGB, and the contents were shaken for a definite time at room temperature. After the beads had settled, the supernatant solution was filtered through a dry sheet of Toyo No. 5B filter paper. Antimony was quantified in aliquots of the filtrate by atomic absorption spectrometry (a.a.s.) at 217.6 nm. The percent retention of antimony was calculated by comparison of the absorbance measured for the filtrate solution and the untreated solution.

Procedure for column methods. A glass column was filled with 3 g of thionalide/CGB which was previously soaked in 0.6 mol l^{-1} hydrochloric acid containing 1% of ethanol for 1 day, and a small disc of Toyo No. 5C filter paper was placed on top so that the beads were not disturbed during sample passage. A 50-ml portion of a 3 μg ml^{-1} antimony(III) solution was adjusted to a suitable acid concentration, and then percolated through the column at 1.2 ml min^{-1}. The column was washed with deionized water and

antimony was eluted with 10 ml of 6 mol l^{-1} hydrochloric acid at 1.5 ml min^{-1}. The effluent was diluted to 15 ml in a measuring flask and antimony was quantified as above.

Measurement of the amount of thionalide on glass beads. Dry thionalide/CGB (1 g) was packed in a glass column and 20 ml of THF was passed through to remove the reagent and collodion completely. The effluent was diluted with the solvent to the desired volume. The absorbance of the solution was measured at 285 nm against THF as reference.

Results

The amount of the reagent loaded on the glass beads was found to be 18.8 ± 3.8 mg (86.6 ± 18 μmol) g^{-1}. The complexing capacity for antimony was measured by the break-through method using 300 ml of 3 μg ml^{-1} antimony(III) solution (0.6 mol l^{-1} HCl) and 10 g of thionalide/CGB. In the course of the study, it was found that the retention capacity of the beads increased with increase in the soaking time of the beads in 0.6 mol l^{-1} hydrochloric acid containing 1% of ethanol. This effect is shown in Fig. 1. This can be attributed to a hydrophobic effect of the collodion membrane, which prevents perfect contact between the reagent on the beads and antimony in the aqueous solution. When the beads were soaked in the above solution for 50 h prior to the column operation, the capacity increased by a factor of 2. However, the capacity remains rather low, indicating that a larger portion of thionalide does not react with antimony, because most of the reagent is within the collodion coating, and so has restricted ability to react with the element.

Effect of acid concentration and flow rate on retention of antimony. The retention of antimony(III) ion from aqueous solutions at various acidities was examined by the batch method; 10 ml of 5 μg ml^{-1} antimony solution was equilibrated with 4 g of thionalide/CGB. The results are shown in Fig. 2. Antimony was quantitatively retained from 0.4 to 0.8 mol l^{-1} hydrochloric

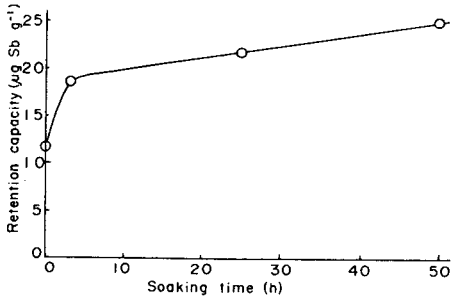

Fig. 1. Relationship between soaking time and retention capacity of thionalide/CGB.

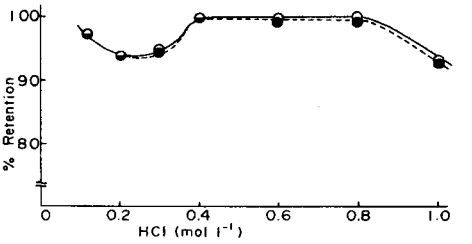

Fig. 2. Effect of hydrochloric acid concentration on retention of antimony(III): (○) 60-s shaking; (●) 30-s shaking.

acid. The retention of antimony from 0.6 mol l^{-1} hydrochloric acid solution was examined at various flow rates using 3 g of the beads. The retained antimony was eluted with 10 ml of 6.0 mol l^{-1} hydrochloric acid and quantified by a.a.s. The results showed that 3 $\mu g\ ml^{-1}$ antimony was collected quantitatively by 3 g of thionalide/CGB at flow rates lower than 1.3 ml min^{-1} from 50 ml of the solution. The retention then decreased gradually up to flow rate of 3.2 ml min^{-1}. However, when 750 and 1000 ml of samples of lower antimony concentrations were passed through the column, a flow rate of 1.0 ml min^{-1} and at least 10 g of the loaded beads provided complete retention (Table 1). The same or larger amounts of sample can be treated more rapidly if a wider column is used with a larger amount of the beads.

Elution of antimony. Several acids were investigated for the elution of antimony. Complete elution was obtained with 10 ml of 6.0 mol l^{-1} hydrochloric acid. The elution curves of antimony obtained with hydrochloric acid of various concentrations are shown in Fig. 3. When 10 ml of 6.0 mol l^{-1} hydrochloric acid was passed through the column, complete elution of up to 30 μg of antimony was achieved at a flow rate of 1.5 ml min^{-1}. The eluting solution did not affect the subsequent determination of antimony by a.a.s.

Several metal ions such as silver(I), bismuth(III), copper(II), mercury(II) and platinum(IV) react with thionalide under the present conditions [7]. However, in general, the concentrations of these metals are very low in natural waters and their interferences are likely to be negligible in practice. With regard to organic materials, their effects also may be neglected, because as shown in Table 1, approximately quantitative recovery of added antimony was achieved from seawater collected near the shore at Atakano-Seki, Ishikawa Prefecture, which is considered to be more polluted by human activities than open sea.

In conclusion, the present method seems promising for application to the preconcentration of antimony in various kinds of natural waters prior to

TABLE 1

Recovery of antimony added to seawater samples by column collection[a]

Sb concn. (ng ml^{-1})	Sample vol. (ml)	Thionalide/CGB (g)	Recovery (%)
40	750	5.0	70.5
40	750	10.0	100
20	1000	5.0	64.9
20	1000	10.0	100

[a]Flow rate of 1.0 ml min^{-1} cm^{-2}.

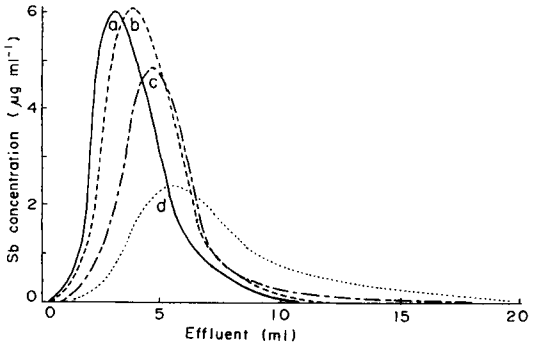

Fig. 3. Elution of antimony retained on thionalide/CGB by hydrochloric acid of various concentrations: (a) 6 mol l^{-1}; (b) 5 mol l^{-1}; (c) 4 mol l^{-1}; (d) 3 mol l^{-1}.

an a.a.s. determination after hydride generation in which the effluent from the column may conveniently be used directly [9].

REFERENCES

1 K. H. Wedepohl, C. W. Correns, D. M. Shaw, K. K. Turekian and J. Zemann (Eds.), Handbook of Geochemistry, II-4, Springer-Verlag, Berlin, 1974, 51-1-1.
2 T. Nakahara and N. Kikui, Anal. Chim. Acta, 172 (1985) 127.
3 M. Thompson, B. Pahlavanpour, S. J. Walton and G. F. Kirkbright, Analyst (London), 103 (1978) 568, 705.
4 R. Berg and E. S. Fahrenkamp, Fresenius Z. Anal. Chem., 107 (1937) 305; 112 (1938) 162.
5 H. Kienitz and L. Rombock, Fresenius Z. Anal. Chem., 117 (1939) 241.
6 W. J. Rogers, F. E. Beamish and D. S. Russell, Ind. Eng. Chem., Anal. Ed., 12 (1940) 561.
7 R. A. Chalmers (Ed.), Handbook of Organic Reagents in Inorganic Analysis, Wiley, New York, 1976, p. 391.
8 K. Terada, K. Matsumoto and T. Inaba, Anal. Chim. Acta, 170 (1985) 225.
9 B. Welz and M. Melcher, Anal. Chem., 57 (1985) 427.

Analytica Chimica Acta, 193 (1987) 387—392
Elsevier Science Publishers B.V., Amsterdam — Printed in The Netherlands

Short Communication

LIQUID/LIQUID EXTRACTION SEPARATION OF HAFNIUM WITH AMBERLITE LA-1 FROM ZIRCONIUM AND OTHER ELEMENTS IN CITRIC ACID SOLUTIONS

C. P. VIBHUTE and S. M. KHOPKAR*
Department of Chemistry, Indian Institute of Technology, Bombay — 400 076 (India)
(Received 19th March 1986)

Summary. Hafnium (10—110 μg ml^{-1}) is quantitatively extracted at pH 4.5 from 0.01 M citric acid with 0.1 M Amberlite LA-1 in xylene; it can be stripped with 0.1 M perchloric acid and determined spectrophotometrically with xylenol orange at 540 nm. Hafnium can be separated from binary and multicomponent mixtures by selective extraction and back-extraction. The method is suitable for determining hafnium in zircon.

Liquid/liquid extraction methods for the separation of zirconium as well as hafnium have been reviewed [1]. Various liquid anion exchangers have been used [2, 3] to separate hafnium, including Aliquat-336S [4], Primine-JMT [5] and Adogen 364 [6], which gave complete extraction. It is shown here that hafnium forms citrate complexes which are extractable with Amberlite LA-1 or Aliquat-336S with xylene as diluent; this extraction separates hafnium from zirconium and similar elements.

Experimental

Apparatus. An Orion Research Microprocessor ion-analyzer 901 with glass and calomel reference electrodes, a GS-866C spectrophotometer (Electronic Corporation of India) with matched 10-mm corex glass cells and a wrist-action flask shaker (Toshniwal, India) were used.

Reagents. Pure hafnium dioxide (ca. 0.5 g; Indian Rare Earths, Alwaye) was dissolved in a (9 + 1) mixture of hydrofluoric acid (26.5 M) and sulphuric acid (18 M, both BDH, AnalaR). After digestion and evaporation, the cooled mass was extracted with hot sulphuric acid and diluted to 100 ml with distilled water, maintaining the total acidity at 0.4 M sulphuric acid. The solution was standardized gravimetrically [7] with mandelic acid; it contained 3.4 mg ml^{-1} hafnium. A solution containing 25 μg ml^{-1} hafnium was prepared by appropriate dilution with water. Xylenol orange (BDH) was used as an aqueous 0.05% (w/v) solution in 0.3 M perchloric acid. Citric acid (AnalaR), Amberlite LA-1 and LA-2 (Rohm and Hass), Aliquat-336S (General Mills Chemicals, Minneapolis, MN) and trioctylamine (Riedel de Haen, Seelze, F.R.G.) were used as received. The exchangers were converted to their citrate forms as described previously [8].

0003-2670/87/$03.50

General procedure. A portion of solution containing 10—110 μg ml^{-1} hafnium was mixed with 5 ml of 0.01 M citric acid. The pH was adjusted to 4.5 with 0.01 M sodium hydroxide or citric acid. The solution was diluted to 10.00 ml with distilled water. The solution was transferred to a 100-ml separatory funnel, and shaken with 10 ml of 0.1 M Amberlite LA-1 in xylene for 5 min. After phase separation, the aqueous phase was discarded. Hafnium was stripped from the organic phase with 10 ml of 0.5 M perchloric acid. After addition of 3 ml of 0.05% xylenol orange solution and dilution to exactly 25 ml, the absorbance of the violet-red complex was measured at 540 nm against a reagent blank. For calibration, solutions containing 10—110 μg ml^{-1} hafnium were taken through the above procedure. The apparent molar absorptivity of the complex was 1.96×10^4 l mol^{-1} cm^{-1}.

Determination of hafnium in zircon. Zircon (ca. 0.4 g) was weighed accurately and fused with 4 g of borax in a platinum crucible. The mass was cooled, and extracted with ca. 50 ml of 2 M hydrochloric acid. The solution was diluted to 250 ml with distilled water. A 25-ml aliquot was mixed with an equal volume of concentrated hydrochloric acid. Silicic acid was filtered off (and weighed as silicon dioxide). After filtration, portion of the solution was extracted as described in the general procedure. Extracted iron and titanium were stripped with 0.5 M sulphuric acid, hafnium with 9 M hydrochloric acid and zirconium with 2 M hydrochloric acid, and each was determined spectrophotometrically with suitable chromogenic reagents (see below).

Results and discussion

Effect of extraction conditions. The best choice of liquid anion exchanger and pH for quantitative extraction of hafnium was ascertained by extraction at pH 1.0—7.0 with 0.1 M Amberlite LA-1, 0.08 M Amberlite LA-2, 0.1 M Aliquat-336S or 0.1 M trioctylamine (TOA) in xylene. Extraction was quantitative with Amberlite LA-1 at pH 3—6, with Aliquat-336S at pH 2.5—5.0 and with Amberlite LA-2 at pH 3—5. The extraction was not complete at any pH with TOA. Hafnium in the organic and aqueous phases was determined spectrophotometrically at 540 nm with xylenol orange (after stripping from the organic phase). From the calibration graph, the amount and proportion of hafnium extracted at each pH were evaluated. The results are shown in Fig. 1. The concentration of citrate used throughout the pH studies was 0.01 M. Variation of the concentration of hafnium indicated that under the conditions for quantitative extraction, 10—110 μg ml^{-1} hafnium can be extracted.

The effect of various diluents on the extraction of 50 μg ml^{-1} hafnium with 0.1 M Amberlite LA-1 was studied. Benzene, toluene, xylene, hexane, cyclohexane, carbon tetrachloride, nitrobenzene and isobutyl methyl ketone were tested. The results (Table 1) show that the extraction was quantitative only with xylene, hexane and cyclohexane as diluent; all of these have low dielectric constants. However, extraction into other solvents of low dielectric constant, such as benzene, toluene and carbon tetrachloride was poor.

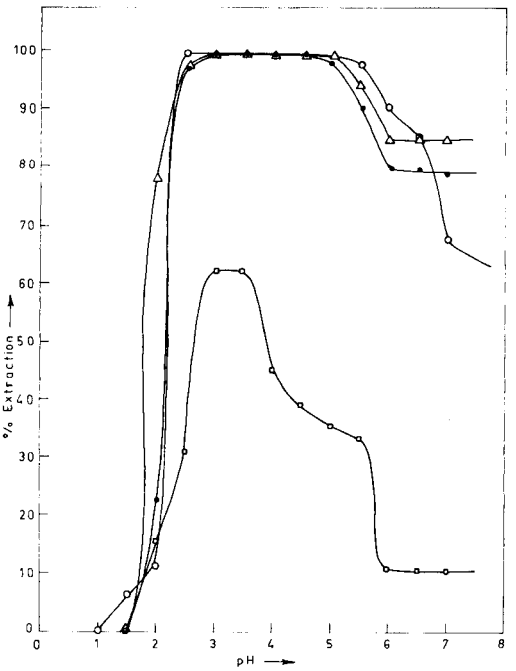

Fig. 1. Extraction of hafnium (50 μg ml^{-1}) as a function of pH: (○) Amberlite LA-1 (0.1 M); (△) Aliquat-336S (0.1 M); (□) TOA (0.1 M); (●) Amberlite LA-2 (0.08 M). Conditions as in Procedure unless otherwise stated.

TABLE 1

Effect of various diluents on extraction of hafnium

Diluent	Dielectric constant	Hafnium extraction (%)	Distribution ratio
Benzene	2.28	56.0	1.30
Toluene	2.38	60.6	1.50
Xylene	2.30	99.9	999
Hexane	1.89	99.9	999
Cyclohexane	2.05	99.9	999
Nitrobenzene	34.8	32.0	0.47
Carbon tetrachloride	2.24	84.0	5.30
Chloroform	4.80	36.0	0.60
Isobutylmethyl ketone	13.10	24.0	0.31

The concentration of citric acid required for the complete extraction of hafnium (50 μg ml^{-1}) was ascertained by extracting hafnium at pH 4.5 with 0.1 M Amberlite LA-1 in xylene from 1×10^{-4}—1×10^{-2} M citric acid. The extraction was quantitative (99.8%) for $\geqslant 8 \times 10^{-4}$ M citric acid, therefore

0.01 M citric acid is recommended for use. Similarly, hafnium (50 μg ml^{-1}) was extracted with 0.01—0.1 M Amberlite LA-1 with xylene as diluent. Extraction was complete with $\geqslant$0.09 M Amberlite LA-1, so 0.10 M is recommended.

After extraction of hafnium from 0.01 M citric acid, the effect of different stripping agents at various concentrations was studied. Back-extraction was quantitative into 10 ml of 1—8 M hydrochloric acid, 2—8 M hydrobromic acid, 4—8 M nitric or sulphuric acid and 0.5—8 M perchloric acid (Table 2). Ammonia and sodium hydroxide were poor stripping agents because they caused hafnium to precipitate. Perchloric acid (0.5 M) was preferred as the stripping agent on account of the ease of spectrophotometric determinations in such media.

Separation of hafnium from binary mixtures. Hafnium was readily separated from alkali and alkaline earths, thallium(I) and silver(I), which were not extracted. Manganese(II), cobalt, nickel, copper, zinc, cadmium, lead, aluminium, cerium(III), chromium(III), lanthanum and yttrium formed weak citrate complexes which could be back-extracted with distilled water. Gallium, thallium, germanium, tin, uranium, mercury and gold were extracted, but could be separated after extraction by stripping hafnium into 5 M hydrochloric acid after the other ions had been stripped into 0.5 M hydrochloric acid. Antimony, bismuth, titanium, vanadium, molybdenum and iron were separated after extraction by first stripping them into 0.5 M sulphuric acid and then stripping hafnium into 0.5 M perchloric acid. Extracted indium and hafnium could be separated by first stripping hafnium into 6 M nitric acid and then indium into 0.5 M hydrochloric acid. Each element separated in this way was determined in the aqueous phase by suitable spectrophotometric methods (Table 3). Separation of hafnium from other elements was possible at ratios of 1:1 to 1:100.

Separation of hafnium from multicomponent mixtures. Cobalt or copper, hafnium and iron were separated after extraction by back-extracting cobalt or copper into water, stripping iron into 0.5 M sulphuric acid, and finally stripping hafnium into 0.5 M perchloric acid. A mixture of nickel, hafnium

TABLE 2

Efficiency of various stripping agents on back-extraction of hafnium

Stripping agent	Back-extraction (%)[a]					
	0.05	0.1	0.5	1.0	2—4	6—8
HCl	15.3	46.7	88.3	98.4	99.9	99.6
HBr	0.0	30.0	70.8	85.4	98.7	99.9
HNO_3	0.0	0.0	65.4	90.5	95.7	99.9
H_2SO_4	0.0	0.0	0.0	48.5	80.4	99.9
$HClO_4$	42.4	80.7	99.9	99.0	99.9	99.8

[a]With different concentrations (0.05—8 M) of the acids listed.

TABLE 3

Spectrophotometric methods for the determination of other elements

Analyte	pH (acidity)	Reagent	λ (nm)	Ref.[a]
Be	2.0—3.0	Erichrome cyanine R	525	675
Mg	7.0	Erichrome black T	520	1932
Sc	3.5	Alizarin red S	525	536
Ti(IV)	3.0	Tiron	380	1114
Zr	(2 M)	Arsenazo-III	665	1143
Th	(3 M)	Arsenazo-III	655	1820
U(VI)	8.0	PAR[b]	530	1390
V(V)	6.2	PAR	550	1226
La	7.2	Arsenazo-I	570	1802
Ce(III)	3.0	Arsenazo-I	655	1795
Cr(VI)	(0.1 M)	Diphenylcarbazide	545	715
Mo(VI)	(5 M)	Phenylfluorone	526	1311
Mn(II)	10.0	PAR	500	1028
Fe(II)	2.0	1,10-Phenanthroline	510	795
Co	4.0	Nitroso-*R* salt	415	953
Ni	8.3	Dithizone	670	901
Cu	8.5	Diethyldithiocarbamate	580	172
Zn	8.0	PAR	495	1059
Cd	9.0	Arsenazo-III	600	292
Al	4.0	Alizarin red S	490	587
Ga	4.0	PAR	505	514
In	4.0	PAR	510	480
Tl(III)	(1.5 M)	Malachite green	635	58
Sn(II)	2.5	Pyrocatechol violet	555	456
Pb	10	PAR	520	34
Sb(III)	(1.2—1.5 M)	Iodide	555	388
Bi	(0.2 M)	Iodide	460	306
Ge	(6 M)	Phenylfluorone	530	570

[a]Reference is given to page numbers in Snell [9]. [b]4-(2-pyridylazo)resorcinol.

and gallium was separated after extraction, by back-extracting nickel into water, hafnium into 5 M hydrochloric acid and gallium into 0.5 M hydrochloric acid. For the separation of extracted titanium, hafnium and zirconium, titanium was stripped into 0.1 M sulphuric acid, hafnium into 9 M hydrochloric acid and zirconium into 2 M hydrochloric acid. Other ternary and quaternary mixtures were separated by using the stripping agents indicated in Table 4; such separations were quantitative. Spectrophotometric measurements were made with the reagents indicated in Table 3.

Separation of hafnium from zirconium. When mixtures of zirconium and hafnium were extracted at pH 3.5 with 0.1 M Aliquat-336S from 0.1 M citric acid, hafnium was not extracted, while zirconium was extracted. Zirconium could be back-extracted into 2 M hydrochloric acid. In this way, it was possible to separate quantitatively zirconium and hafnium in ratios from 1:10 to

TABLE 4

Separation and determination of hafnium in multicomponent mixtures

Sample	Species	Taken (μg)	Found (μg)	Recovery (%)	Stripping agent
1	Co or Cu	475	475	100	H_2O
	Hf	50	50	100	4 M HCl
	Fe(III)	540	540	100	0.5 M H_2SO_4
2	Ni(II)	320	320	100	H_2O
	Hf	490	490	100	4 M HCl
	Ga	190	190	100	0.5 M HCl
3	Ti(IV)	1070	1070	100	0.1 M H_2SO_4
	Hf(IV)	50	50	100	9 M HCl
	Zr(IV)	780	779	99.8	2 M HCl
4	Al	450	450	100	H_2O
	Fe(III)	50	50	100	0.5 M H_2SO_4
	Hf	100	100	100	0.5 M $HClO_4$
5	Fe(III)	520	519	99.8	0.5 M H_2SO_4
	Hf(IV)	410	409	99.7	9 M HCl
	Zr(IV)	385	385	100	2 M HCl
6	Ti(IV)	290	290	100	0.1 M H_2SO_4
	Th(IV)	320	320	100	0.5 M H_2SO_4
	Hf(IV)	50	50	100	9 M HCl
	Zr(IV)	340	340	100	2 M HCl
7	Cr(III)	570	569	99.8	H_2O
	Ti(IV)	160	159	99.4	0.1 M H_2SO_4
	Hf(IV)	130	130	100	9 M HCl
	Zr(IV)	230	230	100	2 M HCl

10:1. The procedure was used to determine hafnium in zircon. The concentrations found were 1.40 and 1.42%; a value of 1.4% was reported by the Indian Standards Institution.

REFERENCES

1 B. Nandi, N. R. Das and S. N. Bhattacharyya, Solvent Extraction and Ion Exchange, 1 (1983) 141.
2 E. Cerrai and Testa, Energ. Nucl. (Milan), 6 (1959) 768.
3 F. L. Moore, Anal. Chem., 29 (1957) 1660.
4 I. S. El-Yamani, M. Y. Farah and F. A. Abd-El-Aleim, J. Radioanal. Chem., 45 (1978) 125.
5 I. S. El-Yamani, M. Y. Farah and F. A. Abd-El-Aleim, Talanta, 25 (1978) 523.
6 I. S. El-Yamani, M. Y. Farah and F. A. Abd-El-Aleim, Radiochem. Radioanal. Lett., 33 (1978) 345.
7 A. K. Mukherji, Analytical Chemistry of Zirconium and Hafnium, Pergamon, Oxford, 1970, p. 36.
8 C. P. Vibhute and S. M. Khopkar, Anal. Lett., 16 (1983) 1037.
9 F. D. Snell, Photometric and Fluorometric Methods of Analysis, Parts I and II, Wiley, New York, 1978.

Analytica Chimica Acta, 193 (1987) 393—411
Elsevier Science Publishers B.V., Amsterdam — Printed in The Netherlands

Book Reviews

A. Knowles and C. Burgess (Eds.), *Practical Absorption Spectrometry*. Chapman and Hall, London, 1984 (ISBN 0-412-24390-3). Price £18.00.

This book will tell you almost everything the analytical chemist needs to know about absorption spectrometry in the u.v.-visible region. It does so with clarity and thoroughness, and bears that stamp of authority that emanates from distinguished practitioners who have spent a lifetime working in the field. The book is a sequel to "Standards in Absorption Spectrometry" and will serve modern spectroscopists in the same way as Edisbury's celebrated "Practical Hints for Absorption Spectrometry" did twenty years ago.

The text covers the various aspects of the subjects in logical sequence: spectra, spectrometer design, light sources, optical components, monochromators, detectors, signal processing, interfacing, cells, spectral measurement, numerical methods of data analysis, derivative and other special techniques, automated sample handling, and instrument maintenance. Appendices detail solvent characteristics and spectra of solvents, optical materials, and wavelength standards.

It is essential that all users of u.v.-visible spectrophotometers should be familiar with the contents of this book. It provides much needed information about the way in which the work-horse of the analytical laboratory should be operated, and the consequences of treating it merely as an eternally reliable black box! The UV Spectrometry Group are to be congratulated for sponsoring a very useful and timely series of books.

Zygmunt Marczenko, *Separation and Spectrophotometric Determination of Elements*. Horwood, Chichester, 1986 (ISBN 0-85312-903-7). 678 pp. Price £69.50.

To those, like myself, who found Professor Marczenko's previous book "Spectrophotometric Determination of Elements" (1976) particularly useful, the new text will be more than welcome. It not only updates the considerable information on spectrophotometry found in the earlier book, but also includes reviews on separation procedures; extraction, ion-exchange and precipitation are the most popular. The first three chapters comprise Part I (101 pp.), which provides detailed discussions of Separation and Preconcentration Processes, Principles and Practice of Spectrophotometric Analysis, and Spectrophotometric Reagents. Part II is arranged in chapters, in alphabetical order of the elements or groups of elements (e.g. alkali metals). Most elements are included, even oxygen, but not hydrogen. The chapters have similar formats: a brief description of the element in various oxidation states, reviews of separation methods and spectrophotometric procedures, practical details of the most useful spectrophotometric pro-

cedures, summaries of other procedures, and an extensive reference list. The book ends with a comprehensive subject index.

There is no doubt that Professor Marczenko has done a considerable service to analytical chemistry by collecting such a wealth of information in one book. It provides ready access to information that is becoming increasingly useful as interest in spectrophotometry revives. It is an essential text for anyone involved in inorganic trace analysis who uses spectrophotometry, and at a cost of ca. £1 per element, good value.

Alan Townshend

K. Carr-Brion, *Moisture Sensors in Process Control.* Elsevier/Applied Science Publishers, London and New York, 1986 (ISBN 1-85166-005-4). ix + 122 pp. Price £24.00.

The determination of water has always been, and will probably continue to be, one of the most difficult analyses to achieve precisely and accurately under any circumstances. The reliable, accurate determination of water in flowing streams is particularly problematic and if the results of these determinations are to be used for plant process control, the requirements of the sensor in terms of precision, accuracy, reversibility and response time have to be considered very carefully.

In this small book, aimed at providing a concise practical guide to the on-line determination of moisture for process control, Ken Carr-Brion has condensed current thinking and contemporary technology for the on-line determination of water. The author discusses moisture measurement in gases, liquids, slurries, pastes, emulsions and solids in the first half, and the second half of the book considers the determination of moisture form, calibration of sensors, electronics for data transmission, conversion and verification and also how to select and from where to purchase the sensor most appropriate for the reader's needs. All of the commercially available moisture sensors are discussed in practical detail, with useful quantitative and qualitative performance data included. Advantages and disadvantages of the individual sensors are tabulated and comments of the applications in certain industries made. A number of diagrams and photographs complement the text, and, although the treatment is necessarily superficial, the reader is bound to learn a considerable amount from this detailed description.

Whereas the author has purposely left out any detailed theoretical treatment of the sensor response functions, I feel that the text would have benefitted by a slightly more detailed discussion of the physical and chemical principles involved in the sensing process employed by the various systems. Likewise, the chapter on calibration of on-line moisture sensors is remarkably short (8 pp.) for such an important aspect of any sensor operation. For these sensors to be involved closely in process control, it is essential

that precise and true values of water content be fed into the control system, if reasonable control is to be effected. The ability to calibrate the sensors in a variety of matrix compositions is an essential part of their reliable operation. The chapter on the selection of on-line moisture sensors will be extremely useful to the engineer or scientist who is bewildered by the range of different, and expensive, equipment available to him, and the chapter on sources of moisture sensors will prove equally helpful.

Overall, this modest book achieves a great deal and is clearly written by a person who has experience in the field and has thus been able to give useful practical advice. Perhaps later editions will be able to treat some aspects in greater depth and discuss some of the thornier problems in practical water determinations where complex matrices and high accuracy requirements conspire to defeat the analyst.

J. F. Alder

Allen J. Bard (Ed.), *Electroanalytical Chemistry: A Series of Advances, Vol. 14*. M. Dekker, New York and Basel, 1986 (ISBN 0-8247-7608-9). xvi + 459 pp. Price $84.75 (U.S.A. and Canada), $101.50 (other countries).

It is well known that, with few exceptions, the electroanalytical chemistry of this series is not mainline analytical chemistry, but rather fundamentals of the development of instrumentation, events at electrodes, reaction mechanisms, etc. This volume is not very different, and readers who expect to find straightforward hints and directions for carrying out actual analysis will be disappointed. Nevertheless, there are four interesting articles here, namely, Precision in Linear Sweep and Cyclic Voltammetry, Conformational Change and Isomerization Associated with Electrode Reactions, Square Wave Voltammetry, and Infrared Vibrational Spectroscopy of the Electrode-Solution Interface.

The first chapter, by Vernon D. Parker (Trondheim, Norway), is typical of articles in the series, and is an informative discourse on the principles and apparatus of linear sweep and cyclic voltammetry (LSV and CV) and recognition of the fact that measurement precision is a severe problem. After consideration of this weakness and of ways of improving precision, the chapter goes on to deal with the kind of problems that can be solved by LSV and CV in their various forms, and comparison with other approaches.

The second chapter, by D. H. Evans and Kathleen M. O'Connell (Wisconsin), is essentially concerned with the various electrochemical properties of different conformations of a molecule. This includes attention to conformational change that precedes electron transfer as illustrated by tetraalkylhydrazines and vicinal dibromides, and change or isomerization that follows electron transfer as illustrated by *cis/trans* isomerization and torsion about double bonds and isomerization of organometallic complexes, and changes that are concurrent with electron transfer as illustrated by cyclooctatetrane and methoxyazocines.

Analytical chemists will be more at home with square-wave voltammetry, by Janet Osteryoung and J. J. O'Dea (Buffalo), a technique which was primarily responsible for the renaissance of electroanalysis. Barker's idea of rejecting the capacity current in linear scan voltammetry, by employing a staircase potential-time waveform and sampling the current once on each tread of the staircase after the capacity current had decayed to a negligible value, was imaginative in concept, with the bonus of considerable gains in sensitivity. This, with developments in electronics, led to many analytical chemist users of the new polarography who will avidly read this chapter which has been so well put together; it details the theory before passing on to the experimental side of instrumental considerations and applications.

The final chapter, by J. K. Foley, Carol Korzeniewski, J. L. Daschbach and S. Pons (Utah) is essentially concerned with putting infrared vibrational spectroscopy to work for elucidating events at the electrode-solution interface. After the theory and methodology it deals with adsorption, double layer, surface coverage, electrocatalytic oxidation-reduction and other application areas.

The volume succeeds in its stated objectives of in-depth, authoritative reviewing; but, except for the very expert, it is not bed-time reading. It is a characteristic of electrochemistry to have many acronyms. This book is full of them; usually they are defined, but the reader coming across DPSC on page 11 has to wade through to page 56 to find that it means "double-potential-step chronopotentiometry". However, errors are not easy to find. Collectors of the series will need to have this for themselves and for their graduate students to read what is relevant and a little more as well.

J. D. R. Thomas

G. Henze and R. Neeb. *Elektrochemische Analytik*. Springer, Berlin, 1986 (ISBN 3-540-15048-X). x + 383 pp. Price DM 298.

The scarcity of modern electroanalytical texts in the German language makes this volume a welcome addition to the analytical chemist's bookshelf, even though the price appears to be very high. The text is arranged into four chapters. Chapter 1 gives the electrochemical background, Chapter 2 describes the various electroanalytical methods, Chapter 3 discusses polarographic and voltammetric determination of inorganic and organic materials and Chapter 4 deals with the practical application of electroanalytical techniques. A list of symbols and abbreviations is provided, besides the usual table of contents and index. Printing and layout is exemplary, and the figures and the numerous and detailed tables are clearly presented.

There is a great deal of material covered in this book, though it can be rather difficult to find particular items. To me, the arrangement of the material into the above chapters is rather unsatisfactory. The split between

Chapters 3 and 4 is not clear, as there are numerous applications of voltammetry described in the 4th Chapter. While the inorganic material in Chapter 3 is excellently covered, I found the organic section rather sketchy. The arrangement of Chapter 2 is somewhat unclear: pulse-, inverse- and a.c.-voltammetry are treated in separate sections (not under "voltammetry"), oscillopolarography appears under "miscellaneous methods", as do amperometric titrations. Again, the section on "instrumentation, evaluation and sources of errors of polarographic methods" seems to me out of place at the end of Chapter 2. But, in spite of these shortcomings, I have no hesitation in recommending this book to the analytical public, who will find here a wealth of information, which can be located via the excellent and detailed index.

G. Svehla

R. E. Kaiser (Ed.), *Planar Chromatography, Vol. 1.* Hüthig, Heidelberg, 1986 (ISBN 3-7785-0780-X). ix + 265 pp. Price DM 88.

This is the first volume in a specialised series of texts purposely designed to exclude classical TLC because it has been treated in detail elsewhere (e.g. Touchstone and Dobbins, recently reviewed here) and also because of "non-controllability" in its simple modes. The material is a collection of independent essays on a range of theoretical, technique and application areas, in a variety of styles; some sections require major deconvolution prior to consideration of their content.

The contents are summarized as follows. Definitions, introduction, comparisons (R. E. Kaiser); Optimization in chromatographic analysis (S. Turina); HPTLC compared critically with TLC, OPLC and HPLC (R. E. Kaiser); Equilibrium sandwich TLC chambers (E. Soczewiński); Instrumental preparative planar chromatography (Sz. Nyiredi, C. A. J. Erdelmeier and O. Sticher); HPTL circular chromatography — a new dimension in analytical chromatography ranging from GC to LC? (R. E. Kaiser and R. I. Rieder), Automatic multiple development (K. D. Burger and H. Tengler); Image processing of HPTLC (R. M. Belchamber, H. Read and J. D. M. Roberts); Image processing evaluation of some sugars (M. Prosek, M. Medja, J. Korsic and M. Pristar); Computer-aided evaluation of continuous development two-dimensional TLC (J. E. Steinbrunner, E. K. Johnson, S. Habibi-Goudarzi and D. Nurok); Cyclodextrin mobile phases for mycotoxins (H. M. Stahr and M. Domoto).

With such a diverse range of content it is perhaps invidious to pick out any sections for comment since the views expressed are as likely to reflect as much on the reviewer as the author(s). However, the chapters dealing with the mathematical basis of optimization in chromatography and the critical comparison of HPTLC with other LC methods were found to be of great interest. No doubt others will find that different sections appeal since there is much of quality therein.

D. T. Burns

K. Grob, *Making and Manipulating Capillary Columns for Gas Chromatography*. Hüthig, Heidelberg, 1986 (ISBN 3-7785-1312-5). iii + 232 pp. Price DM 68.

In the preface the author explains that this book evolved in response to appeals from fellow chromatographers for a complete description of his way of working. The result is a book which is more a laboratory guide for individual column makers than a theoretical text. Chapter 1 (Introduction) is related to practical column technology rather indirectly through ideas, concepts and critical comparisons. It begins by considering why chromatographers prefer to make their own columns and ends by offering words of advice to those entering this vast field. It is the only chapter that can be read from beginning to end. Chapter 2 (General Column Preparation) considers the materials and tools required for column manufacture. Manipulations of general importance are classified such as producing and handling capillaries, cutting techniques, handling plastics, filling and rinsing and permanent connection of capillary columns. Chapter 3 (Special Column Preparation) should be considered as the principal part of the book and should be used as a laboratory guide to column manufacture. The user first finds the column of interest in the preparation scheme inside the rear cover, together with the preparation steps involved. Each step carries a number corresponding to a specific working direction, given in the text.

The book is innovative in its mode of presentation. It has wide margins, key sentences produced in heavy type for emphasis, and diagrams and figures, all clearly presented. The author deals with technical description in a clear, down-to-earth manner which holds the reader's attention. The usefulness of this book to those who merely wish to collect information on capillary columns, however, is limited. It is written for the practising chromatographer wanting to make a specific kind of capillary column, who will find a wealth of practical and technical information therein.

Michael J. Cope

B. G. Belenkii and L. Z. Vilenchik, *Modern Liquid Chromatography of Macromolecules, Vol. 25* in the series, *Journal of Chromatography Library*. Elsevier, Amsterdam, 1984 (ISBN 0-444-42075-4). xviii + 432 pp. Price $110.75.

Despite the title, this book is largely concerned with separations of polymers by gel permeation chromatography (GPC), also known as gel filtration chromatography (GFC) and size exclusion chromatography, which is covered in detail in Chapters 3, 4, 5 and 6. The other techniques for polymer separations are: thin-layer chromatography (TLC) in Chapter 7, and field-flow fractionation (FFF) and hydrodynamic chromatography (HDC) in the final chapter.

The first chapter is concerned with the general theory of the kinetics of the chromatographic process, including consideration of efficiency, selectivity and resolution in order to choose the optimum chromatographic conditions. Thermodynamic aspects of macromolecular retention in GPC and in adsorption chromatography with rigid packings are discussed in Chapter 2, and extended to interpret the separation behaviour of polymers with swollen gel packings. Both these chapters are clearly presented, and a thorough treatment of separation mechanisms is given in Chapter 2 including fundamental concepts proposed by Belenkii and his group. The following four chapters on GPC/GFC provide extensive details on data analysis (calibration methods and correction methods for chromatogram broadening), on column packings, polymer standards, solvents, instrumentation and operating procedures, on GPC for characterisation (e.g. oligomers, polyelectrolytes, branched polymers, copolymers), and on GFC with rigid packings for characterizing water-soluble polymers. Much of the information in these chapters will be valuable to practitioners of GPC. Chapter 7 contains details on TLC of polymers, with particular emphasis on studies of structural variations and composition distribution in copolymers. Chapter 8 provides only brief surveys of FFF and HDC.

This book is highly recommended. It should be purchased by a library serving laboratories involved with the chromatography of polymers, but the price may deter chromatographers purchasing personal copies.

J. V. Dawkins

R. L. Grob (Ed.), *Modern Practice of Gas Chromatography, 2nd edn.*, Wiley, New York, 1985 (ISBN 0-471-87157-5). xvi + 897 pp. Price £75.20.

The first edition of what has become a standard book was based on an annual short course in gas chromatography and ran to eight reprints. After such a proven success the updated second edition was thus welcome in principle, and on perusal was found to live up to the expectation. It is highly recommended for those who need either a basic course or an update in the subject. The material is logically divided into three sections, theory and basics, techniques and instrumentation, and finally, applications. The treatments of the various topics and areas are detailed and all follow current IUPAC nomenclature and terminology. The overall level is at advanced postgraduate/serious non-empirical practitioner level.

The editor is to be doubly congratulated, firstly for assembling the distinguished set of authors and secondly for their uniformly high performance. The publishers have also done a first class job on the layout, diagrams, indexing etc. An interesting and useful appendix is that on gas chromatographic acronyms and symbols and their definitions, a great aid and defence against those who try to exclude the uninitiated via over use of jargon. It is an essential purchase for all higher level teachers of analytical chemistry

and their institutional libraries, chromatographers in industry and the public services. It is the best current book on the subject.

D. T. Burns

Ervin Jungreis, *Spot Test Analysis. Clinical, Environmental, Forensic and Geochemical Applications.* Wiley-Interscience, New York, 1985 (ISBN 0-471-86524-9). xi + 315 pp. Price £76.00.

To many 'older' analytical chemists, their interest in analytical chemistry arose from the classical studies of chromogenic reactions collected and rationalized by Fritz Feigl in his famous books on Spot Tests in Inorganic and Organic Analysis. It is particularly pleasing to see that such spot tests have not entirely disappeared under the pressure of modern instrumental techniques. The present book shows that there are still numerous situations where the simple spot test provides, at little expense, a rapid, sensitive and selective answer to an analytical problem. Most of these are qualitative tests but some quantitative procedures are given, (although some of these, such as oxygen demands, are hardly spot tests). Thus, tests as intriguing as those for chillproofing agents in beer, for differentiation of butter and margerine, and for mammalian faeces in food, rub shoulders with screening tests for sugars and artificial sweeteners, tests for explosives and for the quality and composition of flour. Experimental details for each test are included. With the current growing trend to carrying out increasing numbers of analyses in the field (i.e. at the riverside, the doctor's surgery or at the shop counter), the appearance of this book is a timely reminder of the continuing value of a knowledge of chemical reactions and observational skill in analytical chemistry, and that high-powered instrumentation is not the sole answer to analytical problems.

Alan Townshend

Sidney Williams (Ed.), *Official Methods of Analysis of the Association of Official Analytical Chemists, 14th edn.*, AOAC, Arlington VA, 1984 (ISBN 0-935584-24-2). xxvi + 1141 pp. Price $148.50 (U.S.A.), $151.50 (all other countries).

This centennial edition will be welcomed throughout the analytical community. It presents, as in previous editions, an immense collection of collaboratively tested and validated methods of analysis for a very wide range of materials. These are arranged in 49 sections, covering various foodstuffs, beverages and additives, drugs, pesticides and other toxic materials, agricultural materials and cosmetics, forensic and biological methods, and radioactivity. As always, clear procedures for solution preparation and the analytical method are given, with appropriate references, including

J.A.O.A.C. papers, at the end of each method. There are also chapters on standards, reference materials and laboratory safety, and extensive tabulated data, mostly relating to ethanol and sugar solutions.

Advances in analytical technology will always be slow to appear in authoritative collections of this sort. However, in this edition, inductively-coupled plasma atomic emission spectrometry is introduced for multielement analysis. In addition, one of the automated methods has been written in generic terms i.e. by listing performance specifications, rather than referring to a specific type of instrument. A total of 167 new methods is included in this edition, of which ca. 25% are based on HPLC or GLC. This is a trend which will undoubtedly accelerate. I congratulate the Association of Official Analytical Chemists on reaching their centenary, and thoroughly recommend this new edition of their compendium of methods to all analytical chemists.

Alan Townshend

W. Dennis Pocklington, *Guidelines for the Development of Standard Methods by Collaborative Study, 2nd edn.*, Laboratory of the Government Chemist, London, 1986. ca. 132 pp. Price £25.

The value of collaborative testing of analytical methods has long been recognized, but the collaborative testing and harmonization of such collaborative studies has taken much longer. Even now, there is no complete agreement as to how such studies should be carried out, but the present document presents the considerably improved situation that has arisen since the Symposium on the Harmonization of Collaborative Studies, in Washington, 1984, and subsequent ISO and IUPAC deliberations. Complete international agreement on the most suitable model has not yet been achieved, however, so that the present text describes a number of alternative models. It is hoped that an agreed model will be finalized before the end of 1987.

The Guidelines are in two sections. The first deals with the organization of the collaborative study, covering the number of participants, the text of the method, samples, instructions for participants and the report of the coordinator. It is emphasized that all these items must be agreed in great detail before embarking on the measurement stage. The inclusion of a specimen 'Agreement' form is most welcome. The second section gives detailed instructions for the statistical analysis of the results obtained by the various study models, and includes numerical examples of the calculations involved. Together they provide an extremely comprehensive account of the organization of the collaborative development of analytical methods, and all participants (especially the organizer) of such exercises cannot be recommended too strongly to follow all the guidelines given.

G. Brubacher, W. Müller-Mulot and D. A. T. Southgate, *Methods for the Determination of Vitamins in Food, Recommended by COST 91*, Elsevier

Applied Science, London, 1985 (ISBN 0-85334-339-X). x + 166 pp. Price £20.00.

This book is essentially the outcome of the first step in establishing tested and recommended methods for the determination of vitamins in foods. It comprises recommended methods for vitamins A, B, C, E and carotene and tentative methods for vitamins B_2, B_6 and D, and briefly describes procedures for niacin and folacin. The methods were selected by a group of European experts working under the aegis of the COST 91 project (effects of thermal processing and distribution on the quality and nutritive value of food). The methodology is described in detail, the methods having been selected for accuracy, precision and reasonable robustness. Many of them involve liquid chromatography or spectrophotometric measurement. The editors freely admit the quite large areas where more testing and standardization are necessary, hence the inclusion of tentative as well as recommended methods. Such areas include sampling, where too often all that can be said is that "the proportional composition .... must be representative of the material ... to be analyzed". Hopefully, therefore, the book should provide the starting point for much needed improvements in methods for determination of vitamins, as well as providing information as to best current practice.

H. G. Jerrard and D. B. McNeill, *A Dictionary of Scientific Units, Including Dimensionless Numbers and Scales, 5th edn.*, Chapman and Hall, London, 1986 (ISBN 0-412-28090-6 or -28100-7 paperback). ix + 222 pp. Price £18.00 (hardback), £8.95 (paperback).

This new edition updates a book whose intention has been to list "any scientific unit .... which has appeared in print." This time more than 850 units and dimensionless numbers are included, covering all scientific disciplines, units that are currently acceptable and those of yesteryear. As well as the expected, you will find, for example, pencil hardness, the Beaufort scale, the misery index and wood screw sizes, and units such as the clo, the ce, the mel, the kip and the drex. The only major omission seems to be the proof scale for spiritous liquors! Most analytically useful units are present, although optical density is defined in preference to absorbance. Appendices include a list of fundamental constants, standardization committees and conferences, tables of weights and measures, conversion tables and factors and a list of references. The description of the work of IUPAC is certainly dated, referring to "recent" reports issued in 1957, and still labouring under the assumption that columbium is scientifically acceptable in the USA.

B. J. Finlayson-Pitts and J. N. Pitts, Jr., *Atmospheric Chemistry*, Wiley, New York, 1986 (ISBN 0-471-88227-5). xxviii + 1098 pp. Price £57.45.

This is a large and ambitious book in a rapidly developing area of chemistry. The authors have wisely chosen to confine themselves predominantly to a consideration of the chemistry of the troposphere, with only a token incursion, in the final chapter, into its interaction with the chemistry of the stratosphere.

The bulk of the early chapters deal with the photochemical and kinetic backgrounds to laboratory studies of atmospheric systems. The scientific approach is soundly based, following the pattern of, and updating, the classic book in this field, "Photochemistry of Air Pollution" by Philip Leighton published in 1961. Useful chapters follow on monitoring techniques for atmospheric pollutants and techniques for smog chamber studies of simulated atmospheres, both of which contain clear and readable accounts of the battery of spectroscopic and other techniques presently being brought to bear in tropospheric chemistry. The next three chapters focus on the real atmosphere, covering the modelling of photochemical air pollution, acid deposition and atmospheric particulate matter. There follows a long chapter on the chemistry and mutagenic activity of polycyclic aromatic hydrocarbons together with a chapter on the chemistry of the natural troposphere.

This book is well written and well presented. It is clearly centred on the large volume of research work and publications which have emanated from the Riverside Air Pollution Research Center. It is consequently not difficult to find gaps in the coverage, and unevenness in the treatment of some topics. Nevertheless, I would predict that this book will form the backbone of undergraduate and post-graduate teaching in tropospheric chemistry for some time to come.

J. A. Kerr

R. E. Hester (Ed.), *Understanding our Environment*, Royal Society of Chemistry, London, 1986 (ISBN 0-85186-907-6). xiii + 333 pp. Price £42.50/$77.00.

The stated aim of this book is to provide a wide-ranging and authoritative coverage of topics which are fundamental to our understanding and appreciation of the nature of our environment. The result is an interesting and extremely readable publication, containing six chapters which collectively demonstrate the multi-disciplinary nature of environmental issues such as acid rain, water quality and the dumping of toxic wastes.

The topics covered are monitoring (C. N. Hewitt and R. M. Harrison), the air (A. G. Clarke), water (H. Fish), land contamination (E. E. Finney and K. W. Pearce), assessing the ecological and health effects of pollution (S. Smith) and regulation and the economics of pollution control (P. Burrows, N. Highton and A. I. Ogus). The book is therefore aimed at a general audience and not directly towards analytical chemists, but the information it contains provides a useful background for those in the area of environmental analysis.

Of the material presented, the chapter on monitoring is of most immediate interest to analytical chemists, and covers in detail the establishment of environmental monitoring programmes (particularly sampling techniques) for air, water, soil and sediments, remote sensing and several case studies are also included.

The price is a little high, but this book is nonetheless recommended reading for any chemist with an interest in environmental issues.

P. J. Worsfold

P. M. Lonn (Ed.), *Methods in Enzymology, Vol. 124*, Academic Press, Orlando FL, 1986 (ISBN 0-12-182024-6). 679 pp. Price $77.50.

One of the most exciting developments in pharmaceutical chemistry has been the advances which have occurred with the neuroendocrine peptides. Perhaps the best known examples of these neuropeptides are the enkephalins and the endorphins which exert morphine-like actions. This current volume of Methods in Enzymology provides an invaluable experimental basis for investigating many of these peptides. It should be indispensable for all those who work in pharmaceutical laboratories, whether these be in industry or academia.

There are some 41 separate articles covering five separate sections: the longest section covers the measurement of the various neuroendocrine substances including the genes which are responsible for coding for many of the polypeptide hormones. There are shorter sections on the preparation of chemical probes and the equipment and technology which are involved with these studies. There is a short section on the preparation and maintenance of biological materials which would be helpful in just a few specialized instances and the final section covers a miscellaneous collection of techniques aimed at the localization of the neuroendocrine substances.

Altogether, this is a highly specialized techniques volume which will give valuable insight into those areas which are as yet peripheral to the principal interests of those people who are already involved in neuroendocrine research.

Colin Ratledge

H. U. Bergmeyer (Editor-in-Chief), *Methods of Enzymatic Analysis Vol. IX: Proteins and Peptides*, VCH, Weinheim, FRG, 1986 (ISBN 3-527-26049-8). xxv + 571 pp. Price DM 310.

This book is one of twelve volumes in the recently revised and expanded third edition of Bergmeyer's "Methods of Enzymatic Analysis". As with the previous English editions (1963 and 1974), the third edition is clearly written, well presented and contains a wealth of information on practical aspects of enzymatic analysis.

Volume IX on proteins and peptides is one of several volumes in the latest edition to cover applications based on the technique of enzyme immunoassay. There is a useful introductory chapter, with the section on practical considerations in enzyme immunoassays being particularly recommended for readers unfamiliar with the technique. An ELISA procedure for the proteinase inhibitor aprotinin is used as a model system and all of the steps in the development of the assay are discussed.

The other four chapters cover the determination of particular proteins within the following group areas: transport proteins (6 applications), carcinoembryonic and pregnancy proteins (4 applications), structural and regulatory proteins (12 applications) and hormonal proteins and peptides (15 applications). Each of the applications is written by experts in that particular field but the editors have managed to achieve a uniform presentation of information throughout the volume, and indeed the series. For each determination there is a general introduction, details of the assay procedure, a method validation and an appendix.

This volume therefore provides an excellent reference source for laboratories involved in the determination of proteins and peptides by enzyme immunoassay procedures, and the twelve volume series is recommended for its comprehensive coverage of enzymatic analysis.

H. U. Bergmeyer (Editor-in-Chief), *Methods of Enzymatic Analysis Vol. X: Antigens and Antibodies 1.* VCH, Weinheim, FRG, 1986 (ISBN 3-527-26050-1). xxii + 509 pp. Price: (single volume) £115.00, (series subscription) £84.00.

This is another of the twelve volumes that constitute the third edition of Bergmeyer's "Methods of Enzymatic Analysis". The new edition has been extensively revised and expanded, and includes two volumes (X and XI) on the topic of enzyme immunoassays. Previous editions have provided clear and comprehensive coverage of enzymatic methods, with particular emphasis on practical considerations, and this volume is in the same category.

The methodologies described in this particular volume are all based on solid phase immunoassays, either competitive binding enzyme immunoassays or sandwich assays. The introduction outlines the rapid growth of enzyme immunoassay techniques over the last decade and emphasises the need for a standardized approach, e.g. in terms of methodology, the use of reference preparations and the presentation of data. This is followed by a series of specific applications, which are designed to serve as model systems for related species. Each application contains a clearly illustrated diagram of the assay principle, detailed instructions on the preparation of reagents and experimental procedures, and a discussion of method validation.

The applications considered fall into three main areas: immonoglobulins and immune complexes, antigens and antibodies in allergic and autoimmune

diseases, e.g. red blood cell autoantibodies and rheumatoid factors, and antigens and antibodies in viral diseases, e.g. cytomegalovirus antibodies and hepatitis B virus. Only three enzyme labels: peroxidase, alkaline phosphatase and β-galactosidase, are used in the thirty-four applications covered.

As with previous editions, this volume is likely to become a primary reference source for workers in the field because of its comprehensive coverage of enzyme immunoassay techniques for antigens and antibodies, but it is not an appropriate text for anyone requiring a general introduction to the subject.

P. J. Worsfold

B. A. Morris and M. N. Clifford (Eds.), *Immunoassays in Food Analysis.* Elsevier Applied Science Publishers, London, 1985 (ISBN 0-85334-321-7), xxi + 222 pp. Price £25.00.

Interest in the application of immunoassays to the analysis of foodstuffs led to the organisation of the first symposium on the subject at the University of Surrey in September 1983. This book presents the proceedings of that conference in an expanded and well organised form, and contains papers from three sessions covering the principles of immunoassays and their application to macromolecules and to small molecules.

The first section outlines the principles of classical and immunometric assays and discusses the various non-isotopic labels that are used, with particular reference to enzyme labels. There are also useful practical details, extensive reference lists and a glossary, which combine to make a very readable introduction to the subject.

In recent years there has been a growing interest in the application of immunoassay procedures to non-clinical samples, e.g. food and environmental analysis and forensic and veterinary science; the heterogeneous nature of the samples, particularly in the food industry, has presented problems that were not encountered in the clinical area. These are discussed in some detail in the second section, which contains applications of immunoassays, predominantly ELISA techniques, to the analysis of food, e.g., the identification of meat, and the determination of soya protein in meat and amyloglucosidase in beer. Experimental conditions and results are given for most applications and the cross-reactivity of antisera is also considered. The final section provides similar coverage of the determination of small molecules in foods, e.g., anabolic steroids in meat.

The growing importance of immunoassay techniques in the food industry is illustrated by the recent introduction of immunoassay kits for specific determinands. This book therefore provides a useful and well presented source of material for workers in the field and at the same time is appropriate for a wider audience wishing to become more acquainted with the general principles of immunoassays.

P. J. Worsfold

S. B. Pal (Ed.), *Immunoassay Technology, Vol. 2.* de Gruyter, Berlin, 1986 (ISBN 3-11-010948-4). 247 pp. Price DM 148 (paperback).

This is the second volume of a series of review articles and methods dealing with nonisotopic immunoassay techniques of biological, commercial and environmental importance. The first volume (in 1985) contained six contributed papers (see review in Anal. Chim. Acta, 183 (1986) 326) and this issue (which is dedicated to Professor Michael Finkelstein) contains ten contributions covering a wide range of topics. There are review papers on conjugation procedures in enzyme immunoassay, immunoselective electrodes, therapeutic drug monitoring by automated fluorescence polarization immunoassay, antibody synthesis *in vitro*, liposome immunoassay and the use of detergent solubilized antigens. The four methodology papers discuss the determination of antibodies to insulin, DNA and sperm.

The edited articles are reproduced directly by photo-printing, leading to quick publication of contributed material, which is particularly important for a subject developing as rapidly as nonisotopic immunoassays. The quality of the printing is good, but the clarity of figures is variable. There is also a brief biography of the contributors and a small section on commercially available immunoassay reagents.

The increased number of contributions in this volume and the breadth of material covered suggest that this series will become a useful literature source for those who are actively engaged in any aspect of immunoassay work.

C. Engelmann, G. Kraft, J. Pauwels and C. Vandecasteele, *Modern Methods for the Determination of Non-metals in Non-ferrous Metals. Application to Particular Systems of Metallurgical Importance.* de Gruyter, Berlin, 1985 (ISBN 3-11-010342-7). xii + 410 pp. Price DM 190.

The determination of non-metals in metal samples has always been necessary but often difficult and unreliable, as well as requiring methodology quite unlike that used for any other metallurgical analyses. This book is unusual in that it brings together descriptions of the determination of all common non-metals in a wide variety of non-ferrous metals, using procedures and samples tested collaboratively under the auspices of the EEC Bureau of Reference. It begins with a useful summary of the influence of oxygen, nitrogen, carbon, boron, sulphur and phosphorus on the technological properties of non-ferrous metals. The second and third chapters cover basic concepts and practicabilities of nuclear methods of analysis and sample preparation for surface analysis. These are followed by individual chapters on the determination of each of the above elements in a wide variety of non-ferrous metals. The methods are based on neutron, charged-particle or photon activation analysis and chemical procedures. Each chapter has a section dealing with the evaluation of the methods and an extensive refer-

ence list. This is a most useful compilation that will be of value in any laboratory where metal analysis is routinely carried out.

A. Townshend

D. T. E. Hunt and A. L. Wilson, *The Chemical Analysis of Water: General Principles and Techniques, 2nd edn.* Royal Society of Chemistry, London, 1986 (ISBN 0-85186-797-9). xxi + 683 pp. Price £55.00.

This edition, like the first, contains a comprehensive discussion of all aspects of water quality measurement, with particular reference to fresh, natural waters and drinking waters. There are thirteen chapters, each with an extensive reference list, covering every stage of the analytical process from the definition of information requirements, through sampling and analytical techniques, to the estimation and control of errors and the reporting of results. A detailed table of contents is included, but not a general index.

The authors are to be commended for paying particular attention to aspects of sampling and to the estimation and control of bias and precision. Indeed, the first half of the book is devoted to these topics and provides a detailed but readable account of the application of a wide range of statistical tests to water analysis. The second half of the book describes the various techniques available for the chemical analysis of water and includes a critical appraisal of automatic and on-line analysis. By design, detailed written procedures for substances of interest are not included.

This book contains useful information on all the steps involved in the analytical process, and as such, is appropriate as a general analytical text. The broad, yet authoritative coverage of water analysis in particular also makes it a highly recommended primary reference source for specialists in the field.

P. J. Worsfold

J. W. Robinson, *Undergraduate Instrumental Analysis*, M. Dekker, New York, *4th revised edn.*, 1987 (ISBN 0-8247-7406). xxviii + 640 pp. Price $34.75 (USA and Canada), $41.50 (all other countries).

The fourth edition of this book is revised and expanded. It presents a discussion of the basic principles of almost all instrumental methods currently used in analytical chemistry. After an introductory chapter on the concepts of analytical chemistry, spectroscopic methods are discussed in the next ten chapters in order of decreasing wavelength of the radiation involved. The final five chapters deal with surface analysis, chromatography, thermal analysis, mass spectrometry and electrochemistry. Titrimetric and gravimetric methods are not included, because the author felt them to be

superfluous in view of the many good books available on these topics. The various subjects are clearly treated and the author has succeeded in making each chapter as self-explanatory as possible. Each chapter ends with a number of problems and many of the chapters have some suggested experiments as well.

The book will be of value not only for undergraduate students, but it can be recommended to every analytical chemist who wants to refresh his knowledge. In this respect the newly added chapter on surface analysis is particularly useful. The very great number of techniques discussed has one drawback: the length of the various parts do not reflect their relative importance in analytical chemistry. As an example only a few pages deal with HPLC whereas an equal number of pages is devoted to conductometric analysis. The reviewer also objects to the definition used for sensitivity, which is not in accordance with the recommendations of IUPAC and ISO. The book is well-printed and has a clear, but rather conventional lay-out. In some cases the figures are rather schematic and too rough. However, these minor points of criticism do not affect the overall positive impression.

W. E. van der Linden

Clifford W. Hand and Harry L. Blewit, *Acid—Base Chemistry*. Macmillan, New York, 1986 (ISBN 0-333-0234 99 109). 273 pp. Price £15.50.

Acid—base chemistry plays an important role in introducing undergraduate students to the theoretical foundations of solution equilibria. In most textbooks the Arrhenius concept and the Brønsted-Lowry theory are treated extensively in contrast to the theory of Lewis which usually is only defined. For organic chemists, however, the Lewis theory is very profitable as it provides a useful hatrack on which to hang seemingly unrelated systematic organic reactions. This book is meant to bridge this gap and to show the mutual relation of these concepts to both fields of chemistry.

The book contains excellent material insofar as is related to organic chemistry. The treatment of the aqueous equilibria, however, is far from systematic. pH calculations and calculations of titration curves are demonstrated through many examples, but the mathematical treatment is poor and inconsistent. Moreover, the fact that approximate methods can generally be used, as most experimentally determined equilibrium constants are fairly inaccurate and medium dependent (on ionic strength), is hardly indicated. Instead error discussions appear which are far from realistic. Therefore although the book is well printed and reasonably free from typing errors it suffers from a split level treatment. The Lewis concept is treated well; for the common pH calculations and titration curves much better textbooks are available. At the end of the book some BASIC software programs are given for the exact calculation of the pH of buffers and polyprotic acids. The calculation of a titration curve, however, fails. It is a pity that the con-

sistent treatment advocated in the introduction has not been achieved. Starting from the viewpoint that only the best books should come into the hands of students, this one is on the borderline for introduction in curriculae.

J. Kragten

J. Zupan (Ed.), *Computer-supported Spectroscopic Databases.* Ellis Horwood, Chichester, 1986 (ISBN 0-85312-941-X). viii + 166 pp. Price £28.50.

Have you ever used a modern spectrometer with its own data base to identify an unknown compound? Maybe as the possible structures are printed out you have wondered, how does it do it? This multi-author book expounds the principles of organisation and searching of such data bases. While storage of a mass spectrum (mass numbers and intensities) in a computer is simple, the storage in digital form of high resolution IR and NMR spectra with their complex peak shapes is more daunting. Each chemical substance needs to be stored in a way that will allow correlations between its structural elements and the corresponding spectrum to be drawn. When a spectroscopist examines a spectrum and attempts to relate it to a chemical structure, much complex reasoning is involved. A spectroscopic data base needs a complex management program, which will attempt to carry out similar assignments, but yet is easy for a chemist to use. Solutions to problems like these are discussed in detail in eight chapters, of which four cover general problems of spectroscopic data bases, and four deal with the individual techniques of IR, NMR and mass spectrometry.

If you make use of spectrometers with data bases this book is sure to increase your understanding of the way such systems work, and give you a good idea of likely developments in the next few years.

J. R. Chipperfield

O. Strouf, *Chemical Pattern Recognition*, Research Studies Press (distributed by Wiley), 1986 (ISBN 0-86380-044-0). xvi + 202 pp. Price £26.65.

This is number 11 in the Chemometrics series of monographs published by RSP and marketed worldwide by Wiley. The stated aim of the book is to summarize and discuss the achievements in chemical pattern recognition since 1979. The most important contribution of this monograph is the collection of 350 references covering the methodologies and a wide range of applications. Any chemist with even a passing interest in the topic is likely to find 10—20 references to follow up. The introduction, survey of applications, and recent trends chapters, although very readable, are not much more than a guide to the references.

The heart of the text is the detailed exposition of the various techniques that are available. In the supervised classification section, good explanations

of discriminant, learning machine, *K*-nearest neighbours, probability density, SIMCA and some extensions are given. Two methods new to the reviewer were the deviation-pattern and SPHERE methods (the latter looks very similar to SIMCA). The unsupervised classification section describes hierarchical cluster analysis including a new method called fractal clustering and some recent extensions of non-hierarchical clustering by the Massart School. Selection of features and visualisation are also discussed.

On the negative side there are no detailed descriptions of regression, partial least squares, or target factor analysis. I would have liked to have seen more on the recognition of patterns among the features as opposed to the samples. Nevertheless, at the price, I would recommend this book to the chemist as an up-to-date introduction, and to the chemometrician for the new methods and the reference collection.

H. J. H. MacFie

ANALYTICA CHIMICA ACTA, VOL. 193 (1987)

AUTHOR INDEX

INFORMATION FOR AUTHORS

Detailed "Information for Authors" was published in Vol. 190, No. 2, pp. 375–378. A free reprint is available from the Editors or from:

Elsevier Editorial Services Ltd., Mayfield House, 256 Banbury Road, Oxford OX2 7DH (Great Britain)

Types of contribution. The journal welcomes original research papers, short communications and reviews. Reviews are written by invitation of the editors, who welcome suggestions for subjects. Short communications are usually complete descriptions of limited investigations, and should generally not exceed six printed pages. Preliminary communications of important urgent work can be printed within four months of submission, if the authors are prepared to forgo proofs.

Manuscripts. The preferred language of the journal is English, but French and German manuscripts are also acceptable. For authors whose first language is not English, French or German, linguistic improvement is provided as part of the normal editorial processing. Authors should submit three copies of the manuscript in double-spaced typing on one side of the paper only, with a margin of 4 cm, on pages of uniform size. If any variety of machine copying is used (e.g. xerox), authors should ensure that all copies are easily legible and that the paper used can be written on with both ink and pencil. Authors are advised to retain at least one copy of the manuscript. Manuscripts should be preceded by a sheet of paper carrying (a) the title of the paper, (b) the name and full postal address of the person to whom proofs are to be sent, (c) the number of pages, tables and figures.

Information on the *submission of papers* is given on the inside front cover.

Summary. Research papers and reviews begin with a Summary (50–250 words) which should comprise a brief factual account of the contents of the paper, with emphasis on new information. Short communications and preliminary communications require summaries, which should not exceed 50 words. Uncommon abbreviations, jargon and reference numbers must not be used. The Summary should be suitable for use by abstracting services without rewriting. Papers in French or German require a Résumé or Zusammenfassung preceded by a Title and Summary in English; authors are encouraged to provide translations where necessary.

Introduction. The first paragraphs of the paper should contain an account of the reasons for the work, any essential historical background (as briefly as possible and with key references only) and preliminary experimental work.

Figures. Figures should be prepared in black waterproof drawing ink on drawing or tracing paper of the same size as that on which the manuscript is typed. One original (or sharp glossy print) and two photostat (or other) copies are required. Attention should be given to line thickness, lettering (which should be kept to a minimum) and spacing on axes of graphs, to ensure suitability for reduction during printing. Axes of a graph should be clearly labelled, along the axes, and outside the graph itself.

All figures should be numbered with Arabic numerals, and require descriptive legends. Explanatory information should be placed not in the figure, but in the legend, which should be typed on a separate sheet of paper. Simple straight-line graphs are not acceptable, because they can readily be described in the text by means of an equation or a sentence. Claims of linearity should be supported by regression data that include slope, intercept, standard deviations of the slope and intercept, standard error, and the number of data points; correlation coefficients are optional.

Photographs should be glossy prints and be as rich in contrast as possible; colour photographs cannot be accepted. In general, line diagrams are more informative and less liable to dating than photographs of equipment, which are therefore not usually acceptable.

Computer outputs for reproduction as figures must be good quality on blank paper, and should preferably be submitted as glossy prints.

Nomenclature, abbreviations and symbols. In general, the recommendations of the International Union of Pure and Applied Chemistry (IUPAC) should be followed, and attention should be given to the recommendations of the Analytical Chemistry Division in the journal *Pure and Applied Chemistry* (see also *IUPAC Compendium of Analytical Nomenclature*, 1978).

References. The references should be collected at the end of the paper, numbered in the order of their appearance in the text (*not* arranged alphabetically), and typed on a separate sheet.

In the list of references, the following forms should be adopted.

Journals

1 W. Lund and M. Salberg, Anal. Chim. Acta, 76 (1975) 131.

2 M. McDaniel, A. D. Shendrikar, K. D. Reizneir and P. W. West, Anal. Chem., 48 (1976) 2240.

The title of the journal must be abbreviated as in the Bibliographic Guide for Editors and Authors.

Books

1 D. D. Perrin, Masking and Demasking of Chemical Reactions, Interscience–Wiley, New York, 1970, p. 188.

2 S. Hofmann, in G. Svehla (Ed.), Wilson and Wilson's Comprehensive Analytical Chemistry, Vol. 9, Elsevier, Amsterdam, 1979, p. 89.

Titles of papers are unnecessary. Citations of reports which are not widely available (e.g., reports from government research centres) should be avoided if possible. Authors' initials should not be used in the text, unless real confusion could be caused by their omission. If the reference cited contains three or more names, only the first author's name followed by et al. (e.g., McDaniel et al.) should be used in the text; but the reference list must contain the initials and names of *all* authors.

ANABIOTEC '88

2nd INTERNATIONAL SYMPOSIUM ON ANALYTICAL METHODS AND PROBLEMS IN BIOTECHNOLOGY

Noordwijkerhout, The Netherlands, 29–31 March, 1988

FIRST ANNOUNCEMENT AND CALL FOR PAPERS

Organized under the auspices of the Royal Netherlands Chemical Society (KNCV), Section for Analytical Chemistry, and the Netherlands Biotechnological Society (NBV)

ANABIOTEC '88

Analytical methods and systems for biotechnological applications are becoming increasingly important. The development of these methods and systems therefore calls for an interdisciplinary approach.

The use of analytical methods in daily practice in biotechnological research, development and industrial production is coming to be seen as essential for progress in biotechnology in general.

Close cooperation is needed between experts in analytical methodology, system development, and biotechnology.

The purpose of this second ANABIOTEC Symposium is to outline the progress already made through interdisciplinary discussion and cooperation and to deal with the rapid developments taking place.

The Symposium is intended for analytical chemists and both industrial and academic biotechnologists.

Topics

Topics covered will include:

- State-of-the-art analytical techniques already successfully applied in biotechnology.
- Strategies for the selection of analytical procedures with regard to optimum process control in industrial biotechnology, for environmental biotechnology and for fundamental and developmental research.
- Development of new analytical techniques for the above-mentioned areas.

Sessions are planned on: Sampling strategies, biosensors, mass spectrometry in process control, application of computers in analysis and process control, prospects for practical application of new analytical techniques, analytical problems in biotechnology.

The programme will consist of invited plenary lectures, invited and submitted papers (both oral and poster presentations) and discussion sessions.

Organizing Committee

Ir. B. te Nijenhuis
(Gist-brocades N.V.)
Dr. Ir. C. van Dijk
(TNO-Biotechnology)
Ir. W. A. Scheffers
(Delft University of Technology)
Dr. J. Kragten
(University of Amsterdam)

Call for Papers

Participants wishing to present a paper should submit an abstract, in English, of about 250 words before 15 October 1987 to the Symposium Secretariat.

In conjunction with the Symposium, an exhibition of instruments within its scope will be held.

For further information contact:

Symposium Secretariat
ANABIOTEC '88
c/o QLT Convention Services
Keizersgracht 792
1017 EC Amsterdam,
The Netherlands
Telephone: (31-20) 261372
Telefax: (31-20) 259574
Telex: 31578 inter nl attn. qlt

11A029 /381

ELSEVIER THE SCIENCE PUBLISHER
P O BOX 211 • 1000 AE AMSTERDAM • THE NETHERLANDS
P O BOX 1663 • GRAND CENTRAL STATION • NEW YORK • NY 10163